The Role of Branching Topology on Rheological Properties and its Effect on Film-Casting Performance

Christopher W. Seay

Dissertation submitted to the Faculty of
Virginia Polytechnic Institute and State University
in partial fulfillment of the requirements for the degree of

DOCTOR OF PHILOSOPHY
IN
CHEMICAL ENGINEERING

Advisory Committee:

Dr. Donald G. Baird, Chairman
Dr. Richey M. Davis
Dr. Timothy E. Long
Dr. John Y. Walz

April 24, 2008
Blacksburg, VA

Keywords: polyethylene, pom-pom model, film-casting, step-strain rheology

The Role of Branching Topology on Rheological Properties and its Effect on Film-Casting Performance

Christopher W. Seay

Abstract

With this research, we work towards the overall objective of customizing polymer molecules in terms of their molecular structure to optimize processing performance. The work includes analysis of the rheology in shear and shear-free flows for sparsely long-chain branched, LCB, polyethylene, PE, resins; determination of the consistency of the molecular based constitutive model, the pom-pom model; for these flows, and evaluation of the same PE resins in film-casting. As we progress towards molecular systems with defined molecular structural characteristics, we transition from a linear low density polyethylene, LLDPE, based series of PE resins to a high density polyethylene, HDPE, based series of PE resins, each with materials of varying degrees of sparse LCB.

Evaluation of the shear step-strain rheology for the series of LLDPE-based PE resins allows for the assessment of any inadequacies associated with the step-strain experiments and the ability of the K-BKZ analog of the pom-pom constitutive model to predict step-strain rheological behavior. Finite rise time and wall slip are addressed to ensure the accuracy of the experimental step-strain measurements and eliminated as factors contributing to the stress relaxation moduli response. Analysis of the K-BKZ analog of the pom-pom constitutive model includes comparisons between experimental stress relaxation moduli and predictions from the model using pom-pom model parameters determined from extensional rheology. The results show inconsistencies in the model

predictions, where the predictions fail to capture the short time behavior and accurately dampen at larger strains. Pom-pom model parameters are determined using the K-BKZ analog of the pom-pom constitutive model and fitting the stress relaxation moduli. These results are qualitatively consistent indicating that branching occurs on the longest backbone segments, but the values appear to be unrealistic with respect to the molecular theory.

Analysis of film-width reduction or necking during film-casting for the series of LLDPE-based resins determines whether uniaxial extensional rheological characteristics, in particular strain-hardening, that are a result of LCB influence the film-necking properties. At the lowest drawdown ratio necking is observed to be reduced with increasing LCB, and thus strain-hardening characteristics. At the higher drawdown ratios it is observed that LCB no longer reduces necking and the curves merge to the results found for linear PE, except in the case of LDPE, which shows reduced necking at all drawdown ratios. Furthermore, comparisons of film necking are also made to separate the effects of molecular weight distribution, MWD, and LCB. The results indicate that both broadening the MWD and the addition of sparse LCB reduce the degree of necking observed. It is established that film necking is more significantly reduced by LCB than by broadening the MWD. Analysis of the uniaxial extensional and dynamic shear rheology with the pom-pom constitutive model reveals that a distribution of branches along shorter relaxation time modes is important in reducing necking at higher drawdown ratios. Factors such as shear viscosity effects, extrudate swell, and non-isothermal behavior were eliminated as contributing factors because of the similar shear viscosity curves, N_1 curves, and activation energies among the sparsely LCB PE resins.

The same experimental concepts have been extended to the series of HDPE-based resins, but the lack of adequate uniaxial extensional data prevents a thorough analysis with respect to uniaxial extensional characteristics. Regardless, in the context of step-strain rheology, the results were found to be similar with those of the LLDPE-based series of resins, where a distinctive shape at short times was observed for any of the PE resins possessing some level of LCB that was not apparent in the linear PE resins. Film-casting revealed similar results to those of the LLDPE-based materials as well, but a broader spectrum of drawdown ratios revealed greater insight into how the distribution of branching controls the film-casting response. At low drawdown ratios all materials exhibit the same necking behavior. At intermediate drawdown ratios separation occurs where the linear PE resins experiences the most drastic necking, the sparsely LCB PE resins show reduced necking, and the LDPE shows an even greater reduction in necking. Progression then to the higher drawdown ratios results in similar necking behavior for the linear and sparsely LCB PE resins and greatly reduced necking for the LDPE. These results support the idea that to reduce necking the backbone segments that dominate the film-casting behavior must contain some level of LCB.

Acknowledgements

The author would like to acknowledge Dr. Donald G. Baird for his support and guidance that resulted in the completion of this work. The author would also like to acknowledge the members of his research committee: Dr. Richey M. Davis, Dr. Timothy E. Long, and Dr. John Y. Walz.

The author also wishes to acknowledge the following persons:

- His wife and son for their continued support and patience through the completion of this process.
- His parents and sister for their continued support.
- Everyone that at some point during my tenure was involved with the Polymer Processing Lab for helping accomplish this work and more importantly for providing welcomed distractions.
- All the departmental staff members for making this work easier over the years.

Original Contributions

The following list highlights the significant original contributions of this research:

1. It has been established that the addition of sparse long-chain branching helps reduce necking commonly observed in the film-casting process at low drawdown ratios, but is insignificant in reducing necking at higher drawdown ratios.

2. Film necking has been determined to depend on the distribution of branches. To reduce necking at all drawdown ratios, branches must be distributed along all of the polymer chains and not occur on only the longest backbone segments.

3. Shear step-strain rheology is an effective tool to characterize the molecular structure associated with a polymer resin. Branched polyethylene resins show a distinctive behavior in the short time region of the stress relaxation modulus.

4. Comparisons are made to the experimental shear step-strain measurements and inconsistencies are found in the K-BKZ analog of the pom-pom constitutive model for predicting the stress relaxation modulus.

Table of Contents

Volume 1

List of Figures

Chapter 2.0

List of Tables

Chapter 3.0

Chapter 4.0

Chapter 5.0

Volume 1

1.0 Introduction

1.0 Introduction

Polyethylene chemistry is constantly evolving through the process of ever-changing catalysis yielding the possibility of a vast array of molecular topologies and providing mechanical and processing properties to fit the specific need over time. The introduction of constrained geometry single-site catalysts such as metallocenes have sparked an interest in controlling molecular architecture and providing the ability to tailor design molecularly the structure of polyethylene that benefits the needed processing situation whether it be for processability issues or for specific mechanical properties. In an effort to bridge the gap between a specific molecular architecture and its effect on the final processing characteristics and mechanical properties, two vital areas of interest present themselves: understanding the relationship between molecular architecture and rheological properties and understanding the relationship between rheological properties and processing characteristics and mechanical properties. Polyethylene materials containing varying levels of long-chain branching exhibit rheological differences as well as changes in the processing behavior of the material and thus will be the focus of this research. Much of the discrepancy in processing characteristics stems from the extensional rheological features and as a result extensional flow dominated processes such as film-casting, film-blowing, and fiber-spinning experience to a greater degree the effects of changing molecular topology.

1.1 Molecular architecture and rheology

Variations in molecular structure are typically classified by branching characteristics such as length and density given that all the subtypes of polyethylene must retain the

same C_2H_4 repeat unit and that changes in rheological properties are a matter of how the repeat units are organized. Common molecular topologies, where the referred topological name is derived from the molecules shape, include: linear, star, comb, H, and randomly branched materials. Polymers that are used in processing operations are generally combinations of multiple topologies and to fully understand the rheology of these types of materials some insight into the rheology of the components as well as the distribution of the components must be gained.

Distinct differences exist in the rheological behavior of a polymeric material containing long-chain branching, LCB, versus short-chain branching, SCB [1-4]. LCB occurs when the molecular weight of the branch arm exceeds the molecular weight for entanglements, M_e [5], and alters polymer melt rheology through suppression of molecular mobility [6] and by offering the opportunity for entanglements, whereas SCB is descriptive of branches that are of significantly lower molecular weight and fail to entangle with surrounding polymer chains. Rheological behavior is also dependent on the density of branching. For the case of LCB two regimes exist: sparse LCB, where less than 1 LCB exists per 1000 carbon atoms; and dense LCB, where the number of LCB is greater than 1 LCB per 1000 carbon atoms. Commonly LCB is characterized by comparing the relative size of a branched polymer to that of its linear counterpart based on the concept of finding a reduction in the radius of gyration with increased branching where typical analytical techniques include ^{13}C NMR and SEC-MALLS. Janzen and Colby [7] argue the effectiveness of the current analytical methods to quantitatively describe the branching content and look to studying the differences in shear rheological behavior as a viable alternative, but the efforts of Doerpinghaus and Baird [8] have shown the inability with

shear rheology alone to distinguish slight differences in LCB content in sparsely LCB metallocene polyethylenes.

Much of the literature on shear rheological behavior focuses on the dependence of viscosity, both in the limit of zero-shear viscosity as well as the complex viscosity as a function of frequency, on molecular topological effects and the separation of these effects from the effects experienced by changing molecular weight, M_w, and molecular weight distribution, MWD. Doerpinghaus and Baird [8] have shown the ability to correct for differences in M_w and MWD through data shifting and see that in the case of zero-shear viscosity the progression from linear to highly branched materials proceeds through a maximum as concluded by Janzen and Colby [7] and that the onset of shear-thinning occurs at lower frequencies.

Analysis of extensional flows coupled with shearing flows can provide insight into molecular structure and aid in distinguishing between branching levels that are too sparse and too similar for analytical techniques and shear rheological behavior alone. Extensional rheological work [5, 9-13] confirms that increasing long-chain branching content results in a pronounced strain-hardening effect. Bin Wadud and Baird [9], Doerpinghaus and Baird [11], and La Mantia and coworkers [10] all show distinguishable strain-hardening characteristics at low LCB concentrations for polyethylene confirming experimentally the characterization potential of extensional rheological measurements.

1.2 Film-casting process

Film-casting is a widely used processing technique that has applications ranging from packaging films to barrier coatings where films are cast onto a substrate with the majority

of the interest in polyethylene. Taking cue from literature terminology necking and edge-bead are considered instabilities, hence film-casting suffers from three primary instabilities: necking phenomenon, defined as the reduction in film width compared to the original die width that is generated as a result of the conservation of mass when drawing a film sample at a greater rate than it is being extruded; edge-bead phenomenon, defined as the non-uniformity across the width of the sample where the edges are thicker than the central region; and draw resonance, an oscillatory instability where film width and thickness vary periodically above a critical draw ratio. A better fundamental understanding of how rheological characteristics affect these film instabilities can lead to the production of more usable film and increase profitability in an industrial setting.

Film-casting instabilities are dependent on processing conditions such as extrusion rate, drawdown ratio, and air gap length as well as material viscoelastic properties. Experimental data probing the affects of these conditions is rather limited in the literature including only the efforts of Canning and Co [14] and Canning and coworkers [15], but numerous film-casting simulations [16-28] have shed light on the subject. It is shown that the viscoelastic nature of the material plays a large role in the film behavior and in particular the strain-hardening features of the material act to stabilize all of the film-casting instabilities, but there is debate that the stabilization is attributed to the difference in uniaxial and planar strain-hardening based on the ideas of Dobroth and Erwin [29] who conclude that planar extension is the primary flow in the central region of the film and uniaxial extension exists on the film edges.

1.3 Numerical simulation and rheological modeling

The industrial interest in predicting film-casting instabilities has led to much work in the area of numerical simulations. Complexity of the simulation varies and as with all numerical work is largely dependent on the allowable computation time. Simple one-dimensional isothermal Newtonian predictions are capable of being performed on-line, but suffer from losses in accuracy when compared to more complex three-dimensional non-isothermal viscoelastic predictions. The accuracy of the numerical work is largely a function of the constitutive equation used to represent the viscoelastic behavior of the material, where the decision of the constitutive equation rests in the hands of the simulators and the primary criterion is the ability of the constitutive equation to fit the rheological data both in shear and extensional flows.

Numerical simulations begin with a one-dimensional approach. The primary concern here is the inability to predict both edge-bead and necking. Two approaches are taken, one in which the width remains constant and only thickness is allowed to vary and the other specifies the width reduction extraneously and then evaluates thickness changes. A general progression towards two-dimensional simulations has been taken and with success. Two-dimensional simulations allow for the consideration of both edge-bead and necking and have improved upon the accuracy of the predictions especially with the introduction of constitutive equations to represent the viscoelastic behavior. Finally, three-dimensional simulations have been considered and all possible flow directions are represented. No considerable improvements from using a three-dimensional approach are documented, but the natural progression of science led to three-dimensional simulations.

The use of viscoelastic constitutive equations has added a great deal of realism and accuracy to numerical simulations of film-casting. The upper convected Maxwell, modified Giesekus, Phan-Thien Tanner, Bird Carreau, and Larson models have all been employed to describe the viscoelastic behavior of polymer melts. The pom-pom model developed by McLeish and Larson [1] has been shown to model the rheological behavior of polyethylene extremely well and provides the possibility of extracting information regarding molecular structure from the model fits. An attempt at numerical simulations with the multi-mode pom-pom model may produce a more accurate depiction of film-casting instabilities and will be one step closer to having the ability to tailor design resins for particular applications.

The pom-pom model is derived from the ideas of the tube model presented by Doi and Edwards [30]. Molecular constraints from entanglements in the tube model are represented by confining the polymer chain to a hypothetical tube and relaxation occurs through retraction and reptation. Retraction is described as the contraction of a chain segment after a stretch is imposed due to elasticity within the chain and occurs on faster timescales than reptation, which is chain motion within the confines of the tube constraints through a diffusive process. Extension of these concepts to branched polymers produces a model that has the potential to explain the nonlinear rheology associated with these branched materials. Backbone segments with more than one branch-point exhibit strain-hardening characteristics that are explained by the stretch component of the backbone, which has a retarded relaxation because in order to relax the stretch the attached arms must completely relax first and, therefore act as pinning points.

Real molecules are modeled by taking a multi-mode approach with the pom-pom model introduced by Inkson and coworkers [31], where real molecules are treated as combinations of much simpler theoretical pom-pom molecules. The ideas of seniority, the smallest number of chain segments required to reach a free end, and priority, the smallest number of free chain ends that are visible from an inner layer backbone segment, are used to physically describe the structure of a real molecule and suggest the relative relaxation order of individual segments in the polymer chain. The multi-mode approach has improved the diversity of the pom-pom model and generates predictions representative of real complex molecular structures. The pom-pom model is expressed in a full integro-differential form [1], a differential form [1], and an extended form [32], with the majority of the modeling emphasis placed on the differential form, because of its prediction capabilities and less complex computational efforts required.

1.4 Research objectives

Our work evaluates the fundamental relationships between molecular architecture and rheological behavior and rheological behavior and processing characteristics in order to create a method in which a polymer can be tailored for a specific processing application. The emphasis of this research is to determine what and how rheological characteristics affect film-casting instabilities and effectively model the film-casting process with a viscoelastic constitutive equation that explains both the shear and extensional rheological features of the material. The three objectives required to accomplish this goal are stated below.

1. Analyze and characterize the rheological behavior of the HDB series of resins including model fitting with the pom-pom model constitutive equation to find model parameters and determine the consistency of the model with this well-controlled series of materials.

2. Determine what and how rheological characteristics affect film-casting instabilities such as necking and edge-bead formation using conventional industrial polyethylene resins with varying degrees of branching and well-controlled high-density polyethylenes, HDPE, with varying degrees of branching.

3. Determine the feasibility for modeling the film-casting process using Polyflow® flow simulation software using the multi-mode pom-pom model to describe the viscoelastic behavior of the materials used.

1.5 References

1. McLeish, T. C. B.; Larson, R. G., Molecular constitutive equations for a class of branched polymers: The pom-pom polymer. *Journal of Rheology* **1998,** 42, (1), 81-110.

2. Meissner, J. M., Modification of the Weissenberg Rheogoniometer for measurements of transient rheological properties of molten polyethylene under shear, Comparison with tensile data. *Journal of Applied Polymer Science* **1972,** 16, 2877-2899.

3. McLeish, T. C. B., On the trail of topological fluids. *Physics World* **1995,** 8, 32-35.

4. Larson, R. G., *Constitutive Equations for Polymer Melts and Solutions*. Butterworths: Boston, 1988.

5. Lohse, D. J.; Milner, S. T.; Fetters, L. J.; Xenidou, M.; Hadjichristidis, N.; Mendelson, R. A.; Garcia-Franco, C. A.; Lyon, M. K., Well-Defined, Model Long Chain Branched Polyethylene. 2. Melt Rheological Behavior. *Macromolecules* **2002,** 35, 3066-3075.

6. Ferri, D.; Lomellini, P., Melt rheology of randomly branched polystyrenes. *Journal of Rheology* **1999,** 43, (6), 1355-1372.

7. Janzen, J.; Colby, R. H., Diagnosing long-chain branching in polyethylenes. *Journal of Molecular Structure* **1999,** 485-486, 569-584.

8. Doerpinghaus, P. J.; Baird, D. G., Separating the effects of sparse long-chain branching on rheology from those due to molecular weight in polyethylenes. *Journal of Rheology* **2003,** 47, (3), 717-736.

9. Bin Wadud, S. E.; Baird, D. G., Shear and extensional rheology of sparsely branched metallocene-catalyzed polyethylenes. *Journal of Rheology* **2000,** 44, (5), 1151-1167.

10. La Mantia, F. P.; Scaffaro, R.; Carianni, G.; Mariani, P., Rheological Properties of Different Film Blowing Polyethylene Samples Under Shear and Elongational Flow. *Macromolecular Materials and Engineering* **2005,** 290, 159-164.

11. Doerpinghaus, P. J.; Baird, D. G., Assessing the Branching Architecture of Sparsely Branched Metallocene-Catalyzed Polyethylenes Using the Pompom Constitutive Model. *Macromolecules* **2002,** 35, (27), 10087-10095.

12. Barroso, V. C.; Maia, J. M., Influence of Long-Chain Branching on the Rheological Behavior of Polyethylene in Shear and Extensional Flow. *Polymer Engineering and Science* **2005,** 45, (7), 984-997.

13. Bourrigaud, S.; Marin, G.; Poitou, A., Shear Modification of Long-Chain Branched Polymers: A Theoretical Approach Using the Pom-Pom Model. *Macromolecules* **2003,** 36, (4), 1388-1394.

14. Canning, K.; Co, A., Edge Effects in Film Casting of Molten Polymers. *Journal of Plastic Film & Sheeting* **2000,** 16, 188-203.

15. Canning, K.; Bian, B.; Co, A., Film Casting of a Low Density Polyethylene Melt. *Journal of Reinforced Plastics and Composites* **2001,** 20, (5), 366-376.

16. Kim, J. M.; Lee, J. S.; Shin, D. M.; Jung, H. W.; Hyun, J. C., Transient solutions of the dynamics of film casting process using 2-D viscoelastic model. *Journal of Non-Newtonian Fluid Mechanics* **2005,** 132, 53-60.

17. Sakaki, K.; Katsumoto, R.; Kajiwara, T.; Funatsu, K., Three-Dimensional Flow Simulation of a Film-Casting Process. *Polymer Engineering and Science* **1996,** 36, (13), 1821-1831.

18. Zheng, H.; Yu, W.; Zhou, C.; Zhang, H., Three-Dimensional Simulation of the Non-Isothermal Cast Film Process of Polymer Melts. *Journal of Polymer Research* **2006,** 13, 433-440.

19. Silagy, D.; Demay, Y.; Agassant, J. F., Study of the Stability of the Film Casting Process. *Polymer Engineering and Science* **1996,** 36, (21), 2614-2625.

20. Silagy, D.; Demay, Y.; Agassant, J. F., Stationary and stability analysis of the film casting process. *Journal of Non-Newtonian Fluid Mechanics* **1998,** 79, 563-583.

21. Lee, J. S.; Jung, H. W.; Song, H.-S.; Lee, K.-Y.; Hyun, J. C., Kinematic waves and draw resonance in film casting process. *Journal of Non-Newtonian Fluid Mechanics* **2001,** 101, 43-54.

22. Satoh, N.; Tomiyama, H.; Kajiwara, T., Viscoelastic Simulation of Film Casting Process for a Polymer Melt. *Polymer Engineering and Science* **2001,** 41, (9), 1564-1579.

23. Ito, H.; Doi, M.; Isaki, T.; Takeo, M., A Model of Neck-in Phenomenon in Film Casting Process. *Journal of the Society of Rheology, Japan* **2003,** 31, (3), 157-163.

24. Kajiwara, T.; Yamamura, M.; Asahina, T., Relationship between Neck-in Phenomena and Rheological Properties in Film Casting. *Nihon Reoroji Gakkaishi* **2006,** 34, (2), 97-103.

25. Smith, S.; Stolle, D., Numerical Simulation of Film Casting Using an Updated Lagrangian Finite Element Algorithm. *Polymer Engineering and Science* **2003,** 43, (5), 1105-1122.

26. Iyengar, V. R.; Co, A., Film Casting of a Modified Giesekus Fluid: Stability Analysis. *Chemical Engineering Science* **1996,** 51, (9), 1417-1430.

27. Pis-Lopez, M. E.; Co, A., Multilayer film casting of modified Giesekus fluids Part 1. Steady-state analysis. *Journal of Non-Newtonian Fluid Mechanics* **1996,** 66, 71-93.

28. Pis-Lopez, M. E.; Co, A., Multilayer film casting of modified Giesekus fluids Part 2. Linear stability analysis. *Journal of Non-Newtonian Fluid Mechanics* **1996,** 66, 95-114.

29. Dobroth, T.; Erwin, L., Causes of edge beads in cast films. *Polymer Engineering and Science* **1986,** 26, (7), 462-467.

30. Doi, M.; Edwards, S. F., *The Theory of Polymer Dynamics*. Oxford University Press: 1988.

31. Inkson, N. J.; McLeish, T. C. B.; Harlen, O. G.; Groves, D. J., Predicting low density polyethylene melt rheology in elongational and shear flows with "pom-pom" constitutive equations. *Journal of Rheology* **1999,** 43, (4), 873-896.

32. Verbeeten, W. M. H.; Peters, G. W. M.; Baaijens, F. P. T., Differential constitutive equations for polymer melts: The extended Pom-Pom model. *Journal of Rheology* **2001,** 45, (4), 823-843.

2.0 Literature Review

Preface

This chapter provides a review of the literature relevant to this research. The major topics include: the dependence of molecular architecture on rheology, how rheological features affect film-casting, a review of film-casting simulation efforts, and the concepts behind the McLeish-Larson pom-pom model.

2.0 Literature Review

This literature review covers the relevant issues associated with rheology as a function of molecular structure and experimental and numerically simulated film-casting instabilities. Section 2.1 focuses on the dependence of molecular architecture on rheological characteristics in both shear and shear-free flows. Section 2.2 evaluates the experimental efforts of film-casting, evaluating necking and edge-bead instabilities. Section 2.3 is concentrated with the evolution of numerically simulating the film-casting process emphasizing the ability to predict necking, edge-bead, and draw resonance. Section 2.4 evaluates the different forms of the McLeish-Larson pom-pom model and the published literature on their ability to fit the rheological behavior of various materials. Section 2.5 discusses the potential of a new extensional rheometer dubbed the SER.

2.1 Dependence of molecular architecture on rheology

Rheological characteristics of polymers in both shear and extensional flows are significantly affected by the fundamental molecular architecture. These changing rheological features determine the behavior in polymer processing applications. In subsection 2.1.1 the vast array of possible molecular structures is probed and differences in branching type and density are discussed. In subsections 2.1.2 and 2.1.3 the effects of molecular architecture on rheological properties are evaluated with respect to shear and extensional flows, respectively. Preceding the discussion of rheological behavior in these subsections, a brief review of the fundamental concepts of rheology for each flow condition is provided.

2.1.1 Molecular structures

Control over polymerization conditions and catalyst selection provides a means for the generation of greatly differing molecular structures. Architecture at the molecular level has increased in importance because it significantly affects the rheological characteristics and influences the processing behavior of a polymeric material. Variations in molecular structure are determined through the addition of branches and the characteristics associated with those branches.

Common molecular topologies include: linear, star, comb, H, pom-pom, and random. Generally, the structural names are derived from their shape in the molecular sense. A linear material is a backbone segment with no branching; all of the subsequent chain building occurs at one of the original two free ends. Star polymers may have as many branches as desired, but the characteristic feature of a star polymer is that all of the branches emanate from a single branch point. Comb structured polymers require that all branches are directly connected to the backbone segment at a branch point, resulting in the absence of branches emanating from other branches. The pom-pom structure consists of two branch points along the backbone at which any number of branches can exist and no branches may occur on other previously established branches. In randomly branched structures, branches have more freedom in their location of attachment and can occur on the backbone segment or on other branches.

The natural progression of structural changes in polyethylene is depicted by Doerpinghaus [1] adapted from Kim and coworkers [2] in Figure 2.1.1. Low density polyethylene, LDPE, is produced under high temperature and high pressure conditions providing a highly or densely-branched structure with both short and long-chain

branching. Coordination catalysts, notably Zieglar-Natta and Phillips type catalysts, generate linear polymer structures of which an example is high density polyethylene, HDPE. Linear low density polyethylene, LLDPE, retains a molecular structure more linear in nature with branching only of the short-chain variety. Polyethylene resins that are generated from metallocene type catalysts, MCPE, provide better control of molecular structure and thus allow for the production of resins of a specific molecular architecture incorporating sparse amounts of long-chain branching. The variations in molecular structures that are experienced by polyethylene provide a descriptive representation of the branching possibilities and provide examples of short-chain branching, long-chain branching, densely-branched structures, and sparsely-branched structures all of which are discussed in further detail.

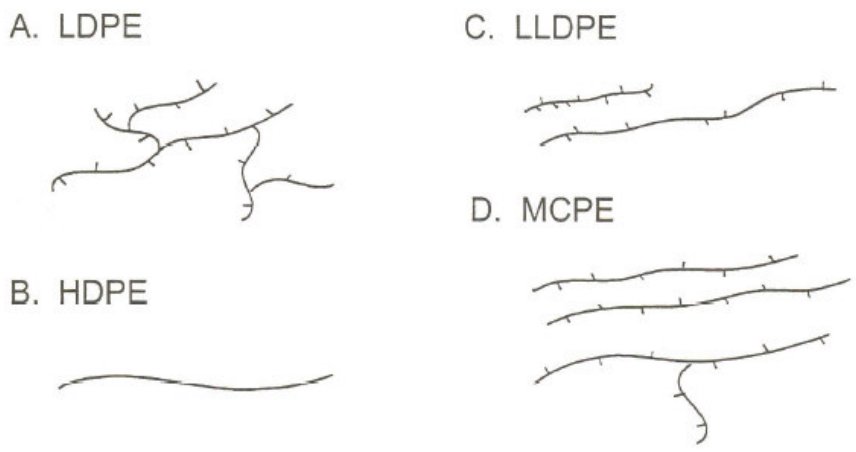

Figure 2.1.1 Common molecular structures for polyethylene [1].

There is a distinct difference in the rheological behavior of polymer melts containing long-chain branching in comparison to those that are linear or have only short-chain

branching [3-6]. Long-chain branches alter polymer melt rheology by suppressing molecular mobility [7] and providing the opportunity for entanglements. A long-chain branch is generally described as a branch arm with a molecular weight greater than the molecular weight for entanglements, M_e [8]. Wood-Adams and coworkers [9] summarize the work of Jordan and coworkers [10] and Gell and coworkers [11] where they determine the length required for a long-chain branch based on its impact towards rheological behavior. Based on self-diffusion experiments, the findings indicate for branching to significantly affect the rheological behavior of a polymeric material branch lengths need to be 2-3 times M_e. Short-chain branches are of significantly lower molecular weight and do not entangle with surrounding polymer chains. The differing rheological effects of both long-chain and short-chain branching are discussed in detail in subsections 2.1.2 and 2.1.3.

Characterization of long-chain branching content is typically expressed as some variation of a g-ratio analysis where quantitatively molecular size sensitive measurements of branched polymers are related to those of their linear counterparts. Typical analytical techniques are, ^{13}C nuclear magnetic resonance, ^{13}C NMR, and size exclusion chromatography, SEC, coupled with multi-angle laser light scattering, MALLS. The relationship defining g' is shown in equation 2.1.1 where methods of determination produce ratios of either intrinsic viscosities or mean square radii of gyration of branched to linear polymer materials.

$$g' = \frac{[\eta]_{branched}}{[\eta]_{linear}} = \frac{\left(\langle s^2 \rangle_0\right)_{branched}}{\left(\langle s^2 \rangle_0\right)_{linear}} = g^k \qquad (2.1.1)$$

Zimm and Kilb [12] have originally shown the value of k to be 0.5, but it is noted by Barth and Mays [13] that the actual value of k can lie anywhere between 0.5 and 1.5. Janzen and Colby [14] argue the possibility of using ^{13}C NMR. ^{13}C NMR suffers from two main problems when evaluating branching content for sparsely long-chain branched polymers that make its results somewhat inaccurate: branch concentrations below 1 LCB per 10,000 carbons are undetectable and all branches larger than 6 carbons are not distinguishable from one another, but those branches that are rheologically relevant must be long enough to entangle and are, therefore, much larger than 6 carbons long.

The ineffectiveness of analytical techniques to quantify the extent of LCB has led to the work of Janzen and Colby [14] to use shear rheology as an alternative. They show that SEC coupled with melt viscometry is sensitive to low concentrations of LCB and that this method works for polyethylenes that are linear in nature, sparsely-branched, as well as highly-branched. Piel and coworkers [15] suggest the inability of shear viscosity measurements as indicators of LCB because of the similar effects of M_w and MWD. Doerpinghaus and Baird [16] have published results to normalize the effects of M_w and MWD, but still were unable to distinguish slight differences in LCB content present in metallocene polyethylenes.

2.1.2 Effects on shear rheological properties

Rheology describes the flow behavior of a polymeric material when subjected to a particular deformation. This subsection focuses on the rheological response for differing molecular topologies when a material is subjected to shear flow deformations. When coupled with the rheological response from extensional flows, insight into material

information may be gained. Shear deformation is described in figure 2.1.2 where a cube of material is deformed at some shear rate, $\dot{\gamma}$. To fully understand the relevance of shear rheological measurements a brief review of the characteristic velocity field and material functions for common simple shear flows is provided.

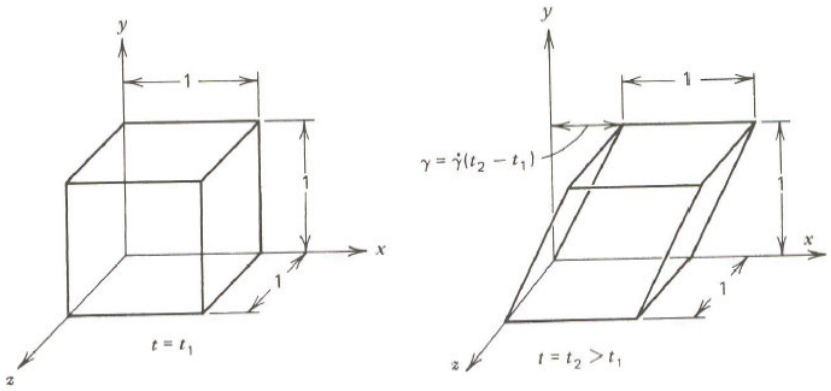

Figure 2.1.2 The deformation of a unit cube of material from time t_1 to t_2 ($t_2 > t_1$) in steady simple shear flow. Recall that material conservation must be observed [17].

Shear flows are common in practice and experimentation and as an example can be generated in parallel plate geometries by simply moving the top plate at some rate while holding the bottom plate stationary. The velocity field for simple shear flow is expressed in equations 2.1.2, 2.1.3, and 2.1.4 as well as the rate of deformation tensor for simple shear flow shown in equation 2.1.5.

$$v_x = \dot{\gamma}_{yx} y \tag{2.1.2}$$

$$v_y = 0 \tag{2.1.3}$$

$$v_z = 0 \tag{2.1.4}$$

$$\dot{\gamma}_{ij} = \dot{\gamma}(t)\begin{pmatrix} 0 & 1 & 0 \\ 1 & 0 & 0 \\ 0 & 0 & 0 \end{pmatrix} \tag{2.1.5}$$

Equation 2.1.6 defines the distance between neighboring fluid particles initially separated by a distance l_0 for simple shear flows.

$$l = l_0\sqrt{1+(\dot{\gamma}\Delta t)^2} \sim l_0\dot{\gamma}\Delta t \tag{2.1.6}$$

Various shear flow experiments are used to characterize the viscous and elastic nature of polymer melts and liquids [1, 17, 18]. Experiments such as steady shear flow, small-amplitude oscillatory flow, and stress relaxation after a sudden shearing displacement are the most common and of greatest interest when probing molecular architectural differences. The corresponding velocity gradients and resulting material functions for these experiments are summarized in figure 2.1.3 adapted from Bird and coworkers [17]. Small-amplitude oscillatory experimental results in literature generally report complex viscosity, η^*, which is related to the real and imaginary portions, η' and η'', respectively shown in figure 2.1.3 through equation 2.1.7

$$\eta^* = \eta' - i\eta'' \tag{2.1.7}$$

a. Steady shear flow

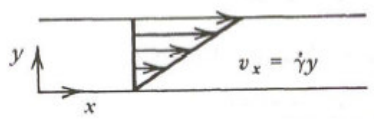

v_x = velocity in x–direction
$\dot{\gamma}$ = shear rate

Flow	Material Function	Defining Equation
Steady shear flow $\dot{\gamma}_{yx} = \dot{\gamma} =$ constant	$\eta(\dot{\gamma})$ $\Psi_1(\dot{\gamma})$ $\Psi_2(\dot{\gamma})$	$\tau_{yx} = -\eta\dot{\gamma}_{yx}$ $\tau_{xx} - \tau_{yy} = -\Psi_1\dot{\gamma}_{yx}^2$ $\tau_{yy} - \tau_{zz} = -\Psi_2\dot{\gamma}_{yx}^2$

b. Small–amplitude oscillatory shear

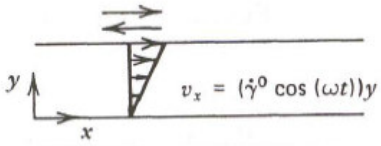

$\dot{\gamma}^0$ = shear rate amplitude
ω = angular frequency

Flow	Material Function	Defining Equation
Small-amplitude oscillatory shear $\dot{\gamma}_{yx} = \dot{\gamma}^0 \cos \omega t$ $= \gamma^0 \omega \cos \omega t$	$\eta'(\omega)$ $\eta''(\omega)$ $G'(\omega) = \eta''\omega$ $G''(\omega) = \eta'\omega$	$\tau_{yx} = -\eta'\dot{\gamma}^0 \cos \omega t$ $-\eta''\dot{\gamma}^0 \sin \omega t$ $\tau_{yx} = -G'\gamma^0 \sin \omega t$ $-G''\gamma^0 \cos \omega t$

c. Stress relaxation after a sudden shearing displacement

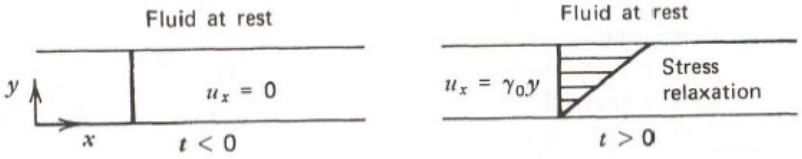

Flow	Material Function	Defining Equation
Stress relaxation after a sudden shearing displacement $\dot{\gamma}_{yx} = \gamma_0 \delta(t)$	$G(t, \gamma_0)$ $G_{\Psi_1}(t, \gamma_0)$	$\tau_{yx} = -G\gamma_0$ $\tau_{xx} - \tau_{yy} = -G_{\Psi_1}\gamma_0^2$

Figure 2.1.3 Description of the velocity gradient and material functions for steady shear flow, small-amplitude oscillatory shear flow, and stress relaxation after a sudden shearing displacement flow experiments [17].

The processing behavior of various polyethylene materials throughout the years has proven the importance of rheology and the role of certain molecular characteristics. Differences are seen in shear rheological behavior as a result of changes in the molecular weight, molecular weight distribution, and molecular topology. Recent catalysis efforts provide considerable control over these molecular features and enhance the efforts of separating the effects of branched structures from those of molecular weight and molecular weight distribution.

Long-chain branching has been deemed the primary cause of rheological behaviors associated with the changes experienced in zero-shear viscosity and the viscosity dependence on shear rate. Due to the lack of entanglements generated in short-chain branching it is seen that rheological behavior is relatively unaffected by the presence of short-chain branching [9]. Steady shear normal stress difference data along with dynamic evaluations on storage and loss moduli, phase angle, and Van Gurp-Palmen analyses are also presented in the literature and discussed in the following paragraphs. Much of the remainder of this section focuses on the effects for branched materials where the branching is of a random nature, but the rheological behavior of linear, star, and H polymers are briefly considered because randomly LCB materials are theoretically explained as combinations of simpler molecule types.

The relaxation of orientation in linear polymers is attributed to reptation process of Doi and Edwards [19], where chain motion is limited to the confining tube that is imposed as a result of molecular motion constraints from neighboring molecules. Modifying the original reptation theory by including path-length fluctuation has led to the dependence of

$M_w^{3.4}$ that is commonly observed experimentally for linear polymers. The tube theories also correctly describe the linear and non-linear rheological properties.

McLeish and Larson [20] state three observations on the behavior of monodisperse star polymer systems: the range of relaxation times is much broader than that of monodisperse linear systems; the range of timescales varies exponentially with the number of entanglements of the arms , M_a/M_e; and the terminal time and zero-shear viscosity are dependent only on the molecular weight of the arm, M_a, and not the number of arms. Star polymers have also shown no strain-hardening in elongational flows. Relaxation only occurs through the reptation of the one free end, while the remaining end is fixed at the one common branch point. The tube theory still applies to stars, but with a different relaxation modulus and distribution of relaxation times.

Roovers [21] made three observations for H-polystyrenes: the crossbar provided relaxations at lower frequencies than a melt of pure stars suggesting that a longer relaxation process existed, the low-frequency contribution appeared Rouse-like, and the zero-shear viscosity depended exponentially on M_a, much like that of stars, but with a greater slope on a log-log plot. The rheological spectra indicate two distinct timescales that appear to be identified with the relaxation of the arms, fast, and the relaxation of the crossbar, slow. Non-linear deformations have led to three more important observations: the relaxation modulus does not show time-strain separability at times later that the pure Rouse time as in the case of linear polymers, strong shear-stress overshoots at high strain rates, and the presence of strain-hardening in extensional flows. McLeish [20] proposed a theoretical explanation incorporating the ideas of two separate relaxation timescales and a hierarchical relaxation mechanism in which the crossbar or backbone segment may not

relax until the arms first relax. These ideas led to the development of the pom-pom model [3] which is the discussion of section 2.4.

Wood-Adams and coworkers [9] evaluate the effect of short-chain branching on rheological behavior for three linear metallocene-catalyzed polyethylenes with similar polydispersities but differing short-chain branching contents. Complex viscosity data has been normalized to the zero-shear viscosity in order to eliminate M_w effects for the three polyethylene resins that are shown in figure 2.1.4. Little to no deviation is seen in these curves and the slight deviations are attributed to the slight differences in MWD. At least for this set of materials Wood-Adams and coworkers [9] confirm that short-chain branching doesn't affect the rheological response.

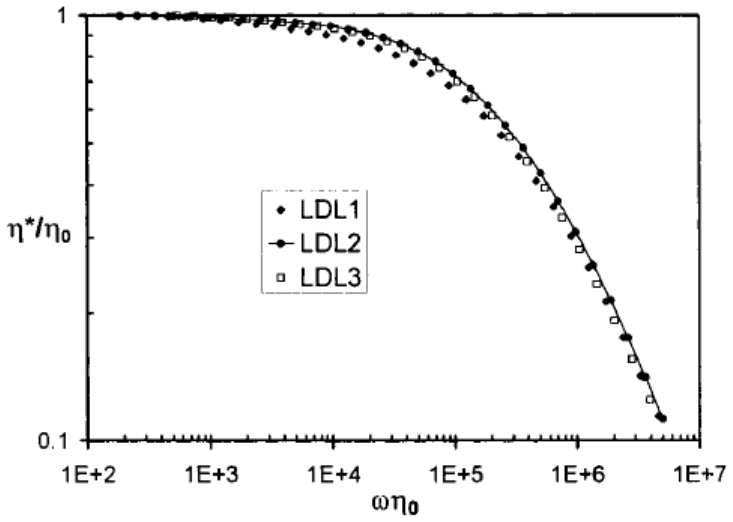

Figure 2.1.4 Effect of SCB on complex viscosity. The units for η_0 and ω are Pa-s and rad/s, respectively [9].

Much of the literature on shear rheological behavior is focused on the effect long-chain branching has on the zero-shear viscosity of a material. The results can be different

and are dependent on the density of the long-chain branching in the molecule. According to Janzen and Colby [14] polymers experience an increase in zero-shear viscosity with increasing long-chain branching content until a critical maximum value is reached at which point further increasing of the branching density suppresses the zero-shear viscosity. The behavior for both sparsely-branched and densely-branched structures is discussed along with the idea of reaching a maximum zero-shear viscosity in the following paragraphs.

For sparsely-branched polyethylenes, accounts of an increase in zero-shear viscosity with increasing branching content are established by Doerpinghaus and Baird [16], Bin Wadud and Baird [22], Wood-Adams and coworkers [9], Gabriel and coworkers [23], and Piel and coworkers [15]. The steady shear and dynamic rheological data of Doerpinghaus and Baird [16] is shown in figures 2.1.5 and 2.1.6, where unshifted results are shown in the former and to correct for differences in M_w and MWD results shifted to a reference M_w are shown in the latter. Progression in the branching density from linear to sparsely-branched leads to increased values of the zero-shear viscosity. Linear materials include NTX101 and Exact 3132, and sparsely-branched materials include Affinity PL1880 (0.18 LCB/10^4 C), Affinity PL1840 (0.57 LCB/10^4 C), and Exact 0201 (0.79 LCB/10^4 C). The most densely-branched polyethylene, NA952, has a suppressed zero-shear viscosity, which other literature supports and is discussed in further detail later.

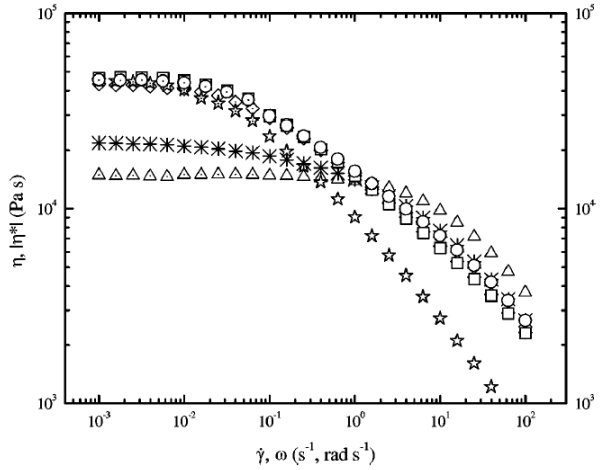

Figure 2.1.5 Steady shear and complex viscosities at 150°C. (◊) Exact 0201, (Δ) Exact 3132, (☆) NA952, (✳) NTX101, (□) Affinity PL1840, and (○) Affinity PL1880. Dotted symbols represent steady shear measurements; open symbols represent dynamic oscillatory measurements [16].

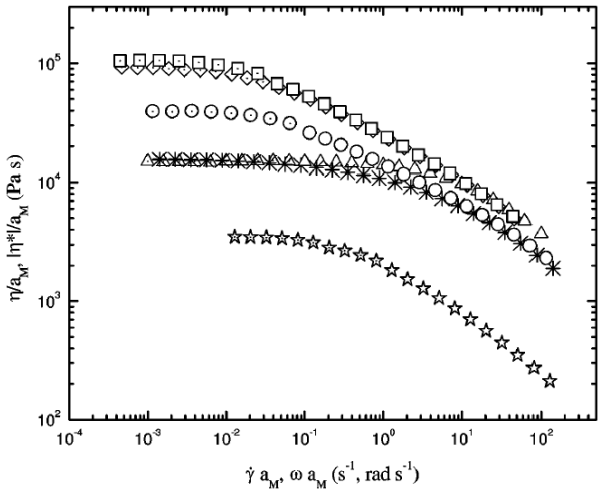

Figure 2.1.6 Shifted steady shear and complex viscosities to M_{ref} = 111,000 g/mol. (◊) Exact 0201, (Δ) Exact 3132, (☆) NA952, (✳) NTX101, (□) Affinity PL1840, and (○) Affinity PL1880. Dotted symbols represent steady shear measurements; open symbols represent dynamic oscillatory measurements [16].

The results of Wood-Adams and coworkers [9] for long-chain branched polyethylenes are presented in figures 2.1.7 and 2.1.8. The materials that are tested range in long-chain branching content: HDL1, linear; HDB1, 0.26 LCB/10,000 C; HDB2, 0.37 LCB/10,000 C; HDB3, 0.42 LCB/10,000 C; HDB4, 0.80 LCB/10,000 C. Viscosity of complex viscosity as a function of shear rate or frequency for HDL1, HDB1, HDB2, HDB3, and HDB4 is presented in figure 2.1.7. With increasing LCB content, increases in the zero-shear viscosity are noticed. The ratio of zero-shear viscosity of a branched polymer to that of a linear polymer versus the LCB content is displayed in figure 2.1.8. Up to LCB concentrations of 0.8 LCB/10,000 C increases in this ratio are seen indicating that LCB contributes to increases in zero-shear viscosity.

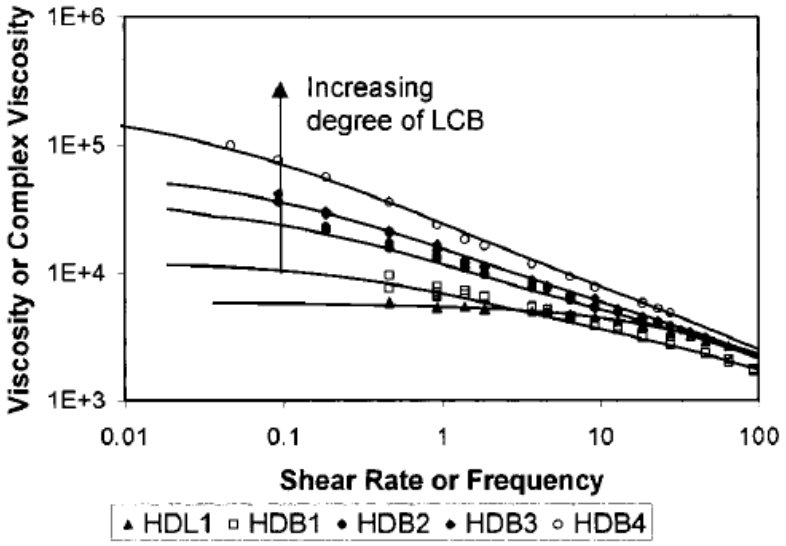

Figure 2.1.7 Viscosity and complex viscosity data for high-density mPEs. Solid lines are complex viscosity data, and symbols are viscosity data [9].

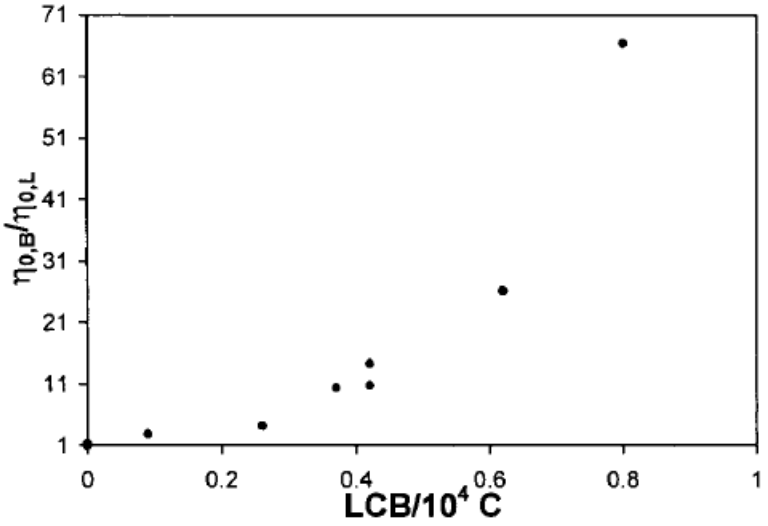

Figure 2.1.8 Effect of LCB on zero shear viscosity (150°C): HD series and LD series [9].

In the case of highly-branched molecular systems, where LCB concentrations are greater on average than two LCB per chain, the zero-shear viscosity is suppressed relative to linear systems. This behavior is noted by Janzen and Colby [14], Doerpinghaus and Baird [16], Piel and coworkers [15], Romanini and coworkers [24], and Patil and coworkers [25] where highly-branched polyethylenes have exhibited lower zero-shear viscosities than those of their linear counterparts. The work of Janzen and Colby [14] along with Bersted and coworkers [26] predict this type of behavior in polyethylenes. Doerpinghaus and Baird [16] have explored the results of Janzen and Colby [14] in figure 2.1.9 for a system of fixed M_W, where zero-shear viscosity is evaluated as a function of LCB per molecule. A maximum value for zero-shear viscosity is reached at a branching level less than one LCB per molecule, but the exact curve is also dependent on the molecular weight.

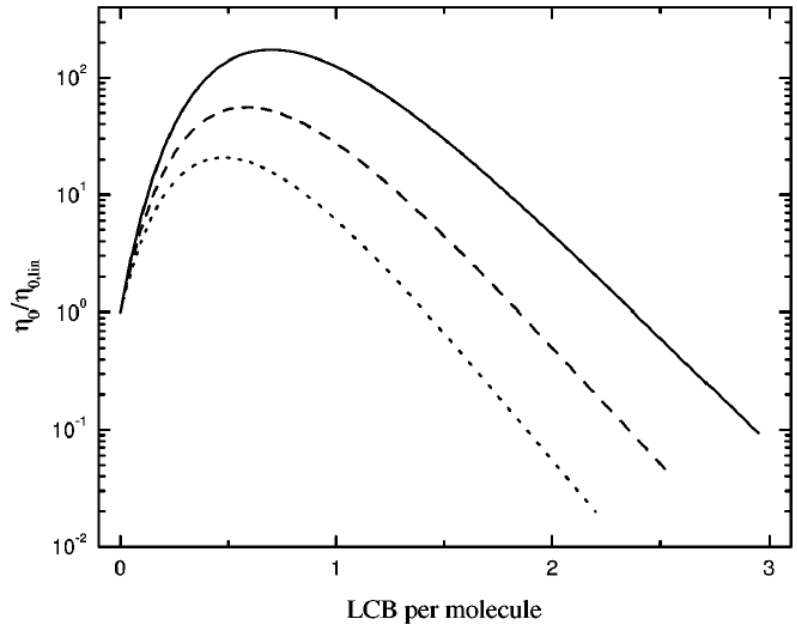

Figure 2.1.9 Predicted zero-shear viscosity versus long chain branches per molecule using the Janzen and Colby (1999) viscosity relation. (-) M_w = 100,000 g/mol, (...) M_w = 88,000 g/mol, (---) M_w = 120,000 g/mol [16].

Robertson and coworkers [27] have generated predictions for zero-shear viscosity curves as functions of LCB/10^4 C for both the Janzen and Colby [14] and Bersted and coworkers [26] approaches, which are shown in figure 2.1.10. The original work of Janzen and Colby [14] has proposed a B value of 3.9 for polyesters with known molecular weights and number of branches per molecule whereas a B value of 6 is proposed for polyethylenes with LCB in order to account for the characteristically high zero-shear viscosities. The model of Bersted and coworkers [26] is more similar to that of Janzen and Colby [14] when B is 3.9, but the curve is shifted to where the maximum in zero-shear viscosity occurs at slightly higher LCB densities.

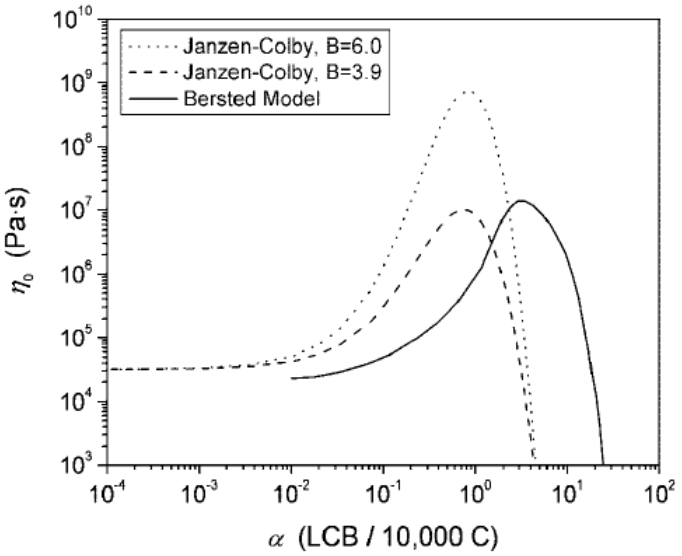

Figure 2.1.10 Predictions of the Janzen-Colby and Bersted's model for branched polyethylene with M_w = 200 kg/mol [27].

Long-chain branching influences the rheology in multiple ways creating a competition between forces that control the rheological behavior. Lohse and coworkers [8] along with La Mantia and coworkers [28] state that the approach of Janzen and Colby [14] and Bersted and coworkers [26] stems from the competition between the rheological effects generated from a rise in the number of entanglements and the reduction in size as apparent in the decreased radius of gyration.

The dependence of viscosity on shear rate including both the onset and degree of shear-thinning behavior is also influenced by long-chain branching content. The work of Doerpinghaus and Baird [16], Bin Wadud and Baird [22], and La Mantia and coworkers [28] has shown that increases in the long-chain branching density results in the onset of shear-thinning occurring at much lower shear rates. Doerpinghaus and Baird [16] present data for polyethylenes with varying degrees of branching in the previously shown figure 2.1.5.

Here it is seen that materials with any extent of long-chain branching enter the shear-thinning regime at shear rates two decades lower than those for linear polyethylenes. Differences between sparsely long-chain branched materials are indistinguishable and thus this in only another effect of long-chain branching on the rheological behavior. This rheological characteristic of long-chain branching is also shown by La Mantia and coworkers [28] in figure 2.1.11 where the two branched polyethylenes, m-bPE and LDPE, experience shear-thinning behavior approximately one decade lower in shear rate than polyethylenes with no long-chain branching present, m-PE and LLDPE.

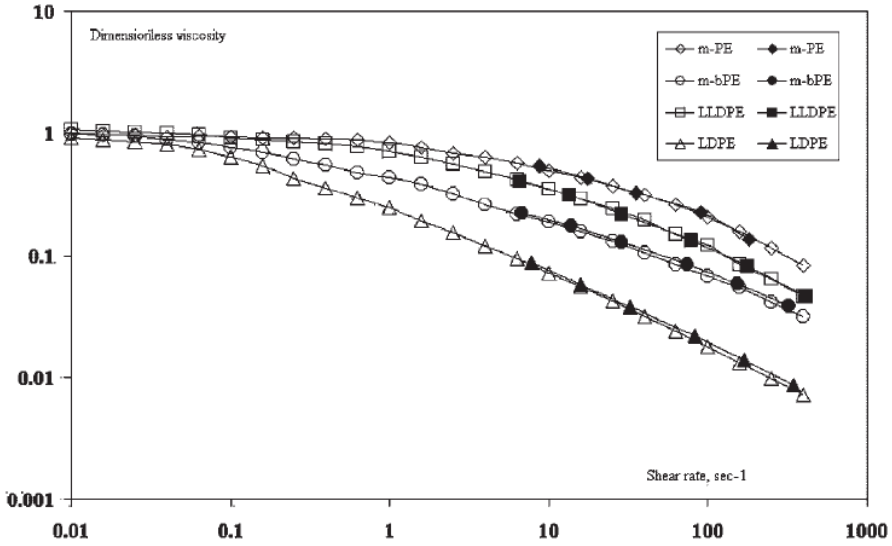

Figure 2.1.11 Dimensionless flow curves of the three samples. Open symbols are referred to parallel-plate measured viscosity and full symbols to capillary viscometer measured viscosity [28].

Another shear rate dependent rheological behavior that is affected by long-chain branching content is the degree of shear-thinning or the rate at which a material deviates from Newtonian behavior. Increasing long-chain branching content has been seen by Doerpinghaus and Baird [16], La Mantia and coworkers [28], Lohse and coworkers [8], and Kim and coworkers [2] to increase gradient of shear-thinning. Doerpinghaus and Baird [16] show this rheological behavior in the previously referenced figure 2.1.5 where the most highly branched polyethylene, NA952, has a viscosity that deviates from Newtonian behavior the most severely and the other materials follow suit with the three sparsely branched polyethylenes deviating to a slightly less degree and the two linear polyethylenes showing even less deviation.

Steady shear experiments allow for the investigation of primary normal stress differences which measure elasticity within the material. Increasing long-chain branching content has been found by Doerpinghaus and Baird [16] as well as Jabbarzadeh and coworkers [29] to increase the primary normal stress differences. Doerpinghaus and Baird show in figure 2.1.12 that the most highly branched polyethylene yields the highest values for N_1. The three sparsely branched polyethylenes are indistinguishable from each other, but do have N_1 values that are noticeably lower than those of the highly branched polyethylene and higher than those of the two linear polyethylenes. The difference experienced between the two linear materials is attributed to the higher molecular weight distribution in NTX101 when compared to Exact 3132. Increases in molecular weight distribution lead to increases in the primary normal stress difference.

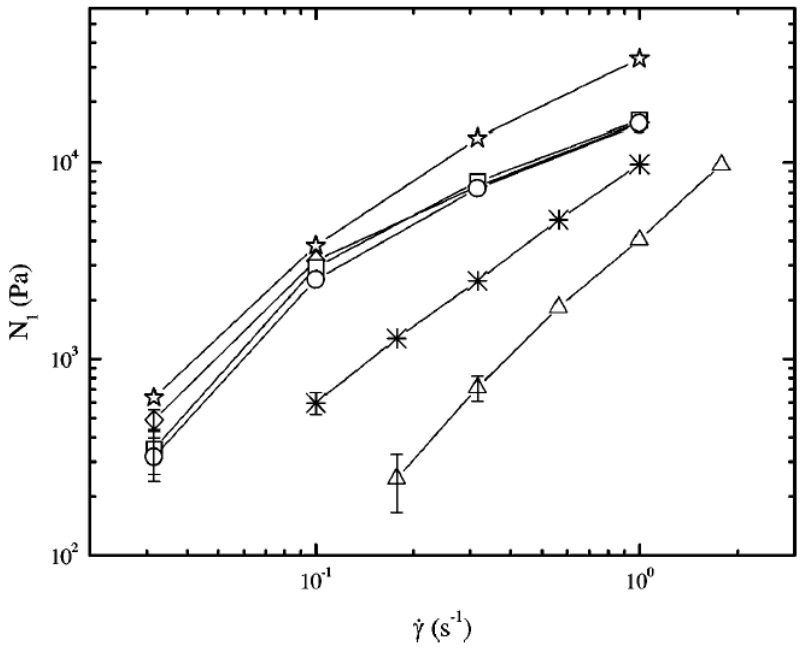

Figure 2.1.12 Primary normal stress differences (N_1) at 150°C. (◊) Exact 0201, (Δ) Exact 3132, (☆) NA952, (✳) NTX101, (□) Affinity PL1840, and (○) Affinity PL1880. Lines have been drawn to aid the eye [16].

Increases in molecular weight and broadening of the molecular weight distribution produce similar effects to those of long-chain branching on rheological behavior. Most of the work in the literature takes these contributions into effect and either uses materials that are very similar on both fronts or normalizes results to alleviate the effects of these particular molecular characteristics. Rheological behavior is complex and dependent on multiple molecular characteristics and, therefore, shear rheology should be coupled with extensional rheology to fully understand the results of long-chain branching.

2.1.3 Effects on extensional rheological properties

Shear-free flows also provide information relevant to material structure that is distinctly different to that obtained from shear flows. This subsection focuses on the rheological response of differing molecular topologies when a material is subjected to shear-free flow deformations. Various shear-free flows occur and a representation of elongational flow, biaxial stretching flow, and planar elongational flow of a unit cube of material is provided in figure 2.1.13.

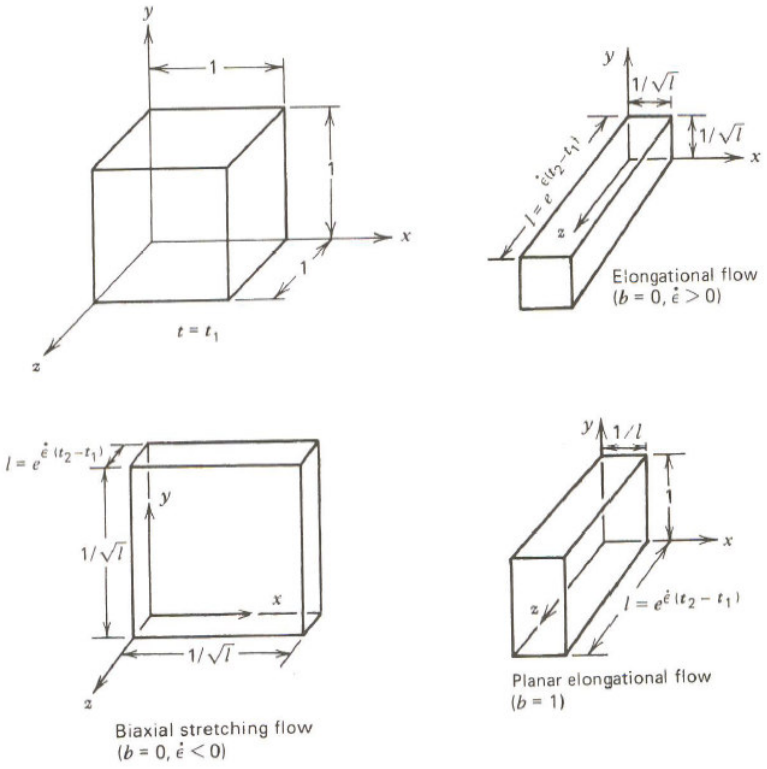

Figure 2.1.13 The deformation of a unit cube of material from time t_1 to t_2 ($t_2 > t_1$) for three kinds of shear-free flow: elongational flow, biaxial stretching flow, and planar elongational flow. Recall that material conservation must be observed [17].

The velocity field for simple shear-free flow is expressed in equations 2.1.8, 2.1.9, and 2.1.10 as well as the rate of deformation tensor for simple shear-free flow shown in equation 2.1.11. The parameter b is dependent on the type of shear-free flow experienced. Elongational flow occurs when a material is stretched from one direction allowing contraction of the material in the other two directions to account for the elongational deformation. For elongational flow b = 0 and $\dot{\varepsilon} > 0$. Biaxial stretching flow is when a material is stretched from two directions only allowing the contraction of the material in the final third direction. For biaxial stretching flow b = 0 and $\dot{\varepsilon} < 0$. Planar elongational flow is similar to elongational flow except for one of the two directions where contraction is allowable is held constant at its original dimension causing contraction to occur in only one direction. For planar elongational flow b = 1.

$$v_x = --\frac{1}{2}\dot{\varepsilon}(1+b)x \tag{2.1.8}$$

$$v_y = -\frac{1}{2}\dot{\varepsilon}(1-b)y \tag{2.1.9}$$

$$v_z = \dot{\varepsilon}z \tag{2.1.10}$$

$$\dot{\gamma}_{ij} = \dot{\varepsilon}(t)\begin{pmatrix} -(1+b) & 0 & 0 \\ 0 & -(1-b) & 0 \\ 0 & 0 & 2 \end{pmatrix} \tag{2.1.11}$$

Equation 2.1.12 defines the separation of neighboring fluid particles initially separated a distance l_0 for simple shear-free flows.

$$l = l_0 e^{\dot{\varepsilon}(\Delta t)} \tag{2.1.12}$$

Shear-free flows are characterized as strong flows conversely to shear flows, which are referred to as weak flows. Experiments involving shear-free flows are similar to those involving shear flows and of primary importance when evaluating molecular structure are steady shear-free flow and stress growth on the inception of steady shear-free flow. The resulting material functions for these experiments are summarized in figure 2.1.14 adapted from Bird and coworkers [17]. Uniaxial extension or elongational flow is the preferred shear-free flow for experimentation. For this particular case the elongational viscosity established through steady shear-free flow is shown in equation 2.1.13.

$$\bar{\eta}(\dot{\varepsilon}) = \bar{\eta}_1(\dot{\varepsilon},0) = \tau_{xx} - \tau_{zz} \tag{2.1.13}$$

Flow	Material Function	Defining Equation
a. Steady shearfree flow $\dot{\varepsilon}$ = constant	$\bar{\eta}_1(\dot{\varepsilon})$ $\bar{\eta}_2(\dot{\varepsilon})$	$\tau_{zz} - \tau_{xx} = -\bar{\eta}_1\dot{\varepsilon}$ $\tau_{yy} - \tau_{xx} = -\bar{\eta}_2\dot{\varepsilon}$
b. Stress growth on inception of steady shearfree flow $\dot{\varepsilon} = \begin{cases} 0 & t < 0 \\ \dot{\varepsilon}_0 & t \geq 0 \end{cases}$	$\bar{\eta}_1^+(t, \dot{\varepsilon}_0)$ $\bar{\eta}_2^+(t, \dot{\varepsilon}_0)$	$\tau_{zz} - \tau_{xx} = -\bar{\eta}_1^+\dot{\varepsilon}_0$ $\tau_{yy} - \tau_{xx} = -\bar{\eta}_2^+\dot{\varepsilon}_0$

Figure 2.1.14 Material functions for steady shear-free flow and stress growth on inception of steady shear-free flow experiments [17].

Difficulty in reaching steady-state is observed in shear-free flows and as a result transient data is extremely important for rheological analysis. For Newtonian fluids and at low elongation rates the Trouton ratio holds in which the extensional viscosity is three times that of the shear viscosity. This value of three times the shear viscosity also provides a lower limit to which the extensional viscosity will follow or deviate depending on its rheological features.

Shear-free flows are inherently more difficult to measure and thus extensional rheological behavior has not been investigated in the literature with as much rigor. Analysis of shear-free flows coupled with shear flows can provide great insight into molecular structure and aid in distinguishing between branching levels that are too sparse and too similar for analytical techniques and shear rheological behavior alone. To probe the molecular architecture uniaxial elongation experiments are performed and the degree of strain-hardening or deviation from the Newtonian Trouton ratio is observed.

Extensional rheological work [8, 22, 28, 30-32] confirms that increasing long-chain branching content results in a pronounced strain-hardening effect. Bin Wadud and Baird [22], Doerpinghaus and Baird [30], and La Mantia and coworkers [28] show strain-hardening characteristics at low long-chain branching concentrations for polyethylene. Lohse and coworkers [8] also show strain-hardening characteristics at low long-chain branching concentrations, but through the efforts of blends of linear and branched polymers. Doerpinghaus and Baird [30], Bin Wadud and Baird [22], and Barroso [31] all comment on the ability to either qualitatively or quantitatively define long-chain branching based on extensional rheological measurements.

Bin Wadud and Baird [22] have analyzed the extensional behavior of two metallocene-catalyzed polyethylenes and the results are provided in figure 2.1.15. Affinity PL1880 contains long-chain branching on the order of 0.18 LCB/10^4 C and Affinity PL1840 on the order of 0.57 LCB/10^4 C. Strain-hardening characteristics are present for both materials, but more intriguingly is that the materials provide noticeably different extensional stress growth curves especially at higher extension rates where greater degrees of strain-hardening occurs. Recall that these same two materials had no noticeable differences in their viscosity curves that are previously shown in figure 2.1.5.

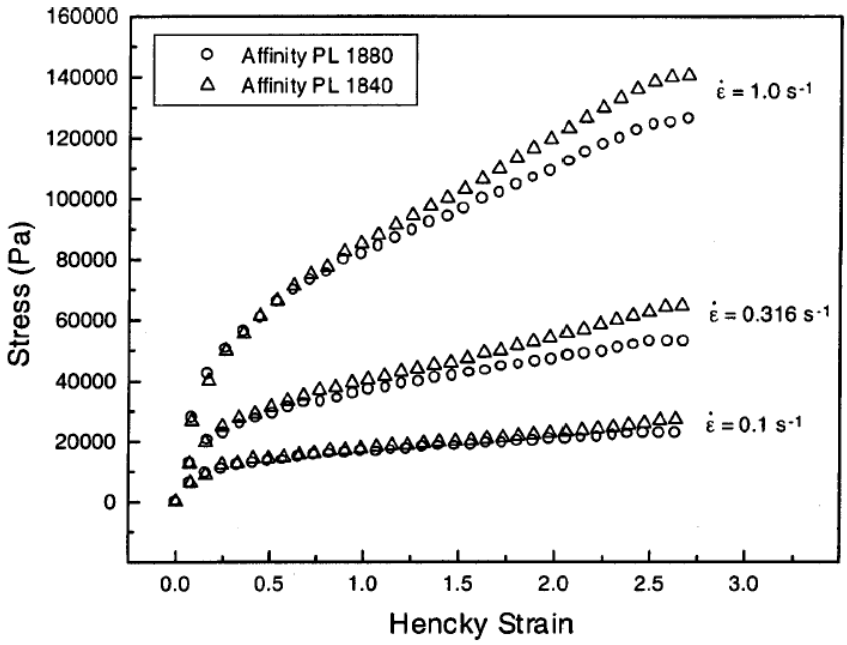

Figure 2.1.15 Extensional stress growth of PL 1840 and PL 1880 at 135°C [22].

Transient extensional viscosities for a highly-branched LDPE, NA952, a sparsely-brached metallocene-catalyzed polyethylene, Exact 0201, and two linear polyethylenes, Exact 3132 and NTX101 are presented in figure 2.1.16 taken from Doerpinghaus and

Baird [1]. The evolution of strain-hardening behavior is demonstrated as the transition is made from linear to highly-branched polyethylene. This same progression is shown by La Mantia and coworkers [28] and explicitly illustrates the drastic differences that are obtained in extensional rheological measurements fueling the idea of identifying long-chain branching content from the sensitivity of elongational results.

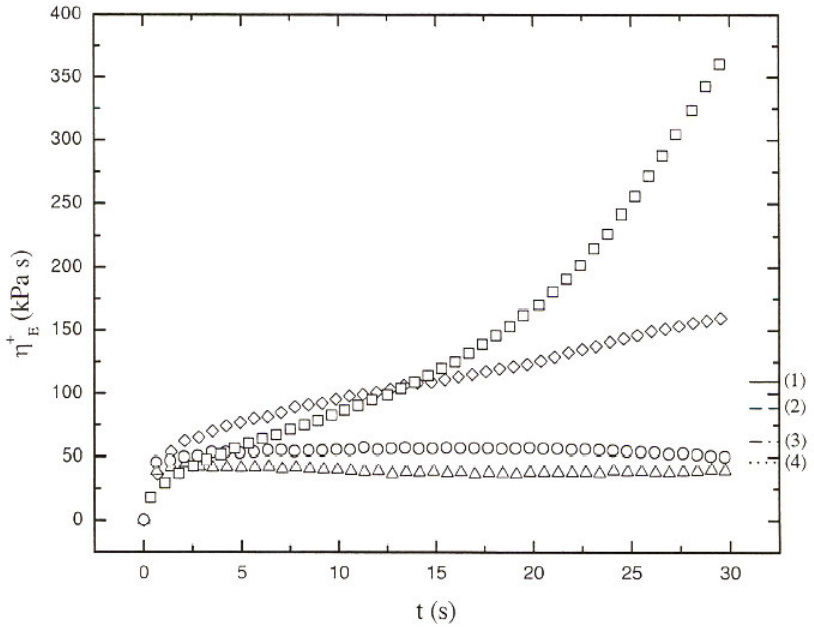

Figure 2.1.16 Transient extensional viscosities obtained at 150°C. (□) NA952, (◇) Exact 0201, (○) NTX101, (△) Exact 3132. Values of $3\eta^+(t)$ at t = 30 s for (1) Exact 0201, (2) NA952, (3) NTX101, (4) Exact 3132 [1].

Lohse and coworkers [8] reported extensional behavior of blends of linear and branched molecules, including stars and combs, for varying topological effects. Figure 2.1.17 presents the extensional viscosity measurements obtained by Lohse and coworkers [8] for their base polymer resin and for blends of 3% star and comb polymers. Clearly, only

blends with long-chain branched molecules of the comb topology experience strain-hardening, which is in accordance with the theory proposed by McLeish and Larson [3] where strain-hardening is limited to molecules with more than one branch point. Some discrepancies have arisen where linear materials show strain-hardening characteristics and this is an artifact of primarily high molecular weight tails in the molecular weight distribution, but could also result from poor rheometer design.

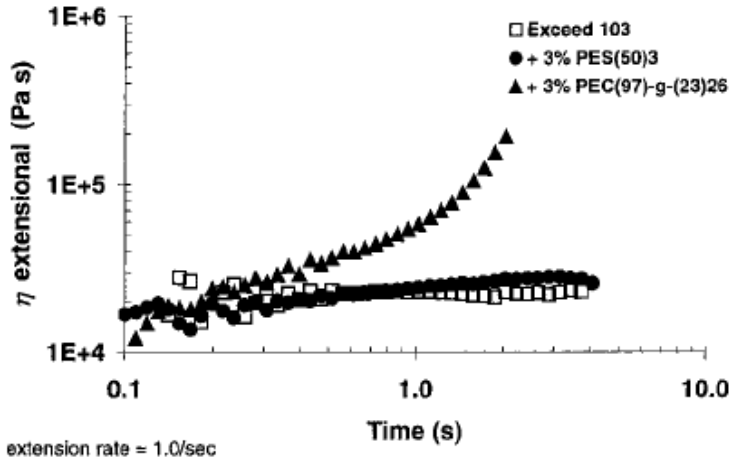

Figure 2.1.17 Extensional viscosity for Exceed 1018 and blends with star and comb polymers [8].

Malmberg and coworkers [33] note that high molecular weight and broadening of the molecular weight distribution contribute to the extensional rheological behavior as well and tend to generate the same strain-hardening characteristics due to the longer relaxation times. Here it is important to realize that many molecular characteristics influence rheological behavior, but with well-defined materials the effects of long-chain branching can be isolated providing correlation between rheology and molecular structure. The literature also includes work on shear and shear-free flow rheology for other materials

such as polybutadiene by Kasehagen and Macosko [34], polypropylene by Gotsis and coworkers [35], and polystyrene by Hepperle and Munstedt [36] and Ferri and Lomellini [7] among others. The net result is that much of this work is in agreement with the work reviewed for polyethylene and the behavioral trends transcend over polymeric material.

Molecular architecture influences rheological characteristics in both shear and shear-free flows. The work considered here concentrates on the effects of random long-chain branching of highly branched materials as well as the use of rheology to distinguish sparsely long-chain branched materials. LCB influences the onset of shear-thinning, the zero-shear viscosity, and strain-hardening properties. Sparsely LCB polymers that show similar flow behavior in shear flows are distinctly different in extensional flows and, thus, indicating that when shear and extensional flow behavior are coupled a better understanding of molecular architectures is gained.

2.2 Controlling rheological features for the film-casting process

Film-casting is a widely used processing technique that has applications ranging from packaging films to barrier coatings where films are cast onto a substrate with the majority of the interest in polyethylene. Other production methods for films exist for example blown films, but the focus of this work is on casting of molten polymer through a film-die. Subsection 2.2.1 discusses the instabilities associated with processing in this manner and subsection 2.2.2 presents the affect of rheological features on these instabilities. A better fundamental understanding of how molecular flow properties that can be related to molecular architecture perturb the instabilities in film-casting can lead to the production of more usable film and from an industrial point of view increase profitability. This section investigates the experimental observations although limited regarding these instabilities leaving the bulk of the discussion on simulation efforts to section 2.3.

2.2.1 Potential instabilities in film-casting

Instabilities, the terminology commonly used in the literature, prevalent in film-casting include necking phenomenon, the subject of subsection 2.2.1.1, edge-bead phenomenon, the subject of subsection 2.2.1.2, and draw resonance, the subject of subsection 2.2.1.3. The instabilities are discussed from a physical standpoint including the type of flow phenomenon that is occurring and the common operating conditions that enhance its growth. All of these instabilities take away from the ability to get the most usable from a given die geometry.

2.2.1.1 Necking phenomenon

Necking is defined as the reduction in film width compared to the original die width that is generated as a result of the conservation of mass when drawing a film sample at a greater rate than it is being extruded. Figure 2.2.1 is a schematic of the film-casting process through a flat die, which in this case is being cast onto a substrate, and illustrates the concept of necking. Evaluation of a film width profile leads to the conclusion that necking occurs more rapidly in a region closest to the die exit and tapers off until a steady width is reached or the film contacts the chill roll.

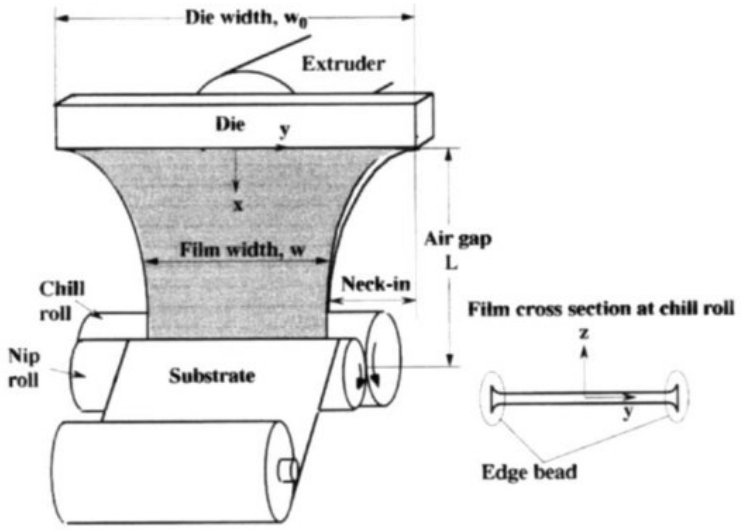

Figure 2.2.1 Schematic of film-casting onto a substrate [37].

Necking is affected by processing conditions such as extrusion rate, drawdown ratio, and air gap length as well as material viscoelastic properties, the latter of most importance and the discussion of subsection 2.2.2. In general it is seen through the simulation efforts of Kim and coworkers [38], Sakaki and coworkers [39], and Zheng and coworkers [40] that increasing drawdown ratio and increasing air gap length lead to more

drastic necking results. Canning and Co [41] and Canning and coworkers [42] have shown experimentally for the necking to both increase and decrease with increasing drawdown ratio. This is shown in figure 2.2.2 for polymers A, B, and C, where polymer A is a LDPE and B and C are LLDPE. The LDPE exhibits increases in film width with increasing drawdown ratio, but both LLDPE materials experience reductions in film width with increasing drawdown ratio. The results of Canning and Co [41] identify that material characteristics also play a role in final film dimensions and that necking is affected differently by processing conditions depending on the molecular structure and viscoelasticity associated with the polymer. Experimental verification of necking as a function of air gap length is unavailable, but nothing suggests any deviation from the predicted relationship from simulations.

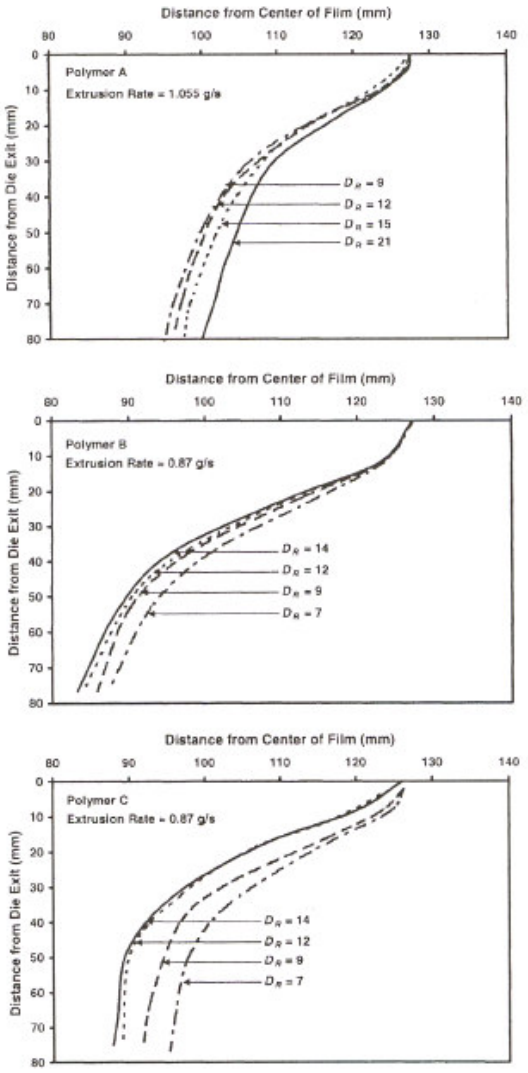

Figure 2.2.2 The dependence of film width profiles on draw ratio for a LDPE material, polymer A, and two LLDPE materials, polymers B and C [41].

2.2.1.2 Edge-bead phenomenon

Edge-bead defines the non-uniformity in the cross-section of a film sample and occurs according to Dobroth and Erwin [43] due to differing means of flow across the width of the film where the central film experiences planar extension and the edges uniaxial extension. An illustration of edge-bead is included in figure 2.2.1 as is seen when the

edges of a sample are substantially thicker than the primary central regions average thickness. Two main considerations prevail when evaluating edge-bead: the magnitude or difference between edge thickness and central thickness and the rate of growth of edge-bead; in other words the distance inward from the edge at which the edge-bead ceases to exist.

Like necking, edge-bead is also affected by processing conditions and material rheological properties. The effects of draw ratio and air gap length are discussed here whereas the role of rheological properties is considered in subsection 2.2.2. The simulations of Kim and coworkers [38], Sakaki and coworkers [39], and Zheng and coworkers [40] have shown that edge-bead forms immediately upon exiting the die and that the magnitude of the bead increases with increasing draw ratio. With regards to an increasing air gap length minor increases are experienced in the magnitude, but the gradient displays noticeably slower edge-bead growth leading to less usable film. Canning and Co [41] and Canning and coworkers [42] illustrate the effects seen experimentally for LDPE in figure 2.2.3 where normalized edge-bead profiles are presented at different draw ratios. It is found that increasing draw ratio does in fact increase the magnitude of the edge-bead, but to counteract the increasing magnitude is a steeper gradient for the transition to the edge-bead region resulting in more usable film. No experimental results are presented that illustrate the effect of varying air gap length on edge-bead so the simulation efforts for now must suffice.

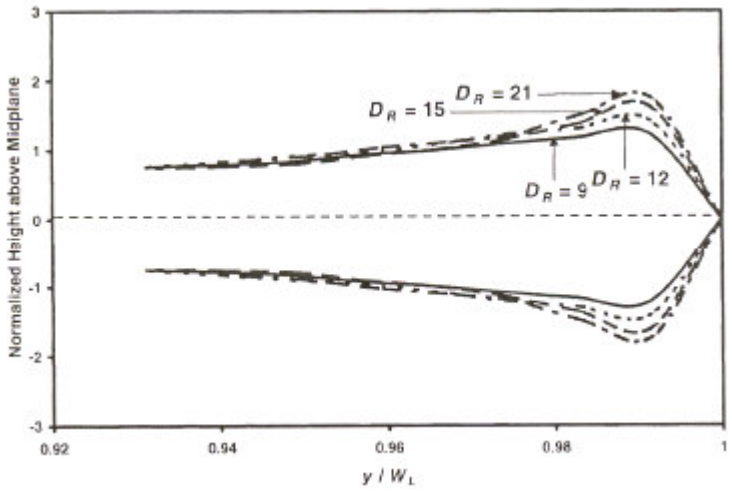

Figure 2.2.3 The normalized edge bead profiles of the LDPE, polymer A, at various draw ratios ranging from 9-21 [41].

2.2.1.3 Draw resonance

Draw resonance is an oscillatory instability where film width and thickness vary periodically above a critical draw ratio generating a non-uniform film. Lee and coworkers [44] indicate that draw resonance in cast films takes on the same mechanism of formation as that of fiber spinning. The onset of draw resonance is characteristic to a critical draw ratio and, therefore, draw resonance is quantified in terms of the maximum draw ratio where stability is present and draw resonance is about to occur.

The critical draw ratio that defines draw resonance is a function of the air gap length and viscoelastic behavior of the material, the latter of which is discussed in subsection 2.2.2. No experimental results indicating the effect of air gap length on the critical draw ratio have been presented in the literature, but the simulations efforts of Silagy and coworkers [45, 46], Lee and coworkers [44], and Kim and coworkers [38] provide insight on the situation. Figure 2.2.4 illustrates the effect of changing air gap length on the critical draw

ratio by showing the stable and unstable regions for a Newtonian fluid. Critical draw values range from 20-40 and the dependence on air gap length is observed as it is noted that in terms of draw resonance an optimal air gap length exists. Lee and coworkers [44] find that when in the unstable regime width behavior is different from the thickness behavior and is more sensitive to air gap length and viscoelastic properties.

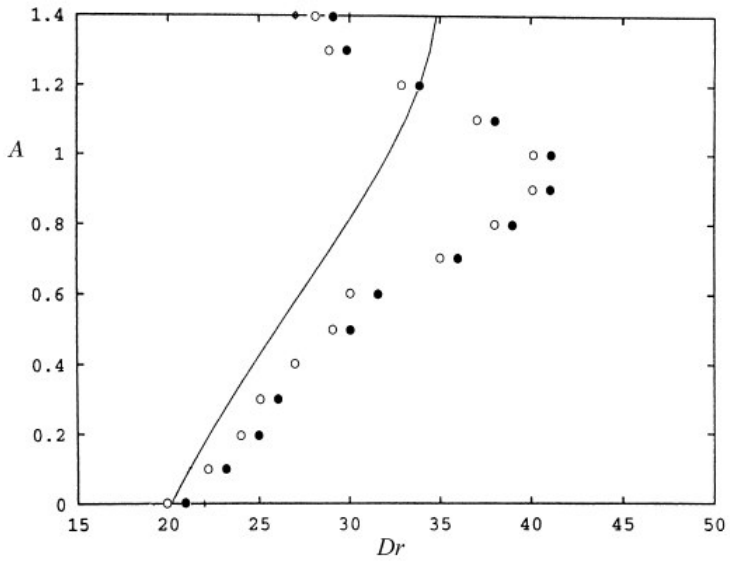

Figure 2.2.4 Influence of the air gap length on the critical draw ratio for a Newtonian fluid, where A is the aspect ratio defined as the distance from the die exit to the chill roll divided by the die width. The straight line represents the 1-D model critical curve and the symbols represent the 2-D, where the stable regime is left of the unfilled symbols and the unstable regime is right of the filled symbols [46].

2.2.2 The effects of rheological properties on film-casting instabilities

The topic of much discussion is the relationship between molecular features and rheological properties and the importance of this is to also distinguish the rheological

properties that cause differing processing behaviors. Both shear and extensional rheology are accounted for including the effects of shear-thinning, extensional-thinning, and strain-hardening, but commonly the enigma is materials that are identical in shear process differently especially in extensional dominated flows and, thus, the variations in processability are generally a result of extensional behavior. The effects of these rheological features on film-casting instabilities are considered. Limited experimental work is available, but simulation efforts have shown dependencies. Further detail of the simulation work is provided in section 2.3, but the trends concerning the viscoelastic nature of a material are discussed here.

Necking has been shown by numerous authors [37, 38, 41, 45-49] to decrease as the strain-hardening capabilities of a material increase, but groups such as Satoh and coworkers [37], Ito and coworkers [49], and Kajiwara and coworkers [47] attribute the behavior to the difference in uniaxial and planar strain-hardening based on the ideas of Dobroth and Erwin [43]. Canning and Co [41] have shown experimentally the changes in necking behavior for a LDPE and two LLDPE materials, where LDPE exhibits strain-hardening characteristics and LLDPE does not. Figure 2.2.5 illustrates the streamlines for the LDPE, polymer A, and the two LLDPE materials, polymer B and C, at a constant drawdown and polymer A is seen to have less necking than polymers B and C. Strain-hardening characteristics also affect the trend for necking behavior as a function of draw ratio extracted from figure 2.2.3. The LDPE exhibits reductions in necking with increasing draw ratio whereas the two LLDPE materials exhibit increases in necking with increasing draw ratio. Shear rheological effects are not considered because the materials exhibit similar shear rheological characteristics.

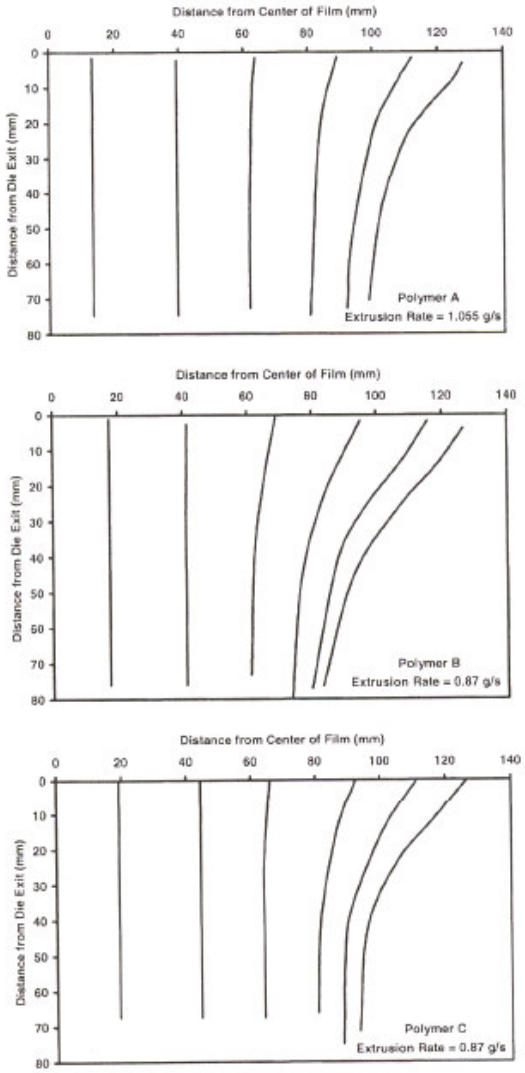

Figure 2.2.5 Streamlines for the LDPE, polymer A, and the two LLDPEs, polymers B and C, at a draw ratio of 12 [41].

Edge-bead as a function of viscoelastic behavior has only been addressed through comparison of simulation results as no experimental results making comparisons between different materials exist. The general trend like in the case of necking appears to only depend on the extensional rheological characteristics. The simulation work of Kim and

coworkers [38], Silagy and coworkers [45, 46], and Ito and coworkers [49] indicate that increasing strain-hardening slightly increases the magnitude of the edge-bead, but also increases the gradient or rate at which the edge-bead grows resulting in a higher area of usable film.

Draw resonance is another instability that is probed with simulation results and suffers from a lack of experimental observations to verify the findings. The work of Kim and coworkers [38], Silagy and coworkers [45, 46], Smith and Stolle [48], Iyengar and Co [50], and Pis-Lopez and Co [51, 52] show that strain-hardening properties act to stabilize the process and push the critical draw ratio to higher values and that both extensional-thinning and shear-thinning destabilize the process acting to enhance the draw resonance behavior.

2.3 Modeling the film-casting process for Newtonian and non-Newtonian fluids

The industrial applicability of the film-casting process has led to a thrust in modeling the flow behavior with particular interest in prediction of the aforementioned instabilities. Film-casting modeling has progressed from simple one-dimensional isothermal Newtonian predictions to fully developed three-dimensional non-isothermal viscoelastic predictions. The transformation entails a transition from simple to rather complex modeling features and can provide for expedient on-line predictions or full analysis of film features such as final film dimensions, velocity profiles, and stress profiles. Constitutive relationships such as the upper convected Maxwell model, modified Giesekus, Phan-Thien Tanner, Bird-Carreau, and Larson models have been employed to describe the viscoelastic behavior characteristic to polymer melts.

The current modeling approaches and successes are discussed in detail in subsection 2.3.1. Model predictions are evaluated by their ability to predict instabilities and in some instances compared to experimental observations. Linear and non-linear stability analyses provide insight to the stable operating regions with respect to draw ratio and Deborah number.

2.3.1 Review of current modeling success

Moderate success has been achieved for modeling instabilities especially within the framework of understanding the potential effects of process variables, but comparisons of model predictions and experimental data are rather limited. Subsections 2.3.1.1, 2.3.1.2, and 2.3.1.3 proceed through the evolution of film-casting modeling from simple to increasingly complex considerations. Each subsection focuses on the considered spatial

kinematics and the subsequent analysis in the isothermal and non-isothermal cases as well as the Newtonian and non-Newtonian cases.

2.3.1.1 One-dimensional spatial analysis

Inspired by modeling of the fiber-spinning process, one-dimensional film-casting analyses only consider material flow in the stretching direction. Two approaches are taken: one in which the width remains constant and only the thickness suffers a reduction, a true one-dimensional model, and one in which the width does not remain constant and generally takes on a fixed final dimension, sometimes referred to as the 1.5-dimensional model. The second approach is in accordance with observations and subsequently is a more realistic modeling approach.

Pearson [53] along with Yeow [54] provide a one-dimensional analysis for Newtonian fluids. Barq and coworkers [55] and Iyengar and Co [50] extend this research and include Maxwell and modified Giesekus constitutive equations, respectively, to account for viscoelasticity. True one-dimensional analyses are ineffective given the inability to account for both the necking and edge bead instabilities. Regarding draw resonance, it is shown in this work that for Newtonian fluids under isothermal conditions the critical draw ratio is similar to that found for melt-spinning based on a linear stability analysis of steady flow. Viscoelastic properties are shown to affect the stability and the final critical draw achieved. Extensional-hardening features provide a stabilizing effect and increase the value for critical draw ratio whereas shear-thinning and extensional-thinning characteristics create a destabilizing effect and reduce the critical draw ratio.

Silagy and coworkers [45] treat the one-dimensional set of ordinary differential equations implicitly and allow for the final film width to be determined computationally hypothesizing constant thickness across the width of the film. The Maxwell model is used to describe viscoelasticity in the simulations and the resulting free surfaces for both the Newtonian and viscoelastic cases are presented in figure 2.3.1. Newtonian fluid simulations generate a linear profile whereas the Maxwell model simulations are nonlinear producing a profile that depicts a highly necking region close to the die that then dampens out to a steady film width. Experimental observations support the viscoelastic model and qualitatively confirm the benefits of the inclusion of viscoelasticity in the model simulation. Elasticity is seen to lead to the production of wider, thinner films and, therefore, suppresses the necking instability as well as providing process stability through a reduction in draw resonance. Increasing elasticity does yield competing efforts and has a negative effect for highly elastic materials. Newtonian materials suffer from draw resonance and consequently have small stability regions which increase with elasticity until a material becomes too elastic and suffers from film breakage. Stability and in turn critical draw are determined to then be functions not only of processing conditions like draw ratio and the distance to the chill roll, but material properties like their viscoelastic nature.

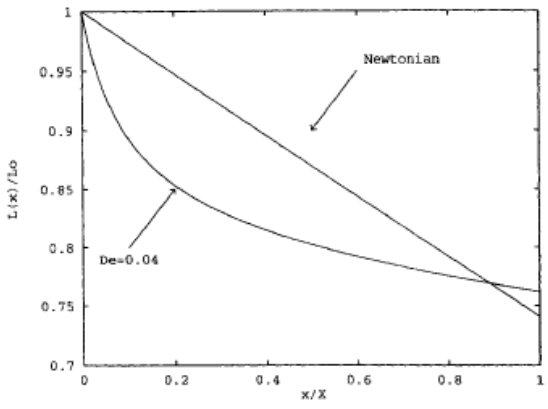

Figure 2.3.1 Comparison of the free surfaces for the one-dimensional simulations of Newtonian and viscoelastic fluids [45].

Contrary to the typical Eulerian approach Smith and Stolle [48] simulate the film-casting process using an updated Lagrangian algorithm and evaluate stability by the rate of energy dissipation. Similar results are seen regarding viscoelasticity effects, but they conclude that a one-dimensional simulation is better suited than a 1.5-dimensional simulation because of the restraining influence inherent to the edge-bead defect. Non-isothermal evaluation reveals an increase in the critical draw ratio and a stabilizing effect with higher values for the heat transfer coefficient, and thus greater heat transfer.

Process stabilization encountered when using materials with more elastic characteristics yields the idea of attempting to stabilize a viscous material like HDPE by encapsulating the free surfaces with a more elastic material such as LDPE as shown in figure 2.3.2 where the white material is HDPE and the shaded material is LDPE. Lee and coworkers [56] simulate the encapsulated film-casting experiment for an isothermal one-dimensional model of both Newtonian and viscoelastic materials where viscoelasticity is described by the Phan-Thien Tanner constitutive equation. Increased elastic behavior and

increased width of encapsulant increase stability and decrease the degree of necking qualitatively agreeing with experimental results. Lee and coworkers [56] attempt to extend this idea to the encapsulation of PET with LDPE, but the decreased viscosity of LDPE at processing temperatures of PET yield LDPE ineffective requiring temperature compatibility between the encapsulant and the primary film material.

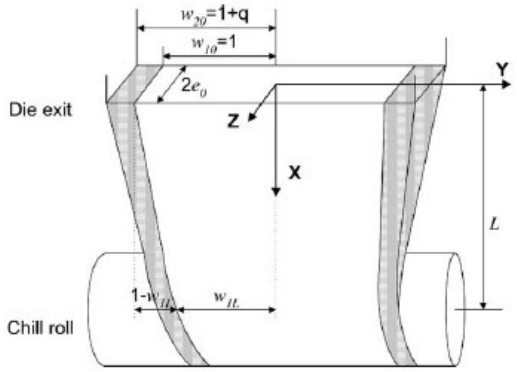

Figure 2.3.2 Illustration of the encapsulation method where the white part of the film represents the more viscous material and the shaded regions represent the more elastic material [56].

2.3.1.2 Two-dimensional spatial analysis

The inability of the one-dimensional model to predict the edge-bead defect has led to the generation of a two-dimensional model in which flow in the width direction is also considered. d'Halewyu and coworkers [57] introduced the ideas of the membrane approximation for two-dimensional modeling where the width is considered much larger than the thickness and components such as velocity and stress are constant throughout the thickness. The coupled system of partial differential equations lends itself to the use of finite element method calculations. Two approaches to meshing are employed for

calculations along the free surface: tracking strategy or deforming mesh and fixed meshing. Tracking leads to induced mesh degeneration and loss of accuracy requiring remeshing at high draw ratios. Calculations on a fixed mesh induce diffusion and yield difficulties when dealing with the large changes on the free surface.

d'Halewyu and coworkers [57] introduce the membrane approximation to formulate a two-dimensional simulation considering Newtonian fluids and an isothermal approach. The ability of a two-dimensional model to simultaneously predict both the necking and edge-bead instabilities as well as the capability to probe draw resonance thresholds is proven. d'Halewyu and coworkers [57] neglect the effects of surface tension, non-isothermal behavior, and most importantly viscoelasticity as was previously shown in the one-dimensional models.

Silagy and coworkers [45, 46] address the issue of viscoelasticity by employing a Maxwell model constitutive equation. As in the one-dimensional case it is found that increasingly elastic behavior provides a stabilizing effect on the draw resonance and affects the film dimensions by promoting enhanced film width and reduced edge-bead. Draw resonance is evaluated and the relationship between dimensions while experiencing this instability is observed where interior film thickness increases with decreases in width and exterior thickness and oscillations with the converse occur. Comparisons are made to experimental data for LDPE and LLDPE with the results for the film width profile and film thickness shown respectively in figures 2.3.3 and 2.3.4. Relatively good agreement is established, but some differences are noticed. The model predictions for film width show a slightly delayed necking behavior and predictions for final film width that are slightly less than the experimental values. For edge-bead evaluation the model predicts a

less abrupt increase in thickness at the edge and a slightly larger value for thickness across the central part of the film.

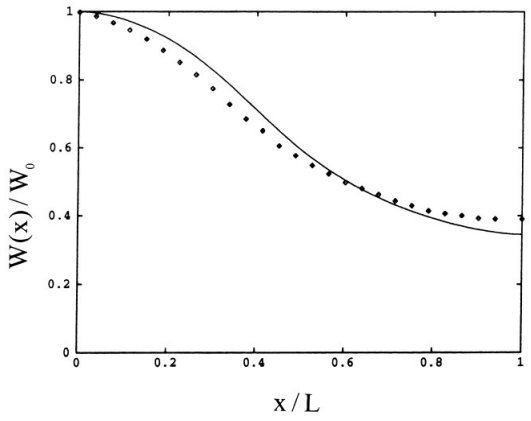

Figure 2.3.3 Film width profile illustrating the necking phenomenon through a comparison of (-) the 2-D numerical Newtonian simulation and (◇) experimental results for linear low density polyethylene [46].

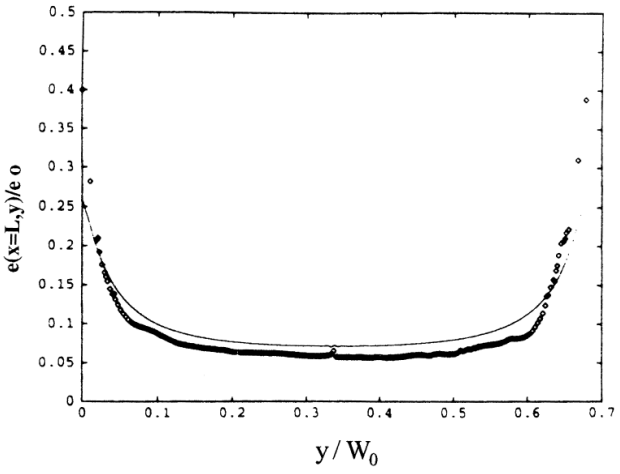

Figure 2.3.4 Film thickness profile illustrating the edge-bead instability through a comparison of (-) the 2-D numerical viscoelastic simulation and (◇) experimental results for low density polyethylene [46].

Other works by Smith and Stolle [58], Kim and coworkers [38], and Sollogoub and coworkers [59] incorporate a non-isothermal evaluation along with the 2-D modeling approach. Smith and Stolle [58] exclude viscoelasticity and exclusively evaluate Newtonian fluids and how they are affected by a non-isothermal approach along with self-weight, localized cooling, and a non-constant die thickness. All simulations infer the conclusion that lengthening relaxation times of a material leads to larger edge-bead, but less necking and more uniform film thickness across the width. For example, increasing the heat transfer coefficient increases the viscosity of the material effectively lengthening the relaxation time and produces the previously discussed results. The results are explained according to the ideas of Dobroth and Erwin [43] by suggesting that the restraining influence generated by edge-bead increases with increasing edge-bead and the width of the plane strain region must increase. The plane strain region is the central part of the film thus preventing necking.

Kim and coworkers [38] add the effects of viscoelasticity by incorporating the upper-convected Maxwell constitutive equation while retaining a non-isothermal 2-D approach. They also consider variations in draw ratio and aspect ratio determined by comparing the distance between the die and the chill roll to the width of the die. The effects of draw ratio, aspect ratio, and viscoelasticity on final film dimensions are shown respectively in figure 2.3.5 a-c. Increasing viscoelasticity and decreasing aspect ratio and to a lesser extent draw ratio lead to less necking while decreasing draw significantly reduces edge-bead and reductions in aspect ratio slightly decrease the magnitude of the edge-bead as well as increase the gradient form central film thickness to edge thickness. Viscoelasticity doesn't appear to affect the magnitude of the edge-bead, but increases in

viscoelasticity cause increases in the gradient for edge-bead formation leading to more usable film. Draw resonance stabilization is confined to a critical draw ratio that increases with increasing viscoelasticity and occurs at some intermediate aspect ratio. The inherent rheological inadequacies associated with the constitutive equation may influence the simulations, but the authors point out that their approach can be extended to other constitutive equations.

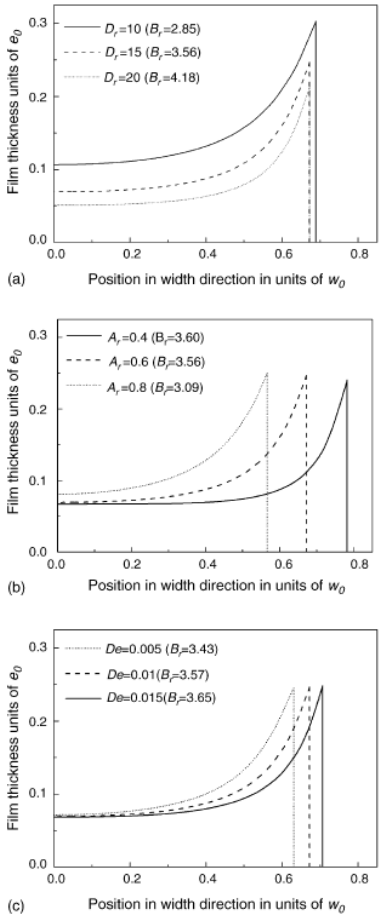

Figure 2.3.5 The effects of various processing conditions on the steady-state film dimensions: (a) the effect of draw ratio, (b) the effect of aspect ratio, and (c) the effect of viscoelasticity in the form of changing Deborah number [38].

Similar work is presented by Sollogoub and coworkers [59] where modeling of a non-isothermal 2-D viscoelastic fluid is performed. The viscoelastic constitutive equation is the upper convected Maxwell model and this work differs from that of Kim and coworkers [38] in the solution algorithm. Sollogoub and coworkers [59] define the free surface by surrounding the polymer with a ficticious fluid. The results generated are the same indicating that increases in elastic behavior and heat transfer abilities produce reduced necking. These operating conditions concentrate the stretching to the area very near the die.

2.3.1.3 Three-dimensional spatial analysis

Two-dimensional analyses appear to accurately depict film behavior provided the constitutive equation adequately describes a materials rheological features, but in the interest of completeness Sakaki and coworkers [39], Satoh and coworkers [37], and Zheng and coworkers [40] have all taken a three-dimensional approach to the kinematics. A number of articles authored by Lamberti, Titomanlio, and Brucato [60-64] evaluate the role of crystallization and material solidification also using three-dimensional kinematics. This now includes flow in the film thickness direction neglecting the membrane approximation. Increases in computational speed make the efforts of a full three-dimensional analysis including complex viscoelastic constitutive equations and heat transfer now accessible. Providing flow information prior to the die exit is considered, features such as die swell may also now be evaluated.

Sakaki and coworkers [39] model the simplest three-dimensional case for Newtonian fluids and the assumption of isothermal behavior. The potential effects of changing draw

ratios, air gap length, and die width are evaluated with respect to the necking and edge-bead instabilities. Increasing draw ratio and air gap length provide for greater necking and thus decreased productivity, however, die width has no effect on the necking behavior. Studies on particle path-lines and velocity and stress profiles confirm that flow in the thickness direction doesn't contribute to the film behavior. Particle path-lines in the x-z plane at various thicknesses of the film are shown in figure 2.3.6 to be the same regardless of position in the thickness direction. The ideas of Dobroth and Erwin [43] are also represented where flow in the length direction is constant along the width direction for the majority of the central film, but differs near the edges illustrating possibly two types of flow: planar at the center and uniaxial at the edges. Figure 2.3.7 provides a cross-sectional representation of the film at progressively larger distances from the die exit. It is observed that edge-bead forms close to the die exit and the film from that point forward thins fairly uniformly, where necking appears to occur after the edge-bead is initially formed. The authors do find discrepancies between their three-dimensional model and the two-dimensional model of d'Halewyu and coworkers [57] shown in figure 2.3.8. A suggestion is made to evaluate the effect of the finite element mesh pattern on the final film shape.

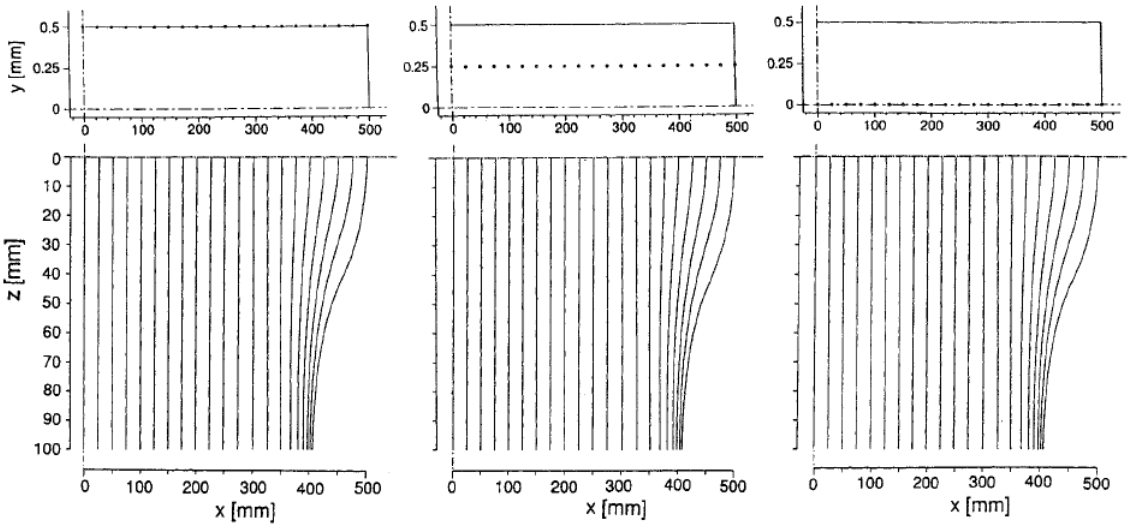

Figure 2.3.6 Particle path-lines projected in the x-z plane originating at varying thicknesses for the following case: $D_R = 50$, die width = 100 mm, die thickness = 1 mm, air gap length = 100 mm, velocity at die exit = 5 cm/s [39].

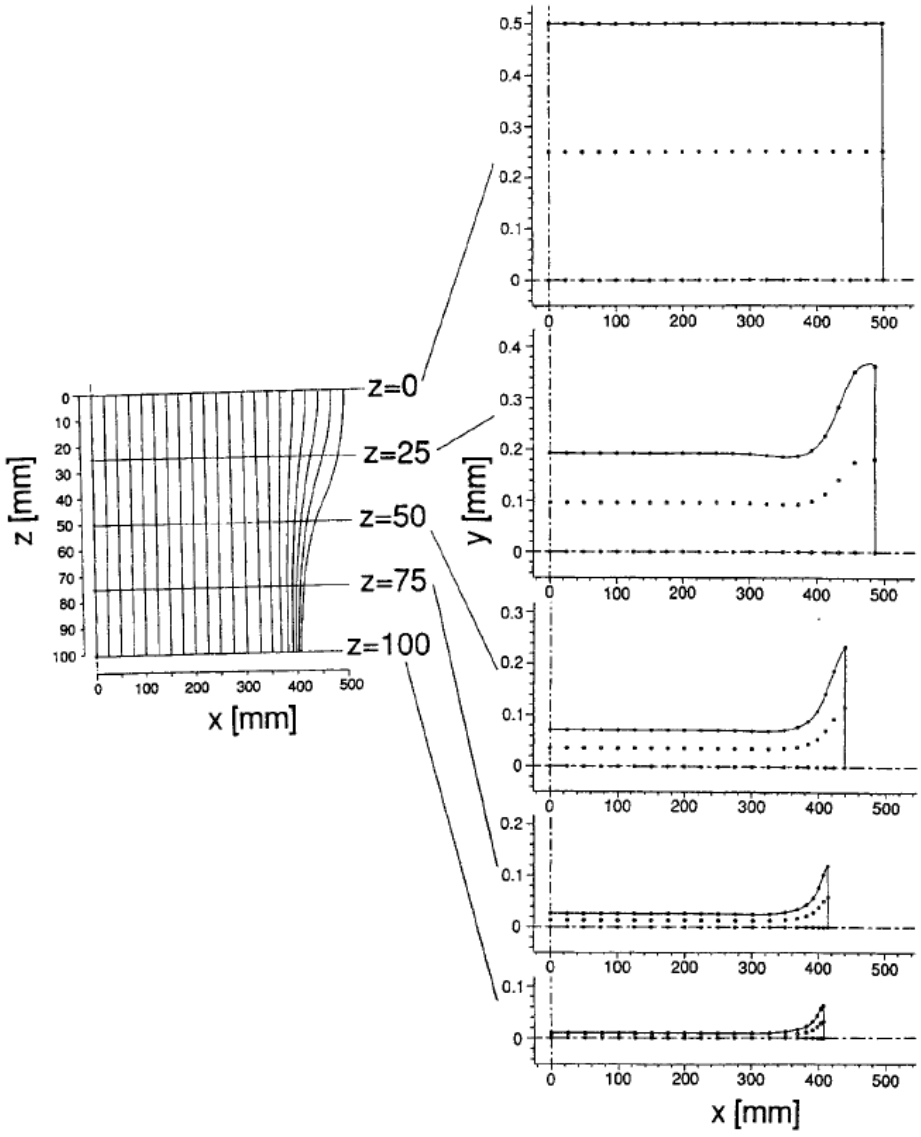

Figure 2.3.7 Cross-sectional film shape and position of particle path-lines at differing distances from the die exit for the following case: D_R = 50, die width = 100 mm, die thickness = 1 mm, air gap length = 100 mm, velocity at die exit = 5 cm/s [39].

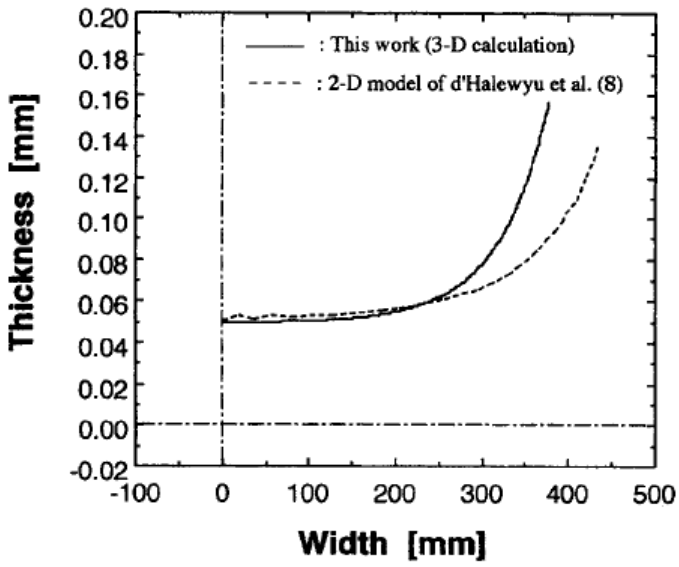

Figure 2.3.8 Comparison of the final film thickness distributions for the 3-D calculation of Sakaki and coworkers and the 2-D model of d'Halewyu and coworkers. Processing parameters are as follows: die width = 1000 mm, die thickness = 1 mm, air gap length = 200 mm, draw ratio = 10 [39].

Extension to viscoelastic simulations along with Newtonian behavior is provided by Satoh and coworkers [37] in their quasi three-dimensional simulations. They use a multi-mode Larson model constitutive equation for viscoelasticity due to the ability to model the rheological behavior of LDPE. The simulations are compared to experimental results for several LDPE resins featuring different amounts of strain-hardening behavior, which have been shown to stabilize instabilities. Satoh and coworkers [37] compare their simulation to that of Sakaki and coworkers [39] and find excellent agreement verifying the simulation scheme. Simulations and experimental results for changes in film thickness and film width for the various polyethylene resins are shown in figure 2.3.9. The simulations appear to be in agreement with the experimental results especially in the film

width predictions. A more gradual edge-bead is noted in contrast to the steep gradient seen experimentally when evaluating the film thickness profile. To illustrate the effects of strain-hardening the authors provide in figure 2.3.10 film profiles for, in order of increasing strain-hardening, Newtonian, Model-B, Model-A, and LDPE-B. It is observed that increases in strain-hardening lead to increases in film width and a larger usable film area. No changes in thickness or edge-bead evolution can be distinguished for the strain-hardening materials; however, when compared to the Newtonian simulation it is seen that in general strain-hardening reduces film thickness and generates a more abrupt transition to the edge-bead region. Satoh and coworkers [37] also discuss the ideas of Dobroth and Erwin [43] where planar flow occurs in the central film and uniaxial flow occurs on the edges and look at film simulation results with respect to a ratio of η_{EU}/η_{EP} also stated by Ito and coworkers [49] and Kajiwara and coworkers [47]. The viscosity relationship for LDPE-B, Model-A, and Model-B is provided in figure 2.3.11. It is observed that the most highly strain-hardening material also has the largest ratio of viscosities and the necking behavior may also be influenced by differences in viscosities for these two different extensional flows. In regards to thermal effects Satoh and coworkers [37] show in figure 2.3.12 that commercially heat transfer is negligible due to the high flow rates and processing temperatures, but this is not the case in a laboratory scale experiment. Heat transfer effects depend on the temperature change between the die exit and the chill roll.

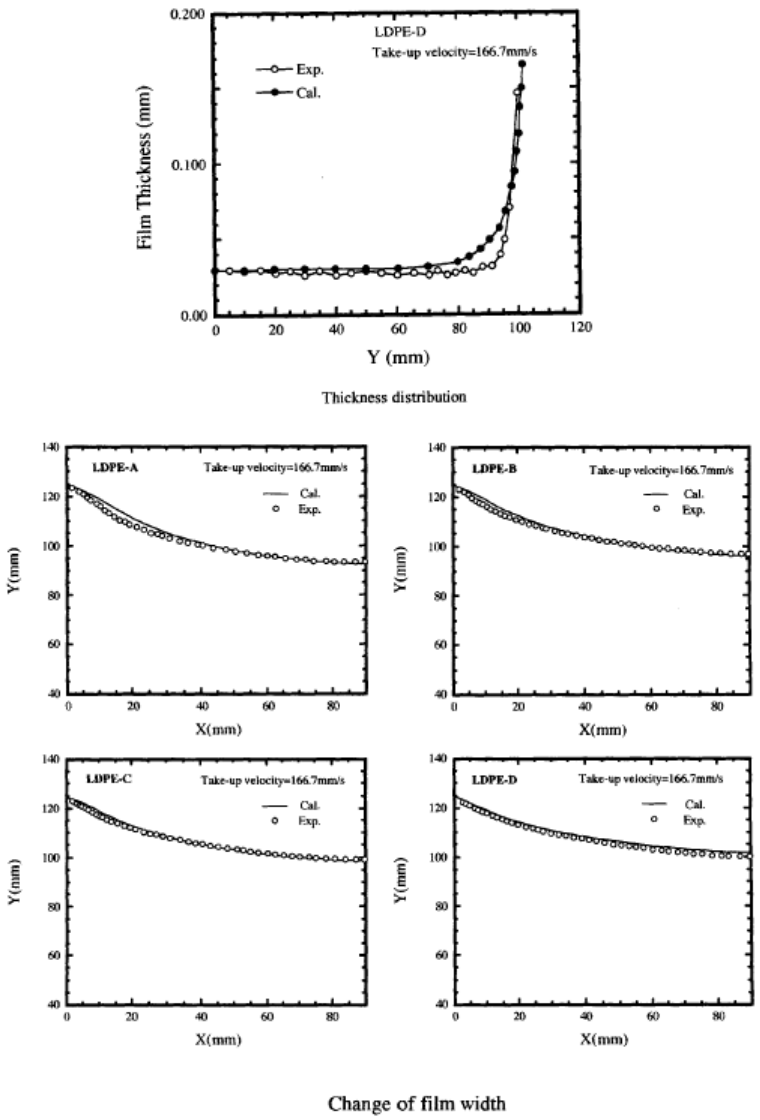

Figure 2.3.9 Comparisons for the simulation results and experimental data for the final film thickness and width distributions at the chill roll for a laboratory-scale process [37].

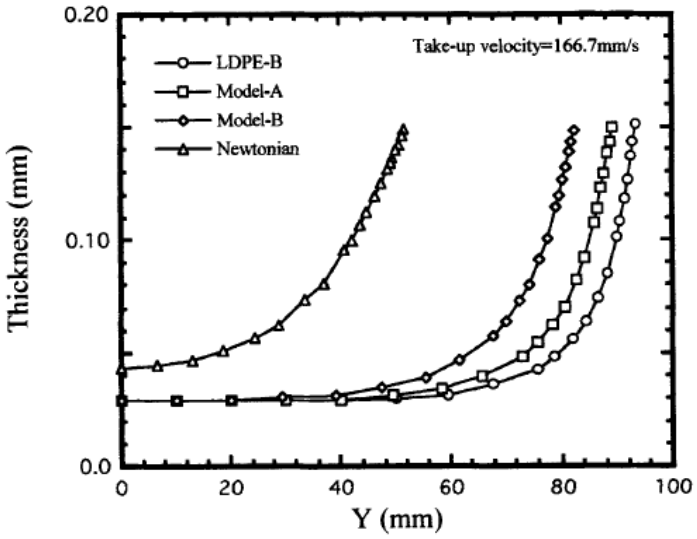

Figure 2.3.10 Predicted final film dimensions at the chill roll for, in order of increasing strain-hardening behavior; LDPE-B, Model-A, Model-B, and Newtonian fluids [37].

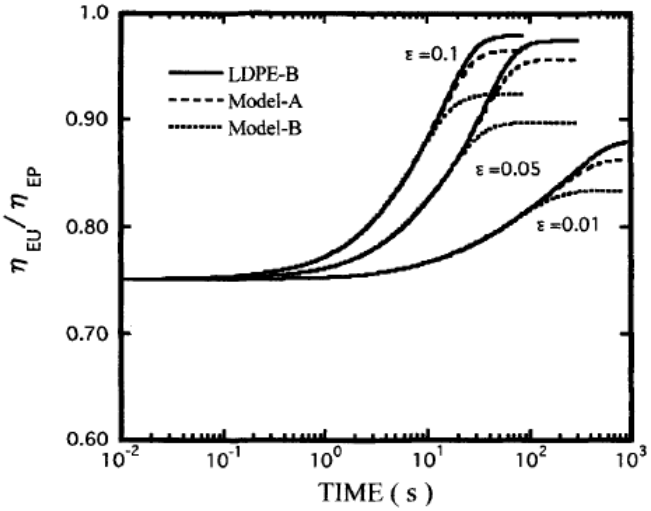

Figure 2.3.11 The ratio of uniaxial elongational viscosity to planar elongational viscosity at elongational rates of $\varepsilon = 0.01\ s^{-1}$, $0.05\ s^{-1}$, and $0.1\ s^{-1}$ for LDPE-B and the two Model fluids [37].

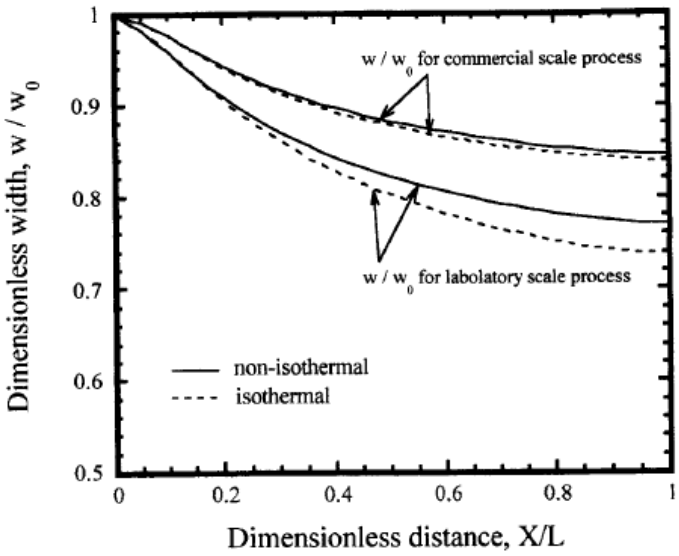

Figure 2.3.12 The change of film width predicted for LDPE-B under isothermal and non-isothermal conditions at 166.7 mm/s take-up velocity for the laboratory-scale process, and 3333.3 mm/s for the commercial-scale process [37].

Zheng and coworkers [40] have also performed a three-dimensional analysis for isothermal and non-isothermal viscoelastic materials, in which viscoelasticity is described with the Bird-Carreau model. Model simulations are compared to experimental data of PET cast films. In agreement with other works Zheng and coworkers [40] observe increases in the severity of both necking and edge-bead with increasing draw ratio and distance between the die exit and chill roll. The comparison between experimental results and the simulation are provided in figure 2.3.13 where the film edge is shown as distance from the die versus distance from the centerline. This only provides insight to the width dimension identifying the necking, but no comparisons of film thickness are made leaving to wonder the capabilities of edge-bead predictions. The film width prediction is reasonable although the experimental film experiences more drastic necking

close to the die than the simulation predicts. Temperature and velocity profiles are lower on the edges of the film than in the center. This result, which contributes greatly to the edge-bead defect, is verified with both simulation and experimental observations. Zheng and coworkers [40] find that provided the distances between the die exit and chill roll is short enough the non-isothermal assumption is negligible because of insufficient cooling. When incorporating heat transfer it is observed that increasing the rate of heat transfer results in less necking and larger edge-bead.

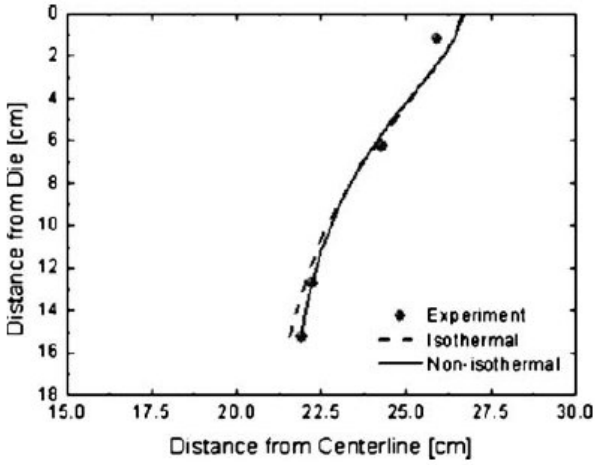

Figure 2.3.13 Comparison of experimental and simulation results for the film width including the differences between an isothermal and non-isothermal approach where α = 1.37 w/m^2°C for non-isothermal and α = 0 for isothermal simulations [40].

Lamberti, Titomanlio, and Brucato [60-64] have also investigated and contributed to film-casting simulation efforts with an emphasis on solidification of the film whether it be through cooling or crystallization. Spatially a 3-dimensional approach is taken and with regards to heat transfer a 1-dimensional approach is taken including both natural and forced convection as well as radiation where emissivity is a function of film thickness.

The authors find on the front of heat transfer improved model predictions especially under high deformations by also including radiant heating of the film from the die acting to suppress the cooling rate. Crystallization kinetics are dependent on elongational flow behavior and flow-induced crystallization is relevant. To effectively incorporate the effects into the model such that the model accurately predicts crystallization both relaxation time and number of monomers between entanglements must be variable.

2.4 Evaluation of the effectiveness of the pom-pom model

An increase in the importance of the link between molecular architecture and rheological features for branched polymeric materials has led to the proposal of the pom-pom model by McLeish and Larson [3]. In subsection 2.4.1 the theoretical concepts behind the pom-pom model equations are reviewed. The ideas are discussed in their application to the idealized pom-pom molecule as well as the extension to real molecules, which can be thought of as an ensemble of pom-pom molecules. An integro-differential form and a simplified differential form, that lacks the mathematical complexity of the former, were both developed by McLeish and Larson [3]. The extended pom-pom model was also developed as an improvement on the original by Verbeeten and coworkers [65]. The potential ramifications of any simplifications and subsequent additions through this chronological evolution are discussed in detail in the subsections 2.4.2, 2.4.3 and 2.4.4.

2.4.1 Theory behind the McLeish-Larson pom-pom model

The tube model developed by Doi and Edwards [19] has been applied by McLeish and Larson [3] to the pom-pom molecular structure to create a model that has the potential to explain the nonlinear rheology associated with branched polymers. Molecular constraints from entanglements in the tube model are represented by confining the polymer chain to a hypothetical tube. Two relaxation mechanisms are permitted within the tube model theory: reptation and retraction. Chain motion is allowed within the tubes constraints through a diffusive process deemed reptation. Retraction is described as the contraction of a chain segment after a stretch is imposed due to elasticity within the chain segment.

The relaxation of a linear polymer chain through its reptation process is shown in Figure 2.4.1. The chain moves about its primitive path confined by the tube diameter, which represents chain entanglements. As an end of the polymer chain frees itself from the tube, the remaining empty tube is disregarded. This process continues at both ends of the polymer until the tube is completely disregarded. The physical representation of the reptation process remains the same when extended to branched polymers except for the reptation can only occur at the one free end.

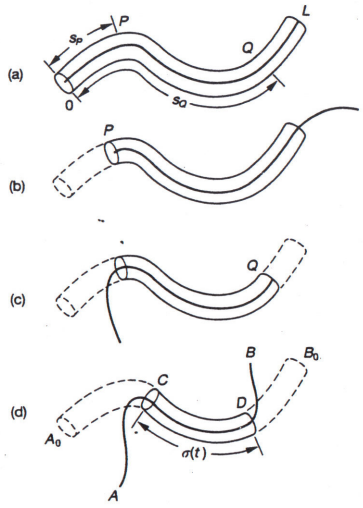

Figure 2.4.1 Mechanism for chain relaxation through reptation. (a) Initial conformation of the primitive chain in its tube. (b) and (c) Chain reptation beyond the tube on the left then right sides to relieve the original tube constraints. (d) Conformation at a later time with reduced tube length [19].

Small step strains do not invoke any stretch in the polymer chain and are not discussed here as they are not nearly as interesting as large step strains. Stress relaxation after a large step strain is described in Figure 2.4.2 again for a linear polymer chain.

Upon deformation the polymer chain first takes on a new conformation. Before reptation begins the polymer chain retracts to its original contour length, but retains its new conformation. After the time for retraction the chain relaxes through reptation.

This stretching of the polymer chain is interesting when extended to polymers with multiple branch points. The branch points serve as pins that restrict the backbone segment from relaxation until the branch arms first relax. This delayed relaxation of the imposed stretch contributes to the rheology of the material yielding nonlinear effects such as extensional strain-hardening.

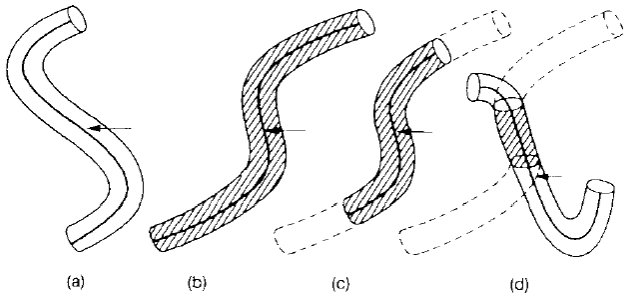

Figure 2.4.2 Stress relaxation after a large step strain. (a) Initial conformation of the chain in its equilibrium state. (b) Deformation results in chain stretching and changing orientation. (c) Retraction of chain stretch after τ_R in order to return to its original contour length. (d) Relaxation through reptation after τ_d [19].

2.4.1.1 Idealized pom-pom molecule

The pom-pom model was introduced by McLeish and Larson [3] as an attempt to effectively account for the shear strain-softening properties and the extensional strain-hardening properties exhibited by branched polyolefins. An idealized pom-pom molecule was envisioned to illustrate the needed molecular complexity to achieve the nonlinear rheological features characteristic of branched polymers. The pom-pom molecule is described as an extension of the H-polymer [66] in which two branch points consisting of q arms are attached by a single backbone segment. The pom-pom molecular structure is illustrated in Figure 2.4.3 where q = 3.

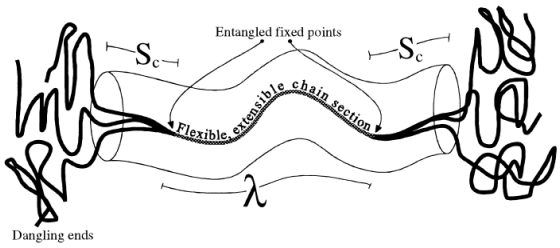

Figure 2.4.3 Representative pom-pom molecule with q = 3. Chain stretch and branch-point withdrawal are indicated by λ and s_c, respectively [67].

The nonlinear rheological features characteristic to branched polymers are created upon deformation by restrictions of relaxation motions to the backbone connecting segment. This segment is subjected to impeded retraction due to the arms attached at the branch points, and the segment is prohibited to relax via reptation until the attached arms are completely relaxed. McLeish and Larson [3] are able to incorporate the ideas of

relaxation times for stretch as well as orientation, the concept of time-dependent backbone stretch, and branch-point withdrawal into their pom-pom model.

Pom-pom molecules relax from the outermost regions to the innermost regions resulting in different relaxation timescales. The arm segments of a pom-pom molecule relax rapidly as star polymer arms would through path length fluctuations. The backbone segment is restricted from any relaxation processes until the free arms first relax, yielding a delayed retraction mechanism for the backbone. After the arms completely relax the backbone then undergoes an immediate retraction to alleviate any accrued stretch, which correlates to the relaxation time for stretch. Finally, the backbone relaxes through reptation corresponding to the orientational relaxation time [20].

Branch-point withdrawal is a product of the finite extensibility associated with a polymer backbone segment. Physically the backbone segment cannot extend infinitely and at some point it is entropically favored for the arm segments to become withdrawn into the backbone tube. The maximum tension in the backbone is directly related to the number of arm segments and the primitive path of the backbone may not exceed q times its equilibrium length. At this level of stretch the branch point and arm segments withdraw into the tube a distance s_c. There are now three distinct regimes that summarize the stretch deformation of a branched polymer. When $\lambda < q$, s_c remains zero and the backbone segment stretches until $\lambda = q$. Accumulated tension beyond $\lambda = q$ designates the growth of s_c. A pictorial description of a pom-pom molecule is represented in Figure 2.4.4 for the three different regimes discussed.

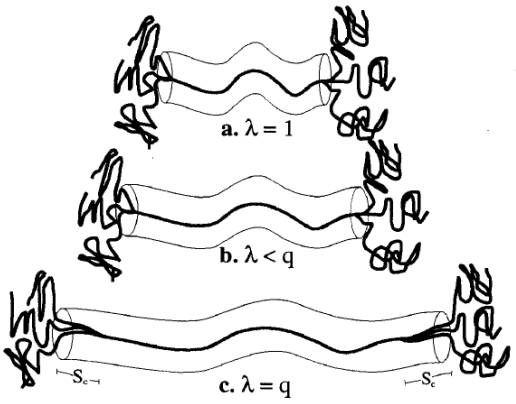

Figure 2.4.4 A pom-pom molecule with q = 3 under different stretch situations. (a) $\lambda = 1$, equilibrium state; (b) $\lambda < q$, chain stretching occurs until a maximum stretch is achieved at $\lambda = q$; (c) $\lambda = q$, branch-point withdrawal occurs [3].

Blackwell and coworkers [68] examine the exponential dependence the primitive path length of the arm segments has on arm relaxation times. They find that branch-point withdrawal less than the tube diameter affects the arm length enough to significantly influence the arm relaxation times. Reduction in the arm length outside of the tube generates reduced arm relaxation times, which entails faster stretch relaxation as well. Blackwell and coworkers also note that the withdrawn arm material is now oriented, but neglect the reduction in the backbone orientation relaxation time, τ_b. They justify the approximation because the convective term is the main contributor in the orientation integral when flow rates high enough to produce significant stretch are reached.

2.4.1.2 Extension to real molecules

The pom-pom model must be adjusted so that it is effective for real branched molecular structures. Real molecules consist of multiple branch points where it is likely

that branches occur off of other branches. The ideas of seniority and priority are used to describe a particular segments topological placement on the molecule and its effect on the total relaxation mechanism. Precise structures and true branching topology for many real molecules are still unable to be found accurately by experiment. Multi-mode approaches are taken to solving the pom-pom equation set where real molecules are treated as combinations of much simpler theoretical pom-pom molecules [69].

The ideas of seniority and priority describe the hierarchical nature for the relaxation process of real molecules. The seniority distribution measures the depth of any segment in a molecule and controls the linear rheological response of the material. The value for seniority is simply calculated by counting the minimum number of segments required to reach the exterior of the molecule. A branched molecule labeled with its seniority distribution is provided in Figure 2.4.5 (a). An embedded segment may not relax until all of the exterior segments with lower seniority values first relax. As seniority increases so too does the effective tube diameter. Due to the longer relaxation times for segments that are deeper within the molecule, exterior segments are assumed to no longer entangle and only add a frictional drag to relaxation [70].

The priority distribution describes the effective number of arms any segment experiences and defines the nonlinear rheological properties such as strain-hardening. The priority distribution is calculated by taking the minimum number of free arm segments that any backbone segment can see. A branched molecule labeled with its priority distribution is provided in Figure 2.4.5 (b). A greater priority value translates to higher degrees of stretch and extensional strain-hardening based on the fact that branch-point withdrawal occurs when the stretch is equal to the number of arms. The priority

reveals an upper limit on the amount of stretch that a molecule can endure before branch-point withdrawal occurs [70].

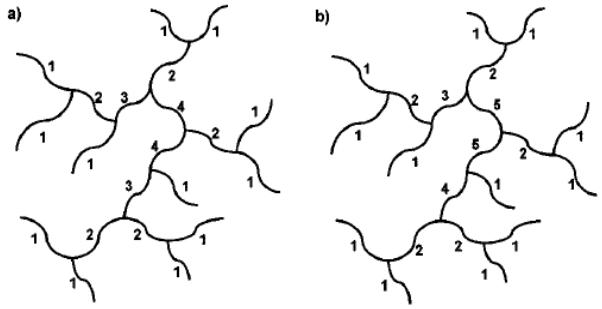

Figure 2.4.5 Branched polymers where labeled numbers indicate topological relevance to rheology. (a) Seniority: Smallest number of chain segments required to reach a free chain end; (b) Priority: Smallest number of free chain ends that are visible from an inner layer backbone segment [70].

A multi-mode pom-pom model is suggested by Inkson and coworkers [69] to apply the ideas of seniority and priority to the original model. The molecular structure for a randomly branched molecule is not always known and if it were calculations for the complete seniority and priority distributions would be undesirable because of computation time. In avoidance of these calculations multiple modes that represent differing seniority and priority segments are used in the pom-pom model calculations. High seniority values as well as high priority values are synonymous with high orientational relaxation times. The primary assumption is that different levels of branching in the molecule can be decoupled. This states that the interactions between segments of different priorities are ignored [69]. The multi-mode approach is widely used, and its mathematical formulation and results are included section 2.4.3.

2.4.2 Full integro-differential form

The full integro-differential form of the pom-pom model as developed by McLeish and Larson [3] is summarized and then reviewed for its abilities to both qualitatively and quantitatively describe the rheological behavior of branched polymers. An attempt is made to express the assumptions taken when modeling and to ensure that the model is mathematically stable.

The constitutive relationship does not directly relate stress to strain as other popular and simpler models do. Stress is determined by evaluating a dynamical system of evolution equations for the orientation $\underline{\underline{S}}(t)$, the stretch λ(t), and the branch-point withdrawal $s_c(t)$ [3]. To eliminate the need for distribution functions about orientation and stretch, McLeish and Larson assume the backbone includes a sufficient number of tube segments such that self-averaging occurs over these variables [3]. In materials with higher backbone molecular weights this assumption is closer to reality than in dilute situations [3].

The derivation for the dynamics of the orientation tensor $\underline{\underline{S}}(t)$, the stretch λ(t), and the branch-point withdrawal $s_c(t)$ can be found in McLeish and Larson's work [3], and will not be discussed here. Instead only a summary of the pom-pom equation set is provided.

Pom-pom equation set [3]

Expression for the stress:

$$\underline{\underline{\sigma}} = \frac{15}{4} G_0 \phi_b \left(\phi_b \lambda^2(t) + \frac{2qs_c(t)}{2qs_a + s_b} \right) \underline{\underline{S}}(t) \qquad \text{with } \phi_b = \frac{s_b}{2qs_a + s_b} \qquad (2.4.1)$$

Evolution of orientation:

$$\underline{\underline{S}}(t) = \int_{-\infty}^{t} \frac{dt'}{\tau_b(t')} \exp\left(- \int_{t'}^{t} \frac{dt''}{\tau_b(t'')} \right) \frac{1}{\left\langle \left| E(t,t') \cdot u \right| \right\rangle} \left\langle \frac{E(t,t') \cdot u E(t,t') \cdot u}{\left| E(t,t') \cdot u \right|} \right\rangle \qquad (2.4.2)$$

Evolution of backbone stretch:

$$\frac{\partial}{\partial t} \lambda = \lambda (K : S) - \frac{1}{\tau_s} (\lambda - 1) \qquad \text{strictly for } \lambda < q \qquad (2.4.3)$$

Evolution of arm-withdrawal measure s_c:

$$\frac{\partial s_c}{\partial t} = \left(q \frac{s_b}{2} + s_c \right) K : S - \frac{1}{2 \tau_a (x_c)} \qquad \text{strictly for } \lambda = q \qquad (2.4.4)$$

Timescales

Backbone orientation:

$$\tau_b = \frac{4}{\pi^2} s_b^2 \phi_b \tau_a (x_c(t)) q \qquad \text{with } x_c = \frac{s_c}{s_a} \qquad (2.4.5)$$

Arm spectrum:

$$\tau_a(x) = \tau_0 \exp\left[\frac{15}{4} s_a \left(\frac{(1-x)^2}{2} - (1 - \phi_b) \frac{(1-x)^3}{3} \right) \right] \qquad (2.4.6)$$

Backbone stretch:

$$\tau_s = s_b \tau_a (0) q \qquad (2.4.7)$$

Qualitatively the model accounts for both the shear-thinning and extension-hardening properties characteristic to branched polymers. For simplification, McLeish and Larson [3] neglect the role of branch-point withdrawal other than imposing the limit of $\lambda = q$ and approximate the strain tensor appearing in equation 2.4.1 with formulas Currie [71] has previously derived. The approximation by Currie is found by replacing equation 2.4.8

with equation 2.4.9 where equation 2.4.10 is a relationship between the invariants that can be substituted in equation 2.4.9.

$$\frac{15}{4\left\langle\left|\underline{\underline{E}}(t,t')\cdot\underline{u}\right|\right\rangle}\left\langle\frac{\underline{\underline{E}}(t,t')\cdot\underline{u}\,\underline{\underline{E}}(t,t')\cdot\underline{u}}{\left|\underline{\underline{E}}(t,t')\cdot\underline{u}\right|}\right\rangle \tag{2.4.8}$$

$$Q=\left(\frac{5}{J-1}\right)\underline{\underline{B}}-\left(\frac{5}{(J-1)\left(I_2+13/4\right)^{1/2}}\right)\underline{\underline{C}} \tag{2.4.9}$$

$$J=I_1+2\left(I_2+13/4\right)^{1/2} \tag{2.4.10}$$

Figure 2.4.6 demonstrates the models ability to qualitatively predict the phenomenon observed in both shear and extensional deformations. In the figure, the pom-pom model predictions are compared to its K-BKZ analog. To generate these curves structural parameters were selected and are as follows: q = 5, s_a = 3, and s = 30.

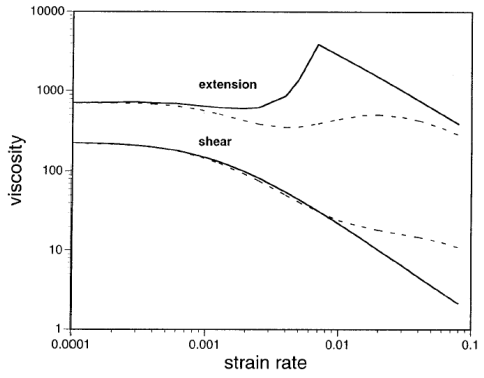

Figure 2.4.6 Steady state shear and extensional viscosities as functions of strain rate. The dashed line indicates the K-BKZ integral equation prediction, which follows the step-strain behavior of the pom-pom model exactly [3].

More evidence for the qualitative agreement of the pom-pom model is presented in Figure 2.4.7 (b) and (c) and Figure 2.4.8 as taken from McLeish and Larson [3]. In Figure 2.4.7 (b) and (c) shear, uniaxial extension, and planar extension predictions are produced using the integro-differential form of the pom-pom model and the curves are similar in shape to experimental data collected by Laun and Schuch [72]. In Figure 2.4.8 start-up transient shear and extensional viscosities are predicted at different shear and extension rates respectively and compared to data taken by Meissner [4] for a LDPE melt designated IUPAC A. The similarity in shapes of the predictions and the experimental observations confirms at least qualitatively the abilities of the pom-pom model for uniaxial and planar extension and shear growth curves at various extension and shear rates. Both sets of data represent LDPE materials and illustrate the advantages of the pom-pom model to predict both strain-hardening and shear-thinning properties characteristic to branched materials.

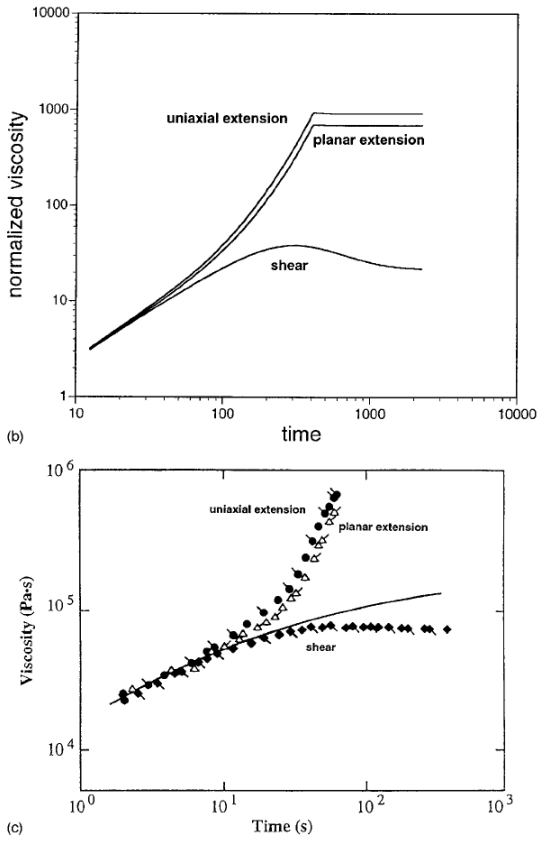

FIG. 5. (*Continued.*)

Figure 2.4.7 (b) Normalized transient shear, uniaxial extensional, and planar extensional viscosities as functions of time at a deformation rate of $\varepsilon = \gamma = 0.01\ s^{-1}$; (c) Transient shear, uniaxial extensional, and planar extensional data for a LDPE from Laun and Schuch [72] at a deformation rate of $\varepsilon = \gamma = 0.05\ s^{-1}$ [3].

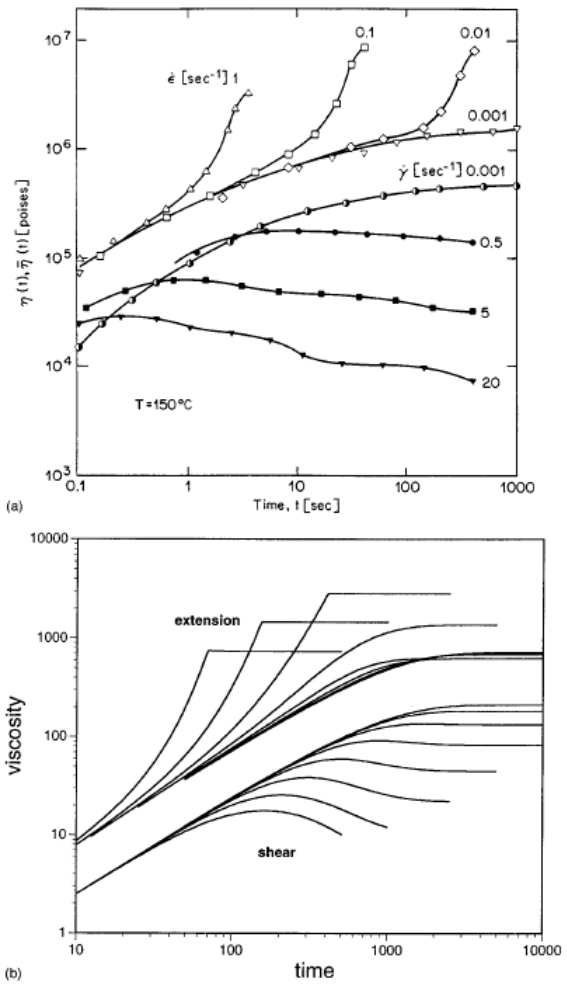

Figure 2.4.8 (a) Transient shear and uniaxial extensional viscosity data as functions of time for IUPAC A at 150°C provided by Meissner [4]; (b) Start-up behavior of the pom-pom model with q = 5, s_a = 3, and s_b = 30 in shear and uniaxial extension [3].

Insight into the effect that molecular structure has on the transient shear and extensional properties is provided by Figure 2.4.9. Maintaining all of the molecular weight parameters constant, McLeish and Larson [3] vary the number of arms, q, from 2 to 8 and evaluate the predicted response. For the shear response, at all times the viscosity decreases as the number of arms increases [3]. It is also noticed that at higher numbers of

branch arms the overshoot peak is shifted to longer times. For the transient response, there are two competing factors that yield different ordering at low versus high extension rates. At short times the diluting effect of the arms on the backbone dominates and viscosity decreases with increasing branch arms. At long times the converse is true because of the introduction of stretch making viscosity proportional to q^{2} [3]. It is also noticed that an increase in the number of branched arms leads to an increased strain-hardening effect.

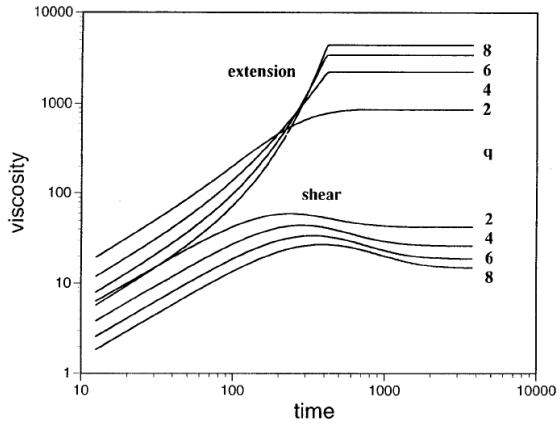

Figure 2.4.9 Transient shear and uniaxial extensional viscosities as functions of time with varying values for q [3].

Thermodynamic admissibility of the pom-pom model is considered by Ottinger [73] by reformulating the equations to fit a non-equilibrium thermodynamic framework GENERIC. GENERIC is also used by Meerveld [74] when looking at the thermodynamic consistency of the pom-pom model. The thermodynamics of the pom-pom model are questioned primarily because of independent arguments for the development of the dynamics for both the configurational variables and the stress tensor [73]. Thermodynamic

admissibility is established for the pom-pom model [73], but the nonequilibrium thermodynamics suggest modifications.

Mathematical stability of the pom-pom model is considered by Lee, Kim, and Kwon [75] in the sense of Hadamard and dissipative stability. Hadamard stability is the focus in viscoelastic constitutive equations, and it defines the stability of differential equations subjected to short and high frequency wave disturbances [75]. Hadamard unstable equations should not be applied to the analysis of viscoelastic flows and represent a non-physical formulation of viscoelastic phenomenon [75]. Two situations are evaluated: $\lambda < q$ and $\lambda = q$. When $\lambda < q$ maximum stretch is not yet achieved and in simple shear flow it is found that the equations are Hadamard stable. When $\lambda = q$ maximum stretch is achieved and the neglecting of branch point withdrawal leads to equations that are Hadamard unstable.

Modifications such as the inclusion of local branch-point withdrawal and the extension to multi-mode expressions for the pom-pom model are discussed in section 2.4.3. Because of the mathematical complexity of the complete integro-differential form of the pom-pom model, others tend to use more mathematically simple forms such as the differential form and an abundance of data is available using the differential equation set. Quantitative results for the integro-differential form of the pom-pom model are provided in section 2.4.3 where the results are compared to those generated by the differential form.

2.4.3 Differential form

The differential equation set for the pom-pom model is more widely used because of its exceedingly less complex computational efforts. McLeish and Larson have already proven that quantitatively the integro-differential model is acceptable contingent on the separation of relaxation times for the backbone and the stretch of the molecule through their neglecting of branch-point withdrawal and arm relaxation. Provided the flow is homogeneous the integration for the orientation tensor, $\underline{\underline{S}}(t)$, is possible, but for inhomogeneous flow conditions such as contraction flows the integral is no longer feasible. The challenge is arriving at a differential formula for the orientation tensor which retains all of the behaviors of the original integro-differential constitutive equations.

McLeish and Larson [3] have achieved a computationally more friendly differential approximate to describe $\underline{\underline{S}}(t)$ by working with another orientation tensor $\underline{\underline{A}}(t)$, which is the convection equation for elements within the flow [3]. This yields the correct asymptotics where the shear response decreases as a function of $\dot{\gamma}^{-1}$ [3]. The simplified differential equation set is provided below in equations 2.4.11 – 2.4.16.

Simplified pom-pom equation set [3]

Expression for the stress:

$$\underline{\underline{\sigma}} = \frac{15}{4} G_0 \phi_b^2 \lambda^2(t) \underline{\underline{S}}(t) \qquad \text{with } \phi_b = \frac{s_b}{2qs_a + s_b} \qquad (2.4.11)$$

Evolution of orientation:

$$\frac{\partial}{\partial t}\underline{\underline{A}}(t) = K \cdot A + A \cdot K^T - \frac{1}{\tau_b}\left(A - \frac{1}{3}I\right) \tag{2.4.12}$$

$$\underline{\underline{S}}(t) = \frac{\underline{\underline{A}}(t)}{trace\left[\underline{\underline{A}}(t)\right]} \tag{2.4.13}$$

Evolution of backbone stretch:

$$\frac{\partial}{\partial t}\lambda = \lambda(K:S) - \frac{1}{\tau_s}(\lambda - 1) \qquad \text{strictly for } \lambda < q \tag{2.4.14}$$

Timescales

Backbone orientation:

$$\tau_b = \frac{4}{\pi^2} s_b^2 \phi_b \tau_a(0) q \tag{2.4.15}$$

Backbone stretch:

$$\tau_s = s_b \tau_a(0) q \tag{2.4.16}$$

Numerous accounts of the differential pom-pom model exist [3, 68, 69, 76, 77], and here the progression is discussed beginning with McLeish and Larson [3] and their qualitative description of material properties through a few universally accepted modifications that enhance the models abilities and modeling predictions compared to real experimental results. Taking a multi-mode approach to represent the distribution of molecular topologies is introduced by Inkson and coworkers [69] and local branchpoint withdrawal is introduced by Blackwell and coworkers [68]. These ideas are discussed in detail along with their contributions to modeling capabilities.

Beginning with McLeish and Larson's [3] results, figure 2.4.10 presents the qualitative solution to the differential set of equations in both uniaxial extension and shear. They find the results in agreement to those found previously for the full integro-differential set of equations. The differential set of equations correctly predicts the extensional-hardening and shear-thinning properties that have escaped other constitutive equations and are characteristic of branched materials.

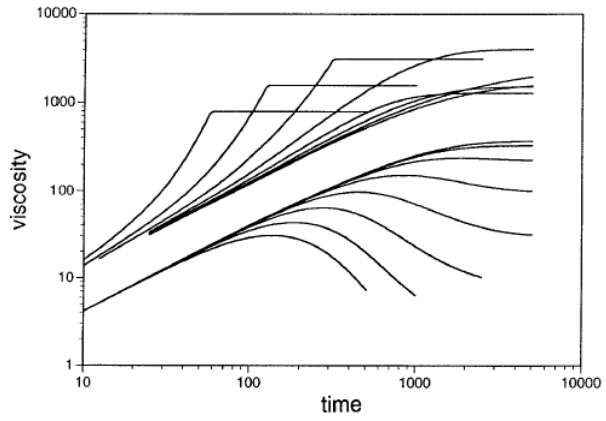

Figure 2.4.10 Transient shear and uniaxial extensional viscosities as functions of time computed using the differential approximation for orientation, $\underline{\underline{S}}(t)$ [3].

Rubio and Wagner [76] performed calculations comparing the predictions of the original Doi-Edwards strain measure in the independent alignment approximation with those of the differential approximation originally proposed by McLeish and Larson [3]. Model predictions for both forms of the pom-pom model in uniaxial extensional, first planar extensional, second planar extensional, and shear viscosities are expressed in Figure 2.4.11. The original Doi-Edwards approach is indicated by solid lines, whereas the differential approximation is indicated by symbols for various deformation rates.

Model fits for uniaxial extensional viscosity and the first planar extensional viscosity are representative of the actual behavior, but in this case the model fails to predict the second planar extensional viscosity and does a poor job predicting the steady-state values of shear viscosity. The model fitting becomes worse, severely under predicting the steady-state shear viscosity with increasing strain rates. Overall, it is observed that the differential approximation is a crude one for the original configuration tensor in the case of high Deborah numbers [76].

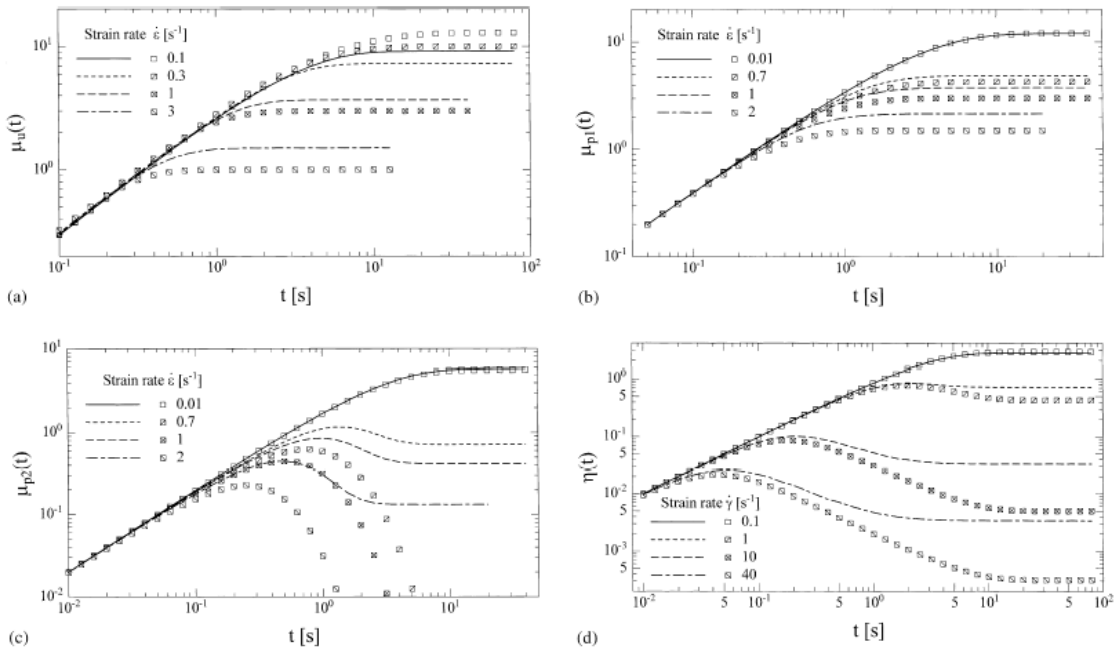

Fig 2.4.11 (a) Uniaxial viscosity μ_u, (b) planar viscosity μ_{p1}, (c) planar viscosity μ_{p2}, and (d) shear viscosity η at various strain rates as predicted by the Doi-Edwards model for a melt with a characteristic relaxation time τ_b of 3 s; lines indicate the use of the DE strain measure and symbols refer to the approximation $S_A(t)$, for the configuration tensor [76].

Inkson and coworkers [69] have developed a multi-mode approach to solving the pom-pom set of equations. Combinations of theoretical pom-pom molecules on different length scales are illustrated by the approach and this yields an advantage when modeling real molecules of unknown or complicated molecular structures. The stress tensor equation in multi-mode form is shown in equation 2.4.17 below.

$$\underline{\underline{\sigma}} = \sum_{i=1}^{n} \underline{\underline{\sigma}}_i = \sum_{i=1}^{n} g_i \lambda_i^2(t) \underline{\underline{S}}_i(t) \qquad (2.4.17)$$

Parameters g_i and τ_{bi} are determined from the linear viscoelastic regime by fitting storage and loss moduli data. Possible instabilities are encountered when selecting too large of a number of modes with a relatively small linear viscoelastic data set. A plot of $g_i\tau_{bi}^2/\Delta\tau_b$ against τ_b originally provided by Inkson and coworkers [69] is found in Figure 2.4.12 illustrates the lack of acceptable data fitting when the number of modes is to large. Selecting the proper number of modes is important and must be compatible with the linear viscoelastic data available. Here it is shown that the quantity $g_i\tau_{bi}^2/\Delta\tau_b$ can oscillate twofold when choosing two many modes.

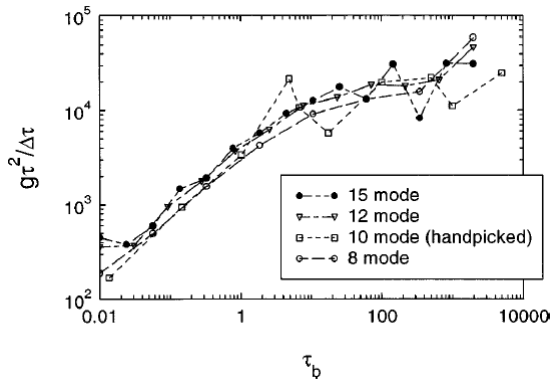

Figure 2.4.12 $g_i\tau_{bi}^2/\Delta\tau_b$ as a function of τ_b using varying numbers of modes for fitting the linear relaxation spectra [69].

In spite of the disagreements between the Doi-Edwards and differential strain measures, quantitative validification of the multi-mode approach is provided in figures 2.4.13 and 2.4.14 where the transient uniaxial extensional viscosity and transient shear viscosity in startup are plotted, respectively, as functions of deformation rate. Excellent predictions are achieved with the multi-mode model in both extensional and shear deformations. Model predictions have correctly captured material characteristics like extensional-hardening, shear-thinning, shear viscosity overshoot, and steady state viscosities in both extension and shear.

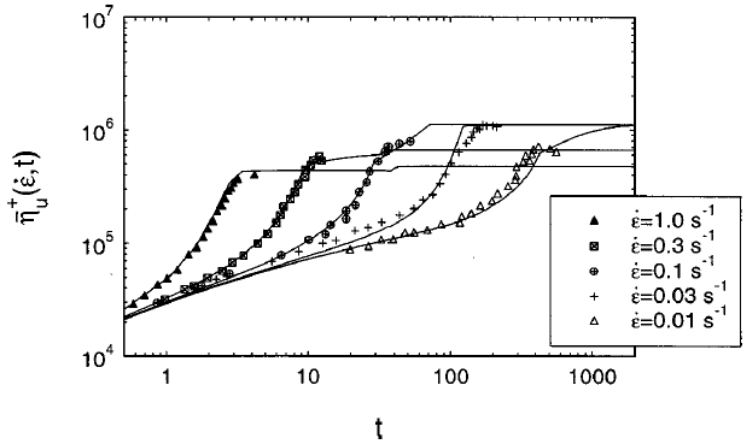

Figure 2.4.13 Transient uniaxial extensional viscosity of a 9 mode pom-pom melt in start-up plotted against data for IUPAC A LDPE. The extension rates range form 0.01 to 1.0 s^{-1} [69].

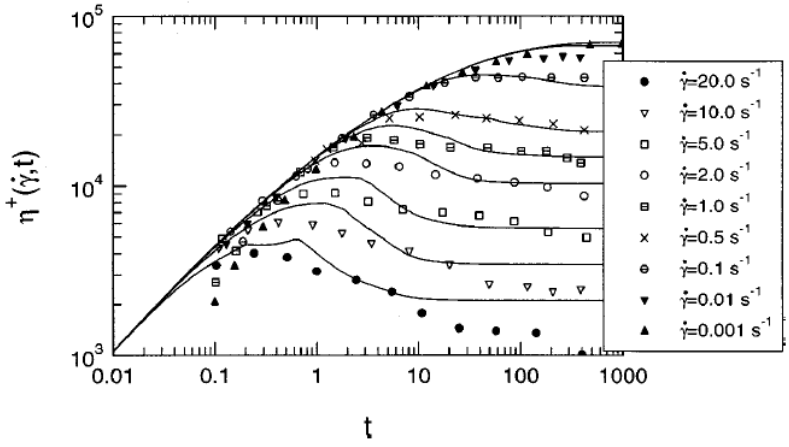

Figure 2.4.14 Transient shear viscosity of a 9 model multimodal pom-pom melt in start-up plotted against data for IUPAC A LDPE. The shear rates range from 0.001 to 20.0 s^{-1} [69].

The idea of branch-point withdrawal has been revisited by Blackwell and coworkers [68] on a local scale where branch-points are withdrawn prior to backbone segments reaching their maximum stretch. The incorporation of local branch-point withdrawal has resulted in the elimination of some physically unrealistic phenomenon like abrupt peaks in extensional viscosity curves. The stretch equation has been modified to represent the effect of local branch-point withdrawal as seen in equation 2.4.18 below.

$$\frac{D\lambda}{Dt}(t) = \lambda(t)K:S - \frac{1}{\tau_s}\left[\lambda(t) - 1\right]e^{\nu^*(\lambda(t)-1)} \qquad (2.4.18)$$

Dependence on the number of branch arms is included in the term ν^*, which is traditionally taken as $2/q_i$.

The advantage of including local branch-point withdrawal is shown in Figure 2.4.15, where transient uniaxial extensional viscosity data for IUPAC A LDPE is plotted along with model predictions with and without the inclusion of local branch-point withdrawal. Modeling without local branch-point withdrawal has led to an underprediction of experimental results at low extension rates and an overprediction of exeperimental results at high extension rates. Excellent fits to the experimental data are obtained when branch-point withdrawal is included correctly predicting the strain-hardening behavior, indicated by deviations from the LVE envelope, as well steady-state extensional viscosity values.

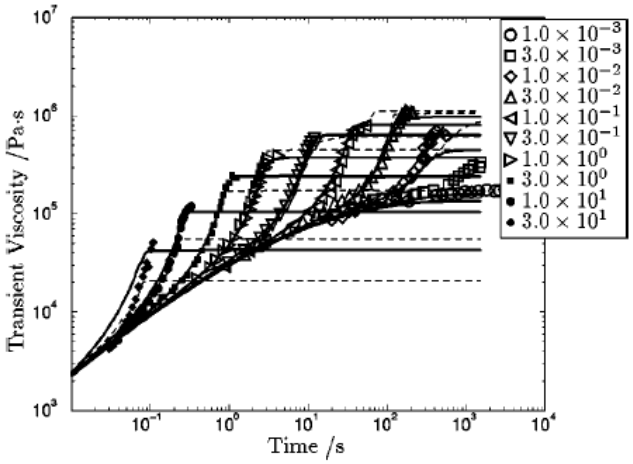

Figure 2.4.15 The best-fit transient viscosity of the IUPAC A LDPE in uniaxial extension startup flow calculated using the multimode pom-pom model with local drag-strain coupling ($\nu^* = 2.0/q_i$, solid) and without local drag-strain coupling (dashed). Strain rates are in reciprocal seconds and the data was taken at 150°C [68].

The smoothing effect on extensional viscosity curves and thus the elimination of an unphysical artifact of the model is represented in Figure 2.4.16. Both uniaxial extensional and shear viscosity are plotted as functions of strain rate, and again model predictions with and without the inclusion of branch-point withdrawal are presented. It is clear that in the case of uniaxial extension including local branch-point withdrawal predicts a smooth curve that follows very nicely the experimental results, whereas without local branch-point withdrawal a physical peaks occurs in the predictions.

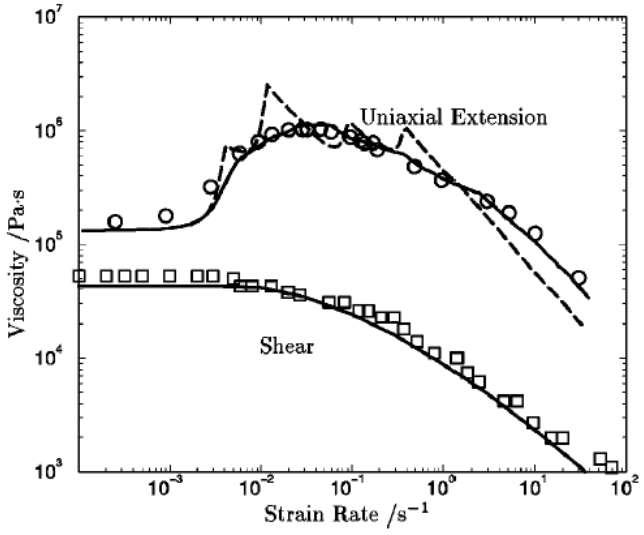

Figure 2.4.16. The steady state viscosity of the IUPAC A LDPE in uniaxial extension and shear calculated using he multimode pom-pom model with local drag-strain coupling ($\nu^* = 2.0/q_i$, solid) and without local drag-strain coupling (dashed) [68].

Blackwell and coworkers [78] utilized Cayley tree topology and have investigated a multi-mode pom-pom approach to predicting rheological behavior. Full Cayley tree calculations as well as the pom-pom model predictions for shear and extensional viscosity are shown in Figure 2.4.17. The data do not directly overlap and the conclusions made by the authors provide insight to possible problems in the pom-pom model that should be rectified within the theory. First, it is seen that the pom-pom model lacks a time-dependent priority and cannot accept the coupling between different levels that occurs because of maximum stretch [78]. Second, outer segments appear to contribute to the stress because of orientation that is generated by advection of the tube between levels [78]. Incorporation of these more complex molecular effects should lead to improvements in model predictions.

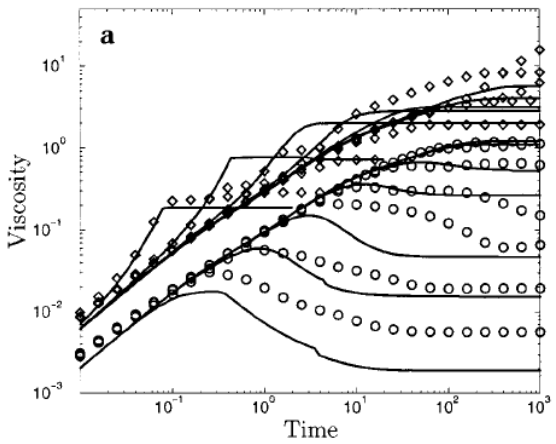

Figure 2.4.17 Multi-mode pom-pom fitting of Cayley tree topology where points indicate full Cayley tree calculations and lines indicate model fits. The general trends are captured but effects of coupling and tube advection are missing [78].

Doerpinghaus and Baird [30] have also shown the ability of the pom-pom model to effectively model shear and extensional viscosity growth curves for polyethylenes with various LCB concentrations including LDPE, a series of metallocene-catalyzed polytheylenes ranging in LCB concentration from linear to 0.79 LCB/10,000 C, and LLDPE. Fitting of the metallocene-catalyzed polyethylene materials illustrates the pom-pom model is capable of representing the behavior of sparsely long-chain branched materials having on average less than two branch points per chain. The model parameters suggest that multiple branches occur on the longest chain and that the frequency of branch points not the number of branch arms dominate the extensional strain-hardening response. Doerpinghaus and Baird [30] do find that the predicted number of branch arms is unrealistically large and does not agree with the dilute solution measurements, but the accuracy of the dilute solution measurements for these particular systems is in question.

A comparison of the original Doi-Edwards strain measure and the differential approximation is evaluated in the multi-mode scheme by Rubio and Wagner [76]. Predictions of uniaxial extension, shear, first planar, and second planar viscosities with the pom-pom model for the two forms of the configuration tensor are illustrated in Figure 2.4.18. In the case of the multi-mode approach experimentally observed stress overshoot is seen only in the differential approximation and is attributed to a strong artificial stretch relaxation [76]. Shear thinning behavior of the melt also disagrees with the original pom-pom model using the Doi-Edwards configuration tensor [76].

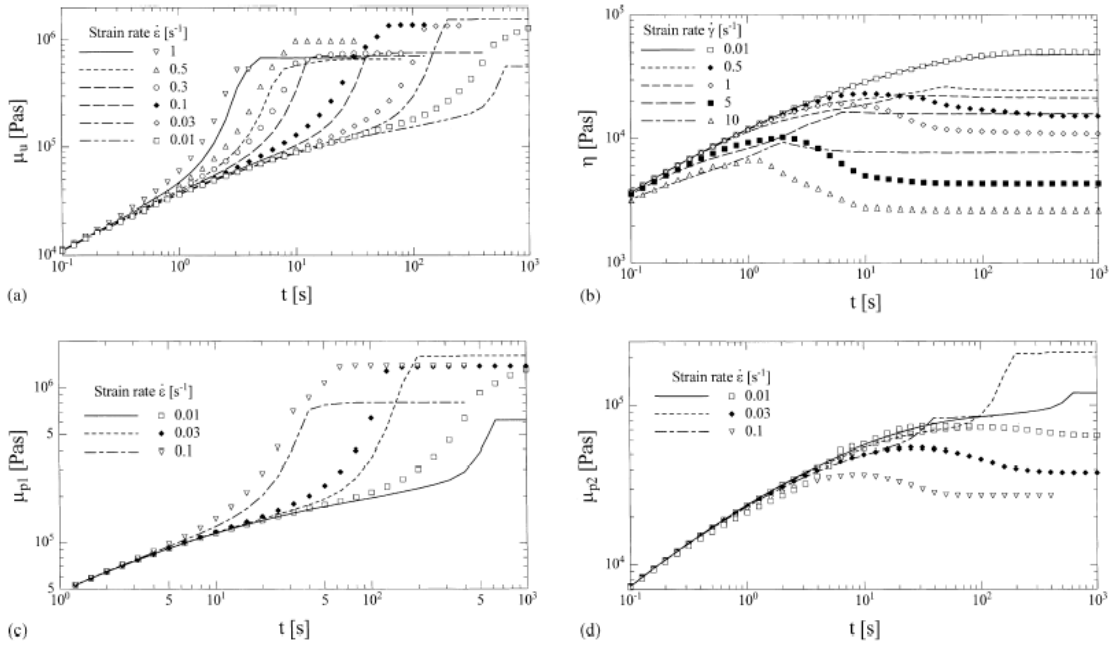

Figure 2.4.18 (a) Uniaxial viscosity μ_u, (b) shear viscosity η, (c) planar viscosity μ_{p1}, and (d) planar viscosity μ_{p2} using the multi-mode pom-pom model for LDPE IUPAC A. Lines indicate the use of the configuration tensor $S_{DE}(t)$ and symbols refer to the approximation $\underline{\underline{S}}_A(t)$ [76].

Consistency between the original integro-differential pom-pom equations with the Doi-Edwards value for Q and with the Currie approximation for Q along with both the differential pom-pom model and the integral MGI is investigated by Wapperom and Keunings [77]. Figure 2.4.19 illustrates a comparison of the different models. Under shear flow the correlation between the models is dependent on the rate of deformation. At low shear rates all of the models correspond well to one another, but as the rate is increased differences in model predictions are exposed. At all shear rates the Currie approximation of Q appears to be valid and corresponds well with the Doi-Edwards approach, but this is not the case when the transition is made to the differential model. The differential pom-pom model accurately predicts the height of the shear viscosity overshoot, but then the fit becomes relatively poor. The integral MGI model fails to predict any stress overshoot and slightly over predicts the steady state viscosity. Under extensional flow all of the pom-pom models tend to agree in their predictions regardless of the extension rate. The MGI model, an elongational-thinning model, fails to predict any strain-hardening and grossly under predicts the steady state elongational viscosity [77].

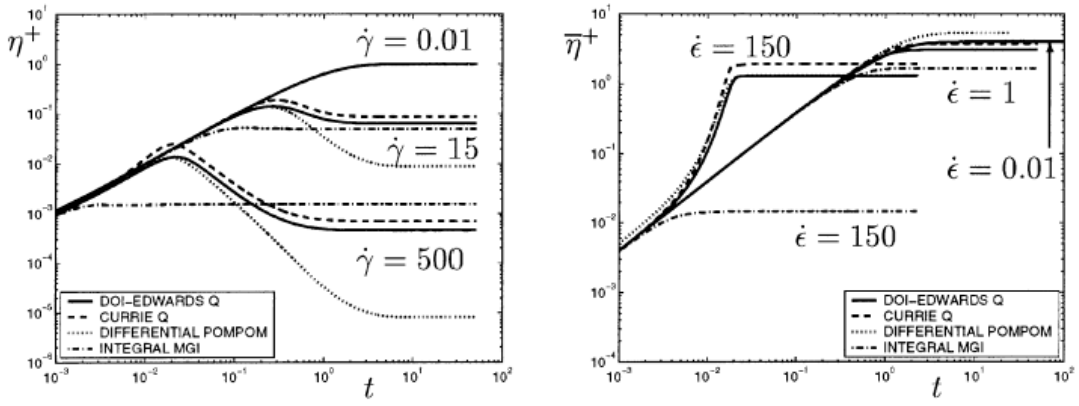

Figure 2.4.19 Transient shear viscosity, η^+, and planar elongational viscosity, η_p^+, for pom-pom and MGI models [77].

Analysis of the mathematical stability of the differential pom-pom constitutive equations is carried out by Lee, Kim, and Kwon [75]. The authors look at three different situations for Hadamard stability: $\lambda < q$, $\lambda = q$ with branch-point withdrawal neglected, and $\lambda = q$ with the inclusion of branch-point withdrawal. The differential pom-pom constitutive equations are Hadamard stable when $\lambda < q$ as long as there is a predefined smooth strain history [75]. Lee, Kim, and Kwon find that when $\lambda = q$ and branch-point withdrawal is neglected the equations are Hadamard unstable if the instantaneous shear strain exceeds $\sqrt{[3]}$ [75]. If branch-point withdrawal is included in the analysis the pom-pom constitutive equations are Hadamard stable regardless of the instantaneous shear strain [75].

Extensive work on modeling more complex flow situations with the pom-pom model has been completed by groups such as Bishko and coworkers [67], Wapperom and Keunings [77], and Chodankar and coworkers [79] among others. Flow through a 4:1 contraction has been evaluated by Bishko and coworkers [67] and along the same general

theme 4:1:4 flow has been examined by Wapperom and Keunings [77]. Double step-strain flow has been modeled using the pom-pom model by Chodankar and coworkers[79]. This work is not discussed here and the readers are referred to the authors' original works. This is by no means a full representation of the work being done with the pom-pom model on complex flows, just a mere sampling of the possibilities and the potential of the pom-pom model as a viable constitutive relationship.

2.4.4 Extended pom-pom model

Inconsistencies exist in the original formulation of the pom-pom model and attempts have been made to rectify some of the issues most notably by Verbeeten and coworkers [65]. They proposed the extended pom-pom model as well as presented other ideas that could lead to improvements from the non-equilibrium thermodynamic work of Ottinger [73]. The successive elimination of the original pom-pom model's inconsistencies, thus leading to the extended pom-pom model, is discussed and both qualitative and quantitative results are presented.

Three distinct problems appear within the original pom-pom model that affect its potential modeling capabilities. The orientation equation is of the form of the upper convected Maxwell model and is unbounded in extension at high elongation rates. This makes numerical analysis not plausible at higher extension rates. With the induction of finite extensibility, where the dynamics of stretch for the backbone segment are limited by $\lambda \leq q$, steady-state elongation suffers from discontinuities. The inclusion of local branch-point withdrawal as suggested by Blackwell and coworkers [68] helps to alleviate some of the discontinuities, but the issue still remains. In shear, the original formulation

of the pom-pom model fails to predict a second normal stress difference, ψ_2. Based on experimental results, the positive influence of ψ_2 on the stability of flow, and the related phenomena that occur in flow-induced crystallization Verbeeten and coworkers [65] argue the need to include ψ_2.

The extended model is still based on the theory that gives rise to the original formulation of the pom-pom model, primarily the separation of two relaxation mechanisms, one for orientation and another for stretch. To eliminate the issues at hand it is first concluded that the requirement that tube orientation for linear polymers strictly follows the Doi-Edwards [19] theory must be relaxed. Finite extensibility as defined by McLeish and Larson [3] produces a discreet maximum stretch where it is more physically reasonable for the maximum stretch to exist as a distribution. The transition from stretch dynamics to a fixed maximum stretch has been removed in the extended pom-pom model to eliminate the unphysical discontinuities seen in extensional fits. The stretch is instead bound indirectly by q through the exponential term $e^{-\nu(\lambda-1)}$ because as the strains increase the stretch relaxes exponentially. To generate ψ_2, a parameter α is incorporated that defines the present amount of anisotropy. This stems from modeling ψ_2 by an anisotropic relaxation and introducing constants of the Giesekus form that contain this α parameter that influences orientation only. When it comes to modeling with the extended pom-pom model, α is fit preferably using second normal stress coefficient data, but if this is unavailable can be fit using second planar viscosity data.

As has been derived by Verbeeten and coworkers [65] the double-equation extended pom-pom equation set, equations 2.4.19 – 2.4.21, and the single-equation extended pom-pom equation set, equations 2.4.22 – 2.4.27, are shown below. Both equation sets remain

in the form of Verbeeten and coworkers [65]. For the full derivation of these sets of equations consult the work of Verbeeten and coworkers [65].

Double-equation extended pom-pom equation set [65]

Viscoelastic stress:

$$\underline{\underline{\tau}} = G_0\left(3\Lambda^2 \underline{\underline{S}} - \underline{\underline{I}}\right) \tag{2.4.19}$$

Evolution of orientation:

$$\frac{\partial}{\partial t}\underline{\underline{S}} - \underline{\underline{D}}\cdot\underline{\underline{S}} - \underline{\underline{S}}\cdot\underline{\underline{D}}^T + 2[D{:}S]S + \frac{1}{\lambda_{0b}\Lambda^2}\left[3\alpha\Lambda^4 S\cdot S + \left(1-\alpha-3\alpha\Lambda^4 I_{S\cdot S}\right)S - \frac{(1-\alpha)}{3}I\right] = 0 \tag{2.4.20}$$

Evolution of the backbone stretch:

$$\Lambda = \Lambda[D{:}S] - \frac{1}{\lambda_{0s}}(\Lambda - 1)e^{-\nu(\Lambda-1)} \qquad \text{where } \nu = \frac{2}{q} \tag{2.4.21}$$

Single-equation extended pom-pom equation set [65]

Viscoelastic stress:

$$\frac{\partial}{\partial t}\underline{\underline{\tau}} - \underline{\underline{D}}\cdot\underline{\underline{\tau}} - \underline{\underline{\tau}}\cdot\underline{\underline{D}}^T + \lambda(\tau)^{-1}\underline{\underline{\tau}} = 2G_0 D \tag{2.4.22}$$

Relaxation time tensor:

$$\lambda(\tau)^{-1} = \frac{1}{\lambda_{0b}}\left\{\frac{\alpha}{G_0}\tau + f(\tau)^{-1} I + G_0\left[f(\tau)^{-1} - 1\right]\tau^{-1}\right\} \tag{2.4.23}$$

Extra function:

$$\frac{1}{\lambda_{0b}} f(\tau)^{-1} = \frac{2}{\lambda_s}\left(1 - \frac{1}{\Lambda}\right) + \frac{1}{\lambda_{0b}\Lambda^2}\left(1 - \frac{\alpha I_{\tau\tau}}{3G_0^2}\right) \tag{2.4.24}$$

Backbone stretch and stretch relaxation time:

$$\Lambda = \sqrt{1 + \frac{I_\tau}{3G_0}} \tag{2.4.25}$$

$$\lambda_s = \lambda_{0s} e^{-\nu(\Lambda - 1)} \tag{2.4.26}$$

$$\nu = \frac{2}{q} \tag{2.4.27}$$

Verbeeten and coworkers [65] first qualitatively test the extended pom-pom model for transient and steady state flows in simple shear, planar elongational, uniaxial elongational, and equibiaxial elongational. The parameters are maintained the same as those of McLeish and Larson [3] and Blackwell and coworkers [68]. Values for the new anisotropy parameter α are changed in order to establish the potential effect of the parameter. Figures 2.4.20 and 2.4.21 graphically summarize both the transient and steady state results for simple shear and planar elongational flows, respectively. It is noted that the transient and steady state viscosities in both uniaxial and equibiaxial elongation have similar behavior to that of planar elongation [65].

Figure 2.4.20 displays viscosity, η/η_0; second normal stress coefficient, $-\psi_2/\psi_1$; and backbone stretch, Λ as a function of time, t/λ_{0b}, and viscosity, η/η_0, and shear orientation, S_{12}, as a function of shear rate, $\gamma\lambda_{0b}$, all in dimensionless form. Three values of α are evaluated at three different shear rates. Simple shear flow is relatively unaffected by α with the exception of the second normal stress coefficient, ψ_2/ψ_1, where a higher anisotropy parameter predicts higher values for ψ_2/ψ_1. This is consistent with the formulation of the model in its ability to predict a second normal stress coefficient. When α is selected to be zero no second normal stress coefficient appears indicating an

improvement on the original pom-pom formulation without sacrificing an influence towards other material parameters in shear flow.

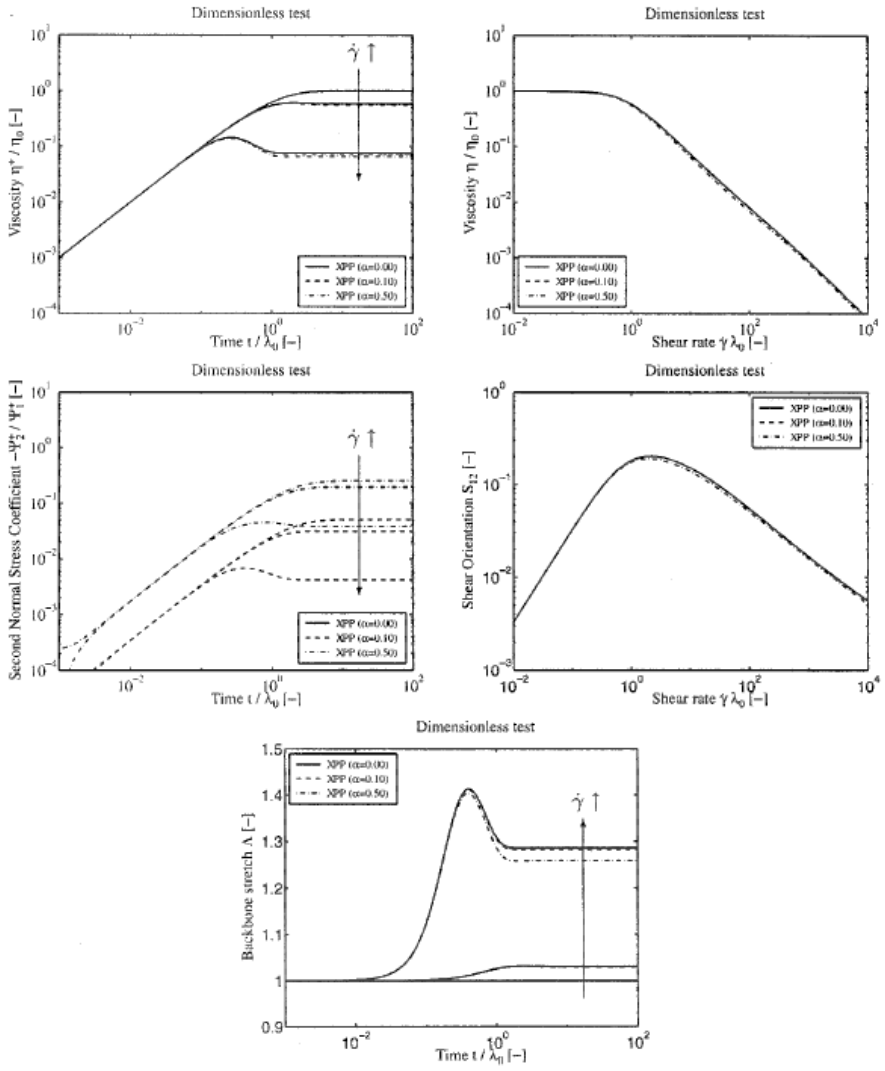

Figure 2.4.20 Dimensionless features in simple shear flow for the XPP model: transient viscosity (left top), steady state viscosity (right top), transient second over first normal stress coefficient ratio $-\psi_2/\psi_1$ (left middle), steady state shear orientation component S_{12} (right middle) and transient backbone stretch Λ (bottom). Parameters: $q = 5$; $\lambda_{0s} = (150/912)\lambda_{0b}$; $\alpha = 0, 0.1, 0.5$. Transient: $\gamma = 10^{-5}, 1, 10$ [65].

First planar viscosity, $\eta_{p1}/(4\eta_0)$; second planar viscosity, $\eta_{p2}/(2\eta_0)$; and backbone stretch, Λ, as a function of time, t/λ_{0b}, and first planar viscosity, $\eta_{p1}/(4\eta_0)$, as a function of strain rate, $\varepsilon\lambda_{0b}$, all in dimensionless form are shown in figure 2.4.21. First planar viscosity is defined in equation 2.4.28 and second planar viscosity is defined in equation 2.4.29.

$$\eta_{p1} = \frac{\tau_{11} - \tau_{33}}{\varepsilon} \tag{2.4.28}$$

$$\eta_{p2} = \frac{\tau_{22} - \tau_{33}}{\varepsilon} \tag{2.4.29}$$

Here it is observed that α has little to no effect on any of the material properties except for the second planar viscosity, $\eta_{p2}/(2\eta_0)$. An increase in α value leads to less overshoot and a higher steady state value for the viscosity. The deviations that result from increasing α are more apparent at higher strain rates and at significantly low strain rates α has no effect at all. The alleviation of the finite extensibility condition is evident in the smooth steady state planar viscosity functions.

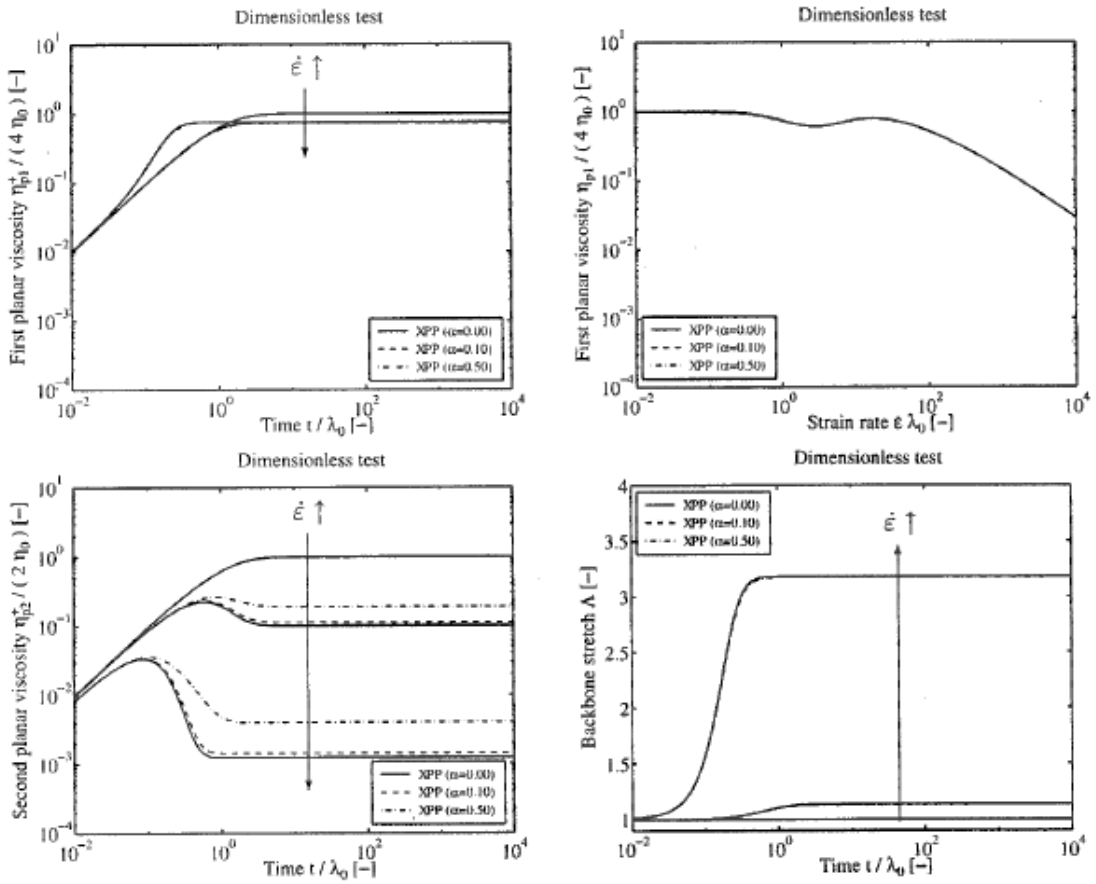

Figure 2.4.21 Dimensionless features in planar elongational flow for the XPP model: transient (left top) and steady state (right top) first planar viscosity η_{p1}, transient second planar viscosity η_{p2} (left bottom), and transient backbone stretch Λ (right bottom). Parameters: $q = 5$; $\lambda_{0s} = (150/912)\lambda_{0b}$; $\alpha = 0, 0.1, 0.5$. Transient: $\varepsilon = 10^{-5}, 1, 10$ [65].

Quantitative analysis is presented by Verbeeten and coworkers [65] for two LDPE melts and an HDPE melt to validify their models capabilities. The original development of the model is for long-chain branched materials, thus the testing on the two LDPE materials, but HDPE is examined to evaluate the extension to other molecular structures. Figures 2.4.22, 2.4.23, and 2.4.24 illustrate the transient and steady state results for the LDPE

melt Lupolen 1810H in uniaxial elongation, planar elongation, and simple shear. Figure 2.4.25 shows the transient and steady state results for the HDPE melt Statoil 870H in uniaxial elongation and simple shear.

Figure 2.4.22 presents uniaxial elongational viscosity as a function of time and Figure 2.4.23 shows the first and second planar elongational viscosities as functions of time. Generally good fits to viscosity data are obtained for elongational flows, both uniaxial and planar, with the exception of the second planar elongational viscosity. In both uniaxial elongational viscosity and first planar elongational viscosity strain-hardening characteristics are experimentally observed and correctly modeled. The model underpredicts the experimental results for the second planar elongational viscosity, but does establish the expected thinning behavior. Figure 2.4.24 depicts the shear viscosity and first normal stress coefficient as functions of time. Model predictions for shear viscosity are good as well captivating the overshoot seen at higher shear rates and the shear-thinning behavior, while the predictions for the first normal stress coefficient fail to predict the correct amount of overshoot. The other LDPE evaluated, IUPAC A, yielded similar results and is not included in any further description.

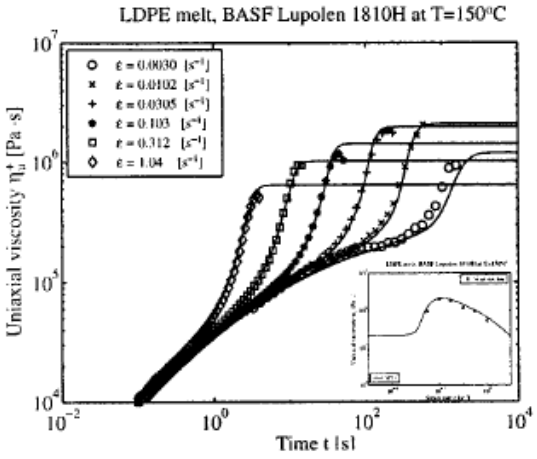

Figure 2.4.22 Transient and quasisteady state (inset) uniaxial elongational viscosity η_u of the XPP model for Lupolen 1810H melt at T = 150°C. $\nu_i = 2/q_i$, ε = 0.0030, 0.0102, 0.0305, 0.103, 0.312, 1.04 s^{-1} [65].

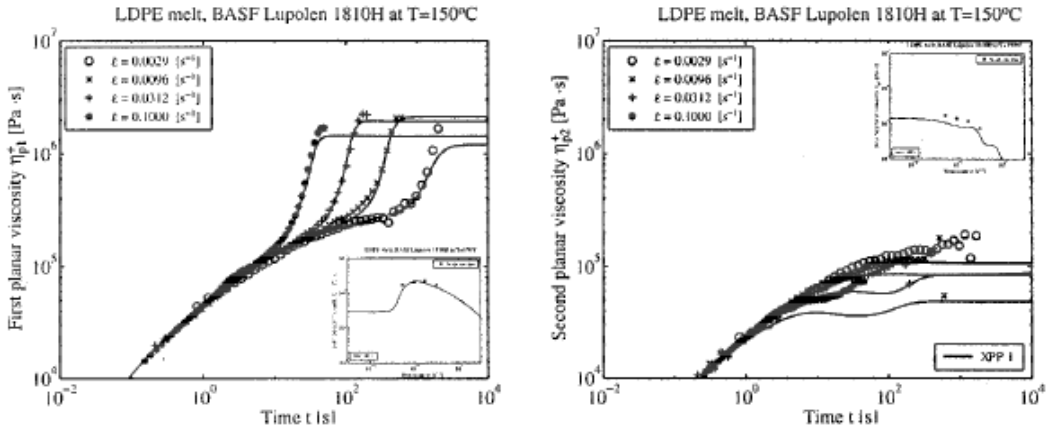

Figure 2.4.23 Transient and quasisteady state (inset) first planar elongational viscosity η_{p1} (left) and second planar elongational viscosity η_{p2} (right) of the XPP model for Lupolen 1810H melt at T = 150°C. $\nu_i = 2/q_i$, ε = 0.0029, 0.0096, 0.0312, 0.1000 s^{-1} [65].

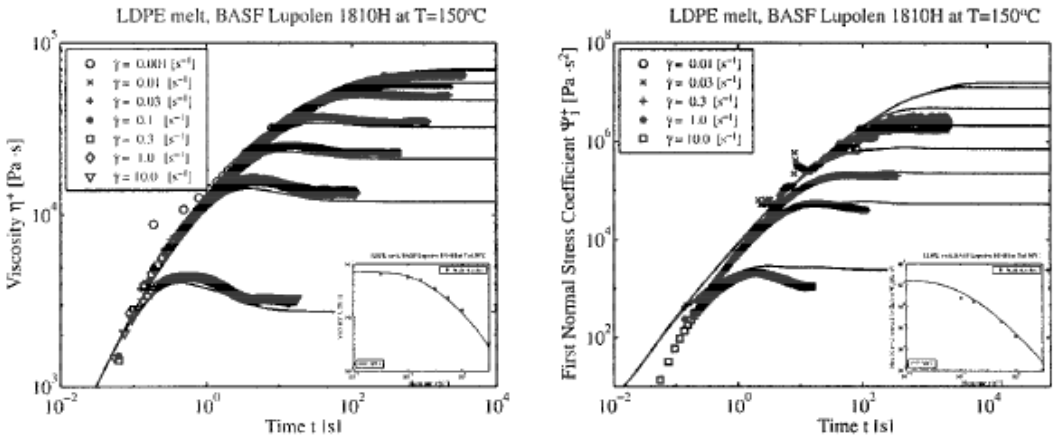

Figure 2.4.24 Transient and steady state (inset) shear viscosity η (left) and first normal stress coefficient ψ_1 (right) of the XPP model for Lupolen 1810H melt at T = 150°C. $\nu_i = 2/q_i$, γ = 0.001, 0.01, 0.03, 0.1, 0.3, 1, 10 s^{-1} [65].

Figure 2.4.25 illustrates the uniaxial elongational viscosity and simple shear viscosity as functions of time for the HDPE material Statoil 870H. The fits are not as convincing as those seen for the LDPE, but the model is developed for long-chain branched materials like LDPE. Still the predictions are relatively good; the model is slightly preemptive in establishing the hardening characteristics and slightly overpredicts the simple shear viscosity results.

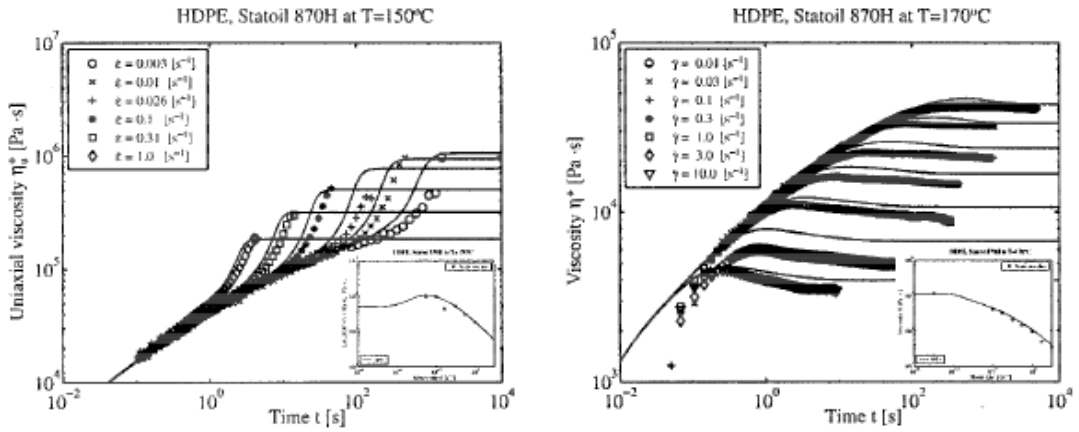

Figure 2.4.25 Transient (left) and quasisteady state (inset) uniaxial elongational viscosity η_u at T = 150°C, and transient (right) and steady state (inset) shear viscosity η_s at T = 170°C of the XPP model for Statoil 870H HDPE melt. $\nu_i = 2/q_i$, ε = 0.003, 0.010, 0.026, 0.10, 0.31, 1.0 s^{-1}, γ = 0.01, 0.03, 0.1, 0.3, 1.0, 3.0, 10.0 s^{-1} [65].

Further evaluation of the extended pom-pom model has been done by Zatloukal [80], where comparisons are made in uniaxial extension and shear viscosities to modified Leonov and modified White-Metzner models. Modification appears in the Leonov model by increasing the dependence of dissipation on the relaxation times [80]. In elongational flows the original White-Metzner model predicts infinite elongational viscosity. Zatloukal uses the modification of Barnes and Roberts [81] that eliminates this unrealistic nature of the original White-Metzner model and is thus dubbed the modified White-Metzner model. Experimental uniaxial and shear viscosity data and model fits for the extended pom-pom model, modified Leonov, and modified White-Metzner models are illustrated in Figures 2.4.26 and 2.4.27 for two different LDPE materials. The results are practically indistinguishable and for predicting uniaxial extensional and shear viscosities

yielding another potential candidate for describing the rheological behavior of these types of materials.

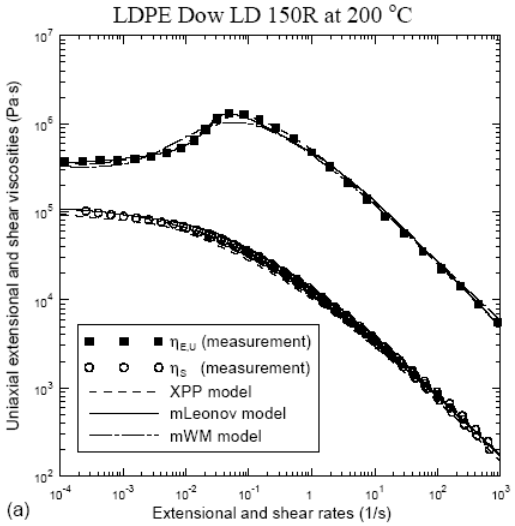

Figure 2.4.26 Experimental data and model predictions in steady shear and uniaxial extensional viscosities for LDPE Dow LD 150R melt at 200°C [80].

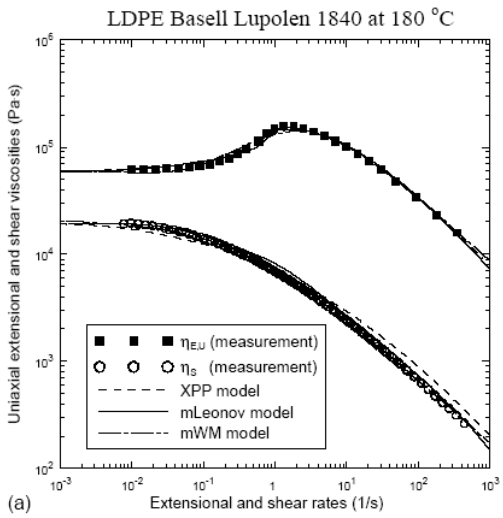

Figure 2.4.27 Experimental data and model predictions in steady shear and uniaxial extensional viscosities fro LDPE Basell Lupolen 1840 melt at 180°C [80].

Other formulations are suggested by Verbeeten and coworkers [65] that better follow the thermodynamic work of Ottinger [73]. Clemeur and coworkers [82] review some of the differential formulations for the pom-pom model including the extended pom-pom model and find mathematical stipulations. The model leads to analytical singularities and multiple solutions under certain conditions. It is suggested by Clemeur and coworkers [82] to further develop and evaluate some of the differential forms mentioned.

2.5 Determine the extensional capabilities of the SER extensional device

Characterization of extensional flow behavior is critical to fully describe most typical polymer processing operations. Extensional flows are strong flows and lead to higher degrees of molecular orientation. Extensional measurements provide a more responsive method to explore molecular characteristics such as crystallinity and long-chain branching that are indistinguishable by shear rheology alone. Experimentally, extensional measurements have been more difficult to obtain and subsections 2.5.1 and 2.5.2 reveal, respectively, the theory and design and experimental results to date for a newly developed extensional rheometer dubbed the SER that conveniently attaches to most conventional rotational rheometers in an effort to determine this new device's capabilities.

2.5.1 Theory and design for the device

Sentmanat [83] has developed an extensional rheometer derived from the previous work of Macosko and Lornston [84], Connelly and coworkers [85], Pearson and Connelly [86], and Padmanabhan and coworkers [87] where a fiber wind-up approach is taken in which a fixture is adapted to a conventional torsional rheometer. Devices of this nature have previously featured materials fixed at one end and stretched from the other free end; however, at moderate strains non-uniform deformations are encountered as a result of the non-slip boundary condition acting on the fixed end. To alleviate these circumstances Sentmanat [88] has proposed the use of dual counter-rotating wind-up drums where rotation is resisted by the stretching material.

A photograph and an illustration of the SER device is provided in figure 2.5.1 to assist visually in the size and operation of the proposed rheometer. Sentmanat's [83] extensional rheometer features a master and slave wind-up drum paired with intermeshing gears. A sample is fixed to each drum with a clamp and then extended through rotation of the master drum and an equal counter-rotation of the slave drum. The applied Hencky strain on the material obeys equation 2.5.1 and depends on the rotation rate, Ω, the radius of the drum, R, and the distance between drums, L_0.

$$\dot{\varepsilon}_H = \frac{2\Omega R}{L_0} \tag{2.5.1}$$

Important material properties are determined by evaluating the resistance of the material to stretch. The resistance is measured with the torque transducer available on conventional torsional rheometers and then used for further calculations and manipulations. Of greatest importance for polymer melts is the extensional viscosity growth explained in equation 2.5.2 for a constant Hencky strain rate,

$$\eta_E^+(t) = \frac{F(t)}{\dot{\varepsilon}_H A(t)} \tag{2.5.2}$$

where F(t) is the instantaneous extensional force, $\dot{\varepsilon}_H$ is the Hencky strain rate, and A(t) is the instantaneous cross-sectional area of the sample.

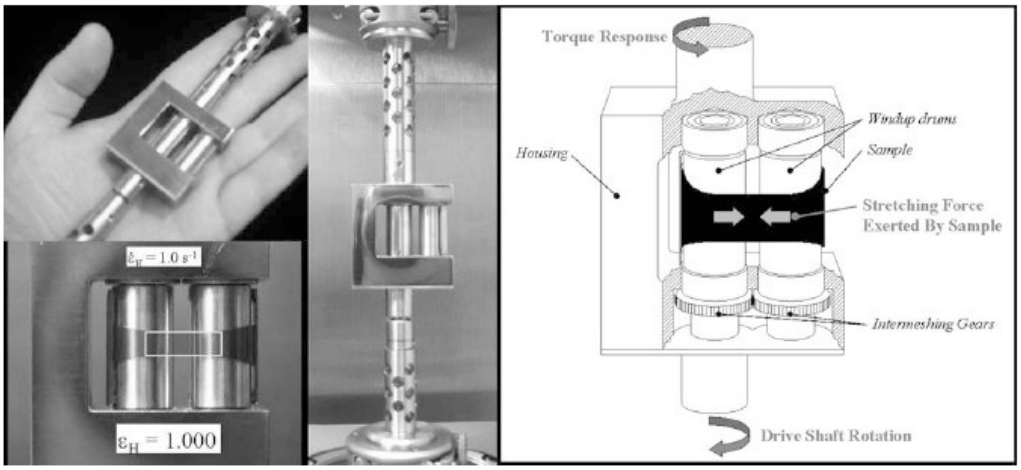

Figure 2.5.1 On the left are photographic images of the SER Universal Testing Platform adapted for an ARES torsional rheometer and on the right is a schematic illustration of the fixture during operation [89].

Sentmanat [83] has provided specifications for certain parameters that inherently point out equipment limitations. For the instrument itself the maximum and minimum torque requirements are 2500 g-cm and < 0.2 g-cm, respectively; the maximum recommended Hencky strain rate is 20 s^{-1}, but it is noted that higher rates may be achieved; the maximum Hencky strain per revolution of the wind-up drum is 4; the operating temperature range is between 0-290°C; the wind-up drum diameter is 1.031 cm; and the stretch zone gauge length is 1.272 cm. For the sample, recommended dimensions and sample mass are provided: width, 0.1-1.27 cm; thickness, 0.005-0.1 cm; mass, 5-200 mg. To prevent material sagging while performing extensional measurements on polymer melts it is recommended that the minimum zero-shear viscosity of the melt at the testing temperature is approximately 10,000 Pa-s.

2.5.2 Experimental results

Theoretically the SER appears to be a viable alternative to conventional extensional rheometers enabling a relatively easy to operate device that can be adapted to many torsional rheometer makes, but experimental validation is somewhat limited in the literature. Sentmanat and coworkers [83, 88-91] have provided validation of applied and actual strain through videography as shown in figure 2.5.2, validation of the Trouton rule, confirmed reproducibility of data, experimental comparisons of results to those obtained with different rheometer host systems as well as different rheometer designs, and mention further applications for which the SER is useful. The only other published indication of SER use is by Stamboulides and Hatzikiriakos [92] who use the SER to characterize poly (methyl methacrylate), PMMA, resins, which contributes to the diversity of materials that have been tested although the results have not been compared to data on previously proven equipment.

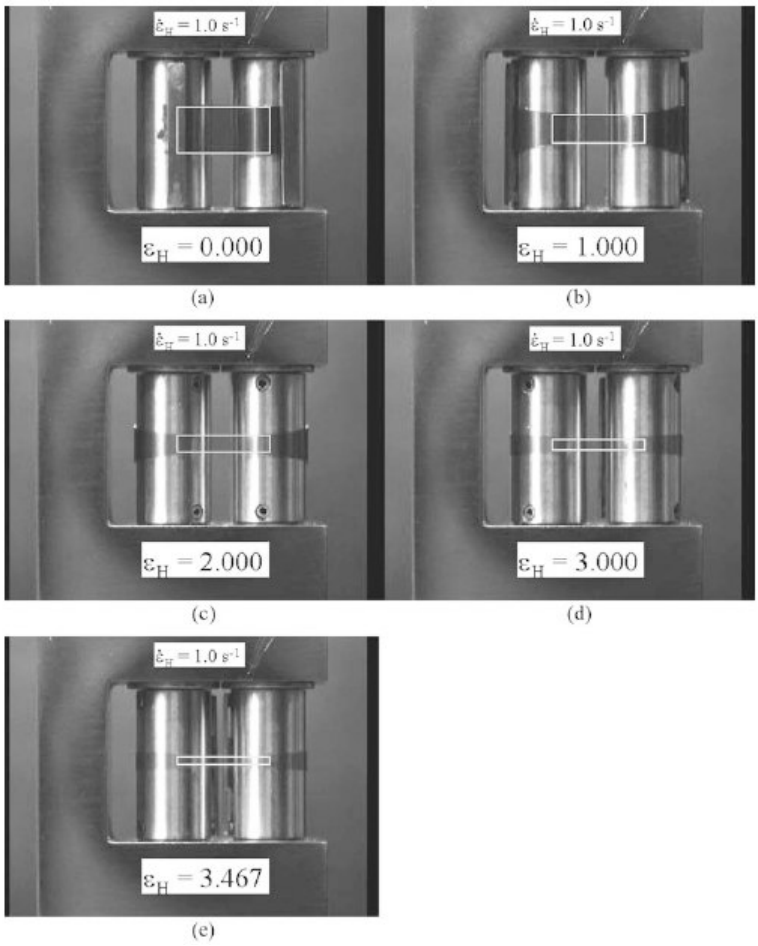

Figure 2.5.2 Stop-frame videographic sequence depicting the evolution of an extensional rheology specimen's width dimension at an applied Hencky strain rate of 1.0 s^{-1} superposed with the theoretical width dimension depicted as a box outline from the instant stretching begins until the moment immediately prior to sample rupture where ε_H is the Hencky strain [83].

Sentmanat and coworkers [83, 88-91] have tested polymer resins including linear low density polyethylene, LLDPE, metallocene linear low density polyethylene, m-LLDPE, both virgin and containing fillers, low density polyethylene, LDPE, both virgin and containing fillers, and polyisobutylene, PIB, and compared to experimental data obtained

with other extensional rheometer designs when applicable to ensure the validity of the SER. Two common materials that have been used as the standard to evaluate extensional measurements are IUPAC A and more recently Lupolen 1840 H both of which are LLDPE materials. Lupolen 1840 H is considered presently because the stability over time of IUPAC A has been questioned given that when originally produced no stabilizers were included. Figure 2.5.3 illustrates the extensional viscosity growth curves of Lupolen 1840 H for two different SER attachments and superposes the experimental data on the linear viscoelastic data. Through experimental testing and analysis Sentmanat and coworkers [90] were able to confirm reproducibility of data, consistency of data regardless of the host torsional rheometer, and concurrence with the linear viscoelastic envelope obtained by $3\eta^{+}(t)$ from cone and plate measurements. Comparison of the SER extensional measurements are made to Munstedt and coworkers [93] results for Lupolen 1840 H in figure 2.5.4 and show excellent agreement. Other extensional tests have been performed such as tensile step strain, stress growth, tensile creep, and stress relaxation for both a m-LLDPE, Affinity 1880, and a LDPE, Lupolen 1840 H, and the results agree with the previously published data [90]. Similar results are shown in the work with other polymeric materials, but only results on the PIB are compared to published data of Meissner [94] and Laun and Schuch [72] obtained using other extensional rheometry devices in which excellent agreement is seen in tensile growth curves. The SER can also be used in applications other than strictly uniaxial extensional rheology including solid tensile, tear, fracture, peel, and friction testing of which success has been seen for all of these testing mechanisms.

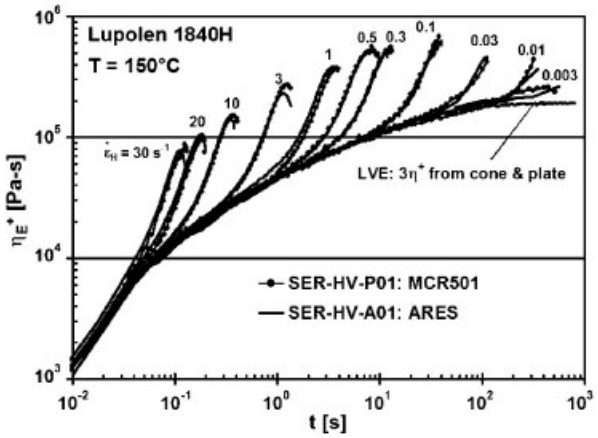

Figure 2.5.3 Tensile stress growth curves for Lupolen 1840H at a melt temperature of 150°C over a range of Hencky strain rates from 0.003 to 30 s^{-1} generated with the SER on two different host platforms, an MCR501 and an ARES, plotted against the LVE curve taken from $3\eta^+(t)$ in shear stress growth data obtained from cone and plate measurements in start-up of steady shear at a shear rate of 0.005 s^{-1} [90].

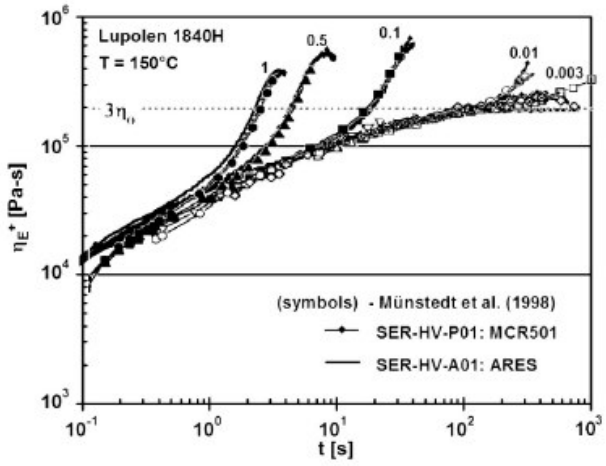

Figure 2.5.4 Comparison of tensile stress growth data at a melt temperature of 150°C over a range of Hencky strain rates from 0.003 to 1 s^{-1} generated with the SER on two different host platforms, designated by solid lines, with extensional data taken from Munstedt and coworkers [93], designated by symbols with lines [90].

The SER has been proven reliable for extensional rheological characterization of molten polymers by Sentmanat and coworkers [83, 88-91] for polyethylene and polyisobutylene materials. Stamboulides and Hatzikiriakos [92] use the SER in their characterization of PMMA and the tensile stress growth at various Hencky strain rates is shown in figure 2.5.5. Interestingly the linear PMMA material exhibits strain-hardening characteristics. The authors designate the behavior as slightly strain-hardening at high Hencky strain rates common to all resins, and of which the origin cannot be explained. No comparisons to extensional data obtained on previously established equipment is available and raises the question of validity of the experimental data and the diversity of the SER on a spectrum of molten polymers.

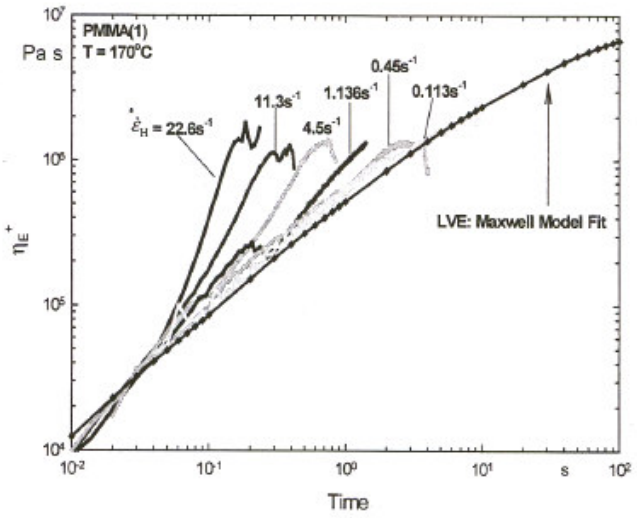

Figure 2.5.5 The tensile stress growth coefficient of PMMA at 170°C for various Hencky strain rates ranging from 0.113 s^{-1} to 22.6 s^{-1} [92].

2.6 References

1. Doerpinghaus, P. J. Flow Behavior of Sparsely Branched Metallocene-Catalyzed Polyethylenes. Virginia Tech, Blacksburg, 2002.

2. Kim, Y. S.; Chung, C. I.; Lai, S. Y.; Hyun, K. S., Melt Rheological and Thermodynamic Properties of Polyethylene Homopolymers and Polyethylene(ethylene/α-olefin) Copolymers with Respect to Molecular Composition and Structure. *Journal of Applied Polymer Science* **1996,** 59, 125-137.

3. McLeish, T. C. B.; Larson, R. G., Molecular constitutive equations for a class of branched polymers: The pom-pom polymer. *Journal of Rheology* **1998,** 42, (1), 81-110.

4. Meissner, J. M., Modification of the Weissenberg Rheogoniometer for measurements of transient rheological properties of molten polyethylene under shear, Comparison with tensile data. *Journal of Applied Polymer Science* **1972,** 16, 2877-2899.

5. McLeish, T. C. B., On the trail of topological fluids. *Physics World* **1995,** 8, 32-35.

6. Larson, R. G., *Constitutive Equations for Polymer Melts and Solutions*. Butterworths: Boston, 1988.

7. Ferri, D.; Lomellini, P., Melt rheology of randomly branched polystyrenes. *Journal of Rheology* **1999,** 43, (6), 1355-1372.

8. Lohse, D. J.; Milner, S. T.; Fetters, L. J.; Xenidou, M.; Hadjichristidis, N.; Mendelson, R. A.; Garcia-Franco, C. A.; Lyon, M. K., Well-Defined, Model Long Chain Branched Polyethylene. 2. Melt Rheological Behavior. *Macromolecules* **2002,** 35, 3066-3075.

9. Wood-Adams, P. M.; Dealy, J. M.; deGroot, A. W.; Redwine, O. D., Effect of Molecular Structure on the Linear Viscoelastic Behavior of Polyethylene. *Macromolecules* **2000,** 33, 7489-7499.

10. Jordan, E. A.; Donald, A. M.; Fetters, L. J.; Klein, J., *ACS Polymer Preprints* **1989**, (30).

11. Gell, C. B.; Graessley, W. W.; Efstratiadis, V.; Pitsikalis, M.; Hadjichristidis, N., Viscoelasticity and self-diffusion in melts of entangled asymmetric star polymers. *Journal of Polymer Science: Part B: Polymer Physics* **1997,** 35, (12), 1943-1954.

12. Zimm, B. H.; Kilb, R. W., Dynamics of branched polymer molecules in dilute solution. *Journal of Polymer Science* **1959,** 37, 19-42.

13. Barth, H. G.; Mays, J. W., *Modern Methods of Polymer Charaterization*. Wiley: New York, 1984.

14. Janzen, J.; Colby, R. H., Diagnosing long-chain branching in polyethylenes. *Journal of Molecular Structure* **1999,** 485-486, 569-584.

15. Piel, C.; Stadler, F. J.; Kaschta, J.; Rulhoff, S.; Munstedt, H.; Kaminsky, W., Structure-Property Relationship of Linear and Long-Chain Branched Metallocene High-Density Polyethylens Characterized by Shear Rheology and SEC-MALLS. *Macromolecular Chemistry and Physics* **2006,** 207, 26-38.

16. Doerpinghaus, P. J.; Baird, D. G., Separating the effects of sparse long-chain branching on rheology from those due to molecular weight in polyethylenes. *Journal of Rheology* **2003,** 47, (3), 717-736.

17. Bird, R. B.; Armstrong, R. C.; Hassager, O., *Dynamics of Polymer Liquids: Fluid Mechanics*. 2 ed.; Wiley Interscience: New York, 1987; Vol. 1.

18. Baird, D. G.; Collias, D. I., *Polymer Processing Principles and Design*. Wiley Interscience: New York, 1998.

19. Doi, M.; Edwards, S. F., *The Theory of Polymer Dynamics*. Oxford University Press: 1988.

20. McLeish, T. C. B., LONG CHAIN BRANCHING: Theory and Experiments on Model Materials. *Trans IChemE* **2000,** 78, (Part A), 12-32.

21. Roovers, J., The melt properties of ring polystyrenes. *Macromolecules* **1985,** 17, 1196-1200.

22. Bin Wadud, S. E.; Baird, D. G., Shear and extensional rheology of sparsely branched metallocene-catalyzed polyethylenes. *Journal of Rheology* **2000,** 44, (5), 1151-1167.

23. Gabriel, C.; Kokko, E.; Lofgren, B.; Seppala, J.; Munstedt, H., Analytical and rheological characterization of long-chain branched metallocene-catalyzed ethylene homopolymers. *Polymer* **2002,** 43, 6383-6390.

24. Romanini, D.; Savadori, A.; Gianotti, G., Long chain branching in low density polyethylene: 2. Rheological behaviour of the polymers. *Polymer* **1980,** 21, 1092-1101.

25. Patil, R.; Colby, R. H.; Read, D. J.; Chen, G.; Guan, Z., Rheology of Polyethylenes with Novel Branching Topology Synthesized by a Chain-Walking Catalyst. *Macromolecules* **2005,** 38, 10571-10579.

26. Bersted, B. H.; Slee, J. D.; Richter, C. A., Prediction of rheological behavior of branched polyethylene from molecular structure. *Journal of Applied Polymer Science* **1981,** 26, 1001-1014.

27. Robertson, C. G.; Garcia-Franco, C. A.; Srinivas, S., Extent of Branching from Linear Viscoelasticity of Long-Chain-Branched Polymers. *Journal of Polymer Science: Part B: Polymer Physics* **2004,** 42, 1671-1684.

28. La Mantia, F. P.; Scaffaro, R.; Carianni, G.; Mariani, P., Rheological Properties of Different Film Blowing Polyethylene Samples Under Shear and Elongational Flow. *Macromolecular Materials and Engineering* **2005,** 290, 159-164.

29. Jabbarzadeh, A.; Atkinson, J. D.; Tanner, R. I., Effect of Molecular Shape on Rheological Properties in Molecular Dynamics Simulation of Star, H, Comb, and Linear Polymer Melts. *Macromolecules* **2003,** 36, 5020-5031.

30. Doerpinghaus, P. J.; Baird, D. G., Assessing the Branching Architecture of Sparsely Branched Metallocene-Catalyzed Polyethylenes Using the Pompom Constitutive Model. *Macromolecules* **2002,** 35, (27), 10087-10095.

31. Barroso, V. C.; Maia, J. M., Influence of Long-Chain Branching on the Rheological Behavior of Polyethylene in Shear and Extensional Flow. *Polymer Engineering and Science* **2005,** 45, (7), 984-997.

32. Bourrigaud, S.; Marin, G.; Poitou, A., Shear Modification of Long-Chain Branched Polymers: A Theoretical Approach Using the Pom-Pom Model. *Macromolecules* **2003,** 36, (4), 1388-1394.

33. Malmberg, A.; Gabriel, C.; Steffl, T.; Munstedt, H.; Lofgren, B., Long-Chain Branching in Metallocene-Catalyzed Polyethylenes Investigated by Low Oscillatory Shear and Uniaxial Extensional Rheometry. *Macromolecules* **2002,** 35, 1038-1048.

34. Kasehagen, L. J.; Macosko, C. W., Nonlinear shear and extensional rheology of long-chain randomly branched polybutadiene. *Journal of Rheology* **1998,** 42, (6), 1303-1327.

35. Gotsis, A. D.; Zeevenhoven, B. L. F.; Tsenoglou, C., Effect of long branches on the rheology of polypropylene. *Journal of Rheology* **2004,** 48, (4), 895-914.

36. Hepperle, J.; Munstedt, H., Rheological properties of branched polystyrenes: nonlinear shear and extensional behavior. *Rheologica Acta* **2006,** 45, 717-727.

37. Satoh, N.; Tomiyama, H.; Kajiwara, T., Viscoelastic Simulation of Film Casting Process for a Polymer Melt. *Polymer Engineering and Science* **2001,** 41, (9), 1564-1579.

38. Kim, J. M.; Lee, J. S.; Shin, D. M.; Jung, H. W.; Hyun, J. C., Transient solutions of the dynamics of film casting process using 2-D viscoelastic model. *Journal of Non-Newtonian Fluid Mechanics* **2005,** 132, 53-60.

39. Sakaki, K.; Katsumoto, R.; Kajiwara, T.; Funatsu, K., Three-Dimensional Flow Simulation of a Film-Casting Process. *Polymer Engineering and Science* **1996,** 36, (13), 1821-1831.

40. Zheng, H.; Yu, W.; Zhou, C.; Zhang, H., Three-Dimensional Simulation of the Non-Isothermal Cast Film Process of Polymer Melts. *Journal of Polymer Research* **2006,** 13, 433-440.

41. Canning, K.; Co, A., Edge Effects in Film Casting of Molten Polymers. *Journal of Plastic Film & Sheeting* **2000,** 16, 188-203.

42. Canning, K.; Bian, B.; Co, A., Film Casting of a Low Density Polyethylene Melt. *Journal of Reinforced Plastics and Composites* **2001,** 20, (5), 366-376.

43. Dobroth, T.; Erwin, L., Causes of edge beads in cast films. *Polymer Engineering and Science* **1986,** 26, (7), 462-467.

44. Lee, J. S.; Jung, H. W.; Song, H.-S.; Lee, K.-Y.; Hyun, J. C., Kinematic waves and draw resonance in film casting process. *Journal of Non-Newtonian Fluid Mechanics* **2001,** 101, 43-54.

45. Silagy, D.; Demay, Y.; Agassant, J. F., Study of the Stability of the Film Casting Process. *Polymer Engineering and Science* **1996,** 36, (21), 2614-2625.

46. Silagy, D.; Demay, Y.; Agassant, J. F., Stationary and stability analysis of the film casting process. *Journal of Non-Newtonian Fluid Mechanics* **1998,** 79, 563-583.

47. Kajiwara, T.; Yamamura, M.; Asahina, T., Relationship between Neck-in Phenomena and Rheological Properties in Film Casting. *Nihon Reoroji Gakkaishi* **2006,** 34, (2), 97-103.

48. Smith, S.; Stolle, D., Numerical Simulation of Film Casting Using an Updated Lagrangian Finite Element Algorithm. *Polymer Engineering and Science* **2003,** 43, (5), 1105-1122.

49. Ito, H.; Doi, M.; Isaki, T.; Takeo, M., A Model of Neck-in Phenomenon in Film Casting Process. *Journal of the Society of Rheology, Japan* **2003,** 31, (3), 157-163.

50. Iyengar, V. R.; Co, A., Film Casting of a Modified Giesekus Fluid: Stability Analysis. *Chemical Engineering Science* **1996,** 51, (9), 1417-1430.

51. Pis-Lopez, M. E.; Co, A., Multilayer film casting of modified Giesekus fluids Part 1. Steady-state analysis. *Journal of Non-Newtonian Fluid Mechanics* **1996,** 66, 71-93.

52. Pis-Lopez, M. E.; Co, A., Multilayer film casting of modified Giesekus fluids Part 2. Linear stability analysis. *Journal of Non-Newtonian Fluid Mechanics* **1996,** 66, 95-114.

53. Pearson, J. R. A., *Mechanical Principles of Polymer Processing*. Elsevier Applied Science: London, 1985.

54. Yeow, Y. L., On the stability of extending films: a model for the film casting process. *Journal of Fluid Mechanics* **1974,** 66, 613-622.

55. Barq, P.; Haudin, J. M.; Agassant, J. F.; Bourgin, P., Stationary and Dynamic Analysis of Film Casting Process: A Viscoelastic Approach. *International Polymer Processing* **1994,** 9, (4), 350-358.

56. Lee, J. S.; Jung, H. W.; Hyun, J. C., Stabilization of film casting by an encapsulation extrusion method. *Journal of Non-Newtonian Fluid Mechanics* **2004,** 117, 109-115.

57. d'Halewyu, S.; Agassant, J. F.; Demay, Y., Numerical simulation of the cast film process. *Polymer Engineering and Science* **1990,** 30, (6), 335-340.

58. Smith, S.; Stolle, D., Nonisothermal Two-Dimensional Film Casting of a Viscous Polymer. *Polymer Engineering and Science* **2000,** 40, (8), 1870-1877.

59. Sollogoub, C.; Demay, Y.; Agassant, J. F., Non-isothermal viscoelastic numerical model of the cast-film process. *Journal of Non-Newtonian Fluid Mechanics* **2006,** 138, 76-86.

60. Lamberti, G.; Titomanlio, G.; Brucato, V., Measurement and modelling of the film casting process 1. Width distribution along draw direction. *Chemical Engineering Science* **2001,** 56, 5749-5761.

61. Lamberti, G.; Titomanlio, G.; Brucato, V., Measurement and modelling of film casting process 2. Temperature distribution along draw direction. *Chemical Engineering Science* **2002,** 57, 1993-1996.

62. Lamberti, G.; Titomanlio, G., Analysis of film casting process: The heat transfer phenomena. *Chemical Engineering and Processing* **2005,** 44, 1117-1122.

63. Lamberti, G.; Brucato, V.; Titomanlio, G., Orientation and Crystallinity in Film Casting of Polypropylene. *Journal of Applied Polymer Science* **2002,** 84, 1981-1992.

64. Titomanlio, G.; Lamberti, G., Modeling flow induced crystallization in film casting of polypropylene. *Rheologica Acta* **2004,** 43, 146-158.

65. Verbeeten, W. M. H.; Peters, G. W. M.; Baaijens, F. P. T., Differential constitutive equations for polymer melts: The extended Pom-Pom model. *Journal of Rheology* **2001,** 45, (4), 823-843.

66. McLeish, T. C. B., Molecular Rheology of H-Polymers. *Macromolecules* **1988,** 21, 1062-1070.

67. Bishko, G. B.; Harlen, O. G.; McLeish, T. C. B.; Nicholson, T. M., Numerical simulation of the transient flow of branched polymer melts through a planar contraction using the 'pom-pom' model. *Journal of Non-Newtonian Fluid Mechanics* **1999,** 82, 255-273.

68. Blackwell, R. J.; McLeish, T. C. B.; Harlen, O. G., Molecular drag-strain coupling in branched polymer melts. *Journal of Rheology* **2000,** 44, (1), 121-136.

69. Inkson, N. J.; McLeish, T. C. B.; Harlen, O. G.; Groves, D. J., Predicting low density polyethylene melt rheology in elongational and shear flows with "pom-pom" constitutive equations. *Journal of Rheology* **1999,** 43, (4), 873-896.

70. Read, D. J.; McLeish, T. C. B., Molecular Rheology and Statistics of Long Chain Branched Metallocene-Catalyzed Polyolefins. *Macromolecules* **2001,** 34, (6), 1928-1945.

71. Currie, P. K. In *Calculations on the Doe-Edwards Model for Concentrated Polymer Systems in Rheology*, Ninth International Congress on Rheology, Acapulco, Mexico, 1984; Acapulco, Mexico, 1984.

72. Laun, H. M.; H., S., Transient elongational viscosities and drawability of polymer melts. *Journal of Rheology* **1989,** 33, 119-175.

73. Ottinger, H. C., Thermodynamic admissibility of the pompom model for branched polymers. *Rheologica Acta* **2001,** 40, 317-321.

74. Meerveld, J. v., Note on the thermodynamic consistency of the integral pom-pom model. *Journal of Non-Newtonian Fluid Mechanics* **2002,** 108, 291-299.

75. Lee, J. W.; Kim, D.; Kwon, Y., Mathematical characteristics of the pom-pom model. *Rheologica Acta* **2002,** 41, 223-231.

76. Rubio, P.; Wagner, M. H., LDPE melt rheology and the pom-pom model. *Journal of Non-Newtonian Fluid Mechanics* **2000,** 92, 245-259.

77. Wapperom, P.; Keunings, R., Numerical simulation of branched polymer melts in transient complex flow using pom-pom models. *Journal of Non-Newtonian Fluid Mechanics* **2001,** 97, 267-281.

78. Blackwell, R. J.; Harlen, O. G.; McLeish, T. C. B., Theoretical Linear and Nonlinear Rheology of Symmetric Tree-like Polymer Melts. *Macromolecules* **2001,** 34, (8), 2579-2596.

79. Chodankar, C. D.; Schieber, J. D.; Venerus, D. C., Pom-Pom theory evaluation in double-step strain flows. *Journal of Rheology* **2003,** 47, (2), 413-427.

80. Zatloukal, M., Differential viscoelastic constitutive equations for polymer melts in steady shear and elongational flows. *Journal of Non-Newtonian Fluid Mechanics* **2003,** 113, 209-227.

81. Barnes, H. A.; Roberts, G. P., A simple empirical model describing the steady-state shear and extensional viscosities of polymer melts. *Journal of Non-Newtonian Fluid Mechanics* **1992,** 44, 113-126.

82. Clemeur, N.; Rutgers, R. P. B.; Debbaut, B., On the evaluation of some differential formulations for the pom-pom constitutive model. *Rheologica Acta* **2003,** 42, 217-231.

83. Sentmanat, M. L., Miniature universal testing platform: from extensional melt rheology to solid-state deformation behavior. *Rheologica Acta* **2004,** 43, 657-669.

84. Macosko, C.; Lorntson, J., The rheology of two blow-molding polyethylenes. *Annual Technical Conference - Society of Plastics Engineering* **1973,** 19, 461-467.

85. Connelly, R. W.; Garfield, L. J.; Pearson, G. H., Local stretch history of a fixed-end-constant-length-polymer-melt stretching experiment. *Journal of Rheology* **1979,** 23, 651-662.

86. Pearson, G. H.; Connelly, R. W., The use of extensional rheometry to establish operating parameters for stretching processes. *Journal of Applied Polymer Science* **1982,** 27, 969-981.

87. Padmanabhan, M.; Kasehagen, L. J.; Macosko, C., Transient extensional viscosity from a rotational shear rheometer using fiber-windup technique. *Journal of Rheology* **1996,** 40, 473-481.

88. Sentmanat, M. L. Dual Windup Extensional Rheometer. 2000.

89. Sentmanat, M.; Hatzikiriakos, S. G., Mechanism of gross melt fracture elimination in the extrusion of polyethylenes in the presence of boron nitride. *Rheologica Acta* **2004,** 43, 624-633.

90. Sentmanat, M.; Wang, B. N.; McKinley, G. H., Measuring the transient extensional rheology of polyethylene melts using the SER universal testing platform. *Journal of Rheology* **2005,** 49, (3), 585-606.

91. Sentmanat, M.; Muliawan, E. B.; Hatzikiriakos, S. G., Fingerprinting the processing behavior of polyethylenes from transient extensional flow and peel experiments in the melt state. *Rheologica Acta* **2004,** 44, 1-15.

92. Stamboulides, C.; Hatzikiriakos, S. G., Rheology and Processing of Molten Poly(methyl methacrylate) Resins. *International Polymer Processing* **2006,** 21, (2), 155-163.

93. Munstedt, H.; Kurzbeck, S.; Egersdorfer, L., Influence of molecular structure on rheological properties of polyethylenes - Part II: Elongational behavior. *Rheologica Acta* **1998,** 37, 21-29.

94. Meissner, J., *Chemical Engineering Communications* **1985,** 33, 159-180.

3.0 Using molecular scale rheology to infer polymeric architectural features

Preface

This chapter is an invited manuscript that assesses the future of rheology as we see it. It highlights the concepts of using rheological analyses and molecular structure based constitutive relationships to deduce molecular structural features. This chapter is organized as a manuscript to be published in a special issue of Journal of Non-Newtonian Fluid Mechanics put together from participants in a congress on "Whither Rheology".

Using Molecular Scale Rheology to Infer Polymeric Architectural Features

Seay, Christopher W.; McGrady, Christopher D.; and Baird, Donald G.

Department of Chemical Engineering, Virginia Tech

Blacksburg, VA 24061

3.1 Evolution of rheology

Certain aspects of rheology as applied to the flow of polymeric materials have reached a mature state (e.g. the sensitivity of viscosity and normal stresses to molecular weight and its distribution). However, the ability to connect molecular features such as branching architecture to processing performance is still an area for continued exploration. For example, adding one long chain branch (LCB), where a LCB refers to a branch of molecular weight greater than the critical molecular weight for entanglements, on as few as one in two chains can lead to a 10 fold increase in the zero shear viscosity but a 1000-fold decrease in the onset of shear-thinning and significant strain-hardening extensional viscosity [1]. Furthermore, the flow stability behavior can be significantly modified with the addition of as few as one branch per 8 chains [2]. Traditional analytical techniques are insufficient for determining the level of branching at levels less than one branch per 10,000 carbon atoms let alone determine the types of branching present especially in commercial polymers. With the aid of a constitutive theory such as the Mcleish-Larson Pom-Pom model [3] and certain non-linear rheological measurements, the possibility of directly connecting molecular architecture to processing performance exists. Furthermore, the possibility of tailoring the production of polymer molecules for processing performance exists. The remainder of this article will discuss briefly the

current efforts in exploiting the molecular-based pom-pom model [3] and the rheological tests required to extract model parameters which have a direct connection to not only molecular architecture but processing performance.

3.1.1 The pom-pom model and branching

The Doi-Edwards tube theory [4] has generated new thoughts on polymer dynamics and motion at the molecular scale resulting in constitutive relationships that define rheology based on extensions of these general ideas developed for linear polymer chains. According to the tube theory, relaxation after some applied strain is comprised of two distinct relaxation processes: relaxation in which a stretched polymer first relieves chain stretch by retracting to its equilibrium length followed by relaxation in which the stresses are relaxed through reptative motion within a tube defined by molecular entanglements and the relative space a chain has to move. The McLeish-Larson pom-pom model [3] was developed through an extension of these ideas to branched polymers where the relaxation of polymer backbone segments is impeded by the relaxation of the branched arm segments that must first relieve their constraints. Subsequent contributions from Inkson *et al* [5] and Blackwell *et al* [6] have resulted in a multi-mode application of the differential form of the pom-pom model depicted in equations 1-4.

$$\underline{\underline{\sigma}} = \sum_i \underline{\underline{\sigma}}_i = 3\sum_i g_i \lambda_i^2 \underline{\underline{S}}_i \tag{1}$$

$$\underline{\underline{S}}_i = \frac{\underline{\underline{A}}_i}{tr\,\underline{\underline{A}}_i} \tag{2}$$

$$\frac{D}{Dt}\underline{\underline{A}}_i = \underline{\underline{K}} \cdot \underline{\underline{A}}_i + \underline{\underline{A}}_i \cdot \underline{\underline{K}}^T - \frac{1}{\tau_{bi}}\left(\underline{\underline{A}}_i - \underline{\underline{I}}\right) \tag{3}$$

$$\frac{D}{Dt}\lambda_i = \lambda_i\left(\underline{\underline{K}}:\underline{\underline{S}}_i\right) - \frac{1}{\tau_{si}}\left(\lambda_i - 1\right)e^{\nu_i^*\left(\lambda_i - 1\right)} \tag{4}$$

This set of constitutive equations has been shown to explain the rheology of highly-branched hierarchical structures present in LDPE rather well [5, 6]. The ideas of seniority and priority distributions allow for this hierarchical description of the molecular structure. A seniority distribution depicts the degree to which a particular backbone segment is embedded within a polymer chain and defines the linear rheological properties, whereas a priority distribution describes the effective number of arms a particular segment experiences and defines the nonlinear rheological properties [7].

The commercial production of branched polymers using metallocene catalysts usually results in a collection of linear, star, pom-pom, and randomly branched chains [8, 9]. The Pom-Pom constitutive relationship that yields insight into molecular features like branching topologies and chain-type distributions may be useful in determining the aforementioned characteristics for commercially produced branched polymers. To effectively evaluate the correlation between molecular characteristics and constitutive relationships, the constitutive relationship must be validated on model systems where the molecular features are controlled. This work includes collaboration between multiple disciplines bringing together polymer chemistry, rheology, and polymer dynamics and is currently underway, but also represents years of future efforts.

3.2 Validation and applications for the McLeish-Larson pom-pom model

3.2.1 Step-strain rheology

Shear step-strain deformations allow for investigation of the nonlinear viscoelastic behavior of polymer melts and solutions. Typically, the relaxation modulus is

determined as a function of time and strain and obeys time-strain separability as noted in McLeish and Larson [3]. Step-strain experiments are conducted by applying a strain instantaneously at time t = 0 and evaluating the relaxation behavior at times t > 0. McLeish and Larson [3] also provide a KBKZ analog solution for the step-strain relaxation modulus that is independent of q allowing for the direct calculation of τ_s, where the relationship for G(t) is given in equation 5.

$$G\left(t, I_1, I_2\right) = G_0 e^{-t/\tau_b} \left\{\left[\lambda\left(I_1, I_2\right) - 1\right] e^{-t/\tau_s}\right\}^2 \tag{5}$$

Much of the literature explores the behavior of varying polymer solutions [10-14], but of greater interest in this discussion are the relatively few publications that evaluate the behavior of polyethylene melts [15-17]. Laun [15] evaluated a LDPE and was interested in using the step-shear generated relaxation curves to explore the nonlinear rheological behavior through the damping function. Chodankar *et al* [16] also explored a LDPE and presented an exhaustive evaluation of constitutive equations for branched polymers subjected to step-strain flow where they ultimately concluded that the multi-mode differential pom-pom model approach was adequately successful at predicting the step-strain behavior. Jiang *et al.* [17] conducted similar work to that of Chodankar *et al* [16] using a LDPE melt, and evaluated various constitutive equations to determine which constitutive relationship adequately predicted the rheological behavior with the outcome being the uncoupled Giesekus multi-mode model.

Shear step-strain experiments are inherently difficult to execute, raising questions of wall slip, imperfect strain history, and transducer compliance [12, 18-20], which fuel the arguments of data validity. Venerus *et al* [12] cite the previous work of Venerus and Kahvand [18] stating that experiments employing different cone angles and diameters can

ensure the avoidance of imperfect strain history as well as transducer compliance. Imperfect strain history is unavoidable in the sense that no machine can instantaneously apply a strain, but commonly the required times to reach an applied strain range from 20-50 ms. Gevgilili and Kalyon [19] express concerns regarding another component of imperfect strain history as well as wall slip evident in experiments with a polyethylene melt. With regards to an imperfect strain history a small reverse step-strain was observed due to apparent recoil induced from the applied step-strain resulting in a different flow than conceptualized. Gevgilili and Kalyon [19] also found evidence of wall slip at strains as low as 2 strain units and conclude that due to wall slip the applied strain is in fact not the actual strain. Without taking these concerns lightly it is still believed that the experimental results presented are absent of these experimental errors due to comparisons between different cone and plate fixtures of different diameters and cone angles as well as no physical evidence of wall slip, but this could be an area of further investigation.

3.3 Experimental techniques

Two inherently different series of PE resins are considered: a LLDPE-based series and a HDPE-based series. Table 3.1 illustrates the molecular weight, $M_{w,}$ molecular weight distribution, M_w/M_n, and the characteristic branching features for the LLDPE-based series. The LLDPE-based series are well characterized with the McLeish-Larson pom-pom model [21] and provide a more typical industrial polymer system with which to evaluate step-strain rheology. The disadvantage with this series is the relative branching concentrations are merely estimates in that there is no proven method to calculate the exact number of branch ends when ^{13}C NMR is not useful due to the short-chain

branching, SCB, present [22]. This series contains six PE resins: NA952, a highly branched LDPE produced using a tubular free radical polymerization process; NTX101, a linear LLDPE produced with traditional Zieglar-Natta catalysts; Exact 3132, a linear LLDPE produced with metallocene-type catalysts; and Exact 3132, Affinity PL1880, and Affinity PL1840, all of which are sparsely LCB LLDPE's produced with metallocene-type catalysts. The HDPE-based series of materials have been provided by Dow chemical and their molecular characteristics along with their linear rheology has been previously studied [23-25]. These materials provide a distinct advantage in that in the absence of SCB, LCB content can be determined with ^{13}C NMR.

Shear step-strain experiments were conducted using a Rheometrics RMS-800 fitted with 25 mm cone and plate fixtures featuring a cone angle of 0.1 radians and 10 mm cone and plate fixtures featuring a cone angle of 0.035 radians. Tests were carried out at 150°C for the LLDPE-based materials and 170°C for the HDPE-based materials under an inert N_2 atmosphere. Strains of 0.01, 0.1, and 1 strain units were evaluated using the 25 mm setup and strains of 1, 5, 7.5, 10, and 12.5 strain units were evaluated using the 10 mm setup. The applied strain is tracked by the machine and reaches the desired value in approximately 50 ms and, therefore, any data at times less than 50 ms is inaccurate and has thus been discarded.

For a full description of the molecular features and to quantitatively apply the McLeish-Larson pom-pom model to the HDPE-based series of PE resins, transient extensional growth must also be evaluated. Extensional measurements are made using a Rheometrics RER-9000 extensional rheometer, which is a vertical filament stretching machine of the Munstedt design in which the material is submerged in a temperature

controlled oil bath containing an oil of density equal to that of the polymer. Difficulties are observed when testing the HDPE-based PE resins and a novel encapsulation method was developed to overcome these difficulties. The difficult HDPE-based material is encapsulated by a more stable outer sheath as concentric cylinders allowing for deformation of the pair to occur. A full evaluation of this technique is underway and will be published at a later date. It is recognized that a complete evaluation of the parameters in the McLeish-Larson pom-pom model requires extensional viscosity as the number of branch arms is determined from this data.

3.4 Results

Model parameter fitting for the McLeish-Larson pom-pom model is somewhat arbitrary for the terms obtained from nonlinear rheological data (i.e. the stretch relaxation time, τ_s, and the number of effective branch arms, q). These two parameters are fit by attempting to minimize the error between model predictions and experimental data in transient extensional experiments or the combination of extensional and transient shear experiments (i.e. startup of steady shear) whether it be in the single or multi-mode approach. The issue is that both parameters are coupled and the combination that best fits is somewhat subjective. In an effort to rectify and possibly clear up this potential issue, shear step-strain rheology is evaluated to confirm the current model parameters and provide insight into molecular dynamics through the stretch relaxation time.

The relaxation modulus as a function of time, G(t), is evaluated for both the LLDPE-based and HDPE-based series of polymers. The results associated with Exact 3132, NTX101, and Affinity PL1880 are highlighted as they exemplify the findings that appear

to be consistent across both series of materials. The focus of the discussion is on the short-time scales after which time-strain separability is achieved. The curves at different strains have been shifted to obtain a damping function h(γ) that is similar to the Doi-Edwards prediction [4], although it does predict slightly less strain dependence upon reaching higher strains.

Relaxation moduli curves shifted through the exploitation of the damping function for Exact 3132 are illustrated in Figure 3.1. Applied strains range form 0.01 strain units, the linear regime, to 12.5 strain units, the nonlinear regime, and it is observed that the curves superimpose on all timescales. For a linear polymer of narrow MWD, the relaxation curves show no indication of a different relaxation mechanism occurring at short time scales which is typical of most linear polymers (i.e. stretch relaxation is very rapid). This is consistent with the ideas of molecular theory because for linear polymers the relaxation of the stretch is instantaneous and not being impeded by the relaxation of the entangled branched arms.

Figure 3.2 is analyzed to evaluate the relaxation response for NTX101, where the data is presented in a similar manner to that of Exact 3132. Recall NTX101 is another linear chain PE, but differs from the Exact 3132 in that it possesses a broader MWD. Upon shifting, the relaxation curves with the damping function, good agreement is established again on long timescales, but on the order of short timescales, in this case $0.05 \text{ s} < t < 0.1 \text{ s}$, the experimental results show slight deviations at the highest applied strains. At higher strains the relaxation modulus takes longer to fall on the superimposed curve and demonstrates a slightly elevated value at shorter times until it reaches the superimposed curve around 0.1 s. This behavior does not correspond with the expected

behavior of linear chain polymers. However, the presence of a few chains with extremely high MW may be responsible for this behavior as their relaxation times may approach the Rouse relaxation time leading to a slight retardation of the stretch relaxation .

The effects of sparse LCB are evaluated by examining the relaxation moduli behavior for Affinity PL1880, which is depicted in Figure 3.3, where the data is presented in a matter similarly to that of Exact 3132 and NTX101. Recall that Affinity PL1880 posses the least degree of sparse LCB of the series of sparsely LCB LLDPE-based resins, but this slight branching content contributes largely in the relaxation behavior. After superimposing the relaxation curves with the damping function, good agreement is established again on the long timescales, but significant deviations exist on the shorter timescales, in this case $0.05 \text{ s} < t < 0.2 \text{ s}$. At the shorter times as the applied strain is increased, the relaxation modulus becomes more inflated. These results suggest that the stretch relaxation time is impeded, which is consistent with the ideas of the McLeish-Larson pom-pom model providing multiple branch points exist. The branch points act as pins that allow for the stretch in the backbone segment to be maintained until the branched arms complete their relaxation mechanism.

Comparisons of the relaxation behavior provide the potential to evaluate and separate the effects of MWD and LCB. Increasing MWD does have an effect on the relaxation behavior, but not nearly to the degree of the effect of increasing LCB. A broader MWD impeded the stretch relaxation mechanisms only at the highest strains and the deviations were nonexistent after 0.1 s. The addition of sparse amounts of LCB accounted for significant deviations at short times that increased as higher strains were applied. The

relaxation curves retarded the relaxation for a longer period of time as indicated by the failure of time-strain separability until after 0.2 s.

The results are consistent with the ideas of the McLeish-Larson pom-pom model providing a cause to probe the model quantitatively, which is currently underway. Relaxation after the imposition of a shear step-strain appears to yield insight into the stretch relaxation mechanism. It is hoped that this behavior coupled with extensional rheology will better describe the McLeish-Larson pom-pom model parameters and provide a unique solution scheme in which τ_s is extracted from step-strain rheology leaving only q to be determined from extensional rheological experiments.

Preliminary encapsulation results are presented in Figures 3.4 and 3.5 for Affinity PL1880 and HDB-3, respectively, both encapsulated by an outer sheath of NA952. Extensional viscosity growth curves for composite samples of Affinity PL1880 and NA952 are shown at extension rates of 0.1 s^{-1} and 1.0 s^{-1}. This experimental setup was designed to evaluate the potential of this encapsulation technique being that extensional data for both of these pure materials has previously been determined [21] allowing for comparison between experimental data of pure Affinity PL1880 (hollow symbols) and extrapolated data for Affinity PL1880 via the composite samples (filled symbols). Excellent agreement is established at an extension rate of 0.1 s^{-1}, but some disagreement is noted at longer times for the data at an extension rate of 1.0 s^{-1}, where the composite model overpredicts the degree of strain-hardening. This could be attributed to the extreme differences in the extensional viscosities of these two materials at long times and perhaps slight deviations in the volume fraction of sheath material magnifying the strain-hardening effect. HDB-3 although proving extremely difficult in extension by itself

leading to necking and premature material failure, was able to be run to the full strain of 3.0 strain units when encapsulated with the sheath material. The extensional viscosity calculated from the composite sample for this material is difficult to comprehend. The plateau of the extensional viscosity for the pure sample could very well be an artifact of the necking behavior observed and the strain-hardening behavior is possibly real, but due to what was seen with the Affinity PL1880 composites this artificial strain-hardening response could be a trend due to sheath material selection. For this reason current experimentation is underway evaluating the effect of sheath material selection and attempting to find the optimum composite to generate representative extensional data.

3.5 Conclusions

The results of this step-strain rheological evaluation are promising in regards to agreement with the ideas behind the molecular dynamics and potentially provide another piece of the puzzle when attempting to extract molecular topological information from rheology and corresponding constitutive relationships. There is a distinct difference in relaxation behavior for linear and sparsely LCB PEs that is currently being evaluated as a source for determining the associated stretch relaxation times. Moreover, it is observed that the behavior generated by increasing MWD isn't on the same scale as that of increasing LCB content. Rheological analysis with this type of focus on molecular characteristics should prove to be extremely useful for ultimately connecting polymer processing to the underlying polymer chemistry.

3.6 Acknowledgements

This research is a collaborative effort for the World Wide Network of Materials – UK Leeds and is supported financially by the National Science Foundation DMI-052198. Gratitude is given as well to Dow Chemical for supplying a series of sparsely long-chain branched PEs.

3.7 References

1. Doerpinghaus, P. J.; Baird, D. G., Separating the effects of sparse long-chain branching on rheology from those due to molecular weight in polyethylenes. *Journal of Rheology* **2003,** 47, (3), 717-736.

2. Doerpinghaus, P. J.; Baird, D. G., Comparison of the Melt Fracture Behavior of Metallocene and Conventional Polyethylenes. *Rheologica Acta* **2003,** 42, 544-556.

3. McLeish, T. C. B.; Larson, R. G., Molecular constitutive equations for a class of branched polymers: The pom-pom polymer. *Journal of Rheology* **1998,** 42, (1), 81-110.

4. Doi, M.; Edwards, S. F., *The Theory of Polymer Dynamics*. Oxford University Press: 1986.

5. Inkson, N. J.; McLeish, T. C. B.; Harlen, O. G.; Groves, D. J., Predicting low density polyethylene melt rheology in elongational and shear flows with "pom-pom" constitutive equations. *Journal of Rheology* **1999,** 43, (4), 873-896.

6. Blackwell, R. J.; McLeish, T. C. B.; Harlen, O. G., Molecular drag-strain coupling in branched polymer melts. *Journal of Rheology* **2000,** 44, (1), 121-136.

7. Read, D. J.; McLeish, T. C. B., Molecular Rheology and Statistics of Long Chain Branched Metallocene-Catalyzed Polyolefins. *Macromolecules* **2001,** 34, (6), 1928-1945.

8. Soares, J. B. P.; Hamielec, A. E., Effect of reactor residence time distribution on the size distribution of polymer particles made with heterogeneous Ziegler-Natta and supported metallocene catalysts. A generic mathematical model *Macromolecular Theory and Simulations* **1995,** 4, (6), 1085-1104.

9. Soares, J. B. P.; Hamielec, A. E., The chemical composition component of the distribution of chain length and long chain branching for compolymerization of olefins and polyolefin chains containing terminal double-bonds. *Macromolecular Theory and Simulations* **1997,** 6, (3), 591-596.

10. Einaga, Y.; Osaki, K.; Kurata, M.; Kimura, S.-i.; Tamura, M., Stress Relaxation of Polymer Solutions under Large Strain. *Polymer Journal* **1971,** 2, (4), 550-552.

11. Vrentas, C. M.; Graessley, W. W., Study of Shear Stress Relaxation in Well-Characterized Polymer Liquids. *Journal of Rheology* **1982,** 26, (4), 359-371.

12. Venerus, D. C.; Brown, E. F.; Burghardt, W. R., The Nonlinear Response of a Polydisperse Polymer Solution to Step Strain Deformations. *Macromolecules* **1998,** 31, 9206-9212.

13. Chen, C. Y.; Wu, S. M.; Chen, Z. R.; Huang, T. J.; Hua, C. C., Nonlinear Stress Relaxation of an Entangled Linear Polystyrene in Single Step-Strain Flow: A Quantitative Theoretical Investigation. *Journal of Polymer Science: Part B: Polymer Physics* **2003,** 41, 1281-1293.

14. Venerus, D. C.; Nair, R., Stress relaxation dynamics of an entangled polystyrene solution following step strain flow. *Journal of Rheology* **2006,** 50, (1), 59-75.

15. Laun, H. M., Description of the non-linear shear behaviour of a low density polyethylene melt by means of an experimentally determined strain dependent memory function. *Rheologica Acta* **1978,** 17, (1), 1-15.

16. Chodankar, C. D.; Schieber, J. D.; Venerus, D. C., Evaluation of rheological constitutive equations for branched polymers in step shear strain flows. *Rheologica Acta* **2003,** 42, 123-131.

17. Jiang, B.; Kamerkar, P. A.; Keffer, D. J.; Edwards, B. J., Using Multiple-Mode Models for Fitting and Predicting the Rheological Properties of Polymer Melts. II. Single and Double Step-Strain Flows. *Journal of Applied Polymer Science* **2007,** 105, 2884-2892.

18. Venerus, D. C.; Kahvand, H., Normal stress relaxation in reversing double-step strain flows. *Journal of Rheology* **1994,** 38, (5), 1297-1315.

19. Gevgilili, H.; Kalyon, D. M., Step strain flow: Wall slip effects and other error sources. *Journal of Rheology* **2001,** 45, (2), 467-475.

20. Venerus, D. C., A critical evaluation of step strain flows of entangled linear polymer liquids. *Journal of Rheology* **2005,** 49, (1), 277-295.

21. Doerpinghaus, P. J.; Baird, D. G., Assessing the Branching Architecture of Sparsely Branched Metallocene-Catalyzed Polyethylenes Using the Pompom Constitutive Model. *Macromolecules* **2002,** 35, (27), 10087-10095.

22. Janzen, J.; Colby, R. H., Diagnosing long-chain branching in polyethylenes. *Journal of Molecular Structure* **1999,** 485-486, 569-584.

23. Wood-Adams, P. M.; Dealy, J. M., Using Rheological Data to Determine the Branching Level in Metallocene Polyethylenes. *Macromolecules* **2000,** 33, 7481-7488.

24. Wood-Adams, P. M.; Dealy, J. M.; deGroot, A. W.; Redwine, O. D., Effect of Molecular Structure on the Linear Viscoelastic Behavior of Polyethylene. *Macromolecules* **2000,** 33, 7489-7499.

25. Das, C.; Inkson, N. J.; Read, D. J.; Kelmanson, M. A.; McLeish, T. C. B., Computational linear rheology of general branch-on-branch polymers. *Journal of Rheology* **2006,** 50, (2), 207-235.

Table 3.1. Molecular characteristics including M_w, M_w/M_n, and LCB/10,000 C for the LLDPE-based series of polyethylene resins.

Polymer Resin ID	*M_W*	*M_W/M_N*	*LCB/10,000 C [[a] as determined from GPC-LALLS [b] as determined from ^{13}C NMR]*
Exxon Exact 0201	88,700	2.14	0.79 [a]
Exxon Exact 3132	111,000	2.04	---
Dow Affinity PL1840	87,400	2.43	0.57 [a]
Dow Affinity PL1880	115,800	2.12	0.18 [a]
Equistar NA952	235,500	17.1	39 [b]
Mobil NTX101	122,700	3.44	---

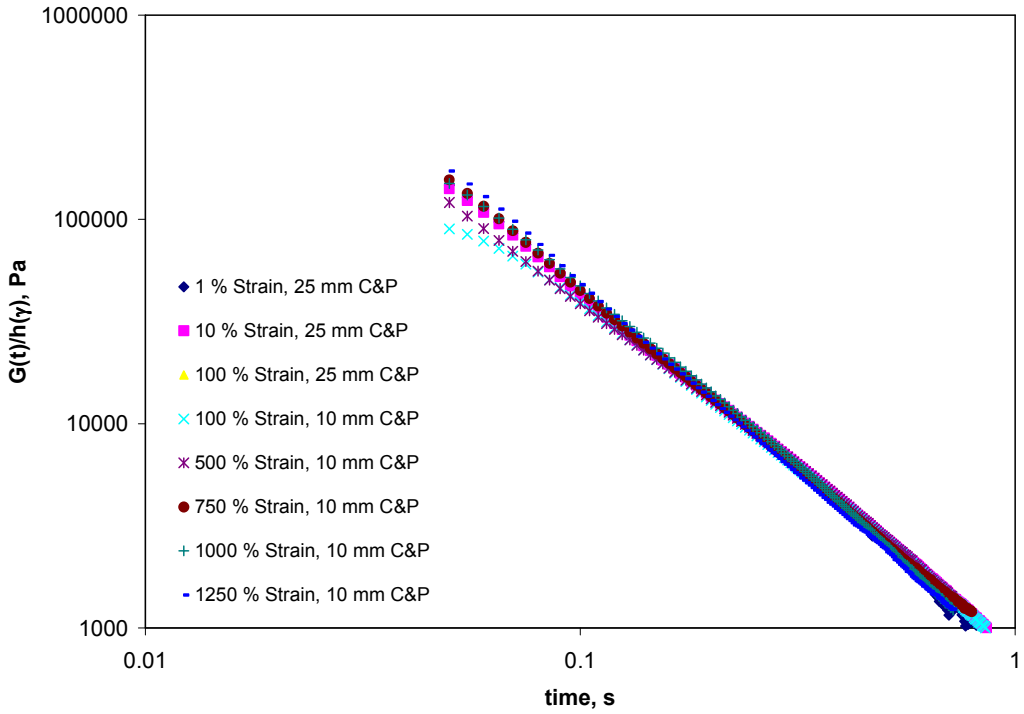

Figure 3.1. Relaxation modulus as a function of time for Exact 3132 at various applied strains ranging from 0.01-12.5 strain units. The data begins at 0.05 s and is shown only out to 1 s after which time-strain separability is confirmed for all polyethylene melts tested.

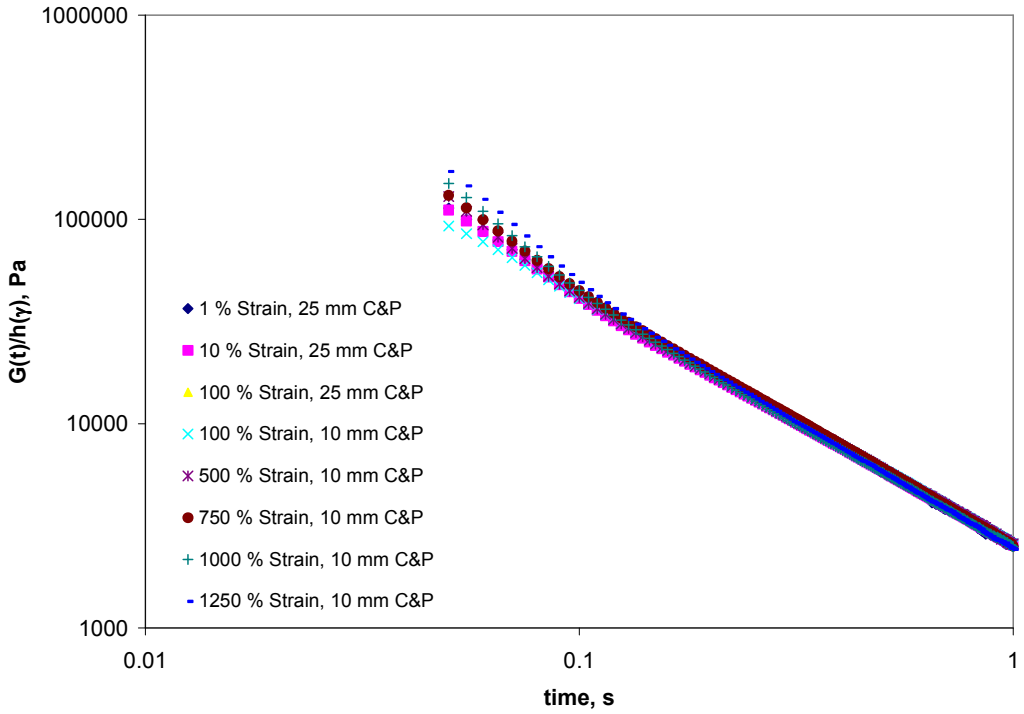

Figure 3.2. Relaxation modulus as a function of time for NTX101 at various applied strains ranging from 0.01-12.5 strain units. The data begins at 0.05 s and is shown only out to 1 s after which time-strain separability is confirmed for all polyethylene melts tested.

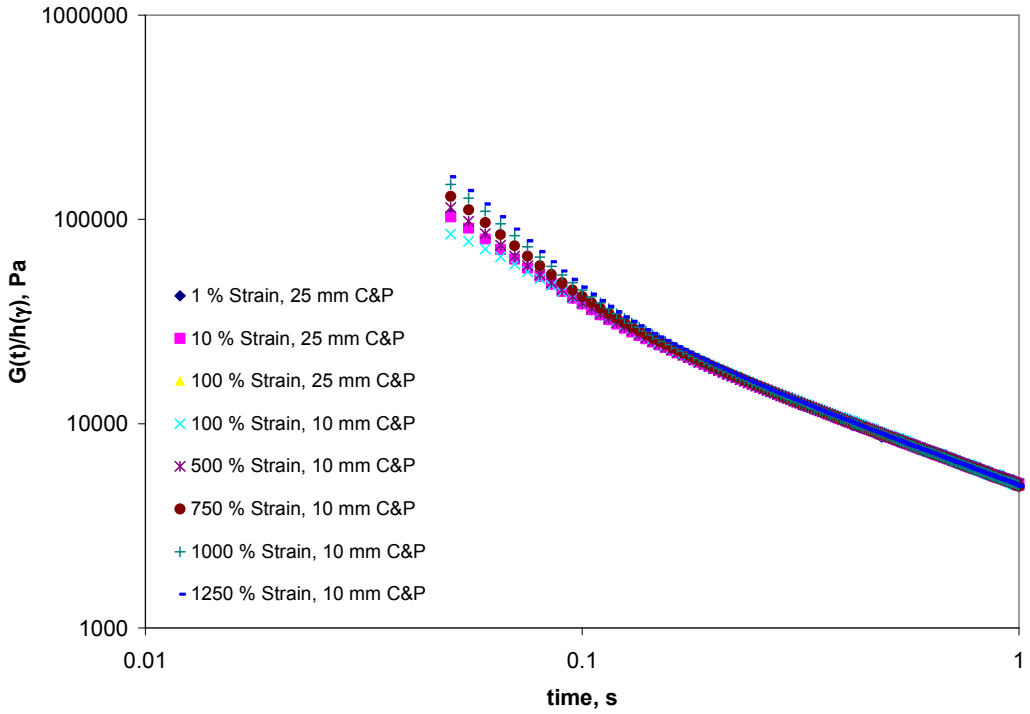

Figure 3.3. Relaxation modulus as a function of time for Affinity PL1880 at various applied strains ranging from 0.01-12.5 strain units. The data begins at 0.05 s and is shown only out to 1 s after which time-strain separability is confirmed for all polyethylene melts tested.

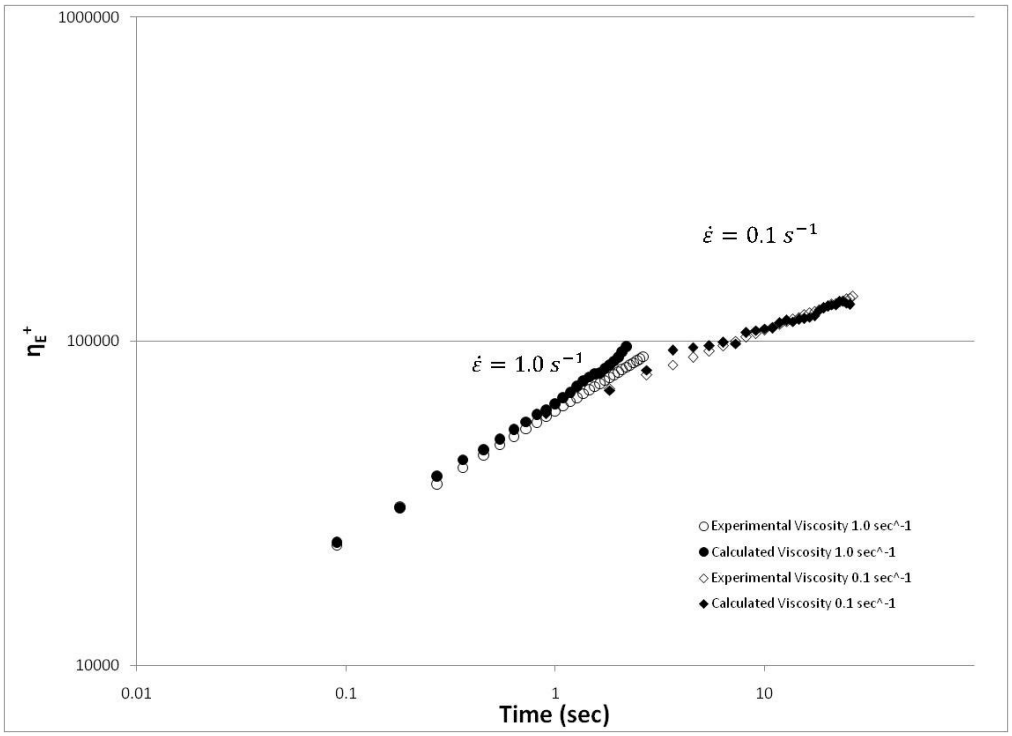

Figure 3.4. Extensional viscosity of Affinity PL1880 at ε = 1.0 s^{-1} and 0.1 s^{-1} calculated from the encapsulated composite method (solid) and compared with data from Doerpinghaus *et al* [21] (hollow).

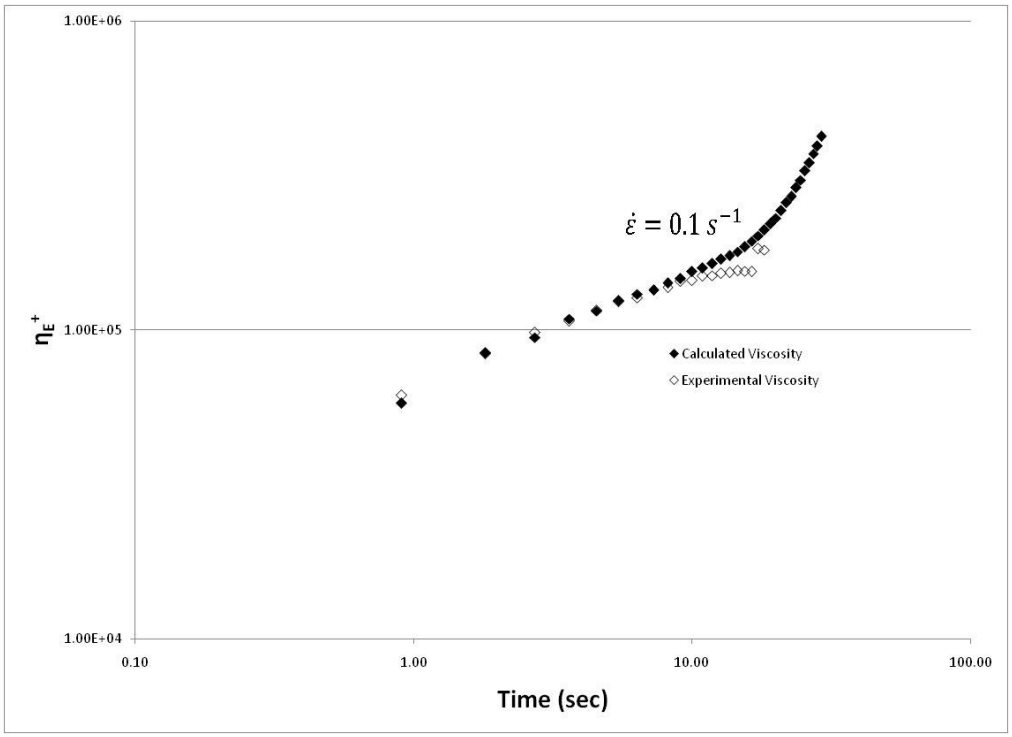

Figure 3.5. Extensional viscosity of HDB-3 at $\varepsilon = 0.1\ s^{-1}$ calculated from the encapsulated composite method (solid) and compared with pure HDB-3 resin (hollow). The pure HDB-3 resin necks to the point of material failure at Hencky strains larger than 1.8 and makes it difficult to obtain repeatable extensional data at longer times.

4.0 An analysis of shear step-strain rheology on sparsely long-chain branched metallocene-catalyzed linear low density polyethylene resins

Preface

This chapter addresses the analysis of a series of linear low density polyethylene resins in shear step-strain rheology. The behavior of the stress relaxation moduli is evaluated to deduce information regarding the molecular structural features. This chapter is organized as a manuscript for publication.

An Analysis of Shear Step-Strain Rheology on Sparsely Long-Chain Branched Metallocene-Catalyzed Linear Low Density Polyethylene Resins

Seay, Christopher W.; McGrady, Christopher D.; Baird, Donald G.

Department of Chemical Engineering, Virginia Tech

Blacksburg, VA 24061

4.1 Abstract

Shear step-strain rheology for a series of metallocene-catalyzed linear low-density polyethylene, LLDPE, resins with varying degree of branching is evaluated. The objectives of this research include the assessment of the inadequacies associated with the step-strain experiments and the ability of the K-BKZ analog of the pom-pom constitutive model to predict step-strain rheological behavior. Finite rise times associated with the inability of present rheological equipment to instantaneously impose a strain are compared to the Rouse relaxation times of the PE resins and are found to be at least an order of magnitude smaller. The potential for wall slip exists, thus the experiments were monitored and found to be devoid of any wall slip. Analysis of the K-BKZ analog of the pom-pom constitutive model includes comparisons between experimental stress relaxation moduli and predictions from the model using pom-pom model parameters determined from extensional rheology. The results show inconsistencies in the model predictions, where the predictions fail to capture the short time behavior and accurately dampen at larger strains. Pom-pom model parameters are determined using the K-BKZ analog of the pom-pom constitutive model and fitting the stress relaxation moduli. These results are qualitatively consistent indicating that branching occurs on the longest

backbone segments, but the values appear to be unrealistic with respect to the molecular theory.

4.2 Introduction

The McLeish-Larson pom-pom constitutive model has been shown to effectively model the shear and extensional rheological behavior of LDPE [1] as well as sparsely long-chain branche, LCB, PE [2], but the fitting technique results in nonlinear parameters that are not entirely unique. Fitting is accomplished by evaluating uniaxial extensional viscosity growth curves to find two unknown nonlinear parameters, namely the stretch relaxation time and the number of branch arms associated with each relaxation time, using a least squared fitting analysis. The major limitation is that variations in the parameter fits are possible leading to potential inconsistency in the determination of model parameters. Evaluation of the pom-pom model in shear step-strain flows for LDPE and sparsely LCB PE resins could allow for an independent determination of one of the two unknown nonlinear parameters, thus making the solution scheme potentially more unique. However, this depends on whether the stress relaxation modulus can accurately be measured at short times where the stretch relaxation is dominant.

The Doi-Edwards tube theory [3] has spurned new thoughts on polymer dynamics and motion at the molecular scale resulting in constitutive relationships that define rheology based on extensions of these general ideas developed for linear polymer chains. According to the tube theory, relaxation after some applied strain is comprised of two distinct relaxation processes: relaxation of the stretched polymer segment confined in a tube representing the entanglement constraints followed by relaxation of the orientation of the backbone segment in which the stresses are relaxed through reptative motion

within the tube defined by molecular entanglements. For linear polymers the stretch relaxation occurs nearly instantaneously.

The McLeish-Larson pom-pom model [1] was developed through an extension of the ideas of Doi and Edwards to branched polymers where the relaxation of polymer backbone segments is impeded by the relaxation of the branched arm segments that must first relieve their constraints. Subsequent contributions from Inkson *et al* [4] and Blackwell *et al* [5] have resulted in a multi-mode application of the differential form of the pom-pom model depicted in Eqs. 1-4.

$$\underline{\underline{\sigma}} = \sum_i \underline{\underline{\sigma}}_i = 3\sum_i g_i \lambda_i^2 \underline{\underline{S}}_i \tag{1}$$

$$\underline{\underline{S}}_i = \frac{\underline{\underline{A}}_i}{tr\,\underline{\underline{A}}_i} \tag{2}$$

$$\frac{D}{Dt}\underline{\underline{A}}_i = \underline{\underline{K}} \cdot \underline{\underline{A}}_i + \underline{\underline{A}}_i \cdot \underline{\underline{K}}^T - \frac{1}{\tau_{bi}}\left(\underline{\underline{A}}_i - \underline{\underline{I}}\right) \tag{3}$$

$$\frac{D}{Dt}\lambda_i = \lambda_i\left(\underline{\underline{K}} : \underline{\underline{S}}_i\right) - \frac{1}{\tau_{si}}\left(\lambda_i - 1\right)e^{\nu_i^*\left(\lambda_i - 1\right)} \tag{4}$$

Four unknown parameters at each mode exist: g, which is the individual contribution to the plateau modulus; τ_b, which is the characteristic relaxation time associated with the backbone orientation; τ_s, which is the characteristic relaxation time associated with the stretch; and q, which is the number of branch arms.

This set of equations has been shown to explain the rheology of highly-branched hierarchical structures present in LDPE rather well [4, 5]. The ideas of seniority and priority distributions allow for this hierarchical description of the molecular structure. A seniority distribution depicts the degree to which a particular backbone segment is embedded within a polymer chain and defines the linear rheological properties, whereas a

priority distribution describes the effective number of arms a particular segment experiences and defines the nonlinear rheological properties [6].

Shear step-strain deformations allow for investigation of the nonlinear viscoelastic behavior of polymer melts and solutions. Typically, the relaxation modulus is determined as a function of time and strain and obeys time-strain separability as noted in McLeish and Larson [1]. Step-strain experiments are conducted by applying a strain instantaneously at time t = 0 and evaluating the relaxation behavior at times t > 0. McLeish and Larson [1] also provide a K-BKZ analog solution for the relaxation modulus obtained from step-strain measurements that is independent of q allowing for the direct calculation of τ_s, where the relationship for G(t) is given in Eq. 5.

$$G\left(t, I_1, I_2\right) = G_0 e^{-t/\tau_b} \left\{ \left[\lambda\left(I_1, I_2\right) - 1 \right] e^{-t/\tau_s} \right\}^2 \qquad (5)$$

It is noted that in the case of a branched polymer that at short times the corresponding relaxation modulus is a function of the stretch relaxation unlike linear polymers where stretch relaxation occurs rapidly.

Much of the literature explores the behavior of varying polymer solutions [7-11], but of greater interest in this discussion are the relatively few publications that evaluate the behavior of polyethylene melts [12-16]. Laun [13] evaluated a LDPE and was interested in using the step-shear generated relaxation curves to explore the nonlinear rheological behavior through the damping function. Vega and Milner [16] and Stadler *et al* [12] were also interested in the damping behavior, but extended the evaluation to branched polymers. Vega and Milner [16] found that diluted samples of combs and LDPE showed damping functions with a weaker dependence on strain than predicted by Doi-Edwards, which they attribute to marginally entangled polymer chains. Stadler *et al* [12] turned their efforts to

the effect of LCB on the damping function. They found that higher degrees of LCB lead to a weaker dependence of the damping function of stain.

Chodankar *et al* [14] also explored a LDPE and presented an exhaustive evaluation of constitutive equations for branched polymers subjected to step-strain flow where they ultimately concluded that the multi-mode differential pom-pom model approach was adequately successful at predicting the step-strain behavior. Jiang *et al.* [15] conducted similar work to that of Chodankar *et al* [14] using a LDPE melt, and evaluated various constitutive equations to determine which constitutive relationship adequately predicted the rheological behavior with the outcome being the uncoupled Giesekus multi-mode model.

Shear step-strain experiments are inherently difficult to execute, raising questions of wall slip, imperfect strain history, and transducer compliance [9, 16-19], which fuel the arguments of data validity. Venerus *et al* [9] cite the previous work of Venerus and Kahvand [17] stating that experiments employing different cone angles and diameters can ensure the avoidance of imperfect strain history as well as transducer compliance. Imperfect strain history is unavoidable in the sense that no machine can instantaneously apply a strain, but commonly the required times to reach an applied strain range from 20-50 ms. Measurements should not suffer any influence from the finite rise time provided that the Rouse relaxation time, τ_R, is significantly greater than the finite rise time. Gevgilili and Kalyon [18] express concerns regarding another component of imperfect strain history as well as wall slip evident in experiments with a polyethylene melt. With regards to an imperfect strain history a small reverse step-strain was observed due to apparent recoil induced from the applied step-strain resulting in a different flow than

conceptualized. Gevgilili and Kalyon [18] also found evidence of wall slip at strains as low as 2 strain units and conclude that due to wall slip the applied strain is in fact not the actual strain.

In the present study, shear step-strain rheology measurements are evaluated for a series of resins including metallocene-catalyzed linear and sparsely LCB PE resins and LDPE with respect to the pom-pom constitutive model. It has been shown that the pom-pom constitutive model is effective for modeling the rheology of sparsely LCB PE resins [2] and LDPE [4], but the determination of pom-pom model parameters is in no way unique when using uniaxial extensional growth curves to find both τ_s and q. Initial parameters for the pom-pom constitutive model were determined following the techniques of Blackwell *et al* [5] and Inkson *et al* [4]. The goal of this study is to investigate differences in stress relaxation moduli curves among the resins and evaluate the consistency of these parameters with the shear step-strain rheological measurements. Using the K-BKZ approximation for the relaxation modulus, as defined by McLeish and Larson, τ_s is determined from shear step-strain data to present a more unique method of determination of the nonlinear parameters in the pom-pom constitutive model.

4.3 Experimental materials and methods

4.3.1 Materials

Six commercially available PE resins developed were selected for this study. The series consists of four metallocene-catalyzed materials featuring different degrees of sparse LCB ranging from linear to 0.79 LCB/10,000 CH_2 along with two reference systems consisting of a LLDPE and a LDPE. This series of resins has also been characterized rheologically at a temperature of 150°C for both steady and dynamic

oscillatory shear and uniaxial extensional flows [2, 20, 21]. Physical properties for this series of resins including density; melt flow index; weight-average molecular weight; molecular weight distribution, MWD; and LCB concentration are tabulated in Table 4.1.

Exact 3132, Exact 0201, Affinity PL1880, and Affinity PL1840 are all metallocene-catalyzed polyethylene resins. These materials were selected to evaluate the effects of sparse LCB on step-shear rheology. Exact 3132 is a ethylene-hexene copolymer while Exact 0201 is an ethylene-octene copolymer both manufactured by ExxonMobil Chemical using EXXPOL® catalyst technology. Affinity PL1880 and Affinity PL1840 are ethylene-octene copolymers manufactured by Dow Chemical using INSITE® catalyst technology. Exact 3132 is specified as a linear metallocene-catalyzed copolymer, while Exact 0201, Affinity PL1880, and Affinity PL1840 are identified to contain sparse LCB analytically quantified using GPC-LALLS [22, 23]. Typical of metallocene-catalyzed polyethylene resins the MWD for these materials is relatively narrow falling between 2.0 and 2.5.

The remaining two materials, NTX101 and NA952, are a conventional LLDPE and LDPE, respectively. NTX101 is an ethylene-hexene copolymer manufactured by ExxonMobil using a Zieglar-Natta gas-phase polymerization process. NA952 is an ethylene homopolymer manufactured by Equistar using a high-pressure, high-temperature tubular free-radical polymerization process. NTX101 exhibits a broader MWD of approximately 3.5 and provides a resin that allows us to assess the effects of broadening the MWD on shear step-strain rheology. NA952 was selected as a highly branched reference material providing an extreme case scenario for the addition of LCB. The level of LCB for NA952 is quantified analytically using ^{13}C NMR. A major

limitation of this technique is its inability to distinguish branches longer than six carbon atoms in length [24, 25], and therefore, the value of LCB includes LCB as well as short-chain branches.

4.3.2 Shear step-strain rheology

Shear step-strain experiments were conducted using a Rheometrics RMS-800 fitted with 25 mm cone and plate fixtures featuring a cone angle of 0.1 radians and 10 mm cone and plate fixtures featuring a cone angle of 0.035 radians, which is in the appropriate range to achieve a constant shear rate within the polymer sample [26]. Tests were carried out at a temperature of 150°C under an inert N_2 atmosphere. Strains of 0.01, 0.1, and 1 strain units were evaluated using the 25 mm diameter plates and strains of 1, 5, 7.5, 10, and 12.5 strain units were evaluated using the 10 mm diameter plates. Wall slip was evaluated by measuring the displacement of a stained line drawn perpendicular to the flow direction. No evidence of wall slip was experienced for any of the six PE resins on either set of cone and plate fixtures.

4.3.3 Parameter fitting

The experimental data is fit using a multimode form of Eq. 5 with five modes. Values of τ_{bi} and g_i are fit from the linear relaxation spectrum of each material listed in Table 4.2. Values of the initial stretch are approximated using the Doi-Edwards relationship shown in Eq. 7 developed for linear polymer chains.

$$\lambda = \left[1 + \left(\frac{\gamma}{3}\right)^2\right]^{\frac{1}{2}} \tag{6}$$

This leaves only the τ_{si} at each mode to be fit. A linear least squares analysis is used to determine the optimum values of each τ_{si} across all strains simultaneously. The ratio τ_{bi}

$/\tau_{si}$ is bounded by a lower limit of one, corresponding to a perfectly unentangled segment. Realistic upper limits of τ_{bi}/τ_{si} are on the order of ten [Inkson *et al.* (1999)], but are not constrained here in order to evaluate the qualitative nature of the model and parameters.

4.4 Results and discussion

The shear step-strain results and subsequent discussions are presented in three distinct groups according to polymer resin branching properties. The key findings from experiments on two linear PE resins are discussed concerning the general shape of the relaxation modulus as well as the discerned effects of a broadening MWD. The sparsely LCB PE resins are considered with respect to the general shape of their relaxation moduli and how the curves compare to each other and the results from the linear PE resins. The highly branched structure of LDPE is then evaluated for any differences in observations when compared with the five other PE resins. In each case the relaxation moduli predictions using the pom-pom constitutive model are discussed and unique parameters for the spectrum of τ_{si} are considered. Preceding these results is an analysis of the Rouse relaxation time and how it compares to the finite rise time. This analysis proves the lack of influence of the finite rise time for the timescales studied. Finally, the behavior of the damping function is evaluated for all of the PE resins and compared to previous results.

4.4.1 Finite rise time

Finite rise time stems from the inability to instantaneously apply a strain to polymeric material, which can affect the stress relaxation modulus output by artificially damping the results due relaxation occurring prior to complete deformation [13]. Imperfect strain history is considered through evaluation of the applied strain at early times for each applied strain. Table 4.3 shows the time required for 95% of the desired applied strain to be

achieved experimentally. The time required ranges from 0.055-0.065 s and increases with increasing strain. All experimental data is truncated at lower times according to this 95% strain time interval. Applied strain as a function of time for the greatest applied strain of 12.5 strain units is presented in Fig. 4.1. It is seen that in the most extreme case, strain grows relatively quickly with respect to time. The importance of the finite rise time lies in its comparison to the Rouse relaxation time, τ_R, for the tested PE resins. For the relaxation modulus curves to be unaffected by relaxation that takes place prior to reaching the applied strain, τ_R must be sufficiently greater than the finite rise time. τ_R for each PE resin was calculated following the method of Elbirli and Shaw [27] shown in Eq. 6.

$$\tau_R = \frac{6\eta_0 M_w}{\pi^2 \rho R T} \tag{7}$$

The values of τ_R for each PE resin are tabulated in Table 4.4 and range from 0.327-1.19 s. In all cases, τ_R is approximately at least an order of magnitude greater than the finite rise time.

4.4.2 Linear PE resins

The relaxation moduli for two linear PE resins are considered. The molecular characteristics for these two materials are presented in Table 4.1. The results for Exact 3132 are presented first followed by the results for NTX101. Comments are made regarding the shapes and time-strain separable region for each of the linear materials. Comparisons to pom-pom model predictions are made and values for τ_{si} are determined from fitting the relaxation moduli curves. Differences when comparing the two PE resins are evaluated as effects of a broadening molecular weight distribution.

The relaxation modulus for shear step-strain experiments as a function of time is presented in Fig. 4.2a,b at strains of 0.01, 0.1, 1.0, 5.0, 7.5, 10.0, and 12.5 strain units for Exact 3132. The data is presented as $G(t,\gamma)$ in Fig. 4.2a as well as shifted by dividing through by the damping function in Fig. 4.2b. The damping function represents the suppression of the relaxation modulus in the time-strain separable region that occurs with increasing applied strains. All of the subsequent data for the remainder of the PE resins is simply presented in the shifted form as $G(t,\gamma)/h(\gamma)$ versus time because of our interest in differences in the short time region prior to the occurrence of time-strain separability. As expected for a linear material after shifting, the data superimpose over the entire time scale evaluated. Time-strain separability occurs over the entire spectrum and no differences are observed with increasing strain at short timescales.

The relaxation modulus for Exact 3132 at 0.01, 5.0, and 12.5 strain units along with the pom-pom model predictions generated by taking a multi-mode approach to the K-BKZ analog shown in Eq. 6 are presented in Fig. 4.3. The predictions are shifted using the experimentally determined damping behavior. The predictions are in relatively good agreement with the experimental data, but it is observed that at short times the model predictions change less with time than the experimental data and at the highest strain of 12.5 strain units the model overpredicts the experimental result. For a linear material, the model predictions agreeing with the experimental results reveal nothing in terms of the accuracy of fitting τ_{si} and q_i with the original approach as the material fails to contain LCB.

τ_{si} values for Exact 3132 are determined from the stress relaxation moduli curves using the approach outlined in the experimental materials and methods section and are

presented in Table 4.5. The values determined from this approach do not agree with the values determined from the original approach using transient extensional growth curves. Qualitatively, the new τ_{si} parameters are reasonable showing negligible increase in τ_{si} with increasing τ_{bi} except for the case of the smallest τ_{bi}. Because there is no LCB present in the molecule it stands to reason that τ_{si} would be the similar for all backbone segments. τ_{si} values are also on the order of the finite rise time raising the question whether they are truly representative of the stretch relaxation or negligible inferring that the stretch relaxes faster than the finite rise time, where the latter argument is the most probable.

Shifted relaxation moduli curves for shear step-strain experiments as a function of time are presented in Fig. 4.4 at strains of 0.01, 0.1, 1.0, 5.0, 7.5, 10.0, and 12.5 strain units for NTX101. Separation at short times is observed in the case of the highest applied strains of 10.0 and 12.5 strain units indicating the failure of time-strain separability until times of approximately 0.15 s. The shifted relaxation modulus for applied strains of 10.0 and 12.5 strain units is initially larger than the other experimental applied strains and decreases rapidly until the time-strain separable regime is reached. This is not the anticipated response for a linear PE resin, and it is concluded that broadening the MWD does in fact affect the relaxation process following a shear step-strain deformation. The results may be due to explained by the higher molecular weight polymer chains that exist in a material with a broadened MWD.

The relaxation modulus for NTX101 at 0.01, 5.0, and 12.5 strain units along with the pom-pom model predictions generated by taking a multi-mode approach to the K-BKZ analog shown in Eq. 6 are presented in Fig. 4.5. The predictions reasonably agree with

the experimental results, but again fail to represent the data at the earliest times and overpredict the experimental results at higher strains. In this case the model predictions overpredict the experimental results at both 5.0 and 12.5 strain units. Interestingly, the experimentally observed damping behavior does not dampen the model prediction to the correct degree. Again, the linear nature of the material does not provide any insight into the accuracy of the original method of determination for τ_{si} and q_i values, but by increasing the MWD of the polymer the model predictions become less accurate perhaps providing insight into the behavior of sparsely LCB resins.

τ_{si} values for NTX101 are determined from the stress relaxation moduli curves using the approach outlined in the experimental materials and methods section and are presented in Table 4.6. The values determined from this approach do not agree with the values determined from the original approach using transient extensional growth curves. Again it is observed that, qualitatively, the τ_{si} parameters determined from step-strain measurements are reasonable showing negligible increase in τ_{si} with increasing τ_{bi} except for the case of the smallest τ_{bi}. Because there is no LCB present in the molecule it stands to reason that τ_{si} would be the similar for all backbone segments. The τ_{si} values determined from step-strain measurements for both linear resins are similar, which is reasonable, but somewhat unexpected after the observed separation in $G(t,\gamma)/h(\gamma)$ curves at the higher strains.

4.4.3 Sparsely LCB PE resins

The relaxation moduli for the three PE resins with sparse LCB are evaluated. The molecular characteristics for these three materials are presented in Table 4.1. The materials are presented in order of increasing degree of LCB: Affinity PL1880, Affinity

PL1840, and Exact 0201. The general shape of the relaxation moduli curves is investigated along with comparisons to predictions from the pom-pom constitutive model. The relative shapes of the relaxation moduli curves are observed to be similar for all three materials and any differences observed are established by evaluation of the fitted τ_s values.

Shifted relaxation moduli curves for shear step-strain experiments as a function of time are presented in Figs. 4.6 through 4.8 at strains of 0.01, 0.1, 1.0, 5.0, 7.5, 10.0, and 12.5 strain units for Affinity PL1880, Affinity PL1840, and Exact 0201, respectively. Results for the three materials with sparse LCB are presented simultaneously due to the relative similarities in the stress relaxation behavior. Failure of time-strain separability is observed at short times consistent with the molecular theory predictions for branched polymers. Separation is observed at all strains greater than and including 5.0 strain units, where a larger degree of separation is observed at the higher strains. The inflection in the stress relaxation moduli curves at short times is noticeably larger than those present in the NTX101. This inflection is also observed at all applied strains contrary to what was seen in the case of NTX101 where an inflection only occurred on the larger strains. In the previous section we established that broadening the MWD does affect the stress relaxation moduli curves, but it is observed that the addition of sparse LCB results in stress relaxation moduli curves that have a different shape altogether and exhibit an inflection in the data at all strains. It is concluded that through the addition of sparse LCB and subsequent lengthening of the stretch relaxation times associated with the branched arms contributes to the general shape of the stress relaxation moduli curves at short times.

The relaxation modulus for Affinity PL1880, Affinity PL1840, and Exact 0201 at 0.01, 5.0, and 12.5 strain units, respectively, along with the pom-pom model predictions generated by taking a multi-mode approach to the K-BKZ analog shown in Eq. 6 are presented in Figs. 4.9 through 4.11. Similar behavior is observed in all three cases, where the model predictions fail to predict the experimental results at short times and grossly overpredict the experimental results at the higher strains of 5.0 and 12.5 strain units. Comparisons between the model predictions and the experimental data illustrate the inability of the K-BKZ analog to the pom-pom constitutive model to accurately predict the stress relaxation behavior after a shear step-strain deformation for sparsely LCB PE resins. The damping behavior is underpredicted due to the response of λ following the Doi-Edwards approximation. Inspection of Eq. 6 shows that to accurately portray the damping observed, λ must be less than originally predicted. This is expected with branched polymers because of the increasing number of entanglements and resistance to stretch.

τ_{si} values for Affinity PL1880, Affinity PL1840, and Exact 0201 are determined from the stress relaxation moduli curves using the approach outlined in the experimental materials and methods section and are presented in Tables 4.7 through 4.9, respectively. The values determined from this approach do not agree with the values determined from the original approach using transient extensional growth curves. The results for Affinity PL1880 are very similar to those of the two linear materials showing no τ_{si} values that are significantly long. This is unexpected due to the LCB present in the polymer. The results for Affinity PL1840 and Exact 0201, however, qualitatively yield the expected behavior. For these two materials the τ_{si} associated with the longest τ_{bi} was observed to

be an order of magnitude larger than all other τ_{si}'s. From the parameters determined from the original fitting approach we would expect that longer τ_{si} values will occur on the τ_{bi} values that contain branch arms. This qualitatively makes sense because the incorporation of LCB inhibits the stretch relaxation of the material. Quantitatively the values for τ_{si} are unrealistic. This is most likely a product of incorrectly approximating λ using the Doi-Edwards approach.

4.4.4 LDPE

Finally, the stress relaxtion moduli curves for a highly branched LDPE are considered. The molecular characteristics for this material are included in Table 4.1. The results for NA952 are evaluated and compared to the results of the previous resins discussed. The predictions from the pom-pom constitutive model are examined and values for τ_s are also calculated. NA952 provides an extreme case illustrating the maximum effect of LCB on the stress relaxation moduli curves.

Shifted relaxation moduli curves for shear step-strain experiments as a function of time are presented in Fig. 4.12 at strains of 0.01, 0.1, 1.0, 5.0, 7.5, 10.0, and 12.5 strain units for NA952. The general shape of the stress relaxation moduli curves are similar to the results of the sparsely LCB PE resins, showing failure of time-strain separability on the same timescales and a similar degree of inflection in the curves at short times that occurs for all strains contrary to the results of Vega and Milner [16]. The observed results are expected due to the presence of LCB in the polymer chains.

The relaxation modulus for NA952 at 0.01, 5.0, and 12.5 strain units along with the pom-pom model predictions generated by taking a multi-mode approach to the K-BKZ analog shown in Eq. 6 are presented in Fig. 4.13. The model predictions again fail to

predict the relaxation behavior at short times as well as drastically overpredict the relaxation moduli curves at the higher strains of 5.0 and 12.5 strain units. The same arguments that apply to the sparsely LCB PE resins also apply here. It is found that the as we progress from linear to sparsely LCB and finally to highly branched systems the model predictions become more inaccurate at representing the stress relaxation behavior and we can determine that the K-BKZ analog expression for $G(t,\gamma)$ fails when applied using pom-pom model parameters determined from uniaxial extensional viscosity growth curves.

τ_{si} values for NA952 are determined from the stress relaxation moduli curves using the approach outlined in the experimental materials and methods section and are presented in Table 4.10. Like all of the other resins evaluated, the values determined from this approach do not agree with the values determined from the original approach using transient extensional growth curves. The results are similar to those of Affinity PL1840 and Exact 0201 where τ_{si} associated with the longest τ_{bi} is at least an order of magnitude larger than the τ_{si} determined at the other modes. This is consistent with the idea that the branches are found on the longest backbone segments, but for a highly branched resin, such as LDPE, we would expect the branching distribution to incorporate smaller backbone segments as well. The differences found in the τ_{si} values when comparing the PE resins are not great enough to detect differences in the branching concentrations. It is observed that a polymer material either shows a longer τ_{si} at the longest τ_{bi} or it doesn't, which can be viewed as the material contains LCB or it does not. The only exception is Affinity PL1880, which contains sparse LCB but does not show

any longer τ_{si} values perhaps indicating that the LCB is so sparse that it fails to impede the stretch relaxation of the material.

4.4.5 Damping function behavior

The damping function, $h(\gamma)$, as a function of strain is presented in Fig. 4.14 for all of the PE resins discussed in this text. It is observed that all of the materials with the exception of the LDPE display a similar dependence of $h(\gamma)$ on γ as the Doi-Edwards approximation. The LDPE presents a weaker dependence on γ. We expect the linear PE resins to follow the Doi-Edwards approximation of $h(\gamma)$, but the remaining results only partially agree with that of Stadler *et al* [12]. The sparsely branched materials do not show a weakening dependence on γ with increasing degree of branching contrary to Stadler *et al* [12]. Weakening dependence of $h(\gamma)$ on γ may also be a result of wall slip and not achieving the strain that is desired. Agreement is found for the case of LDPE where a weaker dependence of $h(\gamma)$ on γ is observed.

4.5 Conclusions

Step-strain rheology for this series of metallocene-catalyzed LLDPE resins has been validated as being capable of producing experimental results that are not influenced by finite rise time and wall slip. Rouse relaxation times are evaluated and determined to be at least an order of magnitude larger than the finite rise time, suggesting that relaxation is not occurring on the short times associated with the finite rise time. Wall slip is evaluated experimentally, and it is concurred that it does not occur for any of the materials for the strains applied.

The K-BKZ analog of the pom-pom constitutive model was evaluated to determine the consistency of the experimental data and the model predictions. The model failed to

yield predictions which agreed with the experimental data at short times and incorrectly predicted the damping of the stress relaxation moduli curves when pom-pom model parameters determined using extensional rheological measurements were used. To better fit the experimental results and determine a more unique set of the pom-pom model parameters, τ_{si} values are determined using the K-BKZ analog equation to fit the stress relaxation moduli curves. The results are consistent with the ideas that the longest backbone segments contain the bulk of the branching. This is shown in the cases of Affinity PL1840, Exact 0201, and NA952 where τ_{si} associated with the largest τ_{bi} is an order of magnitude larger the τ_{si} values associated with the shorter τ_{bi}'s. The values determined for τ_{si}, however, are unrealistic, which is believed to be associated with the inadequacy of the correct damping behavior. Damping defined by λ and was determined according to the Doi-Edwards approximation, which drastically fails for our systems except the linear materials. A better approximation of λ could reduce the effect on τ_{si} and more realistic values for the series of τ_{si}'s could be generated.

4.6 Acknowledgements

This research is a collaborative effort for the World Wide Network of Materials – UK Leeds and is supported financially by the National Science Foundation DMR-052198. Gratitude is given as well to Dow Chemical Company, ExxonMobil Chemical Company, and Equistar Chemical Company for supplying their respective PE materials.

4.7 References

1. McLeish, T. C. B.; Larson, R. G., Molecular constitutive equations for a class of branched polymers: The pom-pom polymer. *Journal of Rheology* **1998,** 42, (1), 81-110.

2. Doerpinghaus, P. J.; Baird, D. G., Assessing the Branching Architecture of Sparsely Branched Metallocene-Catalyzed Polyethylenes Using the Pompom Constitutive Model. *Macromolecules* **2002,** 35, (27), 10087-10095.

3. Doi, M.; Edwards, S. F., *The Theory of Polymer Dynamics*. Oxford University Press: 1986.

4. Inkson, N. J.; McLeish, T. C. B.; Harlen, O. G.; Groves, D. J., Predicting low density polyethylene melt rheology in elongational and shear flows with "pom-pom" constitutive equations. *Journal of Rheology* **1999,** 43, (4), 873-896.

5. Blackwell, R. J.; McLeish, T. C. B.; Harlen, O. G., Molecular drag-strain coupling in branched polymer melts. *Journal of Rheology* **2000,** 44, (1), 121-136.

6. Read, D. J.; McLeish, T. C. B., Molecular Rheology and Statistics of Long Chain Branched Metallocene-Catalyzed Polyolefins. *Macromolecules* **2001,** 34, (6), 1928-1945.

7. Einaga, Y.; Osaki, K.; Kurata, M.; Kimura, S.-i.; Tamura, M., Stress Relaxation of Polymer Solutions under Large Strain. *Polymer Journal* **1971,** 2, (4), 550-552.

8. Vrentas, C. M.; Graessley, W. W., Study of Shear Stress Relaxation in Well-Characterized Polymer Liquids. *Journal of Rheology* **1982,** 26, (4), 359-371.

9. Venerus, D. C.; Brown, E. F.; Burghardt, W. R., The Nonlinear Response of a Polydisperse Polymer Solution to Step Strain Deformations. *Macromolecules* **1998,** 31, 9206-9212.

10. Chen, C. Y.; Wu, S. M.; Chen, Z. R.; Huang, T. J.; Hua, C. C., Nonlinear Stress Relaxation of an Entangled Linear Polystyrene in Single Step-Strain Flow: A Quantitative Theoretical Investigation. *Journal of Polymer Science: Part B: Polymer Physics* **2003,** 41, 1281-1293.

11. Venerus, D. C.; Nair, R., Stress relaxation dynamics of an entangled polystyrene solution following step strain flow. *Journal of Rheology* **2006,** 50, (1), 59-75.

12. Stadler, F. J.; Auhl, D.; Munstedt, H., Influence of the Molecular Structure of Polyolefins on the Damping Function in Shear. *Macromolecules*.

13. Laun, H. M., Description of the non-linear shear behaviour of a low density polyethylene melt by means of an experimentally determined strain dependent memory function. *Rheologica Acta* **1978,** 17, (1), 1-15.

14. Chodankar, C. D.; Schieber, J. D.; Venerus, D. C., Evaluation of rheological constitutive equations for branched polymers in step shear strain flows. *Rheologica Acta* **2003,** 42, 123-131.

15. Jiang, B.; Kamerkar, P. A.; Keffer, D. J.; Edwards, B. J., Using Multiple-Mode Models for Fitting and Predicting the Rheological Properties of Polymer Melts. II. Single and Double Step-Strain Flows. *Journal of Applied Polymer Science* **2007,** 105, 2884-2892.

16. Vega, D. A.; Milner, S. T., Shear Damping Function Measurements for Branched Polymers. *Journal of Polymer Science: Part B: Polymer Physics* **2007,** 45, 3113-3136.

17. Venerus, D. C.; Kahvand, H., Normal stress relaxation in reversing double-step strain flows. *Journal of Rheology* **1994,** 38, (5), 1297-1315.

18. Gevgilili, H.; Kalyon, D. M., Step strain flow: Wall slip effects and other error sources. *Journal of Rheology* **2001,** 45, (2), 467-475.

19. Venerus, D. C., A critical evaluation of step strain flows of entangled linear polymer liquids. *Journal of Rheology* **2005,** 49, (1), 277-295.

20. Doerpinghaus, P. J. Flow Behavior of Sparsely Branched Metallocene-Catalyzed Polyethylenes. Virginia Tech, Blacksburg, 2002.

21. Doerpinghaus, P. J.; Baird, D. G., Separating the effects of sparse long-chain branching on rheology from those due to molecular weight in polyethylenes. *Journal of Rheology* **2003,** 47, (3), 717-736.

22. Flory, P. J., *Principles of Polymer Chemistry*. Cornell University Press: Ithaca, NY, 1953.

23. Zimm, B. H.; Stockmayer, W. H., *Journal of American Chemical Society* **1949,** 17.

24. Axelson, D. E.; Levy, G. C.; Mandelkern, L., *Macromolecules* **1979,** 12.

25. Janzen, J.; Colby, R. H., Diagnosing long-chain branching in polyethylenes. *Journal of Molecular Structure* **1999,** 485-486, 569-584.

26. Macosko, C. W., *Rheology Principles, Measurements, and Applications*. Wiley-VCH, Inc.: 1994.

27. Elbirli, B.; Shaw, M. T., Time Constants from Shear Viscosity Data. *Journal of Rheology* **1978,** 22, (5), 561-570.

Table 4.1. Molecular characteristics including M_w, M_w/M_n, and LCB/10,000 C for the LDPE and the LLDPE-based series of polyethylene resins.

Polymer Resin ID	*ρ [g/cm^3]*	*M_w [g/mol]*	*M_w/M_n*	*LCB/10,000 C [[a] as determined from GPC-LALLS [b] as determined from ^{13}C NMR*
Exxon Exact 3132	0.900	111,000	2.04	---
Exxon Exact 0201	0.902	88,700	2.14	0.79 [a]
Mobil NTX101	0.917	122,700	3.44	---
Equistar NA952	0.919	235,500	17.1	39 [b]
Dow Affinity PL1880	0.902	115,800	2.12	0.18 [a]
Dow Affinity PL1840	0.909	87,400	2.43	0.57 [a]

Table 4.2. Pom-pom model parameters for the LDPE and the LLDPE-based series of polyethylene resins at T=150°C.

Polymer Resin ID	τ_{bi}	g_i	τ_{si}	q_i
Exxon Exact 3132	0.01	488,000	0.002	1
	0.1	83,800	0.02	1
	1	2,280	0.2	1
	10	36.0	2	1
	100	8.61	20	1
Exxon Exact 0201	0.01	299,000	0.002	1
	0.1	49,700	0.02	1
	1	11,000	0.2	1
	10	1,790	2	4
	100	52.8	28.56	6
Mobil NTX101	0.01	149,000	0.002	1
	0.1	90,500	0.02	1
	1	6,430	0.2	1
	10	353	2	1
	100	22.5	20	1
Equistar NA952	0.01	68,800	0.002	1
	0.1	21,500	0.02	1
	1	8,290	0.2	1
	10	1,820	4.18	7
	100	181	100	12
Dow Affinity PL1880	0.01	344,000	0.002	1
	0.1	56,100	0.02	1
	1	10,600	0.2	1
	10	1,710	2	3
	100	50.2	20	3
Dow Affinity PL1840	0.01	299,000	0.002	1
	0.1	47,300	0.02	1
	1	11,300	0.2	1
	10	1,870	2	3
	100	54.2	28.57	8

Table 4.3. Time required for 95% of the desired strain to be achieved for each experimentally applied strain.

Applied Strain	*Time [s]*
0.01	0.055
0.1	0.055
1	0.055
5	0.06
7.5	0.06
10	0.065
12.5	0.065

Table 4.4. Calculated Rouse relaxation times for the LDPE and the LLDPE-based series of polyethylene resins.

Polymer Resin ID	τ_R *[s]*
Exxon Exact 3132	0.327
Exxon Exact 0201	0.548
Mobil NTX101	0.412
Equistar NA952	1.19
Dow Affinity PL1880	0.735
Dow Affinity PL1840	0.557

Table 4.5. Pom-pom model τ_s parameters determined from shear step-strain experiments for Exact 3132.

τ_{bi}	g_i	τ_{si}
0.01	488,000	0.002
0.1	83,800	0.0327
1	2,280	0.0360
10	36.0	0.0361
100	8.61	0.0364

Table 4.6. Pom-pom model τ_s parameters determined from shear step-strain experiments for NTX101.

τ_{bi}	g_i	τ_{si}
0.01	149,000	0.002
0.1	90,500	0.0276
1	6,430	0.0265
10	353	0.0377
100	22.5	0.0292

Table 4.7. Pom-pom model τ_s parameters determined from shear step-strain experiments for Affinity PL1880.

τ_{bi}	g_i	τ_{si}
0.01	344,000	0.002
0.1	56,100	0.0383
1	10,600	0.0045
10	1,710	0.0432
100	50.2	0.0428

Table 4.8. Pom-pom model τ_s parameters determined from shear step-strain experiments for Affinity PL1840.

τ_{bi}	g_i	τ_{si}
0.01	299,000	0.002
0.1	47,300	0.0332
1	11,300	0.0044
10	1,870	0.0501
100	54.2	0.5336

Table 4.9. Pom-pom model τ_s parameters determined from shear step-strain experiments for Exact 0201.

τ_{bi}	g_i	τ_{si}
0.01	299,000	0.0014
0.1	49,700	0.0375
1	11,000	0.0045
10	1,790	0.0441
100	52.8	0.5428

Table 4.10. Pom-pom model τ_s parameters determined from shear step-strain experiments for NA952.

τ_{bi}	g_i	τ_{si}
0.01	68,800	0.002
0.1	21,500	0.0218
1	8,290	0.0270
10	1,820	0.0443
100	181	0.5918

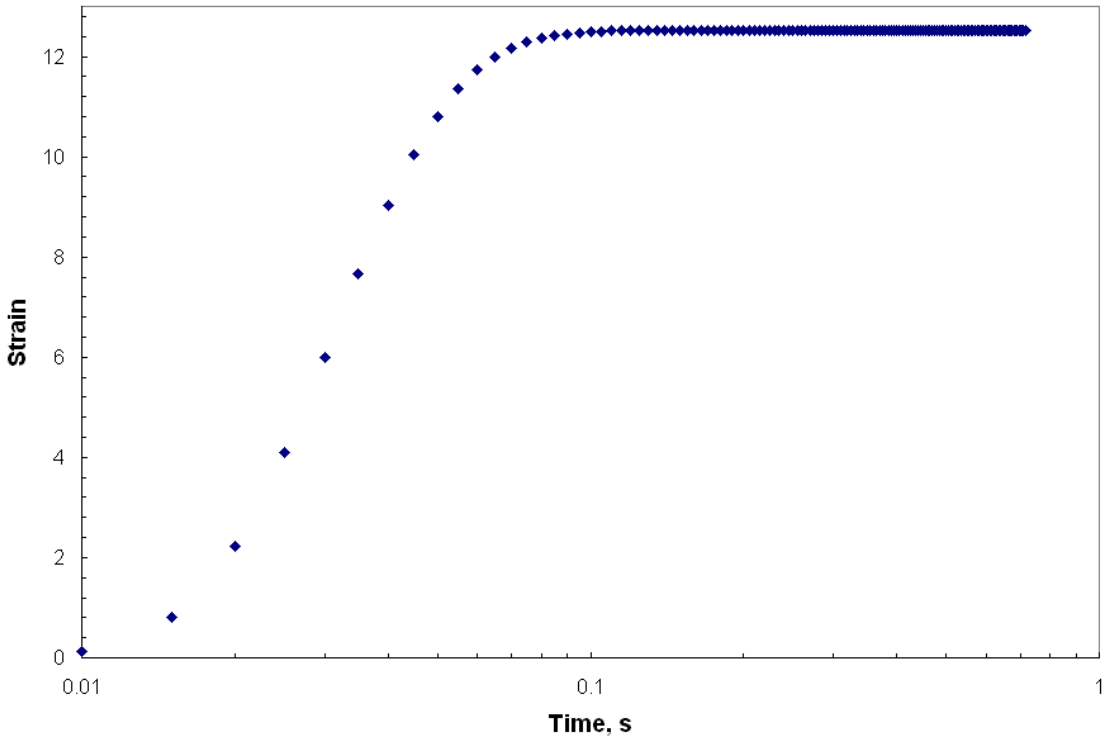

Figure 4.1. Measured strain as a function of time during a step-strain experiment for γ=12.5.

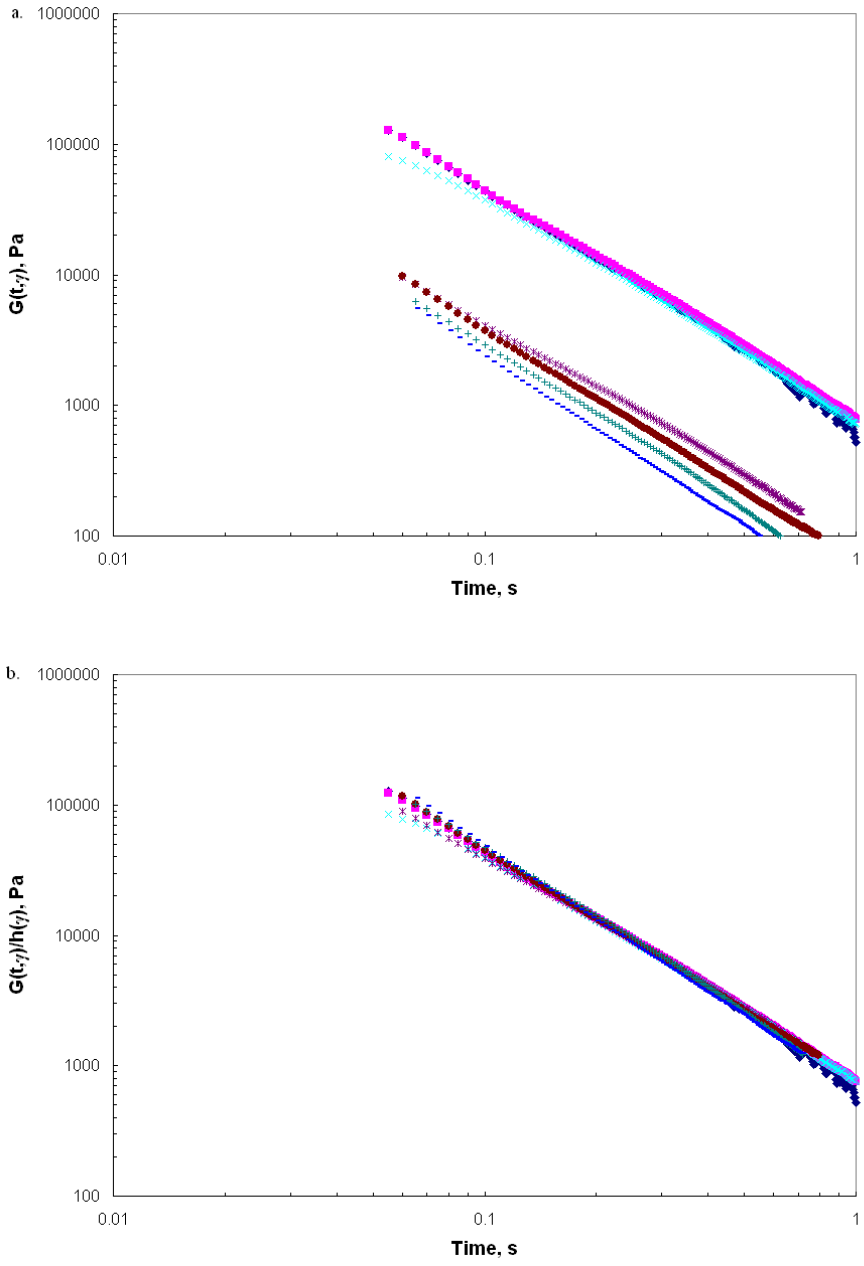

Figure 4.2. (a) G(t,γ) as a function of time at various strains ranging from 0.01-12.5 strain units for Exact 3132 at T=150°C. (b) Shifted stress relaxation moduli curves, G(t,γ)/h(γ) as a function of time for Exact 3132 subjected to the same strains. 0.01 (◆), 0.1 (■), 1.0 (X), 5.0 (*), 7.5 (●), 10.0 (+), 12.5 (-).

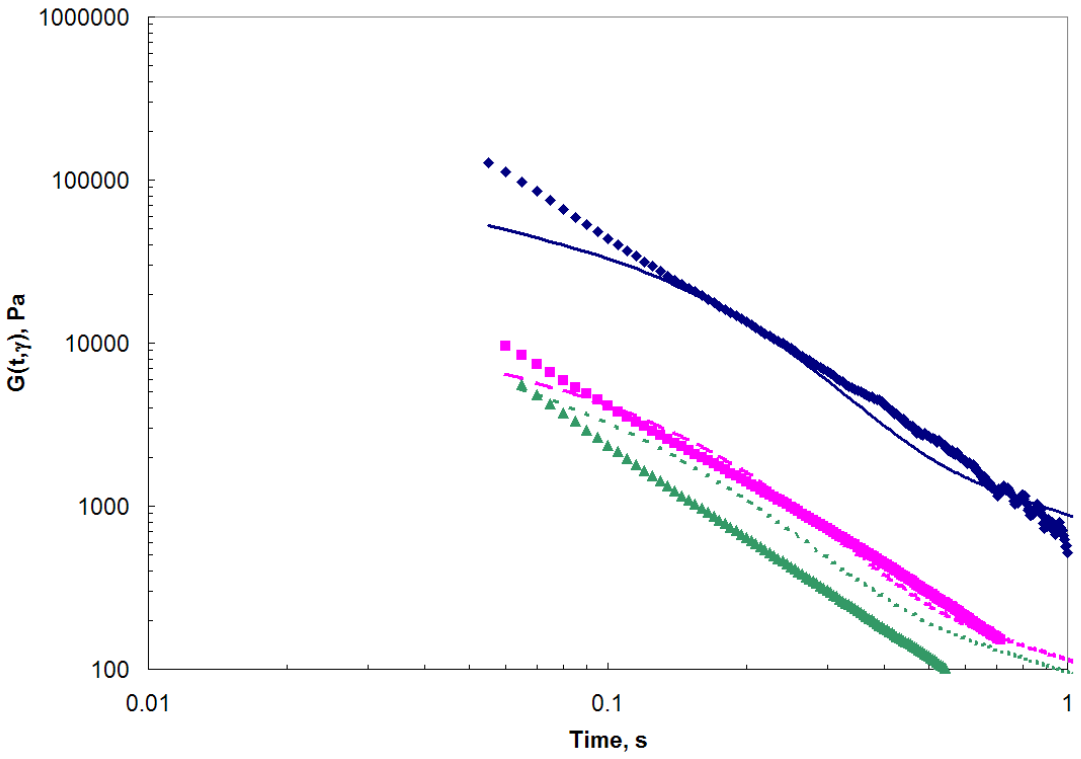

Figure 4.3. Experimental data versus pom-pom model predictions for Exact 3132 at T=150°C for strains of 0.01 [(◆) - experimental data, (——) – pom-pom prediction], 5.0 [(■) - experimental data, (— —) – pom-pom prediction], and 12.5 [(▲) - experimental data, (- - -) – pom-pom prediction].

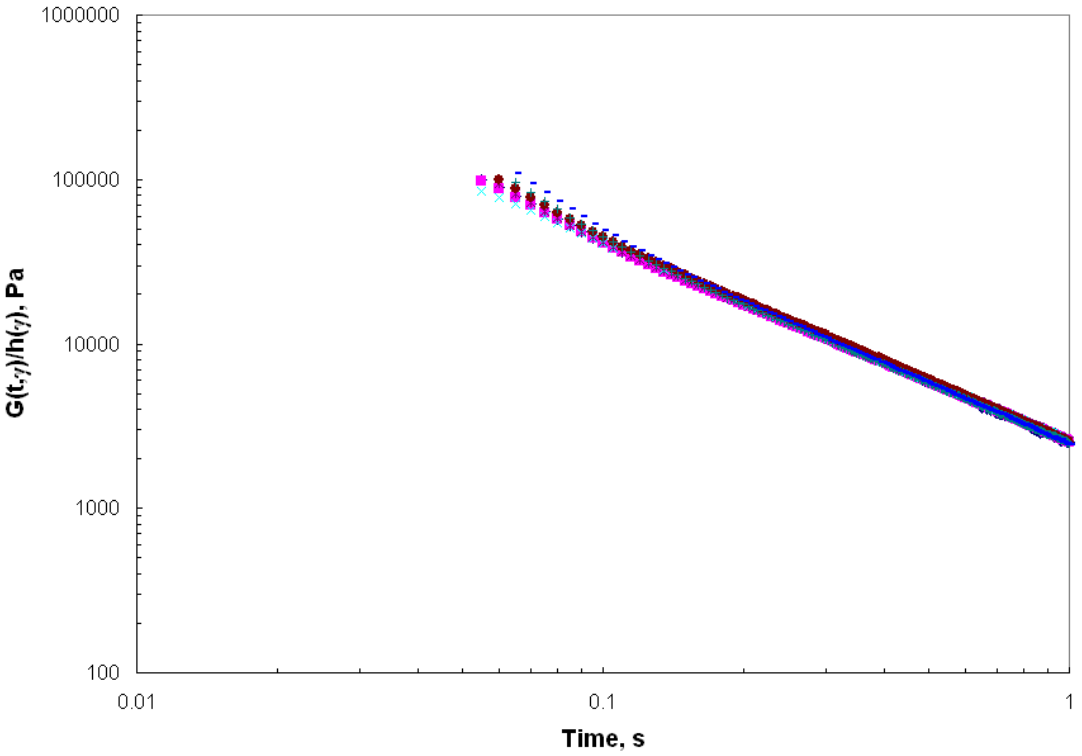

Figure 4.4. G(t,γ)/h(γ) as a function of time at various strains ranging from 0.01-12.5 strain units for NTX101 at T=150°C. 0.01 (◆), 0.1 (■), 1.0 (X), 5.0 (*), 7.5 (●), 10.0 (+), 12.5 (-).

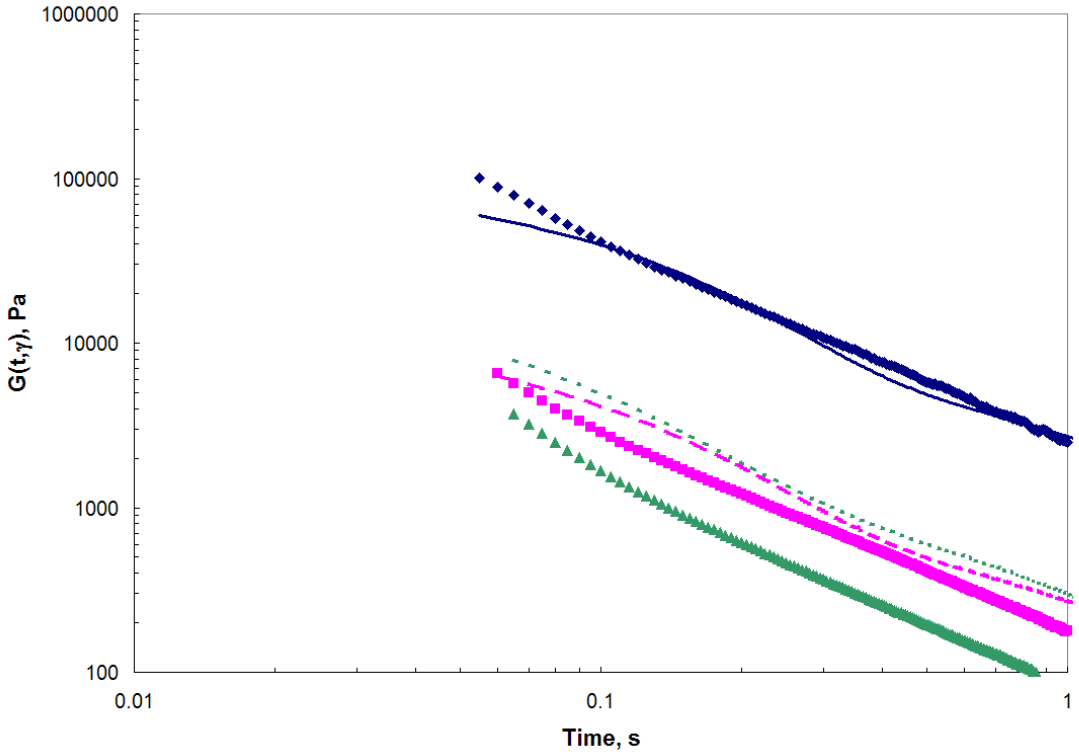

Figure 4.5. Experimental data versus pom-pom model predictions for NTX101 at T=150°C for strains of 0.01 [(◆) - experimental data, (——) – pom-pom prediction], 5.0 [(■) - experimental data, (— —) – pom-pom prediction], and 12.5 [(▲) - experimental data, (- - -) – pom-pom prediction].

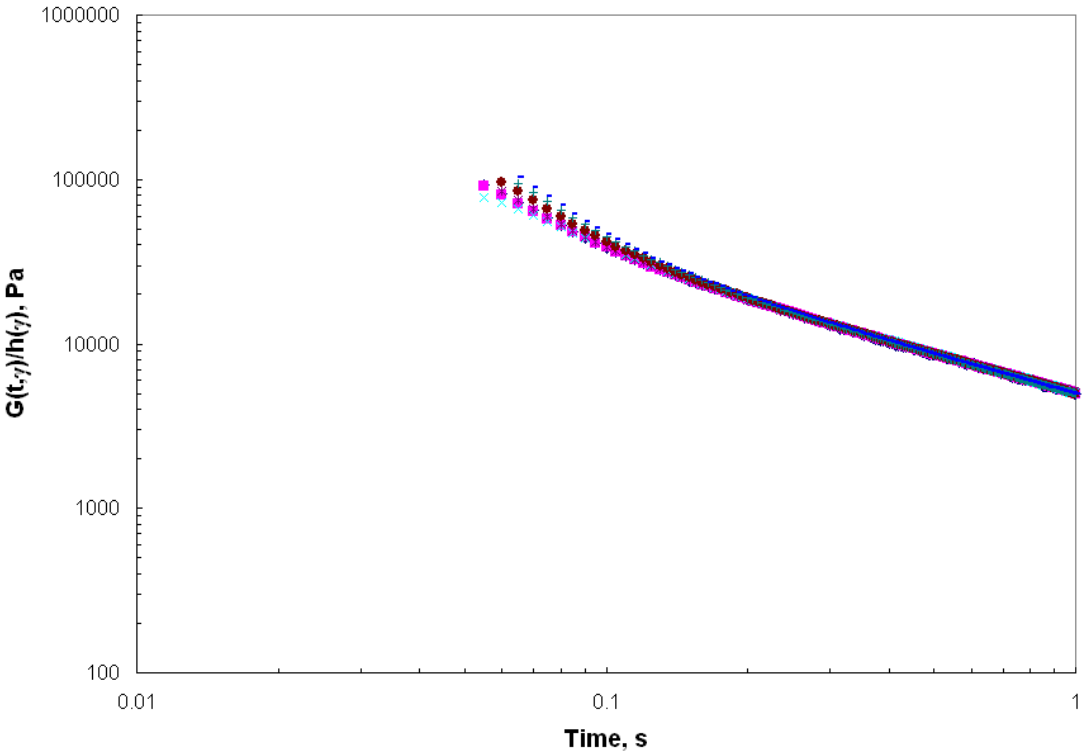

Figure 4.6. G(t,γ)/h(γ) as a function of time at various strains ranging from 0.01-12.5 strain units for Affinity PL1880 at T=150°C. 0.01 (◆), 0.1 (■), 1.0 (X), 5.0 (*), 7.5 (●), 10.0 (+), 12.5 (-).

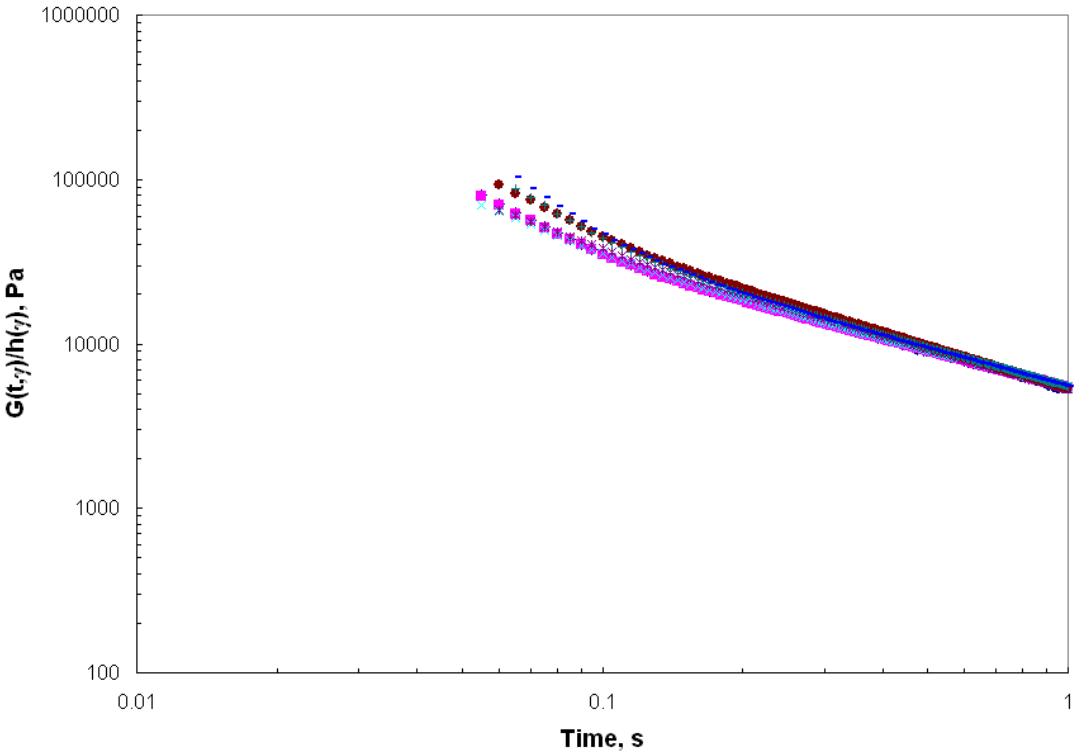

Figure 4.7. G(t,γ)/h(γ) as a function of time at various strains ranging from 0.01-12.5 strain units for Affinity PL1840 at T=150°C. 0.01 (◆), 0.1 (■), 1.0 (X), 5.0 (*), 7.5 (●), 10.0 (+), 12.5 (-).

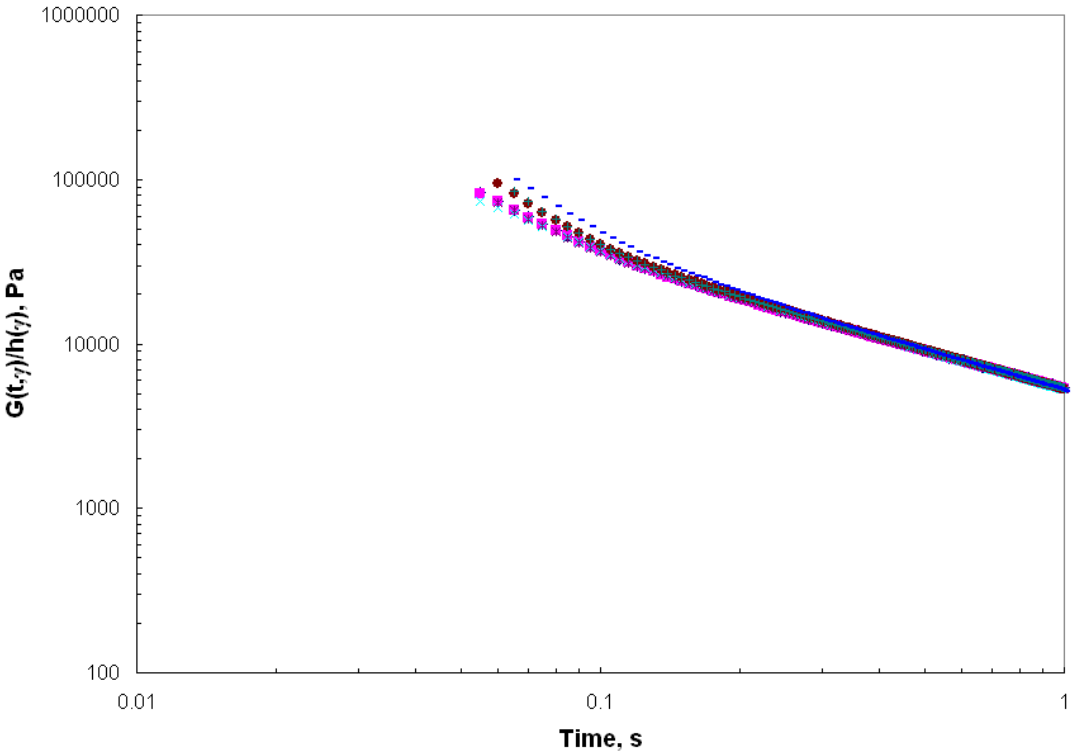

Figure 4.8. G(t,γ)/h(γ) as a function of time at various strains ranging from 0.01-12.5 strain units for Exact 0201 at T=150°C. 0.01 (◆), 0.1 (■), 1.0 (X), 5.0 (*), 7.5 (●), 10.0 (+), 12.5 (-).

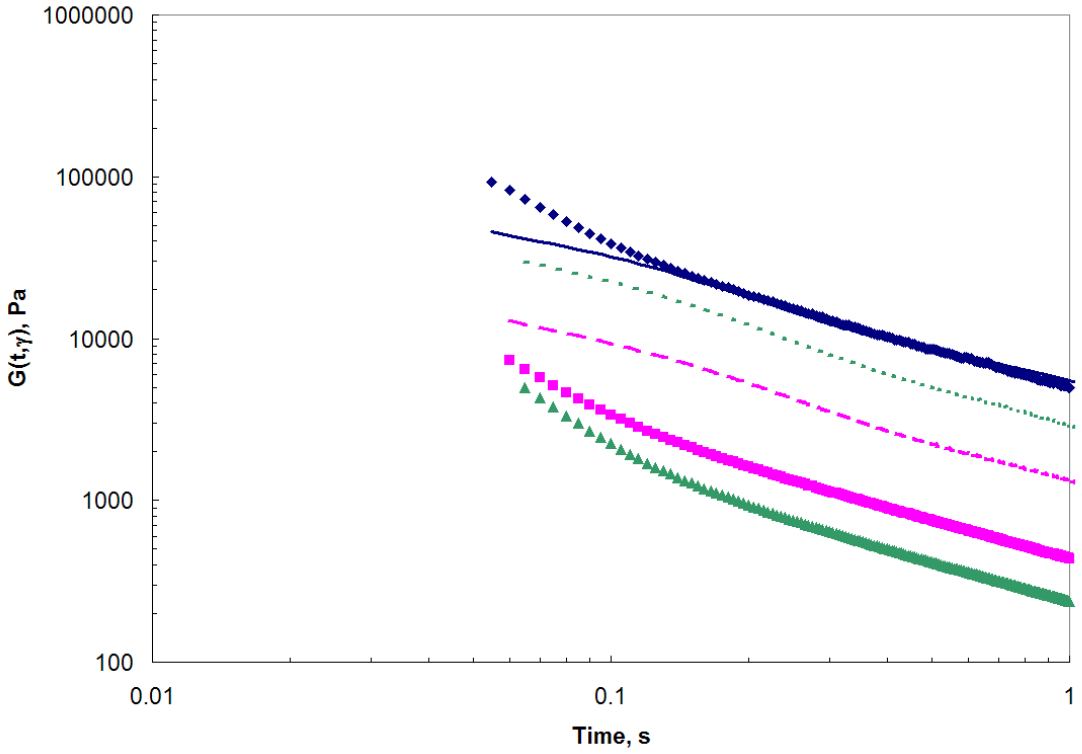

Figure 4.9. Experimental data versus pom-pom model predictions for Affinity PL1880 at T=150°C for strains of 0.01 [(◆) - experimental data, (——) – pom-pom prediction], 5.0 [(■) - experimental data, (— —) – pom-pom prediction], and 12.5 [(▲) - experimental data, (- - -) – pom-pom prediction].

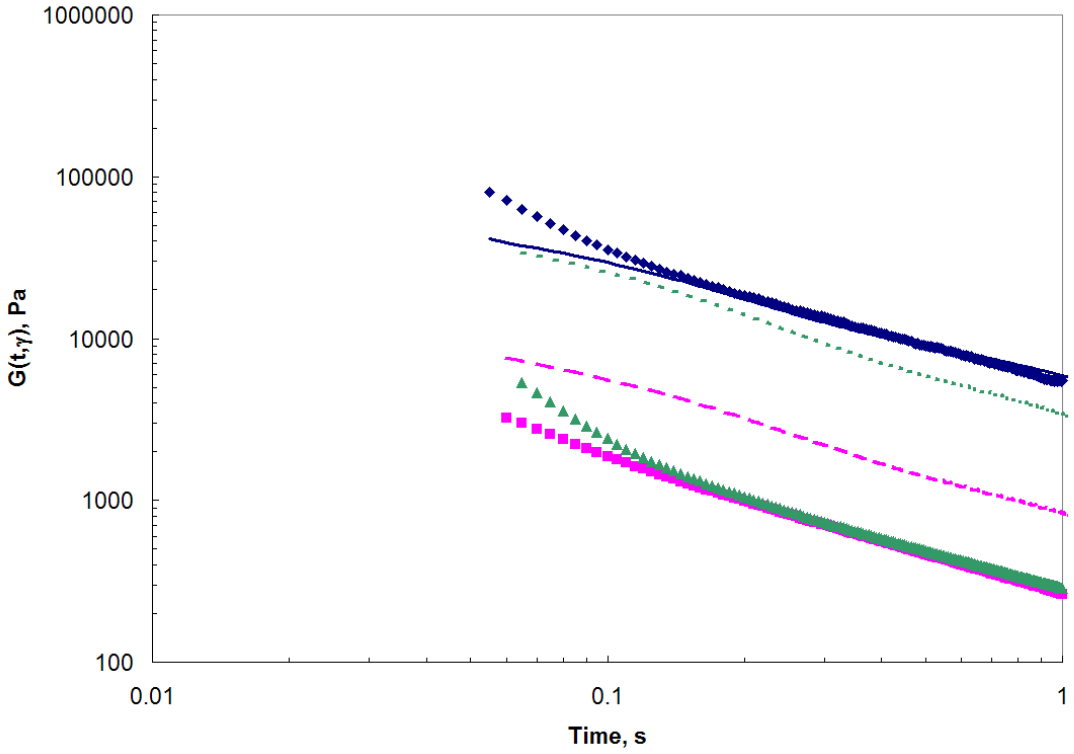

Figure 4.10. Experimental data versus pom-pom model predictions for Affinity PL1840 at T=150°C for strains of 0.01 [(◆) - experimental data, (——) – pom-pom prediction], 5.0 [(■) - experimental data, (— —) – pom-pom prediction], and 12.5 [(▲) - experimental data, (- - -) – pom-pom prediction].

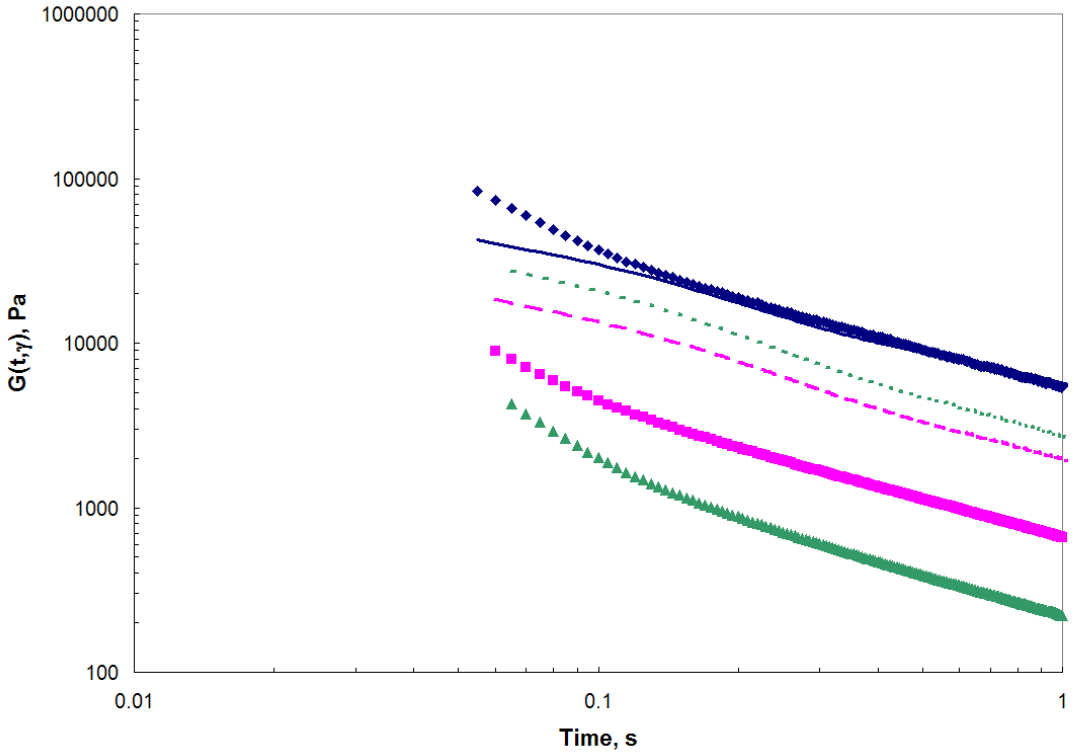

Figure 4.11. Experimental data versus pom-pom model predictions for Exact 0201 at T=150°C for strains of 0.01 [(◆) - experimental data, (——) – pom-pom prediction], 5.0 [(■) - experimental data, (— —) – pom-pom prediction], and 12.5 [(▲) - experimental data, (- - -) – pom-pom prediction].

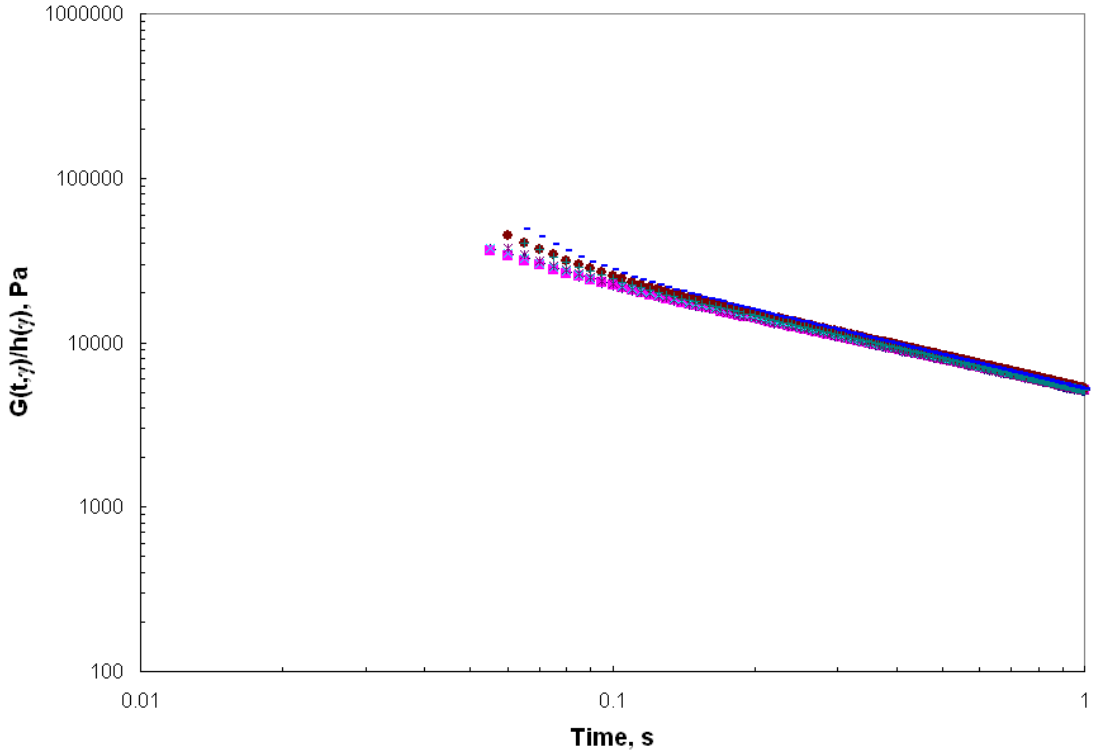

Figure 4.12. G(t,γ)/h(γ) as a function of time at various strains ranging from 0.01-12.5 strain units for NA952 at T=150°C. 0.01 (◆), 0.1 (■), 1.0 (X), 5.0 (*), 7.5 (●), 10.0 (+), 12.5 (-).

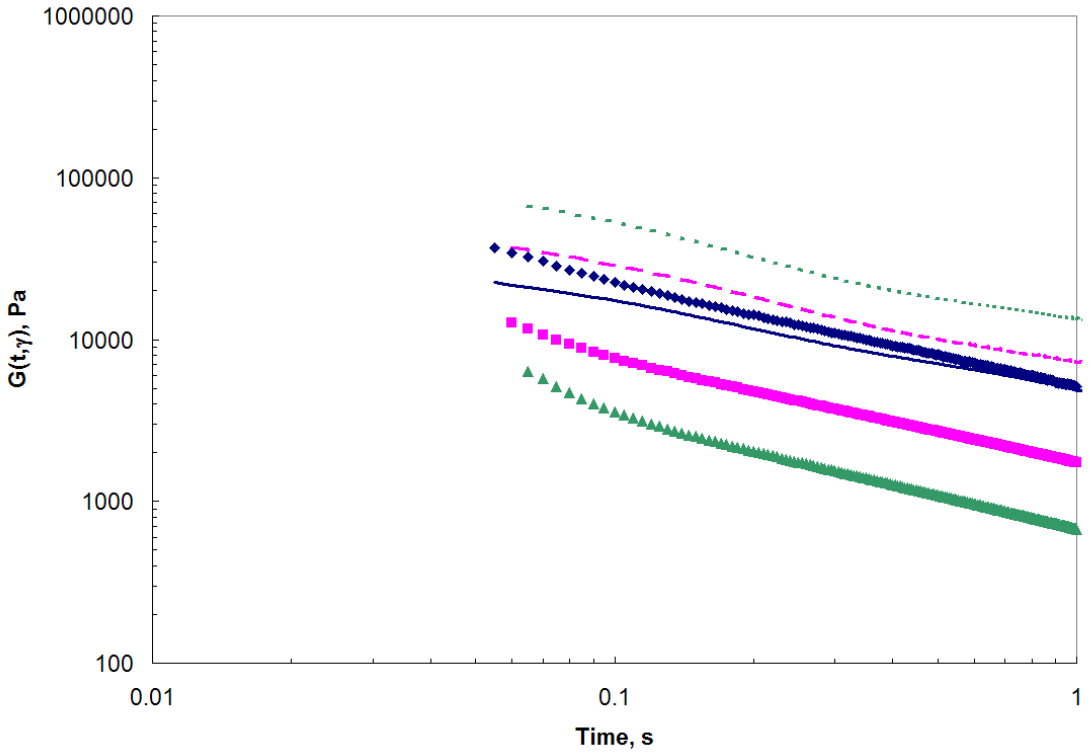

Figure 4.13. Experimental data versus pom-pom model predictions for NA952 at T=150°C for strains of 0.01 [(◆) - experimental data, (——) – pom-pom prediction], 5.0 [(■) - experimental data, (— —) – pom-pom prediction], and 12.5 [(▲) - experimental data, (- - -) – pom-pom prediction].

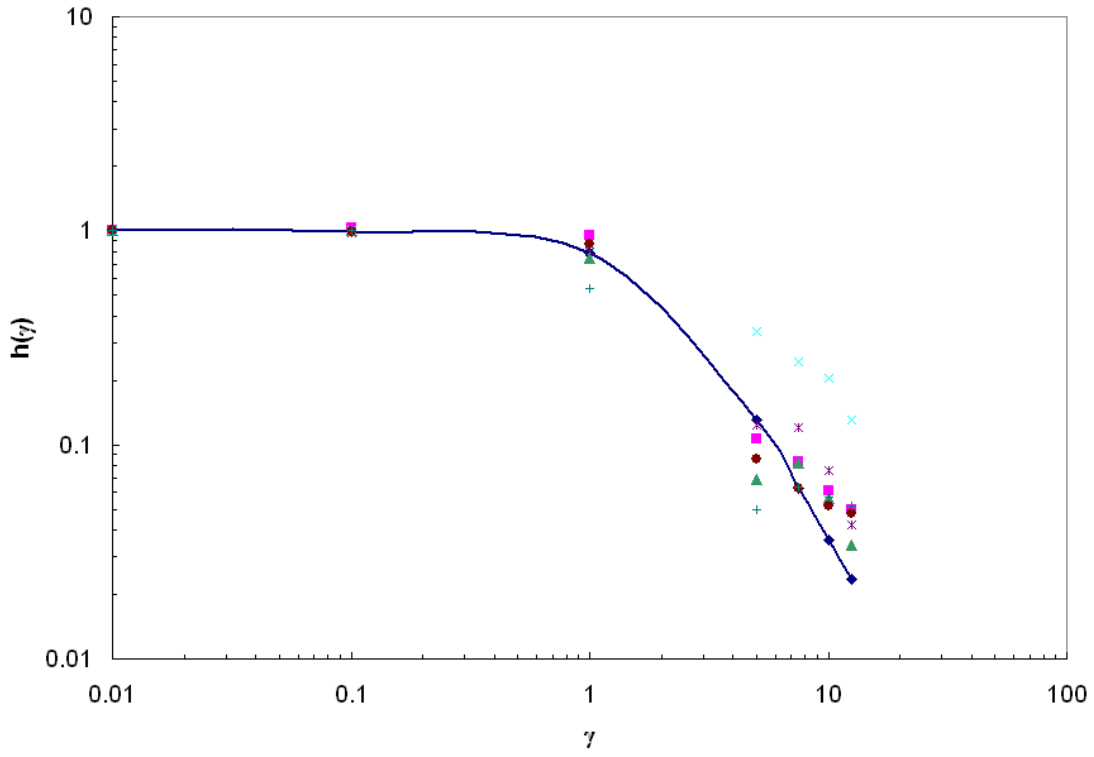

Figure 4.14. Damping function, h(γ), as a function of strain for all of the experimental PE resins compared to the Doi-Edwards approximation. Doi-Edwards approximation (◆), Exact 3132 (■), Exact 0201 (*), NTX101 (▲), NA952 (X), Affinity PL1880 (●), Affinity PL1840 (+).

5.0 Film-casting behavior for metallocene-catalyzed LLDPE resins with various degrees of sparse LCB

Preface

This chapter considers the film-casting behavior for a series of linear low density polyethylene resins with respect to their rheological characteristics, in particular strain-hardening capabilities. This chapter is organized as a manuscript for publication.

Film-casting Behavior for Metallocene-Catalyzed LLDPE Resins with Various Degrees of Sparse LCB

Seay, Christopher W.; Baird, Donald G.

Department of Chemical Engineering, Virginia Tech

Blacksburg, VA 24061

5.1 Abstract

The degree of film-width reduction or necking during film-casting is analyzed for three metallocene-catalyzed linear low density polyethylenes, LLDPE, with varying degrees of sparse long-chain branching, LCB, levels ranging in LCB content from linear to 0.57 LCB/10,000 CH_2 along with a Ziegler-Natta polymerized LLDPE and a tubular free-radical polymerized low density polyethylene, LDPE, that are used as reference materials. The primary objective of this analysis is to evaluate whether uniaxial extensional rheological characteristics, in particular strain-hardening, that are a result of LCB influence the film-necking properties. At the lowest drawdown ratio necking is observed to be reduced with increasing LCB, and thus strain-hardening characteristics. At the higher drawdown ratios it is observed that LCB no longer reduces necking and the curves merge to the results found for linear PE, except in the case of LDPE, which shows reduced necking at all drawdown ratios. Furthermore, comparisons of film necking are also made to separate the effects of molecular weight distribution, MWD, and LCB. The results indicate that both broadening the MWD and the addition of sparse LCB reduce the degree of necking observed. It is established that film necking is more significantly reduced by LCB than by broadening the MWD. Analysis of the uniaxial extensional and

dynamic shear rheology with the pom-pom constitutive model reveals that a distribution of branches along shorter relaxation time modes is important in reducing necking at higher drawdown ratios. Factors such as shear viscosity effects, extrudate swell, and non-isothermal behavior were eliminated as contributing factors because of the similar shear viscosity curves, N_1 curves, and activation energies among the sparsely LCB PE resins.

5.2 Introduction

In film-casting, typical behaviors that negatively impact the production of usable film are necking, edge-bead, and draw resonance. These behaviors are typically referred to as defects from the standpoint that they reduce the amount of usable film [1]. Necking is defined as the reduction in film width compared to the original die width that is generated as a result of drawing a film at higher velocities than it is extruded. Edge-bead represents the non-uniformity in the cross-section of a film sample, where an increase in film thickness on the edge is typically observed. Draw resonance is the only time-dependent instability, which is observed by periodic fluctuations in film width and film thickness occurring after a critical drawdown ratio is achieved.

Film-casting defects are dependent on material viscoelastic properties as well as processing conditions such as extrusion rate, drawdown ratio, and air gap length; the former of which is the primary focus of this work although some discussion is provided on the effect of drawdown ratio and extrusion rate. Differences in viscoelastic behavior become evident in molecular structural features, for example increases in LCB content increase strain-hardening characteristics [2]. Photographic evidence shown in Fig. 5.1 documents the effect of different molecular structures, which are known to have

significant differences in their extensional rheology [2], where linear and highly branched polyethylene resins are compared at identical processing conditions. The highly branched material has drastically reduced necking when compared to the linear resin.

Necking has been shown by numerous authors [3-12] to be affected by both material viscoelastic properties and processing conditions. Increasing the ability for a material to undergo strain-hardening has been shown to reduce the degree of necking observed. Groups such as Satoh et al [8], Ito et al [10], and Kajiwara et al [5] attribute the behavior to the difference in uniaxial and planar strain-hardening based on the ideas of Dobroth and Erwin [13]. Canning and Co [4] have proven the effect of strain-hardening experimentally. Differences in necking behavior for a LDPE and two LLDPE materials are observed, where LDPE exhibits strain-hardening characteristics and neither LLDPE does. LDPE exhibits less necking than either of the two LLDPE's. Canning and Co [4] also observe strain-hardening to have an affect on the dependence of necking on drawdown ratio. LDPE exhibits reductions in necking with increasing drawdown ratio whereas the two LLDPE materials exhibit increases in necking with increasing drawdown ratio. These results identify that material characteristics also play a role in final film dimensions and that necking is affected differently by processing conditions depending on the molecular structure and viscoelasticity associated with the polymer. Simulation efforts of Kim et al [3], Sakaki et al [11], and Zheng et al [12] suggest that necking is always increased by increasing drawdown ratios and air gap lengths.

Edge-bead as a function of viscoelastic behavior has only been addressed through comparison of simulation results because no experimental results making comparisons between different materials exist. The general trend in edge-bead is similar to that of

necking depending primarily on the extensional rheological characteristics. The simulation work of Kim et al [3], Silagy et al [6, 7], and Ito et al [10] indicate that increasing strain-hardening slightly increases the magnitude of edge-bead as well as the gradient, or rate at which edge-bead grows resulting in a greater area of usable film. The simulations of Kim et al [3], Sakaki et al [11], and Zheng et al [12] have shown that edge-bead is dependent on drawdown ratio and air gap length as well. Increases in drawdown ratio and air gap length are directly proportional to edge-bead growth, but the effects relating to drawdown ratio are sufficiently larger. Canning and Co [4] verify these findings experimentally for LDPE. Air gap length predominantly affects the gradient of edge-bead growth causing a noticeably slower transition to the edge-bead region at larger air gap lengths.

Draw resonance is evaluated in the work of Kim et al [3], Silagy et al [6, 7], Smith and Stolle [9], Iyengar and Co [14], and Pis-Lopez and Co [15, 16] who show that strain-hardening properties act to stabilize the process and push the critical draw ratio to higher values. They also state that both extensional-thinning and shear-thinning destabilize the process acting to enhance the draw resonance behavior. Dependence on air gap length is deduced from simulation experiments [3, 6, 7, 17]. It is determined that an optimum air gap length exists when it is equal to the width of the die.

The use of viscoelastic constitutive equations has improved the accuracy of numerical simulations of film-casting. The importance of including viscoelasticity has shown that the accuracy of the numerical work is largely a function of the constitutive equation used to represent the viscoelastic behavior of the material. The pom-pom model developed by McLeish and Larson [18] has been shown to model the rheological behavior of PE extremely well and provides the possibility of extracting information regarding molecular

structure from the model fits. The pom-pom model, therefore, may serve as an excellent link between molecular structure and rheology and could be a valuable tool in assessing the effects of LCB on film necking.

The pom-pom model is derived from the ideas of the tube model presented by Doi and Edwards [19]. Molecular constraints from entanglements in the tube model are represented by confining the polymer chain to a hypothetical tube and relaxation occurs through retraction and reptation. Retraction is described as the contraction of a chain segment after a stretch is imposed due to elasticity within the chain and occurs on faster timescales than reptation, which is chain motion within the confines of the tube constraints through a diffusive process. Extension of these concepts to branched polymers produces a model that has the potential to explain the nonlinear rheology associated with these branched materials. Backbone segments with more than one branch-point exhibit strain-hardening characteristics that are explained by the stretch component of the backbone, which has a retarded relaxation. In order to relax the stretch the branch arms must completely relax causing branch points to act as pinning points.

With limited experimental results, the effects of sparse LCB and MWD on film necking remain unclear. Experimental data of Canning and Co [4] have shown that LCB in the extreme case of LDPE can drastically reduce necking, but nothing is available documenting the significance of sparse LCB and how sparse LCB compares to broadening MWD in terms of reducing necking. Insight into these effects is possible with the set of conventional and metallocene-catalyzed resins available for this study. The conventional resins consist of a free radical polymerized LDPE and a Zieglar-Natta polymerized LLDPE, while the metallocene resins consist of linear and sparsely branched

PE resins of narrow MWD. The primary objective of this work is to determine whether subtle differences in LCB affect the rheology enough to influence film-necking properties. Also considered are the differences in contribution from LCB and broadening MWD for reducing necking behavior. Because processing is performed under identical conditions, we can focus our attention on the differences in shear and uniaxial extensional behavior observed for these polymers. To assess the molecular structure and identify correlations between structure and film-casting performance of the resins, previously made experimental rheological measurements [20] are used. Dynamic oscillatory shear measurements are reproduced using the Bird-Carreau model and uniaxial extensional viscosity growth measurements are generated using pom-pom model parameters defined by Doerpinghaus and Baird [2].

5.3 Experimental materials and methods

5.3.1 Materials

Five commercially available polyethylene resins developed for film-blowing applications were selected for this study. The series consists of three metallocene-catalyzed materials featuring different degrees of sparse LCB ranging from linear to 0.57 LCB/10,000 CH_2 along with two reference systems consisting of a LLDPE and a LDPE. This series of resins has also been characterized rheologically at a temperature of 150°C for both shear and uniaxial extensional flows [2, 20, 21]. Physical properties for this series of resins including density, melt flow index, weight-average molecular weight, MWD, and degree of LCB are tabulated in Table 5.1.

Exact 3132, Affinity PL1880, and Affinity PL1840 are all metallocene-catalyzed polyethylene resins. These materials were selected to evaluate the effect of sparse LCB

on film-casting stability properties, in particular film necking. Exact 3132 is an ethylene-hexene copolymer manufactured by ExxonMobil Chemical using EXXPOL® catalyst technology. Affinity PL1880 and Affinity PL1840 are ethylene-octene copolymers manufactured by Dow Chemical using INSITE® catalyst technology. Exact 3132 is specified as a linear metallocene-catalyzed copolymer, while Affinity PL1880 and Affinity PL1840 are identified to contain sparse LCB analytically quantified using GPC-LALLS [22, 23]. Typical of metallocene-catalyzed polyethylene resins the MWD for these materials is relatively narrow falling between 2.0 and 2.5.

The remaining two materials, NTX101 and NA952, are a conventional LLDPE and LDPE, respectively. NTX101 is an ethylene-hexene copolymer manufactured by ExxonMobil using a Zieglar-Natta gas-phase polymerization process. NA952 is an ethylene homopolymer manufactured by Equistar using a high-pressure, high-temperature tubular free-radical polymerization process. NTX101 exhibits a broader MWD of approximately 3.5 and provides a resin that allows us to assess the effects of broadening the molecular distribution on film-casting properties. NA952 was selected as a highly branched reference material providing an extreme case scenario for the addition of LCB. The level of LCB for NA952 is quantified analytically using ^{13}C NMR. A major limitation of this technique is its inability to distinguish branches longer than six carbon atoms in length [24, 25], and therefore, the value of LCB includes LCB as well as short-chain branches.

5.3.2 Film-casting

Film-casting experiments were performed by vertically extruding each polyethylene resin directly through an adjustable thickness slit die with a coathanger manifold. The

width of the slit die was 101.6 mm and its thickness was 0.57 mm. The extruded films were then drawn by a chill roll positioned 141.4 mm away from the die. This distance was selected to enhance film stability and due to limitations of the current equipment setup. A non-isothermal process is expected because of the distance from the die exit to the chill roll. The polymer was extruded at a temperature of 150°C.

Processing conditions generated in the film-casting process such as shear rate, strain, and extension rate were calculated as described in the subsequent text. Every polyethylene resin was extruded at a velocity in the z-direction of 0.8217 mm/s. NA952 was also extruded at a velocity in the z-direction of 3.148 mm/s to evaluate the effect of suppressing the shear viscosity for this particular material. Mass flow rate was monitored to maintain a constant throughput for the extruder. The initial velocity was calculated using the density of each polyethylene resin and the cross-sectional area at the die exit. The apparent shear rate was determined using the exit velocity from the die and parallel plate flow following Eq. 1.

$$\dot{\gamma} = \frac{6Q}{WH^2} \tag{1}$$

For each polyethylene resin drawdown ratios of 5, 10, 15, and 20 were applied resulting in strains ranging from 1.61-3.00. Strains, γ, were calculated by multiplying the residence time of the polymer melt between the extrusion die and the chill roll by the extension rate. Residence time of the polymer melt was determined according to Eq. 2 where the average velocity was calculated by taking the integral of the velocity in the z-direction over the total length of the material.

$$\gamma = \frac{\dot{\varepsilon}L}{v_{zAVG}} = \frac{\dot{\varepsilon}L}{\frac{\int_0^L v_{z0}(DR)^{\frac{z}{L}}dz}{\int_0^L zdz}} = \frac{\dot{\varepsilon}L}{v_{z0}\left[\frac{DR}{\ln(DR)} - \frac{1}{\ln(DR)}\right]} \quad (2)$$

Extension rates are defined by subtracting the speed at which the polymer is extruded from the speed at which the polymer is taken up and dividing over the distance in which the polymer is subjected to stretching. Applied extension rates range from 0.024-0.13 1/s and are tabulated in Table 5.2 for each polyethylene resin at all applied drawdown ratios.

Digital photographs were taken of the films after steady state conditions were reached for each extrusion speed and drawdown ratio scenario. Measurements of the evolution of film-width were then made using a pixel counting software to determine film-widths at various positions in the z-direction. Analysis of the photographs allowed for measurements to the nearest one hundredth of a millimeter. Combined error for the experimental casting and measurements falls within +/-3%.

5.4 Results

5.4.1 Film-casting

Necking is evaluated by analyzing the film half-width as a function of the distance from the die until contact with the chill roll occurs. The film-casting experimental results are shown in Figs. 5.2 through 5.5 with each figure corresponding to the four applied drawdown ratios in order of increasing drawdown ratio. Observations from previous experimental and simulated film-casting studies suggest that increases in the strain-hardening properties of the material will lead to a reduction in necking [3-10]. Therefore, it is expected that materials will experience less necking as the level of LCB and strain-hardening behavior increase.

The results in Fig. 5.2 include film-width profiles for the five polyethylene resins at a constant drawdown ratio of 5. As expected the degree of necking is inversely proportional to the LCB content with the greatest overall film-widths occurring in the densely branched NA952. The two sparsely branched resins, Affinity PL1880 and Affinity PL1840, experience a much higher degree of necking than NA952, but not the degree of necking observed in the two linear materials, Exact 3132 and NTX101. The sparsely branched resins also separate according to the slight differences observed in their respective LCB content with Affinity PL1840, the more highly branched of the two, experiencing less necking than Affinity PL1880. It is also observed that the two linear materials exhibit the highest degree of necking, and that breadth in MWD impacts the final film dimensions in a similar fashion to LCB. However, the effect of broadening the MWD shows less influence than LCB on reducing the degree of necking.

The results in Figs. 5.3 through 5.5 include film-width profiles for the five polyethylene resins at constant drawdown ratios of 10, 15, and 20, respectively. As increasing drawdown ratios are applied the film-width profiles become indistinguishable with the exception of NA952. The trend of reduced necking with increasing LCB is still observed, but the results now fall within the experimental error.

5.5 Discussion

We are interested in evaluating film necking results with respect to the rheological behavior of the five PE resins. A thorough analysis of the shear and uniaxial extensional rheological features has previously been discussed for this series of resins [2, 20, 21]. The data is reproduced using relevant relationships of the Bird-Carreau and pom-pom models,

respectively. The effects of decreasing shear viscosity, primary normal stress differences, and strain-hardening with LCB are considered.

5.5.1 Rheological analysis

5.5.1.1 Shear rheology

Dynamic oscillatory measurements for the five PE resins at a temperature of 150°C have previously been reported [20]. The experimental data was fit to the Bird-Carreau model [26] using non-linear least squares regression. The Bird-Carreau parameters are tabulated in Table 5.3 and the resulting shear viscosity flow curves are presented in Fig. 5.6 covering the frequency range of 0.1-100 1/s. The Cox-Merz relationship has been shown [21] to be valid for these materials. In the Bird-Carreau model, λ represents the onset of shear-thinning and n represents the degree of shear-thinning. Both the sparsely and highly branched PE resins exhibit an earlier onset of shear-thinning than either of the two linear PE resins, while the degree of shear-thinning is similar for all of the PE resins with the one exception of the LDPE. The zero-shear viscosity is the lowest fro the two linear PE resins followed by the LDPE and the highest for the two sparsely LCB PE resins. Our primary focus is to establish any significant difference in processing behavior as a result of slightly different degrees of sparse LCB. In most cases, operating conditions are identical and only the absolute value for the shear viscosity at the operating conditions is considered. It is possible to envision that more pronounced shear-thinning characteristics would result in a greater dependence of necking on extrusion rate.

Under operating conditions of γ=8.62 1/s, the shear viscosities for all of the materials are similar with the exception of NA952 and to some extent Exact 3132. The NA952 melt is well into its shear-thinning regime and it exhibits a lower viscosity. Exact 3132

demonstrates the weakest shear-thinning characteristics as well as an onset of shear-thinning that occurs at higher shear rates as shown by a small λ and large n in the Bird-Carreau parameters. Evaluation of the dependence of film necking on the apparent shear rate at the die wall was conducted for NA952 by comparing the results at 8.62 1/s with those at 33.05 1/s as presented in Fig. 5.7. Film half-width profiles are shown for NA952 produced at the two respective shear rates. The drawdown ratio was adjusted to maintain constant extension rates between the two comparative films. Film necking for NA952 has already been shown to be independent of drawdown ratio, making the comparison at γ=8.62 1/s and γ=33.05 1/s reasonable. The NA952 film produced at higher shear rates and therefore lower shear viscosities suffered more necking than the film produced at lower shear rates and therefore higher shear viscosities. These results would suggest that if films were cast of NA952 at the same shear viscosity of the other polyethylene resins, they would experience a lower degree of necking. NA952, however, exhibits the least necking of any of the tested PE resins confirming that the suppressed values of shear viscosity at γ=8.62 1/s for NA952 are not the cause for its reduced necking.

Extrudate swell is another factor that could influence the necking results; in particular polymer materials with higher degrees of extrudate swell may exhibit more necking.. The magnitude of extrudate swell has been shown to correlate to increases in the primary normal stress difference, N_1 [27]. N_1 is approximated using Laun's approximation [26] shown in Eq. 4 and plotted as a function of shear rate for the series of polyethylene resins in Fig. 5.8.

$$N_1 = 2G'\left[1+\left(\frac{G'}{G''}\right)^2\right]^{0.7} \qquad (4)$$

At a shear rate of 8.62 1/s, N_1 is nearly identical for all of the tested resins. These results suggest that extrudate swell N_1 should be similar for all of the tested resins and, therefore, should not be a factor in the differences observed in film necking for these PE resins.

5.5.1.2 Extensional rheology

Transient extensional growth measurements at a temperature of 150°C for this series of polyethylene resins have previously been made [20]. Rates examined were 0.01, 0.1, and 1 1/s. The results were then fit with a multi-mode pom-pom model following the methods of Inkson et al [28] and Blackwell et al [29]. The parameters found by Doerpinghaus and Baird [2] and shown in Table 5.4 were used to generate extensional viscosity growth curves under the film-casting experimental operating conditions. These curves are presented in Figs. 5.9 through 5.12 for each applied drawdown ratio and reveal the strain-hardening properties for the PE resins.

The pom-pom model is a constitutive relationship that we are using as a characterization tool to link the extensional rheology to molecular architectural features. Four unknown parameters at each mode exist: g, which is the individual contribution to the plateau modulus; τ_b, which is the characteristic relaxation time associated with the backbone orientation; τ_s, which is the characteristic relaxation time associated with the stretch; and q, which is the number of branch arms. The key conclusions from Doerpinhaus and Baird [2] are that the branching arms all appear on the longest τ_b for metallocene-catalyzed sparsely LCB PE resins, which indicates that the majority of the chains in these systems are linear. Alternatively, LDPE experiences a distribution of branches among multiple backbone relaxation times.

Extensional viscosity growth curves are indicative of the strain-hardening behavior a material possesses. Strain-hardening in extension is defined as the deviation from the linear viscoelastic behavior. In Figs. 5.9 through 5.12 the extensional viscosity is plotted as a function of time. At all drawdown ratios the strain-hardening regime is reached. It is also observed that strain-hardening behavior increases with the degree of LCB present in each respective resin. The highly strain-hardening resins exhibit higher q_i values or number of branch arms when analyzed with the pom-pom model.

The film-width profiles show that the degree of necking is inversely proportional to the degree of branching. Therefore, the degree of necking is inversely proportional to the degree of strain-hardening as well. The discussions presented by Dobroth and Erwin [13] analyze the final film dimensions with respect to the differences in planar and uniaxial extensional viscosities. Whether a film undergoes planar or uniaxial deformation is material dependent and is observed in the degree of necking. Reduced necking as seen in the LDPE is more reminiscent of planar extension, while samples that experience enhanced necking like the linear PE resins more closely resemble uniaxial extension. Regardless, the ability of a material to strain-harden, which is a direct result of the molecular structure of the polymer chains enhances the ability for that material to suffer less necking during film-casting of polymer melts.

The sparsely LCB PE resins as well as the linear PE resins are comprised of mainly linear polymer chains. Conversely, for the densely branched LDPE resin practically every chain has some branching associated with it. This is indicated by the distribution of q_i among multiple τ_{bi} for the LDPE and q_i occurring on only one τ_{bi} for the sparsely LCB PE resins. As drawdown ratios are increased, and, therefore, extension rates are

increased, film-width profiles for the sparsely-branched PE resins are collapsing towards the linear resins behavior as a consequence of linear chains dominating the processing behavior. Film-width profiles for NA952 remain relatively unchanged regardless of drawdown ratio, whereas with all of the other PE resins necking is largely a function of drawdown ratio. These results suggest that in terms of molecular structure to minimize the degree of necking, LCB should be distributed among more polymer backbone segments. Sparse LCB reduces the degree of necking, but only when the branched chains are active. To reduce necking at all extension rates q_i must be distributed among all τ_{bi}'s.

5.5.2 Non-isothermal behavior

In the case of slow line speeds, frost lines were observed before the film made contact with the chill roll resulting in a non-isothermal process. A non-isothermal process raises concern in large part to the increase in viscosity observed during cooling, which resembles strain-hardening behavior [30]. Activation energy is reflective of a material's viscosity dependence on temperature. Dynamic oscillatory measurements at temperatures of 150°C and 190°C have previously been made [20]. Activation energies for each polyethylene resin were calculated by obtaining a shift factor from zero-shear viscosities found by fitting viscosity data with the Bird-Carreau model at 150°C and 190°C and are presented in Table 5.5. Higher activation energies indicate a larger dependence of viscosity on temperature. The activation energies differ slightly with NA952 having the largest and NTX101 the smallest. The remaining three materials have similar activation energies with $\Delta H/R \sim 4500$ K. Differences in film-width profiles are ruled out due to the non-isothermal nature of the process on the context that differences are still observed between these three materials that have similar activation energies.

5.6 Conclusions

Film necking for five commercially available PE resins appears to be influenced by molecular structure and the resulting rheological behavior. The lowest drawdown ratio, and therefore lowest extension rate, provided the most obvious separation distinguishing the necking on the order of LCB despite only slight differences in the degree of LCB. As drawdown ratios were increased the film profiles merge with the exception of LDPE, indicating that linear chains are dominating the processing behavior. Sparsely LCB systems more comparable in structure to LDPE with branches present on a spectrum of backbone segments may provide stabilization across a broader range of extension rates. Increasing MWD reduced necking as well, but fails to offer the same degree of reduced necking.

Other processing factors that could potentially affect the film-casting response such as shear-thinning behavior, extrudate swell, and non-isothermal testing conditions were eliminated in effort to evaluate strictly the effect of extensional rheological behavior. All materials exhibit similar flow curves under shear deformation. Differences are observed in the zero-shear viscosity and both the onset and degree of shear-thinning, but under experimental conditions shear viscosities are similar. Die swell is predicted using N_1 as an indicator. N_1 values for all tested materials are similar, thus nullifying the argument that die swell has an appreciable effect. Non-isothermal behavior is also observed. Based on activation energies, however, is not considered due the relatively similar viscosity dependence on temperature. The Dow resins exhibit nearly identical activation energies, yet separate in film necking consistent with LCB.

5.7 Acknowledgements

This research is a collaborative effort for the World Wide Network of Materials – UK Leeds and is supported financially by the National Science Foundation DMR-052198. Gratitude is given as well to Dow Chemical Company, ExxonMobil Chemical Company, and Equistar Chemical Company for supplying their respective PE materials.

5.8 References

1. Sollogoub, C.; Demay, Y.; Agassant, J. F., Non-isothermal viscoelastic numerical model of the cast-film process. *Journal of Non-Newtonian Fluid Mechanics* **2006,** 138, 76-86.

2. Doerpinghaus, P. J.; Baird, D. G., Assessing the Branching Architecture of Sparsely Branched Metallocene-Catalyzed Polyethylenes Using the Pompom Constitutive Model. *Macromolecules* **2002,** 35, (27), 10087-10095.

3. Kim, J. M.; Lee, J. S.; Shin, D. M.; Jung, H. W.; Hyun, J. C., Transient solutions of the dynamics of film casting process using 2-D viscoelastic model. *Journal of Non-Newtonian Fluid Mechanics* **2005,** 132, 53-60.

4. Canning, K.; Co, A., Edge Effects in Film Casting of Molten Polymers. *Journal of Plastic Film & Sheeting* **2000,** 16, 188-203.

5. Kajiwara, T.; Yamamura, M.; Asahina, T., Relationship between Neck-in Phenomena and Rheological Properties in Film Casting. *Nihon Reoroji Gakkaishi* **2006,** 34, (2), 97-103.

6. Silagy, D.; Demay, Y.; Agassant, J. F., Study of the Stability of the Film Casting Process. *Polymer Engineering and Science* **1996,** 36, (21), 2614-2625.

7. Silagy, D.; Demay, Y.; Agassant, J. F., Stationary and stability analysis of the film casting process. *Journal of Non-Newtonian Fluid Mechanics* **1998,** 79, 563-583.

8. Satoh, N.; Tomiyama, H.; Kajiwara, T., Viscoelastic Simulation of Film Casting Process for a Polymer Melt. *Polymer Engineering and Science* **2001,** 41, (9), 1564-1579.

9. Smith, S.; Stolle, D., Numerical Simulation of Film Casting Using an Updated Lagrangian Finite Element Algorithm. *Polymer Engineering and Science* **2003,** 43, (5), 1105-1122.

10. Ito, H.; Doi, M.; Isaki, T.; Takeo, M., A Model of Neck-in Phenomenon in Film Casting Process. *Journal of the Society of Rheology, Japan* **2003,** 31, (3), 157-163.

11. Sakaki, K.; Katsumoto, R.; Kajiwara, T.; Funatsu, K., Three-Dimensional Flow Simulation of a Film-Casting Process. *Polymer Engineering and Science* **1996,** 36, (13), 1821-1831.

12. Zheng, H.; Yu, W.; Zhou, C.; Zhang, H., Three-Dimensional Simulation of the Non-Isothermal Cast Film Process of Polymer Melts. *Journal of Polymer Research* **2006,** 13, 433-440.

13. Dobroth, T.; Erwin, L., Causes of edge beads in cast films. *Polymer Engineering and Science* **1986,** 26, (7), 462-467.

14. Iyengar, V. R.; Co, A., Film Casting of a Modified Giesekus Fluid: Stability Analysis. *Chemical Engineering Science* **1996,** 51, (9), 1417-1430.

15. Pis-Lopez, M. E.; Co, A., Multilayer film casting of modified Giesekus fluids Part 1. Steady-state analysis. *Journal of Non-Newtonian Fluid Mechanics* **1996,** 66, 71-93.

16. Pis-Lopez, M. E.; Co, A., Multilayer film casting of modified Giesekus fluids Part 2. Linear stability analysis. *Journal of Non-Newtonian Fluid Mechanics* **1996,** 66, 95-114.

17. Lee, J. S.; Jung, H. W.; Song, H.-S.; Lee, K.-Y.; Hyun, J. C., Kinematic waves and draw resonance in film casting process. *Journal of Non-Newtonian Fluid Mechanics* **2001,** 101, 43-54.

18. McLeish, T. C. B.; Larson, R. G., Molecular constitutive equations for a class of branched polymers: The pom-pom polymer. *Journal of Rheology* **1998,** 42, (1), 81-110.

19. Doi, M.; Edwards, S. F., *The Theory of Polymer Dynamics*. Oxford University Press: 1988.

20. Doerpinghaus, P. J. Flow Behavior of Sparsely Branched Metallocene-Catalyzed Polyethylenes. Virginia Tech, Blacksburg, 2002.

21. Doerpinghaus, P. J.; Baird, D. G., Separating the effects of sparse long-chain branching on rheology from those due to molecular weight in polyethylenes. *Journal of Rheology* **2003,** 47, (3), 717-736.

22. Flory, P. J., *Principles of Polymer Chemistry*. Cornell University Press: Ithaca, NY, 1953.

23. Zimm, B. H.; Stockmayer, W. H., *Journal of American Chemical Society* **1949,** 17.

24. Axelson, D. E.; Levy, G. C.; Mandelkern, L., *Macromolecules* **1979,** 12.

25. Janzen, J.; Colby, R. H., Diagnosing long-chain branching in polyethylenes. *Journal of Molecular Structure* **1999,** 485-486, 569-584.

26. Bird, R. B.; Armstrong, R. C.; Hassager, O., *Dynamics of Polymer Liquids: Fluid Mechanics*. 2 ed.; Wiley Interscience: New York, 1987; Vol. 1.

27. Tanner, R. I., Theory of Die Swell. *Journal of Polymer Science* **1970,** A, (8).

28. Inkson, N. J.; McLeish, T. C. B.; Harlen, O. G.; Groves, D. J., Predicting low density polyethylene melt rheology in elongational and shear flows with "pom-pom" constitutive equations. *Journal of Rheology* **1999,** 43, (4), 873-896.

29. Blackwell, R. J.; McLeish, T. C. B.; Harlen, O. G., Molecular drag-strain coupling in branched polymer melts. *Journal of Rheology* **2000,** 44, (1), 121-136.

30. Minoshima, W.; White, J. L., Instability phenomena in tubular film, and melt spinning of rheologically characterized high density, low density and linear low density polyethylenes. *Journal of Non-Newtonian Fluid Mechanics* **1986,** 19, (3), 275-302.

Table 5.1. Molecular characteristics including ρ, MFI, M_w, M_w/M_n, and LCB/10,000 C for the LDPE and the LLDPE-based series of polyethylene resins.

Polymer Resin ID	*ρ [g/cm^3]*	*MFI [dg/min]*	*M_w [g/mol]*	*M_w/M_n*	*LCB/10,000 C [[a] as determined from GPC-LALLS [b] as determined from ^{13}C NMR]*
Exxon Exact 3132	0.900	1.2	111,000	2.04	---
Mobil NTX101	0.917	0.9	122,700	3.44	---
Equistar NA952	0.919	2.0	235,500	17.1	39 [b]
Dow Affinity PL1880	0.902	1.0	115,800	2.12	0.18 [a]
Dow Affinity PL1840	0.909	1.0	87,400	2.43	0.57 [a]

Table 5.2. Operating extensional parameters for the LDPE and the LLDPE-based series of polyethylene resins including material extension rates at DR = 5, 10, 15, and 20 and the corresponding true strains achieved for each DR at T=150°C.

Polymer Resin ID	DR = 5 Strain = 1.61	DR = 10 Strain = 2.30	DR = 15 Strain = 2.71	DR = 20 Strain = 3.00
	ε [1/s]	ε [1/s]	ε [1/s]	ε [1/s]
Exxon Exact 3132	0.024	0.052	0.081	0.11
Mobil NTX101	0.037	0.066	0.082	0.11
Equistar NA952	0.050	0.075	0.081	0.11
Dow Affinity PL1880	0.044	0.075	0.12	0.13
Dow Affinity PL1840	0.054	0.079	0.10	0.13

Table 5.3. Pom-pom model parameters for the LDPE and the LLDPE-based series of polyethylene resins at T=150°C as taken from Doerpinghaus and Baird [2].

Polymer Resin ID	τ_{bi}	g_i	τ_{si}	q_i
Exxon Exact 3132	0.01	488,000	0.001	1
	0.1	83,800	0.01	1
	1	2,280	0.1	1
	10	36.0	1	1
	100	8.61	10	1
Mobil NTX101	0.01	149,000	0.001	1
	0.1	90,500	0.01	1
	1	6,430	0.1	1
	10	353	1	1
	100	22.5	10	1
Equistar NA952	0.01	60,700	0.00333	1
	0.1	22,800	0.0333	1
	1	7,900	0.333	1
	10	1,880	4	7
	100	110	76.9	12
	1000	5.2	1000	20
Dow Affinity PL1880	0.01	208,000	0.001	1
	0.1	55,000	0.01	1
	1	9,880	0.1	1
	10	2,010	1	1
	100	63.5	12.5	7
Dow Affinity PL1840	0.01	246,000	0.001	1
	0.1	49,000	0.01	1
	1	10,600	0.1	1
	10	2,020	1	1
	100	76.1	25	10

Table 5.4. Parameters in the Bird-Carreau model for the LDPE and the LLDPE-based series of polyethylene resins at T=150°C.

Polymer Resin ID	η_0 *[Pa-s]*	λ *[s]*	*n*
Exxon Exact 3132	15,326	0.33	0.64
Mobil NTX101	17,813	1.62	0.68
Equistar NA952	26,869	9.61	0.51
Dow Affinity PL1880	33,084	9.74	0.66
Dow Affinity PL1840	33,480	9.43	0.63

Table 5.5. Activation energies, ΔH/R, for the LDPE and the LLDPE-based series of polyethylene resins.

Polymer Resin ID	*η_0, T=150°C [Pa-s]*	*η_0, T=190°C [Pa-s]*	*ΔH/R [K]*
Exxon Exact 3132	15,326	6,636	4,101.4
Mobil NTX101	17,813	9,152	3,262.8
Equistar NA952	26,869	8,896	5,416.0
Dow Affinity PL1880	33,084	13,123	4,530.5
Dow Affinity PL1840	33,480	12,948	4,654.6

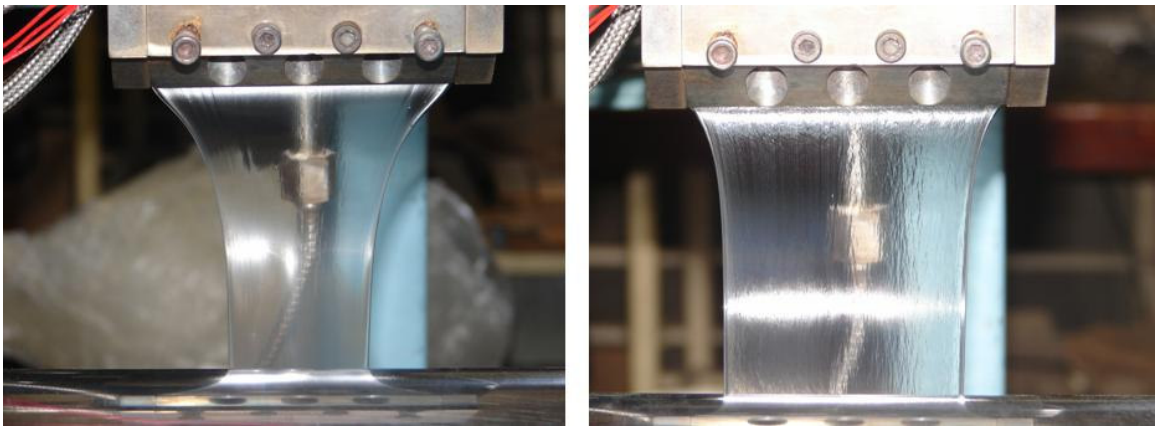

Figure 5.1. Photograph depicting the drastic differences in film dimensions under the same experimental conditions for materials with different molecular topologies. Experimental results for our linear metallocene-catalyzed polyethylene (Exact 3132) on the left and for our highly branched, high MWD control polyethylene (NA952) on the right. The materials were extruded corresponding to a shear rate of 1.33 1/s and taken up at a drawdown ratio of 10 at T=150°C.

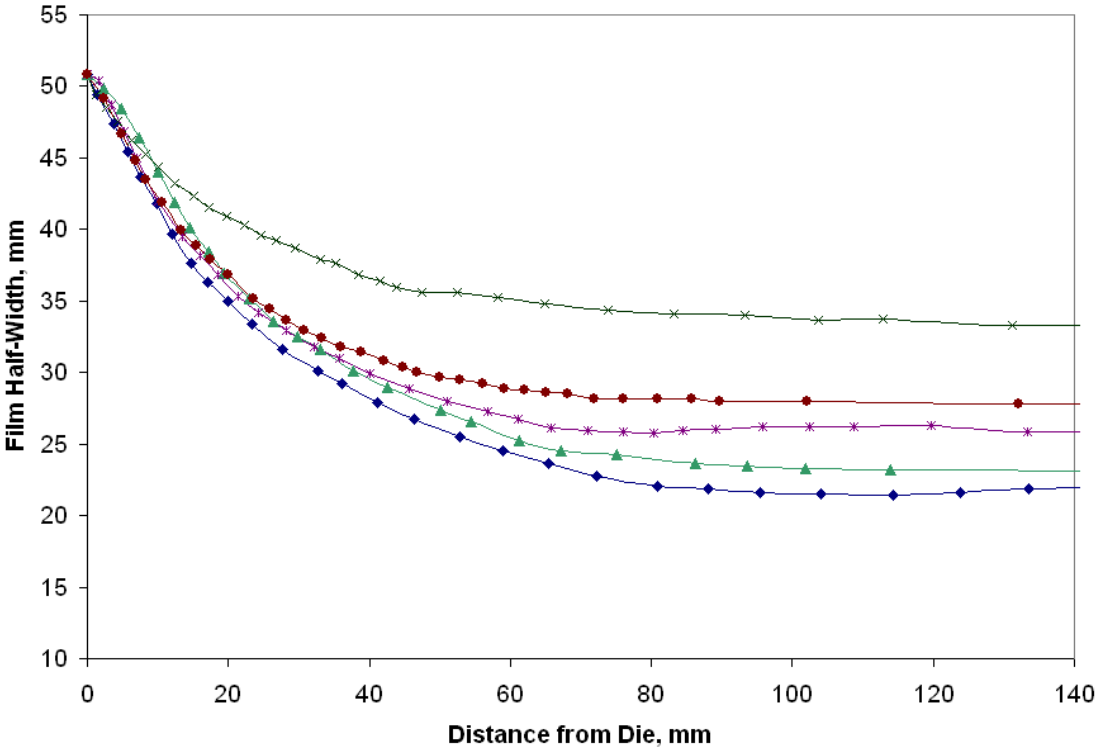

Figure 5.2. Film half-width profile for the LDPE and the LLDPE-based series of polyethylene resins at a DR=5, true strain of 1.61, and T=150°C. The corresponding shear rate is 8.62 1/s and the extension rates are defined in Table 5.2. Exact 3132 (◆), NTX101 (▲), NA952 (X), Affinity PL1880 (*), and Affinity PL1840 (●).

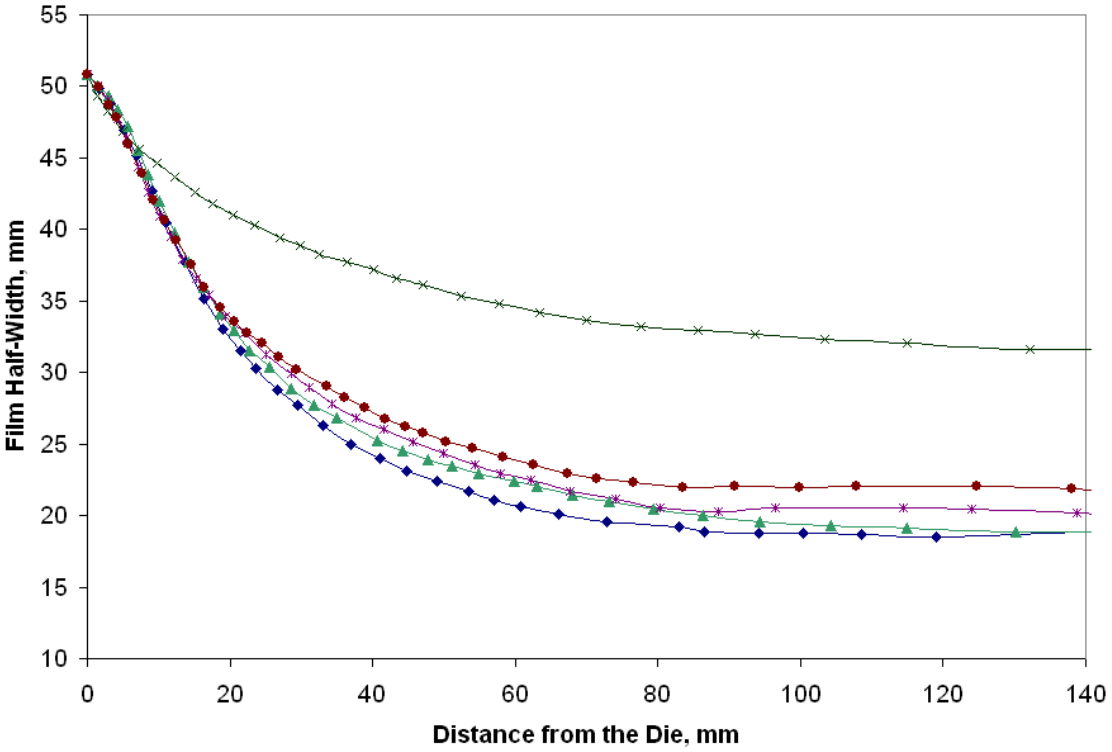

Figure 5.3. Film half-width profile for the LDPE and the LLDPE-based series of polyethylene resins at a DR=10, true strain of 2.30, and T=150°C. The corresponding shear rate is 8.62 1/s and the extension rates are defined in Table 5.2. Exact 3132 (◆), NTX101 (▲), NA952 (X), Affinity PL1880 (*), and Affinity PL1840 (●).

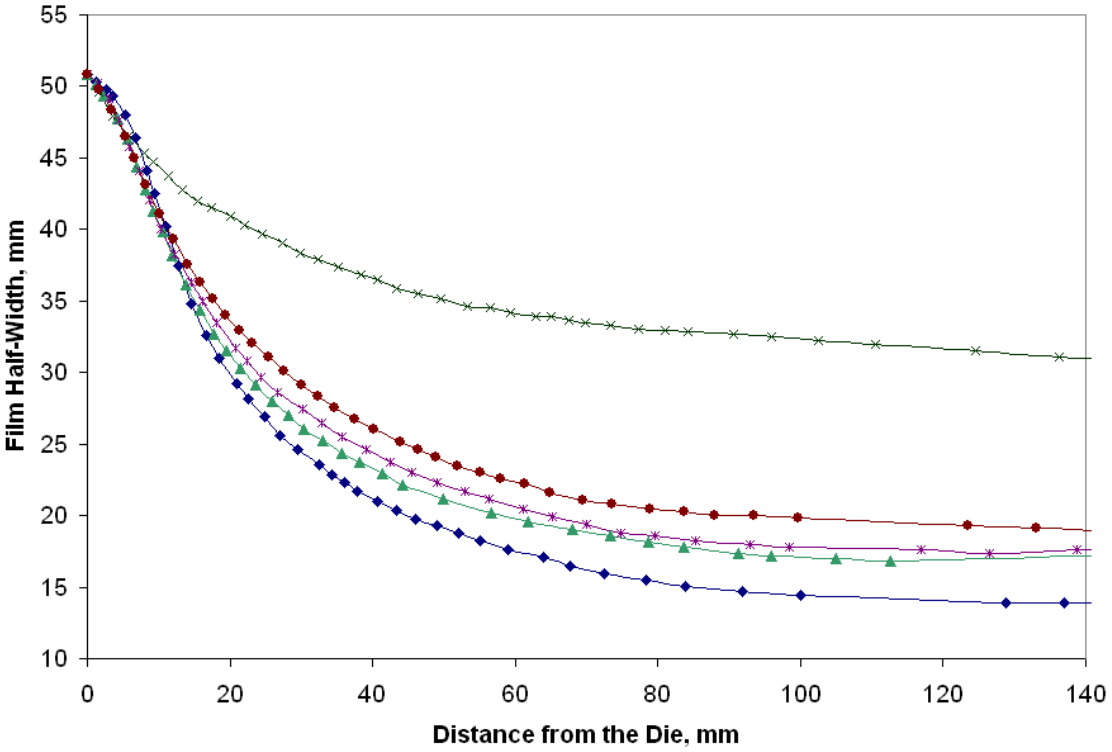

Figure 5.4. Film half-width profile for the LDPE and the LLDPE-based series of polyethylene resins at a DR=15, true strain of 2.71, and T=150°C. The corresponding shear rate is 8.62 1/s and the extension rates are defined in Table 5.2. Exact 3132 (◆), NTX101 (▲), NA952 (X), Affinity PL1880 (*), and Affinity PL1840 (●).

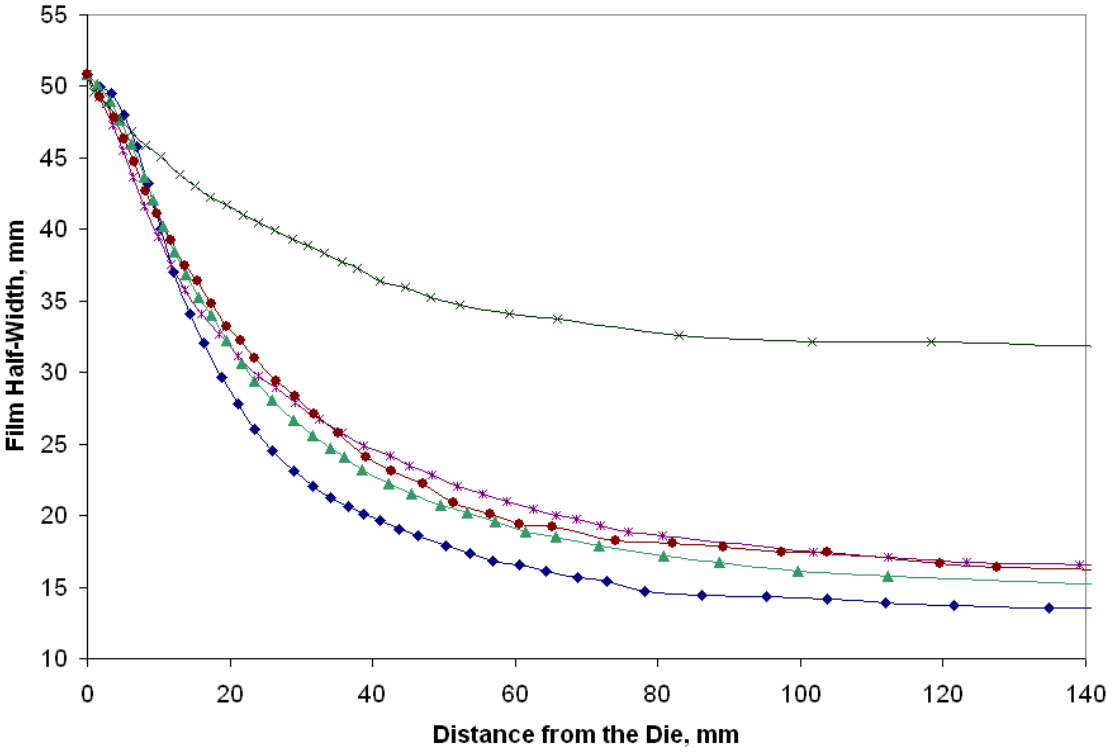

Figure 5.5. Film half-width profile for the LDPE and the LLDPE-based series of polyethylene resins at a DR=20, true strain of 3.00, and T=150°C. The corresponding shear rate is 8.62 1/s and the extension rates are defined in Table 5.2. Exact 3132 (◆), NTX101 (▲), NA952 (X), Affinity PL1880 (*), and Affinity PL1840 (●).

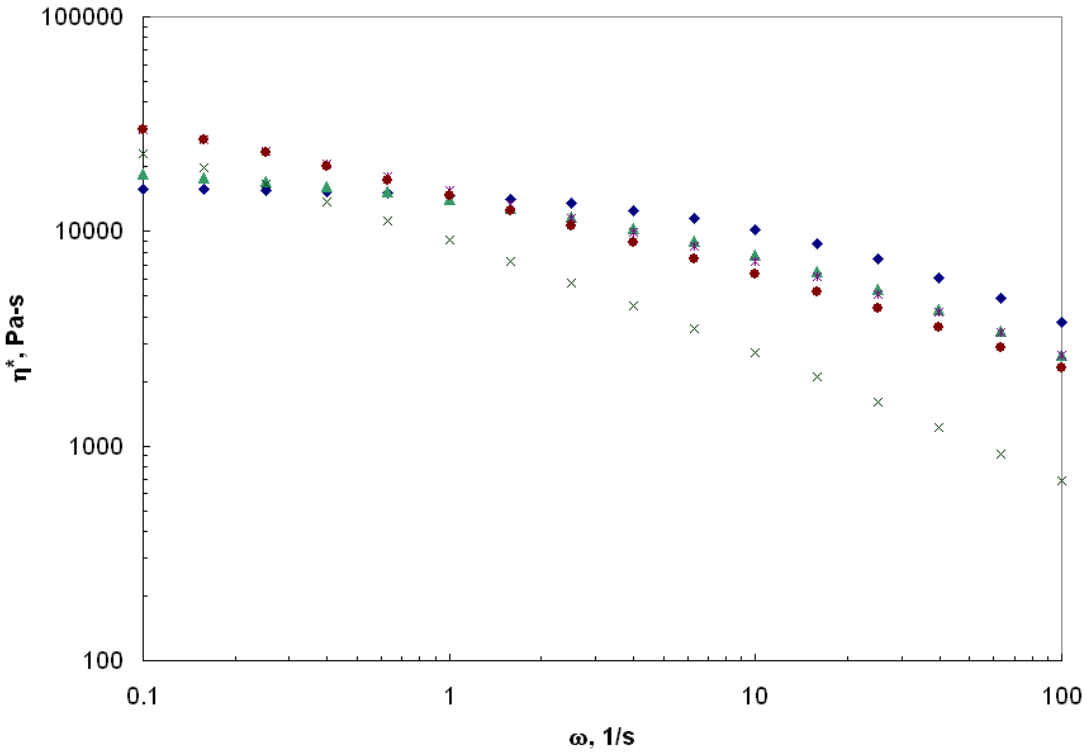

Figure 5.6. Complex viscosity as a function of frequency for the LDPE and the LLDPE-based PE's at T=150°C. Exact 3132 (◆), NTX101 (▲), NA952 (X), Affinity PL1880 (*), and Affinity PL1840 (●).

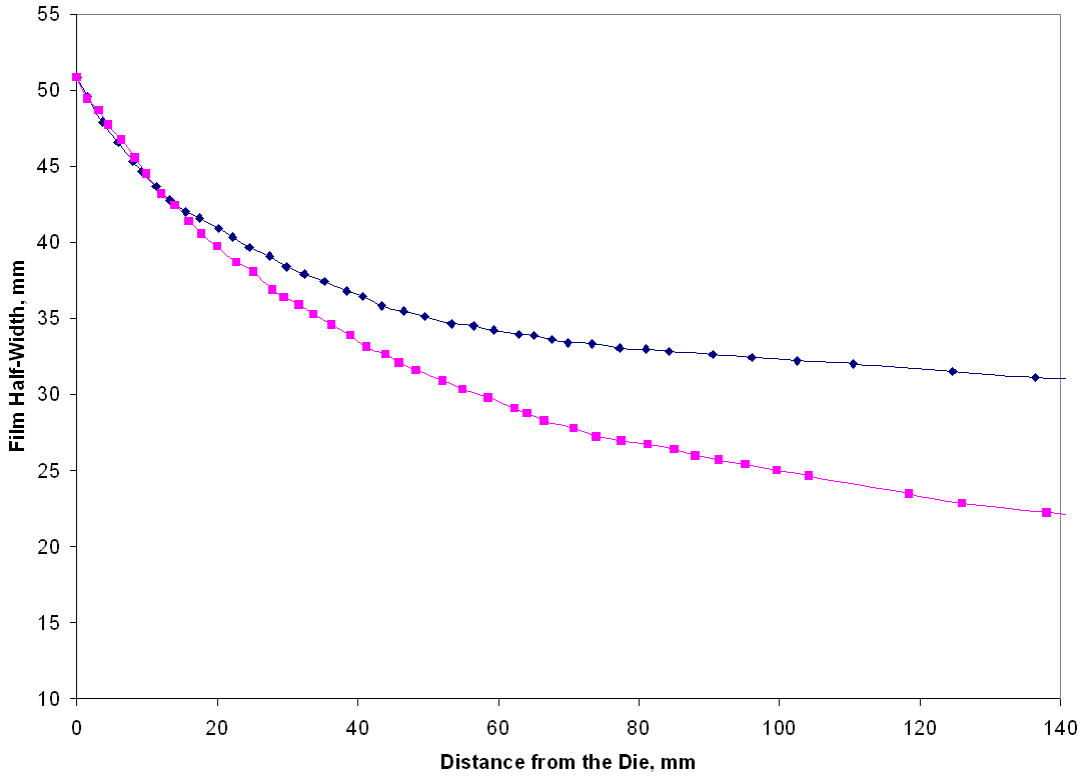

Figure 5.7. Film half-width profile for NA952 at two different shear rates and similar extension rates at T=150°C. (◆) – NA952 at γ= 8.62, DR=15, and ε=0.081, (■) – NA952 at γ=33.05, DR=5, and ε=0.089.

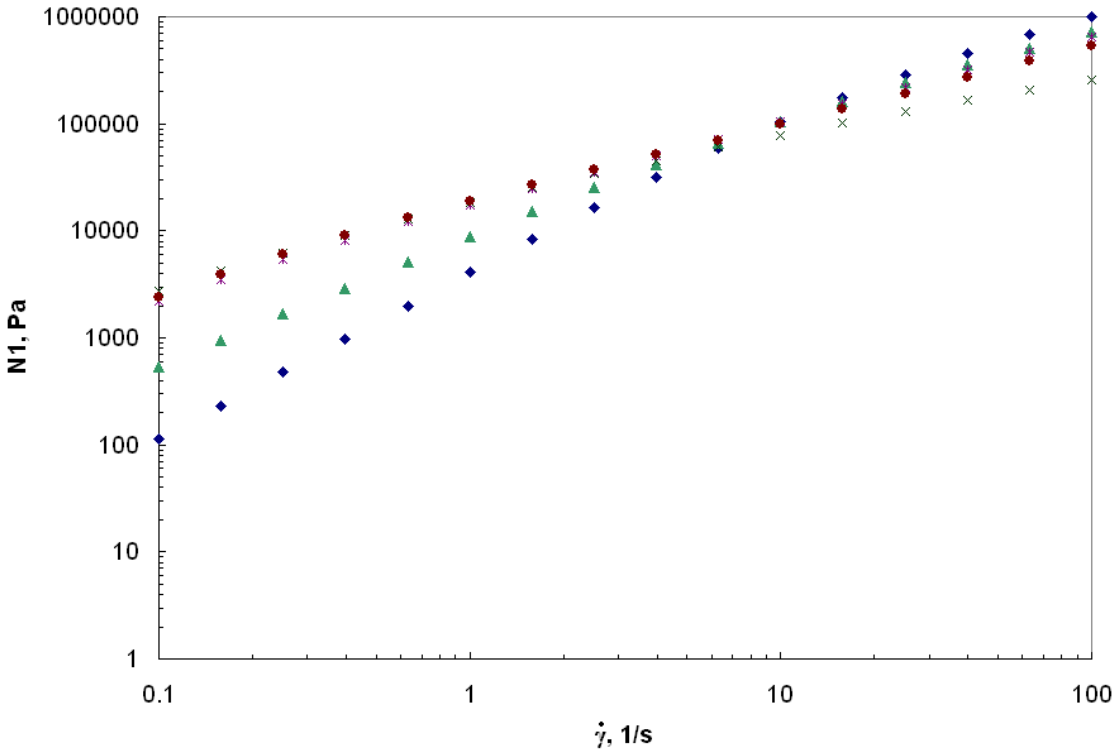

Figure 5.8. Primary normal stress difference estimates using Laun's approximation as a function of shear rate for the LDPE and the LLDPE-based PE's at T=150°C. Exact 3132 (◆), NTX101 (▲), NA952 (X), Affinity PL1880 (*), and Affinity PL1840 (●).

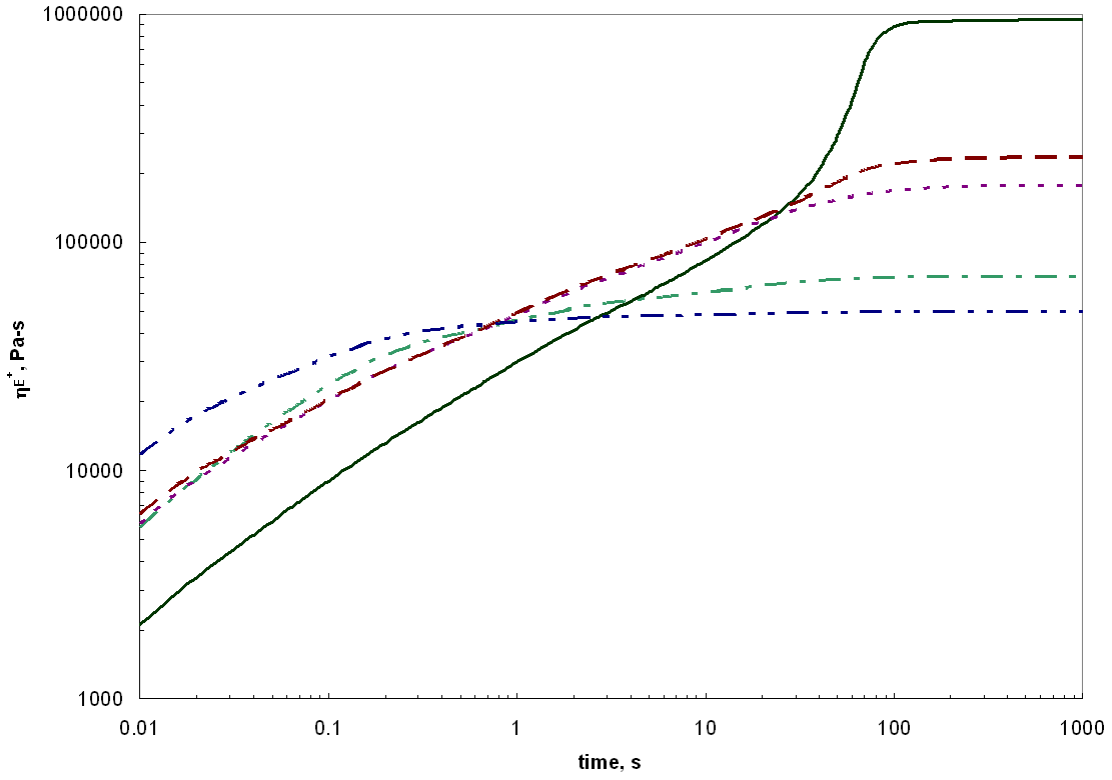

Figure 5.9. Extensional viscosity growth curves for the LDPE and the LLDPE-based series of polyethylene resins at a DR=5, true strain of 1.61, and T=150°C predicted using previously determined pom-pom model parameters shown in Table 5.3 [2] and the operating extension rates defined in Table 5.2. Exact 3132 (— - - —), NTX101 (— - —), NA952 (——), Affinity PL1880 (- - -), and Affinity PL1840 (— —).

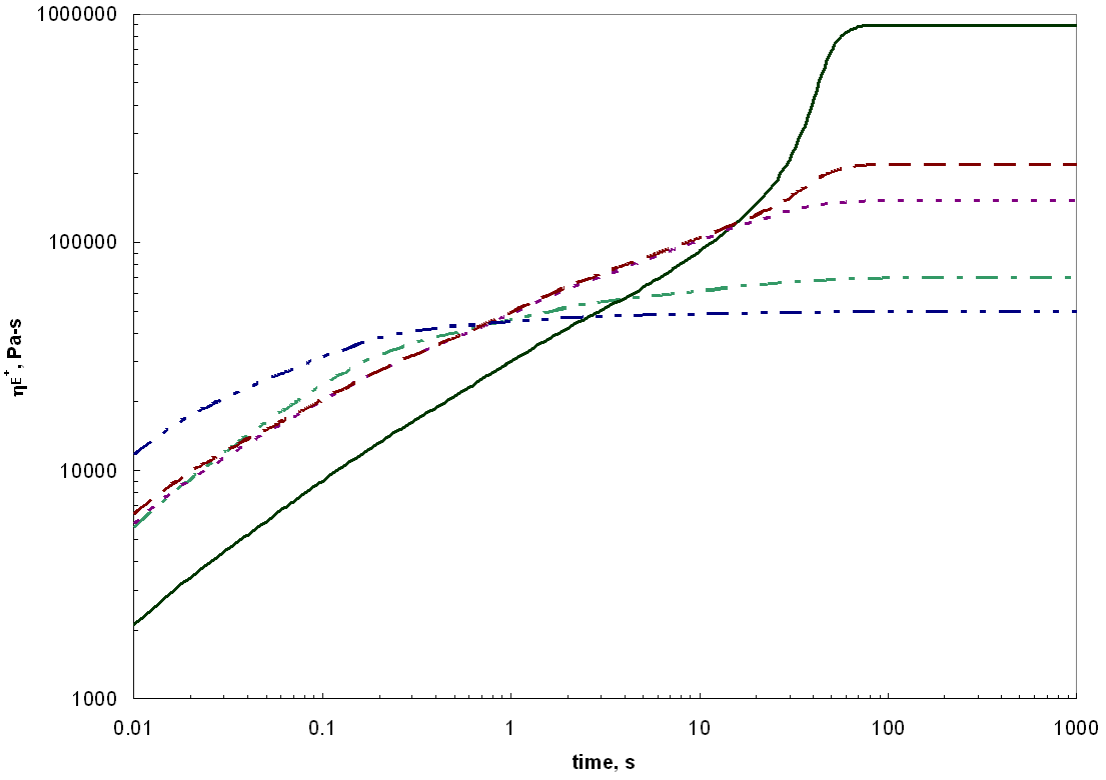

Figure 5.10. Extensional viscosity growth curves for the LDPE and the LLDPE-based series of polyethylene resins at a DR=10, true strain of 2.30, and T=150°C predicted using previously determined pom-pom model parameters shown in Table 5.3 [2] and the operating extension rates defined in Table 5.2. Exact 3132 (— - - —), NTX101 (— - —), NA952 (——), Affinity PL1880 (- - -), and Affinity PL1840 (— —).

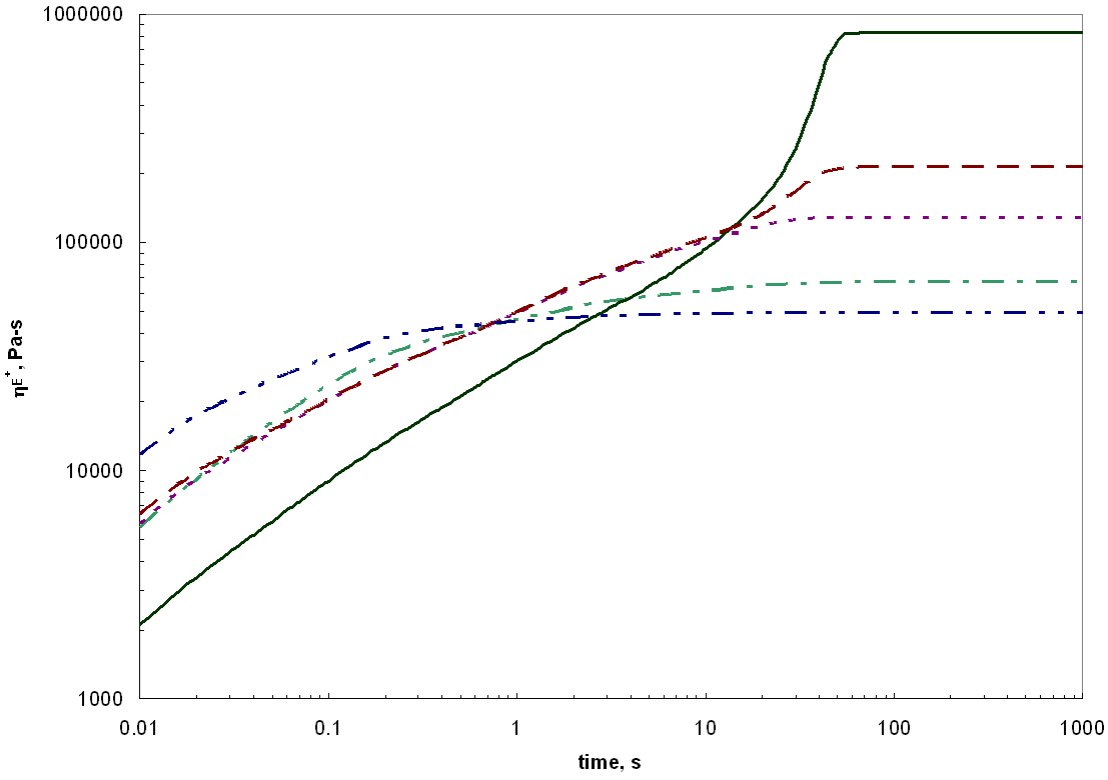

Figure 5.11. Extensional viscosity growth curves for the LDPE and the LLDPE-based series of polyethylene resins at a DR=15, true strain of 2.71, and T=150°C predicted using previously determined pom-pom model parameters shown in Table 5.3 [2] and the operating extension rates defined in Table 5.2. Exact 3132 (— - - —), NTX101 (— - —), NA952 (——), Affinity PL1880 (- - -), and Affinity PL1840 (— —).

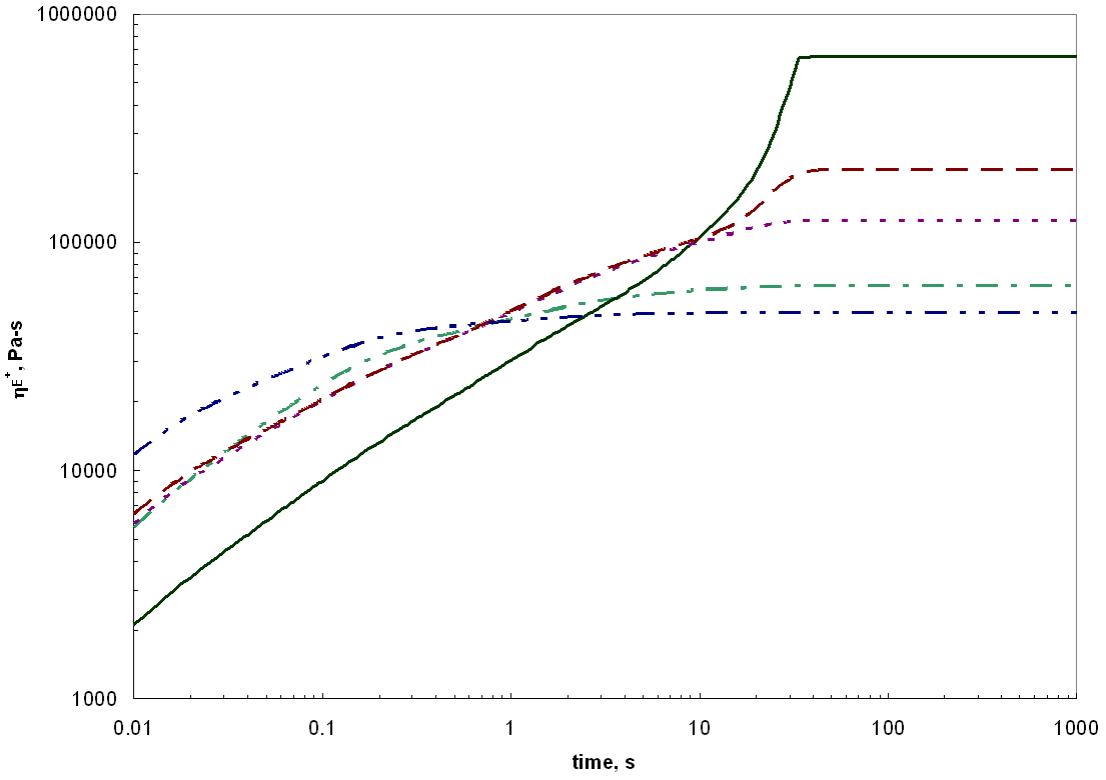

Figure 5.12. Extensional viscosity growth curves for the LDPE and the LLDPE-based series of polyethylene resins at a DR=20, true strain of 3.00, and T=150°C predicted using previously determined pom-pom model parameters shown in Table 5.3 [2] and the operating extension rates defined in Table 5.2. Exact 3132 (— - - —), NTX101 (— - —), NA952 (——), Affinity PL1880 (- - -), and Affinity PL1840 (— —).

6.0 Rheological and film-casting analysis for the HDPE-based series of resins

Preface

This chapter presents the results of an analysis of both rheological and film-casting properties for a series of high density polyethylene resins. This series of materials more closely resembles a model system and the total work requires the contributions of many within the World Wide Network of Polymers research group. My contribution is included in this chapter, but prior to publication requires the results of others including a thorough analysis of the extensional rheology and film-casting simulations.

6.1 Experimental Materials and Methods

6.1.1 Materials

Dow has provided a set of materials that includes sparsely long-chain branched and linear metallocene-catalyzed high density polyethylene homopolymers, where the predicted branching frequency is more exact. These materials are available in limited quantities and provide the opportunity to take a more fundamental approach to the rheological analysis and characterization as well as the film-casting process due to their more well-defined nature. The sparsely long-chain branched metallocene-catalyzed polyethylene resins include HDB1, HDB2, HDB3, HDB4, HDB5, HDB6, and HDB7 and are synthesized using a constrained geometry catalyst of the type described by Stevens [1, 2] in a continuous, stirred-tank reactor as described by Lai and coworkers [3]. No information is provided on the method of synthesis for the linear resin, linear HDB. Both the sparsely-branched resins and the linear resin are homopolymers with narrow molecular weight distributions, MWD, characteristic to metallocene type catalysts. The characteristic M_w, M_w/M_n, LCB/10,000 C, and average number of branches per chain for all of these materials are provided in Table 6.1. Branching concentration is determined using ^{13}C NMR, and ranges from 0.26 LCB/10,000 C to 3.33 LCB/10,000 C. These materials are well-defined in their branching concentrations because the typical pitfalls of ^{13}C NMR measurements do not apply due to the lack of any short-chain branching. The linear rheology for HDB1, HDB3, HDB4, and the linear HDB have been previously studied [4-6]. This set of materials provides the opportunity to compare the details of molecular structure produced with the predictions of the pom-pom model based on rheological results and those of calculated actual branching concentrations. The

similarities of these materials in M_w and MWD should also enable for a non-convoluted comparison of branching effects.

6.1.2 Shear rheology

Dynamic shear measurements were conducted using a Rheometrics RMS-800 fitted with 25 mm cone and plate fixtures featuring a cone angle of 0.1 radians. Tests were carried out for HDB1, HDB3, HDB4, and the linear HDB at temperatures of 150°C, 170°C, 190°C, 230°C, 270°C, and 320°C, while for HDB2, HDB5, HDB6, and HDB7 the dynamic rheology was only measured at 170°C. All tests were performed under an inert N_2 atmosphere in order to prevent oxidative degradation. The test samples were prepared by compression molding preforms at 170 °C under nominal pressure and allowing them to cool slowly under no pressure. This method provided homogenous samples with minimal residual stress.

6.1.3 Film-casting

Film-casting experiments were performed by vertically extruding each polyethylene resin directly through an adjustable thickness slit die with a coathanger manifold. The width of the slit die was 101.6 mm and its thickness was 0.57 mm. The extruded films were then drawn by a chill roll positioned 141.4 mm away from the die. This distance was selected to enhance film stability and due to limitations of the current equipment setup. A non-isothermal process is expected because of the distance from the die exit to the chill roll. The polymer was extruded at a temperature of 190°C.

Processing conditions generated in the film-casting process such as shear rate, strain, and extension rate were calculated as described in the subsequent text. Every polyethylene resin was extruded at a velocity in the z-direction of 1.385 mm/s. Mass flow rate was monitored to maintain a constant throughput for the extruder. The initial velocity was calculated using the density of each polyethylene resin and the cross-sectional area at the die exit. The apparent shear rate was determined using the exit velocity from the die and parallel plate flow following Eq. 1.

$$\dot{\gamma} = \frac{6Q}{WH^2} \tag{1}$$

For each polyethylene resin drawdown ratios of 1.18, 1.76, 2.96, 5.93, 8.89, 11.86, 14.82, 17.79, 20.75, 23.72, and 20.50 were applied resulting in strains ranging from 0.17-3.24. Strains, γ, were calculated by multiplying the residence time by the extension rate. Residence time of the polymer was determined according to Eq. 2 where the average velocity was calculated by taking the integral of the velocity in the z-direction over the total length of the material.

$$\gamma = \frac{\dot{\varepsilon}L}{v_{zAVG}} = \frac{\dot{\varepsilon}L}{\frac{\int_0^L v_{z0}(DR)^{\frac{z}{L}}dz}{\int_0^L zdz}} = \frac{\dot{\varepsilon}L}{v_{z0}\left[\frac{DR}{\ln(DR)} - \frac{1}{\ln(DR)}\right]} \tag{2}$$

Extension rates are defined by subtracting the speed at which the polymer is extruded from the speed at which the polymer is taken up and dividing over the distance in which the polymer is subjected to stretching. Applied extension rates ranged from 0.0036-1.3214 1/s and are tabulated in Table 6.2 for each polyethylene resin at all applied drawdown ratios.

Digital photographs were taken of the films after steady state conditions were reached for each extrusion speed and drawdown ratio scenario. Measurements of the evolution of film-width were then made using a pixel counting software to determine film-widths at various positions in the z-direction. Analysis of the photographs allowed for measurements to the nearest one hundredth of a millimeter. Combined error for the experimental casting and measurements falls within +/-3%.

6.2 Results

6.2.1 Shear rheology

Dynamic oscillatory measurements for HDB1, HDB2, HDB3, HDB4, HDB5, HDB6, HDB7, and the linear HDB were made at a temperature of 170°C, and the resulting shear viscosity curves are presented in Fig. 6.1. The data covers a range in frequency from 0.01-100 1/s. Analysis of the shear viscosity curves indicates that molecular structure influences the onset and degree of shear-thinning as well as the zero-shear viscosity. The onset of shear-thinning is observed to occur at lower frequencies as the branching concentration increases, which is consistent with what Doerpinghaus and Baird [7] observed for a series of LLDPE-based PE resins. The degree of shear-thinning is also observed to increase with increasing branching concentration.

The ratio of the zero-shear viscosity for the sparsely branched HDB series of polymers divided by the zero-shear viscosity for the linear HDB as a function of LCB/10,000 CH_2 is presented in Fig. 6.2. The ratio of zero-shear viscosities increases with increasing branching concentration until a critical value is observed at 0.8 LCB/10,000 CH_2 after which the zero-shear viscosity decreases. This is similar to the

results of Janzen and Colby [8], but we fail to observe suppression of the zero-shear viscosity below that of the linear HDB resin. Subsequently, after the initial reduction in the ratio of zero-shear viscosities that occurs at 0.8 LCB/10,000 CH_2, we observe a leveling of the ratio around 5 for the three highest branched HDB resins.

N_1 is approximated using Laun's approximation [9] shown in Eq. 4 and plotted as a function of shear rate for the series of polyethylene resins in Fig. 6.3.

$$N_1 = 2G'\left[1+\left(\frac{G'}{G''}\right)^2\right]^{0.7} \tag{3}$$

It is observed that at lower shear rates N_1 values are distinctly different exhibiting behavior similar to that of the zero-shear viscosity, where N_1 appears to increase with increasing branching concentration and then subsequently decrease yielding identical curves for HDB3, HDB5, HDB6, and HDB7. As the shear rate increases, it is found that the approximations for N_1 begin to merge towards a single curve.

6.2.2 Film-casting

Necking is evaluated by analyzing the film half-width as a function of the distance from the die until the frostline is reached. The film-casting experimental results are shown in Figs. 6.4 through 6.14 with each figure corresponding to one of the eleven applied drawdown ratios in order of increasing drawdown ratio. Observations from previous experimental and simulated film-casting studies suggest that increases in the strain-hardening properties of the material will lead to a reduction in necking [10-17]. Therefore, it is expected to experience less necking as the level of LCB and strain-hardening behavior increase.

The results in Figs. 6.4 and 6.5 include film-width profiles for the polyethylene resins at constant drawdown ratios of 1.18 and 1.76, respectively. For both drawdown ratios the polyethylene resins fail to show any differences in their necking behavior. This is the anticipated result after analysis of the applied strains achieved, 0.17 and 0.57, respectively, because of the failure to achieve strains high enough where differences in extensional viscosities are present.

The results in Figs. 6.6 through 6.8 include film-width profiles for the polyethylene resins at constant drawdown ratios of 2.96, 5.93, and 8.89, respectively. At these three intermediate drawdown ratios, separation is observed between the LDPE resins, HDB series of resins, and the linear HDB resin. The two LDPE resins experience the least degree of necking followed by the series of HDB resins, which contain sparse LCB, and finally the linear resin, which suffers from the greatest degree of necking. Separation among the sparsely LCB materials was not observed as they all experienced the same degree of necking.

The results in Figs. 6.9 through 6.14 include film-width profiles for the polyethylene resins at constant drawdown ratios of 11.86, 14.82, 17.79, 20.75, 23.72, and 25.50, respectively. For the six drawdown ratios listed above only the LDPE materials experienced reduced necking behavior. The HDB series of resins yield similar film width results to that of the linear HDB resin.

The observations indicate that at low drawdown ratios high enough strains are not achieved to reach any significant differences in the PE resins extensional behavior. At moderate drawdown ratios separation is observed and is accounted for by the differences in their molecular structure. However, at higher drawdown ratios the sparsely LCB PE

resins merge with the linear resin revealing that sparsely LCB is no longer effective at reducing the necking at these drawdown ratios, but the highly branched LDPE still experiences reduced necking. LDPE has a distribution of branches on many different length backbone segments, where it is characteristic for sparsely branched PE resins to have branches on the longest backbone segments. At the highest drawdown ratios we are exploring the shorter backbone segments, which in the case of the sparsely LCB PE resins do not contain any branches and yield the same result as the linear material.

6.3 References

1. Stevens, J., *Journal of Studies in Surface Science and Catalysis* **1994,** 89.

2. Stevens, J., *Journal of Studies in Surface Science and Catalysis* **1996,** 101.

3. Lai, S. Y.; Wilson, J. R.; Knight, J. R.; Stevens, G. W. 1993.

4. Wood-Adams, P. M.; Dealy, J. M., Using Rheological Data to Determine the Branching Level in Metallocene Polyethylenes. *Macromolecules* **2000,** 33, 7481-7488.

5. Wood-Adams, P. M.; Dealy, J. M.; deGroot, A. W.; Redwine, O. D., Effect of Molecular Structure on the Linear Viscoelastic Behavior of Polyethylene. *Macromolecules* **2000,** 33, 7489-7499.

6. Das, C.; Inkson, N. J.; Read, D. J.; Kelmanson, M. A.; McLeish, T. C. B., Computational linear rheology of general branch-on-branch polymers. *Journal of Rheology* **2006,** 50, (2), 207-235.

7. Doerpinghaus, P. J.; Baird, D. G., Separating the effects of sparse long-chain branching on rheology from those due to molecular weight in polyethylenes. *Journal of Rheology* **2003,** 47, (3), 717-736.

8. Janzen, J.; Colby, R. H., Diagnosing long-chain branching in polyethylenes. *Journal of Molecular Structure* **1999,** 485-486, 569-584.

9. Bird, R. B.; Armstrong, R. C.; Hassager, O., *Dynamics of Polymer Liquids: Fluid Mechanics*. 2 ed.; Wiley Interscience: New York, 1987; Vol. 1.

10. Smith, S.; Stolle, D., Numerical Simulation of Film Casting Using an Updated Lagrangian Finite Element Algorithm. *Polymer Engineering and Science* **2003,** 43, (5), 1105-1122.

11. Kim, J. M.; Lee, J. S.; Shin, D. M.; Jung, H. W.; Hyun, J. C., Transient solutions of the dynamics of film casting process using 2-D viscoelastic model. *Journal of Non-Newtonian Fluid Mechanics* **2005,** 132, 53-60.

12. Canning, K.; Co, A., Edge Effects in Film Casting of Molten Polymers. *Journal of Plastic Film & Sheeting* **2000,** 16, 188-203.

13. Kajiwara, T.; Yamamura, M.; Asahina, T., Relationship between Neck-in Phenomena and Rheological Properties in Film Casting. *Nihon Reoroji Gakkaishi* **2006,** 34, (2), 97-103.

14. Silagy, D.; Demay, Y.; Agassant, J. F., Study of the Stability of the Film Casting Process. *Polymer Engineering and Science* **1996,** 36, (21), 2614-2625.

15. Silagy, D.; Demay, Y.; Agassant, J. F., Stationary and stability analysis of the film casting process. *Journal of Non-Newtonian Fluid Mechanics* **1998,** 79, 563-583.

16. Satoh, N.; Tomiyama, H.; Kajiwara, T., Viscoelastic Simulation of Film Casting Process for a Polymer Melt. *Polymer Engineering and Science* **2001,** 41, (9), 1564-1579.

17. Ito, H.; Doi, M.; Isaki, T.; Takeo, M., A Model of Neck-in Phenomenon in Film Casting Process. *Journal of the Society of Rheology, Japan* **2003,** 31, (3), 157-163.

Table 6.1. Molecular characteristics including M_w, M_w/M_n, LCB/10,000 C, and the average number of branches per chain for the HDB series of PE resins.

Polymer Resin ID	*M_w [g/mol]*	*M_w/M_n*	*LCB/10,000 C [[a] as determined from GPC-LALLS [b] as determined from ^{13}C NMR]*	*Avg. # of branches per chain*
HDB1	77,100	2.0	0.26	0.14
HDB2	82,000	1.9	0.37	0.22
HDB3	85,700	2.0	0.42	0.26
HDB4	96,300	2.1	0.80	0.55
HDB5	79,000	-	0.9	0.51
HDB6	68,000	-	1.88	0.91
HDB7	70,000	-	3.33	1.66
Linear HDB	113,000	2.5	Linear	-

Table 6.2. Operating extensional parameters for the HDB series and two LDPE PE resins including material extension rates at DR = 1.18, 1.76, 2.96, 5.93, 8.89, 11.86, 14.82, 17.79, 20.75, 23.72, 25.50 and the corresponding true strains achieved for each DR at T=190°C.

Poly-mer Resin ID	DR= 1.18 Strain= 0.17	DR= 1.76 Strain= 0.57	DR= 2.96 Strain= 1.09	DR= 5.93 Strain= 1.78	DR= 8.89 Strain= 2.18	DR= 11.86 Strain= 2.47	DR= 14.82 Strain= 2.70	DR= 17.79 Strain= 2.88	DR= 20.75 Strain= 3.03	DR= 23.72 Strain= 3.17	DR= 25.50 Strain= 3.24
	ε [1/s]	ε [1/s]	ε [1/s]	ε [1/s]	ε [1/s]	ε [1/s]	ε [1/s]	ε [1/s]	ε [1/s]	ε [1/s]	ε [1/s]
HDB1	0.0086	0.0314	0.0885	0.2136	0.3141	0.3994	0.5263	0.6508	0.7031	0.8645	0.8663
HDB3	0.0079	0.0341	0.0758	0.1884	0.2958	0.4107	-	0.5399	-	0.7669	-
HDB4	0.0112	0.0476	0.1186	0.2136	0.4206	0.5744	0.5306	0.8377	0.9962	1.3214	1.2120
HDB6	0.0091	0.0378	0.0867	0.1619	0.2974	0.4344	0.4964	0.6300	0.8438	0.9228	1.0263
Linear HDB	0.0086	0.0324	0.0750	0.1485	0.2744	0.3459	-	0.5687	-	0.7467	0.7432
Lupolen 1840 H	0.0036	0.0144	0.0347	0.0483	0.0773	0.1064	-	0.1645	-	-	-
LD 150	0.0050	0.0205	0.0503	0.1276	-	-	-	-	-	-	-

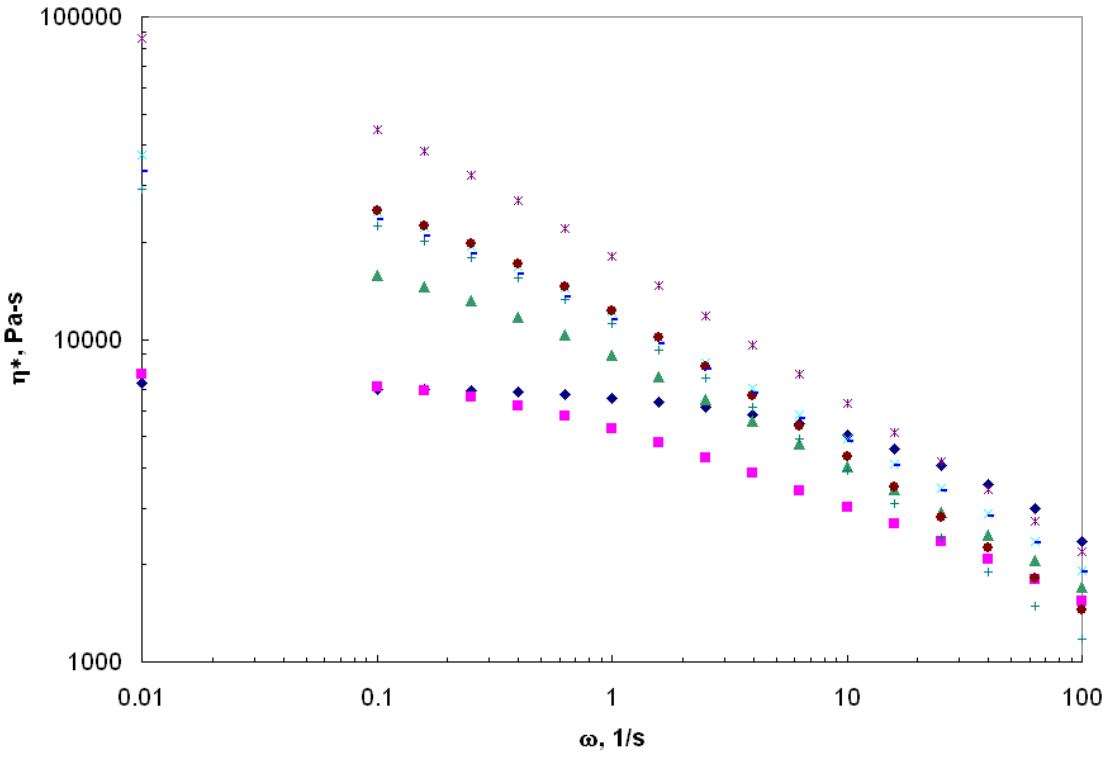

Figure 6.1. Complex viscosity as a function of frequency for the HDB series of PE resins at T=170°C. HDB1 (■), HDB2 (▲), HDB3 (X), HDB4 (*), HDB5 (●), HDB6 (+), HDB7 (-), and Linear HDB (◆).

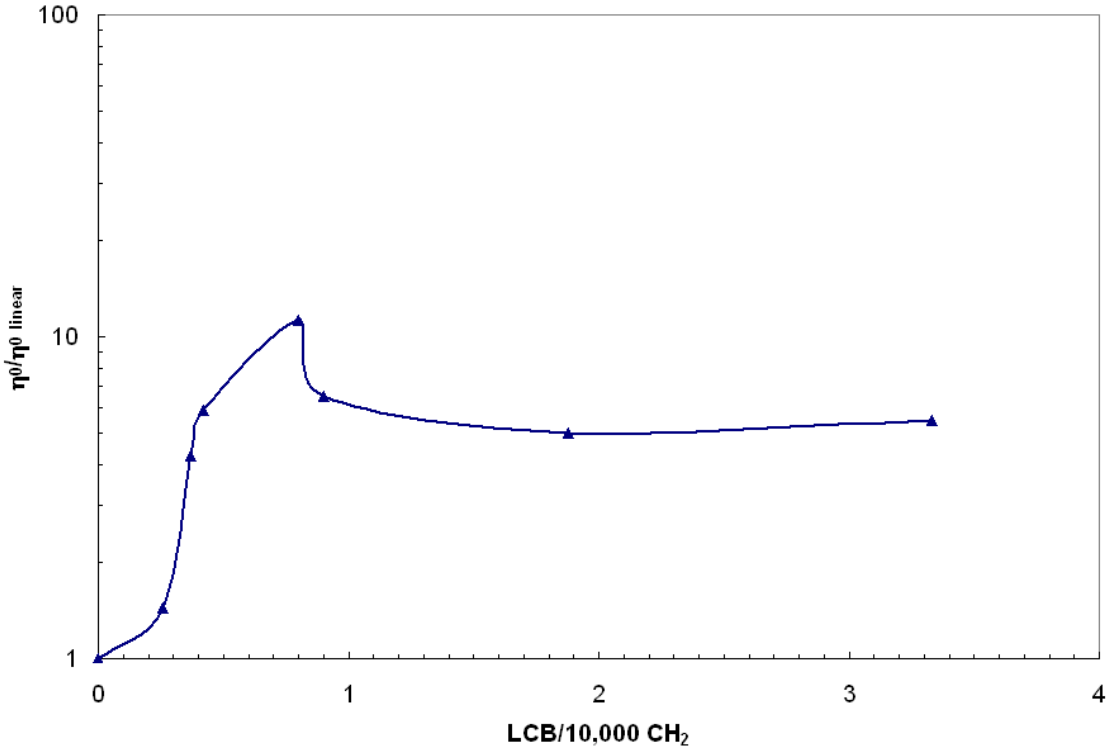

Figure 6.2. The ratio of the zero-shear viscosity for the sparsely branched HDB series of polymers divided by the zero-shear viscosity for the linear HDB as a function of LCB/10,000 CH_2.

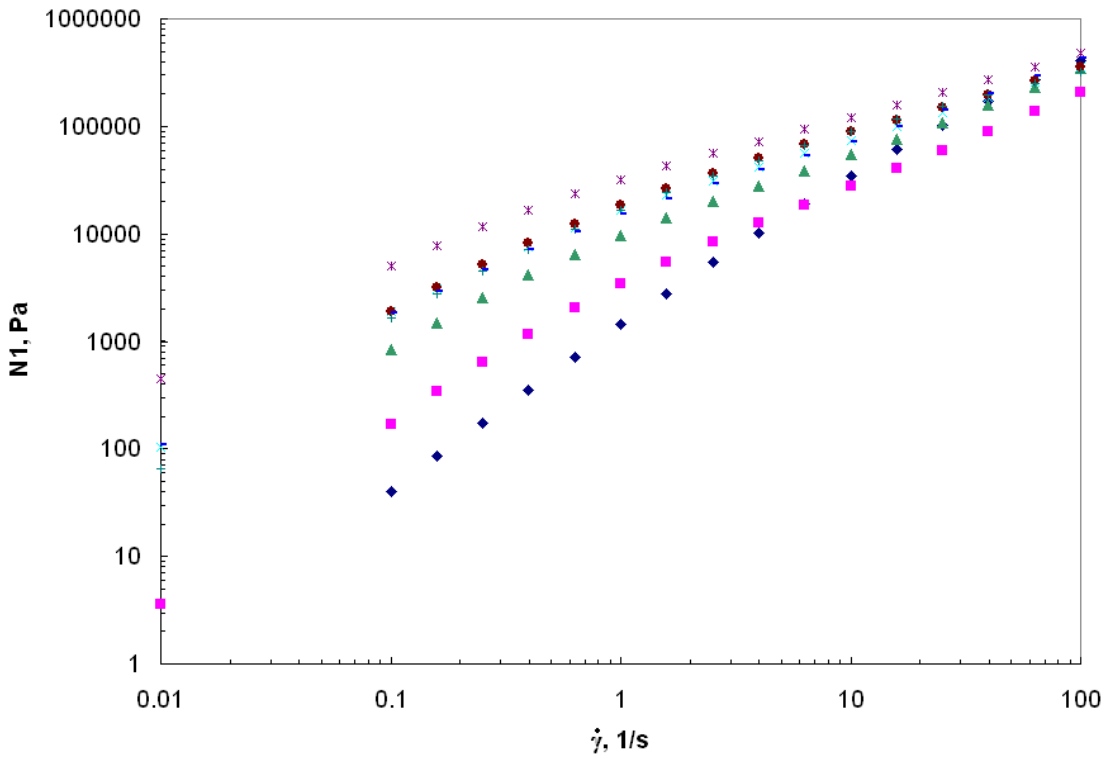

Figure 6.3. Primary normal stress difference estimates using Laun's approximation as a function of shear rate for the HDB series of PE resins at T=170°C. HDB1 (■), HDB2 (▲), HDB3 (X), HDB4 (*), HDB5 (●), HDB6 (+), HDB7 (-), and Linear HDB (◆).

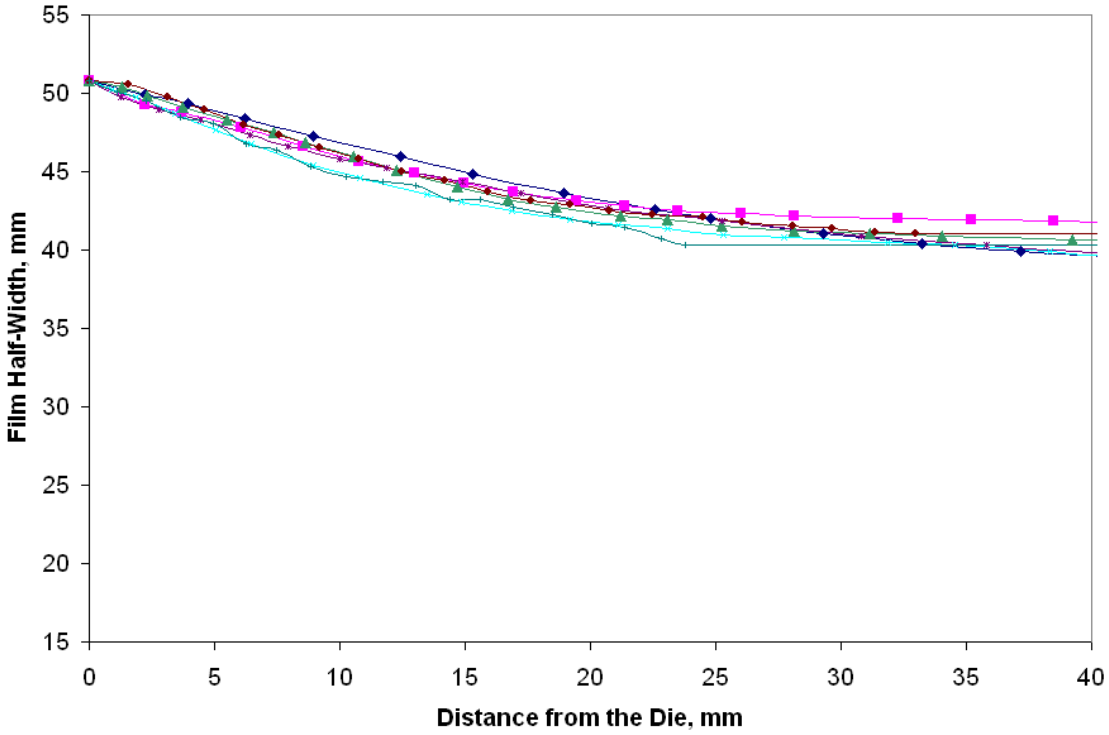

Figure 6.4. Film half-width profile for the HDB series and two LDPE PE resins at a DR=1.18, true strain of 0.17, and T=190°C. The corresponding shear rate is 14.54 1/s and the extension rates are defined in Table 6.2. HDB1 (X), HDB3 (■), HDB4 (●), HDB6 (+), Linear HDB (▲), Lupolen 1840 H (◆), and LD 150 (*).

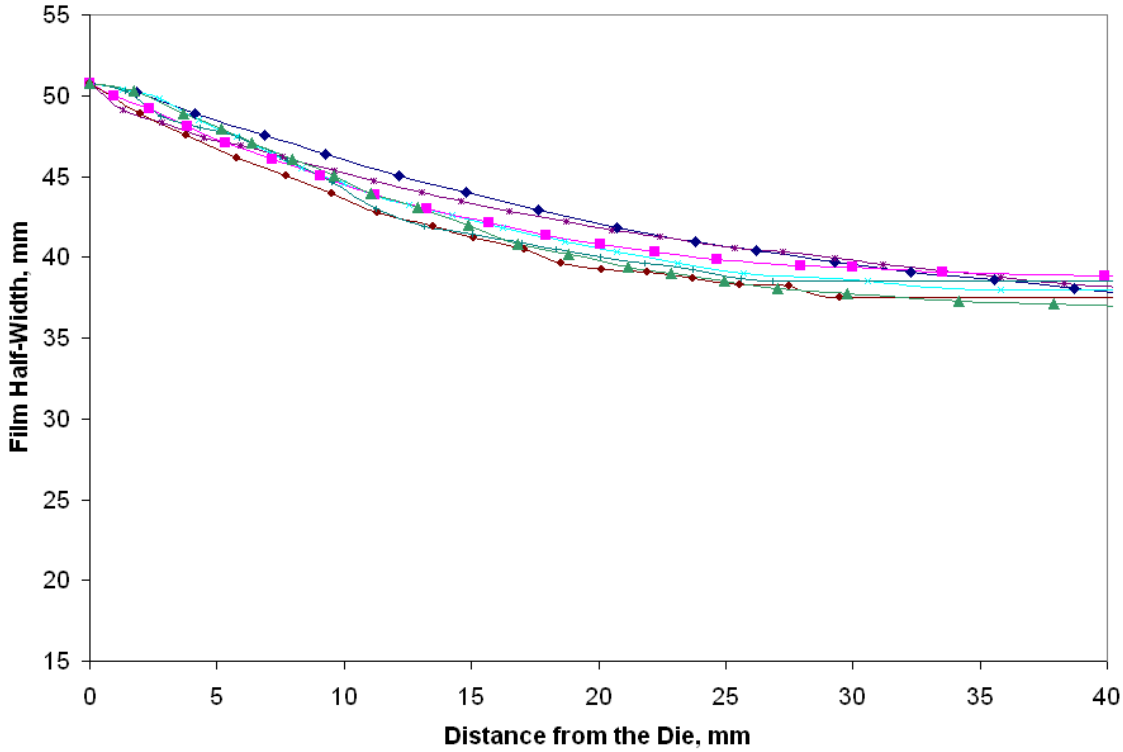

Figure 6.5. Film half-width profile for the HDB series and two LDPE PE resins at a DR=1.76, true strain of 0.57, and T=190°C. The corresponding shear rate is 14.54 1/s and the extension rates are defined in Table 6.2. HDB1 (X), HDB3 (■), HDB4 (●), HDB6 (+), Linear HDB (▲), Lupolen 1840 H (◆), and LD 150 (*).

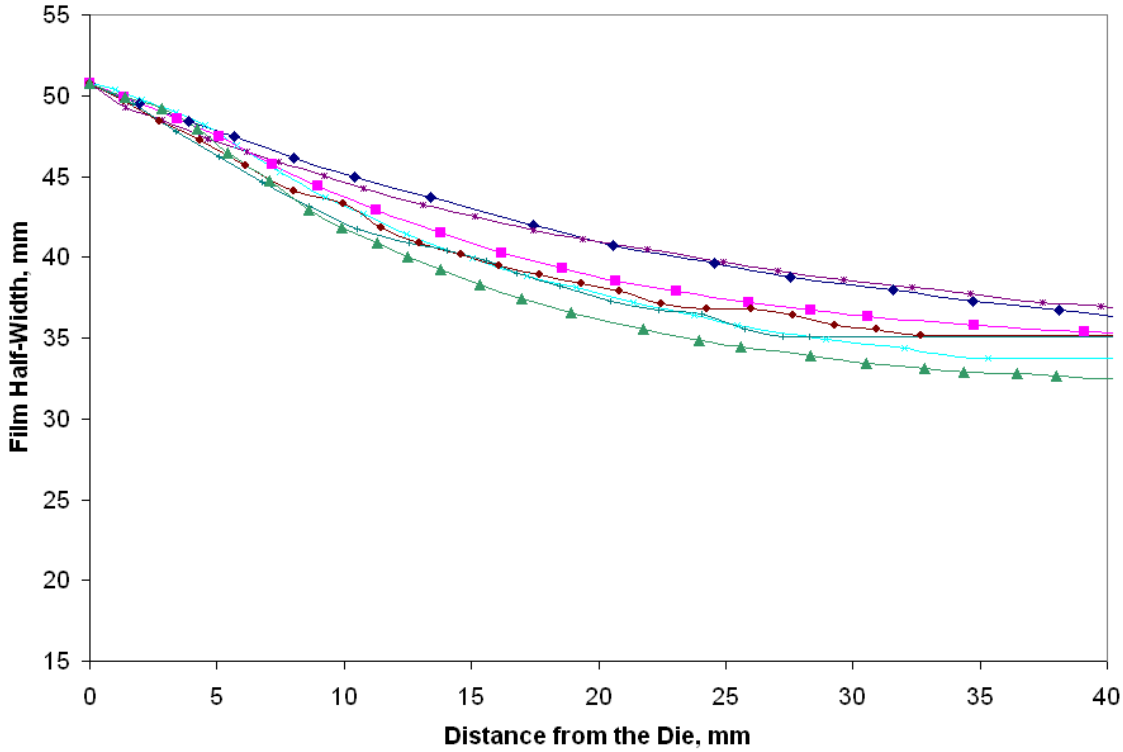

Figure 6.6. Film half-width profile for the HDB series and two LDPE PE resins at a DR=2.96, true strain of 1.09, and T=190°C. The corresponding shear rate is 14.54 1/s and the extension rates are defined in Table 6.2. HDB1 (X), HDB3 (■), HDB4 (●), HDB6 (+), Linear HDB (▲), Lupolen 1840 H (◆), and LD 150 (*).

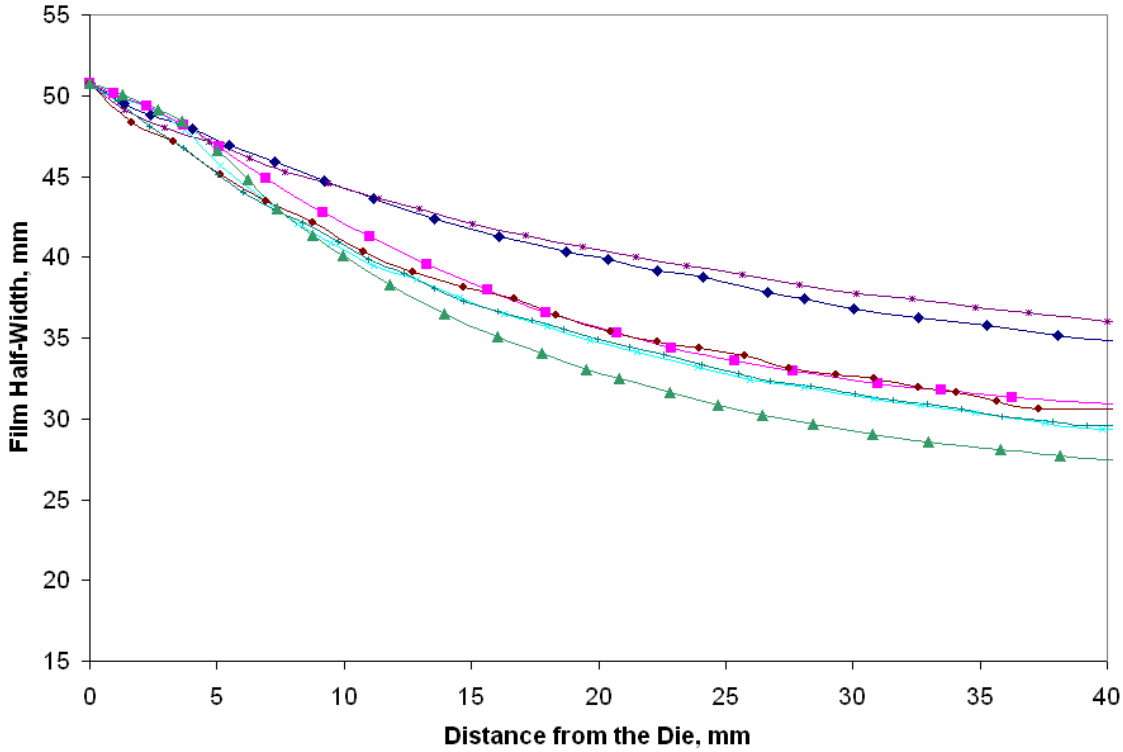

Figure 6.7. Film half-width profile for the HDB series and two LDPE PE resins at a DR=5.93, true strain of 1.78, and T=190°C. The corresponding shear rate is 14.54 1/s and the extension rates are defined in Table 6.2. HDB1 (X), HDB3 (■), HDB4 (●), HDB6 (+), Linear HDB (▲), Lupolen 1840 H (◆), and LD 150 (*).

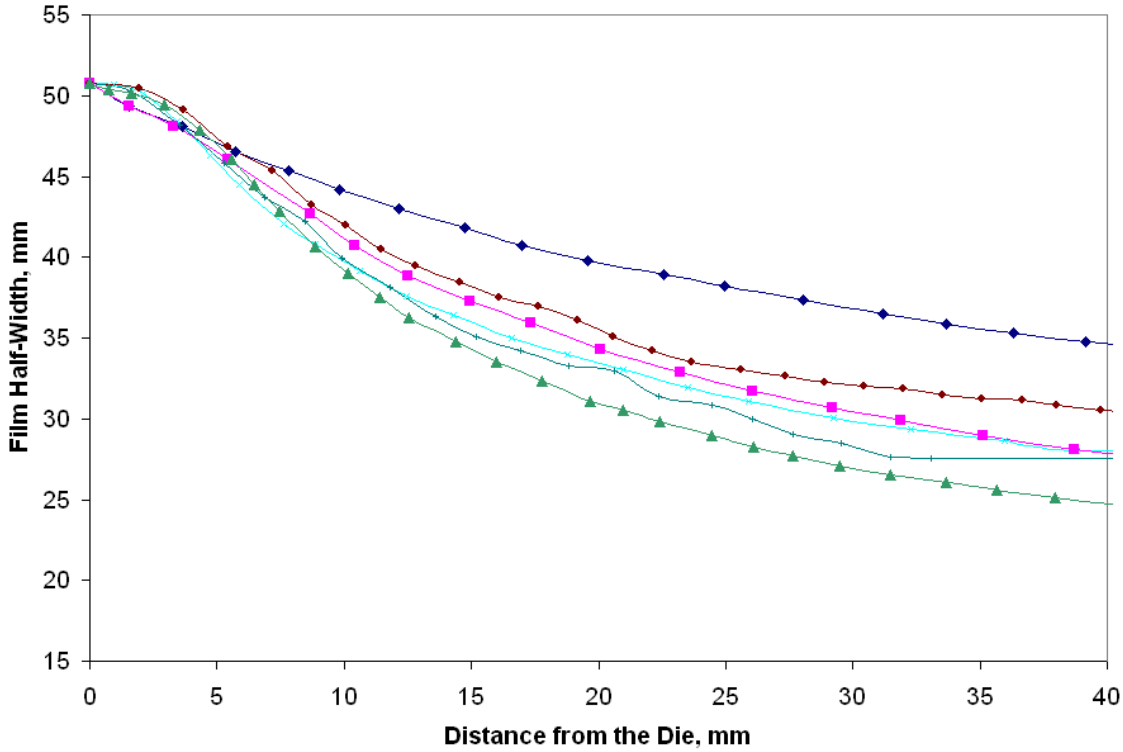

Figure 6.8. Film half-width profile for the HDB series and two LDPE PE resins at a DR=8.89, true strain of 2.18, and T=190°C. The corresponding shear rate is 14.54 1/s and the extension rates are defined in Table 6.2. HDB1 (X), HDB3 (■), HDB4 (●), HDB6 (+), Linear HDB (▲), and Lupolen 1840 H (◆).

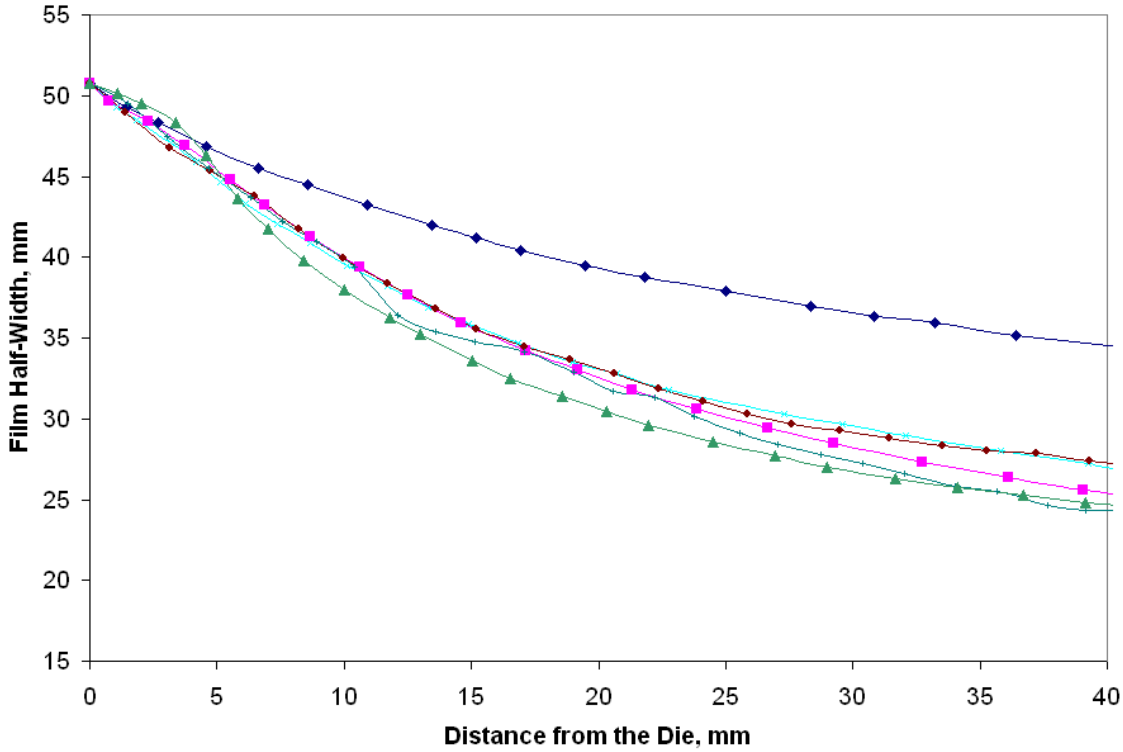

Figure 6.9. Film half-width profile for the HDB series and two LDPE PE resins at a DR=11.86, true strain of 2.47, and T=190°C. The corresponding shear rate is 14.54 1/s and the extension rates are defined in Table 6.2. HDB1 (X), HDB3 (■), HDB4 (●), HDB6 (+), Linear HDB (▲), and Lupolen 1840 H (◆).

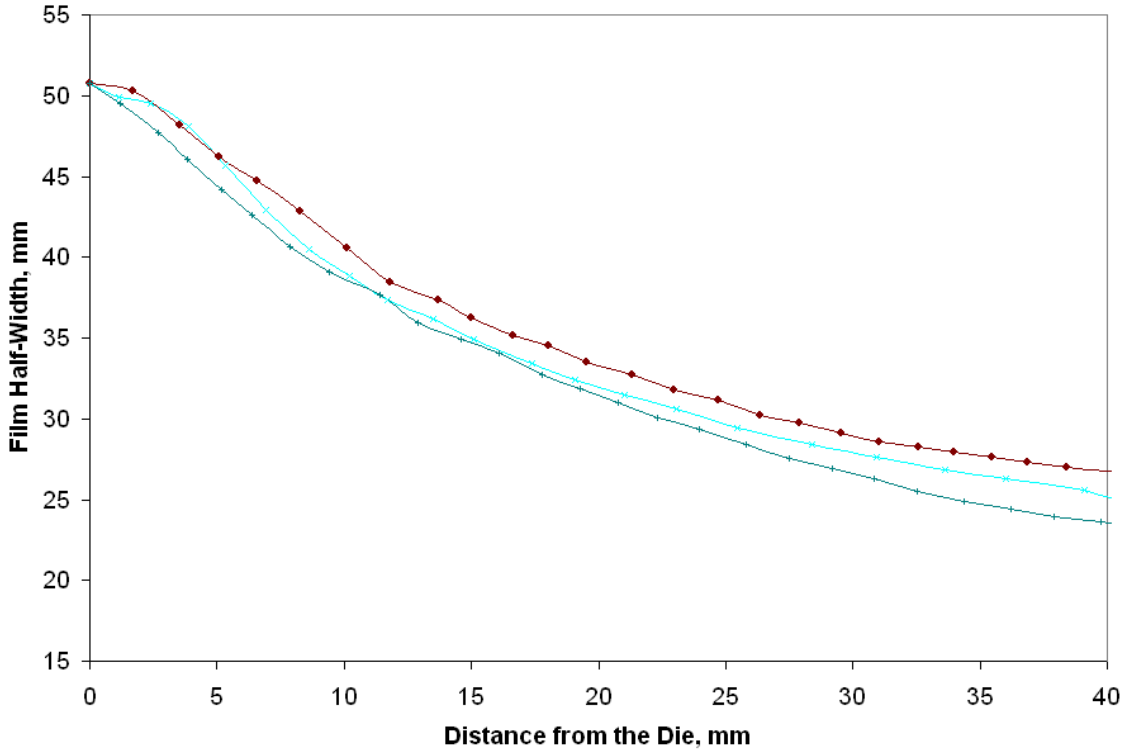

Figure 6.10. Film half-width profile for the HDB series and two LDPE PE resins at a DR=14.82, true strain of 2.70, and T=190°C. The corresponding shear rate is 14.54 1/s and the extension rates are defined in Table 6.2. HDB1 (X), HDB4 (●), and HDB6 (+).

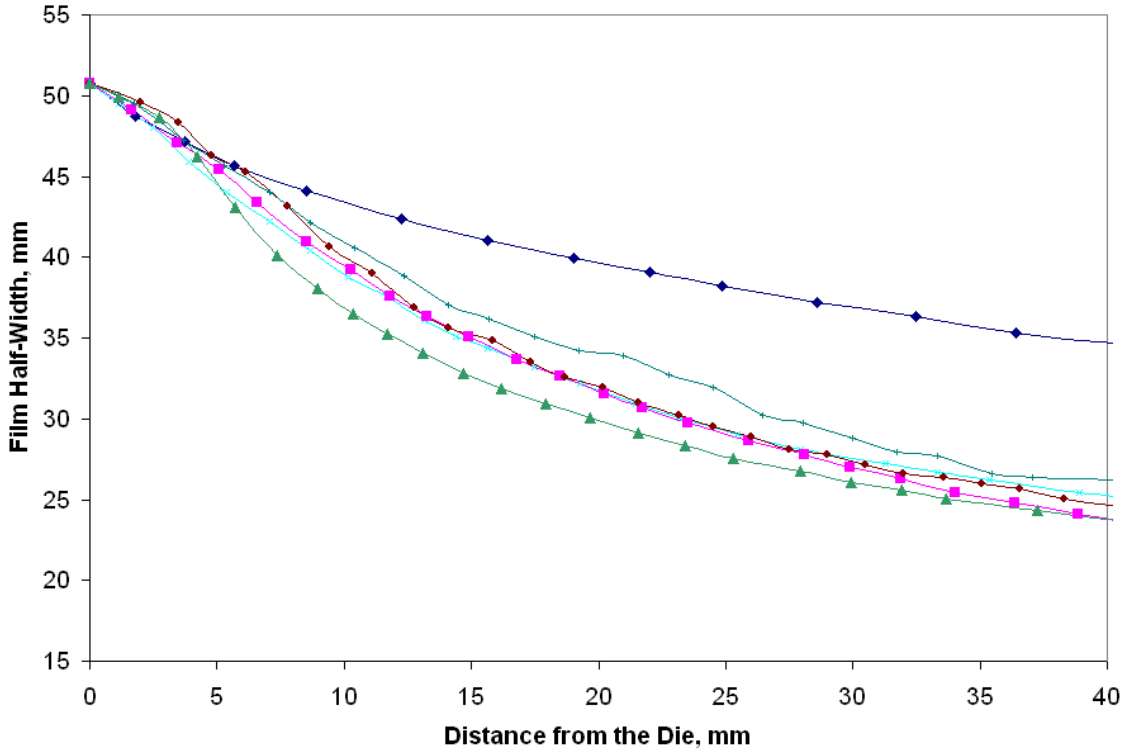

Figure 6.11. Film half-width profile for the HDB series and two LDPE PE resins at a DR=17.79, true strain of 2.88, and T=190°C. The corresponding shear rate is 14.54 1/s and the extension rates are defined in Table 6.2. HDB1 (X), HDB3 (■), HDB4 (●), HDB6 (+), Linear HDB (▲), and Lupolen 1840 H (◆).

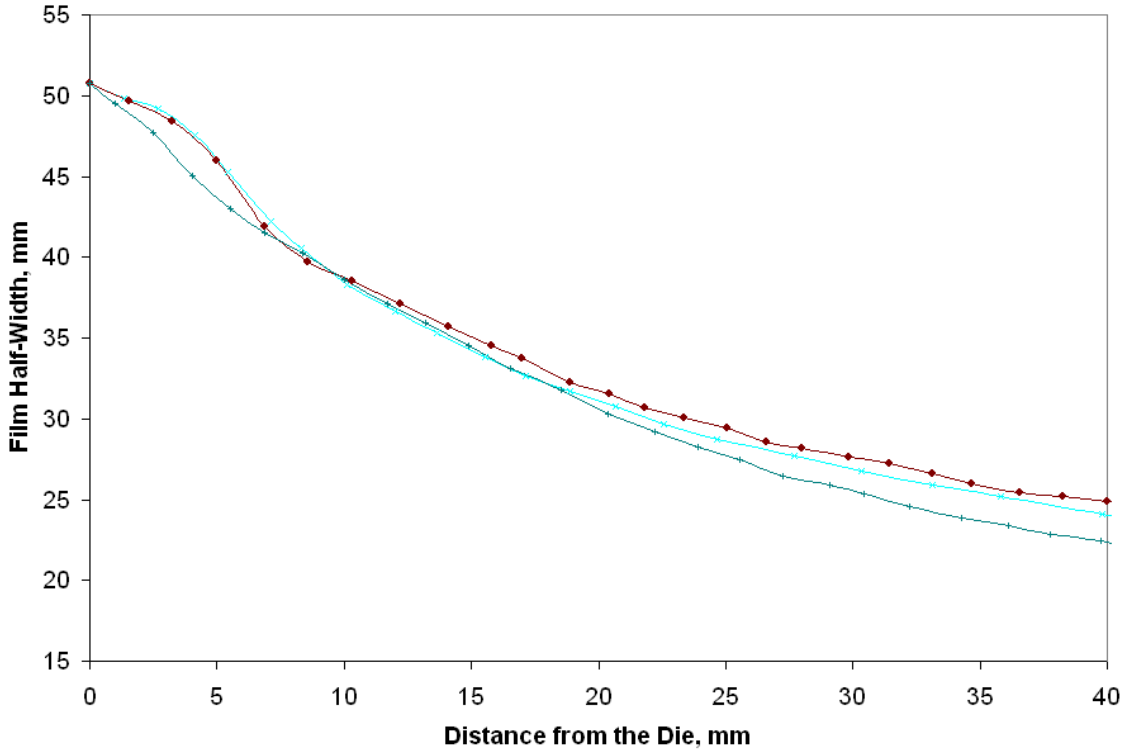

Figure 6.12. Film half-width profile for the HDB series and two LDPE PE resins at a DR=20.75, true strain of 3.03, and T=190°C. The corresponding shear rate is 14.54 1/s and the extension rates are defined in Table 6.2. HDB1 (X), HDB4 (●), and HDB6 (+).

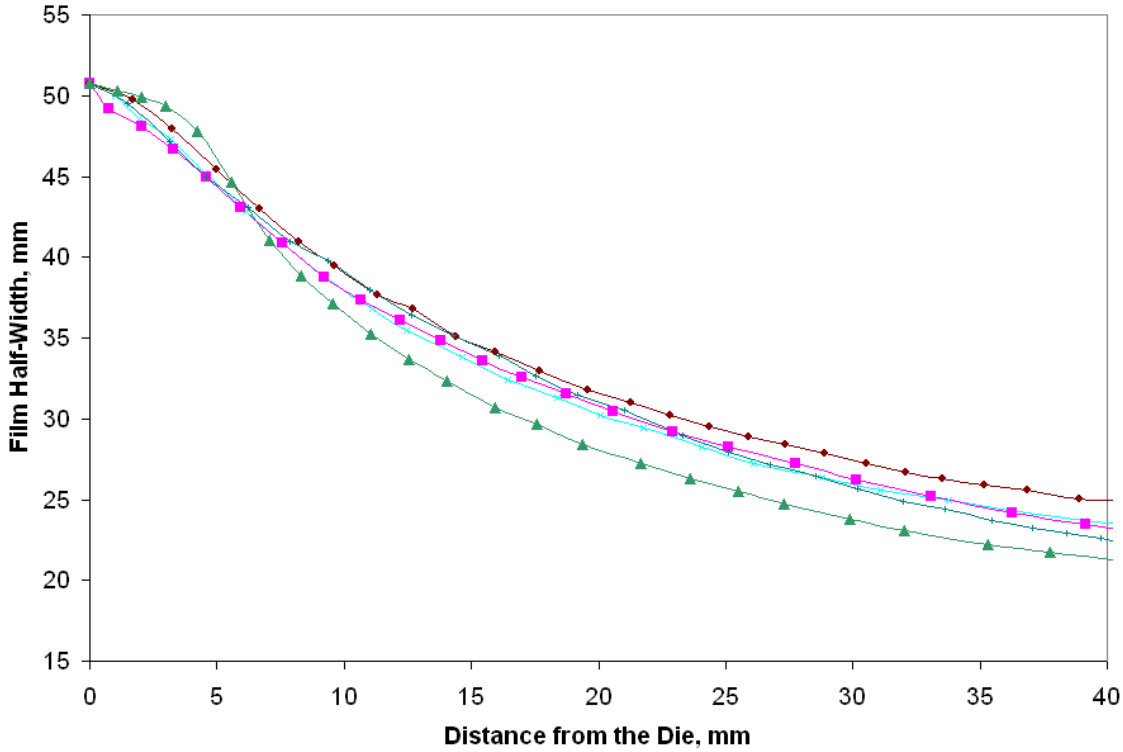

Figure 6.13. Film half-width profile for the HDB series and two LDPE PE resins at a DR=23.72, true strain of 3.17, and T=190°C. The corresponding shear rate is 14.54 1/s and the extension rates are defined in Table 6.2. HDB1 (X), HDB3 (■), HDB4 (●), HDB6 (+), and Linear HDB (▲).

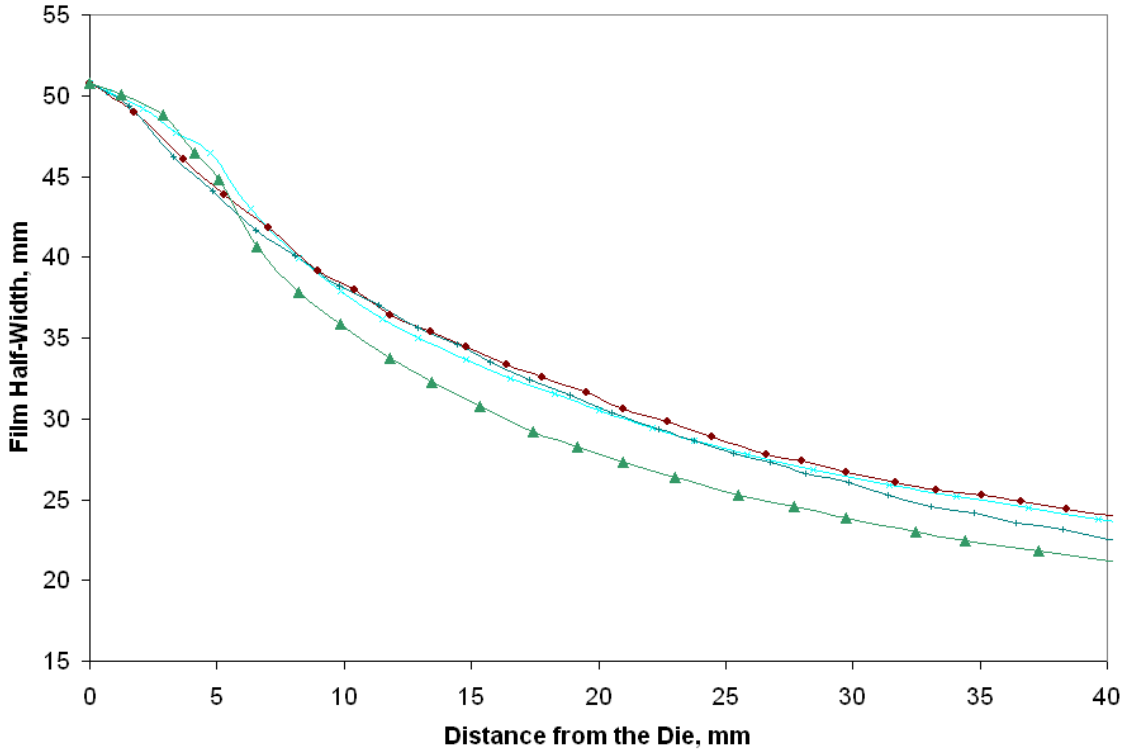

Figure 6.14. Film half-width profile for the HDB series and two LDPE PE resins at a DR=25.50, true strain of 3.24, and T=190°C. The corresponding shear rate is 14.54 1/s and the extension rates are defined in Table 6.2. HDB1 (X), HDB4 (●), HDB6 (+), and Linear HDB (▲).

7.0 Recommendations

7.0 Recommendations

7.1 Material considerations

1. Extend both the rheological and film-casting analysis to polymer systems that are more well-defined in their molecular structure. These types of materials allow for a more useful testing platform of the pom-pom model and could lead to an even better understanding of the film-casting process. Monodisperse systems will allow for a direct analysis of how branching distribution affects the processing characteristics

7.2 Film-casting considerations

1. Decreasing the thickness of the film die may prove useful in more closely resembling an industrial process. Because of a fixed die width the only way to adjust the aspect ratio is to decrease the thickness of the film die. The major limitation here is to not induce any instabilities associated with the thickness being too small.
2. Moving the die exit and the chill rolls closer together not only more closely resembles an industrial process, but it eliminates the non-isothermal behavior as well. Having an isothermal process removes the criterion of comparing materials of similar activation energies.

7.3 Shear step-strain considerations

1. Perform shear step-strain tests in a sliding plate rheometer. This will yield the ability to reach higher strains where the limiting factor becomes wall slip and is not limited to the equipment's operating range. It also gives the possibility of saturating stretch, thus defining the pom-pom parameter q.

Volume 2

Appendix A: Film-Casting Measurements for the LLDPE-based PE Resins

A.1. Exact 3132

Film-Casting

T = 150ºC; DR = 5; γ = 8.62 [1/s]; ε = 0.02379 [1/s]; strain = 1.6091

Distance to frostline = 138.1 [mm]

Dist. from die [mm]	Film width [mm]	Half-width [mm]	Dist. from die [mm] *continued*	Film width [mm] *continued*	Half-width [mm] *continued*
0	101.6	50.8	88.097	43.76	21.88
1.522	98.841	49.4205	95.517	43.285	21.6425
3.71	94.846	47.423	104.079	43.094	21.547
5.708	90.945	45.4725	114.258	42.904	21.452
7.611	87.33	43.665	123.771	43.19	21.595
9.799	83.525	41.7625	133.475	43.761	21.8805
12.082	79.434	39.717	161.063	44.141	22.0705
14.746	75.344	37.672	198.545	43.475	21.7375
17.124	72.68	36.34			
19.978	70.016	35.008			
23.308	66.782	33.391			
27.589	63.262	31.631			
32.726	60.218	30.109			
36.056	58.506	29.253			
41.194	55.747	27.8735			
46.332	53.464	26.732			
52.802	50.99	25.495			
58.986	49.088	24.544			
65.455	47.28	23.64			
72.209	45.568	22.784			
80.962	44.141	22.0705			

A.1. Exact 3132

Film-Casting

T = 150ºC; DR = 10; γ = 8.62 [1/s]; ε = 0.05230 [1/s]; strain = 2.3026

Distance to frostline = 141.4 [mm]

Dist. from die [mm]	Film width [mm]	Half-width [mm]	Dist. from die [mm] *continued*	Film width [mm] *continued*	Half-width [mm] *continued*
0	101.6	50.8	60.753	41.304	20.652
1.602	99.769	49.8845	66.13	40.159	20.0795
3.204	97.595	48.7975	72.88	39.13	19.565
5.149	93.934	46.967	82.948	38.443	19.2215
6.865	90.387	45.1935	86.495	37.642	18.821
9.039	85.353	42.6765	94.161	37.528	18.764
11.098	80.891	40.4455	100.454	37.528	18.764
13.615	75.514	37.757	108.577	37.299	18.6495
16.361	70.25	35.125	119.103	36.956	18.478
18.993	66.132	33.066	154.571	38.1	19.05
21.51	63.042	31.521	199.765	38.558	19.279
23.569	60.525	30.2625			
26.658	57.55	28.775			
29.404	55.377	27.6885			
33.065	52.516	26.258			
36.955	49.885	24.9425			
40.96	47.94	23.97			
44.85	46.223	23.1115			
48.969	44.736	22.368			
53.431	43.363	21.6815			
57.092	42.219	21.1095			

A.1. Exact 3132

Film-Casting

T = 150ºC; DR = 15; γ = 8.62 [1/s]; ε = 0.08136 [1/s]; strain = 2.7082

Distance to frostline = 141.4 [mm]

Dist. from die [mm]	Film width [mm]	Half-width [mm]	Dist. from die [mm] *continued*	Film width [mm] *continued*	Half-width [mm] *continued*
0	101.6	50.8	37.896	43.309	21.6545
1.259	100.593	50.2965	40.666	41.924	20.962
2.644	99.586	49.793	43.31	40.665	20.3325
3.525	98.704	49.352	45.954	39.532	19.766
5.288	96.06	48.03	49.101	38.525	19.2625
6.673	92.787	46.3935	52.125	37.518	18.759
8.436	88.129	44.0645	55.021	36.511	18.2555
9.443	85.107	42.5535	59.05	35.252	17.626
10.954	80.449	40.2245	63.96	34.118	17.059
12.842	74.91	37.455	67.674	32.985	16.4925
14.605	69.622	34.811	72.521	31.852	15.926
16.619	65.215	32.6075	78.312	30.908	15.454
18.507	62.068	31.034	83.852	30.153	15.0765
20.899	58.417	29.2085	91.909	29.397	14.6985
22.536	56.277	28.1385	100.029	28.894	14.447
24.802	53.759	26.8795	128.797	27.824	13.912
27.068	51.241	25.6205	137.043	27.824	13.912
29.46	49.226	24.613	149.255	27.949	13.9745
32.482	47.086	23.543	163.23	28.768	14.384
34.245	45.701	22.8505	199.929	29.02	14.51
36.133	44.694	22.347			

A.1. Exact 3132

Film-Casting

T = 150ºC; DR = 20; γ = 8.62 [1/s]; ε = 0.1104 [1/s]; strain = 2.9954

Distance to frostline = 141.4 [mm]

Dist. from die [mm]	Film width [mm]	Half-width [mm]	Dist. from die [mm] *continued*	Film width [mm] *continued*	Half-width [mm] *continued*
0	101.6	50.8	46.361	37.182	18.591
1.788	99.936	49.968	50.192	35.774	17.887
3.448	99.052	49.526	53.64	34.757	17.3785
5.236	95.995	47.9975	56.833	33.728	16.864
6.896	91.656	45.828	60.537	33.09	16.545
8.556	86.414	43.207	64.368	32.196	16.098
10.344	80.029	40.0145	68.71	31.307	15.6535
12.132	74.015	37.0075	72.797	30.796	15.398
14.431	68.135	34.0675	78.161	29.392	14.696
16.347	64.046	32.023	86.207	28.892	14.446
18.901	59.309	29.6545	95.275	28.631	14.3155
21.072	55.603	27.8015	103.704	28.26	14.13
23.499	52.152	26.076	111.878	27.743	13.8715
25.926	49.08	24.54	121.584	27.494	13.747
28.991	46.262	23.131	134.866	27.1	13.55
31.673	44.084	22.042	200.383	26.347	13.1735
34.1	42.548	21.274			
36.527	41.275	20.6375			
38.698	40.25	20.125			
40.997	39.233	19.6165			
43.679	38.08	19.04			

A.2. Exact 0201

Film-Casting

T = 150ºC; DR = 10; γ = 8.62 [1/s]; ε = 0.05230 [1/s]; strain = 2.3026

Distance to frostline = 141.4 [mm]

Dist. from die [mm]	Film width [mm]	Half-width [mm]	Dist. from die [mm] *continued*	Film width [mm] *continued*	Half-width [mm] *continued*
0	101.6	50.8	77.288	43.272	21.636
1.673	99.816	49.908	83.645	42.38	21.19
3.68	97.362	48.681	92.456	40.595	20.2975
5.911	93.57	46.785	99.036	40.595	20.2975
8.365	88.998	44.499	119.557	38.811	19.4055
11.042	84.202	42.101	127.698	37.919	18.9595
13.607	79.964	39.982	194.613	37.696	18.848
16.618	75.391	37.6955			
19.741	71.488	35.744			
22.306	68.477	34.2385			
25.206	66.023	33.0115			
29.667	62.677	31.3385			
33.682	59.666	29.833			
36.805	57.882	28.941			
41.489	55.205	27.6025			
45.727	53.198	26.599			
49.184	51.636	25.818			
53.199	49.741	24.8705			
57.883	48.068	24.034			
63.571	46.395	23.1975			
69.816	44.722	22.361			

A.2. Exact 0201

Film-Casting

T = 150ºC; DR = 15; γ = 8.62 [1/s]; ε = 0.08136 [1/s]; strain = 2.7082

Distance to frostline = 141.4 [mm]

Dist. from die [mm]	Film width [mm]	Half-width [mm]	Dist. from die [mm] *continued*	Film width [mm] *continued*	Half-width [mm] *continued*
0	101.6	50.8	38.034	55.418	27.709
1.304	100.622	50.311	40.207	53.788	26.894
2.717	99.427	49.7135	42.706	52.702	26.351
4.13	97.797	48.8985	45.64	51.289	25.6445
5.76	95.515	47.7575	49.226	49.55	24.775
7.39	93.016	46.508	53.029	48.029	24.0145
8.911	89.864	44.932	57.05	46.182	23.091
10.541	86.822	43.411	61.614	44.552	22.276
12.062	83.779	41.8895	66.721	43.248	21.624
13.475	81.389	40.6945	74.219	41.618	20.809
15.214	78.346	39.173	81.391	40.097	20.0485
17.17	75.195	37.5975	88.78	39.227	19.6135
18.909	73.022	36.511	100.624	37.815	18.9075
21.082	70.522	35.261	111.925	36.511	18.2555
23.038	67.588	33.794	123.987	35.75	17.875
24.777	65.741	32.8705	143.22	34.012	17.006
26.624	63.785	31.8925	197.443	32.382	16.191
28.689	62.155	31.0775			
31.188	60.091	30.0455			
33.361	58.461	29.2305			
35.426	57.048	28.524			

A.2. Exact 0201

Film-Casting

T = 150ºC; DR = 20; γ = 8.62 [1/s]; ε = 0.1104 [1/s]; strain = 2.9954

Distance to frostline = 141.4 [mm]

Dist. from die [mm]	Film width [mm]	Half-width [mm]	Dist. from die [mm] *continued*	Film width [mm] *continued*	Half-width [mm] *continued*
0	101.6	50.8	43.904	48.155	24.0775
1.456	99.915	49.9575	47.879	46.307	23.1535
3.024	98.012	49.006	52.974	43.954	21.977
4.592	95.211	47.6055	58.629	41.658	20.829
5.824	92.86	46.43	62.884	40.259	20.1295
7.616	89.165	44.5825	67.195	39.027	19.5135
9.296	85.577	42.7885	71.394	38.187	19.0935
11.2	81.654	40.827	74.754	37.403	18.7015
12.992	78.405	39.2025	80.465	36.339	18.1695
14.784	75.158	37.579	87.016	35.219	17.6095
16.688	71.905	35.9525	91.551	34.547	17.2735
18.704	69.214	34.607	98.326	34.155	17.0775
20.832	66.413	33.2065	107.957	33.259	16.6295
22.512	64.845	32.4225	114.676	33.091	16.5455
24.752	62.268	31.134	124.755	32.532	16.266
27.104	59.804	29.902	133.602	32.028	16.014
29.68	57.789	28.8945	147.992	31.356	15.678
32.032	55.66	27.83	159.75	30.964	15.482
34.832	53.53	26.765	195.305	30.236	15.118
37.744	51.626	25.813			
40.544	49.833	24.9165			

A.3. NTX101

Film-Casting

T = 150ºC; DR = 5; γ = 8.62 [1/s]; ε = 0.03687 [1/s]; strain = 1.6095

Distance to frostline = 89.1 [mm]

Dist. from die [mm]	Film width [mm]	Half-width [mm]	Dist. from die [mm] *continued*	Film width [mm] *continued*	Half-width [mm] *continued*
0	101.6	50.8	93.677	46.976	23.488
2.402	99.702	49.851	101.885	46.597	23.2985
4.93	96.917	48.4585	114.009	46.473	23.2365
7.455	92.875	46.4375	195.984	46.092	23.046
10.11	88.071	44.0355			
12.397	83.771	41.8855			
14.547	80.229	40.1145			
17.21	76.813	38.4065			
19.497	73.902	36.951			
22.915	70.361	35.1805			
26.459	67.206	33.603			
29.744	64.934	32.467			
33.155	63.159	31.5795			
37.828	60.246	30.123			
42.507	57.845	28.9225			
50.092	54.692	27.346			
54.513	53.171	26.5855			
61.336	50.515	25.2575			
67.15	49.124	24.562			
75.109	48.493	24.2465			
86.353	47.23	23.615			

A.3. NTX101

Film-Casting

T = 150ºC; DR = 10; γ = 8.62 [1/s]; ε = 0.06555 [1/s]; strain = 2.3027

Distance to frostline = 112.8 [mm]

Dist. from die [mm]	Film width [mm]	Half-width [mm]	Dist. from die [mm] *continued*	Film width [mm] *continued*	Half-width [mm] *continued*
0	101.6	50.8	51.15	46.972	23.486
1.355	100.063	50.0315	54.876	45.843	22.9215
2.936	98.592	49.296	59.844	44.827	22.4135
4.291	96.782	48.391	63.118	44.036	22.018
5.646	94.414	47.207	68.086	42.794	21.397
7.114	91.031	45.5155	73.167	41.891	20.9455
8.582	87.743	43.8715	79.49	40.988	20.494
10.163	83.999	41.9995	86.265	39.971	19.9855
12.195	79.466	39.733	94.395	39.181	19.5905
14.227	75.385	37.6925	104.331	38.616	19.308
16.372	71.864	35.932	114.945	38.165	19.0825
18.63	68.117	34.0585	130.188	37.713	18.8565
20.55	65.845	32.9225	158.755	37.487	18.7435
22.808	63.124	31.562	196.92	37.261	18.6305
25.518	60.754	30.377			
28.68	57.815	28.9075			
31.842	55.441	27.7205			
35.004	53.634	26.817			
40.65	50.472	25.236			
44.15	49.117	24.5585			
47.876	47.762	23.881			

A.3. NTX101

Film-Casting

T = 150ºC; DR = 15; γ = 8.62 [1/s]; ε = 0.08229 [1/s]; strain = 2.7082

Distance to frostline = 139.8 [mm]

Dist. from die [mm]	Film width [mm]	Half-width [mm]	Dist. from die [mm] *continued*	Film width [mm] *continued*	Half-width [mm] *continued*
0	101.6	50.8	38.201	47.406	23.703
1.266	100.334	50.167	41.423	45.795	22.8975
2.302	98.723	49.3615	44.184	44.299	22.1495
4.258	95.502	47.751	49.995	42.343	21.1715
5.639	92.625	46.3125	56.726	40.329	20.1645
6.905	88.828	44.414	61.904	39.179	19.5895
8.171	85.606	42.803	68.06	38.028	19.014
9.322	82.615	41.3075	73.295	37.108	18.554
10.588	79.623	39.8115	78.76	36.36	18.18
11.969	76.286	38.143	83.765	35.669	17.8345
13.925	72.259	36.1295	91.244	34.634	17.317
15.766	68.692	34.346	96.019	34.346	17.173
17.837	65.355	32.6775	105.051	33.943	16.9715
19.563	63.054	31.527	112.703	33.713	16.8565
21.519	60.638	30.319	145.266	34.576	17.288
23.705	58.222	29.111	151.997	34.404	17.202
26.006	55.92	27.96	162.295	34.001	17.0005
28.192	54.079	27.0395	196.296	33.483	16.7415
30.378	52.123	26.0615			
33.024	50.397	25.1985			
35.785	48.671	24.3355			

A.3. NTX101

Film-Casting

T = 150ºC; DR = 20; γ = 8.62 [1/s]; ε = 0.1104 [1/s]; strain = 2.9954

Distance to frostline = 141.4 [mm]

Dist. from die [mm]	Film width [mm]	Half-width [mm]	Dist. from die [mm] *continued*	Film width [mm] *continued*	Half-width [mm] *continued*
0	101.6	50.8	42.198	44.458	22.229
1.507	100.219	50.1095	45.463	43.076	21.538
3.14	97.958	48.979	49.609	41.444	20.722
4.647	95.321	47.6605	53.377	40.313	20.1565
6.28	91.93	45.965	57.27	39.058	19.529
7.913	87.283	43.6415	61.414	37.802	18.901
9.294	84.143	42.0715	65.684	36.923	18.4615
10.675	80.501	40.2505	71.838	35.792	17.896
12.308	76.859	38.4295	80.755	34.285	17.1425
13.941	73.594	36.797	88.667	33.532	16.766
15.699	70.454	35.227	99.593	32.276	16.138
17.332	67.943	33.9715	112.277	31.522	15.761
19.593	64.426	32.213	148.697	30.015	15.0075
21.602	61.287	30.6435	161.256	29.136	14.568
23.486	58.775	29.3875	196.923	28.759	14.3795
25.998	56.137	28.0685			
29.012	53.375	26.6875			
31.649	51.24	25.62			
34.035	49.356	24.678			
36.044	48.225	24.1125			
38.556	46.342	23.171			

A.4. NA952

Film-Casting

T = 150ºC; DR = 5; γ = 8.62 [1/s]; ε = 0.04946 [1/s]; strain = 1.6093

Distance to frostline = 66.4 [mm]

Dist. from die [mm]	Film width [mm]	Half-width [mm]	Dist. from die [mm] *continued*	Film width [mm] *continued*	Half-width [mm] *continued*
0	101.6	50.8	52.406	71.158	35.579
1.284	98.903	49.4515	58.314	70.516	35.258
2.697	97.104	48.552	64.865	69.617	34.8085
4.367	95.049	47.5245	73.856	68.718	34.359
6.294	92.48	46.24	83.232	68.204	34.102
8.221	90.425	45.2125	93.251	67.947	33.9735
10.019	88.755	44.3775	103.655	67.305	33.6525
12.459	86.443	43.2215	112.903	67.434	33.717
15.028	84.645	42.3225	131.142	66.663	33.3315
17.34	83.104	41.552	194.337	66.406	33.203
19.78	81.819	40.9095			
22.349	80.663	40.3315			
24.661	79.122	39.561			
26.716	78.48	39.24			
29.542	77.324	38.662			
33.01	75.782	37.891			
35.194	75.269	37.6345			
38.405	73.599	36.7995			
41.488	72.828	36.414			
43.8	71.929	35.9645			
47.525	71.158	35.579			

A.4. NA952

Film-Casting

T = 150ºC; DR = 10; γ = 8.62 [1/s]; ε = 0.07520 [1/s]; strain = 2.3027

Distance to frostline = 98.3 [mm]

Dist. from die [mm]	Film width [mm]	Half-width [mm]	Dist. from die [mm] *continued*	Film width [mm] *continued*	Half-width [mm] *continued*
0	101.6	50.8	70.038	67.295	33.6475
1.462	98.669	49.3345	77.613	66.371	33.1855
2.791	96.544	48.272	85.72	65.845	32.9225
5.05	93.622	46.811	93.694	65.326	32.663
7.309	91.231	45.6155	103.396	64.645	32.3225
9.701	89.239	44.6195	114.958	64.108	32.054
12.226	87.379	43.6895	132.102	63.306	31.653
15.15	85.117	42.5585	197.091	63.19	31.595
17.675	83.523	41.7615			
20.466	82.052	41.026			
23.523	80.591	40.2955			
26.978	78.851	39.4255			
29.902	77.784	38.892			
32.56	76.589	38.2945			
36.414	75.389	37.6945			
40.135	74.326	37.163			
43.325	73.131	36.5655			
47.046	72.201	36.1005			
52.495	70.74	35.37			
57.811	69.54	34.77			
63.393	68.344	34.172			

A.4. NA952

Film-Casting

T = 150ºC; DR = 15; γ = 8.62 [1/s]; ε = 0.08136 [1/s]; strain = 2.7082

Distance to frostline = 141.4 [mm]

Dist. from die [mm]	Film width [mm]	Half-width [mm]	Dist. from die [mm] *continued*	Film width [mm] *continued*	Half-width [mm] *continued*
0	101.6	50.8	49.564	70.248	35.124
1.561	99.128	49.564	53.337	69.338	34.669
3.642	95.876	47.938	56.459	69.078	34.539
5.854	93.144	46.572	59.321	68.427	34.2135
7.935	90.672	45.336	62.964	67.907	33.9535
9.236	89.372	44.686	65.045	67.777	33.8885
11.317	87.42	43.71	67.517	67.256	33.628
13.268	85.599	42.7995	69.859	66.866	33.433
15.48	84.038	42.019	73.371	66.606	33.303
17.431	83.127	41.5635	77.274	66.086	33.043
20.163	81.826	40.913	81.047	65.955	32.9775
22.114	80.656	40.328	84.299	65.695	32.8475
24.586	79.355	39.6775	90.543	65.305	32.6525
27.448	78.184	39.092	96.007	64.915	32.4575
29.79	76.753	38.3765	102.511	64.394	32.197
32.392	75.842	37.921	110.446	64.004	32.002
35.254	74.802	37.401	124.626	63.093	31.5465
38.376	73.631	36.8155	136.334	62.183	31.0915
40.718	72.98	36.49	158.449	61.532	30.766
43.32	71.679	35.8395	197.476	61.272	30.636
46.442	71.029	35.5145			

A.4. NA952

Film-Casting

T = 150ºC; DR = 20; γ = 8.62 [1/s]; ε = 0.1104 [1/s]; strain = 2.9954

Distance to frostline = 141.4 [mm]

Dist. from die [mm]	Film width [mm]	Half-width [mm]	Dist. from die [mm] *continued*	Film width [mm] *continued*	Half-width [mm] *continued*
0	101.6	50.8	48.191	70.527	35.2635
0.866	99.106	49.553	52.306	69.442	34.721
2.599	97.588	48.794	59.129	68.248	34.124
4.44	95.529	47.7645	65.952	67.5	33.75
6.173	93.686	46.843	82.954	65.217	32.6085
8.122	91.736	45.868	101.689	64.351	32.1755
10.288	90.218	45.109	118.367	64.263	32.1315
12.887	87.619	43.8095	147.39	63.425	31.7125
15.053	86.103	43.0515	196.665	61.839	30.9195
17.219	84.481	42.2405			
19.493	83.396	41.698			
21.767	81.988	40.994			
24.041	81.014	40.507			
26.315	79.826	39.913			
28.698	78.637	39.3185			
30.864	77.769	38.8845			
33.138	76.691	38.3455			
35.629	75.394	37.697			
37.903	74.53	37.265			
41.044	72.801	36.4005			
44.509	71.824	35.912			

A.4. NA952

Film-Casting

T = 150ºC; DR = 5; γ = 33.05 [1/s]; ε = 0.08905 [1/s]; strain = 1.6094

Distance to frostline = 141.4 [mm]

Dist. from die [mm]	Film width [mm]	Half-width [mm]	Dist. from die [mm] *continued*	Film width [mm] *continued*	Half-width [mm] *continued*
0	101.6	50.8	43.897	65.258	32.629
1.563	98.865	49.4325	45.981	64.216	32.108
3.126	97.302	48.651	48.326	63.174	31.587
4.559	95.348	47.674	52.106	61.742	30.871
6.383	93.524	46.762	54.972	60.699	30.3495
8.207	91.179	45.5895	58.619	59.527	29.7635
9.9	88.965	44.4825	62.266	58.225	29.1125
12.114	86.36	43.18	66.565	56.531	28.2655
13.938	84.797	42.3985	70.798	55.554	27.777
15.892	82.713	41.3565	73.989	54.512	27.256
17.716	81.15	40.575	77.506	53.926	26.963
20.061	79.456	39.728	81.283	53.405	26.7025
22.666	77.372	38.686	85.06	52.754	26.377
25.141	76.07	38.035	91.443	51.451	25.7255
27.876	73.725	36.8625	95.09	50.8	25.4
29.569	72.813	36.4065	104.208	49.367	24.6835
31.653	71.771	35.8855	118.536	46.892	23.446
33.737	70.599	35.2995	125.961	45.72	22.86
36.342	69.166	34.583	138.075	44.417	22.2085
38.947	67.733	33.8665	166.081	42.203	21.1015
41.292	66.301	33.1505	196.17	41.812	20.906

A.5. Affinity PL1880

Film-Casting

T = 150ºC; DR = 5; γ = 8.62 [1/s]; ε = 0.04435 [1/s]; strain = 1.6094

Distance to frostline = 74.1 [mm]

Dist. from die [mm]	Film width [mm]	Half-width [mm]	Dist. from die [mm] *continued*	Film width [mm] *continued*	Half-width [mm] *continued*
0	101.6	50.8	75.998	51.669	25.8345
1.58	100.81	50.405	80.264	51.511	25.7555
3.476	97.492	48.746	84.53	51.827	25.9135
5.214	93.7	46.85	89.112	52.143	26.0715
6.952	90.065	45.0325	95.748	52.459	26.2295
10.112	83.903	41.9515	102.384	52.459	26.2295
13.43	79.005	39.5025	108.704	52.459	26.2295
15.958	76.319	38.1595	119.607	52.617	26.3085
18.486	73.632	36.816	133.354	51.669	25.8345
21.33	70.63	35.315	200.35	51.827	25.9135
24.174	68.418	34.209			
28.282	65.89	32.945			
32.232	63.52	31.76			
35.708	61.94	30.97			
40.132	59.886	29.943			
45.662	57.673	28.8365			
51.034	55.935	27.9675			
56.722	54.513	27.2565			
61.146	53.407	26.7035			
65.728	52.301	26.1505			
70.942	51.827	25.9135			

A.5. Affinity PL1880

Film-Casting

T = 150ºC; DR = 10; γ = 8.62 [1/s]; ε = 0.07462 [1/s]; strain = 2.3025

Distance to frostline = 99.1 [mm]

Dist. from die [mm]	Film width [mm]	Half-width [mm]	Dist. from die [mm] *continued*	Film width [mm] *continued*	Half-width [mm] *continued*
0	101.6	50.8	50.012	48.631	24.3155
1.446	100.023	50.0115	54.284	47.054	23.527
2.892	98.183	49.0915	57.965	45.937	22.9685
4.338	95.423	47.7115	62.237	44.951	22.4755
5.521	92.794	46.397	67.626	43.37	21.685
7.098	88.719	44.3595	74.132	42.322	21.161
8.544	85.171	42.5855	80.309	41.074	20.537
10.121	81.753	40.8765	88.458	40.614	20.307
11.698	78.993	39.4965	96.541	41.008	20.504
13.407	75.839	37.9195	114.351	41.008	20.504
15.247	73.21	36.605	124.077	40.877	20.4385
17.087	70.844	35.422	138.668	40.417	20.2085
19.453	67.821	33.9105	155.032	39.497	19.7485
22.016	65.521	32.7605	198.997	38.708	19.354
25.105	62.498	31.249			
28.522	59.803	29.9015			
31.151	57.963	28.9815			
34.24	55.532	27.766			
37.723	53.692	26.846			
41.6	52.049	26.0245			
45.74	50.209	25.1045			

A.5. Affinity PL1880

Film-Casting

T = 150ºC; DR = 15; γ = 8.62 [1/s]; ε = 0.1162 [1/s]; strain = 2.7090

Distance to frostline = 99.0 [mm]

Dist. from die [mm]	Film width [mm]	Half-width [mm]	Dist. from die [mm] *continued*	Film width [mm] *continued*	Half-width [mm] *continued*
0	101.6	50.8	45.473	46.027	23.0135
1.44	100.488	50.244	49.018	44.698	22.349
2.991	98.273	49.1365	52.951	43.424	21.712
4.431	95.279	47.6395	56.385	42.316	21.158
5.871	91.51	45.755	61.204	40.876	20.438
7.2	88.294	44.147	65.137	39.824	19.912
8.751	84.084	42.042	70.066	38.716	19.358
10.302	80.094	40.047	74.719	37.553	18.7765
12.296	76.439	38.2195	79.593	37.11	18.555
14.511	72.562	36.281	85.243	36.39	18.195
16.173	69.902	34.951	92.997	35.946	17.973
18.167	66.911	33.4555	98.425	35.614	17.807
20.715	63.476	31.738	116.869	35.171	17.5855
22.377	61.592	30.796	126.562	34.728	17.364
24.371	59.265	29.6325	138.747	35.282	17.641
26.697	57.16	28.58	149.714	35.171	17.5855
30.131	54.944	27.472	158.244	35.282	17.641
32.9	53.006	26.503	196.295	35.06	17.53
35.725	51.067	25.5335			
39.159	49.184	24.592			
42.482	47.412	23.706			

A.5. Affinity PL1880

Film-Casting

T = 150ºC; DR = 20; γ = 8.62 [1/s]; ε = 0.1322 [1/s]; strain = 2.9953

Distance to frostline = 118.1 [mm]

Dist. from die [mm]	Film width [mm]	Half-width [mm]	Dist. from die [mm] *continued*	Film width [mm] *continued*	Half-width [mm] *continued*
0	101.6	50.8	51.904	44.117	22.0585
1.687	98.486	49.243	55.407	43.079	21.5395
3.504	94.593	47.2965	58.781	42.041	21.0205
5.061	90.96	45.48	62.544	40.874	20.437
6.359	87.327	43.6635	65.791	40.095	20.0475
8.046	83.174	41.587	68.646	39.576	19.788
9.863	79.022	39.511	72.02	38.668	19.334
11.68	75.13	37.565	75.783	37.759	18.8795
13.626	71.496	35.748	80.584	37.175	18.5875
15.962	68.252	34.126	101.799	34.97	17.485
18.427	65.398	32.699	112.309	34.126	17.063
21.152	62.413	31.2065	123.273	33.413	16.7065
24.007	59.429	29.7145	139.104	33.153	16.5765
26.472	57.872	28.936	154.156	32.504	16.252
29.067	55.796	27.898	171.089	32.115	16.0575
32.441	53.46	26.73	201.128	31.791	15.8955
35.685	51.514	25.757			
38.669	49.827	24.9135			
42.432	48.27	24.135			
45.157	46.972	23.486			
48.271	45.675	22.8375			

A.6. Affinity PL1840

Film-Casting

T = 150ºC; DR = 5; γ = 8.62 [1/s]; ε = 0.05146 [1/s]; strain = 1.6094

Distance to frostline = 63.9 [mm]

Dist. from die [mm]	Film width [mm]	Half-width [mm]	Dist. from die [mm] *continued*	Film width [mm] *continued*	Half-width [mm] *continued*
0	101.6	50.8	52.804	58.929	29.4645
2.339	98.252	49.126	56.035	58.372	29.186
4.901	93.351	46.6755	59.043	57.815	28.9075
6.906	89.563	44.7815	61.939	57.592	28.796
8.354	87.001	43.5005	65.058	57.258	28.629
10.582	83.77	41.885	68.177	57.035	28.5175
13.367	79.872	39.936	71.853	56.367	28.1835
15.372	77.755	38.8775	75.975	56.367	28.1835
17.489	75.75	37.875	80.876	56.255	28.1275
19.94	73.633	36.8165	85.777	56.367	28.1835
23.616	70.403	35.2015	89.676	56.033	28.0165
25.844	68.843	34.4215	102.152	56.033	28.0165
28.183	67.284	33.642	132.118	55.698	27.849
30.745	65.836	32.918	195.948	55.921	27.9605
33.196	64.833	32.4165			
35.87	63.608	31.804			
38.878	62.828	31.414			
41.997	61.602	30.801			
44.671	60.711	30.3555			
46.788	60.043	30.0215			
50.019	59.263	29.6315			

A.6. Affinity PL1840

Film-Casting

T = 150ºC; DR = 10; γ = 8.62 [1/s]; ε = 0.07897 [1/s]; strain = 2.3027

Distance to frostline = 93.7 [mm]

Dist. from die [mm]	Film width [mm]	Half-width [mm]	Dist. from die [mm] *continued*	Film width [mm] *continued*	Half-width [mm] *continued*
0	101.6	50.8	44.591	52.379	26.1895
1.633	99.967	49.9835	47.096	51.453	25.7265
3.049	97.353	48.6765	50.2	50.364	25.182
4.138	95.611	47.8055	54.066	49.439	24.7195
5.771	92.017	46.0085	58.258	48.132	24.066
7.622	87.879	43.9395	62.614	47.152	23.576
9.255	84.177	42.0885	67.351	45.845	22.9225
10.78	81.345	40.6725	71.435	45.083	22.5415
12.413	78.514	39.257	76.662	44.538	22.269
14.591	75.029	37.5145	83.522	43.94	21.97
16.333	71.98	35.99	90.872	44.157	22.0785
18.62	69.149	34.5745	99.801	43.994	21.997
20.58	67.08	33.54	107.805	44.103	22.0515
22.322	65.555	32.7775	124.793	44.048	22.024
24.5	64.14	32.07	138.078	43.722	21.861
26.787	62.18	31.09	152.833	42.742	21.371
29.346	60.437	30.2185	193.56	42.796	21.398
33.538	58.15	29.075			
36.097	56.517	28.2585			
38.874	55.101	27.5505			
41.814	53.468	26.734			

A.6. Affinity PL1840

Film-Casting

T = 150ºC; DR = 15; γ = 8.62 [1/s]; ε = 0.09946 [1/s]; strain = 2.7080

Distance to frostline = 115.7 [mm]

Dist. from die [mm]	Film width [mm]	Half-width [mm]	Dist. from die [mm] *continued*	Film width [mm] *continued*	Half-width [mm] *continued*
0	101.6	50.8	43.893	50.372	25.186
1.589	99.522	49.761	46.338	49.272	24.636
3.423	96.71	48.355	48.783	48.171	24.0855
5.257	93.042	46.521	51.84	46.949	23.4745
6.602	89.985	44.9925	55.019	45.971	22.9855
8.191	86.317	43.1585	57.953	45.237	22.6185
10.147	82.16	41.08	61.376	44.381	22.1905
12.103	78.615	39.3075	64.799	43.281	21.6405
14.059	75.069	37.5345	69.445	42.181	21.0905
15.771	72.624	36.312	73.602	41.691	20.8455
17.605	70.301	35.1505	78.859	40.836	20.418
19.317	68.1	34.05	83.627	40.591	20.2955
21.273	65.899	32.9495	88.028	39.98	19.99
23.107	64.065	32.0325	93.408	39.98	19.99
25.43	62.109	31.0545	99.643	39.735	19.8675
27.508	60.153	30.0765	123.484	38.635	19.3175
29.953	58.319	29.1595	133.143	38.268	19.134
32.276	56.73	28.365	158.451	37.29	18.645
34.721	55.018	27.509	197.453	36.801	18.4005
37.411	53.429	26.7145			
40.223	52.084	26.042			

A.6. Affinity PL1840

Film-Casting

T = 150ºC; DR = 20; γ = 8.62 [1/s]; ε = 0.1317 [1/s]; strain = 2.9949

Distance to frostline = 118.5 [mm]

Dist. from die [mm]	Film width [mm]	Half-width [mm]	Dist. from die [mm] *continued*	Film width [mm] *continued*	Half-width [mm] *continued*
0	101.6	50.8	51.374	41.835	20.9175
1.78	98.548	49.274	56.46	40.182	20.091
3.815	95.624	47.812	60.656	38.783	19.3915
5.214	92.572	46.286	65.234	38.402	19.201
6.613	89.52	44.76	74.008	36.495	18.2475
8.139	85.451	42.7255	82.019	36.113	18.0565
9.792	82.145	41.0725	89.14	35.605	17.8025
11.699	78.457	39.2285	97.278	34.969	17.4845
13.734	74.897	37.4485	103.763	34.842	17.421
15.514	72.735	36.3675	119.531	33.316	16.658
17.421	69.683	34.8415	127.542	32.68	16.34
19.583	66.504	33.252	141.021	32.426	16.213
21.49	64.47	32.235	156.28	31.154	15.577
23.525	62.054	31.027	167.216	30.518	15.259
26.452	58.747	29.3735	192.012	30.137	15.0685
29.122	56.586	28.293			
31.792	54.17	27.085			
35.098	51.499	25.7495			
39.04	48.193	24.0965			
42.6	46.159	23.0795			
47.051	44.506	22.253			

Appendix B: Shear Step-Strain Rheology for the LLDPE-based PE Resins

B.1. Exact 3132

Stress Relaxation

T=150°C; strain=0.01 [strain units]; fixture diameter=25 [mm]; cone angle=0.1 [rad]

Time [s]	G(γ,t) [Pa]	γ [%]	Time [s] *cont.*	G(γ,t) [Pa] *cont.*	γ [%] *cont.*	Time [s] *cont.*	G(γ,t) [Pa] *cont.*	γ [%] *cont.*
0.001	0	0	0.145	23056	1.0018	0.285	7309.03	0.99888
0.01	99228.1	0.03745	0.15	21718.6	1.00472	0.29	7101.96	1.00964
0.015	265438	0.1677	0.155	20600.5	1.00571	0.295	6895.61	1.00377
0.02	276250	0.3261	0.16	19538	1.00472	0.3	6698.76	0.9979
0.025	259246	0.48671	0.165	18614.4	1.00377	0.305	6506.02	1.00377
0.03	238872	0.61878	0.17	17721.2	1.00278	0.31	6323.42	1.00278
0.035	214126	0.73081	0.175	16839.4	1.00571	0.315	6073.32	1.0018
0.04	188891	0.8218	0.18	16071.1	1.00278	0.32	5874.3	1.00278
0.045	167762	0.87657	0.185	15300.2	1.0018	0.325	5775.91	1.00278
0.05	147032	0.92061	0.19	14657.9	1.00377	0.33	5565.14	1.00669
0.055	128128	0.95386	0.195	14008.8	1.00472	0.335	5410.89	1.00472
0.06	111744	0.97441	0.2	13436.1	1.0018	0.34	5325.9	1.00964
0.065	97306.7	0.99104	0.205	12875.9	1.00377	0.345	5207.57	1.00377
0.07	85506	0.99691	0.21	12326.1	1.00571	0.35	5107.3	1.0018
0.075	75371.7	1.00082	0.215	11819.9	1.00278	0.355	5007.56	0.99888
0.08	66307.8	1.00866	0.22	11310.9	1.00472	0.36	4900.58	1.00377
0.085	59101.7	1.00866	0.225	11012.7	1.00472	0.365	4799.83	1.0018
0.09	53000	1.01059	0.23	10652	1.00472	0.37	4660.6	1.00377
0.095	48039.3	1.00669	0.235	10316.6	1.00377	0.375	4653.04	1.00964
0.1	43837.4	1.0018	0.24	10010.9	1.00767	0.38	4563.22	1.0018
0.105	39890.8	1.00767	0.245	9579.28	1.00866	0.385	4480.9	1.00082
0.11	36777.4	1.00472	0.25	9249.05	1.00377	0.39	4483.43	1.00377
0.115	34050.3	1.00278	0.255	8937.76	1.00082	0.395	4337.91	1.00377
0.12	31446.2	1.00866	0.26	8501.96	1.00669	0.4	4191.36	1.00964
0.125	29469.7	1.00571	0.265	8276.72	0.99983	0.405	4074.16	1.00767
0.13	27611	1.00377	0.27	7961.53	1.00082	0.41	3952.44	1.00571
0.135	25733.4	1.00964	0.275	7796.38	1.0018	0.415	3815.03	1.00571
0.14	24416.5	1.00472	0.28	7544.03	1.0018	0.42	3686.64	1.00377

Time [s] *cont.*	G(γ,t) [Pa] *cont.*	γ [%] *cont.*	Time [s] *cont.*	G(γ,t) [Pa] *cont.*	γ [%] *cont.*	Time [s] *cont.*	G(γ,t) [Pa] *cont.*	γ [%] *cont.*
0.425	3658.02	1.00082	0.58	2045.72	1.00377	0.735	1269.75	1.00669
0.43	3530.29	1.00571	0.585	2000.45	1.00278	0.74	1290.17	1.00377
0.435	3428.32	1.00278	0.59	1970.93	1.00278	0.745	1250.38	1.00571
0.44	3396.97	0.99691	0.595	1892.77	1.00767	0.75	1216.04	1.00082
0.445	3243.09	1.00767	0.6	1889.93	1.00082	0.755	1162.29	1.00377
0.45	3157.35	1.00377	0.605	1814.77	1.00472	0.76	1150.25	1.00571
0.455	3084.7	1.0018	0.61	1852.74	1.00278	0.765	1078.48	1.00669
0.46	3078.04	0.99691	0.615	1816.49	1.00377	0.77	1024.56	1.00377
0.465	2943.09	1.00571	0.62	1763.91	1.00571	0.775	1060.03	1.00278
0.47	2817.82	1.00767	0.625	1786.69	1.00669	0.78	1041.25	1.00571
0.475	2861.96	1.0018	0.63	1719.79	1.00278	0.785	1056.96	1.00571
0.48	2746.13	1.00377	0.635	1643.96	1.00278	0.79	1085.62	1.00278
0.485	2724.49	1.00377	0.64	1627.78	1.00669	0.795	1165.87	0.99983
0.49	2782.12	1.00571	0.645	1575.94	1.00472	0.8	1166.75	1.00669
0.495	2721.91	1.00472	0.65	1505.63	0.99983	0.805	1104	1.00669
0.5	2680	1.00571	0.655	1460.5	1.00571	0.81	1160.2	1.00472
0.505	2606.48	1.00377	0.66	1512.03	1.00278	0.815	1029.45	1.00669
0.51	2594.39	1.00082	0.665	1417.08	1.00377	0.82	949.734	1.00278
0.515	2563.82	0.99888	0.67	1350.19	1.00669	0.825	973.511	1.00669
0.52	2473.93	1.00964	0.675	1391.89	1.00278	0.83	878.48	0.99983
0.525	2531.68	1.00377	0.68	1314.87	1.00669	0.835	877.989	1.00377
0.53	2467.65	1.0018	0.685	1295.83	1.00472	0.84	895.685	1.00377
0.535	2390.05	1.00377	0.69	1286.79	1.0018	0.845	925.136	1.00278
0.54	2374.64	1.00278	0.695	1262.16	1.0018	0.85	967.665	1.00767
0.545	2272.23	1.00278	0.7	1223.88	1.00571	0.855	968.492	1.00377
0.55	2202.58	1.00669	0.705	1155.55	1.00278	0.86	1032.47	1.00278
0.555	2151.93	1.00377	0.71	1266.34	1.00472	0.865	980.299	1.00377
0.56	2181.79	1.0018	0.715	1249.4	1.00571	0.87	920.274	1.00377
0.565	2118.74	1.0018	0.72	1219.77	1.0018	0.875	953.8	1.00472
0.57	2067.45	1.0018	0.725	1321.97	1.00278	0.88	875.311	1.00571
0.575	2128.37	1.00377	0.73	1285.25	1.00377	0.885	783.655	1.00866

B.1. Exact 3132

Stress Relaxation

T=150°C; strain=0.1 [strain units]; fixture diameter=25 [mm]; cone angle=0.1 [rad]

Time [s]	G(γ,t) [Pa]	γ [%]	Time [s] *cont.*	G(γ,t) [Pa] *cont.*	γ [%] *cont.*	Time [s] *cont.*	G(γ,t) [Pa] *cont.*	γ [%] *cont.*
0.001	0	0	0.145	23470.8	10.0476	0.285	7752.62	10.0398
0.01	87426.9	0.43349	0.15	22247.4	10.0476	0.29	7517.12	10.0398
0.015	258153	1.78837	0.155	21134.9	10.0398	0.295	7318.75	10.0319
0.02	274615	3.40454	0.16	20098.5	10.0398	0.3	7101.13	10.0398
0.025	259195	4.97768	0.165	19125.4	10.0398	0.305	6902.44	10.0319
0.03	236593	6.33559	0.17	18216.5	10.0476	0.31	6721.81	10.0319
0.035	212568	7.42445	0.175	17400.8	10.0476	0.315	6528.14	10.0398
0.04	188633	8.25974	0.18	16645.5	10.0398	0.32	6360.67	10.0319
0.045	166182	8.86866	0.185	15923	10.0398	0.325	6195.39	10.0319
0.05	145672	9.30592	0.19	15240.4	10.0398	0.33	6029.99	10.0319
0.055	127551	9.60251	0.195	14620.3	10.0398	0.335	5875.69	10.0398
0.06	111787	9.79777	0.2	14023.7	10.0398	0.34	5726.25	10.0398
0.065	98057.6	9.93844	0.205	13469.3	10.0319	0.345	5588.97	10.0319
0.07	86303.7	10.0243	0.21	12948.5	10.0398	0.35	5446.88	10.0398
0.075	76352.5	10.0789	0.215	12454	10.0398	0.355	5305.55	10.0319
0.08	67721	10.1101	0.22	11984.7	10.0319	0.36	5183.45	10.0319
0.085	60395.2	10.118	0.225	11535.7	10.0398	0.365	5049.59	10.0319
0.09	54144	10.1101	0.23	11111.9	10.0398	0.37	4923.54	10.0319
0.095	48750.3	10.1101	0.235	10727.9	10.0319	0.375	4813.49	10.0398
0.1	44268.2	10.0944	0.24	10358.8	10.0319	0.38	4703.08	10.0319
0.105	40426.2	10.0867	0.245	10013.1	10.0319	0.385	4592.86	10.0319
0.11	37174.3	10.0789	0.25	9675.35	10.0319	0.39	4486.91	10.0398
0.115	34355	10.071	0.255	9361.1	10.0319	0.395	4396.43	10.0398
0.12	31938.9	10.0631	0.26	9063.26	10.0398	0.4	4293.61	10.0319
0.125	29862.8	10.0555	0.265	8779.87	10.0319	0.405	4195.8	10.0398
0.13	27982.3	10.0555	0.27	8498.3	10.0398	0.41	4113.23	10.0398
0.135	26305.1	10.0555	0.275	8253.57	10.0319	0.415	4014.83	10.0398
0.14	24835.5	10.0476	0.28	8002.18	10.0319	0.42	3928.3	10.0398

Time [s] *cont.*	G(γ,t) [Pa] *cont.*	γ [%] *cont.*	Time [s] *cont.*	G(γ,t) [Pa] *cont.*	γ [%] *cont.*	Time [s] *cont.*	G(γ,t) [Pa] *cont.*	γ [%] *cont.*
0.425	3848.69	10.0319	0.58	2191.11	10.0319	0.735	1397.73	10.0319
0.43	3755.19	10.0398	0.585	2153.68	10.0319	0.74	1382.94	10.0319
0.435	3679.39	10.0319	0.59	2124.18	10.0319	0.745	1369.18	10.0319
0.44	3604.61	10.0319	0.595	2096.59	10.0319	0.75	1357.37	10.0319
0.445	3541.58	10.0319	0.6	2059.53	10.0398	0.755	1341.62	10.0319
0.45	3470.69	10.0319	0.605	2023.73	10.0319	0.76	1329.81	10.0319
0.455	3397.2	10.0398	0.61	1992.24	10.0319	0.765	1305.19	10.0319
0.46	3340.8	10.0319	0.615	1962.74	10.0319	0.77	1289.45	10.0319
0.465	3273.87	10.0319	0.62	1927.73	10.0398	0.775	1266.81	10.0319
0.47	3206.94	10.0319	0.625	1888.39	10.0398	0.78	1260.9	10.0319
0.475	3145.89	10.0319	0.63	1870.2	10.0319	0.785	1237.28	10.0319
0.48	3082.86	10.0319	0.635	1838.69	10.0319	0.79	1209.76	10.0398
0.485	3019.9	10.0319	0.64	1815.09	10.0319	0.795	1214.64	10.0319
0.49	2960.83	10.0319	0.645	1799.32	10.0319	0.8	1190.02	10.0319
0.495	2911.59	10.0319	0.65	1771.76	10.0319	0.805	1175.27	10.0319
0.5	2854.24	10.0398	0.655	1744.21	10.0319	0.81	1164.44	10.0319
0.505	2807.3	10.0319	0.66	1725.13	10.0398	0.815	1152.63	10.0319
0.51	2761.78	10.0398	0.665	1693.02	10.0319	0.82	1129.99	10.0319
0.515	2708.83	10.0319	0.67	1665.46	10.0319	0.825	1122.1	10.0319
0.52	2663.55	10.0319	0.675	1644.47	10.0398	0.83	1117.19	10.0319
0.525	2624.21	10.0319	0.68	1624.12	10.0319	0.835	1096.53	10.0319
0.53	2576.95	10.0319	0.685	1598.54	10.0319	0.84	1078.8	10.0319
0.535	2531.68	10.0319	0.69	1577.85	10.0319	0.845	1075.84	10.0319
0.54	2488.38	10.0319	0.695	1569	10.0319	0.85	1052.21	10.0319
0.545	2454.92	10.0319	0.7	1542.41	10.0319	0.855	1043.36	10.0319
0.55	2413.54	10.0319	0.705	1507.95	10.0319	0.86	1033.53	10.0319
0.555	2368.26	10.0319	0.71	1489.27	10.0319	0.865	1026.63	10.0319
0.56	2329.01	10.0398	0.715	1463.66	10.0319	0.87	1021.9	10.0398
0.565	2289.52	10.0319	0.72	1444.1	10.0243	0.875	1009.11	10.0398
0.57	2248.2	10.0319	0.725	1425.28	10.0319	0.88	1009.9	10.0319
0.575	2216.71	10.0319	0.73	1424.29	10.0319	0.885	995.146	10.0319

B.1. Exact 3132

Stress Relaxation

T=150°C; strain=1.0 [strain units]; fixture diameter=10 [mm]; cone angle=0.035 [rad]

Time [s]	G(γ,t) [Pa]	γ [%]	Time [s] *cont.*	G(γ,t) [Pa] *cont.*	γ [%] *cont.*	Time [s] *cont.*	G(γ,t) [Pa] *cont.*	γ [%] *cont.*
0.001	0	0	0.145	20681.8	100.289	0.285	6882.73	100.199
0.01	51412.1	4.76303	0.15	19583.6	100.289	0.29	6681.16	100.199
0.015	77684.2	20.3716	0.155	18610.1	100.199	0.295	6499.12	100.199
0.02	87087.1	37.3181	0.16	17697.5	100.199	0.3	6322.03	100.199
0.025	90375.2	52.8651	0.165	16838.8	100.289	0.305	6140.13	100.199
0.03	91368.3	65.8924	0.17	16054.6	100.289	0.31	5972.81	100.199
0.035	91560.3	76.0191	0.175	15319.2	100.289	0.315	5820.35	100.199
0.04	91254.2	83.5136	0.18	14652.6	100.289	0.32	5658.13	100.199
0.045	89164.1	88.9564	0.185	14015.4	100.289	0.325	5505.68	100.199
0.05	85474.9	92.703	0.19	13439.2	100.199	0.33	5377.7	100.199
0.055	80346.7	95.2916	0.195	12889.8	100.199	0.335	5230.21	100.199
0.06	74616.7	97.0763	0.2	12369.8	100.199	0.34	5092.47	100.199
0.065	68692.3	98.2343	0.205	11879.2	100.199	0.345	4969.95	100.289
0.07	62989.9	98.9482	0.21	11427.7	100.199	0.35	4842.17	100.289
0.075	57551.3	99.485	0.215	10986.2	100.289	0.355	4724.29	100.289
0.08	52667	99.752	0.22	10583.9	100.199	0.36	4611.21	100.289
0.085	48163.7	99.9319	0.225	10182.4	100.289	0.365	4508.04	100.289
0.09	44150.5	100.109	0.23	9838.27	100.199	0.37	4398.98	100.199
0.095	40617.8	100.199	0.235	9484.54	100.199	0.375	4286.92	100.289
0.1	37458.7	100.199	0.24	9159.96	100.199	0.38	4202.22	100.199
0.105	34672.2	100.199	0.245	8852.06	100.289	0.385	4100.16	100.289
0.11	32199.8	100.199	0.25	8564.85	100.199	0.39	4004.34	100.289
0.115	29955.4	100.289	0.255	8284.58	100.199	0.395	3926.82	100.199
0.12	27975.1	100.289	0.26	8016.63	100.289	0.4	3850.59	100.199
0.125	26210.3	100.289	0.265	7777.94	100.199	0.405	3762.05	100.199
0.13	24622.5	100.289	0.27	7532.06	100.199	0.41	3685.82	100.199
0.135	23171.7	100.289	0.275	7300.75	100.199	0.415	3619.43	100.199
0.14	21857.7	100.289	0.28	7087.86	100.289	0.42	3540.73	100.199

Time [s] *cont.*	G(γ,t) [Pa] *cont.*	γ [%] *cont.*	Time [s] *cont.*	G(γ,t) [Pa] *cont.*	γ [%] *cont.*	Time [s] *cont.*	G(γ,t) [Pa] *cont.*	γ [%] *cont.*
0.425	3466.9	100.199	0.58	1975.43	100.199	0.735	1274.55	100.199
0.43	3400.51	100.199	0.585	1939.76	100.199	0.74	1256.11	100.199
0.435	3326.76	100.199	0.59	1904.12	100.199	0.745	1246.39	100.289
0.44	3253.01	100.199	0.595	1877.05	100.199	0.75	1240.24	100.289
0.445	3189.03	100.199	0.6	1856.17	100.199	0.755	1221.67	100.199
0.45	3127.59	100.199	0.605	1820.49	100.199	0.76	1199.7	100.289
0.455	3056.25	100.199	0.61	1789.74	100.199	0.765	1192.18	100.199
0.46	2994.53	100.289	0.615	1771.3	100.199	0.77	1172.67	100.289
0.465	2950.51	100.199	0.62	1743.03	100.199	0.775	1155.28	100.199
0.47	2889	100.199	0.625	1717.19	100.199	0.78	1144.42	100.289
0.475	2827.43	100.289	0.63	1698.76	100.199	0.785	1131.91	100.199
0.48	2783.24	100.289	0.635	1674.16	100.199	0.79	1114.71	100.199
0.485	2734.06	100.199	0.64	1644.64	100.199	0.795	1102.41	100.199
0.49	2675.11	100.289	0.645	1626.21	100.199	0.8	1091.6	100.289
0.495	2633.28	100.199	0.65	1609.01	100.199	0.805	1071.94	100.289
0.5	2586.56	100.199	0.655	1579.49	100.199	0.81	1054.74	100.289
0.505	2530.15	100.289	0.66	1552.46	100.199	0.815	1050.76	100.199
0.51	2488.18	100.199	0.665	1542.62	100.199	0.82	1033.55	100.199
0.515	2451.55	100.289	0.67	1513.1	100.199	0.825	1016.66	100.289
0.52	2407.32	100.289	0.675	1488.51	100.199	0.83	1015.11	100.199
0.525	2365.56	100.289	0.68	1474.99	100.199	0.835	1001.01	100.199
0.53	2333.6	100.289	0.685	1450.4	100.199	0.84	984.109	100.289
0.535	2294.28	100.289	0.69	1427.04	100.199	0.845	975.755	100.199
0.54	2250.08	100.289	0.695	1409.8	100.199	0.85	971.437	100.199
0.545	2218.12	100.289	0.7	1393.81	100.199	0.855	952.943	100.199
0.55	2183.71	100.289	0.705	1369.25	100.199	0.86	939.387	100.199
0.555	2141.96	100.289	0.71	1350.8	100.289	0.865	938.768	100.199
0.56	2104.53	100.199	0.715	1344.65	100.199	0.87	927.672	100.199
0.565	2079.93	100.199	0.72	1318.82	100.199	0.875	914.735	100.199
0.57	2040.58	100.199	0.725	1297.9	100.199	0.88	912.877	100.199
0.575	2002.46	100.199	0.73	1286.91	100.289	0.885	907.957	100.199

B.1. Exact 3132

Stress Relaxation

T=150°C; strain=5.0 [strain units]; fixture diameter=10 [mm]; cone angle=0.035 [rad]

Time [s]	G(γ,t) [Pa]	γ [%]	Time [s] *cont.*	G(γ,t) [Pa] *cont.*	γ [%] *cont.*	Time [s] *cont.*	G(γ,t) [Pa] *cont.*	γ [%] *cont.*
0.001	0	0	0.145	2312.56	501.232	0.285	792.748	501.232
0.01	83003.7	11.4046	0.15	2194.63	501.232	0.29	773.056	501.232
0.015	109017	66.5164	0.155	2086.57	501.232	0.295	750.888	501.232
0.02	65846.1	150.431	0.16	1992.05	501.232	0.3	729.959	501.232
0.025	41116.8	230.861	0.165	1900.94	501.232	0.305	707.791	501.232
0.03	29234.1	301.526	0.17	1813.51	501.232	0.31	691.794	501.232
0.035	22771.2	357.766	0.175	1737.18	501.232	0.315	672.083	501.232
0.04	18229.1	400.49	0.18	1662.05	501.232	0.32	653.01	501.232
0.045	15207.3	431.815	0.185	1589.39	501.232	0.325	638.231	501.232
0.05	12873	453.886	0.19	1530.32	501.232	0.33	621.596	501.232
0.055	11067.1	469.199	0.195	1468.73	501.232	0.335	605.599	501.232
0.06	9599.48	479.88	0.2	1409.65	501.232	0.34	591.439	501.232
0.065	8407.44	486.997	0.205	1355.45	501.232	0.345	576.661	501.232
0.07	7416.49	491.978	0.21	1307.44	501.232	0.35	559.426	501.232
0.075	6607.64	495.183	0.215	1258.19	501.232	0.355	545.875	501.232
0.08	5930.55	497.319	0.22	1212.64	501.232	0.36	536.029	501.232
0.085	5360.5	498.747	0.225	1172	501.232	0.365	520.023	501.232
0.09	4879.66	499.455	0.23	1130.14	501.232	0.37	508.02	501.232
0.095	4469.04	500.163	0.235	1090.74	501.232	0.375	497.855	501.232
0.1	4111.55	500.523	0.24	1055.03	501.232	0.38	485.852	501.232
0.105	3801.34	500.883	0.245	1023.01	501.232	0.385	473.54	501.232
0.11	3533.41	500.883	0.25	987.306	501.232	0.39	465.232	501.232
0.115	3292.7	501.232	0.255	954.054	501.232	0.395	453.839	501.232
0.12	3083.85	501.232	0.26	926.354	501.232	0.4	443.993	501.232
0.125	2897.21	501.232	0.265	895.578	501.232	0.405	433.828	501.232
0.13	2730.15	501.232	0.27	867.24	501.232	0.41	426.748	501.232
0.135	2575.38	501.232	0.275	843.235	501.232	0.415	415.674	501.232
0.14	2440.28	501.232	0.28	819.229	501.232	0.42	404.899	501.232

Time [s] *cont.*	G(γ,t) [Pa] *cont.*	γ [%] *cont.*	Time [s] *cont.*	G(γ,t) [Pa] *cont.*	γ [%] *cont.*	Time [s] *cont.*	G(γ,t) [Pa] *cont.*	γ [%] *cont.*
0.425	397.819	501.232	0.58	226.972	501.232			
0.43	388.892	501.232	0.585	220.047	501.232			
0.435	378.118	501.232	0.59	216.662	501.232			
0.44	372.576	501.232	0.595	214.66	501.232			
0.445	365.187	501.232	0.6	209.732	501.232			
0.45	357.179	501.232	0.605	206.192	501.232			
0.455	350.718	501.232	0.61	205.269	501.232			
0.46	346.104	501.232	0.615	199.577	501.232			
0.465	337.787	501.232	0.62	194.344	501.232			
0.47	328.86	501.232	0.625	195.113	501.232			
0.475	323.937	501.232	0.63	191.419	501.232			
0.48	316.238	501.232	0.635	186.8	501.232			
0.485	310.087	501.232	0.64	184.494	501.232			
0.49	304.235	501.232	0.645	182.492	501.232			
0.495	300.236	501.232	0.65	179.261	501.232			
0.5	295.004	501.232	0.655	175.567	501.232			
0.505	288.847	501.232	0.66	174.488	501.232			
0.51	286.381	501.232	0.665	172.641	501.232			
0.515	280.535	501.232	0.67	168.946	501.232			
0.52	273.76	501.232	0.675	168.946	501.232			
0.525	269.76	501.232	0.68	165.716	501.232			
0.53	264.832	501.232	0.685	162.331	501.232			
0.535	258.372	501.232	0.69	161.407	501.232			
0.54	256.829	501.232	0.695	160.174	501.232			
0.545	252.366	501.232	0.7	157.712	501.232			
0.55	249.29	501.232	0.705	153.556	501.232			
0.555	243.593	501.232	0.71	152.787	501.232			
0.56	241.441	501.232	0.715	152.478	501.232			
0.565	238.206	501.232						
0.57	232.359	501.232						
0.575	229.434	501.232						

B.1. Exact 3132

Stress Relaxation

T=150°C; strain=7.5 [strain units]; fixture diameter=10 [mm]; cone angle=0.035 [rad]

Time [s]	G(γ,t) [Pa]	γ [%]	Time [s] *cont.*	G(γ,t) [Pa] *cont.*	γ [%] *cont.*	Time [s] *cont.*	G(γ,t) [Pa] *cont.*	γ [%] *cont.*
0.001	0	0	0.145	1939.82	751.847	0.285	611.372	751.15
0.01	82906.5	11.8294	0.15	1831.75	751.847	0.29	592.475	751.15
0.015	108635	74.3678	0.155	1733.53	751.847	0.295	573.991	751.15
0.02	60044.2	187.962	0.16	1644.98	751.15	0.3	555.805	751.847
0.025	38740	310.599	0.165	1559.73	751.15	0.305	542.355	751.15
0.03	27778.6	420.785	0.17	1482.94	751.847	0.31	526.336	751.15
0.035	22138.7	511.553	0.175	1412.53	751.847	0.315	509.492	751.15
0.04	18197.1	581.33	0.18	1345.39	751.847	0.32	497.529	751.847
0.045	15307.4	633.308	0.185	1286.37	751.847	0.325	483.576	751.847
0.05	13018.7	670.681	0.19	1229.74	751.847	0.33	470.023	751.847
0.055	11179.3	696.676	0.195	1177.47	751.15	0.335	457.732	751.15
0.06	9655.23	714.834	0.2	1129.01	751.15	0.34	446.217	751.847
0.065	8396.92	726.932	0.205	1083.63	751.847	0.345	433.502	751.847
0.07	7335.15	735.477	0.21	1038.47	751.847	0.35	422.011	751.847
0.075	6441.56	741.166	0.215	997.432	751.847	0.355	412.572	751.847
0.08	5702.98	744.741	0.22	960.498	751.847	0.36	401.482	751.847
0.085	5083.35	746.877	0.225	922.74	751.847	0.365	390.354	751.15
0.09	4555.9	749.014	0.23	887.431	751.847	0.37	381.318	751.15
0.095	4114.82	749.711	0.235	855.424	751.847	0.375	372.756	751.847
0.1	3740.09	750.431	0.24	824.242	751.847	0.38	362.491	751.847
0.105	3421.81	750.431	0.245	795.498	751.847	0.385	354.696	751.847
0.11	3143.17	751.15	0.25	767.591	751.847	0.39	346.894	751.847
0.115	2900.54	751.15	0.255	744.476	751.15	0.395	338.594	751.15
0.12	2690.74	751.15	0.26	717.517	751.847	0.4	329.246	751.847
0.125	2505.53	751.15	0.265	693.712	751.847	0.405	324.421	751.15
0.13	2339.99	751.15	0.27	671.544	751.847	0.41	315.499	751.847
0.135	2190.38	751.847	0.275	652.044	751.15	0.415	307.904	751.847
0.14	2062.97	751.15	0.28	629.856	751.15	0.42	302.439	751.15

Time [s] *cont.*	G(γ,t) [Pa] *cont.*	γ [%] *cont.*	Time [s] *cont.*	G(γ,t) [Pa] *cont.*	γ [%] *cont.*	Time [s] *cont.*	G(γ,t) [Pa] *cont.*	γ [%] *cont.*
0.425	296.001	751.847	0.58	167.076	751.15	0.735	112.64	751.847
0.43	289.024	751.847	0.585	164.561	751.847	0.74	112.54	751.847
0.435	283.692	751.847	0.59	164.458	751.847	0.745	110.589	751.15
0.44	277.999	751.15	0.595	161.942	751.15	0.75	108.845	751.847
0.445	272.448	751.15	0.6	158.347	751.15	0.755	109.152	751.847
0.45	265.838	751.847	0.605	156.866	751.847	0.76	107.204	751.847
0.455	261.567	751.15	0.61	154.136	751.15	0.765	104.432	751.847
0.46	256.223	751.15	0.615	150.541	751.15	0.77	104.432	751.847
0.465	250.647	751.847	0.62	149.683	751.847	0.775	104.229	751.847
0.47	246.568	751.15	0.625	148.348	751.847	0.78	102.688	751.847
0.475	242.257	751.15	0.63	146.091	751.847	0.785	101.456	751.847
0.48	236.081	751.847	0.635	143.835	751.847	0.79	101.456	751.847
0.485	232.799	751.847	0.64	143.525	751.847	0.795	100.125	751.847
0.49	228.279	751.847	0.645	140.243	751.847			
0.495	223.353	751.847	0.65	137.805	751.15			
0.5	218.021	751.847	0.655	136.369	751.15			
0.505	215.764	751.847	0.66	134.701	751.847			
0.51	211.25	751.847	0.665	131.213	751.847			
0.515	206.53	751.847	0.67	130.822	751.15			
0.52	204.274	751.847	0.675	129.572	751.847			
0.525	201.398	751.847	0.68	126.714	751.15			
0.53	196.472	751.847	0.685	125.981	751.847			
0.535	193.573	751.15	0.69	124.955	751.847			
0.54	190.317	751.847	0.695	123.211	751.847			
0.545	186.623	751.847	0.7	121.876	751.847			
0.55	183.304	751.15	0.705	120.132	751.847			
0.555	180.465	751.847	0.71	119.413	751.847			
0.56	178.002	751.847	0.715	117.26	751.847			
0.565	174.104	751.847	0.72	116.028	751.847			
0.57	172.827	751.15	0.725	116.644	751.847			
0.575	170.203	751.847	0.73	113.977	751.15			

B.1. Exact 3132

Stress Relaxation

T=150°C; strain=10.0 [strain units]; fixture diameter=10 [mm]; cone angle=0.035 [rad]

Time [s]	G(γ,t) [Pa]	γ [%]	Time [s] *cont.*	G(γ,t) [Pa] *cont.*	γ [%] *cont.*	Time [s] *cont.*	G(γ,t) [Pa] *cont.*	γ [%] *cont.*
0.001	0	0	0.145	1521.83	1001.77	0.285	469.686	1001.77
0.01	78707	12.1649	0.15	1437.04	1001.77	0.29	453.668	1001.77
0.015	83547.8	78.9632	0.155	1359.61	1001.77	0.295	440.728	1001.77
0.02	42320.7	211.281	0.16	1288.29	1001.77	0.3	426.868	1001.77
0.025	25580	370.943	0.165	1223.17	1001.77	0.305	413.009	1001.77
0.03	18219.4	521.886	0.17	1162.94	1001.77	0.31	401.917	1001.77
0.035	14469.1	649.678	0.175	1106.4	1001.77	0.315	390.525	1001.77
0.04	12238.5	750.431	0.18	1054.79	1001.77	0.32	378.505	1001.77
0.045	10549.3	825.896	0.185	1005.67	1001.77	0.325	368.342	1001.77
0.05	9212.1	880.719	0.19	960.088	1001.77	0.33	358.79	1001.77
0.055	8076.74	919.869	0.195	918.818	1001.77	0.335	348.937	1001.77
0.06	7091.69	946.943	0.2	878.768	1001.77	0.34	339.075	1001.77
0.065	6241.62	965.45	0.205	840.577	1001.77	0.345	329.531	1001.77
0.07	5504.32	977.548	0.21	806.683	1001.77	0.35	320.908	1001.77
0.075	4882.29	986.093	0.215	774.647	1001.77	0.355	311.665	1001.77
0.08	4342.84	991.782	0.22	743.23	1001.77	0.36	303.656	1001.77
0.085	3894.32	995.357	0.225	714.272	1001.77	0.365	296.262	1001.77
0.09	3510.69	997.493	0.23	688.392	1001.77	0.37	287.019	1001.77
0.095	3182.81	998.91	0.235	662.512	1001.77	0.375	279.629	1001.77
0.1	2902.55	1000.33	0.24	637.27	1001.77	0.38	272.849	1001.77
0.105	2659.4	1001.05	0.245	615.706	1001.77	0.385	266.384	1001.77
0.11	2450.33	1001.05	0.25	593.523	1001.77	0.39	258.375	1001.77
0.115	2266.64	1001.77	0.255	572.569	1001.77	0.395	254.058	1001.77
0.12	2104.41	1001.77	0.26	553.473	1001.77	0.4	247.593	1001.77
0.125	1959.38	1001.77	0.265	534.377	1001.77	0.405	241.433	1001.77
0.13	1834.01	1001.77	0.27	516.511	1001.77	0.41	235.577	1001.77
0.135	1718.48	1001.77	0.275	500.183	1001.77	0.415	230.801	1001.77
0.14	1615.26	1001.77	0.28	484.785	1001.77	0.42	224.335	1001.77

Time [s] *cont.*	G(γ,t) [Pa] *cont.*	γ [%] *cont.*	Time [s] *cont.*	G(γ,t) [Pa] *cont.*	γ [%] *cont.*	Time [s] *cont.*	G(γ,t) [Pa] *cont.*	γ [%] *cont.*
0.425	219.25	1001.77	0.58	117.831	1001.77			
0.43	215.247	1001.77	0.585	115.365	1001.77			
0.435	209.856	1001.77	0.59	112.902	1001.77			
0.44	205.08	1001.77	0.595	111.515	1001.77			
0.445	200.768	1001.77	0.6	110.051	1001.77			
0.45	196.302	1001.77	0.605	107.896	1001.77			
0.455	191.066	1001.77	0.61	106.047	1001.77			
0.46	188.138	1001.77	0.615	104.431	1001.77			
0.465	185.215	1001.77	0.62	102.042	1001.77			
0.47	179.669	1001.77	0.625	100.116	1001.77			
0.475	175.512	1001.77	0.63	98.8849	1001.77			
0.48	172.584	1001.77	0.635	97.5758	1001.77			
0.485	168.273	1001.77	0.64	95.1126	1001.77			
0.49	164.88	1001.77	0.645	94.4182	1001.77			
0.495	161.957	1001.77	0.65	92.9544	1001.77			
0.5	159.494	1001.77	0.655	91.7228	1001.77			
0.505	155.642	1001.77	0.66	90.1838	1001.77			
0.51	153.179	1001.77	0.665	89.6443	1001.77			
0.515	151.176	1001.77	0.67	88.103	1001.77			
0.52	147.324	1001.77	0.675	85.6398	1001.77			
0.525	144.091	1001.77	0.68	85.4849	1001.77			
0.53	141.78	1001.77	0.685	83.4839	1001.77			
0.535	138.852	1001.77	0.69	81.3256	1001.77			
0.54	135.003	1001.77	0.695	81.7878	1001.77			
0.545	132.539	1001.77	0.7	80.711	1001.77			
0.55	130.229	1001.77	0.705	79.0923	1001.77			
0.555	127.301	1001.77	0.71	77.1686	1001.77			
0.56	125.452	1001.77	0.715	77.2461	1001.77			
0.565	124.453	1001.77	0.72	75.0878	1001.77			
0.57	122.22	1001.77						
0.575	118.907	1001.77						

B.1. Exact 3132

Stress Relaxation

T=150°C; strain=12.5 [strain units]; fixture diameter=10 [mm]; cone angle=0.035 [rad]

Time [s]	G(γ,t) [Pa]	γ [%]	Time [s] *cont.*	G(γ,t) [Pa] *cont.*	γ [%] *cont.*	Time [s] *cont.*	G(γ,t) [Pa] *cont.*	γ [%] *cont.*
0.001	0	0	0.145	1160.99	1251.66	0.285	335.028	1251.66
0.01	82044.8	11.9189	0.15	1090.15	1251.66	0.29	323.44	1251.66
0.015	94942.7	79.8106	0.155	1026.22	1251.66	0.295	313.827	1251.66
0.02	46973.9	222.496	0.16	968.17	1251.66	0.3	304.206	1251.66
0.025	27282.3	409.384	0.165	917.025	1251.66	0.305	294.841	1251.66
0.03	18641.4	600.196	0.17	867.833	1251.66	0.31	285.964	1251.66
0.035	14257.6	767.52	0.175	821.6	1251.66	0.315	278.326	1251.66
0.04	11695	902.082	0.18	781.751	1251.66	0.32	268.953	1251.66
0.045	9946.79	1005.32	0.185	742.308	1251.66	0.325	261.555	1251.66
0.05	8534.04	1080.78	0.19	706.318	1251.66	0.33	254.901	1251.66
0.055	7382.79	1134.89	0.195	673.769	1251.66	0.335	248	1251.66
0.06	6399.17	1173.34	0.2	643.203	1251.66	0.34	241.094	1251.66
0.065	5564.13	1198.98	0.205	614.604	1251.66	0.345	234.44	1251.66
0.07	4847.22	1216.78	0.21	587.477	1251.66	0.35	228.522	1251.66
0.075	4242.38	1228.88	0.215	562.828	1251.66	0.355	222.112	1251.66
0.08	3733.69	1236.71	0.22	539.652	1251.66	0.36	215.454	1251.66
0.085	3302.18	1241.7	0.225	517.466	1251.66	0.365	210.771	1251.66
0.09	2936.81	1245.25	0.23	497.745	1251.66	0.37	204.361	1251.66
0.095	2631.73	1247.39	0.235	478.023	1251.66	0.375	200.171	1251.66
0.1	2374.38	1248.81	0.24	459.285	1251.66	0.38	195.364	1251.66
0.105	2153	1250.25	0.245	442.522	1251.66	0.385	191.05	1251.66
0.11	1962.83	1250.94	0.25	426.247	1251.66	0.39	186.239	1251.66
0.115	1801.41	1250.94	0.255	409.973	1251.66	0.395	181.925	1251.66
0.12	1659.69	1250.94	0.26	395.185	1251.66	0.4	177.858	1251.66
0.125	1531.84	1251.66	0.265	382.853	1251.66	0.405	173.915	1251.66
0.13	1423.64	1251.66	0.27	369.049	1251.66	0.41	169.968	1251.66
0.135	1326.24	1251.66	0.275	357.213	1251.66	0.415	166.517	1251.66
0.14	1238.7	1251.66	0.28	345.873	1251.66	0.42	162.327	1251.66

Time [s] *cont.*	G(γ,t) [Pa] *cont.*	γ [%] *cont.*	Time [s] *cont.*	G(γ,t) [Pa] *cont.*	γ [%] *cont.*	Time [s] *cont.*	G(γ,t) [Pa] *cont.*	γ [%] *cont.*
0.425	158.38	1251.66	0.58	87.3164	1251.66			
0.43	156.165	1251.66	0.585	86.1467	1251.66			
0.435	153.945	1251.66	0.59	84.3592	1251.66			
0.44	150.123	1251.66	0.595	83.5575	1251.66			
0.445	147.779	1251.66	0.6	82.4479	1251.66			
0.45	145.932	1251.66	0.605	81.2143	1251.66			
0.455	142.481	1251.66	0.61	79.4269	1251.66			
0.46	139.398	1251.66	0.615	78.6871	1251.66			
0.465	137.55	1251.66	0.62	77.2696	1251.66			
0.47	134.467	1251.66	0.625	76.2219	1251.66			
0.475	131.88	1251.66	0.63	75.0522	1251.66			
0.48	129.537	1251.66	0.635	74.6204	1251.66			
0.485	127.07	1251.66	0.64	73.0169	1251.66			
0.49	124.235	1251.66	0.645	72.4011	1251.66			
0.495	122.263	1251.66	0.65	71.9073	1251.66			
0.5	120.414	1251.66	0.655	71.3534	1251.66			
0.505	116.963	1251.66	0.66	69.4421	1251.66			
0.51	114.992	1251.66	0.665	69.32	1251.66			
0.515	113.264	1251.66	0.67	68.3944	1251.66			
0.52	110.677	1251.66	0.675	66.545	1251.66			
0.525	107.102	1251.66	0.68	65.6832	1251.66			
0.53	106.238	1251.66	0.685	65.1894	1251.66			
0.535	104.143	1251.66	0.69	63.8338	1251.66			
0.54	101.554	1251.66	0.695	63.0321	1251.66			
0.545	99.7665	1251.66	0.7	62.8481	1251.66			
0.55	98.2269	1251.66	0.705	61.8624	1251.66			
0.555	96.4995	1251.66	0.71	60.9987	1251.66			
0.56	93.5424	1251.66	0.715	61.1846	1251.66			
0.565	92.9265	1251.66						
0.57	91.1992	1251.66						
0.575	88.672	1251.66						

B.2. Exact 0201

Stress Relaxation

T=150°C; strain=0.01 [strain units]; fixture diameter=25 [mm]; cone angle=0.1 [rad]

Time [s]	G(γ,t) [Pa]	γ [%]	Time [s] *cont.*	G(γ,t) [Pa] *cont.*	γ [%] *cont.*	Time [s] *cont.*	G(γ,t) [Pa] *cont.*	γ [%] *cont.*
0.001	0	0	0.145	25034.5	0.99691	0.285	14046.4	0.99593
0.01	95622.8	0.02777	0.15	24220.2	0.99593	0.29	13867.6	1.00082
0.015	192678	0.16538	0.155	23477	0.9979	0.295	13761.3	0.99593
0.02	197399	0.32756	0.16	22828.9	0.9979	0.3	13428.7	1.0018
0.025	178623	0.48916	0.165	22179.5	1.00082	0.305	13402.4	0.9979
0.03	158672	0.62759	0.17	21617.5	0.99983	0.31	13270.8	0.99888
0.035	139574	0.73962	0.175	21089.6	0.99495	0.315	13049.7	0.99888
0.04	122773	0.82032	0.18	20621	0.99691	0.32	12948.9	0.99691
0.045	107142	0.88538	0.185	20213.8	0.99593	0.325	12794	0.9979
0.05	94776.5	0.92256	0.19	19631.7	0.99495	0.33	12586.7	1.0018
0.055	83612.5	0.95093	0.195	19181.8	0.99691	0.335	12477.9	0.9979
0.06	73728.2	0.97343	0.2	18859.6	0.99888	0.34	12319.9	0.9979
0.065	65566.7	0.98809	0.205	18501.6	0.99691	0.345	12209.9	0.99396
0.07	59273.2	0.99203	0.21	18062.4	0.99495	0.35	11980.5	1.0018
0.075	53656.7	0.99593	0.215	17692.9	0.9979	0.355	11948.4	0.99593
0.08	48919.8	0.99888	0.22	17505	0.99691	0.36	11829.1	0.99396
0.085	45088.1	0.99983	0.225	17144.1	0.99396	0.365	11703	0.99593
0.09	41797.5	1.00082	0.23	16617.7	0.99983	0.37	11605.2	0.99888
0.095	39082	0.99691	0.235	16444	0.99888	0.375	11390.7	0.99691
0.1	36610.1	0.9979	0.24	16223.3	0.99691	0.38	11251.6	0.99593
0.105	34647.4	0.99888	0.245	15859.6	0.99691	0.385	11223	0.99495
0.11	32784.9	0.99983	0.25	15551.7	0.9979	0.39	11137.6	0.99691
0.115	31208.5	1.00082	0.255	15533	0.99301	0.395	10950.8	0.99593
0.12	30015.4	0.99593	0.26	15196	0.9979	0.4	10821.3	0.99983
0.125	28875.6	0.99593	0.265	14924	0.99495	0.405	10897.6	0.9979
0.13	27735.3	0.99593	0.27	14691.7	0.99888	0.41	10811.1	0.99495
0.135	26695.9	0.99691	0.275	14452	1.0018	0.415	10599.9	0.99691
0.14	25841.3	0.99691	0.28	14260.1	0.99593	0.42	10522	1.00278

Time [s] *cont.*	G(γ,t) [Pa] *cont.*	γ [%] *cont.*	Time [s] *cont.*	G(γ,t) [Pa] *cont.*	γ [%] *cont.*	Time [s] *cont.*	G(γ,t) [Pa] *cont.*	γ [%] *cont.*
0.425	10518.2	0.9979	0.58	8092.63	0.99495	0.735	6808.28	0.99983
0.43	10271.2	0.99888	0.585	8068.86	0.99006	0.74	6880.35	0.99396
0.435	10146.9	0.9979	0.59	8140.07	0.99495	0.745	6784.56	0.99983
0.44	10095.7	0.99983	0.595	8021.41	0.9979	0.75	6642.34	0.99983
0.445	10009	0.99983	0.6	7934.25	0.99593	0.755	6690.83	0.9979
0.45	9864.12	0.99691	0.605	7942.23	0.99593	0.76	6682.84	0.99495
0.455	9830.75	0.9979	0.61	7942.4	0.99888	0.765	6563.23	0.99983
0.46	9842.19	0.99593	0.615	7863.14	0.99691	0.77	6512.62	0.9979
0.465	9717.35	0.99495	0.62	7784.25	0.99888	0.775	6588.45	0.99301
0.47	9612.73	0.99593	0.625	7779.81	0.99691	0.78	6552.2	0.9979
0.475	9458.02	0.99888	0.63	7732.22	0.99691	0.785	6454.04	0.99593
0.48	9473.07	0.99396	0.635	7563.83	1.00082	0.79	6469.02	0.99301
0.485	9343.38	0.99593	0.64	7499.31	0.99888	0.795	6482.68	0.99396
0.49	9305.18	0.99495	0.645	7468.43	0.99983	0.8	6381.83	0.9979
0.495	9142.21	0.99888	0.65	7401.89	0.99495	0.805	6252.65	1.00082
0.5	9094.96	0.99888	0.655	7374.76	0.99593	0.81	6282.9	0.9979
0.505	9029.96	1.00082	0.66	7291.34	0.99593	0.815	6275.48	0.99593
0.51	8973.28	0.99396	0.665	7240.55	0.99691	0.82	6213.73	0.99691
0.515	8850.27	0.99888	0.67	7243.12	0.99983	0.825	6219.87	0.99593
0.52	8802.33	0.99983	0.675	7233.41	0.9979	0.83	6220.3	0.99396
0.525	8751.12	0.99396	0.68	7218.31	0.99396	0.835	6189.94	0.99691
0.53	8621.25	0.99888	0.685	7189.86	0.9979	0.84	6207.61	0.9979
0.535	8646.8	0.99593	0.69	7251.69	0.99593	0.845	6158.3	0.99691
0.54	8624.46	0.99301	0.695	7140.59	0.99593	0.85	6104.69	0.9979
0.545	8494.78	0.99983	0.7	7041.54	0.99983	0.855	6169.79	0.99888
0.55	8385.12	0.99691	0.705	7092.96	0.99593	0.86	6082.9	1.00082
0.555	8447.68	0.99888	0.71	7088.97	0.99593	0.865	6025.47	0.99593
0.56	8353.75	0.99593	0.715	6958.04	0.99593	0.87	5979.95	0.99888
0.565	8203.12	0.9979	0.72	6937.49	0.99888	0.875	6073.13	0.99396
0.57	8275.07	0.99396	0.725	6999.67	0.99396	0.88	5969.86	0.99593
0.575	8234.88	0.99691	0.73	6878.18	0.99888	0.885	5840.17	1.0018

B.2. Exact 0201

Stress Relaxation

T=150°C; strain=0.1 [strain units]; fixture diameter=25 [mm]; cone angle=0.1 [rad]

Time [s]	G(γ,t) [Pa]	γ [%]	Time [s] *cont.*	G(γ,t) [Pa] *cont.*	γ [%] *cont.*	Time [s] *cont.*	G(γ,t) [Pa] *cont.*	γ [%] *cont.*
0.001	0	0	0.145	24273.1	10.0476	0.285	13777.5	10.0319
0.01	63946	0.44967	0.15	23522.7	10.0398	0.29	13589	10.0319
0.015	184632	1.87152	0.155	22831.9	10.0398	0.295	13408.3	10.0319
0.02	188049	3.54152	0.16	22204.4	10.0398	0.3	13237.8	10.0243
0.025	172237	5.12252	0.165	21623.4	10.0398	0.305	13055	10.0319
0.03	153088	6.44514	0.17	21074.7	10.0319	0.31	12897.9	10.0319
0.035	134725	7.48691	0.175	20556.6	10.0319	0.315	12750.4	10.0243
0.04	118468	8.27548	0.18	20053.9	10.0398	0.32	12593.2	10.0243
0.045	103990	8.85316	0.185	19598.5	10.0398	0.325	12436	10.0243
0.05	91553.8	9.25919	0.19	19173.9	10.0319	0.33	12285.2	10.0319
0.055	80814.7	9.54028	0.195	18765.6	10.0319	0.335	12145	10.0243
0.06	71826.3	9.72744	0.2	18372.7	10.0319	0.34	11986.6	10.0319
0.065	64213.2	9.85237	0.205	17981.5	10.0398	0.345	11860.9	10.0319
0.07	57812.1	9.94607	0.21	17634.3	10.0319	0.35	11727.5	10.0319
0.075	52516.4	10.0007	0.215	17304.3	10.0319	0.355	11594.8	10.0243
0.08	48111.8	10.0319	0.22	16958.8	10.0319	0.36	11468.2	10.0319
0.085	44328.5	10.0631	0.225	16660.4	10.0319	0.365	11342.5	10.0319
0.09	41196.1	10.071	0.23	16362	10.0319	0.37	11215.9	10.0398
0.095	38443.6	10.0867	0.235	16078.9	10.0319	0.375	11106.9	10.0319
0.1	36159.5	10.0789	0.24	15812.2	10.0319	0.38	11005.2	10.0243
0.105	34153.8	10.071	0.245	15545	10.0319	0.385	10895.2	10.0243
0.11	32313.5	10.0789	0.25	15301.5	10.0319	0.39	10777.1	10.0319
0.115	30742.1	10.071	0.255	15050.1	10.0319	0.395	10682.8	10.0319
0.12	29341.3	10.0631	0.26	14822.2	10.0319	0.4	10580.6	10.0319
0.125	28109.5	10.0555	0.265	14602.2	10.0319	0.405	10470.5	10.0319
0.13	26960.5	10.0631	0.27	14382.5	10.0319	0.41	10384.4	10.0243
0.135	25998.5	10.0476	0.275	14178.1	10.0319	0.415	10290	10.0243
0.14	25088.4	10.0476	0.28	13974	10.0319	0.42	10180	10.0319

Time [s] *cont.*	G(γ,t) [Pa] *cont.*	γ [%] *cont.*	Time [s] *cont.*	G(γ,t) [Pa] *cont.*	γ [%] *cont.*	Time [s] *cont.*	G(γ,t) [Pa] *cont.*	γ [%] *cont.*
0.425	10093.7	10.0319	0.58	7941.43	10.0319	0.735	6621.73	10.0319
0.43	9999.38	10.0319	0.585	7886.26	10.0319	0.74	6590.3	10.0319
0.435	9920.57	10.0243	0.59	7831.33	10.0319	0.745	6550.96	10.0319
0.44	9818.75	10.0319	0.595	7792.11	10.0319	0.75	6524.5	10.0243
0.445	9740.07	10.0319	0.6	7750.87	10.0243	0.755	6488.11	10.0319
0.45	9653.71	10.0319	0.605	7689.92	10.0319	0.76	6449.25	10.0319
0.455	9575.27	10.0319	0.61	7650.7	10.0319	0.765	6417.83	10.0319
0.46	9511.74	10.0243	0.615	7595.76	10.0319	0.77	6390.24	10.0319
0.465	9425.82	10.0319	0.62	7548.63	10.0319	0.775	6354.74	10.0319
0.47	9347.38	10.0319	0.625	7501.49	10.0319	0.78	6332.09	10.0243
0.475	9268.7	10.0319	0.63	7462.15	10.0319	0.785	6291.77	10.0319
0.48	9190.26	10.0319	0.635	7409.2	10.0398	0.79	6256.39	10.0319
0.485	9111.82	10.0319	0.64	7360.08	10.0319	0.795	6228.8	10.0319
0.49	9041.05	10.0319	0.645	7328.66	10.0319	0.8	6197.26	10.0319
0.495	8977.11	10.0243	0.65	7281.52	10.0319	0.805	6161.87	10.0319
0.5	8899.52	10.0319	0.655	7234.38	10.0319	0.81	6142.2	10.0319
0.505	8836.91	10.0319	0.66	7202.96	10.0319	0.815	6110.66	10.0319
0.51	8774.06	10.0319	0.665	7161.27	10.0243	0.82	6079.11	10.0319
0.515	8711.21	10.0319	0.67	7116.6	10.0319	0.825	6051.65	10.0319
0.52	8640.45	10.0319	0.675	7082.65	10.0243	0.83	6028.02	10.0319
0.525	8584.13	10.0243	0.68	7038.04	10.0319	0.835	6000.43	10.0319
0.53	8514.75	10.0319	0.685	6998.7	10.0319	0.84	5964.93	10.0319
0.535	8451.9	10.0319	0.69	6956.85	10.0243	0.845	5941.42	10.0319
0.54	8389.05	10.0319	0.695	6920.14	10.0319	0.85	5917.79	10.0319
0.545	8334.12	10.0319	0.7	6880.92	10.0319	0.855	5886.25	10.0319
0.55	8279.19	10.0319	0.705	6841.7	10.0319	0.86	5862.62	10.0319
0.555	8216.34	10.0319	0.71	6810.27	10.0319	0.865	5842.95	10.0319
0.56	8161.17	10.0319	0.715	6778.85	10.0319	0.87	5811.41	10.0319
0.565	8106.23	10.0319	0.72	6731.71	10.0319	0.875	5788.22	10.0243
0.57	8043.38	10.0319	0.725	6700.29	10.0319	0.88	5772.5	10.0243
0.575	7994.53	10.0243	0.73	6666.02	10.0243	0.885	5740.52	10.0319

B.2. Exact 0201

Stress Relaxation

T=150°C; strain=1.0 [strain units]; fixture diameter=10 [mm]; cone angle=0.035 [rad]

Time [s]	G(γ,t) [Pa]	γ [%]	Time [s] *cont.*	G(γ,t) [Pa] *cont.*	γ [%] *cont.*	Time [s] *cont.*	G(γ,t) [Pa] *cont.*	γ [%] *cont.*
0.001	0	0	0.145	20212.4	100.199	0.285	11332.8	100.199
0.01	45728.5	4.8469	0.15	19604.1	100.199	0.29	11165.7	100.199
0.015	74377.8	20.6734	0.155	18988.7	100.289	0.295	11018.8	100.199
0.02	80373.7	37.6751	0.16	18465.9	100.199	0.3	10871.6	100.199
0.025	81495.9	53.1771	0.165	17949.3	100.289	0.305	10724.4	100.199
0.03	82499.5	66.1144	0.17	17484.8	100.199	0.31	10586.9	100.199
0.035	79624.4	76.1076	0.175	17043.2	100.199	0.315	10450.1	100.289
0.04	75168	83.6022	0.18	16631	100.199	0.32	10322.2	100.199
0.045	69741.1	88.8665	0.185	16228.8	100.199	0.325	10194.5	100.199
0.05	64118.1	92.6131	0.19	15856	100.199	0.33	10076.8	100.199
0.055	58616.1	95.2016	0.195	15512.6	100.199	0.335	9959.01	100.199
0.06	53572.3	96.8965	0.2	15169.2	100.199	0.34	9831.49	100.199
0.065	49007.8	98.0572	0.205	14832.1	100.289	0.345	9723.64	100.199
0.07	44949.6	98.861	0.21	14538	100.289	0.35	9615.5	100.199
0.075	41422.8	99.3052	0.215	14276.1	100.199	0.355	9502.4	100.199
0.08	38353.9	99.6621	0.22	13991.7	100.199	0.36	9404.01	100.199
0.085	35685.5	99.842	0.225	13736.6	100.199	0.365	9305.63	100.199
0.09	33341.7	100.019	0.23	13491.2	100.199	0.37	9197.34	100.199
0.095	31327.9	100.109	0.235	13256	100.199	0.375	9098.95	100.199
0.1	29553.2	100.199	0.24	13020.4	100.199	0.38	9015.44	100.199
0.105	28003.1	100.199	0.245	12804.5	100.199	0.385	8904.11	100.289
0.11	26648.9	100.199	0.25	12588.5	100.199	0.39	8823.63	100.199
0.115	25432.3	100.199	0.255	12382.7	100.199	0.395	8739.97	100.199
0.12	24333.4	100.199	0.26	12185.2	100.289	0.4	8656.31	100.199
0.125	23352.3	100.199	0.265	12009.6	100.199	0.405	8567.84	100.199
0.13	22429.1	100.289	0.27	11823.3	100.199	0.41	8481.52	100.289
0.135	21625.4	100.289	0.275	11656.6	100.199	0.415	8410.42	100.199
0.14	20899.2	100.199	0.28	11499.5	100.199	0.42	8326.76	100.199

Time [s] *cont.*	G(γ,t) [Pa] *cont.*	γ [%] *cont.*	Time [s] *cont.*	G(γ,t) [Pa] *cont.*	γ [%] *cont.*	Time [s] *cont.*	G(γ,t) [Pa] *cont.*	γ [%] *cont.*
0.425	8248.21	100.199	0.58	6467.7	100.199	0.735	5385.64	100.199
0.43	8174.31	100.199	0.585	6423.39	100.199	0.74	5351.25	100.199
0.435	8095.6	100.199	0.59	6374.28	100.199	0.745	5331.57	100.199
0.44	8021.85	100.199	0.595	6339.73	100.199	0.75	5311.89	100.199
0.445	7953.06	100.199	0.6	6305.33	100.199	0.755	5272.77	100.289
0.45	7884.11	100.199	0.605	6256.22	100.199	0.76	5247.91	100.199
0.455	7815.32	100.199	0.61	6221.82	100.199	0.765	5228.23	100.199
0.46	7751.34	100.199	0.615	6187.28	100.199	0.77	5193.84	100.199
0.465	7697.26	100.199	0.62	6143.12	100.199	0.775	5164.25	100.199
0.47	7628.47	100.199	0.625	6103.76	100.199	0.78	5139.76	100.199
0.475	7552.75	100.289	0.63	6074.17	100.199	0.785	5115.13	100.199
0.48	7510.41	100.199	0.635	6030.01	100.199	0.79	5080.73	100.199
0.485	7446.42	100.199	0.64	5990.66	100.199	0.795	5061.06	100.199
0.49	7377.63	100.199	0.645	5960.68	100.289	0.8	5041.38	100.199
0.495	7323.41	100.199	0.65	5931.63	100.199	0.805	5011.79	100.199
0.5	7258.01	100.289	0.655	5886.99	100.289	0.81	4992.11	100.199
0.505	7200.54	100.199	0.66	5852.48	100.289	0.815	4967.98	100.289
0.51	7135.11	100.289	0.665	5833.25	100.199	0.82	4947.95	100.199
0.515	7087.44	100.199	0.67	5788.94	100.199	0.825	4918.36	100.199
0.52	7028.41	100.199	0.675	5749.59	100.199	0.83	4899.25	100.289
0.525	6963.13	100.289	0.68	5724.95	100.199	0.835	4869.76	100.289
0.53	6925.07	100.199	0.685	5690.56	100.199	0.84	4835.32	100.289
0.535	6871	100.199	0.69	5656.16	100.199	0.845	4819.98	100.199
0.54	6821.73	100.199	0.695	5626.57	100.199	0.85	4796	100.289
0.545	6782.53	100.199	0.7	5597.13	100.199	0.855	4771.46	100.289
0.55	6733.26	100.199	0.705	5562.73	100.199	0.86	4751.19	100.199
0.555	6684.15	100.199	0.71	5533.14	100.199	0.865	4736.39	100.199
0.56	6639.84	100.199	0.715	5508.66	100.199	0.87	4711.84	100.199
0.565	6600.48	100.199	0.72	5474.11	100.199	0.875	4687.2	100.199
0.57	6551.22	100.199	0.725	5444.67	100.199	0.88	4672.48	100.199
0.575	6507.06	100.199	0.73	5420.04	100.199	0.885	4652.81	100.199

B.2. Exact 0201

Stress Relaxation

T=150°C; strain=5.0 [strain units]; fixture diameter=10 [mm]; cone angle=0.035 [rad]

Time [s]	G(γ,t) [Pa]	γ [%]	Time [s] *cont.*	G(γ,t) [Pa] *cont.*	γ [%] *cont.*	Time [s] *cont.*	G(γ,t) [Pa] *cont.*	γ [%] *cont.*
0.001	0	0	0.145	3066.34	501.232	0.285	1736.84	501.232
0.01	59530.3	11.4101	0.15	2970.54	501.232	0.29	1712.24	501.232
0.015	86168.4	66.6049	0.155	2884.57	501.232	0.295	1690.07	501.232
0.02	53671.3	150.52	0.16	2803.48	501.232	0.3	1669.14	501.232
0.025	34801.3	230.861	0.165	2729.81	501.232	0.305	1648.21	501.232
0.03	25681.6	301.526	0.17	2658.54	501.232	0.31	1627.28	501.232
0.035	20350.6	357.766	0.175	2589.83	501.232	0.315	1607.55	501.232
0.04	16519.2	400.49	0.18	2528.39	501.232	0.32	1590.33	501.232
0.045	13884.1	431.815	0.185	2471.9	501.232	0.325	1570.64	501.232
0.05	11841.8	453.886	0.19	2417.85	501.232	0.33	1550.91	501.232
0.055	10250.9	469.548	0.195	2363.8	501.232	0.335	1533.7	501.232
0.06	8983.34	479.88	0.2	2317.14	501.232	0.34	1516.44	501.232
0.065	7967.23	486.997	0.205	2270.44	501.232	0.345	1497.99	501.232
0.07	7140.78	491.978	0.21	2223.78	501.232	0.35	1485.68	501.232
0.075	6467.96	495.183	0.215	2182.03	501.232	0.355	1467.19	501.232
0.08	5915.31	497.319	0.22	2142.72	501.232	0.36	1449.98	501.232
0.085	5463.97	498.747	0.225	2103.41	501.232	0.365	1433.96	501.232
0.09	5081.46	499.455	0.23	2064.11	501.232	0.37	1420.42	501.232
0.095	4754.23	500.163	0.235	2029.71	501.232	0.375	1405.64	501.232
0.1	4480.22	500.523	0.24	1994.19	501.232	0.38	1388.39	501.232
0.105	4241.06	500.883	0.245	1957.24	501.232	0.385	1377.32	501.232
0.11	4029.59	500.883	0.25	1930.16	501.232	0.39	1362.54	501.232
0.115	3842.62	501.232	0.255	1896.93	501.232	0.395	1347.76	501.232
0.12	3680.43	501.232	0.26	1866.13	501.232	0.4	1335.46	501.232
0.125	3530.62	501.232	0.265	1837.82	501.232	0.405	1324.36	501.232
0.13	3397.99	501.232	0.27	1811.97	501.232	0.41	1309.58	501.232
0.135	3280.06	501.232	0.275	1784.89	501.232	0.415	1297.28	501.232
0.14	3169.49	501.232	0.28	1760.25	501.232	0.42	1288.65	501.232

Time [s] *cont.*	G(γ,t) [Pa] *cont.*	γ [%] *cont.*	Time [s] *cont.*	G(γ,t) [Pa] *cont.*	γ [%] *cont.*	Time [s] *cont.*	G(γ,t) [Pa] *cont.*	γ [%] *cont.*
0.425	1275.11	501.232	0.58	1009.16	501.232	0.735	839.841	501.232
0.43	1265.25	501.232	0.585	1003	501.232	0.74	836.765	501.232
0.435	1255.42	501.232	0.59	994.996	501.232	0.745	829.376	501.232
0.44	1241.88	501.232	0.595	987.606	501.232	0.75	825.682	501.232
0.445	1232.01	501.232	0.6	980.217	501.232	0.755	822.606	501.232
0.45	1222.17	501.232	0.605	974.666	501.232	0.76	817.692	501.232
0.455	1213.54	501.232	0.61	966.677	501.232	0.765	811.522	501.232
0.46	1202.47	501.232	0.615	960.506	501.232	0.77	809.684	501.232
0.465	1192.61	501.232	0.62	956.212	501.232	0.775	804.752	501.232
0.47	1184	501.232	0.625	949.441	501.232	0.78	797.981	501.232
0.475	1171.68	501.232	0.63	942.052	501.232	0.785	796.744	501.232
0.48	1161.83	501.232	0.635	938.977	501.232	0.79	793.668	501.232
0.485	1153.21	501.232	0.64	933.425	501.232	0.795	788.754	501.232
0.49	1144.6	501.232	0.645	924.798	501.232	0.8	786.279	501.232
0.495	1132.28	501.232	0.65	921.122	501.232	0.805	783.822	501.232
0.5	1127.36	501.232	0.655	917.428	501.232	0.81	780.127	501.232
0.505	1118.74	501.232	0.66	910.039	501.232	0.815	775.195	501.232
0.51	1108.89	501.232	0.665	904.487	501.232	0.82	772.738	501.232
0.515	1099.04	501.232	0.67	901.412	501.232	0.825	769.662	501.232
0.52	1092.87	501.232	0.675	895.879	501.232	0.83	764.13	501.232
0.525	1085.49	501.232	0.68	889.709	501.232	0.835	761.654	501.232
0.53	1074.4	501.232	0.685	886.014	501.232	0.84	756.741	501.232
0.535	1068.25	501.232	0.69	882.32	501.232	0.845	751.189	501.232
0.54	1062.1	501.232	0.695	875.549	501.232	0.85	747.495	501.232
0.545	1054.71	501.232	0.7	871.255	501.232	0.855	746.876	501.232
0.55	1049.78	501.232	0.705	866.322	501.232	0.86	742.581	501.232
0.555	1042.39	501.232	0.71	860.771	501.232	0.865	736.411	501.232
0.56	1035.02	501.232	0.715	855.857	501.232	0.87	735.192	501.232
0.565	1028.85	501.232	0.72	854.001	501.232	0.875	732.716	501.232
0.57	1025.15	501.232	0.725	849.087	501.232	0.88	727.184	501.232
0.575	1019	501.232	0.73	841.698	501.232	0.885	725.946	501.232

B.2. Exact 0201

Stress Relaxation

T=150°C; strain=7.5 [strain units]; fixture diameter=10 [mm]; cone angle=0.035 [rad]

Time [s]	G(γ,t) [Pa]	γ [%]	Time [s] *cont.*	G(γ,t) [Pa] *cont.*	γ [%] *cont.*	Time [s] *cont.*	G(γ,t) [Pa] *cont.*	γ [%] *cont.*
0.001	0	0	0.145	3167.77	751.847	0.285	1743.04	751.847
0.01	57576	11.874	0.15	3062.95	751.847	0.29	1718.49	751.847
0.015	90265.1	74.5913	0.155	2967.98	751.847	0.295	1695.53	751.847
0.02	62152.7	187.962	0.16	2879.56	751.847	0.3	1672.63	751.847
0.025	44944.6	310.425	0.165	2797.69	751.847	0.305	1648.07	751.847
0.03	34283.6	420.425	0.17	2722.32	751.847	0.31	1630.04	751.847
0.035	27677.1	511.553	0.175	2652.76	751.15	0.315	1608.74	751.847
0.04	22633.9	581.689	0.18	2581.49	751.847	0.32	1585.83	751.847
0.045	18772.4	633.308	0.185	2517.62	751.847	0.325	1566.18	751.847
0.05	15719.2	670.681	0.19	2460.31	751.847	0.33	1548.15	751.847
0.055	13299.6	696.676	0.195	2406.3	751.847	0.335	1528.49	751.847
0.06	11381	714.834	0.2	2352.23	751.847	0.34	1510.49	751.847
0.065	9828.29	727.651	0.205	2301.47	751.847	0.345	1492.49	751.847
0.07	8598.76	735.477	0.21	2255.61	751.847	0.35	1476.11	751.847
0.075	7609.02	741.166	0.215	2208.1	751.847	0.355	1459.73	751.847
0.08	6811.93	744.741	0.22	2165.54	751.847	0.36	1443.35	751.847
0.085	6172.71	746.877	0.225	2124.58	751.847	0.365	1426.97	751.847
0.09	5642.26	749.014	0.23	2085.32	751.847	0.37	1410.59	751.847
0.095	5206.68	749.711	0.235	2046.01	751.847	0.375	1394.21	751.847
0.1	4847.34	750.431	0.24	2009.96	751.847	0.38	1381.11	751.847
0.105	4545.41	750.431	0.245	1977.2	751.847	0.385	1364.73	751.847
0.11	4285.36	751.15	0.25	1946.25	751.15	0.39	1351.63	751.847
0.115	4062.4	751.15	0.255	1911.86	751.15	0.395	1341.08	751.847
0.12	3865.67	751.15	0.26	1880.58	751.847	0.4	1326.3	751.847
0.125	3698.48	751.15	0.265	1851.12	751.847	0.405	1312.34	751.847
0.13	3544.4	751.15	0.27	1821.66	751.847	0.41	1301.67	751.847
0.135	3406.74	751.15	0.275	1795.47	751.15	0.415	1289.36	751.847
0.14	3279.15	751.847	0.28	1769.25	751.847	0.42	1276.21	751.847

Time [s] *cont.*	G(γ,t) [Pa] *cont.*	γ [%] *cont.*	Time [s] *cont.*	G(γ,t) [Pa] *cont.*	γ [%] *cont.*	Time [s] *cont.*	G(γ,t) [Pa] *cont.*	γ [%] *cont.*
0.425	1264.73	751.847	0.58	990.57	751.847	0.735	820.631	751.847
0.43	1254.06	751.847	0.585	983.168	751.847	0.74	815.717	751.847
0.435	1243.38	751.847	0.59	976.592	751.847	0.745	813.254	751.847
0.44	1232.22	751.15	0.595	971.691	751.847	0.75	807.503	751.847
0.445	1221.22	751.847	0.6	963.464	751.847	0.755	802.577	751.847
0.45	1209.72	751.847	0.605	958.602	751.15	0.76	799.301	751.847
0.455	1200.18	751.15	0.61	951.218	751.15	0.765	796.013	751.847
0.46	1187.57	751.847	0.615	945.41	751.847	0.77	791.087	751.847
0.465	1179.63	751.15	0.62	938.033	751.847	0.775	787.798	751.847
0.47	1167.04	751.847	0.625	933.107	751.847	0.78	785.348	751.847
0.475	1158.83	751.847	0.63	927.356	751.847	0.785	779.596	751.847
0.48	1150.05	751.15	0.635	920.779	751.847	0.79	776.308	751.847
0.485	1139.36	751.15	0.64	915.028	751.847	0.795	773.032	751.847
0.49	1128.48	751.847	0.645	910.102	751.847	0.8	768.106	751.847
0.495	1120.25	751.847	0.65	905.215	751.15	0.805	763.18	751.847
0.5	1110.4	751.847	0.655	897.799	751.847	0.81	760.717	751.847
0.505	1100.55	751.847	0.66	893.698	751.847	0.815	756.616	751.847
0.51	1093.99	751.847	0.665	889.597	751.847	0.82	752.503	751.847
0.515	1086.59	751.847	0.67	883.845	751.847	0.825	749.227	751.847
0.52	1076.11	751.15	0.675	878.919	751.847	0.83	745.939	751.847
0.525	1069.36	751.847	0.68	874.818	751.847	0.835	742.65	751.847
0.53	1063.77	751.15	0.685	869.048	751.15	0.84	738.549	751.847
0.535	1053.76	751.847	0.69	861.69	751.847	0.845	736.086	751.847
0.54	1047.21	751.847	0.695	857.589	751.847	0.85	731.985	751.847
0.545	1039.81	751.847	0.7	853.463	751.847	0.855	727.734	751.15
0.55	1033.39	751.15	0.705	847.737	751.847	0.86	723.771	751.847
0.555	1024.2	751.847	0.71	843.611	751.847	0.865	721.308	751.847
0.56	1018.48	751.847	0.715	840.335	751.847	0.87	717.207	751.847
0.565	1011.9	751.847	0.72	832.959	751.847	0.875	713.931	751.847
0.57	1002.87	751.847	0.725	831.254	751.15	0.88	711.468	751.847
0.575	996.296	751.847	0.73	824.732	751.847	0.885	707.355	751.847

B.2. Exact 0201

Stress Relaxation

T=150°C; strain=10.0 [strain units]; fixture diameter=10 [mm]; cone angle=0.035 [rad]

Time [s]	G(γ,t) [Pa]	γ [%]	Time [s] *cont.*	G(γ,t) [Pa] *cont.*	γ [%] *cont.*	Time [s] *cont.*	G(γ,t) [Pa] *cont.*	γ [%] *cont.*
0.001	0	0	0.145	1972.51	1001.77	0.285	1087.57	1001.77
0.01	58909.5	12.0978	0.15	1908.59	1001.77	0.29	1071.6	1001.77
0.015	85627.4	78.6948	0.155	1849.62	1001.77	0.295	1056.85	1001.77
0.02	50672.6	210.392	0.16	1793.06	1001.77	0.3	1043.34	1001.77
0.025	33280.5	370.234	0.165	1743.92	1001.77	0.305	1028.59	1001.77
0.03	24321.1	521.166	0.17	1694.75	1001.77	0.31	1015.05	1001.77
0.035	18895.5	648.97	0.175	1649.26	1001.77	0.315	1002.82	1001.77
0.04	15242.6	749.711	0.18	1608.72	1001.77	0.32	989.268	1001.77
0.045	12480.6	825.896	0.185	1569.39	1001.77	0.325	976.938	1001.77
0.05	10387.2	880.719	0.19	1531.29	1001.77	0.33	965.846	1001.77
0.055	8738.93	919.869	0.195	1496.87	1001.77	0.335	954.755	1001.77
0.06	7428.09	946.943	0.2	1463.69	1001.77	0.34	943.063	1001.77
0.065	6382.76	965.45	0.205	1431.71	1001.77	0.345	933.191	1001.77
0.07	5548.01	977.548	0.21	1402.21	1001.77	0.35	922.719	1001.77
0.075	4875.65	986.093	0.215	1375.18	1001.77	0.355	912.247	1001.77
0.08	4341.17	991.782	0.22	1346.92	1001.77	0.36	901.155	1001.77
0.085	3914.95	995.357	0.225	1319.89	1001.77	0.365	893.16	1001.77
0.09	3565.87	997.493	0.23	1296.51	1001.77	0.37	883.908	1001.77
0.095	3282.26	998.91	0.235	1273.16	1001.77	0.375	873.436	1001.77
0.1	3046.21	1000.33	0.24	1251.05	1001.77	0.38	865.422	1001.77
0.105	2849.68	1001.05	0.245	1230.15	1001.77	0.385	856.808	1001.77
0.11	2682.38	1001.05	0.25	1210.48	1001.77	0.39	847.574	1001.77
0.115	2537.9	1001.77	0.255	1190.83	1001.77	0.395	839.561	1001.77
0.12	2414.97	1001.77	0.26	1171.16	1001.77	0.4	833.386	1001.77
0.125	2304.36	1001.77	0.265	1152.71	1001.77	0.405	824.153	1001.77
0.13	2208.49	1001.77	0.27	1135.5	1001.77	0.41	815.52	1001.77
0.135	2122.46	1001.77	0.275	1118.31	1001.77	0.415	808.144	1001.77
0.14	2043.79	1001.77	0.28	1102.32	1001.77	0.42	801.35	1001.77

Time [s] *cont.*	G(γ,t) [Pa] *cont.*	γ [%] *cont.*	Time [s] *cont.*	G(γ,t) [Pa] *cont.*	γ [%] *cont.*	Time [s] *cont.*	G(γ,t) [Pa] *cont.*	γ [%] *cont.*
0.425	792.736	1001.77	0.58	621.465	1001.77	0.735	519.811	1001.77
0.43	785.961	1001.77	0.585	618.387	1001.77	0.74	517.343	1001.77
0.435	779.186	1001.77	0.59	614.07	1001.77	0.745	514.265	1001.77
0.44	771.792	1001.77	0.595	609.754	1001.77	0.75	513.646	1001.77
0.445	763.778	1001.77	0.6	606.676	1001.77	0.755	509.339	1001.77
0.45	758.242	1001.77	0.605	602.979	1001.77	0.76	506.261	1001.77
0.455	750.847	1001.77	0.61	598.672	1001.77	0.765	504.413	1001.77
0.46	744.072	1001.77	0.615	596.204	1001.77	0.77	501.325	1001.77
0.465	738.517	1001.77	0.62	593.736	1001.77	0.775	497.938	1001.77
0.47	731.742	1001.77	0.625	588.81	1001.77	0.78	495.479	1001.77
0.475	724.967	1001.77	0.63	585.732	1001.77	0.785	493.321	1001.77
0.48	719.412	1001.77	0.635	583.264	1001.77	0.79	491.163	1001.77
0.485	714.495	1001.77	0.64	578.957	1001.77	0.795	487.466	1001.77
0.49	708.94	1001.77	0.645	574.021	1001.77	0.8	484.998	1001.77
0.495	703.403	1001.77	0.65	571.562	1001.77	0.805	483.459	1001.77
0.5	699.706	1001.77	0.655	567.865	1001.77	0.81	480.381	1001.77
0.505	694.17	1001.77	0.66	562.939	1001.77	0.815	478.532	1001.77
0.51	687.376	1001.77	0.665	561.7	1001.77	0.82	476.684	1001.77
0.515	683.679	1001.77	0.67	558.622	1001.77	0.825	473.606	1001.77
0.52	679.381	1001.77	0.675	554.925	1001.77	0.83	470.828	1001.77
0.525	672.606	1001.77	0.68	550.618	1001.77	0.835	469.599	1001.77
0.53	668.289	1001.77	0.685	548.769	1001.77	0.84	467.131	1001.77
0.535	664.592	1001.77	0.69	544.453	1001.77	0.845	464.363	1001.77
0.54	657.817	1001.77	0.695	540.756	1001.77	0.85	463.744	1001.77
0.545	652.881	1001.77	0.7	538.907	1001.77	0.855	461.595	1001.77
0.55	649.184	1001.77	0.705	536.448	1001.77	0.86	459.746	1001.77
0.555	643.029	1001.77	0.71	532.751	1001.77	0.865	457.898	1001.77
0.56	638.712	1001.77	0.715	530.283	1001.77	0.87	456.359	1001.77
0.565	635.015	1001.77	0.72	528.435	1001.77	0.875	453.891	1001.77
0.57	631.318	1001.77	0.725	525.357	1001.77	0.88	451.423	1001.77
0.575	625.781	1001.77	0.73	522.279	1001.77	0.885	450.813	1001.77

B.2. Exact 0201

Stress Relaxation

T=150°C; strain=12.5 [strain units]; fixture diameter=10 [mm]; cone angle=0.035 [rad]

Time [s]	G(γ,t) [Pa]	γ [%]	Time [s] *cont.*	G(γ,t) [Pa] *cont.*	γ [%] *cont.*	Time [s] *cont.*	G(γ,t) [Pa] *cont.*	γ [%] *cont.*
0.001	0	0	0.145	1232.72	1251.66	0.285	631.291	1251.66
0.01	59671.2	12.735	0.15	1187.45	1251.66	0.29	621.918	1251.66
0.015	72804.9	82.5313	0.155	1147.14	1251.66	0.295	612.05	1251.66
0.02	37255.3	226.589	0.16	1107.78	1251.66	0.3	602.196	1251.66
0.025	22042	413.657	0.165	1071.38	1251.66	0.305	593.815	1251.66
0.03	15165.2	604.469	0.17	1038.93	1251.66	0.31	584.938	1251.66
0.035	11519	771.074	0.175	1008.44	1251.66	0.315	576.556	1251.66
0.04	9326.58	904.937	0.18	978.924	1251.66	0.32	569.647	1251.66
0.045	7826.78	1007.46	0.185	952.368	1251.66	0.325	562.257	1251.66
0.05	6640.1	1082.92	0.19	926.788	1251.66	0.33	553.38	1251.66
0.055	5690.85	1136.33	0.195	902.2	1251.66	0.335	547.462	1251.66
0.06	4912.38	1174.06	0.2	880.555	1251.66	0.34	541.048	1251.66
0.065	4265.45	1199.69	0.205	859.887	1251.66	0.345	534.154	1251.66
0.07	3729.86	1217.48	0.21	840.225	1251.66	0.35	528.236	1251.66
0.075	3288.58	1229.58	0.215	819.557	1251.66	0.355	521.822	1251.66
0.08	2927.16	1236.71	0.22	802.885	1251.66	0.36	515.408	1251.66
0.085	2628.35	1242.4	0.225	786.107	1251.66	0.365	509.01	1251.66
0.09	2383.06	1245.25	0.23	769.344	1251.66	0.37	504.068	1251.66
0.095	2179.6	1247.39	0.235	754.564	1251.66	0.375	498.645	1251.66
0.1	2008.32	1249.53	0.24	740.264	1251.66	0.38	492.239	1251.66
0.105	1867.35	1250.25	0.245	725.469	1251.66	0.385	487.305	1251.66
0.11	1746.23	1250.94	0.25	711.665	1251.66	0.39	482.874	1251.66
0.115	1641.89	1250.94	0.255	699.334	1251.66	0.395	476.46	1251.66
0.12	1550.44	1251.66	0.26	686.506	1251.66	0.4	470.054	1251.66
0.125	1471.76	1251.66	0.265	674.189	1251.66	0.405	466.104	1251.66
0.13	1401.92	1251.66	0.27	662.849	1251.66	0.41	460.681	1251.66
0.135	1339.94	1251.66	0.275	651.989	1251.66	0.415	455.259	1251.66
0.14	1284.85	1251.66	0.28	640.649	1251.66	0.42	450.325	1251.66

Time [s] *cont.*	G(γ,t) [Pa] *cont.*	γ [%] *cont.*	Time [s] *cont.*	G(γ,t) [Pa] *cont.*	γ [%] *cont.*	Time [s] *cont.*	G(γ,t) [Pa] *cont.*	γ [%] *cont.*
0.425	447.366	1251.66	0.58	345.302	1251.66	0.735	285.888	1251.66
0.43	442.439	1251.66	0.585	342.59	1251.66	0.74	284.657	1251.66
0.435	438	1251.66	0.59	340.863	1251.66	0.745	283.177	1251.66
0.44	434.546	1251.66	0.595	338.895	1251.66	0.75	280.706	1251.66
0.445	429.123	1251.66	0.6	336.425	1251.66	0.755	278.739	1251.66
0.45	425.676	1251.66	0.605	334.457	1251.66	0.76	277.507	1251.66
0.455	422.221	1251.66	0.61	332.977	1251.66	0.765	275.532	1251.66
0.46	418.279	1251.66	0.615	329.771	1251.66	0.77	273.804	1251.66
0.465	413.344	1251.66	0.62	327.795	1251.66	0.775	273.068	1251.66
0.47	410.881	1251.66	0.625	326.068	1251.66	0.78	270.597	1251.66
0.475	407.426	1251.66	0.63	323.116	1251.66	0.785	269.861	1251.66
0.48	403.236	1251.66	0.635	320.646	1251.66	0.79	268.134	1251.66
0.485	399.541	1251.66	0.64	318.926	1251.66	0.795	266.902	1251.66
0.49	396.829	1251.66	0.645	316.207	1251.66	0.8	264.687	1251.66
0.495	393.622	1251.66	0.65	313.496	1251.66	0.805	264.191	1251.66
0.5	389.68	1251.66	0.655	312.016	1251.66	0.81	263.448	1251.66
0.505	386.721	1251.66	0.66	310.785	1251.66	0.815	261.232	1251.66
0.51	384.009	1251.66	0.665	307.578	1251.66	0.82	260.001	1251.66
0.515	380.066	1251.66	0.67	306.346	1251.66	0.825	260.489	1251.66
0.52	376.86	1251.66	0.675	304.867	1251.66	0.83	258.769	1251.66
0.525	374.637	1251.66	0.68	303.387	1251.66	0.835	257.041	1251.66
0.53	370.446	1251.66	0.685	301.172	1251.66	0.84	256.058	1251.66
0.535	367.487	1251.66	0.69	300.188	1251.66	0.845	255.562	1251.66
0.54	365.519	1251.66	0.695	298.46	1251.66	0.85	253.099	1251.66
0.545	361.817	1251.66	0.7	295.997	1251.66	0.855	252.107	1251.66
0.55	358.865	1251.66	0.705	295.501	1251.66	0.86	250.876	1251.66
0.555	356.89	1251.66	0.71	294.022	1251.66	0.865	249.396	1251.66
0.56	354.427	1251.66	0.715	292.047	1251.66	0.87	248.164	1251.66
0.565	351.715	1251.66	0.72	290.327	1251.66	0.875	246.933	1251.66
0.57	349.245	1251.66	0.725	289.831	1251.66	0.88	245.701	1251.66
0.575	347.765	1251.66	0.73	287.856	1251.66	0.885	243.482	1251.66

B.3. NTX101

Stress Relaxation

T=150°C; strain=0.01 [strain units]; fixture diameter=25 [mm]; cone angle=0.1 [rad]

Time [s]	G(γ,t) [Pa]	γ [%]	Time [s] *cont.*	G(γ,t) [Pa] *cont.*	γ [%] *cont.*	Time [s] *cont.*	G(γ,t) [Pa] *cont.*	γ [%] *cont.*
0.001	0	0	0.145	25637.2	1.02919	0.285	11414.4	1.02821
0.01	51047.4	0.06258	0.15	24696.2	1.02627	0.29	11132.6	1.03017
0.015	189756	0.19345	0.155	23698.2	1.02627	0.295	10972.4	1.02725
0.02	208746	0.3462	0.16	22742.9	1.02919	0.3	10768	1.02919
0.025	195505	0.51117	0.165	21853	1.03214	0.305	10575.9	1.02627
0.03	180620	0.6452	0.17	21282.1	1.0243	0.31	10374.1	1.02725
0.035	163040	0.75526	0.175	20410.9	1.03017	0.315	10107.6	1.03017
0.04	144341	0.84527	0.18	19778.8	1.02725	0.32	9992.91	1.03017
0.045	129268	0.8981	0.185	19226.4	1.02725	0.325	9793.89	1.03017
0.05	113511	0.94799	0.19	18500.9	1.02919	0.33	9637.6	1.02725
0.055	100287	0.97832	0.195	17852.6	1.03214	0.335	9606.99	1.02233
0.06	88866.2	0.9979	0.2	17463.2	1.02627	0.34	9346.18	1.02725
0.065	79192	1.00866	0.205	16878.9	1.02821	0.345	9200.47	1.02725
0.07	71046.5	1.01453	0.21	16434.8	1.02627	0.35	9127.9	1.02332
0.075	63860.7	1.0204	0.215	15943	1.02725	0.355	8941.39	1.02529
0.08	57527.4	1.02821	0.22	15529.9	1.02821	0.36	8781.5	1.02332
0.085	52522.3	1.03017	0.225	15078.7	1.02919	0.365	8578.25	1.02919
0.09	48345.3	1.02725	0.23	14622	1.03116	0.37	8501.8	1.02919
0.095	44338.1	1.03408	0.235	14370.6	1.02725	0.375	8325.97	1.02821
0.1	41455.7	1.02919	0.24	13955.2	1.03017	0.38	8141.65	1.03017
0.105	38668.5	1.02919	0.245	13654.9	1.02627	0.385	8057.75	1.02821
0.11	36248.9	1.02919	0.25	13355.9	1.02919	0.39	7903.73	1.02529
0.115	34164.3	1.03017	0.255	13066.5	1.02725	0.395	7751.15	1.02821
0.12	32267.5	1.03309	0.26	12778.1	1.02332	0.4	7659.17	1.02821
0.125	30794.3	1.02725	0.265	12402.2	1.03017	0.405	7606.65	1.02233
0.13	29136.7	1.03214	0.27	12192.2	1.02919	0.41	7456.15	1.02919
0.135	27922.5	1.03017	0.275	11851.2	1.02821	0.415	7317.35	1.02821
0.14	26800	1.02627	0.28	11593.7	1.02725	0.42	7320.28	1.02725

Time [s] *cont.*	G(γ,t) [Pa] *cont.*	γ [%] *cont.*	Time [s] *cont.*	G(γ,t) [Pa] *cont.*	γ [%] *cont.*	Time [s] *cont.*	G(γ,t) [Pa] *cont.*	γ [%] *cont.*
0.425	7195.61	1.02529	0.58	4909.36	1.02725	0.735	3663.26	1.02627
0.43	7069.47	1.02627	0.585	4921.81	1.02627	0.74	3640.16	1.02627
0.435	7020.56	1.03116	0.59	4839.51	1.02821	0.745	3602.72	1.03309
0.44	6897.32	1.02725	0.595	4769.27	1.0243	0.75	3571.32	1.02725
0.445	6816.87	1.0243	0.6	4701.31	1.02821	0.755	3614.86	1.03017
0.45	6748.71	1.02529	0.605	4675.48	1.02627	0.76	3533.36	1.03214
0.455	6613.21	1.03017	0.61	4571.09	1.02725	0.765	3467.48	1.02725
0.46	6482.71	1.03506	0.615	4549.93	1.03116	0.77	3531.5	1.0243
0.465	6414.52	1.02821	0.62	4642.05	1.0243	0.775	3445.07	1.02821
0.47	6395.07	1.02332	0.625	4489.97	1.02821	0.78	3415.2	1.02332
0.475	6222.49	1.02821	0.63	4430.78	1.02233	0.785	3405.91	1.03017
0.48	6090	1.02529	0.635	4371.47	1.02627	0.79	3344.59	1.03017
0.485	6045.68	1.0243	0.64	4275.44	1.02529	0.795	3357.37	1.02919
0.49	5913.39	1.02919	0.645	4213.32	1.02821	0.8	3335.62	1.03116
0.495	5808.47	1.03214	0.65	4101.73	1.03116	0.805	3377.11	1.02725
0.5	5776.86	1.02821	0.655	4136.56	1.02821	0.81	3309.88	1.02725
0.505	5778.36	1.02725	0.66	4082.86	1.02529	0.815	3241.82	1.02627
0.51	5704.51	1.03017	0.665	4032.74	1.02529	0.82	3250.26	1.02725
0.515	5597.48	1.03506	0.67	4102.35	1.02138	0.825	3165.12	1.0243
0.52	5683.18	1.0243	0.675	3986.6	1.02725	0.83	3074.25	1.03017
0.525	5543.86	1.02725	0.68	3925.32	1.02919	0.835	3054.16	1.02919
0.53	5493.85	1.02725	0.685	3936.9	1.02919	0.84	3042.64	1.02725
0.535	5532.27	1.02725	0.69	3856.23	1.02919	0.845	3007.06	1.0243
0.54	5418.33	1.02627	0.695	3810.38	1.03017	0.85	2959.21	1.03017
0.545	5359.27	1.02725	0.7	3798.94	1.03017	0.855	3003.31	1.02821
0.55	5306.72	1.02627	0.705	3836.68	1.02725	0.86	2936.76	1.02529
0.555	5248.92	1.02627	0.71	3758.43	1.02919	0.865	2883.05	1.02725
0.56	5176.97	1.02529	0.715	3706.58	1.02919	0.87	2963.06	1.03017
0.565	5091.39	1.02233	0.72	3712.37	1.02919	0.875	2931.35	1.02919
0.57	5087.35	1.02627	0.725	3656.72	1.02919	0.88	2948.32	1.02529
0.575	4982.45	1.02725	0.73	3656.78	1.0243	0.885	2980.05	1.0243

B.3. NTX101

Stress Relaxation

T=150°C; strain=0.1 [strain units]; fixture diameter=25 [mm]; cone angle=0.1 [rad]

Time [s]	G(γ,t) [Pa]	γ [%]	Time [s] *cont.*	G(γ,t) [Pa] *cont.*	γ [%] *cont.*	Time [s] *cont.*	G(γ,t) [Pa] *cont.*	γ [%] *cont.*
0.001	0	0	0.145	25183.4	10.071	0.285	11453.3	10.0555
0.01	69332.9	0.484	0.15	24181.7	10.071	0.29	11217.4	10.0631
0.015	204967	1.89402	0.155	23258.4	10.071	0.295	10998.8	10.0555
0.02	213036	3.55916	0.16	22431	10.0631	0.3	10771.2	10.0631
0.025	199174	5.12646	0.165	21647.6	10.0631	0.305	10559.8	10.0631
0.03	179777	6.44908	0.17	20879.9	10.071	0.31	10371.8	10.0631
0.035	160570	7.50253	0.175	20222.8	10.0631	0.315	10183.7	10.0555
0.04	142508	8.29884	0.18	19564.7	10.0631	0.32	9980.36	10.0631
0.045	125898	8.8844	0.185	18954	10.0631	0.325	9800.29	10.0631
0.05	111234	9.29805	0.19	18374.8	10.0631	0.33	9627.88	10.0631
0.055	98306.8	9.58701	0.195	17826.7	10.0631	0.335	9462.87	10.0555
0.06	87214.9	9.78228	0.2	17296.2	10.071	0.34	9298.22	10.0555
0.065	77864.2	9.90721	0.205	16808.4	10.0631	0.345	9149.37	10.0555
0.07	69770.7	9.99304	0.21	16354.6	10.0631	0.35	8984.71	10.0555
0.075	62959.9	10.0555	0.215	15916	10.0631	0.355	8843.76	10.0555
0.08	57174.6	10.0867	0.22	15485.3	10.0631	0.36	8710.46	10.0555
0.085	52241	10.1101	0.225	15085.9	10.0631	0.365	8561.6	10.0555
0.09	47994.4	10.118	0.23	14702.1	10.0631	0.37	8420.64	10.0555
0.095	44318.3	10.118	0.235	14342	10.0631	0.375	8288.95	10.0631
0.1	41110.3	10.118	0.24	13989.5	10.0631	0.38	8155.75	10.0631
0.105	38335.5	10.1101	0.245	13660.7	10.0631	0.385	8024.17	10.071
0.11	35903.8	10.1101	0.25	13331.9	10.0631	0.39	7919.03	10.0555
0.115	33747.9	10.1022	0.255	13018.6	10.0631	0.395	7809.3	10.0555
0.12	31925.5	10.0867	0.26	12754.2	10.0555	0.4	7691.8	10.0555
0.125	30253	10.0867	0.265	12470.5	10.0631	0.405	7582.07	10.0555
0.13	28791.5	10.0789	0.27	12188.6	10.0631	0.41	7474.57	10.0631
0.135	27462.1	10.0789	0.275	11937.9	10.0631	0.415	7362.61	10.0555
0.14	26258.3	10.0789	0.28	11687.3	10.0631	0.42	7255.28	10.0631

Time [s] *cont.*	G(γ,t) [Pa] *cont.*	γ [%] *cont.*	Time [s] *cont.*	G(γ,t) [Pa] *cont.*	γ [%] *cont.*	Time [s] *cont.*	G(γ,t) [Pa] *cont.*	γ [%] *cont.*
0.425	7158.95	10.0555	0.58	4930.15	10.0631	0.735	3717.37	10.0631
0.43	7059.54	10.0631	0.585	4875.27	10.0631	0.74	3674.14	10.0631
0.435	6957.67	10.0631	0.59	4816.32	10.0631	0.745	3654.53	10.0631
0.44	6868.9	10.0555	0.595	4777.1	10.0631	0.75	3611.37	10.0631
0.445	6782.75	10.0555	0.6	4722.22	10.0631	0.755	3579.98	10.0631
0.45	6683.62	10.0631	0.605	4671.16	10.0631	0.76	3559.13	10.0555
0.455	6589.64	10.0631	0.61	4635.46	10.0555	0.765	3531.6	10.0555
0.46	6508.49	10.0555	0.615	4588.31	10.0555	0.77	3496.24	10.0555
0.465	6422.21	10.0555	0.62	4545	10.0555	0.775	3470.04	10.0631
0.47	6340.13	10.0555	0.625	4494.56	10.0631	0.78	3453.05	10.0555
0.475	6261.63	10.0555	0.63	4454.66	10.0555	0.785	3422.99	10.0631
0.48	6190.91	10.0555	0.635	4412.06	10.0631	0.79	3395.49	10.0631
0.485	6112.41	10.0555	0.64	4376.79	10.0631	0.795	3382.33	10.0555
0.49	6033.8	10.0555	0.645	4340.74	10.0555	0.8	3352.32	10.0631
0.495	5978.75	10.0555	0.65	4301.49	10.0555	0.805	3313.05	10.0631
0.5	5900.26	10.0555	0.655	4262.96	10.0631	0.81	3293.44	10.0631
0.505	5825.59	10.0555	0.66	4230.77	10.0555	0.815	3264.52	10.0555
0.51	5758.82	10.0555	0.665	4196.24	10.0631	0.82	3234.55	10.0631
0.515	5688.1	10.0555	0.67	4153.07	10.0631	0.825	3209.02	10.0631
0.52	5621.02	10.0631	0.675	4116.86	10.0555	0.83	3199.67	10.0555
0.525	5554.3	10.0631	0.68	4085.51	10.0555	0.835	3170.23	10.0555
0.53	5499.52	10.0555	0.685	4042.31	10.0555	0.84	3140.33	10.0631
0.535	5432.75	10.0555	0.69	4006.89	10.0555	0.845	3126.64	10.0631
0.54	5369.93	10.0555	0.695	3976.35	10.0631	0.85	3105.44	10.0555
0.545	5314.8	10.0631	0.7	3940.12	10.0555	0.855	3079.89	10.0555
0.55	5252.03	10.0631	0.705	3900.87	10.0555	0.86	3062.18	10.0555
0.555	5189.25	10.0631	0.71	3877.3	10.0555	0.865	3042.22	10.0631
0.56	5138.15	10.0555	0.715	3839.03	10.0631	0.87	3020.96	10.0555
0.565	5079.28	10.0555	0.72	3806.58	10.0555	0.875	2995.41	10.0555
0.57	5028.32	10.0631	0.725	3776.19	10.0631	0.88	2979.45	10.0631
0.575	4973.26	10.0555	0.73	3747.65	10.0555	0.885	2956.16	10.0555

B.3. NTX101

Stress Relaxation

T=150°C; strain=1.0 [strain units]; fixture diameter=10 [mm]; cone angle=0.035 [rad]

Time [s]	G(γ,t) [Pa]	γ [%]	Time [s] *cont.*	G(γ,t) [Pa] *cont.*	γ [%] *cont.*	Time [s] *cont.*	G(γ,t) [Pa] *cont.*	γ [%] *cont.*
0.001	0	0	0.145	19047.6	100.199	0.285	8619.76	100.199
0.01	46459.5	4.81897	0.15	18282.1	100.199	0.29	8457.39	100.199
0.015	74701.3	20.64	0.155	17585.5	100.199	0.295	8290.22	100.199
0.02	81801.3	37.5858	0.16	16928.2	100.199	0.3	8123.04	100.199
0.025	83469	53.0886	0.165	16319.9	100.199	0.305	7980.35	100.199
0.03	84864.2	66.0259	0.17	15736.5	100.289	0.31	7822.94	100.199
0.035	82923	76.1076	0.175	15217	100.289	0.315	7665.52	100.199
0.04	79430.2	83.5136	0.18	14716.9	100.289	0.32	7532.74	100.199
0.045	74292.1	88.8665	0.185	14269	100.199	0.325	7399.96	100.199
0.05	68695.7	92.6131	0.19	13824.9	100.289	0.33	7257.42	100.199
0.055	63027.5	95.2016	0.195	13403.6	100.289	0.335	7129.45	100.199
0.06	57664.2	96.8965	0.2	13022.9	100.199	0.34	7010.06	100.289
0.065	52690.3	98.0572	0.205	12660.1	100.199	0.345	6898.29	100.199
0.07	48203.9	98.861	0.21	12306.8	100.199	0.35	6770.47	100.199
0.075	44187.3	99.3951	0.215	11963.4	100.199	0.355	6667.13	100.199
0.08	40675.4	99.6621	0.22	11659.1	100.199	0.36	6549.07	100.199
0.085	37554.7	99.9319	0.225	11355.1	100.199	0.365	6435.96	100.199
0.09	34868.2	100.019	0.23	11050.8	100.289	0.37	6332.63	100.199
0.095	32459.8	100.109	0.235	10795.7	100.199	0.375	6234.39	100.199
0.1	30350.6	100.199	0.24	10540.7	100.199	0.38	6130.51	100.289
0.105	28506.1	100.199	0.245	10275.7	100.199	0.385	6042.43	100.199
0.11	26857.5	100.199	0.25	10021.3	100.289	0.39	5963.88	100.199
0.115	25366.3	100.199	0.255	9814.62	100.199	0.395	5865.04	100.289
0.12	24070.9	100.199	0.26	9593.52	100.199	0.4	5781.83	100.199
0.125	22874.1	100.199	0.265	9372.28	100.199	0.405	5703.13	100.199
0.13	21755.7	100.289	0.27	9180.47	100.199	0.41	5619.46	100.199
0.135	20775.5	100.289	0.275	8988.66	100.199	0.415	5526.04	100.199
0.14	19873.3	100.289	0.28	8788.96	100.289	0.42	5452.29	100.199

Time [s] *cont.*	G(γ,t) [Pa] *cont.*	γ [%] *cont.*	Time [s] *cont.*	G(γ,t) [Pa] *cont.*	γ [%] *cont.*	Time [s] *cont.*	G(γ,t) [Pa] *cont.*	γ [%] *cont.*
0.425	5383.5	100.199	0.58	3707.89	100.289	0.735	2769.29	100.199
0.43	5309.6	100.199	0.585	3669.38	100.199	0.74	2754.58	100.199
0.435	5231.15	100.289	0.59	3639.87	100.199	0.745	2727.54	100.199
0.44	5172.01	100.199	0.595	3598.04	100.199	0.75	2700.43	100.199
0.445	5098.49	100.289	0.6	3553.8	100.199	0.755	2685.71	100.199
0.45	5024.81	100.289	0.605	3516.93	100.199	0.76	2668.51	100.199
0.455	4975.24	100.199	0.61	3484.93	100.199	0.765	2641.4	100.199
0.46	4911.26	100.199	0.615	3443.1	100.199	0.77	2619.32	100.199
0.465	4837.51	100.199	0.62	3411.19	100.199	0.775	2611.96	100.199
0.47	4774.2	100.289	0.625	3381.11	100.289	0.78	2587.48	100.289
0.475	4710.34	100.289	0.63	3344.8	100.199	0.785	2565.17	100.199
0.48	4650.58	100.199	0.635	3310.32	100.199	0.79	2552.93	100.199
0.485	4587.44	100.289	0.64	3288.17	100.199	0.795	2533.25	100.199
0.49	4542.36	100.199	0.645	3253.77	100.199	0.8	2511.1	100.199
0.495	4474.43	100.289	0.65	3216.9	100.199	0.805	2494.14	100.289
0.5	4415.46	100.289	0.655	3192.27	100.199	0.81	2476.88	100.289
0.505	4375.19	100.199	0.66	3170.19	100.199	0.815	2449.87	100.289
0.51	4322.12	100.289	0.665	3138.19	100.199	0.82	2427.77	100.289
0.515	4271.92	100.199	0.67	3110.84	100.289	0.825	2415.47	100.289
0.52	4222.73	100.199	0.675	3093.96	100.199	0.83	2393.04	100.199
0.525	4178.42	100.199	0.68	3061.96	100.199	0.835	2368.79	100.289
0.53	4129.23	100.199	0.685	3029.97	100.199	0.84	2358.64	100.199
0.535	4080.04	100.199	0.69	3007.89	100.199	0.845	2341.41	100.199
0.54	4045.64	100.199	0.695	2978.38	100.199	0.85	2314.37	100.199
0.545	3990.39	100.289	0.7	2948.86	100.199	0.855	2299.61	100.199
0.55	3949.74	100.199	0.705	2929.19	100.199	0.86	2284.85	100.199
0.555	3912.86	100.199	0.71	2899.47	100.289	0.865	2265.18	100.199
0.56	3875.99	100.199	0.715	2872.63	100.199	0.87	2248.4	100.289
0.565	3829.2	100.199	0.72	2845.52	100.199	0.875	2243.06	100.199
0.57	3792.32	100.199	0.725	2830.8	100.199	0.88	2223.38	100.199
0.575	3752.08	100.289	0.73	2798.81	100.199	0.885	2203.71	100.199

B.3. NTX101

Stress Relaxation

T=150°C; strain=5.0 [strain units]; fixture diameter=10 [mm]; cone angle=0.035 [rad]

Time [s]	G(γ,t) [Pa]	γ [%]	Time [s] *cont.*	G(γ,t) [Pa] *cont.*	γ [%] *cont.*	Time [s] *cont.*	G(γ,t) [Pa] *cont.*	γ [%] *cont.*
0.001	0	0	0.145	1766.71	501.232	0.285	798.288	501.232
0.01	61137.6	11.2033	0.15	1692.85	501.232	0.29	782.89	501.232
0.015	81744.2	66.1594	0.155	1628.79	501.232	0.295	768.731	501.232
0.02	49002.8	150.163	0.16	1570.95	501.232	0.3	753.352	501.232
0.025	31197.4	230.501	0.165	1513.07	501.232	0.305	738.574	501.232
0.03	22160.3	301.166	0.17	1458.87	501.232	0.31	725.033	501.232
0.035	16867.5	357.417	0.175	1412.1	501.232	0.315	712.712	501.232
0.04	13208.5	400.131	0.18	1365.29	501.232	0.32	696.714	501.232
0.045	10776.9	431.455	0.185	1322.23	501.232	0.325	685.011	501.232
0.05	8931.23	453.886	0.19	1281.57	501.232	0.33	674.547	501.232
0.055	7563.95	469.199	0.195	1245.86	501.232	0.335	662.225	501.232
0.06	6492.47	479.88	0.2	1208.93	501.232	0.34	649.922	501.232
0.065	5654.21	486.997	0.205	1170.77	501.232	0.345	640.076	501.232
0.07	4981.34	491.978	0.21	1139.97	501.232	0.35	628.992	501.232
0.075	4441.87	495.183	0.215	1107.96	501.232	0.355	617.908	501.232
0.08	4001.88	497.319	0.22	1077.18	501.232	0.36	609.281	501.232
0.085	3637.44	498.747	0.225	1050.08	501.232	0.365	599.435	501.232
0.09	3336.42	499.455	0.23	1025.46	501.232	0.37	588.352	501.232
0.095	3080.6	500.163	0.235	998.996	501.232	0.375	581.581	501.232
0.1	2861.95	500.523	0.24	974.991	501.232	0.38	573.573	501.232
0.105	2673.05	500.883	0.245	951.585	501.232	0.385	562.499	501.232
0.11	2510.82	500.883	0.25	929.418	501.232	0.39	555.728	501.232
0.115	2365.79	500.883	0.255	907.269	501.232	0.395	548.949	501.232
0.12	2233.95	501.232	0.26	889.415	501.232	0.4	539.722	501.232
0.125	2120.94	501.232	0.265	870.323	501.232	0.405	530.485	501.232
0.13	2020.23	501.232	0.27	848.774	501.232	0.41	523.705	501.232
0.135	1925.55	501.232	0.275	832.758	501.232	0.415	516.935	501.232
0.14	1841.83	501.232	0.28	816.142	501.232	0.42	507.699	501.232

Time [s] *cont.*	G(γ,t) [Pa] *cont.*	γ [%] *cont.*	Time [s] *cont.*	G(γ,t) [Pa] *cont.*	γ [%] *cont.*	Time [s] *cont.*	G(γ,t) [Pa] *cont.*	γ [%] *cont.*
0.425	500.619	501.232	0.58	343.936	501.232	0.735	258.364	501.232
0.43	495.386	501.232	0.585	339.013	501.232	0.74	255.284	501.232
0.435	487.388	501.232	0.59	335.937	501.232	0.745	256.058	501.232
0.44	480.617	501.232	0.595	333.78	501.232	0.75	253.132	501.232
0.445	476.304	501.232	0.6	330.086	501.232	0.755	249.283	501.232
0.45	469.534	501.232	0.605	323.934	501.232	0.76	248.514	501.232
0.455	462.144	501.232	0.61	323.315	501.232	0.765	248.204	501.232
0.46	458.45	501.232	0.615	320.849	501.232	0.77	246.052	501.232
0.465	452.298	501.232	0.62	316.854	501.232	0.775	242.667	501.232
0.47	445.519	501.232	0.625	312.85	501.232	0.78	242.358	501.232
0.475	440.286	501.232	0.63	314.079	501.232	0.785	237.435	501.232
0.48	435.054	501.232	0.635	308.232	501.232	0.79	235.737	501.232
0.485	427.055	501.232	0.64	306.075	501.232	0.795	235.892	501.232
0.49	422.432	501.232	0.645	305.152	501.232	0.8	233.431	501.232
0.495	418.437	501.232	0.65	302.386	501.232	0.805	230.66	501.232
0.5	412.895	501.232	0.655	297.148	501.232	0.81	229.736	501.232
0.505	404.578	501.232	0.66	295.306	501.232	0.815	229.427	501.232
0.51	401.502	501.232	0.665	292.225	501.232	0.82	226.351	501.232
0.515	397.498	501.232	0.67	290.069	501.232	0.825	223.889	501.232
0.52	390.728	501.232	0.675	286.379	501.232	0.83	224.658	501.232
0.525	387.033	501.232	0.68	285.455	501.232	0.835	222.197	501.232
0.53	385.495	501.232	0.685	282.684	501.232	0.84	218.962	501.232
0.535	377.797	501.232	0.69	278.99	501.232	0.845	219.731	501.232
0.54	374.111	501.232	0.695	278.99	501.232	0.85	219.116	501.232
0.545	369.798	501.232	0.7	274.681	501.232	0.855	216.81	501.232
0.55	366.103	501.232	0.705	271.291	501.232	0.86	214.343	501.232
0.555	361.18	501.232	0.71	269.448	501.232	0.865	214.039	501.232
0.56	358.405	501.232	0.715	267.906	501.232	0.87	209.73	501.232
0.565	355.948	501.232	0.72	264.83	501.232	0.875	207.882	501.232
0.57	351.325	501.232	0.725	261.75	501.232	0.88	207.728	501.232
0.575	347.63	501.232	0.73	262.364	501.232	0.885	205.726	501.232

B.3. NTX101

Stress Relaxation

T=150°C; strain=7.5 [strain units]; fixture diameter=10 [mm]; cone angle=0.035 [rad]

Time [s]	G(γ,t) [Pa]	γ [%]	Time [s] *cont.*	G(γ,t) [Pa] *cont.*	γ [%] *cont.*	Time [s] *cont.*	G(γ,t) [Pa] *cont.*	γ [%] *cont.*
0.001	0	0	0.145	2231.74	751.847	0.285	985.617	751.15
0.01	64748.3	11.8631	0.15	2140.02	751.847	0.29	966.72	751.15
0.015	79844.5	74.7248	0.155	2056.5	751.847	0.295	945.293	751.847
0.02	45725.4	188.322	0.16	1976.28	751.847	0.3	928.1	751.15
0.025	30151	310.779	0.165	1902.56	751.847	0.305	910.855	751.15
0.03	22058.5	420.785	0.17	1835.45	751.847	0.31	890.306	751.847
0.035	17799	511.553	0.175	1773.23	751.15	0.315	873.877	751.847
0.04	14757.5	581.689	0.18	1710.97	751.847	0.32	858.298	751.847
0.045	12523.8	633.308	0.185	1655.31	751.847	0.325	842.695	751.847
0.05	10761.1	670.681	0.19	1604.52	751.847	0.33	826.207	751.15
0.055	9341.68	696.676	0.195	1553.76	751.847	0.335	812.313	751.847
0.06	8181.13	714.834	0.2	1506.27	751.847	0.34	797.547	751.847
0.065	7211.26	727.651	0.205	1463.69	751.847	0.345	782.768	751.847
0.07	6411.42	735.477	0.21	1421.13	751.847	0.35	768.815	751.847
0.075	5737.59	741.166	0.215	1381.82	751.847	0.355	755.675	751.847
0.08	5177.7	744.741	0.22	1344.14	751.847	0.36	741.721	751.847
0.085	4707.88	746.877	0.225	1310.58	751.847	0.365	727.768	751.847
0.09	4306.5	749.014	0.23	1274.47	751.847	0.37	718.583	751.15
0.095	3967.46	749.711	0.235	1241.64	751.847	0.375	706.426	751.847
0.1	3678.15	750.431	0.24	1210.43	751.847	0.38	694.11	751.847
0.105	3432.03	750.431	0.245	1181.17	751.15	0.385	685.083	751.847
0.11	3212.4	751.15	0.25	1152.97	751.847	0.39	674.406	751.847
0.115	3022.23	751.15	0.255	1127.76	751.15	0.395	662.916	751.847
0.12	2855.03	751.15	0.26	1100.45	751.847	0.4	653.67	751.15
0.125	2701.75	751.847	0.265	1075.17	751.15	0.405	644.449	751.847
0.13	2564.17	751.847	0.27	1053.82	751.15	0.41	634.184	751.847
0.135	2446.91	751.15	0.275	1029.04	751.847	0.415	623.272	751.15
0.14	2337.08	751.15	0.28	1006.17	751.15	0.42	614.079	751.847

Time [s] *cont.*	G(γ,t) [Pa] *cont.*	γ [%] *cont.*	Time [s] *cont.*	G(γ,t) [Pa] *cont.*	γ [%] *cont.*	Time [s] *cont.*	G(γ,t) [Pa] *cont.*	γ [%] *cont.*
0.425	607.103	751.847	0.58	412.558	751.847	0.735	306.665	751.847
0.43	598.076	751.847	0.585	408.044	751.847	0.74	304.608	751.847
0.435	591.235	751.15	0.59	405.952	751.15	0.745	300.913	751.847
0.44	582.6	751.15	0.595	401.474	751.847	0.75	298.114	751.15
0.445	573.977	751.15	0.6	396.96	751.847	0.755	296.675	751.15
0.45	565.643	751.847	0.605	392.853	751.847	0.76	294.349	751.847
0.455	559.185	751.15	0.61	388.34	751.847	0.765	290.655	751.847
0.46	550.865	751.847	0.615	383.001	751.847	0.77	290.448	751.847
0.465	543.075	751.847	0.62	380.132	751.847	0.775	289.285	751.15
0.47	537.01	751.15	0.625	376.437	751.847	0.78	285.322	751.847
0.475	529.935	751.847	0.63	372.742	751.847	0.785	282.653	751.847
0.48	522.146	751.847	0.635	368.571	751.15	0.79	280.396	751.847
0.485	516.048	751.15	0.64	366.585	751.847	0.795	277.52	751.847
0.49	509.418	751.847	0.645	362.071	751.847	0.8	274.906	751.15
0.495	501.203	751.847	0.65	358.709	751.15	0.805	274.699	751.15
0.5	494.639	751.847	0.655	355.507	751.847	0.81	271.821	751.15
0.505	490.581	751.15	0.66	350.987	751.847	0.815	269.312	751.847
0.51	483.974	751.847	0.665	346.061	751.847	0.82	267.262	751.847
0.515	478.667	751.15	0.67	344.011	751.847	0.825	266.443	751.847
0.52	472.51	751.15	0.675	341.141	751.847	0.83	262.373	751.15
0.525	467.958	751.847	0.68	337.034	751.847	0.835	261.14	751.15
0.53	460.581	751.847	0.685	334.062	751.15	0.84	260.691	751.847
0.535	456.468	751.847	0.69	332.933	751.847	0.845	257.442	751.15
0.54	451.542	751.847	0.695	329.439	751.847	0.85	254.74	751.847
0.545	446.217	751.15	0.7	325.338	751.847	0.855	254.334	751.847
0.55	441.289	751.847	0.705	324.925	751.847	0.86	253.509	751.847
0.555	436.363	751.847	0.71	320.618	751.847	0.865	250.433	751.847
0.56	431.85	751.847	0.715	316.511	751.847	0.87	248.589	751.847
0.565	426.494	751.15	0.72	314.873	751.847	0.875	248.613	751.15
0.57	422.41	751.847	0.725	312.7	751.15	0.88	244.275	751.847
0.575	418.297	751.847	0.73	309.534	751.847	0.885	244.275	751.847

B.3. NTX101

Stress Relaxation

T=150°C; strain=10.0 [strain units]; fixture diameter=10 [mm]; cone angle=0.035 [rad]

Time [s]	G(γ,t) [Pa]	γ [%]	Time [s] *cont.*	G(γ,t) [Pa] *cont.*	γ [%] *cont.*	Time [s] *cont.*	G(γ,t) [Pa] *cont.*	γ [%] *cont.*
0.001	0	0	0.145	1481.12	1001.77	0.285	637.113	1001.77
0.01	63973	12.1761	0.15	1415.96	1001.77	0.29	622.944	1001.77
0.015	74347.1	78.9632	0.155	1356.99	1001.77	0.295	610.004	1001.77
0.02	40921.6	211.101	0.16	1301.67	1001.77	0.3	598.912	1001.77
0.025	26419.6	370.583	0.165	1250.06	1001.77	0.305	585.972	1001.77
0.03	19155.6	521.886	0.17	1204.56	1001.77	0.31	574.27	1001.77
0.035	14903.8	649.678	0.175	1159.09	1001.77	0.315	565.027	1001.77
0.04	12104.1	750.431	0.18	1118.53	1001.77	0.32	554.555	1001.77
0.045	10034.6	825.896	0.185	1081.66	1001.77	0.325	542.854	1001.77
0.05	8466.43	880.719	0.19	1044.8	1001.77	0.33	533.611	1001.77
0.055	7217.28	919.869	0.195	1011.6	1001.77	0.335	524.987	1001.77
0.06	6204.86	946.943	0.2	980.875	1001.77	0.34	515.744	1001.77
0.065	5381.92	965.45	0.205	951.317	1001.77	0.345	505.882	1001.77
0.07	4710.73	977.548	0.21	922.978	1001.77	0.35	497.568	1001.77
0.075	4155.44	986.093	0.215	896.478	1001.77	0.355	488.944	1001.77
0.08	3707.16	991.084	0.22	872.456	1001.77	0.36	480.321	1001.77
0.085	3330.03	995.357	0.225	847.815	1001.77	0.365	472.307	1001.77
0.09	3019.3	997.493	0.23	825.631	1001.77	0.37	465.842	1001.77
0.095	2761.08	998.91	0.235	804.687	1001.77	0.375	458.138	1001.77
0.1	2540.51	1000.33	0.24	783.743	1001.77	0.38	451.363	1001.77
0.105	2351.78	1001.05	0.245	764.018	1001.77	0.385	445.198	1001.77
0.11	2189.4	1001.05	0.25	746.771	1001.77	0.39	437.503	1001.77
0.115	2050.18	1001.77	0.255	728.285	1001.77	0.395	431.028	1001.77
0.12	1924.82	1001.77	0.26	711.038	1001.77	0.4	425.492	1001.77
0.125	1815.44	1001.77	0.265	695.029	1001.77	0.405	418.708	1001.77
0.13	1718.34	1001.77	0.27	680.24	1001.77	0.41	411.933	1001.77
0.135	1632.27	1001.77	0.275	663.594	1001.77	0.415	407.006	1001.77
0.14	1553.64	1001.77	0.28	650.663	1001.77	0.42	400.841	1001.77

Time [s] *cont.*	G(γ,t) [Pa] *cont.*	γ [%] *cont.*	Time [s] *cont.*	G(γ,t) [Pa] *cont.*	γ [%] *cont.*	Time [s] *cont.*	G(γ,t) [Pa] *cont.*	γ [%] *cont.*
0.425	393.456	1001.77	0.58	273.317	1001.77	0.735	204.468	1001.77
0.43	389.14	1001.77	0.585	271.158	1001.77	0.74	203.084	1001.77
0.435	384.213	1001.77	0.59	267.156	1001.77	0.745	201.391	1001.77
0.44	378.667	1001.77	0.595	263.769	1001.77	0.75	200.157	1001.77
0.445	372.812	1001.77	0.6	262.535	1001.77	0.755	198.308	1001.77
0.45	369.424	1001.77	0.605	259.147	1001.77	0.76	195.845	1001.77
0.455	364.498	1001.77	0.61	256.065	1001.77	0.765	194.92	1001.77
0.46	359.262	1001.77	0.615	254.216	1001.77	0.77	194.306	1001.77
0.465	354.636	1001.77	0.62	251.443	1001.77	0.775	191.683	1001.77
0.47	350.638	1001.77	0.625	248.98	1001.77	0.78	189.684	1001.77
0.475	345.393	1001.77	0.63	246.362	1001.77	0.785	189.22	1001.77
0.48	341.086	1001.77	0.635	244.823	1001.77	0.79	186.447	1001.77
0.485	337.698	1001.77	0.64	240.971	1001.77	0.795	184.753	1001.77
0.49	332.772	1001.77	0.645	237.893	1001.77	0.8	183.984	1001.77
0.495	327.836	1001.77	0.65	236.504	1001.77	0.805	183.059	1001.77
0.5	325.687	1001.77	0.655	234.965	1001.77	0.81	181.056	1001.77
0.505	321.68	1001.77	0.66	231.883	1001.77	0.815	179.827	1001.77
0.51	316.134	1001.77	0.665	230.344	1001.77	0.82	179.207	1001.77
0.515	313.357	1001.77	0.67	228.341	1001.77	0.825	177.514	1001.77
0.52	310.898	1001.77	0.675	226.187	1001.77	0.83	175.515	1001.77
0.525	306.582	1001.77	0.68	224.493	1001.77	0.835	175.82	1001.77
0.53	303.504	1001.77	0.685	223.414	1001.77	0.84	173.971	1001.77
0.535	300.116	1001.77	0.69	220.641	1001.77	0.845	171.818	1001.77
0.54	296.419	1001.77	0.695	218.333	1001.77	0.85	170.584	1001.77
0.545	292.722	1001.77	0.7	217.559	1001.77	0.855	170.429	1001.77
0.55	290.259	1001.77	0.705	214.941	1001.77	0.86	167.351	1001.77
0.555	286.871	1001.77	0.71	212.168	1001.77	0.865	166.732	1001.77
0.56	283.479	1001.77	0.715	211.708	1001.77	0.87	166.117	1001.77
0.565	281.016	1001.77	0.72	210.629	1001.77	0.875	164.423	1001.77
0.57	278.553	1001.77	0.725	208.011	1001.77	0.88	163.499	1001.77
0.575	275.47	1001.77	0.73	206.162	1001.77	0.885	163.499	1001.77

B.3. NTX101

Stress Relaxation

T=150°C; strain=12.5 [strain units]; fixture diameter=10 [mm]; cone angle=0.035 [rad]

Time [s]	G(γ,t) [Pa]	γ [%]	Time [s] *cont.*	G(γ,t) [Pa] *cont.*	γ [%] *cont.*	Time [s] *cont.*	G(γ,t) [Pa] *cont.*	γ [%] *cont.*
0.001	0	0	0.145	946.158	1251.66	0.285	392.346	1251.66
0.01	67099.8	12.5337	0.15	902.884	1251.66	0.29	383.221	1251.66
0.015	66083.9	82.2193	0.155	863.53	1251.66	0.295	374.592	1251.66
0.02	33290.1	226.234	0.16	826.144	1251.66	0.3	367.69	1251.66
0.025	20030	413.308	0.165	793.219	1251.66	0.305	359.556	1251.66
0.03	13972.3	603.76	0.17	762.157	1251.66	0.31	351.415	1251.66
0.035	10555.1	770.354	0.175	732.567	1251.66	0.315	344.761	1251.66
0.04	8427.12	904.218	0.18	705.936	1251.66	0.32	338.843	1251.66
0.045	6977.06	1006.74	0.185	681.287	1251.66	0.325	332.189	1251.66
0.05	5858.02	1082.2	0.19	657.134	1251.66	0.33	326.519	1251.66
0.055	4980.86	1136.33	0.195	634.453	1251.66	0.335	320.353	1251.66
0.06	4279.66	1174.06	0.2	615.212	1251.66	0.34	315.179	1251.66
0.065	3703.79	1199.69	0.205	594.995	1251.66	0.345	309.013	1251.66
0.07	3224.89	1217.48	0.21	576.264	1251.66	0.35	304.086	1251.66
0.075	2834.29	1228.88	0.215	559.501	1251.66	0.355	299.152	1251.66
0.08	2509.7	1236.71	0.22	544.706	1251.66	0.36	293.977	1251.66
0.085	2242.53	1242.4	0.225	528.439	1251.66	0.365	288.795	1251.66
0.09	2019.86	1245.25	0.23	514.635	1251.66	0.37	284.357	1251.66
0.095	1832.82	1247.39	0.235	501.312	1251.66	0.375	279.182	1251.66
0.1	1678.9	1248.81	0.24	487.508	1251.66	0.38	274.255	1251.66
0.105	1545	1250.25	0.245	475.184	1251.66	0.385	271.048	1251.66
0.11	1431.93	1250.94	0.25	462.852	1251.66	0.39	266.114	1251.66
0.115	1334.51	1250.94	0.255	451.512	1251.66	0.395	261.676	1251.66
0.12	1249.87	1250.94	0.26	439.683	1251.66	0.4	257.733	1251.66
0.125	1173.39	1251.66	0.265	430.31	1251.66	0.405	254.038	1251.66
0.13	1107.48	1251.66	0.27	420.449	1251.66	0.41	250.087	1251.66
0.135	1048.48	1251.66	0.275	410.588	1251.66	0.415	245.897	1251.66
0.14	994.373	1251.66	0.28	401.223	1251.66	0.42	243.186	1251.66

Time [s] *cont.*	G(γ,t) [Pa] *cont.*	γ [%] *cont.*	Time [s] *cont.*	G(γ,t) [Pa] *cont.*	γ [%] *cont.*	Time [s] *cont.*	G(γ,t) [Pa] *cont.*	γ [%] *cont.*
0.425	238.751	1251.66	0.58	162.199	1251.66	0.735	122.26	1251.66
0.43	234.804	1251.66	0.585	161.335	1251.66	0.74	121.152	1251.66
0.435	232.341	1251.66	0.59	158.872	1251.66	0.745	119.055	1251.66
0.44	229.134	1251.66	0.595	157.145	1251.66	0.75	118.563	1251.66
0.445	225.439	1251.66	0.6	155.913	1251.66	0.755	118.069	1251.66
0.45	223.464	1251.66	0.605	155.173	1251.66	0.76	116.589	1251.66
0.455	221.492	1251.66	0.61	152.83	1251.66	0.765	115.728	1251.66
0.46	218.041	1251.66	0.615	151.106	1251.66	0.77	115.11	1251.66
0.465	215.822	1251.66	0.62	149.871	1251.66	0.775	114.002	1251.66
0.47	213.355	1251.66	0.625	148.147	1251.66	0.78	112.275	1251.66
0.475	209.904	1251.66	0.63	145.928	1251.66	0.785	111.783	1251.66
0.48	206.205	1251.66	0.635	144.941	1251.66	0.79	111.289	1251.66
0.485	203.99	1251.66	0.64	143.709	1251.66	0.795	109.81	1251.66
0.49	201.031	1251.66	0.645	141.737	1251.66	0.8	109.44	1251.66
0.495	198.319	1251.66	0.65	141.49	1251.66	0.805	109.81	1251.66
0.5	195.976	1251.66	0.655	140.258	1251.66	0.81	107.962	1251.66
0.505	193.385	1251.66	0.66	138.531	1251.66	0.815	107.714	1251.66
0.51	190.922	1251.66	0.665	137.423	1251.66	0.82	107.098	1251.66
0.515	188.95	1251.66	0.67	137.175	1251.66	0.825	106.359	1251.66
0.52	186.975	1251.66	0.675	134.836	1251.66	0.83	104.879	1251.66
0.525	184.512	1251.66	0.68	133.848	1251.66	0.835	104.263	1251.66
0.53	182.785	1251.66	0.685	132.74	1251.66	0.84	103.647	1251.66
0.535	180.197	1251.66	0.69	132.121	1251.66	0.845	101.55	1251.66
0.54	177.854	1251.66	0.695	130.149	1251.66	0.85	100.688	1251.66
0.545	175.391	1251.66	0.7	129.285	1251.66	0.855	100.195	1251.66
0.55	174.155	1251.66	0.705	129.165	1251.66	0.86	98.9629	1251.66
0.555	172.06	1251.66	0.71	127.806	1251.66	0.865	98.1612	1251.66
0.56	170.089	1251.66	0.715	126.698	1251.66	0.87	97.9153	1251.66
0.565	167.745	1251.66	0.72	126.574	1251.66	0.875	97.1135	1251.66
0.57	166.885	1251.66	0.725	124.231	1251.66	0.88	95.7579	1251.66
0.575	164.418	1251.66	0.73	123.247	1251.66	0.885	95.3261	1251.66

B.4. NA952

Stress Relaxation

T=150°C; strain=0.01 [strain units]; fixture diameter=25 [mm]; cone angle=0.1 [rad]

Time [s]	G(γ,t) [Pa]	γ [%]	Time [s] *cont.*	G(γ,t) [Pa] *cont.*	γ [%] *cont.*	Time [s] *cont.*	G(γ,t) [Pa] *cont.*	γ [%] *cont.*
0.001	0	0	0.145	17271.6	1.00377	0.285	11359.4	1.00278
0.01	23005.6	0.03954	0.15	17007.3	1.00082	0.29	11177.5	1.00571
0.015	64132.5	0.18242	0.155	16661.3	0.99983	0.295	11040	1.0018
0.02	66528.4	0.33787	0.16	16187.2	1.00669	0.3	10969.1	1.0018
0.025	61594.9	0.49601	0.165	16029.6	0.9979	0.305	10874.9	1.0018
0.03	56170.9	0.63151	0.17	15745.5	0.99888	0.31	10743.6	1.00082
0.035	51955.4	0.7313	0.175	15384.2	1.00082	0.315	10636.1	1.00278
0.04	47520.3	0.81151	0.18	15048.2	1.00377	0.32	10573.2	1.00278
0.045	43419	0.87364	0.185	14833.8	1.0018	0.325	10498.5	0.9979
0.05	40175.3	0.91277	0.19	14531.8	1.00472	0.33	10303.5	1.00377
0.055	37072.8	0.94407	0.195	14270.7	1.00377	0.335	10276.6	1.0018
0.06	34455.6	0.96267	0.2	14155.2	1.00082	0.34	10186.3	0.99983
0.065	32260.6	0.97441	0.205	13942.5	1.00082	0.345	10069.9	0.99888
0.07	30439.4	0.97832	0.21	13618.4	1.00669	0.35	9998.82	0.99888
0.075	28400.7	0.99301	0.215	13490.3	1.00278	0.355	9921.81	0.9979
0.08	26881.7	0.99691	0.22	13273.7	1.00669	0.36	9793.43	0.99888
0.085	25554	1.0018	0.225	13089.3	1.00278	0.365	9703.74	1.00082
0.09	24453.1	0.99983	0.23	12848.8	1.00377	0.37	9683.02	0.99888
0.095	23420.4	1.00082	0.235	12792.1	1.00082	0.375	9541.59	1.00377
0.1	22575.9	0.99983	0.24	12598.6	1.0018	0.38	9473.79	1.0018
0.105	21670.4	1.00377	0.245	12377.4	1.00377	0.385	9434.37	1.0018
0.11	20921.3	1.00278	0.25	12259.5	1.00571	0.39	9330.75	1.00278
0.115	20347.9	1.00082	0.255	12165.7	1.0018	0.395	9198.33	1.0018
0.12	19722.4	1.00377	0.26	11957.5	1.00472	0.4	9158.91	1.0018
0.125	19175.5	1.00278	0.265	11816.7	1.00669	0.405	9103.86	1.0018
0.13	18643.4	1.0018	0.27	11741.2	1.00377	0.41	8983.21	1.00472
0.135	18198.6	1.00377	0.275	11581	1.00472	0.415	8944.48	1.00377
0.14	17726.9	1.00377	0.28	11412.8	1.00571	0.42	9004.16	0.99888

Time [s] *cont.*	G(γ,t) [Pa] *cont.*	γ [%] *cont.*	Time [s] *cont.*	G(γ,t) [Pa] *cont.*	γ [%] *cont.*	Time [s] *cont.*	G(γ,t) [Pa] *cont.*	γ [%] *cont.*
0.425	8899.31	1.0018	0.58	7274.72	1.00472	0.735	6300.01	1.00082
0.43	8784.85	1.00767	0.585	7318.86	1.00082	0.74	6270.15	1.0018
0.435	8845.77	0.99983	0.59	7264.32	1.0018	0.745	6200.75	1.00472
0.44	8776.07	0.9979	0.595	7188.57	1.00082	0.75	6193.04	1.00278
0.445	8638.13	1.00377	0.6	7162.58	1.00278	0.755	6217	1.00082
0.45	8582.96	1.00472	0.605	7127.16	1.00278	0.76	6161.78	1.00082
0.455	8536.18	1.00377	0.61	7045.33	1.00377	0.765	6092.52	1.0018
0.46	8449.46	1.00472	0.615	6928.46	1.01158	0.77	6088.62	1.00571
0.465	8387.56	1.0018	0.62	7003.88	1.0018	0.775	6065	1.0018
0.47	8363.18	1.00472	0.625	6950.81	1.00377	0.78	5988.29	1.00472
0.475	8252.5	1.00866	0.63	6883.88	1.00377	0.785	5996.2	1.00669
0.48	8190.27	1.00571	0.635	6913.14	1.0018	0.79	6027.47	1.00278
0.485	8246.15	1.00082	0.64	6890.63	1.00278	0.795	5968.87	1.00866
0.49	8167.06	1.00278	0.645	6820.91	1.00377	0.8	5980.16	1.00278
0.495	8049.27	1.00669	0.65	6761.89	1.00669	0.805	5986.18	1.00377
0.5	8064.99	1.0018	0.655	6794.88	1.0018	0.81	5948.59	1.00278
0.505	8033.45	1.00082	0.66	6706.71	1.00377	0.815	5869.45	1.00082
0.51	7884.44	1.00472	0.665	6641.27	1.00472	0.82	5868.46	1.00571
0.515	7825	1.00377	0.67	6665.99	1.00278	0.825	5840.44	1.00377
0.52	7836.16	1.00082	0.675	6608.24	1.00377	0.83	5778.07	1.00571
0.525	7761.4	1.0018	0.68	6549.22	1.00377	0.835	5795.59	1.00472
0.53	7721.4	0.99983	0.685	6591.06	1.00278	0.84	5808.03	0.99983
0.535	7698.3	1.0018	0.69	6546.96	1.00472	0.845	5726.95	1.00571
0.54	7658.88	1.0018	0.695	6509.22	1.00082	0.85	5717.78	1.0018
0.545	7553.93	1.00472	0.7	6489.49	1.00082	0.855	5729.56	1.0018
0.55	7536	1.00082	0.705	6476.76	1.00278	0.86	5682.21	1.0018
0.555	7509.45	1.00278	0.71	6446.06	1.00082	0.865	5605.68	1.00278
0.56	7397.26	1.00571	0.715	6350.19	1.00472	0.87	5633.29	1.00278
0.565	7342.19	1.00571	0.72	6419.73	0.99691	0.875	5624.63	1.00082
0.57	7384.85	1.00472	0.725	6383.35	0.99888	0.88	5562.33	1.00278
0.575	7351.81	1.00278	0.73	6308.25	0.99888	0.885	5547.77	1.00472

B.4. NA952

Stress Relaxation

T=150°C; strain=0.1 [strain units]; fixture diameter=25 [mm]; cone angle=0.1 [rad]

Time [s]	G(γ,t) [Pa]	γ [%]	Time [s] *cont.*	G(γ,t) [Pa] *cont.*	γ [%] *cont.*	Time [s] *cont.*	G(γ,t) [Pa] *cont.*	γ [%] *cont.*
0.001	0	0	0.145	17234.2	10.0319	0.285	11319.5	10.0319
0.01	21672.8	0.47002	0.15	16841.8	10.0319	0.29	11201.7	10.0319
0.015	62970.8	1.98602	0.155	16495.9	10.0319	0.295	11083.9	10.0319
0.02	65110.6	3.7059	0.16	16153.1	10.0398	0.3	10973.8	10.0319
0.025	60753.6	5.29466	0.165	15867.4	10.0319	0.305	10856	10.0319
0.03	55713.9	6.59392	0.17	15553.4	10.0319	0.31	10746.2	10.0319
0.035	50935	7.59623	0.175	15270.6	10.0319	0.315	10651.9	10.0319
0.04	46517.1	8.33794	0.18	15011.2	10.0319	0.32	10541.8	10.0319
0.045	42667.6	8.86866	0.185	14760.1	10.0319	0.325	10439.8	10.0319
0.05	39266.2	9.24345	0.19	14508.7	10.0319	0.33	10353.5	10.0319
0.055	36247.1	9.50905	0.195	14280.8	10.0319	0.335	10251.3	10.0319
0.06	33688.7	9.68858	0.2	14068.8	10.0319	0.34	10164.7	10.0243
0.065	31502.4	9.80564	0.205	13848.8	10.0319	0.345	10070.6	10.0319
0.07	29556.2	9.89147	0.21	13644.6	10.0319	0.35	9984.29	10.0319
0.075	27888.5	9.94607	0.215	13456.1	10.0319	0.355	9897.69	10.0319
0.08	26458.7	9.9773	0.22	13259.6	10.0319	0.36	9811.34	10.0319
0.085	25199	10.0007	0.225	13081	10.0243	0.365	9740.3	10.0243
0.09	24089.8	10.0164	0.23	12906.3	10.0319	0.37	9654.21	10.0319
0.095	23111.6	10.0243	0.235	12741.2	10.0319	0.375	9567.86	10.0319
0.1	22230	10.0319	0.24	12560.6	10.0319	0.38	9497.09	10.0319
0.105	21460.5	10.0319	0.245	12411.4	10.0319	0.385	9418.65	10.0319
0.11	20769.1	10.0319	0.25	12254.3	10.0319	0.39	9339.97	10.0319
0.115	20124.8	10.0319	0.255	12105.1	10.0319	0.395	9269.44	10.0319
0.12	19543.8	10.0319	0.26	11963.6	10.0319	0.4	9206.59	10.0319
0.125	18994.5	10.0398	0.265	11830.2	10.0319	0.405	9127.91	10.0319
0.13	18506.6	10.0319	0.27	11688.6	10.0319	0.41	9071.96	10.0243
0.135	18037.1	10.0398	0.275	11555.3	10.0319	0.415	9002.21	10.0319
0.14	17627.2	10.0319	0.28	11453.9	10.0243	0.42	8938.49	10.0243

Time [s] *cont.*	G(γ,t) [Pa] *cont.*	γ [%] *cont.*	Time [s] *cont.*	G(γ,t) [Pa] *cont.*	γ [%] *cont.*	Time [s] *cont.*	G(γ,t) [Pa] *cont.*	γ [%] *cont.*
0.425	8860.92	10.0319	0.58	7313.45	10.0319	0.735	6301.14	10.0243
0.43	8805.99	10.0319	0.585	7268.53	10.0398	0.74	6272.72	10.0319
0.435	8743.14	10.0319	0.59	7234.89	10.0319	0.745	6241.18	10.0319
0.44	8680.29	10.0319	0.595	7182.24	10.0398	0.75	6217.55	10.0319
0.445	8609.53	10.0319	0.6	7169.7	10.0243	0.755	6186.13	10.0319
0.45	8562.51	10.0319	0.605	7117.11	10.0319	0.76	6154.58	10.0319
0.455	8499.66	10.0319	0.61	7077.89	10.0319	0.765	6147.5	10.0243
0.46	8436.81	10.0319	0.615	7046.46	10.0319	0.77	6115.24	10.0319
0.465	8397.47	10.0319	0.62	7007.12	10.0319	0.775	6083.7	10.0319
0.47	8334.63	10.0319	0.625	6967.9	10.0319	0.78	6068.64	10.0243
0.475	8271.78	10.0319	0.63	6944.27	10.0319	0.785	6048.96	10.0243
0.48	8224.76	10.0319	0.635	6905.05	10.0319	0.79	6025.31	10.0243
0.485	8177.5	10.0319	0.64	6878.86	10.0243	0.795	5993.14	10.0319
0.49	8128.75	10.0243	0.645	6842.2	10.0319	0.8	5978.02	10.0243
0.495	8081.46	10.0243	0.65	6802.98	10.0319	0.805	5953.8	10.0319
0.5	8026.48	10.0243	0.655	6776.71	10.0243	0.81	5926.76	10.0243
0.505	7973.36	10.0319	0.66	6740.13	10.0319	0.815	5899.28	10.0243
0.51	7932.14	10.0243	0.665	6716.5	10.0319	0.82	5871.16	10.0319
0.515	7885.09	10.0243	0.67	6685.08	10.0319	0.825	5847.53	10.0319
0.52	7824.04	10.0319	0.675	6645.86	10.0319	0.83	5828.34	10.0243
0.525	7776.9	10.0319	0.68	6614.43	10.0319	0.835	5804.23	10.0319
0.53	7737.68	10.0319	0.685	6590.81	10.0319	0.84	5785.01	10.0243
0.535	7698.34	10.0319	0.69	6559.38	10.0319	0.845	5764.77	10.0319
0.54	7643.41	10.0319	0.695	6525.12	10.0243	0.85	5749.48	10.0243
0.545	7596.27	10.0319	0.7	6496.53	10.0319	0.855	5725.43	10.0319
0.55	7570.6	10.0243	0.705	6465.11	10.0319	0.86	5698.22	10.0243
0.555	7523.43	10.0243	0.71	6438.12	10.0319	0.865	5678.18	10.0319
0.56	7470.57	10.0319	0.715	6410.54	10.0319	0.87	5658.51	10.0319
0.565	7439.15	10.0319	0.72	6378.99	10.0319	0.875	5639.17	10.0243
0.57	7392.01	10.0319	0.725	6352.4	10.0243	0.88	5611.25	10.0319
0.575	7344.87	10.0319	0.73	6327.9	10.0319	0.885	5595.84	10.0243

B.4. NA952

Stress Relaxation

T=150°C; strain=1.0 [strain units]; fixture diameter=25 [mm]; cone angle=0.1 [rad]

Time [s]	G(γ,t) [Pa]	γ [%]	Time [s] *cont.*	G(γ,t) [Pa] *cont.*	γ [%] *cont.*	Time [s] *cont.*	G(γ,t) [Pa] *cont.*	γ [%] *cont.*
0.001	0	0	0.145	14969.7	100.549	0.285	9785.23	100.486
0.01	18229.7	3.41825	0.15	14632	100.549	0.29	9685.03	100.486
0.015	45774.2	17.2223	0.155	14340.8	100.486	0.295	9578.7	100.486
0.02	53935	34.3197	0.16	14040.3	100.486	0.3	9484.82	100.486
0.025	51082.4	50.1211	0.165	13764.8	100.486	0.305	9390.94	100.486
0.03	47791.6	63.73	0.17	13502	100.486	0.31	9290.75	100.486
0.035	44263.4	74.3215	0.175	13264.4	100.486	0.315	9203.19	100.486
0.04	40891.2	82.2961	0.18	13026.5	100.486	0.32	9115.64	100.486
0.045	37659.4	88.0887	0.185	12801.2	100.486	0.325	9027.89	100.486
0.05	34749	92.1379	0.19	12588.5	100.486	0.33	8940.34	100.486
0.055	32133	94.9417	0.195	12388.3	100.486	0.335	8859.1	100.486
0.06	29830.8	96.8739	0.2	12194.2	100.486	0.34	8777.68	100.486
0.065	27836.9	98.1194	0.205	12006.7	100.486	0.345	8702.58	100.486
0.07	26092.7	98.991	0.21	11825	100.486	0.35	8621.15	100.486
0.075	24568.9	99.5518	0.215	11649.9	100.486	0.355	8546.05	100.486
0.08	23256.3	99.9256	0.22	11487.3	100.486	0.36	8470.95	100.486
0.085	22119.8	100.113	0.225	11330.7	100.486	0.365	8402.17	100.486
0.09	21113.1	100.299	0.23	11174.4	100.486	0.37	8333.39	100.486
0.095	20235.1	100.362	0.235	11030.3	100.486	0.375	8264.61	100.486
0.1	19446.4	100.423	0.24	10886.5	100.486	0.38	8195.64	100.486
0.105	18746.1	100.486	0.245	10748.9	100.486	0.385	8133.19	100.486
0.11	18107.7	100.486	0.25	10611.2	100.486	0.39	8064.21	100.486
0.115	17544.4	100.486	0.255	10486	100.486	0.395	8001.76	100.486
0.12	17018.7	100.486	0.26	10360.8	100.486	0.4	7939.11	100.486
0.125	16532.9	100.549	0.265	10235.6	100.486	0.405	7876.65	100.486
0.13	16105.3	100.486	0.27	10116.9	100.486	0.41	7820.33	100.486
0.135	15704.8	100.486	0.275	10004.2	100.486	0.415	7764	100.486
0.14	15319.7	100.549	0.28	9897.69	100.486	0.42	7701.35	100.486

Time [s] *cont.*	G(γ,t) [Pa] *cont.*	γ [%] *cont.*	Time [s] *cont.*	G(γ,t) [Pa] *cont.*	γ [%] *cont.*	Time [s] *cont.*	G(γ,t) [Pa] *cont.*	γ [%] *cont.*
0.425	7645.03	100.486	0.58	6293.39	100.486	0.735	5411.04	100.486
0.43	7595.02	100.486	0.585	6262.16	100.486	0.74	5386.04	100.486
0.435	7538.7	100.486	0.59	6224.61	100.486	0.745	5361.04	100.486
0.44	7482.37	100.486	0.595	6193.29	100.486	0.75	5342.26	100.486
0.445	7432.37	100.486	0.6	6161.96	100.486	0.755	5317.26	100.486
0.45	7382.17	100.486	0.605	6130.73	100.486	0.76	5298.48	100.486
0.455	7325.84	100.486	0.61	6093.18	100.486	0.765	5273.39	100.486
0.46	7282.16	100.486	0.615	6068.08	100.486	0.77	5254.61	100.486
0.465	7231.97	100.486	0.62	6036.86	100.486	0.775	5229.61	100.486
0.47	7181.96	100.486	0.625	6005.53	100.486	0.78	5204.61	100.486
0.475	7131.96	100.486	0.63	5974.3	100.486	0.785	5185.83	100.486
0.48	7088.09	100.486	0.635	5942.98	100.486	0.79	5167.06	100.486
0.485	7044.4	100.486	0.64	5911.65	100.486	0.795	5142.06	100.486
0.49	6994.21	100.486	0.645	5886.65	100.486	0.8	5120.6	100.486
0.495	6950.53	100.486	0.65	5855.33	100.486	0.805	5101.73	100.486
0.5	6912.98	100.486	0.655	5830.33	100.486	0.81	5079.79	100.486
0.505	6869.1	100.486	0.66	5799.1	100.486	0.815	5061.01	100.486
0.51	6825.23	100.486	0.665	5774	100.486	0.82	5042.14	100.486
0.515	6781.55	100.486	0.67	5742.77	100.486	0.825	5020.21	100.486
0.52	6744	100.486	0.675	5717.67	100.486	0.83	5001.34	100.486
0.525	6700.13	100.486	0.68	5686.45	100.486	0.835	4982.56	100.486
0.53	6662.57	100.486	0.685	5661.35	100.486	0.84	4960.62	100.486
0.535	6625.02	100.486	0.69	5636.35	100.486	0.845	4941.75	100.486
0.54	6581.34	100.486	0.695	5611.34	100.486	0.85	4922.98	100.486
0.545	6543.79	100.486	0.7	5586.34	100.486	0.855	4904.11	100.486
0.55	6512.37	100.486	0.705	5561.24	100.486	0.86	4885.33	100.486
0.555	6474.82	100.486	0.71	5536.24	100.486	0.865	4866.46	100.486
0.56	6437.27	100.486	0.715	5511.24	100.486	0.87	4850.85	100.486
0.565	6399.72	100.486	0.72	5486.14	100.486	0.875	4831.97	100.486
0.57	6362.17	100.486	0.725	5461.14	100.486	0.88	4813.2	100.486
0.575	6330.94	100.486	0.73	5436.14	100.486	0.885	4797.49	100.486

B.4. NA952

Stress Relaxation

T=150°C; strain=1.0 [strain units]; fixture diameter=10 [mm]; cone angle=0.035 [rad]

Time [s]	G(γ,t) [Pa]	γ [%]	Time [s] *cont.*	G(γ,t) [Pa] *cont.*	γ [%] *cont.*	Time [s] *cont.*	G(γ,t) [Pa] *cont.*	γ [%] *cont.*
0.001	0	0	0.145	15061.4	100.199	0.285	9861.07	100.199
0.01	20845.5	4.92515	0.15	14727.9	100.199	0.29	9758.33	100.199
0.015	58090.1	20.953	0.155	14423.6	100.199	0.295	9645.23	100.199
0.02	59319.7	37.9203	0.16	14129.2	100.199	0.3	9533.48	100.289
0.025	53665.4	53.3106	0.165	13844.7	100.199	0.305	9453.42	100.199
0.03	49573.5	66.1594	0.17	13599.6	100.199	0.31	9355.04	100.199
0.035	45160.5	76.1076	0.175	13354.2	100.199	0.315	9251.85	100.199
0.04	41250.1	83.5136	0.18	13109.1	100.199	0.32	9168.18	100.199
0.045	37740.8	88.7779	0.185	12883.1	100.199	0.325	9079.57	100.199
0.05	34694.6	92.436	0.19	12677.1	100.199	0.33	8991.1	100.199
0.055	32032	95.0245	0.195	12461.4	100.199	0.335	8907.43	100.199
0.06	29695.5	96.8065	0.2	12265.2	100.199	0.34	8833.68	100.199
0.065	27698.1	97.9673	0.205	12088.6	100.199	0.345	8750.17	100.199
0.07	25999.5	98.7711	0.21	11911.9	100.199	0.35	8671.46	100.199
0.075	24534.8	99.218	0.215	11725.4	100.199	0.355	8602.52	100.199
0.08	23242	99.5749	0.22	11568.6	100.199	0.36	8533.73	100.199
0.085	22116.8	99.842	0.225	11411.5	100.199	0.365	8455.02	100.199
0.09	21114	100.019	0.23	11244.7	100.199	0.37	8391.04	100.199
0.095	20250.7	100.109	0.235	11097.5	100.199	0.375	8327.05	100.199
0.1	19504.2	100.109	0.24	10960.3	100.199	0.38	8248.49	100.199
0.105	18826.4	100.109	0.245	10803.4	100.289	0.385	8179.55	100.199
0.11	18181.7	100.199	0.25	10675.5	100.199	0.39	8120.52	100.199
0.115	17612.4	100.199	0.255	10557.7	100.199	0.395	8046.77	100.199
0.12	17102.3	100.199	0.26	10430.3	100.199	0.4	7973.02	100.199
0.125	16631.3	100.199	0.265	10293.4	100.289	0.405	7913.99	100.199
0.13	16189.7	100.199	0.27	10194.8	100.199	0.41	7854.96	100.199
0.135	15787.5	100.199	0.275	10077.1	100.199	0.415	7786.17	100.199
0.14	15414.7	100.199	0.28	9969.21	100.199	0.42	7736.9	100.199

Time [s] *cont.*	G(γ,t) [Pa] *cont.*	γ [%] *cont.*	Time [s] *cont.*	G(γ,t) [Pa] *cont.*	γ [%] *cont.*	Time [s] *cont.*	G(γ,t) [Pa] *cont.*	γ [%] *cont.*
0.425	7687.79	100.199	0.58	6315.54	100.199	0.735	5430.24	100.199
0.43	7628.76	100.199	0.585	6281.14	100.199	0.74	5415.37	100.199
0.435	7574.54	100.199	0.59	6256.51	100.199	0.745	5395.7	100.199
0.44	7530.38	100.199	0.595	6222.11	100.199	0.75	5366.26	100.199
0.445	7471.35	100.199	0.6	6177.8	100.199	0.755	5351.54	100.199
0.45	7412.32	100.199	0.605	6147.65	100.289	0.76	5331.86	100.199
0.455	7372.96	100.199	0.61	6118.77	100.199	0.765	5297.31	100.199
0.46	7323.7	100.199	0.615	6079.42	100.199	0.77	5277.79	100.199
0.465	7269.62	100.199	0.62	6049.83	100.199	0.775	5262.92	100.199
0.47	7225.46	100.199	0.625	6025.35	100.199	0.78	5238.44	100.199
0.475	7181.15	100.199	0.63	5990.95	100.199	0.785	5213.8	100.199
0.48	7127.08	100.199	0.635	5956.02	100.289	0.79	5194.13	100.199
0.485	7077.82	100.199	0.64	5946.64	100.199	0.795	5179.41	100.199
0.49	7038.46	100.199	0.645	5912.24	100.199	0.8	5149.82	100.199
0.495	6984.39	100.199	0.65	5877.7	100.199	0.805	5135.1	100.199
0.5	6935.27	100.199	0.655	5858.02	100.199	0.81	5110.83	100.289
0.505	6895.92	100.199	0.66	5828.58	100.199	0.815	5085.83	100.199
0.51	6851.61	100.199	0.665	5789.23	100.199	0.82	5066.15	100.199
0.515	6807.3	100.199	0.67	5764.59	100.199	0.825	5046.48	100.199
0.52	6767.95	100.199	0.675	5740.11	100.199	0.83	5021.99	100.199
0.525	6733.55	100.199	0.68	5705.56	100.199	0.835	4992.4	100.199
0.53	6689.24	100.199	0.685	5676.13	100.199	0.84	4977.68	100.199
0.535	6649.89	100.199	0.69	5656.45	100.199	0.845	4958.01	100.199
0.54	6615.49	100.199	0.695	5631.82	100.199	0.85	4933.37	100.199
0.545	6576.14	100.199	0.7	5597.42	100.199	0.855	4914.24	100.289
0.55	6536.79	100.199	0.705	5582.7	100.199	0.86	4908.82	100.199
0.555	6502.39	100.199	0.71	5558.07	100.199	0.865	4884.26	100.199
0.56	6467.99	100.199	0.715	5523.67	100.199	0.87	4864.58	100.199
0.565	6423.68	100.199	0.72	5499.04	100.199	0.875	4859.62	100.199
0.57	6389.29	100.199	0.725	5489.27	100.199	0.88	4830.73	100.289
0.575	6359.7	100.199	0.73	5459.68	100.199	0.885	4805.55	100.199

B.4. NA952

Stress Relaxation

T=150°C; strain=5.0 [strain units]; fixture diameter=10 [mm]; cone angle=0.035 [rad]

Time [s]	G(γ,t) [Pa]	γ [%]	Time [s] *cont.*	G(γ,t) [Pa] *cont.*	γ [%] *cont.*	Time [s] *cont.*	G(γ,t) [Pa] *cont.*	γ [%] *cont.*
0.001	0	0	0.145	5857.76	501.232	0.285	3828.69	501.232
0.01	18454.8	11.3542	0.15	5729.93	501.232	0.29	3786.91	501.232
0.015	42260.5	66.5613	0.155	5607.2	501.232	0.295	3747.6	501.232
0.02	38739.4	150.163	0.16	5489.28	501.232	0.3	3708.29	501.232
0.025	31564.4	230.327	0.165	5381.1	501.232	0.305	3673.93	501.232
0.03	26739.9	301.166	0.17	5278.03	501.232	0.31	3634.62	501.232
0.035	23024.3	357.417	0.175	5179.75	501.232	0.315	3600.27	501.232
0.04	19966.2	400.131	0.18	5091.23	501.232	0.32	3565.83	501.232
0.045	17557.9	431.455	0.185	5007.82	501.232	0.325	3529	501.232
0.05	15583.5	453.886	0.19	4919.29	501.232	0.33	3497.04	501.232
0.055	13983.1	469.199	0.195	4840.75	501.232	0.335	3465.16	501.232
0.06	12676.4	479.88	0.2	4767.08	501.232	0.34	3433.2	501.232
0.065	11601.1	486.997	0.205	4693.34	501.232	0.345	3401.24	501.232
0.07	10712.9	491.978	0.21	4619.68	501.232	0.35	3374.24	501.232
0.075	9967.17	495.183	0.215	4555.76	501.232	0.355	3344.76	501.232
0.08	9350.04	497.319	0.22	4491.92	501.232	0.36	3312.8	501.232
0.085	8839.41	498.747	0.225	4428.08	501.232	0.365	3285.79	501.232
0.09	8393.09	499.455	0.23	4369.12	501.232	0.37	3258.79	501.232
0.095	8006.97	500.163	0.235	4310.15	501.232	0.375	3231.78	501.232
0.1	7676.53	500.523	0.24	4256.14	501.232	0.38	3204.77	501.232
0.105	7380.95	500.883	0.245	4202.05	501.232	0.385	3180.17	501.232
0.11	7125.26	500.883	0.25	4152.92	501.232	0.39	3155.64	501.232
0.115	6889.24	500.883	0.255	4098.91	501.232	0.395	3131.03	501.232
0.12	6673.2	501.232	0.26	4049.77	501.232	0.4	3106.5	501.232
0.125	6486.56	501.232	0.265	4000.63	501.232	0.405	3084.37	501.232
0.13	6309.67	501.232	0.27	3956.45	501.232	0.41	3062.24	501.232
0.135	6147.63	501.232	0.275	3912.19	501.232	0.415	3037.71	501.232
0.14	6000.14	501.232	0.28	3868	501.232	0.42	3018.06	501.232

Time [s] *cont.*	G(γ,t) [Pa] *cont.*	γ [%] *cont.*	Time [s] *cont.*	G(γ,t) [Pa] *cont.*	γ [%] *cont.*	Time [s] *cont.*	G(γ,t) [Pa] *cont.*	γ [%] *cont.*
0.425	2991.05	501.232	0.58	2460.45	501.232	0.735	2119.01	501.232
0.43	2971.4	501.232	0.585	2448.15	501.232	0.74	2111.62	501.232
0.435	2951.74	501.232	0.59	2433.41	501.232	0.745	2099.36	501.232
0.44	2927.13	501.232	0.595	2421.14	501.232	0.75	2091.97	501.232
0.445	2907.48	501.232	0.6	2411.32	501.232	0.755	2082.14	501.232
0.45	2887.83	501.232	0.605	2399.01	501.232	0.76	2072.31	501.232
0.455	2868.25	501.232	0.61	2386.75	501.232	0.765	2062.49	501.232
0.46	2848.59	501.232	0.615	2374.48	501.232	0.77	2057.57	501.232
0.465	2828.94	501.232	0.62	2364.65	501.232	0.775	2047.74	501.232
0.47	2811.68	501.232	0.625	2349.91	501.232	0.78	2037.92	501.232
0.475	2792.03	501.232	0.63	2337.61	501.232	0.785	2030.57	501.232
0.48	2769.97	501.232	0.635	2325.35	501.232	0.79	2023.18	501.232
0.485	2755.2	501.232	0.64	2315.52	501.232	0.795	2013.35	501.232
0.49	2738.02	501.232	0.645	2300.78	501.232	0.8	2007.35	501.232
0.495	2718.36	501.232	0.65	2290.95	501.232	0.805	2001.2	501.232
0.5	2703.66	501.232	0.655	2278.65	501.232	0.81	1990.09	501.232
0.505	2686.4	501.232	0.66	2268.82	501.232	0.815	1983.94	501.232
0.51	2666.75	501.232	0.665	2256.55	501.232	0.82	1976.55	501.232
0.515	2654.52	501.232	0.67	2249.2	501.232	0.825	1969.16	501.232
0.52	2637.27	501.232	0.675	2236.9	501.232	0.83	1960.57	501.232
0.525	2620.09	501.232	0.68	2227.07	501.232	0.835	1954.39	501.232
0.53	2605.39	501.232	0.685	2219.72	501.232	0.84	1948.23	501.232
0.535	2593.08	501.232	0.69	2207.42	501.232	0.845	1938.41	501.232
0.54	2575.9	501.232	0.695	2195.15	501.232	0.85	1931.02	501.232
0.545	2561.13	501.232	0.7	2185.33	501.232	0.855	1924.87	501.232
0.55	2546.42	501.232	0.705	2175.5	501.232	0.86	1915	501.232
0.555	2534.12	501.232	0.71	2165.67	501.232	0.865	1907.61	501.232
0.56	2516.94	501.232	0.715	2155.84	501.232	0.87	1902.7	501.232
0.565	2502.24	501.232	0.72	2148.45	501.232	0.875	1892.83	501.232
0.57	2489.93	501.232	0.725	2138.63	501.232	0.88	1885.44	501.232
0.575	2475.16	501.232	0.73	2128.84	501.232	0.885	1878.05	501.232

B.4. NA952

Stress Relaxation

T=150°C; strain=7.5 [strain units]; fixture diameter=10 [mm]; cone angle=0.035 [rad]

Time [s]	G(γ,t) [Pa]	γ [%]	Time [s] *cont.*	G(γ,t) [Pa] *cont.*	γ [%] *cont.*	Time [s] *cont.*	G(γ,t) [Pa] *cont.*	γ [%] *cont.*
0.001	0	0	0.145	4614.44	751.15	0.285	2936.47	751.847
0.01	18954	12.4554	0.15	4498.83	751.847	0.29	2906.41	751.15
0.015	39670.3	76.5095	0.155	4400.51	751.847	0.295	2870.96	751.847
0.02	36968.7	190.278	0.16	4302.29	751.847	0.3	2841.5	751.847
0.025	30668	312.561	0.165	4210.57	751.847	0.305	2812.04	751.847
0.03	25312.1	422.561	0.17	4128.65	751.847	0.31	2781.87	751.15
0.035	21405.8	512.981	0.175	4046.83	751.847	0.315	2753.08	751.847
0.04	18269.8	582.758	0.18	3971.51	751.847	0.32	2723.57	751.847
0.045	15785.5	634.016	0.185	3899.4	751.847	0.325	2697.37	751.847
0.05	13786.9	671.041	0.19	3830.68	751.847	0.33	2667.91	751.847
0.055	12187.6	697.025	0.195	3761.86	751.847	0.335	2647.46	751.15
0.06	10890.9	715.531	0.2	3699.65	751.847	0.34	2621.23	751.15
0.065	9849.89	727.651	0.205	3640.64	751.847	0.345	2595	751.15
0.07	9001.73	735.477	0.21	3581.72	751.847	0.35	2571.29	751.847
0.075	8301.32	741.166	0.215	3526.01	751.847	0.355	2548.38	751.847
0.08	7719.22	744.741	0.22	3476.9	751.847	0.36	2523.78	751.847
0.085	7242.23	746.877	0.225	3424.49	751.847	0.365	2500.87	751.847
0.09	6827	749.014	0.23	3375.37	751.847	0.37	2481.22	751.847
0.095	6485.62	749.711	0.235	3329.56	751.847	0.375	2460.6	751.15
0.1	6184.07	750.431	0.24	3283.65	751.847	0.38	2439.27	751.15
0.105	5928.13	750.431	0.245	3241.09	751.847	0.385	2417.35	751.847
0.11	5692.99	751.15	0.25	3198.48	751.847	0.39	2397.7	751.847
0.115	5496.26	751.15	0.255	3159.22	751.847	0.395	2376.39	751.847
0.12	5312.75	751.15	0.26	3116.62	751.847	0.4	2356.74	751.847
0.125	5148.76	751.15	0.265	3077.31	751.847	0.405	2340.39	751.847
0.13	4993.35	751.847	0.27	3041.3	751.847	0.41	2320.73	751.847
0.135	4855.82	751.847	0.275	3005.29	751.847	0.415	2304.87	751.15
0.14	4728.09	751.847	0.28	2969.23	751.847	0.42	2284.72	751.847

Time [s] *cont.*	G(γ,t) [Pa] *cont.*	γ [%] *cont.*	Time [s] *cont.*	G(γ,t) [Pa] *cont.*	γ [%] *cont.*	Time [s] *cont.*	G(γ,t) [Pa] *cont.*	γ [%] *cont.*
0.425	2268.32	751.847	0.58	1850.79	751.15	0.735	1582.16	751.847
0.43	2248.66	751.847	0.585	1840.98	751.15	0.74	1575.45	751.15
0.435	2232.31	751.847	0.59	1832.77	751.15	0.745	1567.43	751.847
0.44	2217.96	751.15	0.595	1817.97	751.847	0.75	1559.23	751.847
0.445	2201.6	751.15	0.6	1809.84	751.15	0.755	1554.33	751.847
0.45	2184.8	751.847	0.605	1799.96	751.847	0.76	1546.13	751.847
0.455	2170.1	751.847	0.61	1790.16	751.847	0.765	1537.95	751.847
0.46	2153.69	751.847	0.615	1780.31	751.847	0.77	1533.02	751.847
0.465	2137.34	751.847	0.62	1770.5	751.847	0.775	1527.89	751.15
0.47	2122.59	751.847	0.625	1760.65	751.847	0.78	1518.3	751.847
0.475	2107.83	751.847	0.63	1750.85	751.847	0.785	1513.37	751.847
0.48	2093.08	751.847	0.635	1742.65	751.847	0.79	1506.82	751.847
0.485	2080.03	751.847	0.64	1732.85	751.847	0.795	1500.29	751.847
0.49	2066.92	751.847	0.645	1724.59	751.15	0.8	1492.09	751.847
0.495	2053.82	751.847	0.65	1713.19	751.847	0.805	1485.54	751.847
0.5	2042.32	751.847	0.655	1708.24	751.847	0.81	1480.64	751.847
0.505	2029.21	751.847	0.66	1698.44	751.847	0.815	1474.09	751.847
0.51	2017.76	751.847	0.665	1690.24	751.847	0.82	1469.16	751.847
0.515	2001.41	751.847	0.67	1683.68	751.847	0.825	1462.61	751.847
0.52	1989.95	751.847	0.675	1675.48	751.847	0.83	1457.71	751.847
0.525	1976.85	751.847	0.68	1665.68	751.847	0.835	1451.16	751.847
0.53	1963.75	751.847	0.685	1657.48	751.847	0.84	1446.23	751.847
0.535	1954.06	751.15	0.69	1650.93	751.847	0.845	1439.68	751.847
0.54	1942.6	751.15	0.695	1641.12	751.847	0.85	1433.13	751.847
0.545	1927.69	751.847	0.7	1632.92	751.847	0.855	1428.23	751.847
0.55	1914.59	751.847	0.705	1626.37	751.847	0.86	1421.67	751.847
0.555	1904.79	751.847	0.71	1618.19	751.847	0.865	1415.12	751.847
0.56	1893.33	751.847	0.715	1609.99	751.847	0.87	1410.22	751.847
0.565	1881.83	751.847	0.72	1605.09	751.847	0.875	1406.95	751.847
0.57	1872.03	751.847	0.725	1595.26	751.847	0.88	1400.39	751.847
0.575	1862.3	751.15	0.73	1588.71	751.847	0.885	1393.84	751.847

B.4. NA952

Stress Relaxation

T=150°C; strain=10.0 [strain units]; fixture diameter=10 [mm]; cone angle=0.035 [rad]

Time [s]	G(γ,t) [Pa]	γ [%]	Time [s] *cont.*	G(γ,t) [Pa] *cont.*	γ [%] *cont.*	Time [s] *cont.*	G(γ,t) [Pa] *cont.*	γ [%] *cont.*
0.001	0	0	0.145	3695.32	1001.77	0.285	2360.5	1001.77
0.01	18968.5	12.2207	0.15	3606.81	1001.77	0.29	2333.48	1001.77
0.015	39214.2	79.4537	0.155	3525.66	1001.77	0.295	2306.42	1001.77
0.02	35393.3	211.46	0.16	3446.99	1001.77	0.3	2284.31	1001.77
0.025	28971.3	370.943	0.165	3375.74	1001.77	0.305	2259.72	1001.77
0.03	23547.8	521.886	0.17	3306.91	1001.77	0.31	2235.14	1001.77
0.035	19430.3	649.678	0.175	3243.02	1001.77	0.315	2213.03	1001.77
0.04	16310.9	750.431	0.18	3181.54	1001.77	0.32	2190.88	1001.77
0.045	13856.8	825.896	0.185	3125.01	1001.77	0.325	2171.22	1001.77
0.05	11945.7	880.719	0.19	3068.48	1001.77	0.33	2149.11	1001.77
0.055	10422.6	919.869	0.195	3016.84	1001.77	0.335	2129.44	1001.77
0.06	9211.6	946.943	0.2	2967.67	1001.77	0.34	2109.77	1001.77
0.065	8237.77	964.73	0.205	2920.97	1001.77	0.345	2090.1	1001.77
0.07	7454.63	977.548	0.21	2874.28	1001.77	0.35	2070.43	1001.77
0.075	6820.65	986.093	0.215	2829.99	1001.77	0.355	2053.24	1001.77
0.08	6304.73	991.782	0.22	2788.25	1001.77	0.36	2033.58	1001.77
0.085	5881.36	995.357	0.225	2748.91	1001.77	0.365	2016.35	1001.77
0.09	5532.97	997.493	0.23	2709.58	1001.77	0.37	2001.63	1001.77
0.095	5234.22	998.91	0.235	2672.72	1001.77	0.375	1983.17	1001.77
0.1	4985.64	1000.33	0.24	2633.38	1001.77	0.38	1965.98	1001.77
0.105	4768.98	1000.33	0.245	2598.92	1001.77	0.385	1951.22	1001.77
0.11	4578.57	1001.05	0.25	2567.02	1001.77	0.39	1934.03	1001.77
0.115	4411.34	1001.05	0.255	2535.04	1001.77	0.395	1918.04	1001.77
0.12	4260.66	1001.77	0.26	2503.06	1001.77	0.4	1903.29	1001.77
0.125	4122.99	1001.77	0.265	2471.16	1001.77	0.405	1888.54	1001.77
0.13	4002.58	1001.77	0.27	2444.09	1001.77	0.41	1873.79	1001.77
0.135	3891.92	1001.77	0.275	2414.59	1001.77	0.415	1860.28	1001.77
0.14	3788.7	1001.77	0.28	2387.57	1001.77	0.42	1844.29	1001.77

Time [s] *cont.*	G(γ,t) [Pa] *cont.*	γ [%] *cont.*	Time [s] *cont.*	G(γ,t) [Pa] *cont.*	γ [%] *cont.*	Time [s] *cont.*	G(γ,t) [Pa] *cont.*	γ [%] *cont.*
0.425	1829.54	1001.77	0.58	1497.69	1001.77	0.735	1286.3	1001.77
0.43	1817.26	1001.77	0.585	1490.33	1001.77	0.74	1278.9	1001.77
0.435	1804.95	1001.77	0.59	1481.7	1001.77	0.745	1272.78	1001.77
0.44	1790.2	1001.77	0.595	1474.35	1001.77	0.75	1267.87	1001.77
0.445	1777.93	1001.77	0.6	1465.75	1001.77	0.755	1262.95	1001.77
0.45	1765.62	1001.77	0.605	1458.36	1001.77	0.76	1256.79	1001.77
0.455	1752.1	1001.77	0.61	1449.76	1001.77	0.765	1251.88	1001.77
0.46	1739.83	1001.77	0.615	1443.6	1001.77	0.77	1246.96	1001.77
0.465	1727.52	1001.77	0.62	1436.25	1001.77	0.775	1240.8	1001.77
0.47	1716.48	1001.77	0.625	1427.65	1001.77	0.78	1234.69	1001.77
0.475	1704.17	1001.77	0.63	1420.26	1001.77	0.785	1230.97	1001.77
0.48	1693.14	1001.77	0.635	1414.1	1001.77	0.79	1224.83	1001.77
0.485	1683.3	1001.77	0.64	1406.75	1001.77	0.795	1219.92	1001.77
0.49	1670.99	1001.77	0.645	1398.15	1001.77	0.8	1215	1001.77
0.495	1661.16	1001.77	0.65	1391.99	1001.77	0.805	1210.08	1001.77
0.5	1650.08	1001.77	0.655	1385.84	1001.77	0.81	1205.16	1001.77
0.505	1639.05	1001.77	0.66	1377.24	1001.77	0.815	1199.03	1001.77
0.51	1627.98	1001.77	0.665	1371.09	1001.77	0.82	1196.57	1001.77
0.515	1619.38	1001.77	0.67	1364.97	1001.77	0.825	1190.43	1001.77
0.52	1609.55	1001.77	0.675	1357.57	1001.77	0.83	1185.51	1001.77
0.525	1597.23	1001.77	0.68	1351.42	1001.77	0.835	1181.82	1001.77
0.53	1588.64	1001.77	0.685	1346.5	1001.77	0.84	1176.9	1001.77
0.535	1580.04	1001.77	0.69	1339.14	1001.77	0.845	1170.76	1001.77
0.54	1570.21	1001.77	0.695	1331.75	1001.77	0.85	1167.07	1001.77
0.545	1560.37	1001.77	0.7	1326.83	1001.77	0.855	1163.39	1001.77
0.55	1551.78	1001.77	0.705	1320.72	1001.77	0.86	1158.47	1001.77
0.555	1541.95	1001.77	0.71	1313.32	1001.77	0.865	1154.77	1001.77
0.56	1533.35	1001.77	0.715	1308.4	1001.77	0.87	1151.1	1001.77
0.565	1524.72	1001.77	0.72	1302.29	1001.77	0.875	1146.18	1001.77
0.57	1516.12	1001.77	0.725	1296.13	1001.77	0.88	1141.26	1001.77
0.575	1506.29	1001.77	0.73	1289.97	1001.77	0.885	1137.56	1001.77

B.4. NA952

Stress Relaxation

T=150°C; strain=12.5 [strain units]; fixture diameter=10 [mm]; cone angle=0.035 [rad]

Time [s]	G(γ,t) [Pa]	γ [%]	Time [s] *cont.*	G(γ,t) [Pa] *cont.*	γ [%] *cont.*	Time [s] *cont.*	G(γ,t) [Pa] *cont.*	γ [%] *cont.*
0.001	0	0	0.145	2575.63	1251.66	0.285	1597.86	1251.66
0.01	19094.5	12.6679	0.15	2510.74	1251.66	0.29	1580.14	1251.66
0.015	37578.2	82.7098	0.155	2451.68	1251.66	0.295	1560.46	1251.66
0.02	33137.3	226.589	0.16	2394.67	1251.66	0.3	1543.76	1251.66
0.025	26500.3	413.308	0.165	2341.49	1251.66	0.305	1526.03	1251.66
0.03	21236.7	604.12	0.17	2292.35	1251.66	0.31	1508.34	1251.66
0.035	17113.3	770.354	0.175	2243.14	1251.66	0.315	1491.61	1251.66
0.04	14003.4	904.937	0.18	2197.9	1251.66	0.32	1475.86	1251.66
0.045	11670.1	1006.74	0.185	2154.64	1251.66	0.325	1461.11	1251.66
0.05	9830.38	1082.2	0.19	2115.28	1251.66	0.33	1445.37	1251.66
0.055	8393.79	1136.33	0.195	2075.93	1251.66	0.335	1431.61	1251.66
0.06	7283.24	1173.34	0.2	2038.56	1251.66	0.34	1418.82	1251.66
0.065	6394.23	1199.69	0.205	2005.09	1251.66	0.345	1404.07	1251.66
0.07	5701.34	1216.78	0.21	1971.63	1251.66	0.35	1390.28	1251.66
0.075	5140.22	1228.88	0.215	1938.19	1251.66	0.355	1377.51	1251.66
0.08	4693.47	1236.71	0.22	1908.69	1251.66	0.36	1363.72	1251.66
0.085	4329.63	1241.7	0.225	1879.19	1251.66	0.365	1349.96	1251.66
0.09	4032.47	1245.25	0.23	1851.65	1251.66	0.37	1339.15	1251.66
0.095	3788.7	1247.39	0.235	1824.1	1251.66	0.375	1327.34	1251.66
0.1	3579.29	1248.81	0.24	1798.53	1251.66	0.38	1314.54	1251.66
0.105	3405.79	1250.25	0.245	1772.94	1251.66	0.385	1303.73	1251.66
0.11	3254.26	1250.94	0.25	1747.37	1251.66	0.39	1292.92	1251.66
0.115	3124.35	1250.94	0.255	1725.71	1251.66	0.395	1281.11	1251.66
0.12	3008.21	1250.94	0.26	1702.13	1251.66	0.4	1270.26	1251.66
0.125	2904.22	1251.66	0.265	1678.52	1251.66	0.405	1260.44	1251.66
0.13	2811.75	1251.66	0.27	1658.84	1251.66	0.41	1248.63	1251.66
0.135	2727.1	1251.66	0.275	1637.18	1251.66	0.415	1238.81	1251.66
0.14	2648.45	1251.66	0.28	1617.51	1251.66	0.42	1228.96	1251.66

Time [s] *cont.*	G(γ,t) [Pa] *cont.*	γ [%] *cont.*	Time [s] *cont.*	G(γ,t) [Pa] *cont.*	γ [%] *cont.*	Time [s] *cont.*	G(γ,t) [Pa] *cont.*	γ [%] *cont.*
0.425	1219.13	1251.66	0.58	985.987	1251.66	0.735	837.45	1251.66
0.43	1209.28	1251.66	0.585	981.076	1251.66	0.74	833.515	1251.66
0.435	1200.45	1251.66	0.59	977.14	1251.66	0.745	829.579	1251.66
0.44	1190.6	1251.66	0.595	971.237	1251.66	0.75	824.668	1251.66
0.445	1180.77	1251.66	0.6	964.343	1251.66	0.755	822.7	1251.66
0.45	1171.91	1251.66	0.605	958.44	1251.66	0.76	817.773	1251.66
0.455	1164.04	1251.66	0.61	951.56	1251.66	0.765	814.829	1251.66
0.46	1155.18	1251.66	0.615	945.657	1251.66	0.77	810.894	1251.66
0.465	1146.35	1251.66	0.62	940.746	1251.66	0.775	808.926	1251.66
0.47	1138.47	1251.66	0.625	936.81	1251.66	0.78	804.54	1251.66
0.475	1130.6	1251.66	0.63	930.907	1251.66	0.785	801.101	1251.66
0.48	1121.74	1251.66	0.635	926.972	1251.66	0.79	797.646	1251.66
0.485	1113.87	1251.66	0.64	924.013	1251.66	0.795	794.191	1251.66
0.49	1106	1251.66	0.645	917.133	1251.66	0.8	789.76	1251.66
0.495	1098.13	1251.66	0.65	911.23	1251.66	0.805	787.282	1251.66
0.5	1090.26	1251.66	0.655	907.295	1251.66	0.81	783.346	1251.66
0.505	1085.33	1251.66	0.66	901.392	1251.66	0.815	779.396	1251.66
0.51	1077.46	1251.66	0.665	895.489	1251.66	0.82	776.933	1251.66
0.515	1070.58	1251.66	0.67	891.554	1251.66	0.825	773.478	1251.66
0.52	1063.7	1251.66	0.675	887.618	1251.66	0.83	769.047	1251.66
0.525	1055.83	1251.66	0.68	883.683	1251.66	0.835	766.088	1251.66
0.53	1048.95	1251.66	0.685	879.748	1251.66	0.84	763.129	1251.66
0.535	1043.03	1251.66	0.69	875.812	1251.66	0.845	759.674	1251.66
0.54	1037.15	1251.66	0.695	870.901	1251.66	0.85	756.219	1251.66
0.545	1030.27	1251.66	0.7	865.974	1251.66	0.855	754.747	1251.66
0.55	1024.35	1251.66	0.705	862.039	1251.66	0.86	751.788	1251.66
0.555	1018.46	1251.66	0.71	858.103	1251.66	0.865	747.838	1251.66
0.56	1010.59	1251.66	0.715	853.191	1251.66	0.87	745.375	1251.66
0.565	1002.72	1251.66	0.72	850.247	1251.66	0.875	741.92	1251.66
0.57	996.802	1251.66	0.725	845.321	1251.66	0.88	737.489	1251.66
0.575	990.914	1251.66	0.73	841.385	1251.66	0.885	734.53	1251.66

B.5. Affinity PL1880

Stress Relaxation

T=150°C; strain=0.01 [strain units]; fixture diameter=25 [mm]; cone angle=0.1 [rad]

Time [s]	G(γ,t) [Pa]	γ [%]	Time [s] *cont.*	G(γ,t) [Pa] *cont.*	γ [%] *cont.*	Time [s] *cont.*	G(γ,t) [Pa] *cont.*	γ [%] *cont.*
0.001	0	0	0.145	25236.7	1.02821	0.285	13623.6	1.02725
0.01	51950.6	0.05829	0.15	24262.8	1.03309	0.29	13642.2	1.02529
0.015	172534	0.17298	0.155	23717	1.02627	0.295	13268.5	1.02919
0.02	196629	0.32315	0.16	22957.7	1.02725	0.3	12939.1	1.02919
0.025	188552	0.48182	0.165	22263.4	1.02529	0.305	12877.8	1.02919
0.03	171862	0.62564	0.17	21611.7	1.02919	0.31	12742.2	1.02529
0.035	154279	0.74303	0.175	21089.5	1.02627	0.315	12352.2	1.03214
0.04	136923	0.83352	0.18	20560.1	1.0243	0.32	12234.7	1.02529
0.045	120502	0.89907	0.185	19987.1	1.02529	0.325	12212.1	1.02332
0.05	105961	0.94407	0.19	19628.3	1.02233	0.33	12100	1.02627
0.055	92867.8	0.98028	0.195	18996.6	1.02725	0.335	11850.5	1.02725
0.06	82054.1	0.99983	0.2	18529.5	1.03017	0.34	11754.4	1.02627
0.065	72703.4	1.01158	0.205	18219.3	1.03214	0.345	11670.9	1.02821
0.07	64798.7	1.02138	0.21	17908.7	1.02627	0.35	11443.8	1.02725
0.075	58342.7	1.0243	0.215	17459.2	1.02919	0.355	11269	1.02919
0.08	52933.7	1.02529	0.22	17232.5	1.02627	0.36	11147.4	1.02627
0.085	48151.6	1.03017	0.225	16832	1.02725	0.365	11027.2	1.02529
0.09	44354.6	1.03017	0.23	16510.3	1.02627	0.37	10850.3	1.02821
0.095	41140	1.03017	0.235	16218.4	1.02627	0.375	10735.1	1.02529
0.1	38499.6	1.02627	0.24	15972.1	1.0243	0.38	10587.2	1.02919
0.105	36149	1.03017	0.245	15575.3	1.03017	0.385	10509.6	1.02627
0.11	34067.7	1.03017	0.25	15274.1	1.02725	0.39	10522	1.0243
0.115	32291.2	1.03116	0.255	15104.3	1.02627	0.395	10295.9	1.02919
0.12	31030	1.0243	0.26	14906.4	1.02138	0.4	10175.5	1.02821
0.125	29589.8	1.02725	0.265	14500.7	1.02821	0.405	10173.7	1.02529
0.13	28277.6	1.02919	0.27	14281.5	1.03017	0.41	10046.7	1.02332
0.135	27158.8	1.02919	0.275	14148	1.02821	0.415	9803.84	1.03017
0.14	26252.5	1.02627	0.28	13827.9	1.02919	0.42	9785.77	1.02725

Time [s] *cont.*	G(γ,t) [Pa] *cont.*	γ [%] *cont.*	Time [s] *cont.*	G(γ,t) [Pa] *cont.*	γ [%] *cont.*	Time [s] *cont.*	G(γ,t) [Pa] *cont.*	γ [%] *cont.*
0.425	9753.97	1.02332	0.58	7587.31	1.02919	0.735	6299.5	1.02627
0.43	9607.84	1.02821	0.585	7517.64	1.02821	0.74	6270.38	1.02725
0.435	9497.63	1.03017	0.59	7687.87	1.02138	0.745	6220.64	1.02529
0.44	9558.41	1.02529	0.595	7661.67	1.02332	0.75	6189.51	1.02725
0.445	9499.83	1.02332	0.6	7517	1.02725	0.755	6168.58	1.02627
0.45	9259.62	1.0243	0.605	7492.78	1.02529	0.76	6120.3	1.02919
0.455	9272.61	1.02627	0.61	7553.54	1.02332	0.765	6145.46	1.02627
0.46	9207.92	1.02919	0.615	7433.09	1.02821	0.77	6068.38	1.02627
0.465	9018.06	1.02725	0.62	7236.05	1.02725	0.775	6135.71	1.02725
0.47	8914.13	1.02332	0.625	7266.88	1.02725	0.78	6080.02	1.02821
0.475	8864.03	1.02821	0.63	7251.54	1.02233	0.785	6035.62	1.02725
0.48	8790.14	1.0243	0.635	7078.29	1.02725	0.79	6003.2	1.03017
0.485	8595.89	1.02725	0.64	7164.66	1.0204	0.795	5991.61	1.02821
0.49	8642.6	1.02627	0.645	7125.59	1.02821	0.8	5997.17	1.02725
0.495	8656.45	1.02919	0.65	7065.94	1.03017	0.805	5895.79	1.03017
0.5	8585.74	1.03214	0.655	7047.58	1.02725	0.81	5904.81	1.02725
0.505	8543.33	1.02529	0.66	7092.82	1.02627	0.815	5894.79	1.0243
0.51	8528.25	1.0243	0.665	7101.38	1.02725	0.82	5848.88	1.02627
0.515	8522.42	1.0204	0.67	6923.93	1.03017	0.825	5810.93	1.02821
0.52	8312.01	1.02725	0.675	6893.69	1.02725	0.83	5776.2	1.02138
0.525	8227.62	1.02725	0.68	6847.51	1.02725	0.835	5734.95	1.02529
0.53	8196.91	1.02725	0.685	6728.29	1.03017	0.84	5723.96	1.02725
0.535	8104.74	1.02919	0.69	6657.97	1.02919	0.845	5650.16	1.02529
0.54	8112.46	1.02919	0.695	6638.79	1.02919	0.85	5561.99	1.03017
0.545	8089.58	1.0243	0.7	6645.27	1.03116	0.855	5549.57	1.02821
0.55	7997.43	1.03017	0.705	6598.42	1.02529	0.86	5563.91	1.02627
0.555	8027.85	1.02627	0.71	6540.35	1.03017	0.865	5534.49	1.02529
0.56	7897.57	1.02725	0.715	6536.49	1.03017	0.87	5470.33	1.0243
0.565	7768.48	1.03214	0.72	6465.94	1.0243	0.875	5545.7	1.02821
0.57	7721.73	1.02919	0.725	6411.4	1.03116	0.88	5527.4	1.03017
0.575	7713.2	1.02725	0.73	6331.46	1.02919	0.885	5477.71	1.02725

B.5. Affinity PL1880

Stress Relaxation

T=150°C; strain=0.1 [strain units]; fixture diameter=25 [mm]; cone angle=0.1 [rad]

Time [s]	G(γ,t) [Pa]	γ [%]	Time [s] *cont.*	G(γ,t) [Pa] *cont.*	γ [%] *cont.*	Time [s] *cont.*	G(γ,t) [Pa] *cont.*	γ [%] *cont.*
0.001	0	0	0.145	24919.9	10.0398	0.285	13591.7	10.0243
0.01	70395.8	0.44525	0.15	24107.1	10.0319	0.29	13384.9	10.0319
0.015	202323	1.85197	0.155	23384.1	10.0319	0.295	13198.7	10.0243
0.02	207552	3.52	0.16	22677.4	10.0319	0.3	13000.1	10.0319
0.025	191028	5.0951	0.165	22033.1	10.0319	0.305	12844.8	10.0243
0.03	170367	6.42166	0.17	21436.3	10.0319	0.31	12654.4	10.0319
0.035	150566	7.47916	0.175	20870.6	10.0319	0.315	12491.2	10.0243
0.04	132430	8.27548	0.18	20320.8	10.0319	0.32	12324.6	10.0319
0.045	116261	8.85316	0.185	19833.9	10.0319	0.325	12167.5	10.0319
0.05	101891	9.27469	0.19	19362.7	10.0319	0.33	12019.5	10.0243
0.055	89747.5	9.55578	0.195	18906.9	10.0319	0.335	11869.1	10.0319
0.06	79373.8	9.75104	0.2	18468.4	10.0398	0.34	11727.5	10.0319
0.065	70665.9	9.87597	0.205	18089.9	10.0319	0.345	11595.1	10.0243
0.07	63366.5	9.96181	0.21	17712.8	10.0319	0.35	11453.4	10.0243
0.075	57202.2	10.0164	0.215	17336.2	10.0319	0.355	11327.6	10.0243
0.08	52058.4	10.0555	0.22	16990.3	10.0319	0.36	11193.6	10.0319
0.085	47715.5	10.0789	0.225	16660.7	10.0319	0.365	11067.9	10.0319
0.09	44022.3	10.0867	0.23	16330.6	10.0319	0.37	10949.8	10.0319
0.095	40866	10.0944	0.235	16032.2	10.0319	0.375	10840.3	10.0243
0.1	38179	10.0867	0.24	15749.1	10.0319	0.38	10706.4	10.0319
0.105	35831.7	10.0789	0.245	15458.7	10.0319	0.385	10596.6	10.0243
0.11	33794.2	10.071	0.25	15203.2	10.0243	0.39	10486.4	10.0319
0.115	32004.2	10.0631	0.255	14940.3	10.0319	0.395	10376.5	10.0243
0.12	30453.1	10.0631	0.26	14696.8	10.0319	0.4	10258.7	10.0319
0.125	29081.5	10.0555	0.265	14464.3	10.0243	0.405	10172.4	10.0319
0.13	27865	10.0476	0.27	14236.2	10.0243	0.41	10069.9	10.0243
0.135	26782.9	10.0476	0.275	14005.5	10.0319	0.415	9967.91	10.0243
0.14	25815	10.0398	0.28	13777.8	10.0319	0.42	9873.73	10.0319

Time [s] *cont.*	G(γ,t) [Pa] *cont.*	γ [%] *cont.*	Time [s] *cont.*	G(γ,t) [Pa] *cont.*	γ [%] *cont.*	Time [s] *cont.*	G(γ,t) [Pa] *cont.*	γ [%] *cont.*
0.425	9786.9	10.0243	0.58	7611.65	10.0319	0.735	6323.48	10.0319
0.43	9684.87	10.0243	0.585	7570.27	10.0243	0.74	6300.69	10.0243
0.435	9591.15	10.0319	0.59	7517.37	10.0319	0.745	6264.47	10.0319
0.44	9519.71	10.0243	0.595	7462.32	10.0319	0.75	6225.91	10.0243
0.445	9418.2	10.0319	0.6	7415.19	10.0319	0.755	6202.26	10.0243
0.45	9331.84	10.0319	0.605	7383.76	10.0319	0.76	6166.73	10.0243
0.455	9261.07	10.0319	0.61	7342.21	10.0243	0.765	6127.36	10.0243
0.46	9174.72	10.0319	0.615	7287.23	10.0243	0.77	6091.83	10.0243
0.465	9095.28	10.0243	0.62	7240.06	10.0243	0.775	6064.35	10.0243
0.47	9025.51	10.0319	0.625	7187.42	10.0319	0.78	6036.74	10.0243
0.475	8953.64	10.0243	0.63	7153.64	10.0243	0.785	6001.21	10.0243
0.48	8868.39	10.0319	0.635	7098.54	10.0243	0.79	5977.56	10.0243
0.485	8804.32	10.0243	0.64	7053.92	10.0319	0.795	5945.55	10.0319
0.49	8727.1	10.0319	0.645	7014.58	10.0319	0.8	5918.51	10.0243
0.495	8662.92	10.0243	0.65	6967.45	10.0319	0.805	5886.42	10.0319
0.5	8577.65	10.0319	0.655	6933.5	10.0243	0.81	5862.79	10.0319
0.505	8521.28	10.0243	0.66	6888.88	10.0319	0.815	5835.81	10.0243
0.51	8458.39	10.0243	0.665	6854.88	10.0243	0.82	5808.2	10.0243
0.515	8381.43	10.0319	0.67	6802.53	10.0319	0.825	5772.67	10.0243
0.52	8318.58	10.0319	0.675	6763.31	10.0319	0.83	5748.61	10.0319
0.525	8262.01	10.0243	0.68	6737.01	10.0243	0.835	5713.61	10.0243
0.53	8207.04	10.0243	0.685	6684.75	10.0319	0.84	5686.01	10.0243
0.535	8130.03	10.0319	0.69	6653.32	10.0319	0.845	5662.36	10.0243
0.54	8081.24	10.0243	0.695	6619.01	10.0243	0.85	5630.91	10.0243
0.545	8020.17	10.0319	0.7	6574.76	10.0319	0.855	5603	10.0319
0.55	7955.45	10.0243	0.705	6548.32	10.0243	0.86	5579.66	10.0243
0.555	7902.14	10.0319	0.71	6508.94	10.0243	0.865	5551.79	10.0319
0.56	7831.5	10.0319	0.715	6477.5	10.0243	0.87	5532.36	10.0243
0.565	7784.36	10.0319	0.72	6438.61	10.0243	0.875	5508.72	10.0243
0.57	7729.43	10.0319	0.725	6403.2	10.0243	0.88	5485.07	10.0243
0.575	7680.22	10.0243	0.73	6363.71	10.0243	0.885	5453.31	10.0319

B.5. Affinity PL1880

Stress Relaxation

T=150°C; strain=1.0 [strain units]; fixture diameter=10 [mm]; cone angle=0.035 [rad]

Time [s]	G(γ,t) [Pa]	γ [%]	Time [s] *cont.*	G(γ,t) [Pa] *cont.*	γ [%] *cont.*	Time [s] *cont.*	G(γ,t) [Pa] *cont.*	γ [%] *cont.*
0.001	0	0	0.145	22486.4	100.199	0.285	12026.3	100.289
0.01	49294.1	4.72956	0.15	21702.1	100.289	0.29	11860.5	100.199
0.015	76741	20.4053	0.155	20995.2	100.199	0.295	11703.4	100.199
0.02	84355.6	37.3624	0.16	20329.3	100.289	0.3	11556.2	100.199
0.025	86769.9	52.9101	0.165	19758.7	100.199	0.305	11448.3	100.199
0.03	88116.5	65.8924	0.17	19211.9	100.289	0.31	11291	100.289
0.035	87034.3	76.0191	0.175	18719	100.199	0.315	11114.5	100.289
0.04	84075.1	83.5136	0.18	18208.6	100.199	0.32	10957.7	100.199
0.045	79231.7	88.8665	0.185	17712.1	100.289	0.325	10820.5	100.199
0.05	73690.3	92.6131	0.19	17310.2	100.289	0.33	10663.7	100.289
0.055	67887.4	95.2016	0.195	16927.8	100.289	0.335	10487.2	100.289
0.06	62357.2	96.8965	0.2	16506.1	100.289	0.34	10359.3	100.199
0.065	57127.5	98.0572	0.205	16109.1	100.199	0.345	10281.3	100.289
0.07	52406.5	98.861	0.21	15755.8	100.199	0.35	10183.2	100.289
0.075	48247.5	99.3951	0.215	15432	100.199	0.355	10046	100.289
0.08	44606.3	99.6621	0.22	15084.7	100.289	0.36	9908.85	100.289
0.085	41337.6	99.9319	0.225	14774.4	100.199	0.365	9810.71	100.289
0.09	38490.2	100.019	0.23	14467.3	100.289	0.37	9716.62	100.199
0.095	36020.1	100.109	0.235	14225	100.199	0.375	9613.43	100.199
0.1	33848.9	100.199	0.24	13957.4	100.289	0.38	9485.46	100.199
0.105	31984.6	100.199	0.245	13692.7	100.289	0.385	9377.32	100.199
0.11	30296.9	100.199	0.25	13418.3	100.289	0.39	9337.96	100.199
0.115	28785.9	100.199	0.255	13185	100.199	0.395	9300.03	100.289
0.12	27446.7	100.289	0.26	12978.9	100.199	0.4	9210.14	100.199
0.125	26290	100.289	0.265	12741.8	100.289	0.405	9082.17	100.199
0.13	25211.3	100.289	0.27	12527.7	100.199	0.41	9013.38	100.199
0.135	24192	100.289	0.275	12351	100.199	0.415	8964.11	100.199
0.14	23270.6	100.289	0.28	12192.9	100.289	0.42	8852.97	100.289

Time [s] *cont.*	G(γ,t) [Pa] *cont.*	γ [%] *cont.*	Time [s] *cont.*	G(γ,t) [Pa] *cont.*	γ [%] *cont.*	Time [s] *cont.*	G(γ,t) [Pa] *cont.*	γ [%] *cont.*
0.425	8737.9	100.199	0.58	6755.83	100.199	0.735	5575.34	100.289
0.43	8656.39	100.289	0.585	6677.12	100.199	0.74	5521.32	100.199
0.435	8619.84	100.199	0.59	6626.87	100.289	0.745	5501.66	100.289
0.44	8541.14	100.199	0.595	6617.11	100.289	0.75	5521.32	100.199
0.445	8428.04	100.199	0.6	6564.02	100.199	0.755	5491.75	100.289
0.45	8302.53	100.289	0.605	6474.55	100.289	0.76	5452.37	100.199
0.455	8250.95	100.199	0.61	6441.01	100.199	0.765	5452.37	100.199
0.46	8211.59	100.199	0.615	6431.24	100.199	0.77	5472.05	100.199
0.465	8118.17	100.199	0.62	6396.7	100.199	0.775	5457.33	100.199
0.47	7983.18	100.289	0.625	6327.18	100.289	0.78	5393.46	100.289
0.475	7901.73	100.199	0.63	6288.55	100.199	0.785	5334.31	100.199
0.48	7891.96	100.199	0.635	6263.25	100.289	0.79	5294.96	100.199
0.485	7837.89	100.199	0.64	6268.87	100.199	0.795	5265.52	100.199
0.49	7734.55	100.199	0.645	6239.43	100.199	0.8	5216.4	100.199
0.495	7644.03	100.289	0.65	6185.21	100.199	0.805	5157.55	100.289
0.5	7616.49	100.199	0.655	6160.73	100.199	0.81	5137.7	100.199
0.505	7616.49	100.199	0.66	6160.73	100.199	0.815	5132.74	100.199
0.51	7570.34	100.289	0.665	6136.09	100.199	0.82	5108.11	100.199
0.515	7478.76	100.199	0.67	6056.91	100.289	0.825	5088.43	100.199
0.52	7400.05	100.199	0.675	5983.64	100.199	0.83	5088.82	100.289
0.525	7385.33	100.199	0.68	5959.01	100.199	0.835	5093.39	100.199
0.53	7370.61	100.199	0.685	5924.61	100.199	0.84	5054.04	100.199
0.535	7291.9	100.199	0.69	5880.3	100.199	0.845	4995.01	100.199
0.54	7196.98	100.289	0.695	5835.99	100.199	0.85	4921.8	100.289
0.545	7168.89	100.199	0.7	5801.59	100.199	0.855	4897.18	100.289
0.55	7144.4	100.199	0.705	5771.78	100.289	0.86	4892.23	100.289
0.555	7055.78	100.199	0.71	5757.43	100.199	0.865	4881.9	100.199
0.56	6936.46	100.289	0.715	5722.89	100.199	0.87	4862.74	100.289
0.565	6873.89	100.199	0.72	5693.45	100.199	0.875	4882.4	100.289
0.57	6852.87	100.289	0.725	5673.77	100.199	0.88	4906.54	100.199
0.575	6818.5	100.289	0.73	5644.18	100.199	0.885	4877.53	100.289

B.5. Affinity PL1880

Stress Relaxation

T=150°C; strain=5.0 [strain units]; fixture diameter=10 [mm]; cone angle=0.035 [rad]

Time [s]	G(γ,t) [Pa]	γ [%]	Time [s] *cont.*	G(γ,t) [Pa] *cont.*	γ [%] *cont.*	Time [s] *cont.*	G(γ,t) [Pa] *cont.*	γ [%] *cont.*
0.001	0	0	0.145	2188.05	501.232	0.285	1180.17	501.232
0.01	63621	11.5388	0.15	2111.9	501.232	0.29	1164.17	501.232
0.015	72601.3	67.0518	0.155	2043.11	501.232	0.295	1148.16	501.232
0.02	45033.8	150.967	0.16	1981.75	501.232	0.3	1132.16	501.232
0.025	29595.8	231.215	0.165	1921.4	501.232	0.305	1114.9	501.232
0.03	21946.6	301.7	0.17	1866	501.232	0.31	1102.6	501.232
0.035	17320	358.125	0.175	1817.98	501.232	0.315	1089.06	501.232
0.04	13999.9	400.49	0.18	1769.97	501.232	0.32	1071.83	501.232
0.045	11672.6	431.815	0.185	1724.4	501.232	0.325	1061.96	501.232
0.05	9868.02	453.886	0.19	1683.78	501.232	0.33	1049.66	501.232
0.055	8458.59	469.548	0.195	1644.36	501.232	0.335	1034.88	501.232
0.06	7342.48	479.88	0.2	1603.74	501.232	0.34	1022.56	501.232
0.065	6436.69	487.346	0.205	1570.5	501.232	0.345	1012.71	501.232
0.07	5710.39	491.978	0.21	1537.23	501.232	0.35	997.933	501.232
0.075	5121.4	495.183	0.215	1504	501.232	0.355	986.849	501.232
0.08	4633.96	497.319	0.22	1473.21	501.232	0.36	977.622	501.232
0.085	4230.7	498.747	0.225	1447.36	501.232	0.365	964.7	501.232
0.09	3894.03	499.815	0.23	1420.28	501.232	0.37	954.835	501.232
0.095	3610.68	500.163	0.235	1390.72	501.232	0.375	943.752	501.232
0.1	3369.42	500.523	0.24	1367.32	501.232	0.38	933.287	501.232
0.105	3162.96	500.883	0.245	1343.95	501.232	0.385	922.222	501.232
0.11	2983.94	501.232	0.25	1320.54	501.232	0.39	914.832	501.232
0.115	2829.18	501.232	0.255	1297.14	501.232	0.395	906.206	501.232
0.12	2689.12	501.232	0.26	1277.45	501.232	0.4	895.741	501.232
0.125	2568.8	501.232	0.265	1256.52	501.232	0.405	887.114	501.232
0.13	2458.22	501.232	0.27	1235.59	501.232	0.41	878.505	501.232
0.135	2357.55	501.232	0.275	1219.57	501.232	0.415	869.878	501.232
0.14	2271.54	501.232	0.28	1199.88	501.232	0.42	860.032	501.232

Time [s] *cont.*	G(γ,t) [Pa] *cont.*	γ [%] *cont.*	Time [s] *cont.*	G(γ,t) [Pa] *cont.*	γ [%] *cont.*	Time [s] *cont.*	G(γ,t) [Pa] *cont.*	γ [%] *cont.*
0.425	853.262	501.232	0.58	669.188	501.232	0.735	552.208	501.232
0.43	847.111	501.232	0.585	662.399	501.232	0.74	549.132	501.232
0.435	837.246	501.232	0.59	659.942	501.232	0.745	547.895	501.232
0.44	831.713	501.232	0.595	656.867	501.232	0.75	544.2	501.232
0.445	826.162	501.232	0.6	651.334	501.232	0.755	540.505	501.232
0.45	816.316	501.232	0.605	646.402	501.232	0.76	538.658	501.232
0.455	809.546	501.232	0.61	643.945	501.232	0.765	536.201	501.232
0.46	805.232	501.232	0.615	639.013	501.232	0.77	531.278	501.232
0.465	796.624	501.232	0.62	634.08	501.232	0.775	531.888	501.232
0.47	788.616	501.232	0.625	631.623	501.232	0.78	529.431	501.232
0.475	783.683	501.232	0.63	627.929	501.232	0.785	525.736	501.232
0.48	776.294	501.232	0.635	624.234	501.232	0.79	523.889	501.232
0.485	768.305	501.232	0.64	619.321	501.232	0.795	525.736	501.232
0.49	763.373	501.232	0.645	615.626	501.232	0.8	518.957	501.232
0.495	757.84	501.232	0.65	611.312	501.232	0.805	515.881	501.232
0.5	750.451	501.232	0.655	606.999	501.232	0.81	514.034	501.232
0.505	742.443	501.232	0.66	605.77	501.232	0.815	511.577	501.232
0.51	741.205	501.232	0.665	602.076	501.232	0.82	506.644	501.232
0.515	734.435	501.232	0.67	597.153	501.232	0.825	507.263	501.232
0.52	726.426	501.232	0.675	592.839	501.232	0.83	506.035	501.232
0.525	721.513	501.232	0.68	591.611	501.232	0.835	502.34	501.232
0.53	718.437	501.232	0.685	586.679	501.232	0.84	498.955	501.232
0.535	711.048	501.232	0.69	584.222	501.232	0.845	497.717	501.232
0.54	705.497	501.232	0.695	582.374	501.232	0.85	494.023	501.232
0.545	702.421	501.232	0.7	576.833	501.232	0.855	490.028	501.232
0.55	695.032	501.232	0.705	571.499	501.591	0.86	489.409	501.232
0.555	690.737	501.232	0.71	570.672	501.232	0.865	487.252	501.232
0.56	688.261	501.232	0.715	566.977	501.232	0.87	483.558	501.232
0.565	683.948	501.232	0.72	562.673	501.232	0.875	481.711	501.232
0.57	679.034	501.232	0.725	559.597	501.232	0.88	481.41	501.232
0.575	674.721	501.232	0.73	557.131	501.232	0.885	477.406	501.232

B.5. Affinity PL1880

Stress Relaxation

T=150°C; strain=7.5 [strain units]; fixture diameter=10 [mm]; cone angle=0.035 [rad]

Time [s]	G(γ,t) [Pa]	γ [%]	Time [s] *cont.*	G(γ,t) [Pa] *cont.*	γ [%] *cont.*	Time [s] *cont.*	G(γ,t) [Pa] *cont.*	γ [%] *cont.*
0.001	0	0	0.145	1647.77	751.847	0.285	860.592	751.847
0.01	64638.4	12.1202	0.15	1587.18	751.847	0.29	849.115	751.847
0.015	63114.9	75.3052	0.155	1533.15	751.847	0.295	835.961	751.847
0.02	35638.4	188.85	0.16	1484.01	751.847	0.3	822.833	751.847
0.025	23596.6	311.313	0.165	1436.53	751.847	0.305	811.343	751.847
0.03	17276.3	421.493	0.17	1393.94	751.847	0.31	801.491	751.847
0.035	13849.6	512.272	0.175	1354.63	751.847	0.315	790.826	751.847
0.04	11376.8	582.049	0.18	1317	751.847	0.32	780.149	751.847
0.045	9548.61	633.668	0.185	1280.89	751.847	0.325	771.947	751.847
0.05	8110.94	670.681	0.19	1250.51	751.847	0.33	762.094	751.847
0.055	6970.72	697.025	0.195	1218.5	751.847	0.335	751.417	751.847
0.06	6033.29	715.531	0.2	1188.94	751.847	0.34	744.028	751.847
0.065	5269.51	727.651	0.205	1161.86	751.847	0.345	734.188	751.847
0.07	4647.59	735.477	0.21	1136.41	751.847	0.35	724.336	751.847
0.075	4133.51	741.166	0.215	1112.6	751.847	0.355	716.946	751.847
0.08	3706.93	744.741	0.22	1087.14	751.847	0.36	708.732	751.847
0.085	3360.03	746.877	0.225	1065.81	751.847	0.365	699.705	751.847
0.09	3067.71	749.014	0.23	1045.28	751.847	0.37	692.316	751.847
0.095	2825.07	749.711	0.235	1023.95	751.847	0.375	684.927	751.847
0.1	2620.54	750.431	0.24	1005.08	751.847	0.38	677.537	751.847
0.105	2445.93	751.15	0.245	987.021	751.847	0.385	667.285	751.847
0.11	2298.41	751.15	0.25	968.142	751.847	0.39	661.534	751.847
0.115	2168.91	751.15	0.255	952.538	751.847	0.395	654.97	751.847
0.12	2055.83	751.15	0.26	935.284	751.847	0.4	646.755	751.847
0.125	1955.81	751.15	0.265	918.055	751.847	0.405	641.429	751.847
0.13	1863.92	751.847	0.27	903.277	751.847	0.41	635.678	751.847
0.135	1785.36	751.847	0.275	890.149	751.847	0.415	628.701	751.847
0.14	1714.94	751.847	0.28	875.371	751.847	0.42	622.137	751.847

Time [s] cont.	G(γ,t) [Pa] cont.	γ [%] cont.	Time [s] cont.	G(γ,t) [Pa] cont.	γ [%] cont.	Time [s] cont.	G(γ,t) [Pa] cont.	γ [%] cont.
0.425	617.624	751.847	0.58	481.767	751.847	0.735	396.397	751.847
0.43	610.234	751.847	0.585	478.066	751.847	0.74	395.166	751.847
0.435	604.483	751.847	0.59	475.603	751.847	0.745	392.703	751.847
0.44	601.207	751.847	0.595	471.915	751.847	0.75	391.059	751.847
0.445	595.456	751.847	0.6	468.227	751.847	0.755	388.189	751.847
0.45	588.892	751.847	0.605	464.526	751.847	0.76	386.958	751.847
0.455	584.778	751.847	0.61	461.25	751.847	0.765	384.901	751.847
0.46	580.265	751.847	0.615	457.549	751.847	0.77	381.619	751.847
0.465	574.526	751.847	0.62	454.673	751.847	0.775	380.8	751.847
0.47	569.6	751.847	0.625	453.036	751.847	0.78	378.743	751.847
0.475	566.312	751.847	0.63	450.16	751.847	0.785	376.287	751.847
0.48	560.573	751.847	0.635	445.234	751.847	0.79	375.055	751.847
0.485	553.184	751.847	0.64	444.008	751.847	0.795	375.055	751.847
0.49	551.533	751.847	0.645	442.358	751.847	0.8	372.179	751.847
0.495	545.382	751.847	0.65	437.845	751.847	0.805	371.767	751.847
0.5	540.456	751.847	0.655	435.381	751.847	0.81	370.129	751.847
0.505	536.767	751.847	0.66	433.744	751.847	0.815	368.072	751.847
0.51	533.892	751.847	0.665	430.055	751.847	0.82	365.203	751.847
0.515	528.966	751.847	0.67	427.592	751.847	0.825	363.559	751.847
0.52	524.039	751.847	0.675	426.767	751.847	0.83	362.327	751.847
0.525	521.576	751.847	0.68	424.716	751.847	0.835	359.864	751.847
0.53	516.238	751.847	0.685	421.016	751.847	0.84	357.401	751.847
0.535	511.724	751.847	0.69	421.016	751.847	0.845	357.401	751.847
0.54	509.261	751.847	0.695	417.327	751.847	0.85	353.3	751.847
0.545	505.985	751.847	0.7	415.277	751.847	0.855	352.887	751.847
0.55	501.872	751.847	0.705	412.814	751.847	0.86	351.656	751.847
0.555	498.596	751.847	0.71	411.576	751.847	0.865	349.605	751.847
0.56	496.946	751.847	0.715	407.475	751.847	0.87	347.142	751.847
0.565	492.032	751.847	0.72	404.193	751.847	0.875	346.73	751.847
0.57	488.331	751.847	0.725	402.961	751.847	0.88	343.86	751.847
0.575	485.868	751.847	0.73	400.092	751.847	0.885	342.629	751.847

B.5. Affinity PL1880

Stress Relaxation

T=150°C; strain=10.0 [strain units]; fixture diameter=10 [mm]; cone angle=0.035 [rad]

Time [s]	G(γ,t) [Pa]	γ [%]	Time [s] *cont.*	G(γ,t) [Pa] *cont.*	γ [%] *cont.*	Time [s] *cont.*	G(γ,t) [Pa] *cont.*	γ [%] *cont.*
0.001	0	0	0.145	1405.13	1001.77	0.285	711.241	1001.77
0.01	62439.5	12.1424	0.15	1349.8	1001.77	0.29	701.389	1001.77
0.015	62382.8	79.0518	0.155	1301.87	1001.77	0.295	690.297	1001.77
0.02	33980.5	210.926	0.16	1255.18	1001.77	0.3	679.825	1001.77
0.025	22224.8	370.583	0.165	1212.16	1001.77	0.305	672.43	1001.77
0.03	16392.8	521.526	0.17	1174.06	1001.77	0.31	661.958	1001.77
0.035	12984.7	649.33	0.175	1137.19	1001.77	0.315	652.706	1001.77
0.04	10738.9	750.431	0.18	1104.01	1001.77	0.32	644.092	1001.77
0.045	9006.28	825.896	0.185	1073.26	1001.77	0.325	636.697	1001.77
0.05	7657.19	880.719	0.19	1045	1001.77	0.33	627.445	1001.77
0.055	6560.37	919.869	0.195	1016.74	1001.77	0.335	619.45	1001.77
0.06	5655.05	946.943	0.2	990.932	1001.77	0.34	613.285	1001.77
0.065	4909.01	965.45	0.205	966.91	1001.77	0.345	605.271	1001.77
0.07	4294.06	977.548	0.21	944.126	1001.77	0.35	597.877	1001.77
0.075	3792.33	986.093	0.215	922.562	1001.77	0.355	592.331	1001.77
0.08	3375.83	991.782	0.22	902.218	1001.77	0.36	584.946	1001.77
0.085	3037.09	995.357	0.225	883.132	1001.77	0.365	577.552	1001.77
0.09	2756.61	997.493	0.23	864.027	1001.77	0.37	570.777	1001.77
0.095	2523.39	998.91	0.235	847.399	1001.77	0.375	565.841	1001.77
0.1	2325.37	1000.33	0.24	831.372	1001.77	0.38	557.837	1001.77
0.105	2158.88	1001.05	0.245	815.964	1001.77	0.385	553.52	1001.77
0.11	2014.98	1001.05	0.25	800.574	1001.77	0.39	547.975	1001.77
0.115	1890.6	1001.77	0.255	787.024	1001.77	0.395	541.819	1001.77
0.12	1783.67	1001.77	0.26	772.235	1001.77	0.4	535.044	1001.77
0.125	1690.28	1001.77	0.265	758.685	1001.77	0.405	530.727	1001.77
0.13	1605.45	1001.77	0.27	746.355	1001.77	0.41	524.562	1001.77
0.135	1531.73	1001.77	0.275	734.644	1001.77	0.415	519.026	1001.77
0.14	1466.57	1001.77	0.28	721.094	1001.77	0.42	515.329	1001.77

Time [s] *cont.*	G(γ,t) [Pa] *cont.*	γ [%] *cont.*	Time [s] *cont.*	G(γ,t) [Pa] *cont.*	γ [%] *cont.*	Time [s] *cont.*	G(γ,t) [Pa] *cont.*	γ [%] *cont.*
0.425	509.783	1001.77	0.58	396.118	1001.77	0.735	327.111	1001.77
0.43	503.927	1001.77	0.585	393.031	1001.77	0.74	326.191	1001.77
0.435	499.921	1001.77	0.59	391.182	1001.77	0.745	324.033	1001.77
0.44	495.304	1001.77	0.595	388.105	1001.77	0.75	321.874	1001.77
0.445	489.758	1001.77	0.6	385.336	1001.77	0.755	320.335	1001.77
0.45	485.141	1001.77	0.605	382.868	1001.77	0.76	318.487	1001.77
0.455	482.983	1001.77	0.61	380.71	1001.77	0.765	316.948	1001.77
0.46	479.286	1001.77	0.615	377.013	1001.77	0.77	315.719	1001.77
0.465	474.969	1001.77	0.62	375.164	1001.77	0.775	314.18	1001.77
0.47	471.272	1001.77	0.625	374.245	1001.77	0.78	312.022	1001.77
0.475	467.575	1001.77	0.63	370.548	1001.77	0.785	309.863	1001.77
0.48	462.649	1001.77	0.635	368.08	1001.77	0.79	309.863	1001.77
0.485	458.341	1001.77	0.64	366.85	1001.77	0.795	308.015	1001.77
0.49	455.564	1001.77	0.645	364.082	1001.77	0.8	305.551	1001.77
0.495	451.257	1001.77	0.65	360.995	1001.77	0.805	304.318	1001.77
0.5	446.631	1001.77	0.655	359.766	1001.77	0.81	303.393	1001.77
0.505	444.172	1001.77	0.66	357.608	1001.77	0.815	301.545	1001.77
0.51	440.785	1001.77	0.665	354.22	1001.77	0.82	300.006	1001.77
0.515	436.468	1001.77	0.67	353.3	1001.77	0.825	300.006	1001.77
0.52	433.39	1001.77	0.675	352.371	1001.77	0.83	297.233	1001.77
0.525	430.613	1001.77	0.68	348.984	1001.77	0.835	295.694	1001.77
0.53	425.996	1001.77	0.685	346.826	1001.77	0.84	295.694	1001.77
0.535	423.218	1001.77	0.69	345.287	1001.77	0.845	293.536	1001.77
0.54	420.45	1001.77	0.695	342.519	1001.77	0.85	291.072	1001.77
0.545	416.443	1001.77	0.7	339.741	1001.77	0.855	290.763	1001.77
0.55	413.675	1001.77	0.705	338.512	1001.77	0.86	289.534	1001.77
0.555	410.898	1001.77	0.71	336.973	1001.77	0.865	287.685	1001.77
0.56	407.82	1001.77	0.715	334.505	1001.77	0.87	285.222	1001.77
0.565	403.813	1001.77	0.72	332.656	1001.77	0.875	285.527	1001.77
0.57	401.045	1001.77	0.725	331.737	1001.77	0.88	283.678	1001.77
0.575	399.506	1001.77	0.73	329.269	1001.77	0.885	283.063	1001.77

B.5. Affinity PL1880

Stress Relaxation

T=150°C; strain=12.5 [strain units]; fixture diameter=10 [mm]; cone angle=0.035 [rad]

Time [s]	G(γ,t) [Pa]	γ [%]	Time [s] *cont.*	G(γ,t) [Pa] *cont.*	γ [%] *cont.*	Time [s] *cont.*	G(γ,t) [Pa] *cont.*	γ [%] *cont.*
0.001	0	0	0.145	1327.35	1251.66	0.285	668.463	1251.66
0.01	63896.1	12.4666	0.15	1276.19	1251.66	0.29	658.609	1251.66
0.015	61027.2	82.0409	0.155	1227.97	1251.66	0.295	648.741	1251.66
0.02	33137.2	225.7	0.16	1183.72	1251.66	0.3	639.864	1251.66
0.025	21617.3	412.589	0.165	1144.37	1251.66	0.305	630.987	1251.66
0.03	16256.3	603.052	0.17	1107.96	1251.66	0.31	622.605	1251.66
0.035	12967.2	769.657	0.175	1073.53	1251.66	0.315	614.224	1251.66
0.04	10754.9	904.218	0.18	1042.08	1251.66	0.32	606.338	1251.66
0.045	9132.61	1006.74	0.185	1011.56	1251.66	0.325	597.461	1251.66
0.05	7769.59	1082.2	0.19	984.042	1251.66	0.33	589.08	1251.66
0.055	6659.73	1135.61	0.195	958.447	1251.66	0.335	582.666	1251.66
0.06	5728.45	1174.06	0.2	933.859	1251.66	0.34	574.284	1251.66
0.065	4953.25	1199.69	0.205	911.238	1251.66	0.345	566.894	1251.66
0.07	4310.51	1217.48	0.21	888.617	1251.66	0.35	559.985	1251.66
0.075	3777.59	1228.88	0.215	869.917	1251.66	0.355	553.571	1251.66
0.08	3343.54	1236.71	0.22	850.255	1251.66	0.36	545.19	1251.66
0.085	2983.33	1242.4	0.225	831.555	1251.66	0.365	539.272	1251.66
0.09	2687.75	1245.25	0.23	813.846	1251.66	0.37	533.849	1251.66
0.095	2442.3	1247.39	0.235	799.126	1251.66	0.375	527.451	1251.66
0.1	2240.39	1248.81	0.24	782.858	1251.66	0.38	522.013	1251.66
0.105	2070.41	1250.25	0.245	767.087	1251.66	0.385	516.591	1251.66
0.11	1925.55	1250.94	0.25	753.764	1251.66	0.39	511.169	1251.66
0.115	1803.51	1250.94	0.255	739.464	1251.66	0.395	505.25	1251.66
0.12	1696.22	1251.66	0.26	726.652	1251.66	0.4	501.811	1251.66
0.125	1602.76	1251.66	0.265	713.824	1251.66	0.405	495.893	1251.66
0.13	1522.1	1251.66	0.27	701.988	1251.66	0.41	489.967	1251.66
0.135	1450.31	1251.66	0.275	689.672	1251.66	0.415	486.024	1251.66
0.14	1385.39	1251.66	0.28	679.307	1251.66	0.42	482.081	1251.66

Time [s] *cont.*	G(γ,t) [Pa] *cont.*	γ [%] *cont.*	Time [s] *cont.*	G(γ,t) [Pa] *cont.*	γ [%] *cont.*	Time [s] *cont.*	G(γ,t) [Pa] *cont.*	γ [%] *cont.*
0.425	476.163	1251.66	0.58	368.917	1251.66	0.735	306.049	1251.66
0.43	471.229	1251.66	0.585	367.19	1251.66	0.74	303.586	1251.66
0.435	467.286	1251.66	0.59	363.991	1251.66	0.745	301.859	1251.66
0.44	462.848	1251.66	0.595	361.032	1251.66	0.75	300.875	1251.66
0.445	457.425	1251.66	0.6	359.056	1251.66	0.755	299.395	1251.66
0.45	453.978	1251.66	0.605	357.089	1251.66	0.76	297.42	1251.66
0.455	449.54	1251.66	0.61	354.13	1251.66	0.765	295.452	1251.66
0.46	445.101	1251.66	0.615	351.411	1251.66	0.77	294.221	1251.66
0.465	441.646	1251.66	0.62	350.427	1251.66	0.775	291.998	1251.66
0.47	437.703	1251.66	0.625	348.212	1251.66	0.78	290.03	1251.66
0.475	433.761	1251.66	0.63	345.5	1251.66	0.785	289.286	1251.66
0.48	430.306	1251.66	0.635	344.021	1251.66	0.79	287.807	1251.66
0.485	427.347	1251.66	0.64	341.55	1251.66	0.795	286.08	1251.66
0.49	422.908	1251.66	0.645	338.351	1251.66	0.8	284.848	1251.66
0.495	418.965	1251.66	0.65	336.623	1251.66	0.805	284.112	1251.66
0.5	415.518	1251.66	0.655	334.896	1251.66	0.81	282.632	1251.66
0.505	413.047	1251.66	0.66	332.185	1251.66	0.815	280.905	1251.66
0.51	408.609	1251.66	0.665	329.969	1251.66	0.82	279.921	1251.66
0.515	406.641	1251.66	0.67	328.978	1251.66	0.825	277.45	1251.66
0.52	403.186	1251.66	0.675	326.515	1251.66	0.83	275.483	1251.66
0.525	399.244	1251.66	0.68	324.051	1251.66	0.835	275.235	1251.66
0.53	396.037	1251.66	0.685	323.06	1251.66	0.84	274.491	1251.66
0.535	394.069	1251.66	0.69	321.092	1251.66	0.845	271.78	1251.66
0.54	390.119	1251.66	0.695	318.381	1251.66	0.85	271.78	1251.66
0.545	386.672	1251.66	0.7	317.39	1251.66	0.855	270.548	1251.66
0.55	384.201	1251.66	0.705	316.158	1251.66	0.86	269.069	1251.66
0.555	381.001	1251.66	0.71	312.711	1251.66	0.865	267.342	1251.66
0.56	378.042	1251.66	0.715	311.719	1251.66	0.87	266.853	1251.66
0.565	376.315	1251.66	0.72	310.736	1251.66	0.875	265.622	1251.66
0.57	374.099	1251.66	0.725	309.008	1251.66	0.88	262.663	1251.66
0.575	371.381	1251.66	0.73	306.545	1251.66	0.885	262.415	1251.66

B.6. Affinity PL1840

Stress Relaxation

T=150°C; strain=0.01 [strain units]; fixture diameter=25 [mm]; cone angle=0.1 [rad]

Time [s]	G(γ,t) [Pa]	γ [%]	Time [s] *cont.*	G(γ,t) [Pa] *cont.*	γ [%] *cont.*	Time [s] *cont.*	G(γ,t) [Pa] *cont.*	γ [%] *cont.*
0.001	0	0	0.145	24455.3	0.9979	0.285	14088.2	0.9979
0.01	90418.1	0.03267	0.15	23518.2	1.00278	0.29	13793.7	1.00377
0.015	193982	0.16857	0.155	22938	0.9979	0.295	13731.9	1.00082
0.02	190011	0.32928	0.16	22321.7	0.9979	0.3	13553.8	0.99593
0.025	173720	0.48476	0.165	21589.5	1.0018	0.305	13369.3	0.99495
0.03	154090	0.62369	0.17	20977.4	1.00472	0.31	13195.3	0.9979
0.035	135515	0.73424	0.175	20594.8	0.99888	0.315	13000.8	0.99888
0.04	119233	0.81445	0.18	20109.8	1.0018	0.32	12781.9	1.0018
0.045	104090	0.87854	0.185	19672.4	1.00082	0.325	12686.4	0.99691
0.05	91046.1	0.92354	0.19	19122.4	1.00571	0.33	12624.9	0.99301
0.055	80369.2	0.94995	0.195	18845	1.00377	0.335	12333.8	0.99983
0.06	71369.1	0.96658	0.2	18542.3	0.99888	0.34	12101.2	1.00472
0.065	63251.9	0.98419	0.205	18110.4	1.0018	0.345	11983.6	1.00669
0.07	56719.7	0.99301	0.21	17844.8	1.00082	0.35	11861.1	1.0018
0.075	51333.4	0.99888	0.215	17634.5	0.99396	0.355	11712.1	1.00377
0.08	47257.4	0.99495	0.22	17199.5	0.99983	0.36	11705.4	0.99691
0.085	43270.6	1.00278	0.225	16932.7	0.9979	0.365	11634.4	0.99691
0.09	40338.7	0.99983	0.23	16680.8	0.99691	0.37	11522.6	0.99495
0.095	37666.5	1.00377	0.235	16332.7	0.99593	0.375	11344.9	0.99593
0.1	35467.1	1.00377	0.24	15907	1.00278	0.38	11294.3	0.99691
0.105	33584.9	1.0018	0.245	15748.7	0.99983	0.385	11076.8	1.00082
0.11	31884.9	1.00377	0.25	15425.3	0.99983	0.39	10913.6	1.00278
0.115	30453.8	1.00278	0.255	15123.5	1.00571	0.395	10858.6	1.00278
0.12	29189.8	1.00082	0.26	14948.6	1.00377	0.4	10756.4	0.99691
0.125	27914.9	1.00472	0.265	14815.2	0.9979	0.405	10680	0.99593
0.13	26868.6	1.00571	0.27	14582.9	1.00082	0.41	10624.6	0.99593
0.135	25864.9	1.00571	0.275	14342	1.00278	0.415	10421.6	1.00472
0.14	24986.6	1.00571	0.28	14295.4	0.99888	0.42	10381.3	1.0018

Time [s] *cont.*	G(γ,t) [Pa] *cont.*	γ [%] *cont.*	Time [s] *cont.*	G(γ,t) [Pa] *cont.*	γ [%] *cont.*	Time [s] *cont.*	G(γ,t) [Pa] *cont.*	γ [%] *cont.*
0.425	10250.9	1.00377	0.58	8288.75	0.99691	0.735	6803.32	0.99396
0.43	10284.2	0.99593	0.585	8146.04	0.99983	0.74	6698.77	1.0018
0.435	10125.5	0.99983	0.59	8059.34	0.99983	0.745	6731.7	0.99983
0.44	9977.83	1.00278	0.595	8043.37	0.9979	0.75	6704	0.99983
0.445	9981.8	1.00082	0.6	7933	0.99888	0.755	6702.45	0.99888
0.45	9861.67	1.0018	0.605	7900.89	0.99593	0.76	6644.75	0.99983
0.455	9772.14	0.99888	0.61	7787.93	1.00278	0.765	6707.82	0.99691
0.46	9666.6	1.00082	0.615	7830.66	0.99983	0.77	6591.12	1.00377
0.465	9608.02	0.9979	0.62	7756.03	1.0018	0.775	6545.26	0.99691
0.47	9431.66	0.99983	0.625	7651.34	1.00571	0.78	6544.18	0.99888
0.475	9302.81	1.0018	0.63	7723.03	0.9979	0.785	6426.55	1.0018
0.48	9345.92	0.99888	0.635	7607.83	0.99691	0.79	6324.67	1.00669
0.485	9170.23	1.00082	0.64	7483.82	1.0018	0.795	6362.17	0.99888
0.49	9124.86	0.99888	0.645	7508.67	0.99691	0.8	6372.42	0.9979
0.495	9107.2	1.00082	0.65	7405.52	1.00278	0.805	6348.66	0.9979
0.5	9013.56	0.99983	0.655	7417.49	0.99691	0.81	6286.7	1.00082
0.505	9001.5	0.99593	0.66	7329.79	1.00669	0.815	6362.89	0.99691
0.51	8910.14	1.00082	0.665	7392.52	1.00082	0.82	6249.41	0.99983
0.515	8939	0.99495	0.67	7285.81	1.00082	0.825	6176.14	1.00082
0.52	8865.27	0.9979	0.675	7198.21	0.99983	0.83	6219.57	1.00082
0.525	8752.78	1.00082	0.68	7205.08	0.99888	0.835	6164.37	0.99888
0.53	8817.01	0.99888	0.685	7158.06	0.99495	0.84	6112.76	1.00278
0.535	8729.84	0.99983	0.69	7051.85	1.00377	0.845	6091.12	1.0018
0.54	8675.6	0.9979	0.695	7079.59	0.99983	0.85	6081.3	1.00278
0.545	8625.93	1.0018	0.7	7107.35	0.99593	0.855	6069.39	0.99888
0.55	8507.49	1.00278	0.705	7053.64	0.9979	0.86	5992.57	1.0018
0.555	8396.9	1.00472	0.71	6967.63	0.99888	0.865	6018.18	1.00082
0.56	8349.94	1.00377	0.715	7034.87	0.99495	0.87	5990.16	0.99495
0.565	8334.1	1.00472	0.72	6928.67	0.99593	0.875	5922.79	0.99691
0.57	8328.61	0.99593	0.725	6842.36	0.99983	0.88	5950.57	0.99691
0.575	8216.96	1.00082	0.73	6870.06	0.99983	0.885	5823.33	1.00377

B.6. Affinity PL1840

Stress Relaxation

T=150°C; strain=0.1 [strain units]; fixture diameter=25 [mm]; cone angle=0.1 [rad]

Time [s]	G(γ,t) [Pa]	γ [%]	Time [s] *cont.*	G(γ,t) [Pa] *cont.*	γ [%] *cont.*	Time [s] *cont.*	G(γ,t) [Pa] *cont.*	γ [%] *cont.*
0.001	0	0	0.145	23955.6	10.0398	0.285	13865.1	10.0319
0.01	65326.8	0.45334	0.15	23199.6	10.0476	0.29	13676.5	10.0319
0.015	184562	1.8872	0.155	22556.3	10.0476	0.295	13511.7	10.0319
0.02	186443	3.58848	0.16	21977.7	10.0398	0.3	13330.8	10.0319
0.025	169823	5.16162	0.165	21397.1	10.0398	0.305	13158.1	10.0319
0.03	149904	6.47256	0.17	20878.9	10.0398	0.31	13008.9	10.0319
0.035	131503	7.50253	0.175	20408.3	10.0319	0.315	12851.8	10.0319
0.04	115345	8.27548	0.18	19937.2	10.0319	0.32	12686.8	10.0319
0.045	101070	8.85316	0.185	19466.1	10.0398	0.325	12553.4	10.0319
0.05	88760.3	9.25919	0.19	19058.2	10.0398	0.33	12419.8	10.0319
0.055	78368	9.54028	0.195	18680.2	10.0319	0.335	12262.7	10.0319
0.06	69564.3	9.73531	0.2	18303.1	10.0319	0.34	12138.3	10.0243
0.065	62158.9	9.86811	0.205	17941.9	10.0319	0.345	12011.3	10.0319
0.07	56018	9.95394	0.21	17611.8	10.0319	0.35	11877.9	10.0319
0.075	50925.7	10.0085	0.215	17282.2	10.0319	0.355	11744.3	10.0319
0.08	46649.2	10.0476	0.22	16967.9	10.0319	0.36	11635.3	10.0243
0.085	43100.3	10.0631	0.225	16669.5	10.0319	0.365	11508.7	10.0319
0.09	40031.3	10.0789	0.23	16386.5	10.0319	0.37	11383	10.0319
0.095	37437.7	10.0867	0.235	16103.9	10.0319	0.375	11272.9	10.0319
0.1	35218.9	10.0867	0.24	15852.5	10.0319	0.38	11163	10.0319
0.105	33250.2	10.0867	0.245	15593.2	10.0319	0.385	11052.9	10.0319
0.11	31556.1	10.0789	0.25	15349.7	10.0319	0.39	10951.4	10.0243
0.115	30062.5	10.071	0.255	15106.2	10.0319	0.395	10840.9	10.0319
0.12	28732.5	10.071	0.26	14894.2	10.0319	0.4	10738.9	10.0319
0.125	27564.5	10.0631	0.265	14674.2	10.0319	0.405	10628.8	10.0319
0.13	26504.2	10.0555	0.27	14454.2	10.0319	0.41	10542.5	10.0319
0.135	25548.4	10.0555	0.275	14257.7	10.0319	0.415	10456.1	10.0243
0.14	24721	10.0476	0.28	14069.4	10.0319	0.42	10353.9	10.0319

Time [s] *cont.*	G(γ,t) [Pa] *cont.*	γ [%] *cont.*	Time [s] *cont.*	G(γ,t) [Pa] *cont.*	γ [%] *cont.*	Time [s] *cont.*	G(γ,t) [Pa] *cont.*	γ [%] *cont.*
0.425	10259.6	10.0319	0.58	8132.47	10.0398	0.735	6816.53	10.0243
0.43	10181.2	10.0319	0.585	8091.59	10.0319	0.74	6785.08	10.0243
0.435	10094.6	10.0319	0.59	8042.78	10.0243	0.745	6740.7	10.0319
0.44	10000.6	10.0319	0.595	7989.64	10.0319	0.75	6709.28	10.0319
0.445	9921.89	10.0319	0.6	7950.3	10.0319	0.755	6677.85	10.0319
0.45	9843.45	10.0319	0.605	7895.37	10.0319	0.76	6638.51	10.0319
0.455	9756.85	10.0319	0.61	7840.32	10.0319	0.765	6615	10.0319
0.46	9685.78	10.0243	0.615	7807.04	10.0243	0.77	6591.38	10.0319
0.465	9607.65	10.0319	0.62	7746.04	10.0319	0.775	6544.24	10.0319
0.47	9529.2	10.0319	0.625	7698.91	10.0319	0.78	6520.73	10.0319
0.475	9458.44	10.0319	0.63	7651.77	10.0319	0.785	6489.31	10.0319
0.48	9395.59	10.0319	0.635	7612.55	10.0319	0.79	6449.96	10.0319
0.485	9317.15	10.0319	0.64	7551.7	10.0398	0.795	6426.82	10.0319
0.49	9223.56	10.0398	0.645	7526.19	10.0319	0.8	6399.23	10.0319
0.495	9167.94	10.0319	0.65	7479.06	10.0319	0.805	6363.85	10.0319
0.5	9097.18	10.0319	0.655	7424	10.0319	0.81	6333.16	10.0243
0.505	9026.41	10.0319	0.66	7392.58	10.0319	0.815	6313.48	10.0243
0.51	8956.54	10.0398	0.665	7345.44	10.0319	0.82	6285.05	10.0319
0.515	8900.71	10.0319	0.67	7306.22	10.0319	0.825	6250.46	10.0243
0.52	8837.87	10.0319	0.675	7259.09	10.0319	0.83	6218.89	10.0243
0.525	8766.09	10.0243	0.68	7227.66	10.0319	0.835	6194.49	10.0319
0.53	8704.49	10.0319	0.685	7196.24	10.0319	0.84	6159.11	10.0319
0.535	8649.32	10.0319	0.69	7149.1	10.0319	0.845	6123.61	10.0319
0.54	8585.32	10.0243	0.695	7115.29	10.0243	0.85	6103.94	10.0319
0.545	8523.62	10.0319	0.7	7065	10.0398	0.855	6080.31	10.0319
0.55	8468.69	10.0319	0.705	7031.32	10.0319	0.86	6048.88	10.0319
0.555	8405.84	10.0319	0.71	6991.98	10.0319	0.865	6029.09	10.0319
0.56	8350.91	10.0319	0.715	6960.55	10.0319	0.87	6005.46	10.0319
0.565	8295.97	10.0319	0.72	6921.33	10.0319	0.875	5982.55	10.0243
0.57	8241.04	10.0319	0.725	6881.99	10.0319	0.88	5958.21	10.0319
0.575	8185.87	10.0319	0.73	6850.57	10.0319	0.885	5931.29	10.0243

B.6. Affinity PL1840

Stress Relaxation

T=150°C; strain=1.0 [strain units]; fixture diameter=10 [mm]; cone angle=0.035 [rad]

Time [s]	G(γ,t) [Pa]	γ [%]	Time [s] *cont.*	G(γ,t) [Pa] *cont.*	γ [%] *cont.*	Time [s] *cont.*	G(γ,t) [Pa] *cont.*	γ [%] *cont.*
0.001	0	0	0.145	13286.6	100.199	0.285	7629.64	100.199
0.01	48190.2	4.85252	0.15	12884.3	100.199	0.29	7531.26	100.199
0.015	75977.1	20.7183	0.155	12509.9	100.289	0.295	7432.87	100.199
0.02	68968	37.7636	0.16	12187.7	100.199	0.3	7334.49	100.199
0.025	61113	53.267	0.165	11863.9	100.199	0.305	7239.52	100.289
0.03	59160.5	66.1594	0.17	11549.2	100.289	0.31	7167.31	100.199
0.035	54991.7	76.1076	0.175	11285	100.199	0.315	7072.5	100.289
0.04	50680.2	83.5136	0.18	11010.1	100.289	0.32	6990.23	100.199
0.045	46214.3	88.7779	0.185	10765	100.199	0.325	6916.48	100.199
0.05	41919.4	92.5259	0.19	10539.1	100.199	0.33	6837.77	100.199
0.055	38030.2	95.1117	0.195	10323.4	100.199	0.335	6748.2	100.289
0.06	34581.5	96.8065	0.2	10098.3	100.289	0.34	6680.36	100.199
0.065	31542.3	97.9673	0.205	9902.33	100.289	0.345	6606.61	100.199
0.07	28876.9	98.7711	0.21	9724.96	100.199	0.35	6527.9	100.199
0.075	26602.9	99.3052	0.215	9524.61	100.289	0.355	6454.15	100.199
0.08	24653.2	99.6621	0.22	9347.68	100.289	0.36	6390.17	100.199
0.085	22954.3	99.842	0.225	9198.65	100.199	0.365	6321.37	100.199
0.09	21498.6	100.019	0.23	9041.24	100.199	0.37	6247.62	100.199
0.095	20221.8	100.109	0.235	8878.87	100.199	0.375	6188	100.289
0.1	19131.9	100.109	0.24	8728.5	100.289	0.38	6134.52	100.199
0.105	18153.1	100.199	0.245	8590.89	100.289	0.385	6070.54	100.199
0.11	17299.7	100.199	0.25	8448.32	100.289	0.39	6016.46	100.199
0.115	16544.2	100.199	0.255	8315.66	100.289	0.395	5967.2	100.199
0.12	15857.1	100.199	0.26	8205.06	100.199	0.4	5903.36	100.199
0.125	15258.7	100.199	0.265	8074.95	100.289	0.405	5844.33	100.199
0.13	14699.4	100.199	0.27	7957	100.289	0.41	5795.06	100.199
0.135	14166.7	100.289	0.275	7860.8	100.199	0.415	5730.89	100.289
0.14	13706	100.289	0.28	7747.7	100.199	0.42	5681.96	100.199

Time [s] *cont.*	G(γ,t) [Pa] *cont.*	γ [%] *cont.*	Time [s] *cont.*	G(γ,t) [Pa] *cont.*	γ [%] *cont.*	Time [s] *cont.*	G(γ,t) [Pa] *cont.*	γ [%] *cont.*
0.425	5637.55	100.289	0.58	4467.12	100.199	0.735	3734.29	100.199
0.43	5593.49	100.199	0.585	4428.75	100.289	0.74	3714.61	100.199
0.435	5544.23	100.199	0.59	4404.14	100.289	0.745	3696.57	100.289
0.44	5500.07	100.199	0.595	4384.48	100.289	0.75	3672.78	100.199
0.445	5460.71	100.199	0.6	4354.99	100.289	0.755	3648.22	100.199
0.45	5406.49	100.199	0.605	4325.51	100.289	0.76	3635.9	100.199
0.455	5357.37	100.199	0.61	4305.85	100.289	0.765	3616.23	100.199
0.46	5318.02	100.199	0.615	4280.27	100.199	0.77	3594.15	100.199
0.465	5273.71	100.199	0.62	4245.8	100.199	0.775	3584.31	100.199
0.47	5219.64	100.199	0.625	4226.12	100.199	0.78	3571.99	100.199
0.475	5180.59	100.289	0.63	4197.8	100.289	0.785	3549.84	100.199
0.48	5140.93	100.199	0.635	4168.31	100.289	0.79	3526.99	100.289
0.485	5092.05	100.289	0.64	4138.82	100.289	0.795	3520.32	100.199
0.49	5052.73	100.289	0.645	4124.04	100.289	0.8	3495.76	100.199
0.495	5027.83	100.199	0.65	4093.34	100.199	0.805	3476.09	100.199
0.5	4983.52	100.199	0.655	4065.06	100.289	0.81	3466.25	100.199
0.505	4944.17	100.199	0.66	4050.36	100.289	0.815	3449.05	100.199
0.51	4914.73	100.199	0.665	4029.43	100.199	0.82	3429.37	100.199
0.515	4871	100.289	0.67	3998.73	100.289	0.825	3417.06	100.199
0.52	4831.06	100.199	0.675	3981.55	100.289	0.83	3404.74	100.199
0.525	4801.55	100.199	0.68	3965.45	100.199	0.835	3382.66	100.199
0.53	4772.11	100.199	0.685	3938.41	100.199	0.84	3367.32	100.289
0.535	4728.51	100.289	0.69	3913.85	100.199	0.845	3360.51	100.199
0.54	4699.02	100.289	0.695	3899.06	100.199	0.85	3337.83	100.289
0.545	4678.61	100.199	0.7	3872.02	100.199	0.855	3323.63	100.199
0.55	4644.21	100.199	0.705	3846.41	100.289	0.86	3310.82	100.289
0.555	4610.56	100.289	0.71	3834.11	100.289	0.865	3296.52	100.199
0.56	4590.06	100.199	0.715	3817.87	100.199	0.87	3274.44	100.199
0.565	4555.67	100.199	0.72	3787.44	100.289	0.875	3257.24	100.199
0.57	4521.27	100.199	0.725	3776.12	100.199	0.88	3246.89	100.289
0.575	4496.64	100.199	0.73	3761.32	100.199	0.885	3230.13	100.199

B.6. Affinity PL1840

Stress Relaxation

T=150°C; strain=5.0 [strain units]; fixture diameter=10 [mm]; cone angle=0.035 [rad]

Time [s]	G(γ,t) [Pa]	γ [%]	Time [s] *cont.*	G(γ,t) [Pa] *cont.*	γ [%] *cont.*	Time [s] *cont.*	G(γ,t) [Pa] *cont.*	γ [%] *cont.*
0.001	0	0	0.145	1308.81	501.232	0.285	735.115	501.232
0.01	27645.7	11.3317	0.15	1270.47	501.232	0.29	725.777	501.232
0.015	14318.7	66.6049	0.155	1235.1	501.232	0.295	714.968	501.232
0.02	9272.11	150.52	0.16	1199.7	501.232	0.3	706.605	501.232
0.025	6050.09	230.681	0.165	1167.24	501.232	0.305	698.258	501.232
0.03	5127.06	301.166	0.17	1138.74	501.232	0.31	687.929	501.232
0.035	4776.78	357.417	0.175	1109.23	501.232	0.315	678.591	501.232
0.04	4367.58	400.131	0.18	1082.68	501.232	0.32	671.7	501.232
0.045	4091.51	431.455	0.185	1059.08	501.232	0.325	662.362	501.232
0.05	3785.33	453.886	0.19	1035.48	501.232	0.33	652.528	501.232
0.055	3502.56	469.199	0.195	1011.88	501.232	0.335	645.157	501.232
0.06	3227.9	479.88	0.2	992.246	501.232	0.34	636.794	501.232
0.065	2980.9	486.997	0.205	973.554	501.232	0.345	627.456	501.232
0.07	2758.85	491.978	0.21	952.911	501.232	0.35	620.085	501.232
0.075	2560.34	495.183	0.215	932.253	501.232	0.355	613.689	501.232
0.08	2385.26	497.319	0.22	916.519	501.232	0.36	604.846	501.232
0.085	2232.56	498.747	0.225	897.843	501.232	0.365	597.475	501.232
0.09	2099.46	499.455	0.23	879.167	501.232	0.37	593.046	501.232
0.095	1978.59	500.163	0.235	864.409	501.232	0.375	585.674	501.232
0.1	1876.98	500.523	0.24	849.666	501.232	0.38	578.303	501.232
0.105	1783.39	500.883	0.245	833.932	501.232	0.385	574.37	501.232
0.11	1700.94	500.883	0.25	819.189	501.232	0.39	569.445	501.232
0.115	1625.23	501.232	0.255	806.398	501.232	0.395	562.074	501.232
0.12	1563.59	500.883	0.26	792.646	501.232	0.4	556.669	501.232
0.125	1502.51	501.232	0.265	779.374	501.232	0.405	552.736	501.232
0.13	1446.48	501.232	0.27	768.55	501.232	0.41	546.835	501.232
0.135	1397.33	501.232	0.275	756.254	501.232	0.415	541.431	501.232
0.14	1352.08	501.232	0.28	743.973	501.232	0.42	537.497	501.232

Time [s] *cont.*	G(γ,t) [Pa] *cont.*	γ [%] *cont.*	Time [s] *cont.*	G(γ,t) [Pa] *cont.*	γ [%] *cont.*	Time [s] *cont.*	G(γ,t) [Pa] *cont.*	γ [%] *cont.*
0.425	532.573	501.232	0.58	412.137	501.232	0.735	340.112	501.232
0.43	526.688	501.232	0.585	409.187	501.232	0.74	338.888	501.232
0.435	523.235	501.232	0.59	406.725	501.232	0.745	335.443	501.232
0.44	518.325	501.232	0.595	402.056	501.232	0.75	332.74	501.232
0.445	512.425	501.232	0.6	399.106	501.232	0.755	332.252	501.232
0.45	508.492	501.232	0.605	398.123	501.232	0.76	330.286	501.232
0.455	504.558	501.232	0.61	395.173	501.232	0.765	327.336	501.232
0.46	498.163	501.232	0.615	391.735	501.232	0.77	327.824	501.232
0.465	492.263	501.232	0.62	390.751	501.232	0.775	327.088	501.232
0.47	488.825	501.232	0.625	388.297	501.232	0.78	325.121	501.232
0.475	483.908	501.232	0.63	384.363	501.232	0.785	324.386	501.232
0.48	478.008	501.232	0.635	382.637	501.232	0.79	323.402	501.232
0.485	475.065	501.232	0.64	380.918	501.232	0.795	320.452	501.232
0.49	472.603	501.232	0.645	377.232	501.232	0.8	318.238	501.232
0.495	467.686	501.232	0.65	375.017	501.232	0.805	317.502	501.232
0.5	463.265	501.232	0.655	374.777	501.232	0.81	314.056	501.232
0.505	461.298	501.232	0.66	372.315	501.232	0.815	310.618	501.232
0.51	456.869	501.232	0.665	369.613	501.232	0.82	310.866	501.232
0.515	451.96	501.232	0.67	369.365	501.232	0.825	310.131	501.232
0.52	449.993	501.232	0.675	367.894	501.232	0.83	307.421	501.232
0.525	447.043	501.232	0.68	364.2	501.232	0.835	307.18	501.232
0.53	443.11	501.232	0.685	361.498	501.232	0.84	306.933	501.232
0.535	441.631	501.232	0.69	359.531	501.232	0.845	304.718	501.232
0.54	438.681	501.232	0.695	355.598	501.232	0.85	302.264	501.232
0.545	434.259	501.232	0.7	351.912	501.232	0.855	301.768	501.232
0.55	432.293	501.232	0.705	351.176	501.232	0.86	299.801	501.232
0.555	430.814	501.232	0.71	348.474	501.232	0.865	296.611	501.232
0.56	427.376	501.232	0.715	346.012	501.232	0.87	296.611	501.232
0.565	423.442	501.232	0.72	345.772	501.232	0.875	295.628	501.232
0.57	420.988	501.232	0.725	343.557	501.232	0.88	293.661	501.232
0.575	417.542	501.232	0.73	340.855	501.232	0.885	292.918	501.232

B.6. Affinity PL1840

Stress Relaxation

T=150°C; strain=7.5 [strain units]; fixture diameter=10 [mm]; cone angle=0.035 [rad]

Time [s]	G(γ,t) [Pa]	γ [%]	Time [s] *cont.*	G(γ,t) [Pa] *cont.*	γ [%] *cont.*	Time [s] *cont.*	G(γ,t) [Pa] *cont.*	γ [%] *cont.*
0.001	0	0	0.145	1867.74	751.847	0.285	1000.99	751.15
0.01	27225.7	11.751	0.15	1803.68	751.847	0.29	987.201	751.15
0.015	16368	74.5014	0.155	1747.43	751.847	0.295	971.212	751.847
0.02	12026.6	187.962	0.16	1693.83	751.847	0.3	957.688	751.15
0.025	10639.2	310.245	0.165	1644.35	751.15	0.305	943.688	751.847
0.03	9717.03	420.425	0.17	1597.06	751.847	0.31	931.441	751.15
0.035	9414.53	511.204	0.175	1553.9	751.847	0.315	917.656	751.15
0.04	8732.23	581.33	0.18	1512.07	751.847	0.32	905.014	751.847
0.045	7986.1	633.668	0.185	1475.47	751.847	0.325	894.695	751.15
0.05	7217.02	670.681	0.19	1440.16	751.847	0.33	882.232	751.15
0.055	6487.2	697.025	0.195	1407.44	751.15	0.335	870.264	751.847
0.06	5819.61	714.834	0.2	1373.42	751.15	0.34	859.775	751.847
0.065	5219.79	727.651	0.205	1342.08	751.847	0.345	849.433	751.15
0.07	4704.41	735.477	0.21	1313.29	751.847	0.35	838.934	751.15
0.075	4257.14	741.166	0.215	1284.55	751.847	0.355	829.628	751.847
0.08	3874.97	744.741	0.22	1258.38	751.847	0.36	819.8	751.847
0.085	3555.9	746.877	0.225	1233.54	751.847	0.365	808.65	751.847
0.09	3283.76	748.294	0.23	1208.7	751.847	0.37	800.224	751.15
0.095	3049.35	749.711	0.235	1185.16	751.847	0.375	791.689	751.15
0.1	2849.88	750.431	0.24	1165.32	751.15	0.38	781.851	751.15
0.105	2679.65	751.15	0.245	1142	751.847	0.385	772.598	751.847
0.11	2530.46	751.15	0.25	1121.08	751.847	0.39	765.441	751.15
0.115	2399.55	751.15	0.255	1102.79	751.847	0.395	755.563	751.847
0.12	2286.98	751.15	0.26	1084.47	751.847	0.4	747.036	751.847
0.125	2184.92	751.15	0.265	1065.94	751.15	0.405	739.83	751.847
0.13	2093.28	751.15	0.27	1048.56	751.847	0.41	732.642	751.15
0.135	2010.26	751.847	0.275	1034.45	751.15	0.415	723.435	751.847
0.14	1937.55	751.15	0.28	1016.73	751.15	0.42	716.233	751.15

Time [s] *cont.*	G(γ,t) [Pa] *cont.*	γ [%] *cont.*	Time [s] *cont.*	G(γ,t) [Pa] *cont.*	γ [%] *cont.*	Time [s] *cont.*	G(γ,t) [Pa] *cont.*	γ [%] *cont.*
0.425	708.362	751.847	0.58	539.904	751.847	0.735	438.966	751.847
0.43	700.495	751.847	0.585	535.32	751.847	0.74	437.324	751.847
0.435	693.289	751.847	0.59	531.717	751.847	0.745	435.363	751.847
0.44	687.384	751.847	0.595	527.943	751.15	0.75	432.41	751.847
0.445	679.517	751.847	0.6	523.676	751.15	0.755	430.518	751.15
0.45	671.65	751.847	0.605	521.051	751.15	0.76	428.544	751.15
0.455	665.765	751.847	0.61	518.106	751.15	0.765	425.599	751.15
0.46	660.472	751.15	0.615	513.361	751.847	0.77	422.902	751.847
0.465	652.653	751.847	0.62	510.562	751.15	0.775	421.921	751.847
0.47	648.01	751.15	0.625	507.466	751.847	0.78	420.019	751.15
0.475	641.503	751.847	0.63	503.853	751.847	0.785	417.337	751.847
0.48	634.958	751.847	0.635	500.714	751.15	0.79	416.412	751.15
0.485	629.052	751.847	0.64	497.627	751.847	0.795	414.769	751.15
0.49	625.048	751.15	0.645	494.152	751.15	0.8	411.814	751.15
0.495	619.224	751.847	0.65	489.564	751.15	0.805	410.451	751.847
0.5	613.979	751.847	0.655	486.488	751.847	0.81	408.489	751.847
0.505	609.385	751.847	0.66	484.976	751.15	0.815	405.252	751.15
0.51	604.801	751.847	0.665	481.359	751.15	0.82	402.307	751.15
0.515	598.245	751.847	0.67	478.735	751.15	0.825	401.325	751.15
0.52	594.312	751.847	0.675	475.348	751.847	0.83	398.33	751.847
0.525	589.728	751.847	0.68	471.852	751.15	0.835	396.075	751.15
0.53	583.823	751.847	0.685	468.246	751.15	0.84	394.397	751.847
0.535	577.928	751.847	0.69	466.17	751.847	0.845	393.086	751.847
0.54	573.334	751.847	0.695	463.217	751.847	0.85	390.133	751.847
0.545	568.099	751.847	0.7	459.284	751.847	0.855	389.473	751.847
0.55	563.505	751.847	0.705	457.085	751.15	0.86	388.161	751.847
0.555	559.572	751.847	0.71	454.461	751.15	0.865	385.897	751.15
0.56	555.638	751.847	0.715	450.854	751.15	0.87	382.927	751.847
0.565	550.394	751.847	0.72	448.23	751.15	0.875	381.616	751.847
0.57	547.121	751.847	0.725	446.266	751.15	0.88	379.666	751.15
0.575	544.498	751.847	0.73	442.649	751.15	0.885	377.022	751.847

B.6. Affinity PL1840

Stress Relaxation

T=150°C; strain=10.0 [strain units]; fixture diameter=10 [mm]; cone angle=0.035 [rad]

Time [s]	G(γ,t) [Pa]	γ [%]	Time [s] *cont.*	G(γ,t) [Pa] *cont.*	γ [%] *cont.*	Time [s] *cont.*	G(γ,t) [Pa] *cont.*	γ [%] *cont.*
0.001	0	0	0.145	1586.19	1001.77	0.285	854.059	1001.77
0.01	27272.8	11.9077	0.15	1530.24	1001.77	0.29	843.272	1001.77
0.015	15812.4	78.2943	0.155	1480.18	1001.77	0.295	830.502	1001.77
0.02	11553.5	210.033	0.16	1434.06	1001.77	0.3	817.747	1001.77
0.025	10542.1	369.515	0.165	1389.92	1001.77	0.305	806.96	1001.77
0.03	9959.28	520.458	0.17	1350.65	1001.77	0.31	796.218	1001.77
0.035	9404.16	648.61	0.175	1314.35	1001.77	0.315	785.386	1001.77
0.04	8760.22	749.711	0.18	1279.02	1001.77	0.32	775.065	1001.77
0.045	7944.76	825.177	0.185	1246.63	1001.77	0.325	766.201	1001.77
0.05	7119.12	880	0.19	1216.19	1001.77	0.33	756.361	1001.77
0.055	6332.25	919.172	0.195	1187.73	1001.77	0.335	746.52	1001.77
0.06	5606.74	946.223	0.2	1160.27	1001.77	0.34	738.167	1001.77
0.065	4957.46	965.45	0.205	1134.73	1001.77	0.345	729.799	1001.77
0.07	4405.29	977.548	0.21	1111.2	1001.77	0.35	721.431	1001.77
0.075	3932.44	986.093	0.215	1087.65	1001.77	0.355	713.558	1001.77
0.08	3533.19	991.782	0.22	1066.04	1001.77	0.36	706.182	1001.77
0.085	3200.49	995.357	0.225	1045.43	1001.77	0.365	697.829	1001.77
0.09	2925.55	997.493	0.23	1025.81	1001.77	0.37	689.956	1001.77
0.095	2693.05	998.91	0.235	1006.19	1001.77	0.375	683.06	1001.77
0.1	2496.6	1000.33	0.24	988.521	1001.77	0.38	675.188	1001.77
0.105	2331.77	1001.05	0.245	970.853	1001.77	0.385	667.812	1001.77
0.11	2192.31	1001.05	0.25	953.185	1001.77	0.39	661.412	1001.77
0.115	2070.54	1001.05	0.255	938.462	1001.77	0.395	654.531	1001.77
0.12	1963.04	1001.77	0.26	923.739	1001.77	0.4	646.658	1001.77
0.125	1870.8	1001.77	0.265	909.016	1001.77	0.405	640.258	1001.77
0.13	1788.35	1001.77	0.27	894.292	1001.77	0.41	633.873	1001.77
0.135	1713.77	1001.77	0.275	881.537	1001.77	0.415	627.969	1001.77
0.14	1647.04	1001.77	0.28	867.806	1001.77	0.42	621.073	1001.77

Time [s] *cont.*	G(γ,t) [Pa] *cont.*	γ [%] *cont.*	Time [s] *cont.*	G(γ,t) [Pa] *cont.*	γ [%] *cont.*	Time [s] *cont.*	G(γ,t) [Pa] *cont.*	γ [%] *cont.*
0.425	616.16	1001.77	0.58	482.345	1001.77	0.735	400.436	1001.77
0.43	610.256	1001.77	0.585	478.905	1001.77	0.74	398.716	1001.77
0.435	604.352	1001.77	0.59	476.937	1001.77	0.745	396.748	1001.77
0.44	599.439	1001.77	0.595	474.48	1001.77	0.75	393.796	1001.77
0.445	594.511	1001.77	0.6	470.544	1001.77	0.755	391.828	1001.77
0.45	588.607	1001.77	0.605	467.096	1001.77	0.76	390.356	1001.77
0.455	583.694	1001.77	0.61	464.64	1001.77	0.765	387.892	1001.77
0.46	578.767	1001.77	0.615	460.704	1001.77	0.77	385.435	1001.77
0.465	573.358	1001.77	0.62	456.767	1001.77	0.775	384.203	1001.77
0.47	568.926	1001.77	0.625	454.304	1001.77	0.78	382.235	1001.77
0.475	564.99	1001.77	0.63	451.359	1001.77	0.785	379.283	1001.77
0.48	560.077	1001.77	0.635	447.911	1001.77	0.79	377.811	1001.77
0.485	554.669	1001.77	0.64	445.943	1001.77	0.795	376.331	1001.77
0.49	551.228	1001.77	0.645	442.991	1001.77	0.8	373.875	1001.77
0.495	546.796	1001.77	0.65	440.039	1001.77	0.805	371.907	1001.77
0.5	541.869	1001.77	0.655	437.582	1001.77	0.81	371.17	1001.77
0.505	537.452	1001.77	0.66	436.102	1001.77	0.815	369.691	1001.77
0.51	533.516	1001.77	0.665	432.662	1001.77	0.82	367.723	1001.77
0.515	529.084	1001.77	0.67	429.214	1001.77	0.825	367.234	1001.77
0.52	524.171	1001.77	0.675	427.254	1001.77	0.83	365.754	1001.77
0.525	521.211	1001.77	0.68	424.79	1001.77	0.835	363.298	1001.77
0.53	516.779	1001.77	0.685	421.838	1001.77	0.84	361.818	1001.77
0.535	512.362	1001.77	0.69	420.365	1001.77	0.845	360.098	1001.77
0.54	509.403	1001.77	0.695	418.885	1001.77	0.85	357.642	1001.77
0.545	506.939	1001.77	0.7	415.933	1001.77	0.855	355.426	1001.77
0.55	502.522	1001.77	0.705	413.965	1001.77	0.86	354.69	1001.77
0.555	499.081	1001.77	0.71	412.493	1001.77	0.865	352.474	1001.77
0.56	496.122	1001.77	0.715	410.029	1001.77	0.87	350.017	1001.77
0.565	492.186	1001.77	0.72	407.077	1001.77	0.875	348.537	1001.77
0.57	488.745	1001.77	0.725	405.605	1001.77	0.88	347.065	1001.77
0.575	485.793	1001.77	0.73	403.636	1001.77	0.885	344.849	1001.77

B.6. Affinity PL1840

Stress Relaxation

T=150°C; strain=12.5 [strain units]; fixture diameter=10 [mm]; cone angle=0.035 [rad]

Time [s]	G(γ,t) [Pa]	γ [%]	Time [s] *cont.*	G(γ,t) [Pa] *cont.*	γ [%] *cont.*	Time [s] *cont.*	G(γ,t) [Pa] *cont.*	γ [%] *cont.*
0.001	0	0	0.145	1462.62	1251.66	0.285	765.133	1251.66
0.01	69035.7	12.1649	0.15	1407.56	1251.66	0.29	754.288	1251.66
0.015	70681.4	80.7916	0.155	1358.38	1251.66	0.295	743.939	1251.66
0.02	37211	223.738	0.16	1314.1	1251.66	0.3	732.598	1251.66
0.025	23679.6	410.452	0.165	1271.8	1251.66	0.305	722.73	1251.66
0.03	17635.2	601.264	0.17	1233.44	1251.66	0.31	713.853	1251.66
0.035	14084	767.52	0.175	1198.02	1251.66	0.315	704	1251.66
0.04	11690.7	902.801	0.18	1164.59	1251.66	0.32	694.131	1251.66
0.045	9931.82	1005.32	0.185	1133.1	1251.66	0.325	685.254	1251.66
0.05	8432.68	1081.5	0.19	1103.6	1251.66	0.33	677.864	1251.66
0.055	7200.37	1135.61	0.195	1077.02	1251.66	0.335	668.987	1251.66
0.06	6172.14	1173.34	0.2	1050.46	1251.66	0.34	661.101	1251.66
0.065	5325.53	1198.98	0.205	1025.89	1251.66	0.345	653.215	1251.66
0.07	4620.15	1216.78	0.21	1004.23	1251.66	0.35	645.81	1251.66
0.075	4041.65	1228.88	0.215	982.599	1251.66	0.355	637.925	1251.66
0.08	3574.06	1236.71	0.22	960.954	1251.66	0.36	631.511	1251.66
0.085	3186.86	1241.7	0.225	941.278	1251.66	0.365	624.616	1251.66
0.09	2873.21	1245.25	0.23	923.568	1251.66	0.37	617.211	1251.66
0.095	2617.56	1247.39	0.235	904.883	1251.66	0.375	611.789	1251.66
0.1	2404.18	1249.53	0.24	888.165	1251.66	0.38	604.895	1251.66
0.105	2225.54	1250.25	0.245	873.4	1251.66	0.385	598.481	1251.66
0.11	2076.65	1250.94	0.25	856.682	1251.66	0.39	592.563	1251.66
0.115	1950.68	1250.94	0.255	841.932	1251.66	0.395	587.636	1251.66
0.12	1840.45	1250.94	0.26	828.159	1251.66	0.4	580.727	1251.66
0.125	1746.93	1251.66	0.265	814.385	1251.66	0.405	574.809	1251.66
0.13	1662.33	1251.66	0.27	802.113	1251.66	0.41	569.882	1251.66
0.135	1587.56	1251.66	0.275	789.796	1251.66	0.415	564.955	1251.66
0.14	1521.65	1251.66	0.28	776.969	1251.66	0.42	558.046	1251.66

Time [s] *cont.*	G(γ,t) [Pa] *cont.*	γ [%] *cont.*	Time [s] *cont.*	G(γ,t) [Pa] *cont.*	γ [%] *cont.*	Time [s] *cont.*	G(γ,t) [Pa] *cont.*	γ [%] *cont.*
0.425	553.615	1251.66	0.58	435.269	1251.66	0.735	364.019	1251.66
0.43	548.177	1251.66	0.585	431.326	1251.66	0.74	361.308	1251.66
0.435	543.251	1251.66	0.59	428.862	1251.66	0.745	359.828	1251.66
0.44	537.828	1251.66	0.595	427.383	1251.66	0.75	357.613	1251.66
0.445	534.374	1251.66	0.6	424.424	1251.66	0.755	354.654	1251.66
0.45	528.951	1251.66	0.605	421.953	1251.66	0.76	353.174	1251.66
0.455	524.025	1251.66	0.61	419.49	1251.66	0.765	352.183	1251.66
0.46	520.074	1251.66	0.615	416.531	1251.66	0.77	349.472	1251.66
0.465	515.643	1251.66	0.62	414.067	1251.66	0.775	347.504	1251.66
0.47	510.716	1251.66	0.625	412.092	1251.66	0.78	346.761	1251.66
0.475	507.262	1251.66	0.63	409.133	1251.66	0.785	344.545	1251.66
0.48	503.807	1251.66	0.635	406.182	1251.66	0.79	342.57	1251.66
0.485	499.376	1251.66	0.64	403.223	1251.66	0.795	341.338	1251.66
0.49	495.426	1251.66	0.645	401.495	1251.66	0.8	339.123	1251.66
0.495	492.467	1251.66	0.65	399.032	1251.66	0.805	337.395	1251.66
0.5	488.524	1251.66	0.655	395.825	1251.66	0.81	335.42	1251.66
0.505	484.085	1251.66	0.66	395.081	1251.66	0.815	333.941	1251.66
0.51	481.126	1251.66	0.665	392.37	1251.66	0.82	332.213	1251.66
0.515	477.183	1251.66	0.67	389.907	1251.66	0.825	330.982	1251.66
0.52	472.249	1251.66	0.675	387.932	1251.66	0.83	330.982	1251.66
0.525	469.786	1251.66	0.68	385.964	1251.66	0.835	329.014	1251.66
0.53	466.331	1251.66	0.685	382.757	1251.66	0.84	327.287	1251.66
0.535	462.884	1251.66	0.69	380.782	1251.66	0.845	326.543	1251.66
0.54	459.429	1251.66	0.695	379.062	1251.66	0.85	325.064	1251.66
0.545	456.966	1251.66	0.7	376.343	1251.66	0.855	322.6	1251.66
0.55	453.511	1251.66	0.705	374.128	1251.66	0.86	321.864	1251.66
0.555	449.568	1251.66	0.71	372.401	1251.66	0.865	320.633	1251.66
0.56	446.609	1251.66	0.715	371.169	1251.66	0.87	318.905	1251.66
0.565	444.146	1251.66	0.72	368.458	1251.66	0.875	316.682	1251.66
0.57	440.691	1251.66	0.725	367.474	1251.66	0.88	315.946	1251.66
0.575	437.244	1251.66	0.73	365.747	1251.66	0.885	314.219	1251.66

Appendix C: Film-Casting Measurements for the HDPE-based PE Resins

C.1. Lupolen 1840 H

Film-Casting

T = 190ºC; DR = 1.18; γ = 14.54 [1/s]; ε = 0.003592 [1/s]; strain = 0.1655

Distance to frostline = 69.4 [mm]

Dist. from die [mm]	Film width [mm]	Half-width [mm]	Dist. from die [mm] *continued*	Film width [mm] *continued*	Half-width [mm] *continued*
0	101.6	50.8	90.233	75.25	37.625
2.239	99.885	49.9425	100.565	74.567	37.2835
3.961	98.677	49.3385	117.44	74.056	37.028
6.2	96.779	48.3895	140.864	73.375	36.6875
8.955	94.537	47.2685	163.421	72.338	36.169
12.399	91.953	45.9765	194.072	72.16	36.08
15.326	89.715	44.8575			
18.942	87.303	43.6515			
22.558	85.236	42.618			
24.797	84.032	42.016			
29.274	82.137	41.0685			
33.234	80.759	40.3795			
37.194	79.898	39.949			
42.532	78.865	39.4325			
47.009	78.004	39.002			
50.797	77.316	38.658			
56.307	76.456	38.228			
60.956	75.939	37.9695			
65.092	75.766	37.883			
69.397	75.422	37.711			
75.596	75.423	37.7115			

C.1. Lupolen 1840 H

Film-Casting

T = 190ºC; DR = 1.76; γ = 14.54 [1/s]; ε = 0.01438 [1/s]; strain = 0.5653

Distance to frostline = 73.2 [mm]

Dist. from die [mm]	Film width [mm]	Half-width [mm]	Dist. from die [mm] *continued*	Film width [mm] *continued*	Half-width [mm] *continued*
0	101.6	50.8	63.588	70.908	35.454
1.852	100.453	50.2265	68.968	70.291	35.1455
4.145	97.808	48.904	75.583	69.85	34.925
6.879	95.161	47.5805	87.136	69.056	34.528
9.26	92.78	46.39	96.396	68.879	34.4395
12.17	90.135	45.0675	109.362	68.527	34.2635
14.816	88.018	44.009	126.296	67.91	33.955
17.638	85.813	42.9065	144.552	67.645	33.8225
20.725	83.696	41.848	194.735	66.939	33.4695
23.812	81.932	40.966			
26.193	80.786	40.393			
29.28	79.463	39.7315			
32.279	78.228	39.114			
35.542	77.17	38.585			
38.718	76.112	38.056			
41.805	75.23	37.615			
44.539	74.26	37.13			
48.243	73.378	36.689			
52.035	72.586	36.293			
56.18	71.879	35.9395			
59.884	71.261	35.6305			

C.1. Lupolen 1840 H

Film-Casting

T = 190ºC; DR = 2.96; γ = 14.54 [1/s]; ε = 0.03472 [1/s]; strain = 1.0851

Distance to frostline = 78.2 [mm]

Dist. from die [mm]	Film width [mm]	Half-width [mm]	Dist. from die [mm] *continued*	Film width [mm] *continued*	Half-width [mm] *continued*
0	101.6	50.8	75.651	65.683	32.8415
1.937	99.093	49.5465	82.054	65.531	32.7655
3.873	96.846	48.423	92.18	65.378	32.689
5.66	94.902	47.451	105.88	65.079	32.5395
8.043	92.214	46.107	122.71	64.78	32.39
10.426	89.973	44.9865	141.473	64.481	32.2405
13.404	87.438	43.719	194.189	63.588	31.794
17.425	84.011	42.0055			
20.552	81.48	40.74			
24.573	79.24	39.62			
27.551	77.451	38.7255			
31.572	75.962	37.981			
34.699	74.625	37.3125			
38.124	73.431	36.7155			
42.443	71.934	35.967			
47.357	70.45	35.225			
52.271	69.554	34.777			
57.632	68.369	34.1845			
61.802	67.628	33.814			
65.823	67.029	33.5145			
70.588	66.425	33.2125			

C.1. Lupolen 1840 H

Film-Casting

T = 190ºC; DR = 5.93; γ = 14.54 [1/s]; ε = 0.04829 [1/s]; strain = 1.7801

Distance to frostline = 141.4 [mm]

Dist. from die [mm]	Film width [mm]	Half-width [mm]	Dist. from die [mm] *continued*	Film width [mm] *continued*	Half-width [mm] *continued*
0	101.6	50.8	44.475	68.127	34.0635
1.339	99.069	49.5345	49.235	66.64	33.32
2.38	97.582	48.791	53.846	65.45	32.725
4.016	95.944	47.972	58.606	64.26	32.13
5.503	93.862	46.931	65.3	62.921	31.4605
7.288	91.779	45.8895	70.804	62.029	31.0145
9.222	89.4	44.7	79.134	60.987	30.4935
11.156	87.317	43.6585	86.72	59.946	29.973
13.536	84.788	42.394	94.604	59.202	29.601
16.065	82.556	41.278	101	58.905	29.4525
18.742	80.622	40.311	110.074	58.459	29.2295
20.378	79.73	39.865	120.338	58.459	29.2295
22.312	78.391	39.1955	128.37	58.31	29.155
24.097	77.499	38.7495	145.476	58.31	29.155
26.626	75.714	37.857	197.39	58.161	29.0805
28.113	74.821	37.4105			
30.047	73.631	36.8155			
32.576	72.441	36.2205			
35.253	71.549	35.7745			
38.079	70.359	35.1795			
40.905	69.317	34.6585			

C.1. Lupolen 1840 H

Film-Casting

T = 190ºC; DR = 8.89; γ = 14.54 [1/s]; ε = 0.07728 [1/s]; strain = 2.1849

Distance to frostline = 141.4 [mm]

Dist. from die [mm]	Film width [mm]	Half-width [mm]	Dist. from die [mm] *continued*	Film width [mm] *continued*	Half-width [mm] *continued*
0	101.6	50.8	57.573	63.455	31.7275
1.567	98.74	49.37	62.142	62.541	31.2705
3.656	96.126	48.063	66.842	61.624	30.812
5.745	92.991	46.4955	71.542	60.839	30.4195
7.834	90.638	45.319	74.675	60.449	30.2245
9.792	88.416	44.208	79.766	59.532	29.766
12.142	86.06	43.03	84.074	59.271	29.6355
14.753	83.711	41.8555	89.165	58.487	29.2435
16.972	81.492	40.746	95.692	58.227	29.1135
19.583	79.531	39.7655	102.219	57.313	28.6565
22.586	77.831	38.9155	108.094	57.052	28.526
24.936	76.393	38.1965	117.102	56.529	28.2645
28.069	74.696	37.348	126.371	56.266	28.133
31.202	72.999	36.4995	140.47	55.744	27.872
33.682	71.691	35.8455	193.864	55.222	27.611
36.293	70.647	35.3235			
39.165	69.472	34.736			
42.037	68.556	34.278			
46.215	66.723	33.3615			
51.176	65.154	32.577			
55.354	63.977	31.9885			

C.1. Lupolen 1840 H

Film-Casting

T = 190ºC; DR = 11.86; γ = 14.54 [1/s]; ε = 0.1064 [1/s]; strain = 2.4738

Distance to frostline = 141.4 [mm]

Dist. from die [mm]	Film width [mm]	Half-width [mm]	Dist. from die [mm] *continued*	Film width [mm] *continued*	Half-width [mm] *continued*
0	101.6	50.8	53.33	64.405	32.2025
1.424	98.592	49.296	56.653	63.614	31.807
2.69	96.693	48.3465	61.242	62.506	31.253
4.589	93.689	46.8445	64.882	61.398	30.699
6.646	90.999	45.4995	69.629	60.449	30.2245
8.545	88.94	44.47	74.218	59.658	29.829
10.919	86.406	43.203	77.541	59.183	29.5915
13.451	84.028	42.014	82.13	58.392	29.196
15.192	82.446	41.223	87.194	57.759	28.8795
16.933	80.863	40.4315	95.739	56.968	28.484
19.465	78.964	39.482	103.335	56.493	28.2465
21.839	77.539	38.7695	109.823	56.018	28.009
25.004	75.798	37.899	116.786	55.86	27.93
28.327	73.9	36.95	126.122	55.227	27.6135
30.859	72.634	36.317	200.18	54.119	27.0595
33.233	71.842	35.921			
36.398	70.26	35.13			
40.038	68.994	34.497			
43.045	67.886	33.943			
46.526	66.779	33.3895			
50.007	65.513	32.7565			

C.1. Lupolen 1840 H

Film-Casting

T = 190ºC; DR = 17.79; γ = 14.54 [1/s]; ε = 0.1645 [1/s]; strain = 2.8794

Distance to frostline = 141.4 [mm]

Dist. from die [mm]	Film width [mm]	Half-width [mm]	Dist. from die [mm] *continued*	Film width [mm] *continued*	Half-width [mm] *continued*
0	101.6	50.8	74.06	62.34	31.17
1.776	97.516	48.758	79.921	61.628	30.814
3.73	94.317	47.1585	85.427	61.273	30.6365
5.684	91.295	45.6475	91.11	60.74	30.37
8.526	88.272	44.136	98.036	60.384	30.192
12.256	84.72	42.36	106.738	60.029	30.0145
15.63	82.054	41.027	116.151	59.496	29.748
19.004	79.923	39.9615	128.228	58.612	29.306
22.023	78.147	39.0735	202.82	56.832	28.416
24.865	76.376	38.188			
28.595	74.42	37.21			
32.502	72.644	36.322			
36.409	70.689	35.3445			
40.316	69.445	34.7225			
43.868	68.556	34.278			
47.775	67.135	33.5675			
51.86	66.247	33.1235			
55.767	65.358	32.679			
58.964	64.649	32.3245			
63.404	63.761	31.8805			
69.087	62.875	31.4375			

C.2. LD 150

Film-Casting

T = 190ºC; DR = 1.18; γ = 14.54 [1/s]; ε = 0.004962 [1/s]; strain = 0.1655

Distance to frostline = 50.2 [mm]

Dist. from die [mm]	Film width [mm]	Half-width [mm]	Dist. from die [mm] *continued*	Film width [mm] *continued*	Half-width [mm] *continued*
0	101.6	50.8	112.137	76.091	38.0455
1.279	99.462	49.731	123.769	75.621	37.8105
2.791	97.948	48.974	139.59	75.522	37.761
4.424	96.551	48.2755	198.962	75.076	37.538
6.401	94.689	47.3445			
7.913	93.292	46.646			
10.007	91.661	45.8305			
11.868	90.496	45.248			
14.892	88.634	44.317			
17.221	87.237	43.6185			
20.71	85.377	42.6885			
25.246	83.632	41.816			
30.83	81.771	40.8855			
35.832	80.608	40.304			
40.717	79.561	39.7805			
48.859	78.517	39.2585			
57.467	77.704	38.852			
66.656	77.355	38.6775			
77.939	76.778	38.389			
90.036	76.658	38.329			
99.575	76.435	38.2175			

C.2. LD 150

Film-Casting

T = 190ºC; DR = 1.76; γ = 14.54 [1/s]; ε = 0.02046 [1/s]; strain = 0.5652

Distance to frostline = 51.4 [mm]

Dist. from die [mm]	Film width [mm]	Half-width [mm]	Dist. from die [mm] *continued*	Film width [mm] *continued*	Half-width [mm] *continued*
0	101.6	50.8	40.428	76.348	38.174
1.304	98.281	49.1405	42.799	75.874	37.937
2.845	96.739	48.3695	45.644	75.4	37.7
4.505	94.842	47.421	48.608	74.807	37.4035
5.928	93.775	46.8875	52.757	73.977	36.9885
7.588	92.353	46.1765	56.669	73.384	36.692
9.603	90.693	45.3465	62.715	72.91	36.455
11.144	89.389	44.6945	70.184	72.436	36.218
13.041	87.966	43.983	77.534	71.962	35.981
14.582	86.899	43.4495	86.781	71.725	35.8625
16.479	85.714	42.857	97.688	71.725	35.8625
18.732	84.41	42.205	114.878	71.369	35.6845
20.51	83.343	41.6715	129.223	71.013	35.5065
22.407	82.513	41.2565	145.228	71.369	35.6845
25.371	81.209	40.6045	200.711	70.065	35.0325
27.268	80.616	40.308			
29.283	79.905	39.9525			
31.18	79.075	39.5375			
33.433	78.245	39.1225			
35.804	77.534	38.767			
38.294	76.822	38.411			

C.2. LD 150

Film-Casting

T = 190ºC; DR = 2.96; γ = 14.54 [1/s]; ε = 0.05034 [1/s]; strain = 1.0851

Distance to frostline = 53.9 [mm]

Dist. from die [mm]	Film width [mm]	Half-width [mm]	Dist. from die [mm] *continued*	Film width [mm] *continued*	Half-width [mm] *continued*
0	101.6	50.8	46.438	71.967	35.9835
1.411	98.521	49.2605	49.389	71.325	35.6625
2.822	96.982	48.491	52.596	70.94	35.47
4.618	94.673	47.3365	57.214	70.171	35.0855
6.157	93.133	46.5665	60.934	69.786	34.893
7.44	91.851	45.9255	65.424	69.401	34.7005
9.236	90.055	45.0275	76.2	68.503	34.2515
10.775	88.515	44.2575	90.311	67.862	33.931
13.084	86.463	43.2315	104.422	67.605	33.8025
15.137	85.052	42.526	119.816	67.22	33.61
17.446	83.384	41.692	134.825	66.707	33.3535
19.37	82.229	41.1145	200.634	65.937	32.9685
21.936	80.946	40.473			
24.887	79.407	39.7035			
27.068	78.381	39.1905			
29.634	77.226	38.613			
32.328	76.328	38.164			
34.637	75.559	37.7795			
37.459	74.404	37.202			
39.768	73.891	36.9455			
43.616	72.736	36.368			

C.2. LD 150

Film-Casting

T = 190ºC; DR = 5.93; γ = 14.54 [1/s]; ε = 0.1276 [1/s]; strain = 1.7796

Distance to frostline = 53.5 [mm]

Dist. from die [mm]	Film width [mm]	Half-width [mm]	Dist. from die [mm] *continued*	Film width [mm] *continued*	Half-width [mm] *continued*
0	101.6	50.8	43.702	70.984	35.492
1.358	98.267	49.1335	47.035	69.997	34.9985
2.963	96.045	48.0225	50.368	69.379	34.6895
4.691	94.316	47.158	54.442	68.392	34.196
6.296	92.218	46.109	59.38	67.651	33.8255
7.654	90.613	45.3065	64.565	66.91	33.455
9.382	89.131	44.5655	70.861	66.293	33.1465
11.357	87.28	43.64	80.861	65.552	32.776
12.962	85.922	42.961	89.009	65.059	32.5295
15.061	84.193	42.0965	96.169	64.812	32.406
17.16	82.712	41.356	104.811	64.441	32.2205
19.382	81.231	40.6155	119.378	64.071	32.0355
21.481	79.996	39.998	133.575	63.577	31.7885
23.456	78.885	39.4425	155.179	63.454	31.727
25.678	77.897	38.9485	200.362	62.59	31.295
27.9	76.663	38.3315			
30.122	75.552	37.776			
32.344	74.935	37.4675			
34.813	73.824	36.912			
36.912	73.083	36.5415			
39.998	71.972	35.986			

C.3. HDB-1

Film-Casting

T = 190ºC; DR = 1.18; γ = 14.54 [1/s]; ε = 0.008553 [1/s]; strain = 0.1655

Distance to frostline = 29.1 [mm]

Dist. from die [mm]	Film width [mm]	Half-width [mm]
0	101.6	50.8
0.893	100.484	50.242
1.861	99.59	49.795
3.424	97.432	48.716
5.062	95.348	47.674
6.476	93.524	46.762
8.932	90.826	45.413
10.83	89.151	44.5755
13.51	87.086	43.543
14.85	86.193	43.0965
16.86	85.076	42.538
19.205	83.848	41.924
21.103	83.178	41.589
23.057	82.676	41.338
25.29	81.95	40.975
27.746	81.615	40.8075
31.877	80.945	40.4725
34.557	80.61	40.305
38.353	79.829	39.9145
42.372	79.047	39.5235
203.2	79.047	39.5235

C.3. HDB-1

Film-Casting

T = 190ºC; DR = 1.76; γ = 14.54 [1/s]; ε = 0.03135 [1/s]; strain = 0.5654

Distance to frostline = 33.6 [mm]

Dist. from die [mm]	Film width [mm]	Half-width [mm]
0	101.6	50.8
1.317	100.799	50.3995
2.748	99.597	49.7985
4.293	97.021	48.5105
5.781	94.96	47.48
7.155	92.728	46.364
8.3	91.068	45.534
9.96	89.179	44.5895
11.277	87.634	43.817
12.536	86.546	43.273
14.253	85.172	42.586
16.256	83.684	41.842
18.66	81.852	40.926
20.721	80.593	40.2965
23.125	79.219	39.6095
25.701	78.017	39.0085
30.566	76.987	38.4935
35.832	75.957	37.9785
203.2	75.957	37.9785

C.3. HDB-1

Film-Casting

T = 190ºC; DR = 2.96; γ = 14.54 [1/s]; ε = 0.08853 [1/s]; strain = 1.0852

Distance to frostline = 30.7 [mm]

Dist. from die [mm]	Film width [mm]	Half-width [mm]
0	101.6	50.8
1.018	100.695	50.3475
2.036	99.45	49.725
3.394	97.866	48.933
4.525	96.396	48.198
5.77	93.793	46.8965
7.467	90.512	45.256
9.277	87.457	43.7285
10.748	85.421	42.7105
12.445	82.932	41.466
15.047	79.877	39.9385
17.197	77.614	38.807
19.12	76.257	38.1285
21.383	74.333	37.1665
23.759	72.862	36.431
25.456	71.618	35.809
28.963	69.921	34.9605
32.018	68.676	34.338
35.299	67.432	33.716
203.2	67.432	33.716

C.3. HDB-1

Film-Casting

T = 190ºC; DR = 5.93; γ = 14.54 [1/s]; ε = 0.2136 [1/s]; strain = 1.7802

Distance to frostline = 32.0 [mm]

Dist. from die [mm]	Film width [mm]	Half-width [mm]	Dist. from die [mm] *continued*	Film width [mm] *continued*	Half-width [mm] *continued*
0	101.6	50.8	37.548	59.504	29.752
0.796	99.893	49.9465	39.823	58.707	29.3535
2.275	98.528	49.264	203.3	58.707	29.3535
3.754	95.798	47.899			
5.119	91.36	45.68			
6.712	87.378	43.689			
8.191	84.193	42.0965			
9.443	81.69	40.845			
11.15	78.959	39.4795			
12.857	77.139	38.5695			
14.564	74.977	37.4885			
16.271	73.043	36.5215			
17.978	71.336	35.668			
19.685	69.743	34.8715			
21.505	68.264	34.132			
23.894	66.444	33.222			
25.942	64.851	32.4255			
28.104	63.941	31.9705			
30.835	62.462	31.231			
32.655	61.665	30.8325			
34.817	60.755	30.3775			

C.3. HDB-1

Film-Casting

T = 190ºC; DR = 8.89; γ = 14.54 [1/s]; ε = 0.3141 [1/s]; strain = 2.1848

Distance to frostline = 34.8 [mm]

Dist. from die [mm]	Film width [mm]	Half-width [mm]
0	101.6	50.8
0.922	101.37	50.685
2.074	100.218	50.109
3.456	96.877	48.4385
4.723	92.615	46.3075
5.875	88.929	44.4645
7.603	84.091	42.0455
8.87	81.556	40.778
10.598	78.331	39.1655
12.441	75.221	37.6105
14.284	72.802	36.401
16.588	70.037	35.0185
18.777	67.964	33.982
20.966	66.005	33.0025
23.5	63.817	31.9085
25.919	62.089	31.0445
29.26	60.131	30.0655
32.255	58.748	29.374
35.941	57.251	28.6255
38.821	56.099	28.0495
203.2	56.099	28.0495

C.3. HDB-1

Film-Casting

T = 190ºC; DR = 11.86; γ = 14.54 [1/s]; ε = 0.3994 [1/s]; strain = 2.4732

Distance to frostline = 37.7 [mm]

Dist. from die [mm]	Film width [mm]	Half-width [mm]	Dist. from die [mm] *continued*	Film width [mm] *continued*	Half-width [mm] *continued*
0	101.6	50.8	39.253	54.498	27.249
1.024	98.528	49.264	42.78	52.905	26.4525
1.82	97.049	48.5245	203.2	52.905	26.4525
3.185	94.205	47.1025			
4.209	91.815	45.9075			
5.119	89.312	44.656			
6.143	86.696	43.348			
7.395	84.079	42.0395			
8.647	81.69	40.845			
10.126	78.959	39.4795			
11.719	76.456	38.228			
13.312	73.725	36.8625			
14.905	71.677	35.8385			
16.839	69.402	34.701			
19.001	67.013	33.5065			
20.708	65.534	32.767			
22.756	63.6	31.8			
27.307	60.641	30.3205			
29.582	59.276	29.638			
32.085	57.911	28.9555			
35.84	55.977	27.9885			

C.3. HDB-1

Film-Casting

T = 190ºC; DR = 14.82; γ = 14.54 [1/s]; ε = 0.5263 [1/s]; strain = 2.6959

Distance to frostline = 36.4 [mm]

Dist. from die [mm]	Film width [mm]	Half-width [mm]	Dist. from die [mm] *continued*	Film width [mm] *continued*	Half-width [mm] *continued*
0	101.6	50.8	42.276	49.323	24.6615
1.136	99.782	49.891	203.2	49.323	24.6615
2.386	98.986	49.493			
3.863	96.145	48.0725			
5.34	91.258	45.629			
6.931	85.803	42.9015			
8.636	81.03	40.515			
10.227	77.621	38.8105			
11.704	74.779	37.3895			
13.522	72.279	36.1395			
15.113	69.893	34.9465			
17.386	66.938	33.469			
19.091	64.892	32.446			
21.023	62.96	31.48			
23.069	61.256	30.628			
25.456	58.869	29.4345			
28.411	56.823	28.4115			
30.911	55.232	27.616			
33.639	53.641	26.8205			
36.026	52.618	26.309			
39.094	51.141	25.5705			

C.3. HDB-1

Film-Casting

T = 190ºC; DR = 17.79; γ = 14.54 [1/s]; ε = 0.6508 [1/s]; strain = 2.8786

Distance to frostline = 35.7 [mm]

Dist. from die [mm]	Film width [mm]	Half-width [mm]	Dist. from die [mm] *continued*	Film width [mm] *continued*	Half-width [mm] *continued*
0	101.6	50.8	38.929	50.914	25.457
1.142	98.974	49.487	41.212	50.001	25.0005
2.512	96.006	48.003	46.806	48.289	24.1445
3.882	91.782	45.891	50.117	47.832	23.916
5.366	88.015	44.0075	203.2	47.832	23.916
7.078	84.362	42.181			
8.676	80.823	40.4115			
10.16	77.513	38.7565			
11.644	75.116	37.558			
13.128	72.147	36.0735			
14.384	70.093	35.0465			
15.64	68.723	34.3615			
17.467	66.44	33.22			
19.294	64.385	32.1925			
21.463	61.873	30.9365			
23.175	60.161	30.0805			
25.458	58.106	29.053			
27.969	56.165	28.0825			
31.28	54.453	27.2265			
33.335	53.311	26.6555			
35.39	52.398	26.199			

C.3. HDB-1

Film-Casting

T = 190ºC; DR = 20.75; γ = 14.54 [1/s]; ε = 0.7031 [1/s]; strain = 3.0327

Distance to frostline = 38.9 [mm]

Dist. from die [mm]	Film width [mm]	Half-width [mm]	Dist. from die [mm] *continued*	Film width [mm] *continued*	Half-width [mm] *continued*
0	101.6	50.8	42.909	46.687	23.3435
1.334	99.71	49.855	45.021	46.354	23.177
2.668	98.376	49.188	46.355	46.242	23.121
4.113	95.153	47.5765	48.356	45.687	22.8435
5.447	90.484	45.242	203.2	45.687	22.8435
7.114	84.37	42.185			
8.337	81.147	40.5735			
10.116	76.589	38.2945			
12.006	73.365	36.6825			
13.673	70.586	35.293			
15.563	67.585	33.7925			
17.119	65.362	32.681			
18.898	63.361	31.6805			
20.677	61.582	30.791			
22.567	59.359	29.6795			
24.679	57.47	28.735			
27.68	55.358	27.679			
30.348	53.468	26.734			
33.127	51.8	25.9			
35.795	50.467	25.2335			
39.797	48.132	24.066			

C.3. HDB-1

Film-Casting

T = 190ºC; DR = 23.72; γ = 14.54 [1/s]; ε = 0.8645 [1/s]; strain = 3.1663

Distance to frostline = 36.3 [mm]

Dist. from die [mm]	Film width [mm]	Half-width [mm]	Dist. from die [mm] *continued*	Film width [mm] *continued*	Half-width [mm] *continued*
0	101.6	50.8	39.12	47.398	23.699
1.021	99.899	49.9495	41.73	46.491	23.2455
1.928	97.178	48.589	44.225	45.697	22.8485
3.175	94.57	47.285	46.833	45.017	22.5085
4.536	90.374	45.187	49.554	44.337	22.1685
6.124	85.725	42.8625	203.2	44.337	22.1685
7.598	81.643	40.8215			
9.299	77.447	38.7235			
11.113	73.592	36.796			
12.474	70.984	35.492			
14.628	67.582	33.791			
16.442	64.861	32.4305			
18.37	62.593	31.2965			
20.071	60.438	30.219			
21.772	58.851	29.4255			
24.04	56.47	28.235			
26.081	54.542	27.271			
28.802	52.728	26.364			
31.07	51.14	25.57			
33.791	49.893	24.9465			
36.172	48.646	24.323			

C.3. HDB-1

Film-Casting

T = 190ºC; DR = 25.5; γ = 14.54 [1/s]; ε = 0.8663 [1/s]; strain = 3.2388

Distance to frostline = 39.2 [mm]

Dist. from die [mm]	Film width [mm]	Half-width [mm]	Dist. from die [mm] *continued*	Film width [mm] *continued*	Half-width [mm] *continued*
0	101.6	50.8	39.635	47.516	23.758
0.766	100.396	50.198	42.372	46.311	23.1555
2.08	98.425	49.2125	44.562	45.764	22.882
3.394	95.469	47.7345	47.628	44.778	22.389
4.708	92.841	46.4205	50.256	43.903	21.9515
6.35	86.054	43.027	53.103	43.136	21.568
8.211	79.922	39.961	203.2	43.136	21.568
9.853	75.872	37.936			
11.495	72.368	36.184			
12.918	70.069	35.0345			
14.779	67.332	33.666			
16.531	64.923	32.4615			
18.283	63.062	31.531			
20.035	60.982	30.491			
22.115	58.902	29.451			
23.757	57.369	28.6845			
25.837	55.508	27.754			
28.467	53.647	26.8235			
31.423	51.785	25.8925			
34.051	50.362	25.181			
36.898	48.939	24.4695			

C.4. HDB-3

Film-Casting

T = 190ºC; DR = 1.18; γ = 14.54 [1/s]; ε = 0.007932 [1/s]; strain = 0.1655

Distance to frostline = 31.4 [mm]

Dist. from die [mm]	Film width [mm]	Half-width [mm]	Dist. from die [mm] *continued*	Film width [mm] *continued*	Half-width [mm] *continued*
0	101.6	50.8	86.418	81.906	40.953
2.216	98.589	49.2945	96.758	81.657	40.8285
3.693	97.513	48.7565	115.634	81.906	40.953
6.073	95.698	47.849	132.047	81.82	40.91
8.535	93.153	46.5765	147.968	82.071	41.0355
10.751	91.268	45.634	199.923	82.152	41.076
12.967	89.788	44.894			
14.938	88.477	44.2385			
16.908	87.408	43.704			
19.452	86.257	43.1285			
21.341	85.605	42.8025			
23.475	84.948	42.474			
26.019	84.616	42.308			
28.153	84.289	42.1445			
32.256	83.958	41.979			
35.21	83.793	41.8965			
38.493	83.711	41.8555			
41.611	83.466	41.733			
48.258	83.302	41.651			
60.978	82.972	41.486			
73.534	82.648	41.324			

C.4. HDB-3

Film-Casting

T = 190ºC; DR = 1.76; γ = 14.54 [1/s]; ε = 0.03405 [1/s]; strain = 0.5652

Distance to frostline = 30.9 [mm]

Dist. from die [mm]	Film width [mm]	Half-width [mm]	Dist. from die [mm] *continued*	Film width [mm] *continued*	Half-width [mm] *continued*
0	101.6	50.8	67.143	76.852	38.426
0.934	99.917	49.9585	74.707	76.758	38.379
2.338	98.329	49.1645	83.952	76.291	38.1455
3.832	96.181	48.0905	101.601	75.451	37.7255
5.326	94.22	47.11	118.876	74.891	37.4455
7.194	92.073	46.0365	131.109	74.797	37.3985
9.062	90.112	45.056	196.382	75.358	37.679
11.21	87.777	43.8885			
13.264	86.003	43.0015			
15.692	84.229	42.1145			
17.933	82.735	41.3675			
20.081	81.614	40.807			
22.229	80.68	40.34			
24.657	79.746	39.873			
27.925	78.999	39.4995			
29.979	78.719	39.3595			
33.527	78.159	39.0795			
39.877	77.692	38.846			
46.32	77.412	38.706			
53.23	77.038	38.519			
60.233	76.945	38.4725			

C.4. HDB-3

Film-Casting

T = 190ºC; DR = 2.96; γ = 14.54 [1/s]; ε = 0.07580 [1/s]; strain = 1.0853

Distance to frostline = 35.8 [mm]

Dist. from die [mm]	Film width [mm]	Half-width [mm]	Dist. from die [mm] *continued*	Film width [mm] *continued*	Half-width [mm] *continued*
0	101.6	50.8	100.853	68.483	34.2415
1.349	99.802	49.901	112.092	68.183	34.0915
3.447	97.104	48.552	130.824	68.033	34.0165
5.095	95.006	47.503	198.857	68.632	34.316
7.193	91.56	45.78			
8.991	88.862	44.431			
11.239	85.865	42.9325			
13.786	83.018	41.509			
16.184	80.471	40.2355			
18.582	78.672	39.336			
20.68	77.024	38.512			
23.078	75.825	37.9125			
25.925	74.327	37.1635			
28.323	73.428	36.714			
30.571	72.678	36.339			
34.767	71.629	35.8145			
39.113	70.73	35.365			
44.658	70.131	35.0655			
50.952	69.831	34.9155			
59.943	69.531	34.7655			
76.577	69.082	34.541			

C.4. HDB-3

Film-Casting

T = 190ºC; DR = 5.93; γ = 14.54 [1/s]; ε = 0.1884 [1/s]; strain = 1.7801

Distance to frostline = 36.2 [mm]

Dist. from die [mm]	Film width [mm]	Half-width [mm]	Dist. from die [mm] *continued*	Film width [mm] *continued*	Half-width [mm] *continued*
0	101.6	50.8	58.2	59.96	29.98
0.925	100.304	50.152	66.99	59.682	29.841
2.22	98.73	49.365	86.237	58.572	29.286
3.7	96.324	48.162	99.191	58.017	29.0085
5.088	93.641	46.8205	115.939	57.555	28.7775
6.939	89.755	44.8775	136.296	57.74	28.87
9.16	85.591	42.7955	198.014	57.646	28.823
11.011	82.537	41.2685			
13.232	79.021	39.5105			
15.638	75.968	37.984			
17.951	73.099	36.5495			
20.727	70.601	35.3005			
22.855	68.75	34.375			
25.353	67.177	33.5885			
27.666	65.882	32.941			
30.997	64.309	32.1545			
33.495	63.568	31.784			
36.271	62.643	31.3215			
40.712	61.625	30.8125			
46.819	60.7	30.35			
52.926	60.237	30.1185			

C.4. HDB-3

Film-Casting

T = 190ºC; DR = 8.89; γ = 14.54 [1/s]; ε = 0.2958 [1/s]; strain = 2.1846

Distance to frostline = 36.9 [mm]

Dist. from die [mm]	Film width [mm]	Half-width [mm]	Dist. from die [mm] *continued*	Film width [mm] *continued*	Half-width [mm] *continued*
0	101.6	50.8	61.461	51.5	25.75
1.565	98.749	49.3745	66.156	51.074	25.537
3.272	96.186	48.093	70.424	51.072	25.536
5.406	92.056	46.028	75.688	50.503	25.2515
8.681	85.363	42.6815	84.081	49.934	24.967
10.388	81.524	40.762	92.474	49.223	24.6115
12.522	77.683	38.8415	106.842	48.227	24.1135
14.94	74.554	37.277	196.751	48.369	24.1845
17.358	71.847	35.9235			
20.061	68.579	34.2895			
23.191	65.735	32.8675			
26.036	63.456	31.728			
29.166	61.321	30.6605			
31.869	59.76	29.88			
35.141	57.909	28.9545			
38.698	56.202	28.101			
42.255	55.073	27.5365			
45.812	54.064	27.032			
49.369	53.065	26.5325			
52.356	52.786	26.393			
56.197	51.93	25.965			

C.4. HDB-3

Film-Casting

T = 190ºC; DR = 11.86; γ = 14.54 [1/s]; ε = 0.4107 [1/s]; strain = 2.4734

Distance to frostline = 36.6 [mm]

Dist. from die [mm]	Film width [mm]	Half-width [mm]	Dist. from die [mm] *continued*	Film width [mm] *continued*	Half-width [mm] *continued*
0	101.6	50.8	55.981	47.232	23.616
0.765	99.391	49.6955	62.437	46.807	23.4035
2.294	96.758	48.379	67.279	46.383	23.1915
3.738	93.785	46.8925	78.917	45.958	22.979
5.522	89.622	44.811	89.536	45.533	22.7665
6.881	86.479	43.2395	98.456	45.108	22.554
8.665	82.571	41.2855	112.218	44.854	22.427
10.619	78.748	39.374	127.169	44.089	22.0445
12.488	75.351	37.6755	195.893	44.259	22.1295
14.612	71.868	35.934			
17.16	68.385	34.1925			
19.199	66.006	33.003			
21.323	63.627	31.8135			
23.871	61.249	30.6245			
26.674	58.87	29.435			
29.222	56.916	28.458			
32.705	54.623	27.3115			
36.103	52.754	26.377			
39.076	51.14	25.57			
44.173	49.441	24.7205			
49.865	47.997	23.9985			

C.4. HDB-3

Film-Casting

T = 190ºC; DR = 17.79; γ = 14.54 [1/s]; ε = 0.5399 [1/s]; strain = 2.8788

Distance to frostline = 43.1 [mm]

Dist. from die [mm]	Film width [mm]	Half-width [mm]	Dist. from die [mm] *continued*	Film width [mm] *continued*	Half-width [mm] *continued*
0	101.6	50.8	38.834	48.251	24.1255
1.65	98.163	49.0815	41.515	46.877	23.4385
3.437	94.176	47.088	44.127	45.777	22.8885
5.087	90.875	45.4375	46.945	44.677	22.3385
6.599	86.749	43.3745	49.351	43.852	21.926
8.524	81.938	40.969	52.375	43.027	21.5135
10.242	78.498	39.249	54.781	42.34	21.17
11.823	75.199	37.5995	57.599	41.79	20.895
13.266	72.724	36.362	61.448	40.965	20.4825
14.916	70.111	35.0555	65.572	40.209	20.1045
16.772	67.363	33.6815	69.696	39.591	19.7955
18.49	65.231	32.6155	72.926	38.972	19.486
20.208	63.101	31.5505	77.737	38.354	19.177
21.72	61.382	30.691	81.861	37.804	18.902
23.507	59.525	29.7625	89.559	36.773	18.3865
25.913	57.325	28.6625	100.694	35.604	17.802
28.112	55.537	27.7685	113.547	34.573	17.2865
29.899	53.957	26.9785	200.358	32.167	16.0835
31.892	52.582	26.291			
34.023	50.933	25.4665			
36.36	49.558	24.779			

C.4. HDB-3

Film-Casting

T = 190ºC; DR = 23.72; γ = 14.54 [1/s]; ε = 0.7669 [1/s]; strain = 3.1662

Distance to frostline = 41.0 [mm]

Dist. from die [mm]	Film width [mm]	Half-width [mm]	Dist. from die [mm] *continued*	Film width [mm] *continued*	Half-width [mm] *continued*
0	101.6	50.8	39.142	46.939	23.4695
0.739	98.397	49.1985	43.163	45.134	22.567
2.052	96.263	48.1315	47.102	43.574	21.787
3.283	93.389	46.6945	51.697	42.097	21.0485
4.596	89.86	44.93	55.718	41.277	20.6385
5.909	86.083	43.0415	60.478	40.456	20.228
7.55	81.816	40.908	65.812	39.718	19.859
9.191	77.548	38.774	72.459	38.815	19.4075
10.668	74.758	37.379	78.696	38.158	19.079
12.227	72.132	36.066	89.61	36.763	18.3815
13.786	69.752	34.876	97.898	35.943	17.9715
15.427	67.208	33.604	135.646	33.645	16.8225
16.986	65.074	32.537	146.314	33.235	16.6175
18.709	63.105	31.5525	200.146	32.906	16.453
20.596	60.889	30.4445			
22.894	58.427	29.2135			
25.11	56.458	28.229			
27.736	54.406	27.203			
30.116	52.437	26.2185			
33.07	50.385	25.1925			
36.27	48.416	24.208			

C.5. HDB-4

Film-Casting

T = 190ºC; DR = 1.18; γ = 14.54 [1/s]; ε = 0.01115 [1/s]; strain = 0.1655

Distance to frostline = 22.4 [mm]

Dist. from die [mm]	Film width [mm]	Half-width [mm]	Dist. from die [mm] *continued*	Film width [mm] *continued*	Half-width [mm] *continued*
0	101.6	50.8	203.2	82.111	41.0555
1.576	101.17	50.585			
3.152	99.594	49.797			
4.585	97.874	48.937			
6.161	96.011	48.0055			
7.594	94.722	47.361			
9.17	93.002	46.501			
10.746	91.569	45.7845			
12.466	89.993	44.9965			
14.186	88.846	44.423			
15.906	87.413	43.7065			
17.626	86.267	43.1335			
19.202	85.837	42.9185			
20.778	84.977	42.4885			
22.498	84.547	42.2735			
24.504	84.117	42.0585			
26.08	83.544	41.772			
28.086	83.114	41.557			
29.662	82.684	41.342			
31.382	82.254	41.127			
32.958	82.111	41.0555			

C.5. HDB-4

Film-Casting

T = 190ºC; DR = 1.76; γ = 14.54 [1/s]; ε = 0.04759 [1/s]; strain = 0.5653

Distance to frostline = 22.1 [mm]

Dist. from die [mm]	Film width [mm]	Half-width [mm]
0	101.6	50.8
1.978	97.824	48.912
3.776	95.126	47.563
5.754	92.249	46.1245
7.732	90.091	45.0455
9.53	87.933	43.9665
11.328	85.596	42.798
13.486	83.798	41.899
15.104	82.359	41.1795
17.082	80.92	40.46
18.521	79.302	39.651
20.139	78.403	39.2015
21.937	78.223	39.1115
23.735	77.324	38.662
25.533	76.605	38.3025
27.511	76.425	38.2125
29.489	74.986	37.493
203.2	74.986	37.493

C.5. HDB-4

Film-Casting

T = 190ºC; DR = 2.96; γ = 14.54 [1/s]; ε = 0.1186 [1/s]; strain = 1.0848

Distance to frostline = 22.9 [mm]

Dist. from die [mm]	Film width [mm]	Half-width [mm]	Dist. from die [mm] *continued*	Film width [mm] *continued*	Half-width [mm] *continued*
0	101.6	50.8	203.2	70.276	35.138
1.362	99.285	49.6425			
2.724	96.833	48.4165			
4.358	94.518	47.259			
6.129	91.386	45.693			
8.036	88.253	44.1265			
9.943	86.619	43.3095			
11.441	83.623	41.8115			
12.939	81.716	40.858			
14.573	80.354	40.177			
16.071	78.992	39.496			
17.705	77.902	38.951			
19.339	76.677	38.3385			
20.837	75.86	37.93			
22.471	74.225	37.1125			
24.242	73.68	36.84			
26.013	73.544	36.772			
27.647	72.863	36.4315			
29.281	71.638	35.819			
30.915	71.093	35.5465			
32.686	70.276	35.138			

C.5. HDB-4

Film-Casting

T = 190ºC; DR = 5.93; γ = 14.54 [1/s]; ε = 0.2136 [1/s]; strain = 1.7801

Distance to frostline = 32.0 [mm]

Dist. from die [mm]	Film width [mm]	Half-width [mm]	Dist. from die [mm] *continued*	Film width [mm] *continued*	Half-width [mm] *continued*
0	101.6	50.8	37.294	61.208	30.604
1.652	96.644	48.322	203.2	61.208	30.604
3.304	94.331	47.1655			
5.121	90.201	45.1005			
6.938	86.897	43.4485			
8.755	84.254	42.127			
10.737	80.619	40.3095			
12.719	78.141	39.0705			
14.701	76.324	38.162			
16.683	74.837	37.4185			
18.335	72.855	36.4275			
20.483	70.707	35.3535			
22.3	69.551	34.7755			
23.952	68.725	34.3625			
25.769	67.733	33.8665			
27.504	66.288	33.144			
29.363	65.42	32.71			
30.85	65.049	32.5245			
32.585	63.934	31.967			
34.072	63.19	31.595			
35.683	62.199	31.0995			

C.5. HDB-4

Film-Casting

T = 190ºC; DR = 8.89; γ = 14.54 [1/s]; ε = 0.4206 [1/s]; strain = 2.185

Distance to frostline = 26.0 [mm]

Dist. from die [mm]	Film width [mm]	Half-width [mm]	Dist. from die [mm] *continued*	Film width [mm] *continued*	Half-width [mm] *continued*
0	101.6	50.8	33.541	63.015	31.5075
1.939	100.824	50.412	35.092	62.434	31.217
3.684	98.304	49.152	36.643	62.24	31.12
5.429	93.65	46.825	38	61.658	30.829
7.174	90.742	45.371	39.745	61.076	30.538
8.725	86.476	43.238	41.49	60.689	30.3445
10.082	83.956	41.978	43.235	60.495	30.2475
11.439	81.047	40.5235	45.174	60.107	30.0535
12.796	78.915	39.4575	46.919	59.525	29.7625
14.541	76.976	38.488	48.858	59.137	29.5685
16.092	75.037	37.5185	50.797	58.556	29.278
17.643	73.873	36.9365	52.736	58.75	29.375
19.194	72.128	36.064	55.063	57.974	28.987
20.551	70.189	35.0945	56.808	57.586	28.793
22.102	68.444	34.222	58.747	57.392	28.696
23.653	67.087	33.5435	60.686	57.005	28.5025
25.592	66.118	33.059	62.625	56.811	28.4055
27.337	65.342	32.671	64.37	56.617	28.3085
28.888	64.566	32.283	66.115	56.229	28.1145
30.439	63.985	31.9925	203.2	56.229	28.1145
31.99	63.791	31.8955			

C.5. HDB-4

Film-Casting

T = 190ºC; DR = 11.86; γ = 14.54 [1/s]; ε = 0.5744 [1/s]; strain = 2.4732

Distance to frostline = 26.2 [mm]

Dist. from die [mm]	Film width [mm]	Half-width [mm]	Dist. from die [mm] *continued*	Film width [mm] *continued*	Half-width [mm] *continued*
0	101.6	50.8	37.186	55.688	27.844
1.397	97.934	48.967	39.281	54.815	27.4075
3.143	93.57	46.785	41.027	54.291	27.1455
4.714	90.777	45.3885	42.947	53.942	26.971
6.46	87.634	43.817	44.867	53.593	26.7965
8.206	83.445	41.7225	46.787	52.546	26.273
9.952	79.953	39.9765	203.2	52.546	26.273
11.698	76.811	38.4055			
13.618	73.669	36.8345			
15.189	71.05	35.525			
17.109	68.955	34.4775			
18.855	67.384	33.692			
20.601	65.638	32.819			
22.347	63.718	31.859			
24.093	62.147	31.0735			
25.839	60.576	30.288			
27.585	59.354	29.677			
29.505	58.481	29.2405			
31.425	57.608	28.804			
33.52	56.735	28.3675			
35.266	56.037	28.0185			

C.5. HDB-4

Film-Casting

T = 190ºC; DR = 14.82; γ = 14.54 [1/s]; ε = 0.5306 [1/s]; strain = 2.6961

Distance to frostline = 36.1 [mm]

Dist. from die [mm]	Film width [mm]	Half-width [mm]	Dist. from die [mm] *continued*	Film width [mm] *continued*	Half-width [mm] *continued*
0	101.6	50.8	33.967	55.948	27.974
1.688	100.587	50.2935	35.486	55.188	27.594
3.544	96.368	48.184	36.878	54.682	27.341
5.063	92.486	46.243	38.397	54.049	27.0245
6.582	89.449	44.7245	40.043	53.543	26.7715
8.27	85.736	42.868	41.562	53.036	26.518
10.126	81.179	40.5895	42.828	52.656	26.328
11.814	76.959	38.4795	44.474	52.024	26.012
13.713	74.681	37.3405	46.12	51.644	25.822
14.979	72.529	36.2645	47.512	51.644	25.822
16.625	70.377	35.1885	49.031	50.884	25.442
18.017	69.112	34.556	50.423	50.631	25.3155
19.536	67.086	33.543	203.2	50.631	25.3155
21.308	65.441	32.7205			
22.954	63.542	31.771			
24.726	62.276	31.138			
26.372	60.504	30.252			
27.891	59.492	29.746			
29.537	58.226	29.113			
31.056	57.213	28.6065			
32.575	56.454	28.227			

C.5. HDB-4

Film-Casting

T = 190ºC; DR = 17.79; γ = 14.54 [1/s]; ε = 0.8377 [1/s]; strain = 2.8785

Distance to frostline = 27.8 [mm]

Dist. from die [mm]	Film width [mm]	Half-width [mm]	Dist. from die [mm] *continued*	Film width [mm] *continued*	Half-width [mm] *continued*
0	101.6	50.8	31.976	53.241	26.6205
1.986	99.118	49.559	33.589	52.744	26.372
3.475	96.636	48.318	35.078	52	26
4.799	92.664	46.332	36.567	51.255	25.6275
6.123	90.513	45.2565	38.304	50.138	25.069
7.778	86.377	43.1885	40.166	49.269	24.6345
9.433	81.247	40.6235	41.779	48.649	24.3245
11.088	77.937	38.9685	203.2	48.649	24.3245
12.743	73.842	36.921			
14.108	71.236	35.618			
15.845	69.747	34.8735			
17.334	67.016	33.508			
18.699	65.155	32.5775			
20.188	63.914	31.957			
21.553	62.052	31.026			
23.166	60.439	30.2195			
24.531	59.074	29.537			
26.02	57.833	28.9165			
27.509	56.219	28.1095			
28.998	55.599	27.7995			
30.487	54.358	27.179			

C.5. HDB-4

Film-Casting

T = 190ºC; DR = 20.75; γ = 14.54 [1/s]; ε = 0.9962 [1/s]; strain = 3.0327

Distance to frostline = 27.5 [mm]

Dist. from die [mm]	Film width [mm]	Half-width [mm]	Dist. from die [mm] *continued*	Film width [mm] *continued*	Half-width [mm] *continued*
0	101.6	50.8	34.669	52.001	26.0005
1.545	99.369	49.6845	36.557	50.8	25.4
3.261	96.795	48.3975	38.273	50.457	25.2285
4.977	91.989	45.9945	39.989	49.77	24.885
6.865	83.751	41.8755	41.534	49.427	24.7135
8.581	79.461	39.7305	43.422	48.912	24.456
10.297	77.058	38.529	45.138	47.882	23.941
12.185	74.312	37.156	47.197	47.711	23.8555
14.073	71.395	35.6975	49.085	47.196	23.598
15.789	68.992	34.496	50.973	46.509	23.2545
16.99	67.447	33.7235	203.2	46.509	23.2545
18.878	64.53	32.265			
20.423	63.157	31.5785			
21.796	61.441	30.7205			
23.341	60.068	30.034			
25.057	58.866	29.433			
26.602	57.15	28.575			
27.975	56.292	28.146			
29.863	55.262	27.631			
31.408	54.404	27.202			
33.124	53.203	26.6015			

C.5. HDB-4

Film-Casting

T = 190ºC; DR = 23.72; γ = 14.54 [1/s]; ε = 1.3214 [1/s]; strain = 3.1663

Distance to frostline = 23.8 [mm]

Dist. from die [mm]	Film width [mm]	Half-width [mm]	Dist. from die [mm] *continued*	Film width [mm] *continued*	Half-width [mm] *continued*
0	101.6	50.8	33.511	52.645	26.3225
1.716	99.541	49.7705	35.184	51.873	25.9365
3.261	95.936	47.968	36.857	51.1	25.55
4.977	90.788	45.394	38.916	50.071	25.0355
6.693	85.982	42.991	40.461	49.813	24.9065
8.238	81.864	40.932	42.263	48.912	24.456
9.611	78.946	39.473	43.808	48.397	24.1985
11.327	75.342	37.671	45.224	48.011	24.0055
12.7	73.626	36.813	46.897	47.496	23.748
14.416	70.193	35.0965	48.442	47.11	23.555
15.961	68.305	34.1525	50.115	46.853	23.4265
17.677	65.903	32.9515	51.917	46.467	23.2335
19.565	63.5	31.75	203.2	46.467	23.2335
21.281	62.041	31.0205			
22.826	60.497	30.2485			
24.371	59.081	29.5405			
25.916	57.794	28.897			
27.332	56.764	28.382			
28.877	55.734	27.867			
30.55	54.447	27.2235			
32.095	53.417	26.7085			

C.5. HDB-4

Film-Casting

T = 190ºC; DR = 25.5; γ = 14.54 [1/s]; ε = 1.2120 [1/s]; strain = 3.2387

Distance to frostline = 28.0 [mm]

Dist. from die [mm]	Film width [mm]	Half-width [mm]	Dist. from die [mm] *continued*	Film width [mm] *continued*	Half-width [mm] *continued*
0	101.6	50.8	35.045	50.536	25.268
1.761	97.902	48.951	36.63	49.832	24.916
3.698	92.092	46.046	38.391	48.775	24.3875
5.283	87.689	43.8445	40.152	48.071	24.0355
7.044	83.64	41.82	42.089	47.366	23.683
8.981	78.357	39.1785	43.85	47.014	23.507
10.39	75.892	37.946	45.611	46.662	23.331
11.799	72.898	36.449	47.724	45.782	22.891
13.384	70.785	35.3925	203.2	45.782	22.891
14.793	68.849	34.4245			
16.378	66.736	33.368			
17.787	65.151	32.5755			
19.548	63.214	31.607			
20.957	61.277	30.6385			
22.718	59.692	29.846			
24.479	57.755	28.8775			
26.592	55.642	27.821			
28.001	54.762	27.381			
29.762	53.353	26.6765			
31.699	52.121	26.0605			
33.284	51.24	25.62			

C.6. HDB-6

Film-Casting

T = 190ºC; DR = 1.18; γ = 14.54 [1/s]; ε = 0.009091 [1/s]; strain = 0.1655

Distance to frostline = 27.4 [mm]

Dist. from die [mm]	Film width [mm]	Half-width [mm]
0	101.6	50.8
1.087	100.15	50.075
2.295	99.063	49.5315
3.624	97.009	48.5045
4.953	96.164	48.082
6.282	93.506	46.753
7.49	92.781	46.3905
8.819	90.606	45.303
10.269	89.278	44.639
11.719	88.673	44.3365
13.048	88.19	44.095
14.377	86.499	43.2495
15.585	86.378	43.189
16.914	85.412	42.706
18.485	84.445	42.2225
20.056	83.358	41.679
21.385	82.875	41.4375
22.835	81.425	40.7125
23.801	80.7	40.35
203.2	80.7	40.35

C.6. HDB-6

Film-Casting

T = 190ºC; DR = 1.76; γ = 14.54 [1/s]; ε = 0.03777 [1/s]; strain = 0.5653

Distance to frostline = 27.9 [mm]

Dist. from die [mm]	Film width [mm]	Half-width [mm]
0	101.6	50.8
1.385	100.561	50.2805
2.77	97.446	48.723
4.328	96.061	48.0305
5.886	94.85	47.425
7.79	91.907	45.9535
9.521	89.311	44.6555
11.252	86.022	43.011
13.156	83.772	41.886
15.06	82.907	41.4535
16.964	81.695	40.8475
18.349	81.003	40.5015
20.08	79.965	39.9825
21.811	79.272	39.636
23.715	78.407	39.2035
25.619	77.368	38.684
26.831	77.022	38.511
203.2	77.022	38.511

C.6. HDB-6

Film-Casting

T = 190ºC; DR = 2.96; γ = 14.54 [1/s]; ε = 0.08665 [1/s]; strain = 1.0851

Distance to frostline = 31.3 [mm]

Dist. from die [mm]	Film width [mm]	Half-width [mm]
0	101.6	50.8
1.693	99.06	49.53
3.386	95.504	47.752
5.079	92.456	46.228
6.772	89.239	44.6195
8.635	86.36	43.18
10.498	83.481	41.7405
12.53	81.788	40.894
14.054	80.772	40.386
15.578	79.587	39.7935
16.763	78.063	39.0315
18.456	76.369	38.1845
20.488	74.507	37.2535
22.351	73.491	36.7455
24.044	72.983	36.4915
25.737	71.12	35.56
27.261	70.104	35.052
28.277	70.104	35.052
203.2	70.104	35.052

C.6. HDB-6

Film-Casting

T = 190ºC; DR = 5.93; γ = 14.54 [1/s]; ε = 0.1619 [1/s]; strain = 1.7798

Distance to frostline = 42.2 [mm]

Dist. from die [mm]	Film width [mm]	Half-width [mm]	Dist. from die [mm] *continued*	Film width [mm] *continued*	Half-width [mm] *continued*
0	101.6	50.8	26.755	64.61	32.305
1.11	99.257	49.6285	28.358	63.993	31.9965
2.343	96.175	48.0875	30.084	63.13	31.565
3.699	93.585	46.7925	31.564	62.267	31.1335
5.055	90.256	45.128	32.92	61.897	30.9485
6.041	88.037	44.0185	34.276	61.281	30.6405
7.274	85.817	42.9085	35.879	60.294	30.147
8.384	84.215	42.1075	37.852	59.678	29.839
9.74	81.872	40.936	39.208	59.184	29.592
10.973	79.776	39.888	203.2	59.184	29.592
12.329	78.05	39.025			
13.562	76.077	38.0385			
14.672	74.597	37.2985			
16.028	73.364	36.682			
17.384	72.131	36.0655			
18.617	71.145	35.5725			
19.973	69.788	34.894			
21.206	68.925	34.4625			
22.562	67.939	33.9695			
24.042	66.706	33.353			
25.522	65.596	32.798			

C.6. HDB-6

Film-Casting

T = 190ºC; DR = 8.89; γ = 14.54 [1/s]; ε = 0.2974 [1/s]; strain = 2.1848

Distance to frostline = 36.7 [mm]

Dist. from die [mm]	Film width [mm]	Half-width [mm]
0	101.6	50.8
1.597	100.642	50.321
3.514	96.328	48.164
5.271	91.696	45.848
6.868	87.382	43.691
8.465	84.507	42.2535
9.903	79.874	39.937
11.82	76.2	38.1
13.577	72.686	36.343
15.174	70.13	35.065
16.931	68.372	34.186
18.848	66.615	33.3075
20.605	65.976	32.988
22.362	62.781	31.3905
24.439	61.663	30.8315
26.036	59.906	29.953
27.633	58.148	29.074
29.55	57.03	28.515
31.467	55.273	27.6365
33.064	55.113	27.5565
203.2	55.113	27.5565

C.6. HDB-6

Film-Casting

T = 190ºC; DR = 11.86; γ = 14.54 [1/s]; ε = 0.4344 [1/s]; strain = 2.4730

Distance to frostline = 34.6 [mm]

Dist. from die [mm]	Film width [mm]	Half-width [mm]	Dist. from die [mm] *continued*	Film width [mm] *continued*	Half-width [mm] *continued*
0	101.6	50.8	34.017	51.707	25.8535
1.512	99.03	49.515	35.68	50.951	25.4755
3.024	94.948	47.474	37.645	49.288	24.644
4.687	91.017	45.5085	39.157	48.683	24.3415
6.35	87.388	43.694	203.2	48.683	24.3415
7.56	84.364	42.182			
8.921	81.945	40.9725			
10.433	78.77	39.385			
12.096	72.874	36.437			
13.608	70.757	35.3785			
15.12	69.548	34.774			
17.085	68.338	34.169			
19.05	65.768	32.884			
20.562	63.349	31.6745			
22.225	62.593	31.2965			
23.737	60.325	30.1625			
25.551	58.208	29.104			
27.063	56.848	28.424			
28.726	55.638	27.819			
30.389	54.429	27.2145			
32.052	53.219	26.6095			

C.6. HDB-6

Film-Casting

T = 190ºC; DR = 14.82; γ = 14.54 [1/s]; ε = 0.4964 [1/s]; strain = 2.6961

Distance to frostline = 38.6 [mm]

Dist. from die [mm]	Film width [mm]	Half-width [mm]	Dist. from die [mm] *continued*	Film width [mm] *continued*	Half-width [mm] *continued*
0	101.6	50.8	32.53	50.968	25.484
1.174	99.085	49.5425	34.374	49.794	24.897
2.683	95.397	47.6985	36.218	48.788	24.394
3.857	92.044	46.022	37.895	47.95	23.975
5.198	88.355	44.1775	39.739	47.279	23.6395
6.372	85.17	42.585	41.583	46.273	23.1365
7.881	81.314	40.657	43.427	45.435	22.7175
9.39	78.128	39.064	45.104	44.932	22.466
11.402	75.278	37.639	203.2	44.932	22.466
12.911	71.925	35.9625			
14.588	69.913	34.9565			
16.097	68.069	34.0345			
17.774	65.386	32.693			
19.283	63.71	31.855			
20.792	62.033	31.0165			
22.301	60.189	30.0945			
23.978	58.68	29.34			
25.822	56.836	28.418			
27.499	55.159	27.5795			
29.176	53.818	26.909			
30.853	52.644	26.322			

C.6. HDB-6

Film-Casting

T = 190ºC; DR = 17.79; γ = 14.54 [1/s]; ε = 0.6300 [1/s]; strain = 2.8785

Distance to frostline = 36.9 [mm]

Dist. from die [mm]	Film width [mm]	Half-width [mm]	Dist. from die [mm] *continued*	Film width [mm] *continued*	Half-width [mm] *continued*
0	101.6	50.8	37.045	52.74	26.37
1.764	98.954	49.477	45.248	51.991	25.9955
3.704	94.544	47.272	47.1	50.8	25.4
5.292	91.369	45.6845	48.952	50.006	25.003
7.056	88.018	44.009	50.54	49.477	24.7385
8.644	84.314	42.157	51.995	48.948	24.474
10.408	81.139	40.5695	53.583	48.022	24.011
12.348	77.611	38.8055	55.567	47.096	23.548
14.112	74.083	37.0415	57.155	46.831	23.4155
15.7	72.319	36.1595	58.743	46.037	23.0185
17.464	70.203	35.1015	60.331	45.376	22.688
19.228	68.439	34.2195	61.919	44.847	22.4235
20.992	67.733	33.8665	63.507	44.715	22.3575
22.756	65.44	32.72	203.2	44.715	22.3575
24.52	63.853	31.9265			
26.46	60.501	30.2505			
28.048	59.443	29.7215			
29.988	57.679	28.8395			
31.752	55.915	27.9575			
33.34	55.386	27.693			
35.457	53.269	26.6345			

C.6. HDB-6

Film-Casting

T = 190ºC; DR = 20.75; γ = 14.54 [1/s]; ε = 0.8438 [1/s]; strain = 3.0326

Distance to frostline = 32.4 [mm]

Dist. from die [mm]	Film width [mm]	Half-width [mm]	Dist. from die [mm] *continued*	Film width [mm] *continued*	Half-width [mm] *continued*
0	101.6	50.8	34.256	47.792	23.896
1.003	99.093	49.5465	36.094	46.789	23.3945
2.507	95.417	47.7085	37.765	45.62	22.81
4.011	90.07	45.035	39.77	44.951	22.4755
5.515	86.059	43.0295	41.441	43.782	21.891
6.852	83.051	41.5255	43.279	43.113	21.5565
8.356	80.545	40.2725	44.95	42.111	21.0555
10.027	77.203	38.6015	203.2	42.111	21.0555
11.698	74.195	37.0975			
13.202	71.855	35.9275			
14.873	69.014	34.507			
16.544	66.174	33.087			
18.549	63.5	31.75			
20.387	60.659	30.3295			
22.225	58.32	29.16			
23.896	56.482	28.241			
25.567	54.978	27.489			
27.238	52.972	26.486			
29.076	51.803	25.9015			
30.413	50.633	25.3165			
32.251	49.129	24.5645			

C.6. HDB-6

Film-Casting

T = 190ºC; DR = 23.72; γ = 14.54 [1/s]; ε = 0.9228 [1/s]; strain = 3.1663

Distance to frostline = 34.1 [mm]

Dist. from die [mm]	Film width [mm]	Half-width [mm]	Dist. from die [mm] *continued*	Film width [mm] *continued*	Half-width [mm] *continued*
0	101.6	50.8	35.446	47.435	23.7175
1.477	98.974	49.487	37.046	46.409	23.2045
3.118	94.378	47.189	38.4	45.917	22.9585
4.595	89.946	44.973	39.754	45.178	22.589
6.236	86.171	43.0855	41.477	44.194	22.097
7.877	81.904	40.952	42.954	43.578	21.789
9.354	79.606	39.803	44.308	43.086	21.543
10.995	75.995	37.9975	45.785	42.347	21.1735
12.636	72.876	36.438	47.632	41.608	20.804
14.277	70.25	35.125	203.2	41.608	20.804
16.082	67.788	33.894			
17.559	65.326	32.663			
19.2	62.864	31.432			
21.005	61.058	30.529			
23.303	57.94	28.97			
25.108	55.806	27.903			
26.749	54.329	27.1645			
28.554	52.852	26.426			
30.195	51.374	25.687			
32	49.733	24.8665			
33.641	48.748	24.374			

C.6. HDB-6

Film-Casting

T = 190ºC; DR = 25.5; γ = 14.54 [1/s]; ε = 1.0263 [1/s]; strain = 3.2387

Distance to frostline = 33.1 [mm]

Dist. from die [mm]	Film width [mm]	Half-width [mm]	Dist. from die [mm] *continued*	Film width [mm] *continued*	Half-width [mm] *continued*
0	101.6	50.8	33.066	49.207	24.6035
1.55	98.673	49.3365	34.745	48.303	24.1515
3.272	92.473	46.2365	36.424	47.141	23.5705
4.822	88.168	44.084	38.232	46.237	23.1185
6.544	83.346	41.673	40.04	45.074	22.537
8.094	80.247	40.1235	41.719	44.428	22.214
9.816	76.458	38.229	43.527	43.654	21.827
11.366	74.134	37.067	45.335	42.879	21.4395
12.916	71.292	35.646	46.885	42.362	21.181
14.466	69.226	34.613	48.693	41.975	20.9875
15.758	67.03	33.515	50.501	41.329	20.6645
17.308	64.835	32.4175	203.2	41.329	20.6645
18.858	62.897	31.4485			
20.537	60.702	30.351			
22.345	58.764	29.382			
23.766	57.344	28.672			
25.316	55.665	27.8325			
26.737	54.632	27.316			
28.158	53.211	26.6055			
29.837	52.048	26.024			
31.387	50.499	25.2495			

C.7. Linear HDB

Film-Casting

T = 190ºC; DR = 1.18; γ = 14.54 [1/s]; ε = 0.008594 [1/s]; strain = 0.1655

Distance to frostline = 29.0 [mm]

Dist. from die [mm]	Film width [mm]	Half-width [mm]	Dist. from die [mm] *continued*	Film width [mm] *continued*	Half-width [mm] *continued*
0	101.6	50.8	60.034	79.661	39.8305
1.299	100.731	50.3655	72.012	78.94	39.47
2.309	99.721	49.8605	91.639	78.796	39.398
3.752	98.278	49.139	110.688	79.228	39.614
5.484	96.547	48.2735	132.046	78.363	39.1815
7.36	94.959	47.4795	199.585	78.074	39.037
8.659	93.66	46.83			
10.535	91.928	45.964			
12.267	90.196	45.098			
14.72	88.032	44.016			
16.74	86.444	43.222			
18.616	85.434	42.717			
21.214	84.424	42.212			
23.09	83.846	41.923			
25.255	83.125	41.5625			
28.141	82.403	41.2015			
31.172	82.115	41.0575			
34.058	81.826	40.913			
39.253	81.249	40.6245			
44.593	80.96	40.48			
51.087	80.239	40.1195			

C.7. Linear HDB

Film-Casting

T = 190ºC; DR = 1.76; γ = 14.54 [1/s]; ε = 0.03242 [1/s]; strain = 0.5654

Distance to frostline = 32.5 [mm]

Dist. from die [mm]	Film width [mm]	Half-width [mm]	Dist. from die [mm] *continued*	Film width [mm] *continued*	Half-width [mm] *continued*
0	101.6	50.8	53.136	72.817	36.4085
1.722	100.615	50.3075	59.409	72.448	36.224
3.69	97.786	48.893	69.126	72.079	36.0395
5.166	95.818	47.909	79.335	72.079	36.0395
6.396	94.096	47.048	89.298	71.956	35.978
7.995	92.128	46.064	100.737	71.833	35.9165
9.594	90.037	45.0185	121.77	70.726	35.363
11.07	87.946	43.973	198.646	70.48	35.24
12.915	86.101	43.0505			
14.883	83.887	41.9435			
16.851	81.55	40.775			
18.819	80.32	40.16			
21.156	78.721	39.3605			
22.878	77.983	38.9915			
24.969	77.122	38.561			
27.06	76.138	38.069			
29.766	75.523	37.7615			
34.194	74.539	37.2695			
37.884	74.17	37.085			
41.82	73.801	36.9005			
47.97	73.309	36.6545			

C.7. Linear HDB

Film-Casting

T = 190ºC; DR = 2.96; γ = 14.54 [1/s]; ε = 0.07502 [1/s]; strain = 1.0851

Distance to frostline = 36.2 [mm]

Dist. from die [mm]	Film width [mm]	Half-width [mm]	Dist. from die [mm] *continued*	Film width [mm] *continued*	Half-width [mm] *continued*
0	101.6	50.8	36.439	65.541	32.7705
1.416	99.799	49.8995	37.984	65.283	32.6415
2.832	98.383	49.1915	40.946	64.897	32.4485
4.248	95.806	47.903	44.036	64.768	32.384
5.407	92.845	46.4225	47.255	64.511	32.2555
7.081	89.494	44.747	49.83	64.511	32.2555
8.626	85.887	42.9435	53.307	64.511	32.2555
9.914	83.697	41.8485	56.784	64.382	32.191
11.33	81.767	40.8835	61.291	64.382	32.191
12.489	79.963	39.9815	65.798	64.253	32.1265
13.777	78.418	39.209	70.434	64.124	32.062
15.322	76.615	38.3075	79.447	63.867	31.9335
16.996	74.812	37.406	90.263	63.738	31.869
18.927	73.138	36.569	103.397	63.352	31.676
21.76	71.078	35.539	124.257	63.094	31.547
23.949	69.661	34.8305	199.198	63.352	31.676
25.623	68.889	34.4445			
28.327	67.73	33.865			
30.516	66.829	33.4145			
32.834	66.313	33.1565			
34.379	65.798	32.899			

C.7. Linear HDB

Film-Casting

T = 190ºC; DR = 5.93; γ = 14.54 [1/s]; ε = 0.1485 [1/s]; strain = 1.7804

Distance to frostline = 46.0 [mm]

Dist. from die [mm]	Film width [mm]	Half-width [mm]	Dist. from die [mm] *continued*	Film width [mm] *continued*	Half-width [mm] *continued*
0	101.6	50.8	35.822	56.184	28.092
1.288	100.078	50.039	38.163	55.365	27.6825
2.693	98.206	49.103	42.201	54.312	27.156
3.629	96.801	48.4005	46.649	53.551	26.7755
5.034	93.289	46.6445	51.448	53.141	26.5705
6.205	89.661	44.8305	55.779	52.79	26.395
7.376	86.032	43.016	59.993	52.556	26.278
8.781	82.638	41.319	63.739	52.263	26.1315
9.952	80.18	40.09	69.065	51.971	25.9855
11.825	76.551	38.2755	74.391	51.678	25.839
13.932	73.04	36.52	79.132	51.327	25.6635
16.039	70.23	35.115	87.15	50.859	25.4295
17.795	68.124	34.062	92.651	50.624	25.312
19.551	66.134	33.067	97.86	50.39	25.195
20.839	64.963	32.4815	108.453	50.039	25.0195
22.829	63.324	31.662	115.71	49.922	24.961
24.702	61.686	30.843	121.855	49.864	24.932
26.458	60.398	30.199	129.756	49.981	24.9905
28.448	59.345	29.6725	139.998	50.39	25.195
30.789	58.057	29.0285	153.751	51.034	25.517
32.954	57.121	28.5605	200.337	50.859	25.4295

C.7. Linear HDB

Film-Casting

T = 190ºC; DR = 8.89; γ = 14.54 [1/s]; ε = 0.2744 [1/s]; strain = 2.1853

Distance to frostline = 39.8 [mm]

Dist. from die [mm]	Film width [mm]	Half-width [mm]	Dist. from die [mm] *continued*	Film width [mm] *continued*	Half-width [mm] *continued*
0	101.6	50.8	29.466	54.229	27.1145
0.762	100.711	50.3555	31.498	53.023	26.5115
1.651	100.203	50.1015	33.657	52.134	26.067
2.921	98.933	49.4665	35.689	51.181	25.5905
4.318	95.758	47.879	37.975	50.292	25.146
5.588	92.075	46.0375	40.134	49.467	24.7335
6.477	89.027	44.5135	42.103	48.832	24.416
7.493	85.725	42.8625	44.643	48.133	24.0665
8.89	81.28	40.64	46.929	47.562	23.781
10.16	77.978	38.989	49.406	47.054	23.527
11.43	75.057	37.5285	52.01	46.609	23.3045
12.573	72.517	36.2585	54.169	46.228	23.114
14.415	69.533	34.7665	58.868	45.593	22.7965
16.003	66.993	33.4965	66.171	44.704	22.352
17.781	64.707	32.3535	78.808	43.625	21.8125
19.686	62.23	31.115	88.079	43.18	21.59
20.956	61.024	30.512	96.08	42.926	21.463
22.417	59.627	29.8135	113.543	42.736	21.368
24.449	57.849	28.9245	132.657	42.736	21.368
26.1	56.579	28.2895	152.152	44.514	22.257
27.624	55.436	27.718	199.523	45.784	22.892

C.7. Linear HDB

Film-Casting

T = 190ºC; DR = 11.86; γ = 14.54 [1/s]; ε = 0.3459 [1/s]; strain = 2.4732

Distance to frostline = 43.5 [mm]

Dist. from die [mm]	Film width [mm]	Half-width [mm]	Dist. from die [mm] *continued*	Film width [mm] *continued*	Half-width [mm] *continued*
0	101.6	50.8	36.711	50.529	25.2645
1.084	100.245	50.1225	39.149	49.581	24.7905
2.032	99.026	49.513	41.723	48.903	24.4515
3.387	96.723	48.3615	44.432	48.091	24.0455
4.606	92.524	46.262	46.735	47.549	23.7745
5.825	87.241	43.6205	50.122	47.007	23.5035
7.044	83.447	41.7235	54.186	46.33	23.165
8.399	79.519	39.7595	59.063	45.652	22.826
10.025	75.997	37.9985	64.346	44.975	22.4875
11.786	72.475	36.2375	70.713	44.298	22.149
13.005	70.443	35.2215	79.112	43.62	21.81
15.037	67.191	33.5955	88.73	42.672	21.336
16.527	65.024	32.512	101.599	41.724	20.862
18.559	62.857	31.4285	113.926	41.317	20.6585
20.32	60.825	30.4125	134.246	40.775	20.3875
21.946	59.199	29.5995	199.541	41.588	20.794
24.52	57.167	28.5835			
26.958	55.406	27.703			
28.99	54.051	27.0255			
31.699	52.561	26.2805			
34.137	51.477	25.7385			

C.7. Linear HDB

Film-Casting

T = 190ºC; DR = 17.79; γ = 14.54 [1/s]; ε = 0.5687 [1/s]; strain = 2.8786

Distance to frostline = 40.9 [mm]

Dist. from die [mm]	Film width [mm]	Half-width [mm]	Dist. from die [mm] *continued*	Film width [mm] *continued*	Half-width [mm] *continued*
0	101.6	50.8	37.275	48.618	24.309
1.122	99.855	49.9275	40.828	47.309	23.6545
2.743	97.237	48.6185	44.256	46.063	23.0315
4.239	92.5	46.25	47.747	45.19	22.595
5.735	86.142	43.071	53.107	44.068	22.034
7.356	80.158	40.079	58.031	43.258	21.629
8.977	76.169	38.0845	62.27	42.572	21.286
10.348	72.928	36.464	69.874	41.824	20.912
11.719	70.434	35.217	82.59	40.765	20.3825
13.09	68.066	34.033	93.623	39.892	19.946
14.711	65.573	32.7865	102.91	39.331	19.6655
16.207	63.703	31.8515	113.756	38.583	19.2915
17.952	61.833	30.9165	128.03	37.586	18.793
19.697	60.087	30.0435	161.502	37.399	18.6995
21.567	58.217	29.1085	198.963	37.773	18.8865
23.437	56.597	28.2985			
25.307	55.101	27.5505			
27.925	53.48	26.74			
29.92	52.109	26.0545			
31.915	51.112	25.556			
33.66	50.114	25.057			

C.7. Linear HDB

Film-Casting

T = 190ºC; DR = 23.72; γ = 14.54 [1/s]; ε = 0.7467 [1/s]; strain = 3.1662

Distance to frostline = 42.1 [mm]

Dist. from die [mm]	Film width [mm]	Half-width [mm]	Dist. from die [mm] *continued*	Film width [mm] *continued*	Half-width [mm] *continued*
0	101.6	50.8	35.32	44.459	22.2295
1.091	100.645	50.3225	37.775	43.504	21.752
2.046	99.827	49.9135	40.639	42.345	21.1725
3.001	98.736	49.368	45.003	40.708	20.354
4.228	95.599	47.7995	49.913	39.481	19.7405
5.592	89.326	44.663	54.823	38.663	19.3315
7.092	82.098	41.049	60.619	37.844	18.922
8.319	77.734	38.867	69.142	37.026	18.513
9.546	74.188	37.094	77.665	36.14	18.07
11.046	70.506	35.253	88.098	35.253	17.6265
12.546	67.37	33.685	99.963	34.299	17.1495
14.046	64.642	32.321	116.124	32.662	16.331
15.955	61.369	30.6845	159.696	31.571	15.7855
17.592	59.323	29.6615	199.313	31.366	15.683
19.365	56.869	28.4345			
21.683	54.414	27.207			
23.592	52.641	26.3205			
25.501	51.005	25.5025			
27.274	49.504	24.752			
29.865	47.595	23.7975			
32.047	46.231	23.1155			

C.7. Linear HDB

Film-Casting

T = 190ºC; DR = 25.5; γ = 14.54 [1/s]; ε = 0.7432 [1/s]; strain = 3.2387

Distance to frostline = 45.7 [mm]

Dist. from die [mm]	Film width [mm]	Half-width [mm]	Dist. from die [mm] *continued*	Film width [mm] *continued*	Half-width [mm] *continued*
0	101.6	50.8	40.105	42.368	21.184
1.234	100.092	50.046	43.19	41.202	20.601
2.879	97.624	48.812	46.481	40.174	20.087
4.113	92.962	46.481	49.84	39.214	19.607
5.073	89.671	44.8355	53.199	38.391	19.1955
6.581	81.307	40.6535	57.792	37.637	18.8185
8.226	75.686	37.843	62.454	36.952	18.476
9.871	71.71	35.855	66.293	36.472	18.236
11.791	67.459	33.7295	73.972	35.649	17.8245
13.436	64.443	32.2215	80.622	34.964	17.482
15.356	61.563	30.7815	87.34	34.278	17.139
17.413	58.41	29.205	92.276	34.004	17.002
19.195	56.49	28.245	99.269	33.455	16.7275
20.977	54.571	27.2855	105.645	33.044	16.522
23.034	52.788	26.394	115.311	32.427	16.2135
25.502	50.594	25.297	151.92	31.124	15.562
27.696	49.086	24.543	162.683	31.604	15.802
29.753	47.715	23.8575	199.429	32.084	16.042
32.495	45.933	22.9665			
34.415	44.973	22.4865			
37.294	43.602	21.801			

Appendix D: Dynamic Shear Rheology for the HDPE-based PE Resins

D.1. HDB-1

Dynamic Oscillatory

T = 150ºC

ω rad/s	G' Pa	G" Pa	η* Pa-s
0.1	160.371	981.641	9946.51
0.15849	298.823	1462.5	9418.42
0.25119	531.534	2157.34	8845.3
0.39811	908.384	3130.06	8186.72
0.63097	1486.18	4468.86	7463.96
1.00003	2326.25	6306.35	6721.51
1.58496	3518.63	8822.01	5992.46
2.51202	5177.82	12303.5	5313.91
3.98132	7539.87	17100.2	4694.1
6.31006	10832.2	23768.9	4139.54
10.0007	15636.8	33021	3653.35
15.8501	22570.2	45742.4	3218.13
25.1206	32898.3	62811.2	2822.59
39.8135	48137.4	85200.2	2457.92
63.1006	70117.7	113395	2112.86
100	100839	147061	1783.12

D.1. HDB-1

Dynamic Oscillatory

T = 170ºC

ω rad/s	G' Pa	G" Pa	η* Pa-s
0.01	1.78437	78.2138	7823.43
0.1	83.7222	709.955	7148.72
0.15849	166.239	1086.33	6934.05
0.25119	313.748	1632.48	6617.92
0.39811	564.493	2413.61	6226.27
0.63097	971.012	3520.4	5787.73
1.00003	1590.01	5054.99	5299
1.58496	2514.61	7173.59	4796.05
2.51202	3840.7	10101.3	4302.04
3.98132	5686.57	14169.5	3834.9
6.31006	8345.11	19794.9	3404.41
10.0007	12153.7	27633.8	3018.62
15.8501	17691.6	38548.8	2675.99
25.1206	25942.6	53364.5	2362.05
39.8135	38176.1	73192	2073.42
63.1006	56067.1	98770.8	1799.9
100	81714.3	130254	1537.64

D.1. HDB-1

Dynamic Oscillatory

T = 190ºC

ω rad/s	G' Pa	G" Pa	η* Pa-s
0.63097	513.527	2410.55	3906.14
1.00003	900.43	3534.54	3647.31
1.58496	1491.05	5111.89	3359.65
2.51202	2398.2	7303.11	3060
3.98132	3701.55	10360.7	2763.42
6.31006	5581.41	14599.5	2477
10.0007	8293.11	20586	2219.2
15.8501	12236.2	28851.3	1977.2
25.1206	18084.5	40300.3	1758.4
39.8135	26816.4	55840.9	1555.91
63.1006	39759.9	76353.3	1364.26
100	58625	102373	1179.71

D.1. HDB-1

Dynamic Oscillatory

T = 230ºC

ω rad/s	G' Pa	G" Pa	η* Pa-s
0.01	0.55771	30.7184	3072.35
0.1	22.4627	282.294	2831.85
0.15849	43.2292	436.61	2768.3
0.25119	82.6347	672.583	2697.72
0.39811	155.224	1023.53	2600.38
0.63097	284.145	1544.05	2488.21
1.00003	507.912	2294.69	2350.16
1.58496	875.001	3362.73	2192.3
2.51202	1442.03	4861.48	2018.63
3.98132	2314.15	6933.77	1836.01
6.31006	3581.2	9824.11	1657.11
10.0007	5401.34	13798.7	1481.71
15.8501	8019.22	19333.6	1320.54
25.1206	11808.3	27003.9	1173.25
39.8135	17376.8	37526.9	1038.71
63.1006	25538.2	51694	913.751
100	37497.9	70159.3	795.514

D.1. HDB-1

Dynamic Oscillatory

T = 270ºC

ω rad/s	G' Pa	G" Pa	η* Pa-s
0.01	2.30437	19.1025	1924.1
0.15849	18.5666	257.253	1627.38
0.25119	33.8465	396.295	1583.41
0.39811	62.807	612.163	1545.75
0.63097	119.482	938.957	1500.13
1.00003	217.516	1427.38	1443.81
1.58496	392.558	2148.48	1377.98
2.51202	692.098	3195.58	1301.61
3.98132	1171.18	4691.18	1214.46
6.31006	1919.93	6806.09	1120.7
10.0007	3038.28	9784.87	1024.5
15.8501	4674.28	13970.6	929.447
25.1206	7015.54	19858.2	838.396
39.8135	10373.1	28117.5	752.757
63.1006	15080.9	39576.4	671.188
100	21480.2	55267.2	592.947

D.1. HDB-1

Dynamic Oscillatory

T = 320ºC

ω rad/s	G' Pa	G" Pa	η* Pa-s
0.01	19.0887	15.3903	2452.02
0.1	15.1721	91.804	930.489
0.15849	24.4833	138.241	885.816
0.25119	33.0798	211.841	853.569
0.39811	45.4433	327.405	830.284
0.63097	66.4096	505.968	808.772
1.00003	103.855	779.563	786.426
1.58496	172.136	1195.01	761.748
2.51202	295.017	1817.52	732.999
3.98132	513.405	2736.79	699.399
6.31006	877.536	4071.66	660.082
10.0007	1469.14	5993.05	617.004
15.8501	2387.93	8727.09	570.842
25.1206	3771.12	12596.4	523.426
39.8135	5810.84	18049.7	476.27

D.2. HDB-2

Dynamic Oscillatory

T = 170ºC

ω rad/s	G' Pa	G" Pa	η* Pa-s
0.1	402.619	1520.17	15725.8
0.15849	700.306	2193.64	14529.2
0.25119	1154.29	3095.44	13152
0.39811	1827.27	4290.38	11713.6
0.63097	2778.12	5858.39	10275.9
1.00003	4095.56	7912.89	8909.69
1.58496	5857.59	10620	7652.12
2.51202	8199.35	14225.2	6536.18
3.98132	11345.7	19031.8	5565.24
6.31006	15571	25478	4732.04
10.0007	21460.6	34175.1	4035.16
15.8501	29730.5	45668.5	3438.04
25.1206	41523.2	60460.2	2919.75
39.8135	58391.7	78926.2	2465.95
63.1006	81964	100881	2059.9
100	114470	125530	1698.86

D.3. HDB-3

Dynamic Oscillatory

T = 150ºC

ω rad/s	G' Pa	G" Pa	η* Pa-s
0.1	1324.16	3039.38	33152.9
0.15849	2021.15	4124.84	28982.4
0.25119	3013.65	5535.37	25090.8
0.39811	4347.77	7331.53	21410.6
0.63097	6090.7	9626.88	18054.6
1.00003	8348.48	12600.7	15114.9
1.58496	11198.2	16542.1	12603.4
2.51202	14896.8	21741.7	10491.8
3.98132	19769	28779.8	8769.81
6.31006	26175.8	38235.9	7343.43
10.0007	35025.8	50891.1	6177.5
15.8501	47237.1	67579.9	5202.01
25.1206	64238.6	89045.6	4370.85
39.8135	87835.9	115890	3652.41
63.1006	119661	148422	3021.38
100	161324	185251	2456.49

D.3. HDB-3

Dynamic Oscillatory

T = 170ºC

ω rad/s	G' Pa	G" Pa	η* Pa-s
0.01	51.3635	368.77	37233
0.1	865.142	2323.37	24792.1
0.15849	1386.34	3228.81	22170.9
0.25119	2134.54	4396.46	19456.3
0.39811	3190.94	5897.38	16842.9
0.63097	4613.54	7804.32	14368.4
1.00003	6489.78	10247.5	12129.3
1.58496	8888.26	13406.6	10148.7
2.51202	11991.9	17515.7	8450.35
3.98132	16004.3	22974.2	7032.61
6.31006	21197.2	30278.6	5857.47
10.0007	28156.9	40094.9	4899.05
15.8501	37586.8	53085.6	4103.76
25.1206	50538.3	70111.4	3440.5
39.8135	68352.2	91678.9	2872.27
63.1006	92167.4	117483	2366.41
100	123748	147701	1926.89

D.3. HDB-3

Dynamic Oscillatory

T = 190ºC

ω rad/s	G' Pa	G" Pa	η* Pa-s
0.01	16.2911	197.455	19812.6
0.1	529.603	1717.81	17975.9
0.15849	883.624	2432.43	16328.9
0.25119	1423.69	3390.22	14638.4
0.39811	2208.26	4632.56	12890.8
0.63097	3300.41	6238.38	11185.4
1.00003	4778.52	8289.74	9568.09
1.58496	6733.44	10939.4	8104.7
2.51202	9238.46	14381.7	6804.61
3.98132	12536.1	18945	5705.91
6.31006	16812	24969.3	4770.43
10.0007	22506.9	33073.3	4000.22
15.8501	30102	43853.3	3355.85
25.1206	40521.6	58111.7	2820.18
39.8135	54880.3	76676.4	2368.36
63.1006	74586.3	100098	1978.29
100	101175	128305	1633.97

D.3. HDB-3

Dynamic Oscillatory

T = 230ºC

ω rad/s	G' Pa	G" Pa	η* Pa-s
0.01	9.8878	111.051	11149
0.1	223.949	1001.98	10267
0.15849	399.568	1473	9629.85
0.25119	683.606	2126.98	8894.2
0.39811	1123.2	3004.04	8055.96
0.63097	1776.83	4171.94	7186.69
1.00003	2718.4	5700.96	6315.72
1.58496	4034.83	7686.38	5477.13
2.51202	5805.33	10244.4	4687.46
3.98132	8164.22	13624.6	3989.48
6.31006	11244.5	18027.1	3367.1
10.0007	15327.8	23904.3	2839.43
15.8501	20712.5	31707.6	2389.46
25.1206	27971.8	42146.2	2013.64
39.8135	37884.9	55978.8	1697.76
63.1006	51466.7	73912.8	1427.34
100	70014	96346.8	1190.99

D.3. HDB-3

Dynamic Oscillatory

T = 270ºC

ω rad/s	G' Pa	G" Pa	η* Pa-s
0.01	10.4729	64.5335	6537.78
0.1	79.4916	567.602	5731.4
0.15849	148.497	849.941	5444
0.25119	272.607	1263.37	5145.28
0.39811	482.955	1853.5	4811.2
0.63097	823.975	2676.4	4438.22
1.00003	1354.13	3796.81	4030.94
1.58496	2147.5	5301.53	3608.9
2.51202	3284.33	7303.05	3187.7
3.98132	4859.75	9945.32	2780.27
6.31006	7009.34	13436.4	2401.69
10.0007	9853.68	18108.1	2061.4
15.8501	13610.7	24389	1762.12
25.1206	18525.9	32884.5	1502.5
39.8135	24964.2	44489.2	1281.34
63.1006	33198.5	60227.2	1089.86
100	43217.6	81364.3	921.299

D.3. HDB-3

Dynamic Oscillatory

T = 320ºC

ω rad/s	G' Pa	G" Pa	η* Pa-s
0.01	28.4748	35.6612	4563.49
0.1	38.3495	252.583	2554.76
0.15849	62.2754	381.235	2437.31
0.25119	99.5324	574.857	2322.58
0.39811	163.944	869.918	2223.59
0.63097	278.852	1301.44	2109.43
1.00003	473.182	1925.56	1982.79
1.58496	794.189	2805.4	1839.57
2.51202	1303.67	4030.06	1686.16
3.98132	2075.27	5707.3	1525.35
6.31006	3208.31	7980.9	1363.16
10.0007	4825.03	11043.7	1205.09
15.8501	7048.15	15165.4	1055.08
25.1206	10080.8	20755.8	918.543
39.8135	14157.7	28354.2	796.02
63.1006	19542.3	38639.1	686.205
100	26463.1	52496.8	587.895

D.4. HDB-4

Dynamic Oscillatory

T = 150ºC

ω rad/s	G' Pa	G" Pa	η* Pa-s
0.1	3510.62	5392.93	64349
0.15849	4927.36	6956.9	53789.8
0.25119	6771.17	8887.51	44480.4
0.39811	9099.38	11231.6	36309.2
0.63097	11967.9	14147.1	29368
1.00003	15527.3	17867.4	23670.8
1.58496	19921.3	22610.4	19012.8
2.51202	25434.6	28802.3	15296.5
3.98132	32434.9	36874.5	12335
6.31006	41508.4	47382.1	9982.82
10.0007	53358.2	60974	8101.83
15.8501	68973.1	78375.3	6586.9
25.1206	89709	99992	5347.63
39.8135	117028	126470	4327.89
63.1006	152389	157791	3476.42
100	196796	192881	2755.57

D.4. HDB-4

Dynamic Oscillatory

T = 170ºC

ω rad/s	G' Pa	G" Pa	η* Pa-s
0.01	212.095	832.493	85908.7
0.1	2111.51	3918.81	44514.5
0.15849	3126.05	5196.25	38261.9
0.25119	4471.96	6760.93	32270.7
0.39811	6232.86	8699.3	26881.3
0.63097	8473.92	11083.1	22111.2
1.00003	11283.3	14101	18059.1
1.58496	14806.7	17873.5	14643.9
2.51202	19221.2	22760.6	11859.3
3.98132	24778.7	29081.7	9596.41
6.31006	31860.5	37362.7	7781.64
10.0007	41051.8	48108.5	6323.84
15.8501	53100.4	62008.2	5150.6
25.1206	69100.8	79578.9	4195.49
39.8135	90120.5	101503	3409.32
63.1006	117142	127338	2742.04
100	151932	157338	2187.21

D.4. HDB-4

Dynamic Oscillatory

T = 190ºC

ω rad/s	G' Pa	G" Pa	η* Pa-s
0.01	104.468	528.87	53908.9
0.1	1306.75	2904.52	31849.3
0.15849	1995.52	3927.29	27794.9
0.25119	2976.4	5230.74	23959
0.39811	4313.18	6864.55	20364.1
0.63097	6072.73	8893.33	17067.3
1.00003	8331.94	11426.7	14141.3
1.58496	11213.6	14599.7	11614.9
2.51202	14822	18617.5	9473.28
3.98132	19414.7	23782.5	7711.2
6.31006	25244.7	30492.4	6273.54
10.0007	32749.1	39196	5107.3
15.8501	42401	50495.6	4160.02
25.1206	55124.4	64984.8	3392.27
39.8135	71975.2	83240.5	2763.96
63.1006	93985.6	105921	2244.15
100	122517	132792	1806.76

D.4. HDB-4

Dynamic Oscillatory

T = 230ºC

ω rad/s	G' Pa	G" Pa	η* Pa-s
0.01	46.5039	270.127	27410.1
0.1	662.882	1900.78	20130.4
0.15849	1086.14	2670.34	18189.1
0.25119	1708.24	3672.07	16123.1
0.39811	2593.79	4957.35	14053.7
0.63097	3816.37	6591.02	12070.7
1.00003	5459.68	8646.14	10225.3
1.58496	7593.04	11249	8562.9
2.51202	10374.9	14531.5	7107.85
3.98132	13903.6	18771	5867.24
6.31006	18412.4	24237.6	4823.75
10.0007	24239.2	31407.4	3967.03
15.8501	31788.7	40761.3	3261.27
25.1206	41745.7	52977.7	2685
39.8135	54990.1	68694.9	2210.15
63.1006	72590.6	88579.1	1814.94
100	95713.1	112722	1478.76

D.4. HDB-4

Dynamic Oscillatory

T = 270ºC

ω rad/s	G' Pa	G" Pa	η* Pa-s
0.01	40.1916	195.215	19931
0.1	295.203	1126.32	11643.6
0.15849	489.737	1599.17	10552.6
0.25119	802.961	2257.93	9540.42
0.39811	1283.22	3150.07	8543.92
0.63097	1988.95	4333.24	7556.5
1.00003	2989.4	5865.56	6583.21
1.58496	4375.72	7849.62	5670.07
2.51202	6230.88	10396.7	4825.13
3.98132	8667.94	13693.6	4070.61
6.31006	11833.1	17974.5	3410.41
10.0007	15912.5	23612.6	2847.19
15.8501	21137.9	31094.2	2372.14
25.1206	27839.1	41093	1975.87
39.8135	36353	54507.3	1645.62
63.1006	46939.9	72434.2	1367.88
100	59124.1	96206.7	1129.22

D.4. HDB-4

Dynamic Oscillatory

T = 320ºC

ω rad/s	G' Pa	G" Pa	η* Pa-s
0.01	33.4703	69.6148	7724.31
0.1	83.0886	484.937	4920.02
0.15849	146.961	707.853	4561.49
0.25119	250.613	1038.34	4252.37
0.39811	421.087	1514.58	3948.72
0.63097	696.109	2180.13	3627.08
1.00003	1122.23	3093.4	3290.57
1.58496	1763.59	4325.86	2947.42
2.51202	2702.56	5962.95	2606.19
3.98132	4027.58	8118.46	2276.28
6.31006	5849.75	10947.3	1967.06
10.0007	8302.65	14655.5	1684.27
15.8501	11545.3	19533.7	1431.57
25.1206	15807.8	26004.4	1211.44
39.8135	21355.5	34623.8	1021.77
63.1006	28418.5	46100.2	858.244
100	37126.9	61271	716.417

D.5. HDB-5

Dynamic Oscillatory

T = 170ºC

ω rad/s	G' Pa	G" Pa	η* Pa-s
0.1	865.031	2362.01	25154.1
0.15849	1404.28	3282.08	22524.4
0.25119	2205.98	4468.06	19837.4
0.39811	3343.61	5961.45	17168.9
0.63097	4907.19	7807.57	14615.1
1.00003	6963.17	10062.3	12236.2
1.58496	9635.39	12823	10119.9
2.51202	12995.8	16186	8263.29
3.98132	17249	20346.9	6699.88
6.31006	22499.3	25544.2	5394.57
10.0007	29092.9	32152.3	4335.77
15.8501	37476.3	40515	3482
25.1206	48222.3	51130.8	2797.84
39.8135	62320.8	64401.9	2250.96
63.1006	80897.1	80552.6	1809.21
100	105649	99572.6	1451.77

D.6. HDB-6

Dynamic Oscillatory

T = 170ºC

ω rad/s	G' Pa	G" Pa	η* Pa-s
0.01	31.9876	290.113	29187.1
0.1	755.624	2106.76	22381.7
0.15849	1238.65	2955.64	20220.2
0.25119	1947.4	4047.74	17882.2
0.39811	2964.98	5422.69	15524.2
0.63097	4375.84	7146.25	13280.5
1.00003	6299.87	9256.53	11196.6
1.58496	8814.42	11800.8	9293.18
2.51202	12086.7	14827.2	7615.12
3.98132	16191.1	18448.1	6165.18
6.31006	21269.2	22725.3	4932.74
10.0007	27538	27874.6	3918.05
15.8501	35187.6	34065.3	3089.92
25.1206	44510.9	41637.8	2426.3
39.8135	56043.1	50946	1902.33
63.1006	70439.5	62403	1491.36
100	88948.6	76372.3	1172.37

D.7. HDB-7

Dynamic Oscillatory

T = 170ºC

ω rad/s	G' Pa	G" Pa	η* Pa-s
0.01	54.2027	328.314	33275.8
0.1	827.903	2189.99	23412.5
0.15849	1312.84	3038.83	20886.5
0.25119	2022.21	4144.79	18359.7
0.39811	2999.81	5571.2	15893.8
0.63097	4314.68	7402.87	13579.9
1.00003	6048.4	9775.56	11495.1
1.58496	8288.77	12872.7	9659.82
2.51202	11228.1	16964.3	8098.45
3.98132	15066.4	22453.5	6791.67
6.31006	20238.5	29775	5705.5
10.0007	27340	39544.3	4807.18
15.8501	37330.2	52204.7	4049.09
25.1206	51376.1	68233.8	3400.11
39.8135	71108.6	87738	2836.61
63.1006	98105.6	110171	2337.86
100	134240	134471	1900.08

D.8. Linear HDB

Dynamic Oscillatory

T = 150ºC

ω rad/s	G' Pa	G" Pa	η* Pa-s
0.1	31.1608	929.223	9297.42
0.15849	63.6474	1465.89	9257.89
0.25119	133.796	2300.22	9172.77
0.39811	268.581	3594.54	9054.2
0.63097	540.37	5574.62	8876.47
1.00003	1068.64	8581.07	8647.1
1.58496	2076.44	13077.4	8354.28
2.51202	3944.15	19672.1	7987.02
3.98132	7306.32	29087.9	7533.05
6.31006	12990.1	42102.4	6982.63
10.0007	22490.1	59700.5	6379.15
15.8501	37311	82403.6	5707.03
25.1206	59446.4	110478	4994.16
39.8135	90976.2	143757	4273.07
63.1006	133273	181435	3567.69
100	187138	221324	2898.36

D.8. Linear HDB

Dynamic Oscillatory

T = 170ºC

ω rad/s	G' Pa	G" Pa	η* Pa-s
0.01	0.46275	73.3039	7330.54
0.1	19.8712	701.898	7021.77
0.15849	42.5353	1109.3	7004.33
0.25119	86.7106	1739.73	6934.54
0.39811	175.721	2722.74	6853.41
0.63097	353.894	4234.14	6733.96
1.00003	707.883	6549.65	6587.59
1.58496	1383.82	10049.8	6400.54
2.51202	2650.22	15212.6	6147.12
3.98132	4978.41	22769.8	5854.25
6.31006	9132.86	33407.3	5488.56
10.0007	16076.6	48086.4	5069.89
15.8501	27248.5	67455.2	4589.93
25.1206	44505.2	92188.4	4075.1
39.8135	69754.2	122360	3537.66
63.1006	104833	157611	2999.84
100	145219	185807	2358.24

D.8. Linear HDB

Dynamic Oscillatory

T = 190ºC

ω rad/s	G' Pa	G" Pa	η* Pa-s
0.01	0.28639	51.1574	5115.82
0.1	11.3449	489.417	4895.46
0.15849	24.4242	770.883	4866.38
0.25119	48.6548	1212.82	4832.17
0.39811	99.7253	1906.54	4795.52
0.63097	203.837	2980.06	4734.05
1.00003	411.104	4632.35	4650.42
1.58496	816.709	7151.78	4541.6
2.51202	1619.03	10921.6	4395.24
3.98132	3078.01	16540.4	4225.82
6.31006	5736.58	24597.6	4002.76
10.0007	10400.6	35893.4	3736.71
15.8501	18117.8	51221.8	3427.84
25.1206	30404.2	71249.5	3083.75
39.8135	48971.4	96517	2718.43
63.1006	75662.3	126810	2340.18
100	111919	161184	1962.3

D.8. Linear HDB

Dynamic Oscillatory

T = 230ºC

ω rad/s	G' Pa	G" Pa	η* Pa-s
0.01	0.04326	30.9169	3091.7
0.1	4.34732	299.604	2996.34
0.15849	10.2594	473.517	2988.39
0.25119	21.5785	747.354	2976.49
0.39811	46.1188	1176.98	2958.7
0.63097	94.9118	1846.92	2931
1.00003	195.732	2887.45	2893.99
1.58496	396.853	4491.36	2844.77
2.51202	793.048	6934.1	2778.36
3.98132	1542.28	10604.6	2691.61
6.31006	2961.33	16024.8	2582.57
10.0007	5539.02	23869	2450.15
15.8501	9966.03	34866.9	2287.89
25.1206	17401.9	49877.2	2102.89
39.8135	29186.7	69596.9	1895.57

D.8. Linear HDB

Dynamic Oscillatory

T = 270ºC

ω rad/s	G' Pa	G" Pa	η* Pa-s
0.01	1.02495	21.929	2195.3
0.1	1.43265	210.1	2101.04
0.15849	3.8796	325.655	2054.89
0.25119	8.84428	510.308	2031.86
0.39811	20.1623	803.149	2018.04
0.63097	45.3911	1260.1	1998.39
1.00003	96.8627	1974.21	1976.53
1.58496	198.685	3081.5	1948.25
2.51202	405.4	4784.55	1911.48
3.98132	801.864	7380.03	1864.57
6.31006	1545.37	11273.9	1803.36
10.0007	2907.8	17041.6	1728.66
15.8501	5284.92	25408.6	1637.36
25.1206	9264.29	37306.8	1530.21
39.8135	15435.2	53870.4	1407.52

D.8. Linear HDB

Dynamic Oscillatory

T = 320ºC

ω rad/s	G' Pa	G" Pa	η* Pa-s
0.01	20.0267	19.8745	2821.46
0.1	15.3626	139.959	1407.99
0.15849	23.9188	211.977	1345.97
0.25119	34.1337	325.486	1302.88
0.39811	48.6057	503.19	1269.83
0.63097	73.0356	779.202	1240.35
1.00003	113.96	1206.53	1211.87
1.58496	187.122	1865.52	1182.92
2.51202	316.806	2877.31	1152.34
3.98132	551.226	4418.59	1118.43
6.31006	972.507	6748.44	1080.52
10.0007	1727.1	10223.5	1036.76
15.8501	3043.84	15327.2	985.891
25.1206	5293	22701.9	927.953
39.8135	8968.76	33138.8	862.295
63.1006	14662.9	47486.1	787.605
100	22786.3	66614.6	704.04

Appendix E: Pom-pom model Matlab numerical code

E.1 FinalPomPomModelExact0201

```
% M-File to calculate the stress tensor of long-chain branched
polymeric materials using the multi-mode Pom-Pom model constitutive
equation

clear all

% Experimental Shear Rheology Data

exact0201w =
[0.1,0.15849,0.25119,0.39811,0.63097,1,1.585,2.512,3.9813,6.3101,10.001
,15.850,25.121,39.813,63.101,100];
exact0201eta =
[29202,26121,23006,20013,17251,14744,12565,10665,9034.2,7630.1,6418.3,5
366.2,4440.8,3631.8,2925.4,2314];
exact0201Gprime =
[1062.9,1622.7,2467.8,3644.4,5255.6,7406.6,10324,14261,19628,27005,3720
2,51150,70096,95180,127370,167090];
exact0201Gdoubleprime =
[2733.6,3808.6,5225.4,7085,9532,12749,17030,22679,30141,39860,52308,679
55,86783,108850,133600,160080];
loglog(exact0201w,exact0201Gprime,'*')
hold
loglog(exact0201w,exact0201Gdoubleprime,'.')
loglog(exact0201w,exact0201eta,'o')

% Model Parameters

g = [10000;10000;10000;10000;10000];
LB = [0;0;0;0;0];
UB = [1000000;1000000;1000000;1000000;1000000];
g = [246000;49000;10600;2020;76.1];
ptaub = [0.01;0.1;1;10;100];
taubtaus = [10;10;10;10;4];
pq = [1;1;1;1;10];
s = size(ptaub);
c = s(1,1);
q = size(exact0201w);
r = q(1,2);

% Linear Viscoelastic Curve Fitting

options = optimset('MaxFunEvals',10000,'MaxIter',10000,'TolFun',1e-
6,'TolX',1e-6)
[g,fval,exitflag] = fminsearchbnd(@(g)
minimizationexact0201(g,exact0201w,exact0201eta,exact0201Gprime,exact02
01Gdoubleprime,ptaub,r),g,LB,UB,options)

for i = 1:r
    exact0201Gprimecalculated(i) =
exact0201w(i)^2*g(1)*ptaub(1)^2/(1+(exact0201w(i)*ptaub(1))^2)+exact020
1w(i)^2*g(2)*ptaub(2)^2/(1+(exact0201w(i)*ptaub(2))^2)+exact0201w(i)^2*
g(3)*ptaub(3)^2/(1+(exact0201w(i)*ptaub(3))^2)+exact0201w(i)^2*g(4)*pta
```

```
ub(4)^2/(1+(exact0201w(i)*ptaub(4))^2)+exact0201w(i)^2*g(5)*ptaub(5)^2/
(1+(exact0201w(i)*ptaub(5))^2);
    exact0201Gdoubleprimecalculated(i) =
exact0201w(i)*g(1)*ptaub(1)/(1+(exact0201w(i)*ptaub(1))^2)+exact0201w(i
)*g(2)*ptaub(2)/(1+(exact0201w(i)*ptaub(2))^2)+exact0201w(i)*g(3)*ptaub
(3)/(1+(exact0201w(i)*ptaub(3))^2)+exact0201w(i)*g(4)*ptaub(4)/(1+(exac
t0201w(i)*ptaub(4))^2)+exact0201w(i)*g(5)*ptaub(5)/(1+(exact0201w(i)*pt
aub(5))^2);
end
for i = 1:r
    exact0201etacalculated(i) =
((exact0201w(i)*g(1)*ptaub(1)^2/(1+(exact0201w(i)*ptaub(1))^2)+exact020
1w(i)*g(2)*ptaub(2)^2/(1+(exact0201w(i)*ptaub(2))^2)+exact0201w(i)*g(3)
*ptaub(3)^2/(1+(exact0201w(i)*ptaub(3))^2)+exact0201w(i)*g(4)*ptaub(4)^
2/(1+(exact0201w(i)*ptaub(4))^2)+exact0201w(i)*g(5)*ptaub(5)^2/(1+(exac
t0201w(i)*ptaub(5))^2))^2+(g(1)*ptaub(1)/(1+(exact0201w(i)*ptaub(1))^2)
+g(2)*ptaub(2)/(1+(exact0201w(i)*ptaub(2))^2)+g(3)*ptaub(3)/(1+(exact02
01w(i)*ptaub(3))^2)+g(4)*ptaub(4)/(1+(exact0201w(i)*ptaub(4))^2)+g(5)*p
taub(5)/(1+(exact0201w(i)*ptaub(5))^2))^2)^(1/2);
end
loglog(exact0201w,exact0201Gprimecalculated,'-')
loglog(exact0201w,exact0201Gdoubleprimecalculated,'-')
loglog(exact0201w,exact0201etacalculated,'-')

% Experimental Extensional Rheology Data

exact0201t1 =
[2.34,4.69,7.03,9.38,11.72,14.06,16.41,18.75,21.09,23.44,25.78,28.13,30
.47,32.81,35.16,37.5,39.84,42.19,44.53,46.88,49.22,51.56,53.91,56.25,58
.59,60.94,63.28,65.63,67.97,70.31,72.66,75,77.34,79.69,82.03,84.38,86.7
2,89.06,91.41,93.75,96.1,98.44,100.8,103.1,105.5,107.8,110.2,112.5,114.
9,117.2,119.5,121.9,124.2,126.6,128.9,131.3,133.6,135.9,138.3,140.6,143
,145.3,147.7,150,152.4,154.7,157,159.4,161.7,164.1,166.4,168.8,171.1,17
3.4,178.1,180.5,182.8,185.2,187.5,189.9,192.2,194.5,196.9,199.2,201.6,2
03.9,206.3,208.6,210.9,213.3,215.6,218,220.3,222.7,225,227.4,229.7,232,
234.4,236.7,239.1,241.4,243.8,246.1,248.4,250.8,253.1,255.5,257.8,260.2
,262.5,264.8,267.2,269.5,271.9,274.2,276.6,278.9,281.3,283.6,285.9,288.
3,290.6,293,295.3,297.7];
exact0201v1 =
[20820,70860,80600,933400,101100,103700,107200,108900,110400,110100,113
600,113700,114100,116700,121700,121300,121600,119900,121500,123500,1235
00,125300,127200,126200,124700,127800,125800,126800,126600,127200,12790
0,128700,129700,130500,129300,129800,132600,129900,129700,133000,133400
,134200,132300,132800,133800,136000,136600,136300,134800,132300,134600,
137400,137400,136800,135800,136400,136900,137100,136800,138100,138600,1
37600,138500,139400,141100,142100,140100,141600,140100,138500,140800,13
9400,139800,140900,140700,140000,142200,140100,139400,139600,141200,140
800,140300,139800,140500,141100,138200,143100,141500,140900,142600,1429
00,143300,140800,142300,141700,143100,142500,143200,142000,143800,14330
0,144500,145100,144100,141500,140500,144800,140800,140100,142800,144600
,140700,139500,141000,138300,142300,142200,145300,140200,138700,141600,
140300,144900,144700,144200];
exact0201t2 =
[0.234,0.469,0.703,0.938,1.172,1.406,1.641,1.875,2.109,2.344,2.578,2.81
3,3.047,3.281,3.516,3.750,3.984,4.219,4.453,4.688,4.922,5.156,5.391,5.6
25,5.859,6.094,6.328,6.563,6.797,7.031,7.266,7.500,7.734,7.969,8.203,8.
```

```
438,8.672,8.906,9.141,9.375,9.610,9.844,10.08,10.31,10.55,10.78,11.02,1
1.25,11.49,11.72,11.95,12.19,12.42,12.66,12.89,13.13,13.36,13.59,13.83,
14.06,14.30,14.53,14.77,15,15.24,15.47,15.7,15.94,16.17,16.41,16.64,16.
88,17.11,17.34,17.58,17.81,18.05,18.28,18.52,18.75,18.99,19.22,19.45,19
.69,19.92,20.16,20.39,20.63,20.86,21.09,21.33,21.56,21.80,22.03,22.27,2
2.5,22.74,22.97,23.2,23.44,23.67,23.91,24.14,24.38,24.61,24.84,25.08,25
.31,25.55,25.78,26.02,26.25,26.49,26.72,26.95,27.19,27.42,27.66,27.89,2
8.13,28.36,28.60,28.83,29.06,29.30,29.53,29.77];
exact0201v2 =
[17410,27230,36370,46890,47160,53550,59030,59950,62220,62950,65130,6476
0,65500,67170,69830,70520,72020,74060,73780,75800,76700,77940,78780,798
70,81120,81430,81280,83310,84990,84620,85680,87850,89140,89690,88870,90
910,91160,91520,91980,92870,93240,95380,96170,96340,97790,97520,98690,9
8910,99900,99460,100670,101600,102410,103050,104460,104190,106100,10691
0,107150,108150,108300,108150,108900,110050,110480,110950,111380,111880
,113200,113130,113580,115150,115430,116630,117380,117750,118530,119450,
119180,120700,121350,121580,122880,122930,125150,125630,125830,127450,1
27930,128930,131330,131930,132480,133730,134030,134780,136450,136250,13
7380,138350,138900,140900,141900,142880,143500,144300,144850,146280,146
950,148030,149480,149830,151180,151280,152150,154100,153500,154150,1549
00,155950,156780,157450,157700,158650,159250,159550,160300];
exact0201t3 =
[0.018,0.0401,0.0617,0.0870,0.1117,0.1358,0.1593,0.1823,0.2048,0.2304,0
.2518,0.2763,0.3001,0.3234,0.3462,0.3684,0.3933,0.4145,0.4383,0.4643,0.
4869,0.5090,0.5333,0.5570,0.5802,0.6028,0.6250,0.6466,0.6702,0.6954,0.7
178,0.7398,0.7634,0.7864,0.8109,0.8329,0.8583,0.8792,0.9035,0.9271,0.95
03,0.9728,0.9966,1.02,1.044,1.066,1.089,1.114,1.137,1.1160,1.1183,1.206
,1.229,1.253,1.276,1.3,1.323,1.346,1.369,1.392,1.415,1.439,1.462,1.486,
1.509,1.532,1.555,1.578,1.601,1.625,1.648,1.671,1.695,1.718,1.741,1.765
,1.788,1.811,1.835,1.858,1.881,1.904,1.928,1.950,1.974,1.997,2.02,2.044
,2.067,2.09,2.114,2.137,2.160,2.183,2.206,2.230,2.253,2.276,2.299,2.323
,2.346,2.369,2.393,2.416,2.439,2.462,2.486,2.509,2.532,2.555,2.578,2.60
2,2.625,2.648,2.672,2.695,2.718,2.741,2.765,2.788,2.811,2.834,2.858,2.8
81,2.904,2.927,2.951];
exact0201v3 =
[3780,15688,20825,21940,25518,28283,29295,30593,32415,34103,35375,36470
,37653,38725,39495,40478,41485,42235,43220,44710,45143,46015,46903,4771
8,48295,48755,49525,50308,49743,51173,53060,52270,52665,54175,54558,550
50,55535,55958,56220,56930,57605,58188,58713,59145,59903,60215,60360,61
048,61868,62090,62500,62943,63410,64070,64563,64873,65493,65983,66588,6
6925,67710,68348,68678,69015,69438,70003,70388,70830,71325,71810,72360,
72845,73390,73873,74313,75050,75575,75860,76333,77003,77253,77693,78388
,78943,79283,79885,80500,81235,81805,82430,82940,83760,84310,84770,8536
5,85905,86590,87450,87780,88315,89135,89670,90590,91165,91290,92675,929
45,93040,93705,94985,95095,95950,97120,97420,97470,98295,98840,99040,99
330,99635,99915,99950,100800,101000,100600,101150,101200];
loglog(exact0201t1,exact0201v1,'o')
loglog(exact0201t2,exact0201v2,'o')
loglog(exact0201t3,exact0201v3,'o')

% Produce zero matrices for K, sum, and tsum

K = [0 0 0; 0 0 0; 0 0 0];
sum = zeros(461,4);
tsum = zeros(461,4);
```

```
% For shear flow gamma is defined and epsilon = 0; For extensional flow
epsilon is defined and gamma = 0

gamma = 0;
epsilon = 0.1317;

% For elongational flow b = 0; For planar elongational flow b = 1

b = 0;

% Multi-mode Pom-Pom model constitutive equation solution for shear
flow

if gamma ~= 0
    K = [0 1 0; 0 0 0; 0 0 0]*gamma;
    K1 = K(1,1);
    K2 = K(1,2);
    K5 = K(2,2);
    K9 = K(3,3);
    lambda = zeros(461,1);
    lambda(1) = 1;

% Solution for the orientation tensor S and the backbone stretch lambda
at each mode

    for i = 1:c(1,1)
        i
        taub = ptaub(i);
        taus = ptaub(i)/taubtaus(i);
        q = pq(i);
        tspan =
[0.01,0.011,0.012,0.013,0.014,0.015,0.016,0.017,0.018,0.019,0.02,0.021,
0.022,0.023,0.024,0.025,0.026,0.027,0.028,0.029,0.03,0.031,0.032,0.033,
0.034,0.035,0.036,0.037,0.038,0.039,0.04,0.041,0.042,0.043,0.044,0.045,
0.046,0.047,0.048,0.049,0.05,0.051,0.052,0.053,0.054,0.055,0.056,0.057,
0.058,0.059,0.06,0.061,0.062,0.063,0.064,0.065,0.066,0.067,0.068,0.069,
0.07,0.071,0.072,0.073,0.074,0.075,0.076,0.077,0.078,0.079,0.08,0.081,0
.082,0.083,0.084,0.085,0.086,0.087,0.088,0.089,0.09,0.091,0.092,0.093,0
.094,0.095,0.096,0.097,0.098,0.099,0.1,0.11,0.12,0.13,0.14,0.15,0.16,0.
17,0.18,0.19,0.2,0.21,0.22,0.23,0.24,0.25,0.26,0.27,0.28,0.29,0.3,0.31,
0.32,0.33,0.34,0.35,0.36,0.37,0.38,0.39,0.4,0.41,0.42,0.43,0.44,0.45,0.
46,0.47,0.48,0.49,0.5,0.51,0.52,0.53,0.54,0.55,0.56,0.57,0.58,0.59,0.6,
0.61,0.62,0.63,0.64,0.65,0.66,0.67,0.68,0.69,0.7,0.71,0.72,0.73,0.74,0.
75,0.76,0.77,0.78,0.79,0.8,0.81,0.82,0.83,0.84,0.85,0.86,0.87,0.88,0.89
,0.9,0.91,0.92,0.93,0.94,0.95,0.96,0.97,0.98,0.99,1,1.1,1.2,1.3,1.4,1.5
,1.6,1.7,1.8,1.9,2,2.1,2.2,2.3,2.4,2.5,2.6,2.7,2.8,2.9,3,3.1,3.2,3.3,3.
4,3.5,3.6,3.7,3.8,3.9,4,4.1,4.2,4.3,4.4,4.5,4.6,4.7,4.8,4.9,5,5.1,5.2,5
.3,5.4,5.5,5.6,5.7,5.8,5.9,6,6.1,6.2,6.3,6.4,6.5,6.6,6.7,6.8,6.9,7,7.1,
7.2,7.3,7.4,7.5,7.6,7.7,7.8,7.9,8,8.1,8.2,8.3,8.4,8.5,8.6,8.7,8.8,8.9,9
,9.1,9.2,9.3,9.4,9.5,9.6,9.7,9.8,9.9,10,11,12,13,14,15,16,17,18,19,20,2
1,22,23,24,25,26,27,28,29,30,31,32,33,34,35,36,37,38,39,40,41,42,43,44,
45,46,47,48,49,50,51,52,53,54,55,56,57,58,59,60,61,62,63,64,65,66,67,68
,69,70,71,72,73,74,75,76,77,78,79,80,81,82,83,84,85,86,87,88,89,90,91,9
2,93,94,95,96,97,98,99,100,110,120,130,140,150,160,170,180,190,200,210,
220,230,240,250,260,270,280,290,300,310,320,330,340,350,360,370,380,390
```

```
,400,410,420,430,440,450,460,470,480,490,500,510,520,530,540,550,560,57
0,580,590,600,610,620,630,640,650,660,670,680,690,700,710,720,730,740,7
50,760,770,780,790,800,810,820,830,840,850,860,870,880,890,900,910,920,
930,940,950,960,970,980,990,1000,1100,1200,1300,1400,1500,1600,1700,180
0,1900,2000];
        lambdazero = [1];
        options = odeset('RelTol', 1e-6, 'AbsTol', 1e-6);

        for j = 1:461
            A1 = 1+2*gamma^2*taub^2*(1-exp(-tspan(j)/taub)-
tspan(j)/taub*exp(-tspan(j)/taub));
            A2 = 1;
            A3 = 1;
            A4 = gamma*taub*(1-exp(-tspan(j)/taub));
            S(j,1) = A1/(A1+A2+A3);
            S(j,2) = A2/(A1+A2+A3);
            S(j,3) = A3/(A1+A2+A3);
            S(j,4) = A4/(A1+A2+A3);
        end

        [t,lambda] =
ode15s(@ShearSolve,tspan,lambdazero,options,gamma,taub,taus,q);

% Solution for the stress sigma at each mode

        for l = 1:461
            for k = 1:4
                sum(l,k) = g(i)*lambda(l)^2*S(l,k);
                tsum(l,k) = tsum(l,k)+sum(l,k);
            end
        end
    end

% Calculation for the total stress tensor sigma

    sigma = 3*tsum;

    for n = 1:461
        etaS(n) = sigma(n,4)/gamma;
    end

    loglog(t,etaS)

end

% Multi-mode Pom-Pom model constitutive equation solution for uniaxial
elongational flow

if epsilon ~= 0 & b == 0
    K = [-0.5*(1+b) 0 0; 0 -0.5*(1-b) 0; 0 0 1]*epsilon;
    K1 = K(1,1);
    K2 = K(1,2);
    K5 = K(2,2);
    K9 = K(3,3);
```

```
% Solution for the orientation tensor S and the backbone stretch lambda
at each mode

    for x = 1:c(1,1)
        x
        taub = ptaub(x);
        taus = ptaub(x)/taubtaus(x);
        q = pq(x);
        tspan =
[0.01,0.011,0.012,0.013,0.014,0.015,0.016,0.017,0.018,0.019,0.02,0.021,
0.022,0.023,0.024,0.025,0.026,0.027,0.028,0.029,0.03,0.031,0.032,0.033,
0.034,0.035,0.036,0.037,0.038,0.039,0.04,0.041,0.042,0.043,0.044,0.045,
0.046,0.047,0.048,0.049,0.05,0.051,0.052,0.053,0.054,0.055,0.056,0.057,
0.058,0.059,0.06,0.061,0.062,0.063,0.064,0.065,0.066,0.067,0.068,0.069,
0.07,0.071,0.072,0.073,0.074,0.075,0.076,0.077,0.078,0.079,0.08,0.081,0
.082,0.083,0.084,0.085,0.086,0.087,0.088,0.089,0.09,0.091,0.092,0.093,0
.094,0.095,0.096,0.097,0.098,0.099,0.1,0.11,0.12,0.13,0.14,0.15,0.16,0.
17,0.18,0.19,0.2,0.21,0.22,0.23,0.24,0.25,0.26,0.27,0.28,0.29,0.3,0.31,
0.32,0.33,0.34,0.35,0.36,0.37,0.38,0.39,0.4,0.41,0.42,0.43,0.44,0.45,0.
46,0.47,0.48,0.49,0.5,0.51,0.52,0.53,0.54,0.55,0.56,0.57,0.58,0.59,0.6,
0.61,0.62,0.63,0.64,0.65,0.66,0.67,0.68,0.69,0.7,0.71,0.72,0.73,0.74,0.
75,0.76,0.77,0.78,0.79,0.8,0.81,0.82,0.83,0.84,0.85,0.86,0.87,0.88,0.89
,0.9,0.91,0.92,0.93,0.94,0.95,0.96,0.97,0.98,0.99,1,1.1,1.2,1.3,1.4,1.5
,1.6,1.7,1.8,1.9,2,2.1,2.2,2.3,2.4,2.5,2.6,2.7,2.8,2.9,3,3.1,3.2,3.3,3.
4,3.5,3.6,3.7,3.8,3.9,4,4.1,4.2,4.3,4.4,4.5,4.6,4.7,4.8,4.9,5,5.1,5.2,5
.3,5.4,5.5,5.6,5.7,5.8,5.9,6,6.1,6.2,6.3,6.4,6.5,6.6,6.7,6.8,6.9,7,7.1,
7.2,7.3,7.4,7.5,7.6,7.7,7.8,7.9,8,8.1,8.2,8.3,8.4,8.5,8.6,8.7,8.8,8.9,9
,9.1,9.2,9.3,9.4,9.5,9.6,9.7,9.8,9.9,10,11,12,13,14,15,16,17,18,19,20,2
1,22,23,24,25,26,27,28,29,30,31,32,33,34,35,36,37,38,39,40,41,42,43,44,
45,46,47,48,49,50,51,52,53,54,55,56,57,58,59,60,61,62,63,64,65,66,67,68
,69,70,71,72,73,74,75,76,77,78,79,80,81,82,83,84,85,86,87,88,89,90,91,9
2,93,94,95,96,97,98,99,100,110,120,130,140,150,160,170,180,190,200,210,
220,230,240,250,260,270,280,290,300,310,320,330,340,350,360,370,380,390
,400,410,420,430,440,450,460,470,480,490,500,510,520,530,540,550,560,57
0,580,590,600,610,620,630,640,650,660,670,680,690,700,710,720,730,740,7
50,760,770,780,790,800,810,820,830,840,850,860,870,880,890,900,910,920,
930,940,950,960,970,980,990,1000,1100,1200,1300,1400,1500,1600,1700,180
0,1900,2000];
        lambdazero = [1];
        options = odeset('RelTol', 1e-6, 'AbsTol', 1e-6);
        p = 0;
        if epsilon == 0.5/taub
            p = epsilon/1000;
        end

        for y = 1:461
            if tspan(y)*(2*(epsilon+p)-1/taub) < 44
                A1 = 1/(1-2*(epsilon+p)*taub)*(1-
exp(tspan(y)*(2*(epsilon+p)-1/taub)))+exp(tspan(y)*(2*(epsilon+p)-
1/taub));
            else A1 = 1/(2*(epsilon+p)*taub-
1)*12850000000000000000+12850000000000000000;
            end
            A2 = 1/(1+epsilon*taub)*(1-exp(-
tspan(y)*(epsilon+1/taub)))+exp(-tspan(y)*(epsilon+1/taub));
```

```
            A3 = 1/(1+epsilon*taub)*(1-exp(-
tspan(y)*(epsilon+1/taub)))+exp(-tspan(y)*(epsilon+1/taub));
            A4 = 0;
            S(y,1) = A1/(A1+A2+A3);
            S(y,2) = A2/(A1+A2+A3);
            S(y,3) = A3/(A1+A2+A3);
            S(y,4) = A4/(A1+A2+A3);
        end

        [t,lambda] =
ode15s(@ExtSolve,tspan,lambdazero,options,epsilon,p,taub,taus,q);

% Solution for the stress sigma at each mode

        for w = 1:461
            for z = 1:4
            sum(w,z) = g(x)*lambda(w)^2*S(w,z);
            tsum(w,z) = tsum(w,z)+sum(w,z);
            end
        end
    end

% Calculation for the total stress tensor sigma

    sigma = 3*tsum;

    for m = 1:461;
        etaE(m) = (sigma(m,1)-sigma(m,3))/epsilon;
    end

    loglog(t,etaE)

end
```

E.2 MinimizationExact0201

```
function LVEfit =
minimizationexact0201(g,exact0201w,exact0201eta,exact0201Gprime,exact02
01Gdoubleprime,ptaub,r)

LVEfit1 = 0;
LVEfit2 = 0;

for i = 1:r
    exact0201Gprimecalculated(i) =
exact0201w(i)^2*g(1)*ptaub(1)^2/(1+(exact0201w(i)*ptaub(1))^2)+exact020
1w(i)^2*g(2)*ptaub(2)^2/(1+(exact0201w(i)*ptaub(2))^2)+exact0201w(i)^2*
g(3)*ptaub(3)^2/(1+(exact0201w(i)*ptaub(3))^2)+exact0201w(i)^2*g(4)*pta
ub(4)^2/(1+(exact0201w(i)*ptaub(4))^2)+exact0201w(i)^2*g(5)*ptaub(5)^2/
(1+(exact0201w(i)*ptaub(5))^2);
    exact0201Gdoubleprimecalculated(i) =
exact0201w(i)*g(1)*ptaub(1)/(1+(exact0201w(i)*ptaub(1))^2)+exact0201w(i
)*g(2)*ptaub(2)/(1+(exact0201w(i)*ptaub(2))^2)+exact0201w(i)*g(3)*ptaub
(3)/(1+(exact0201w(i)*ptaub(3))^2)+exact0201w(i)*g(4)*ptaub(4)/(1+(exac
t0201w(i)*ptaub(4))^2)+exact0201w(i)*g(5)*ptaub(5)/(1+(exact0201w(i)*pt
aub(5))^2);
    LVEfit2 = LVEfit2+(exact0201Gprimecalculated(i)/exact0201Gprime(i)-
1)^2+(exact0201Gdoubleprimecalculated(i)/exact0201Gdoubleprime(i)-1)^2;
end

for j = 1:r
    exact0201etacalculated(j) =
((exact0201w(j)*g(1)*ptaub(1)^2/(1+(exact0201w(j)*ptaub(1))^2)+exact020
1w(j)*g(2)*ptaub(2)^2/(1+(exact0201w(j)*ptaub(2))^2)+exact0201w(j)*g(3)
*ptaub(3)^2/(1+(exact0201w(j)*ptaub(3))^2)+exact0201w(j)*g(4)*ptaub(4)^
2/(1+(exact0201w(j)*ptaub(4))^2)+exact0201w(j)*g(5)*ptaub(5)^2/(1+(exac
t0201w(j)*ptaub(5))^2))^2+(g(1)*ptaub(1)/(1+(exact0201w(j)*ptaub(1))^2)
+g(2)*ptaub(2)/(1+(exact0201w(j)*ptaub(2))^2)+g(3)*ptaub(3)/(1+(exact02
01w(j)*ptaub(3))^2)+g(4)*ptaub(4)/(1+(exact0201w(j)*ptaub(4))^2)+g(5)*p
taub(5)/(1+(exact0201w(j)*ptaub(5))^2))^2)^(1/2);
    LVEfit1 = LVEfit1+(exact0201etacalculated(j)-exact0201eta(j))^2;
end

LVEfit = LVEfit1+LVEfit2;
```

E.3 ShearSolve

```
function lambdaprime = ShearSolve(t,lambda,gamma,taub,taus,q)

A1 = 1+2*gamma^2*taub^2*(1-exp(-t/taub)-t/taub*exp(-t/taub));
A2 = 1;
A3 = 1;
A4 = gamma*taub*(1-exp(-t/taub));
lambdaprime = lambda*gamma*A4/(A1+A2+A3)-((lambda-
1)/taus)*exp(2*(lambda-1)/q);

if lambda >= q & lambdaprime > 0
    lambdaprime = [0];
else lambdaprime = [lambda(1)*gamma*A4/(A1+A2+A3)-((lambda(1)-
1)/taus)*exp(2*(lambda(1)-1)/q)];
end
```

E.4. ExtSolve

```
function lambdaprime = ExtSolve(t,lambda,epsilon,p,taub,taus,q)

if t*(2*(epsilon+p)-1/taub) < 44
    A1 = 1/(1-2*(epsilon+p)*taub)*(1-exp(t*(2*(epsilon+p)-
1/taub)))+exp(t*(2*(epsilon+p)-1/taub));
else A1 = 1/(2*(epsilon+p)*taub-
1)*12850000000000000000+12850000000000000000;
end
A2 = 1/(1+epsilon*taub)*(1-exp(-t*(epsilon+1/taub)))+exp(-
t*(epsilon+1/taub));
A3 = 1/(1+epsilon*taub)*(1-exp(-t*(epsilon+1/taub)))+exp(-
t*(epsilon+1/taub));
A4 = 0;
lambdaprime = lambda*(epsilon*A1/(A1+A2+A3)-epsilon*A2/(2*(A1+A2+A3))-
epsilon*A3/(2*(A1+A2+A3)))-(lambda-1)/taus*exp(2*(lambda-1)/q);

if lambda >= q & lambdaprime > 0
    lambdaprime = [0];
else lambdaprime = [lambda(1)*(epsilon*A1/(A1+A2+A3)-
epsilon*A2/(2*(A1+A2+A3))-epsilon*A3/(2*(A1+A2+A3)))-(lambda(1)-
1)/taus*exp(2*(lambda(1)-1)/q)];
end
```

Appendix F: Nomenclature

Provided in this appendix is the nomenclature associated with all of the equations presented in the literature review portion of this text. The variables are organized by their respective equation.

F.1 Nomenclature

Equation 2.1.1

g'	ratio of branched to linear intrinsic viscosities
$[\eta]_{branched}$	intrinsic viscosity for a branched material
$[\eta]_{linear}$	intrinsic viscosity for a linear material
$\left(\langle s^2 \rangle_0\right)_{branched}$	radius of gyration for a branched material
$\left(\langle s^2 \rangle_0\right)_{linear}$	radius of gyration for a linear material
g^k	ratio of branched to linear mean-square radii of gyration

Equation 2.1.2

v_x	velocity component in the x direction
$\dot{\gamma}_{yx}$	velocity gradient
y	position in the y direction

Equation 2.1.3

v_y	velocity component in the y direction

Equation 2.1.4

v_z	velocity component in the z direction

Equation 2.1.5

$\dot{\gamma}_{ij}$	velocity gradient
$\dot{\gamma}(t)$	shear rate

Equation 2.1.6

l	distance between two neighboring fluid particles
l_0	initial separation of two neighboring fluid particles on the y-axis
$\dot{\gamma}$	shear rate
Δt	time interval

Equation 2.1.7

η^*	complex viscosity
η'	viscoelastic material function related to the loss modulus
i	imaginary root
η''	viscoelastic material function related to the storage modulus

Equation 2.1.8

v_x	velocity component in the x direction
$\dot{\varepsilon}$	elongation rate
b	shear-free flow parameter where b = 0 for elongational and biaxial stretching flows and b = 1 for planar elongational flows
x	position in the x direction

Equation 2.1.9

v_y	velocity component in the y direction
$\dot{\varepsilon}$	elongation rate
b	shear-free flow parameter where b = 0 for elongational and biaxial stretching flows and b = 1 for planar elongational flows
y	position in the y direction

Equation 2.1.10

v_z	velocity component in the z direction
$\dot{\varepsilon}$	elongation rate
z	position in the z direction

Equation 2.1.11

$\dot{\gamma}_{ij}$	velocity gradient
$\dot{\varepsilon}(t)$	elongation rate
b	shear-free flow parameter where b = 0 for elongational and biaxial stretching flows and b = 1 for planar elongational flows

Equation 2.1.12

l	distance between two neighboring fluid particles
l_0	initial separation of two neighboring fluid particles on the z-axis
$\dot{\varepsilon}$	elongation rate
Δt	time interval

Equation 2.1.13

$\overline{\eta}(\dot{\varepsilon})$	elongational viscosity
$\overline{\eta}_1(\dot{\varepsilon},0)$	viscosity function describing normal stress differences
τ_{xx}	stress component in the x,x direction
τ_{zz}	stress component in the z,z direction

Equation 2.4.1

σ	viscoelastic stress tensor
G_0	plateau modulus
ϕ_b	volume fraction of backbone material
λ	stretch ratio of the backbone
q	number of dangling arms on each branch point
$s_c(t)$	number of entanglement segments of arms drawn into the backbone tube
s_a	molecular weight of dangling arms in terms of the entanglement molecular weight
s_b	molecular weight of the backbone segment in terms of the entanglement molecular weight
$S(t)$	Second moment of the orientation distribution of backbone segments

Equation 2.4.2

$S(t)$	Second moment of the orientation distribution of backbone segments
$\tau_b(t')$	relaxation time for backbone orientation at t'
t'	time, t'
$\tau_b(t'')$	relaxation time for backbone orientation at t''
t''	time, t''
$E(t,t')$	deformation gradient tensor
u	orientation

Equation 2.4.3

λ	stretch ratio of the backbone
t	time
K	rate of deformation tensor
S	Second moment of the orientation distribution of backbone segments
τ_s	relaxation time for stretch
q	number of dangling arms on each branch point

Equation 2.4.4

s_c	number of entanglement segments of arms drawn into the backbone tube
t	time
q	number of dangling arms on each branch point
s_b	molecular weight of the backbone segment in terms of the entanglement molecular weight
K	rate of deformation tensor
S	Second moment of the orientation distribution of backbone segments
τ_a	relaxation time for an arm segment
x_c	fraction of arm withdrawn into a backbone tube

Equation 2.4.5

τ_b	relaxation time for backbone orientation
s_b	molecular weight of the backbone segment in terms of the entanglement molecular weight
ϕ_b	volume fraction of backbone material
τ_a	relaxation time for an arm segment
$x_c(t)$	fraction of arm withdrawn into a backbone tube
q	number of dangling arms on each branch point

Equation 2.4.6

$\tau_a(x)$	relaxation time for an arm segment a fraction x from the branch point to the free end
τ_0	attempt time for deep retractions of the entangled dangling arm
s_a	molecular weight of dangling arms in terms of the entanglement molecular weight
x	fractional distance from the branch point to the free end
ϕ_b	volume fraction of backbone material

Equation 2.4.7

τ_s	relaxation time for stretch
s_b	molecular weight of the backbone segment in terms of the entanglement molecular weight
$\tau_a(0)$	longest relaxation time of an arm segment
q	number of dangling arms on each branch point

Equation 2.4.8

$E(t,t')$	deformation gradient tensor
u	orientation

Equation 2.4.9

Q	Currie tensor
J	function of the first and second invariants of E
B	Finger tensor
I_2	second invariant of E
C	Cauchy tensor

Equation 2.4.10

J	function of the first and second invariants of E
I_1	first invariant of E
I_2	second invariant of E

Equation 2.4.11

σ	viscoelastic stress tensor
G_0	plateau modulus
ϕ_b	volume fraction of backbone material
$\lambda\ (t)$	stretch ratio of the backbone
$S(t)$	second moment of the orientation distribution of backbone segments
s_b	molecular weight of the backbone segment in terms of the entanglement molecular weight
q	number of dangling arms on each branch point
s_a	molecular weight of dangling arms in terms of the entanglement molecular weight

Equation 2.4.12

$A(t)$	auxiliary orientation tensor
t	time
K	rate of deformation tensor
τ_b	relaxation time for backbone orientation
I	identity matrix

Equation 2.4.13

$S(t)$	second moment of the orientation distribution of backbone segments
$A(t)$	auxiliary orientation tensor

Equation 2.4.14

λ	stretch ratio of the backbone
t	time
K	rate of deformation tensor
S	second moment of the orientation distribution of backbone segments
τ_s	relaxation time for stretch
q	number of dangling arms on each branch point

Equation 2.4.15

τ_b	relaxation time for backbone orientation
s_b	molecular weight of the backbone segment in terms of the entanglement molecular weight
ϕ_b	volume fraction of backbone material
$\tau_a(0)$	longest relaxation time of an arm segment
q	number of dangling arms on each branch point

Equation 2.4.16

τ_s	relaxation time for stretch
s_b	molecular weight of the backbone segment in terms of the entanglement molecular weight
$\tau_a(0)$	longest relaxation time of an arm segment
q	number of dangling arms on each branch point

Equation 2.4.17

σ	viscoelastic stress tensor
g_i	fraction of stress relaxing
$\lambda_i(t)$	evolution of stretch
$S_i(t)$	evolution of orientation

Equation 2.4.18

$\lambda(t)$	stretch ratio of the backbone
t	time
K	rate of deformation tensor
S	second moment of the orientation distribution of backbone segments
τ_s	relaxation time for stretch
ν^*	parameter taken to be 2/q

Equation 2.4.19

τ	stress tensor
G_0	plateau modulus
Λ	backbone tube stretch
S	orientation tensor
I	unit tensor

Equation 2.4.20

S	orientation tensor
t	time
D	rate of deformation tensor
λ_{0b}	relaxation time of the backbone tube orientation
Λ	backbone tube stretch
α	material parameter defining the anisotropy
$I_{S\cdot S}$	first invariant of $\underline{\underline{S}} \cdot \underline{\underline{S}}$
I	unit tensor

Equation 2.4.21

Λ	backbone tube stretch
D	rate of deformation tensor
S	orientation tensor
λ_{0s}	relaxation time for the stretch
ν	parameter taken to be 2/q
q	amount of arms at the end of the backbone

Equation 2.4.22

τ	stress tensor
t	time
D	rate of deformation tensor
$\lambda(\tau)$	relaxation time of the backbone orientation
G_0	plateau modulus

Equation 2.4.23

$\lambda(\tau)$	relaxation time of the backbone orientation
λ_{0b}	relaxation time of the backbone tube orientation
α	material parameter defining the anisotropy
G_0	plateau modulus
τ	stress tensor
$f(\tau)$	function of the stress tensor
I	unit tensor

Equation 2.4.24

λ_{0b}	relaxation time of the backbone tube orientation
$f(\tau)$	function of the stress tensor
λ_s	stretch relaxation time
Λ	backbone tube stretch
α	material parameter defining the anisotropy
$I_{\tau\tau}$	first invariant of $\underline{\underline{\tau}} \cdot \underline{\underline{\tau}}$
G_0	plateau modulus

Equation 2.4.25

Λ	backbone tube stretch
I_τ	first invariant of the stress tensor
G_0	plateau modulus

Equation 2.4.26

λ_s	stretch relaxation time
λ_{0s}	relaxation time for the stretch
ν	parameter taken to be 2/q
Λ	backbone tube stretch

Equation 2.4.27

ν	parameter taken to be 2/q
q	amount of arms at the end of the backbone

Equation 2.4.28

η_{p1}	first planar viscosity
τ_{11}	1,1 component of the stress tensor
τ_{33}	3,3 component of the stress tensor
ε	extension rate

Equation 2.4.29

η_{p2}	second planar viscosity
τ_{22}	2,2 component of the stress tensor
τ_{33}	3,3 component of the stress tensor
ε	extension rate

Equation 2.5.1

$\dot{\varepsilon}_H$	applied Hencky strain
Ω	rotation rate of the drum
R	radius of the drum
L_0	distance between drums

Equation 2.5.2

$\eta_E^+(t)$	extensional viscosity growth
$F(t)$	instantaneous extensional force
$\dot{\varepsilon}_H$	Hencky strain rate
$A(t)$	instantaneous cross-sectional area of the sample